THE OHIO STATE UNIVERSITY

SATCOM ANTENNA SITING STUDY ON A P-3C USING THE NEC-BSC V3.1

D. Bensman and R. J. Marhefka

The Ohio State University

ElectroScience Laboratory

Department of Electrical Engineering
Columbus, Ohio 43212

Technical Report 721711-2
Grant No. NAG2-542
April 1990

Naval Air Test Center
Patuxent River, MD 20670
and
NASA - Ames Research Center
Moffett Field, CA 94035

NOTICES

When Government drawings, specifications, or other data are used for any purpose other than in connection with a definitely related Government procurement operation, the United States Government thereby incurs no responsibility nor any obligation whatsoever, and the fact that the Government may have formulated, furnished, or in any way supplied the said drawings, specifications, or other data, is not to be regarded by implication or otherwise as in any manner licensing the holder or any other person or corporation, or conveying any rights or permission to manufacture, use, or sell any patented invention that may in any way be related thereto.

50272-101

REPORT DOCUMENTATION PAGE	1. REPORT NO.	2.	3. Reciplent's Accession No.

4. Title and Subtitle SATCOM Antenna Siting Study on a P-3C Using the NEC-BSC V3.1	5. Report Date April 1990 6.
7. Author(s) D. Bensman and R.J. Marhefka	8. Performing Org. Rept. No. 721711-2
9. Performing Organization Name and Address The Ohio State University ElectroScience Laboratory 1320 Kinnear Road Columbus, OH 43212	10. Project/Task/Work Unit No. 11. Contract(C) or Grant(G) No. (C) (G) NAG2-542
12. Sponsoring Organization Name and Address University Affairs Branch, NASA - Ames Research Center M/S 241-25 Moffett Field, CA 94035	13. Report Type/Period Covered Technical Report 14.

15. Supplementary Notes

16. Abstract (Limit: 200 words)

The location of a UHF SATCOM antenna on a P-3C aircraft is studied using the NEC-Basic Scattering Code V3.1 (NEC-BSC3). The NEC-BSC3 is a computer code based on the Uniform Geometrical Theory of Diffraction. The code is first validated for this application using scale model measurements. In general, the comparisons are good except in 10 degree regions near the nose and tail of the aircraft. Patterns for various antenna locations are analyzed to achieve a prescripted performance.

17. Document Analysis a. Descriptors

b. Identifiers/Open-Ended Terms

c. COSATI Field/Group

18. Availability Statement A. Approved for public release; Distribution is unlimited.	19. Security Class (This Report) Unclassified	21. No. of Pages 330
	20. Security Class (This Page) Unclassified	22. Price

(See ANSI-Z39.18) *See Instructions on Reverse* OPTIONAL FORM 272 (4-77)
Department of Commerce

Contents

List of Figures

Chapter 1

Introduction

The purpose of this effort is to study the performance of SATCOM antennas on aircraft. The potential locations of the antenna system to achieve a desired pattern and polarization coverage is being assessed on a P-3C aircraft. A circular polarized antenna composed of crossed dipoles is being considered. The aircraft is being modeled using a computer code based on the Uniform Geometrical Theory of Diffraction (UTD), which is the NEC-BSC Version 3.1 [1].

In particular, the antenna modeled in this study represents a Dorne & Margolin DM 1501341 "Batwing" airborne UHF satellite communications antenna. The objective is to try to find a location for the antenna on the P-3C that will provide a minimum coverage of 330° azimuth, from zenith to 10° above the horizon of the aircraft. It is desired for the system to provide performace to maintain the satellite link in areas of high signal fading due to multipath effects. The results are referenced to a circular polarized isotropic radiator.

In Chapter 2, some of the relevent background of the modeling effort pertaining to UTD and the NEC-BSC are discussed. The model used to describe the UHF satelite antenna in this study is validated in Chapter 3. The P-3C computer model is validated in Chapter 4 by comparing with scale model measurements taken independently by Boeing and Lockheed. The extensive study of alternate locations is presented in Chapter 5. Chapter 6 presents a brief summary.

Chapter 2

Background

The use of computer codes based on UTD to analyze antenna system performance has a long history at The Ohio State University ElectoScience Laboratory. This has included the modeling of aircraft, ships and many other structures [2]. The accuracy of the modeling is dependent on many factors. They may be grouped into three broad categories, that is, theoretical completeness, modeling capabilities, and numerical considerations.

The issue of theoretical completeness in the context of UTD is associated with UTD being an asymptotic theory. The scattered field is assumed to come from local scattering centers or combination of centers. It is not necessary that all terms be considered, only the ones that are largest for the given application under study. For most antenna pattern prediction work, this has been determined to be no more than second order interaction terms. The diffraction coefficients for these terms also must be known at least approximately. In addition, the size of the objects should be around a wavelength in extent. Good engineering results, however, are obtainable with distances as small as a quarter wavelength.

The issue of modeling capabilities of the code are associated with the how accurately the individual building blocks of the code match the actual object being modeled. The building blocks of the NEC-BSC are discussed in the next section. Experience has shown that the model only needs to match the real scattering object near the antenna and in the general proximity of the pattern cut desired. The details necessary to be included for a given application can be determined by a modeling sensitivity study. The model is started simple and then features are added to it. If the patterns change

significantly, then more details are added until little change is detected.

The issue of numerical considerations are present in all computer codes. It is dependent on the computer used as well as the algorithms used. Numerical difficulties do not generally affect the entire pattern of a UTD code. It usually manifests itself as a logical consistency near shadow boundaries or at start up locations for approximate ray tracing algorithms for a given field term.

All of the above situations need to be kept in mind when a new class of applications is being considered. It is best to start simple from known situations and slowly build up to the ultimate solution. Ideally, scale model measurements or alternative calculations are available for a couple of cases. This allows bounds to be placed on the accuracy of the patterns of the rest of the unknown situations. If there are discrepancies, they are limited to small regions of the patterns of interest. The following sections of this report attempt to address the application under question based on these considerations.

2.1 NEC-BSC Modeling Capabilities

The analysis is based on uniform asymptotic techniques formulated in the Uniform Geometrical Theory of Diffraction (UTD) [3,4,5], sometimes referred to as the modern Geometrical Theory of Diffraction (GTD). The UTD approach is ideal for a general high frequency study of antennas in a complex environment. Only the most basic structural features of an otherwise very complicated structure need to be modeled. This is because ray optical techniques are used to determine components of the field incident on and diffracted by the various structures. Components of the diffracted fields are found using the UTD solutions for individual rays. They are summed with the geometrical optics terms in the far zone of the scattering centers, but, they can be in the near zone of the entire structure. The rays from a given scatterer interact with other structures causing various higher-order terms. One can trace out the various possible combinations of rays that interact between scatterers and determine and include only the dominant terms. Thus, one need only be concerned with the important scattering components and neglect all other higher-order terms. This method normally leads to accurate and efficient computer codes that can

be systematically written and tested. Complex problems can be built up from simpler problems in manageable pieces.

The limitations associated with the computer code result mainly from the basic nature of the analysis. The solution is derived using the UTD which is a high frequency approach. For the scattering from plate structures, this means that each plate should have edges at least a wavelength long. If a dielectric slab is used, the source must be at least a wavelength from the surface. Also, the incident field should not strike the slab too close to grazing. In addition, each antenna element should be at least a wavelength from all edges. For curved surfaces, the antenna can not be mounted directly on the curved part of the structure. The active element should be approximately a wavelength off the curved surface. In many cases, the wavelength limit can be reduced to a quarter wavelength for engineering purposes.

Note that the NEC-BSC is meant to complement other design techniques such as scale model measurements. It is a fast and cost effective means of anticipating problems at the early design stages of a system and to optimize design parameters such as antenna placement. In addition, it can be used at the measurement stage of development to confirm the experimental results. Also, near zone measurements can be projected into far zone patterns when it is very difficult to obtain the necessary range to be in the far zone of a whole structure.

A summary of the basic capabilities of the code are listed here:

- User oriented command word based input structure.
- Pattern calculations.
  - Near zone source fixed or moving.
  - Far zone observer.
  - Near zone observer.
- Single or multiple frequencies.
- Antenna to antenna spacial coupling calculations.
  - Near zone receiver fixed or moving.
- Efficient representation of antennas.

  - Infinitesimal Green's function representation.
  - Six built in antenna types.
  - Linear interpolation of table look up data.
  - Method of Moments code or Reflector Code interface.

- Multiple sided flat plates.
  - Separate or joined.
  - Infinite ground plane.
  - Limited dielectric plate capability.
- Multiple elliptic cylinders.
- UTD single and multiple interactions included.
  - Second order plate terms not including double diffraction.
  - First order cylinder terms only.
  - Presently no plate - cylinder interactions.

2.2 Plate - Cylinder Interactions

As noted above, presently the NEC-BSC V3.1 does not include any plate - cylinder interactions. However these plate - cylinder interactions have been found to play a significant role in various pattern cuts for some of the antenna locations which have been studied in this report. Most notably these interactions are significant when the antenna is located on the surface of the fuselage of the aircraft rotated down from the center line of the aircraft. These antenna locations are illustrated on the computer models which are used to compare with the Boeing and Lockheed measured results as shown in Sections 4.2, 4.3, 4.4, 4.5, 4.6,and 4.7 and the computer models used for Test Location 6 and Test Location 7 as shown in Sections 5.6 and 5.7 .

For the above antenna locations, the two most dominant terms which are missing from the calculations are: 1) the fields which are reflected from the cylinder (fuselage) then reflected from the plates (wings,stabilizers,etc.) and 2) the fields which are reflected from the cylinder (fuselage) then

diffracted from the plates (wings,stabilizers,etc.). In order to simulate these plate - cylinder interactions, a three step procedure is followed. Initially the first order UTD patterns containing the present UTD terms are calculated for the antenna located in the presence of the complete aircraft model. Secondly, the fuselage is removed and an image of the original antenna with respect to the fuselage is located in the presence of the plates only. The patterns are then calculated for the plate interactions due to the image source alone. Finally, these two patterns are added in order to create a pattern which includes these simulated plate - cylinder interactions. This same procedure is followed for all of the antenna locations in which these plate - cylinder interactions play a significant role as noted in the sections above. Any discontinuities which occur at $\phi = 0^o$ or $\phi = 180^o$ in the azimuth plane or conic planes in the above mentioned sections are also due to this imaging process. The imaging process is only valid in the half plane which contains the antenna. Therefore, the plate - cylinder interactions are only added in the half plane containing the antenna which causes the slight discontinuities which may be seen when crossing from this half plane to the other. This procedure is temporary, as the necessary terms will be added to the code as soon as possible.

2.3 Polarization Definition

In this report, the patterns are plotted according to right hand circular polarization and left hand circular polarization. The procedure used to define right hand circular polarization and left hand circular polarization is shown below. The direction vectors for the right hand and left circular polarized fields denoted by $\hat{R}$ and $\hat{L}$, respectively, are

$$\hat{R} = \frac{1}{\sqrt{2}}(\hat{\theta} - j\hat{\phi}) \tag{2.1}$$

$$\hat{L} = \frac{1}{\sqrt{2}}(\hat{\theta} + j\hat{\phi}). \tag{2.2}$$

The total $\vec{E}$ field at any point in the pattern is defined by

$$\vec{E}^{Tot} = \hat{R}E_R + \hat{L}E_L \tag{2.3}$$

where E_R is the right hand circular polarized field component and E_L is the left hand circular polarized field component. The magnitude for the right hand and left hand circular polarized field components are

$$E_R = \frac{1}{\sqrt{2}}(E_\theta + jE_\phi) \tag{2.4}$$

$$E_L = \frac{1}{\sqrt{2}}(E_\theta - jE_\phi) \tag{2.5}$$

where E_θ and E_ϕ are the field components in the $\hat{\theta}$ and $\hat{\phi}$ directions, respectively. These definitions for the right hand and left hand circular polarized fields given by equations (2.4) and (2.5), respectively, are used throughout the remainder of this report.

2.4 Normalization Procedures

The NEC-BSC is not an antenna code per se. It does not know the current distribution of the antenna as a whole that it is modeling. It just knows the pattern factor based on the type chosen and the amplitude and phase of each of the elements representing the antenna. Therefore, it does not know the power radiated or the input impedance of the antenna unless it is provided the information.

If the information of the antenna is obtained by a method of moments code, than the power budget along with the appropriate currents provided will be sufficient to normalize the code to a gain quantity. If the antenna is described by built in factors with user supplied currents, then the user must also supply an estimate of the power budget. This is accomplished by integrating the volumetric pattern of the fields radiated by the antenna as supplied by the code. The best results are provided by calculating the volumetric pattern of the antenna at its location on the model of the aircraft being used. This can be quite costly, however, since only a portion of the pattern may be of interest even though a complete volumetric pattern is being calculated for each location. It has been determined, however, that sufficiently accurate results are obtainable by determining the power radiated by integrating the volumetric pattern provided by the code for the antenna in free space or over an infinite ground plane which ever is more appropriate. It is obvious that the current distribution will not change for

the NEC-BSC antenna model. Hence, if one assumes that power is conserved when the model is changed, the same number can be used for all the different antenna positions and aircraft models. This concept is confirmed here by the good overall results for the gain obtained by comparing with measured results.

Chapter 3

Antenna Model Validation

The first step has been to analyze the present candidate UHF SATCOM antenna system and validate the antenna model which has been used in the NEC-BSC code [1]. In order to validate the antenna model, NEC-BSC calculated antenna patterns have been compared to measured antenna patterns provided by the manufacturer and measured patterns provided by Naval Air Test Center. Also, the NEC-BSC calculated antenna patterns have been compared to antenna patterns calculated using other methods. All the results found throughout this report have been referenced to an isotropic radiator. In order to reference these results to an isotropic radiator, the average power level of the antenna model in free space is first calculated. This average power level is then subtracted in dB from the absolute levels calculated for the various patterns to give the isotropic levels shown in the patterns throughout this report. The results found during these comparisons are discussed in this chapter. In all cases, the results confirm the antenna model used in the NEC-BSC code.

3.1 Dorne & Margolin Results

Naval Air Test Center has provided antenna system information for the Dorne & Margolin DM 1501341 (Batwing) airborne UHF satellite communication antenna shown in Figure 3.1. A simple crossed dipole has been used in the code with the corresponding dimensions given in the figure. The calculated result in Figure 3.2 at 244 MHz can be compared with the measured result supplied by the manufacturer in Figure 3.3 for the antenna

on a 8 foot ground plane in the principal elevation cut for the antenna. The results compare very well.

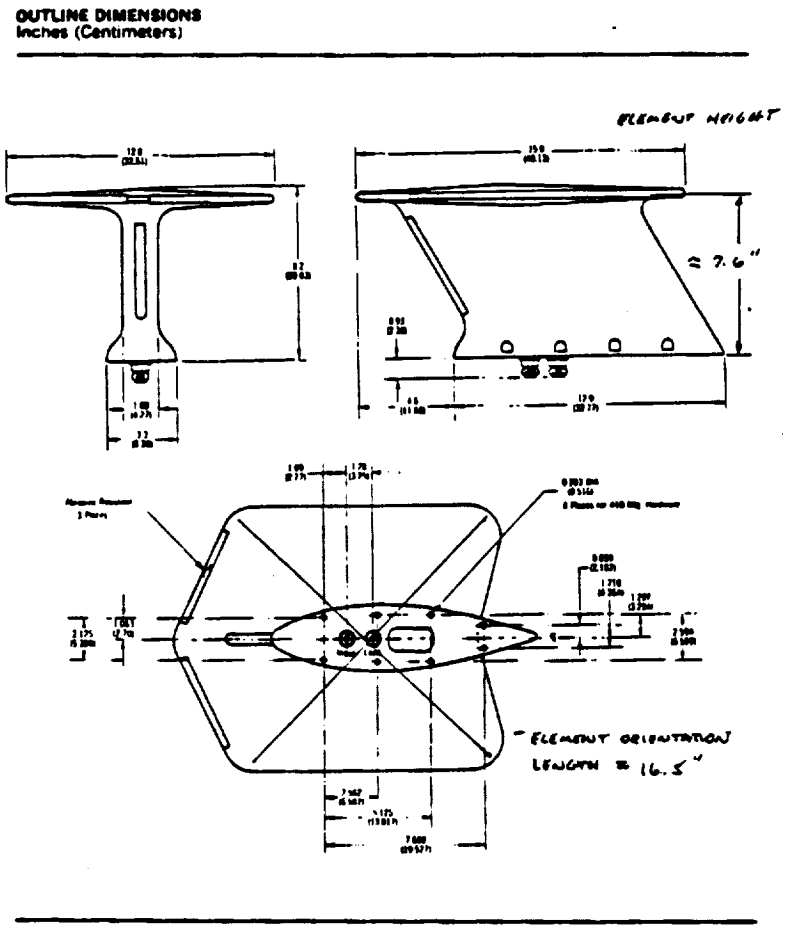

Figure 3.1: Batwing airborne UHF satellite communication antenna of Dorne & Margolin.

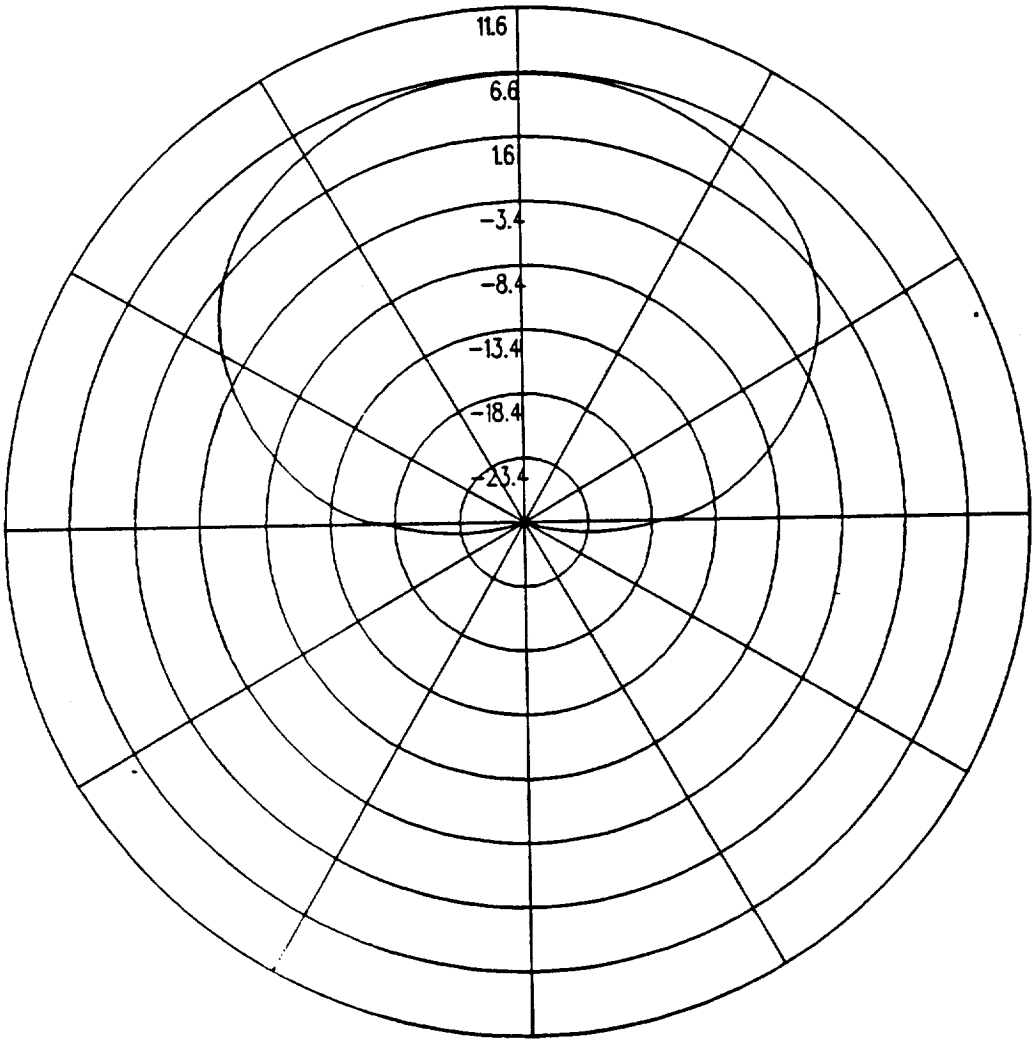

Figure 3.2: Calculated Batwing right hand circular polarized antenna pattern in principal elevation cut at 244 MHz on a 8' ground plane using the NEC-BSC.

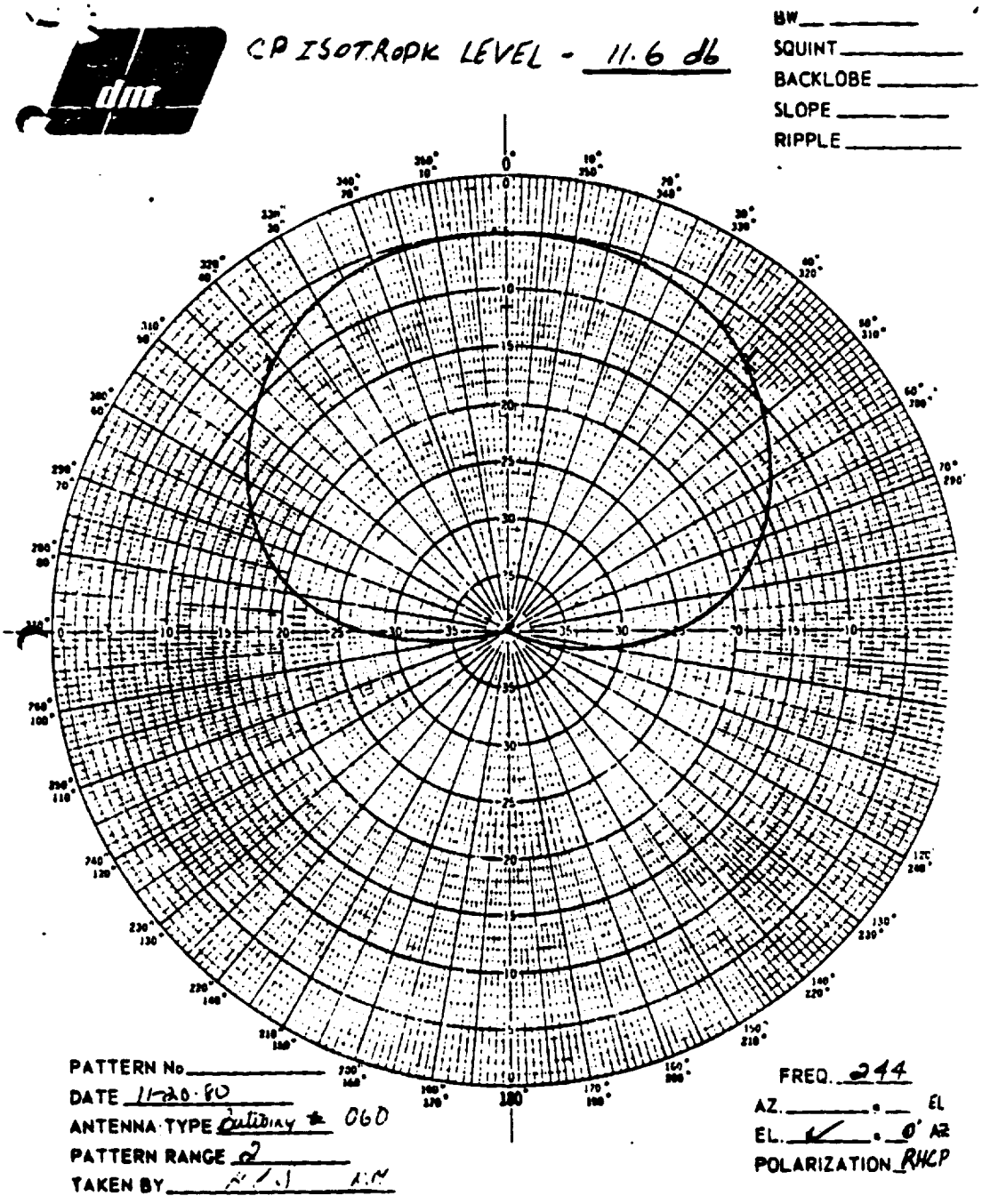

Figure 3.3: Measured Batwing right hand circular polarized antenna pattern in principal elevation cut at 244 MHz on a 8' ground plane. (Pattern supplied by Dorne & Margolin.)

3.2 Method of Moments Results

Because the manufacturer has only provided information in the principal elevation cut, a moment method approach using the electromagnetic surface patch code [6] must be used in order to test the NEC-BSC's representation of the antenna for a pattern taken along the length of one of the dipole arms. Therefore, the free space pattern along the length of one of the dipole arms at 300 MHz using the NEC-BSC code shown in Figure 3.4 can be compared with the method of moments result shown in Figure 3.5. Again quite good agreement is obtained. To ensure that the NEC-BSC representation along the dipole in the presence of an infinite ground plane is also valid, the pattern at 300 MHz using the NEC-BSC code shown in Figure 3.6 can be compared with the method of moments result shown in Figure 3.7. Above the ground plane the results compare very well. The field present below the ground plane in the method of moments pattern is caused by an imaging technique used to simulate the infinite ground plane in the ESP code.

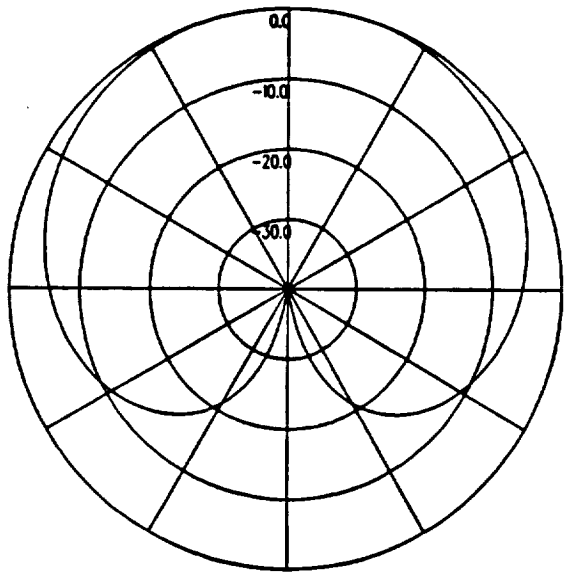

Figure 3.4: Calculated Batwing right hand circular polarized antenna pattern along one of the dipole arms at 300 MHz in free space using the NEC-BSC.

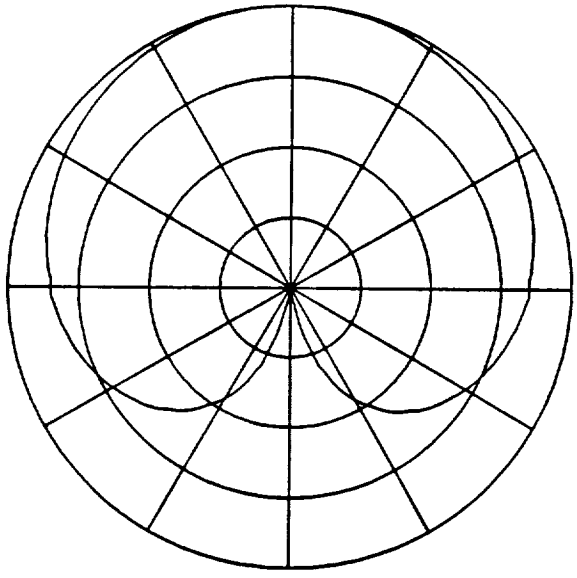

Figure 3.5: Calculated Batwing right hand circular polarized antenna pattern along one of the dipole arms at 300 MHz in free space using the ESP code.

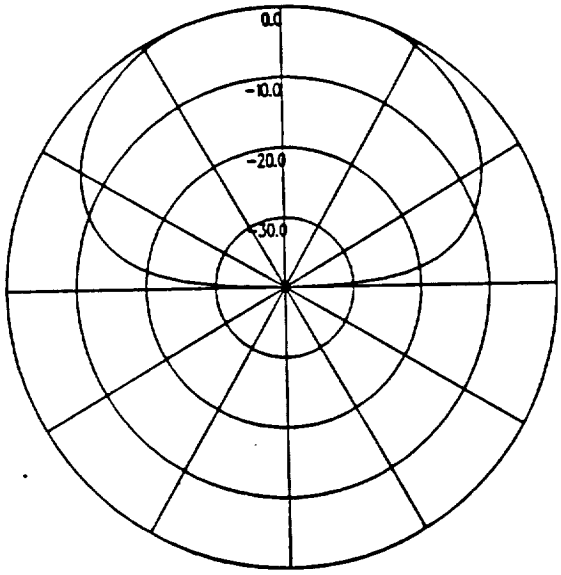

Figure 3.6: Calculated Batwing right hand circular polarized antenna pattern along one of the dipole arms at 300 MHz on an infinite ground plane using the NEC-BSC.

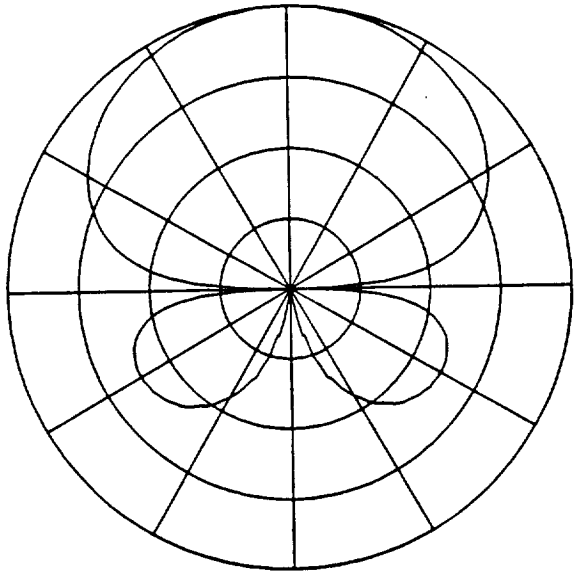

Figure 3.7: Calculated Batwing right hand circular polarized antenna pattern along one of the dipole arms at 300 MHz on an infinite ground plane using the ESP code.

3.3 Naval Air Test Center Results

Naval Air Test Center has also provided measured antenna radiation patterns for the full-sized DM 1501341 Batwing antenna on a 6 foot ground plane. These radiation patterns for the vertical and horizontal polarizations have been taken at 300 MHz for various elevation cuts of the antenna. The calculated results for the vertical and horizontal polarizations in the principal elevation cut shown in Figure 3.8 and Figure 3.10, respectively, can be compared to the measured results shown in Figure 3.9 and Figure 3.11. The calculated results for the vertical and horizontal polarizations in the elevation cut along one of the dipoles shown in Figure 3.12 and Figure 3.14, respectively, can be compared to the measured results shown in Figure 3.13 and Figure 3.15. Again there is good agreement between the calculated results and the measured results for both the vertical and horizontal polarizations in each of the elevation pattern cuts studied.

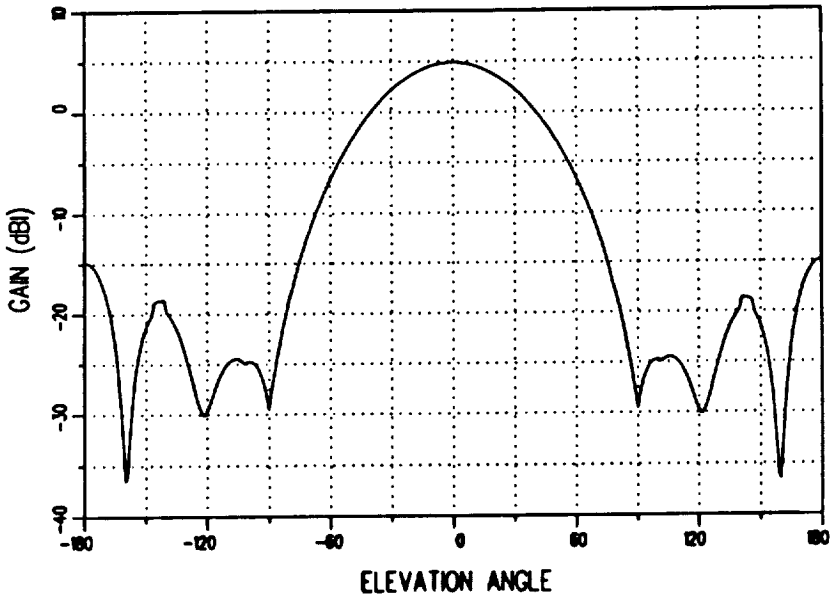

Figure 3.8: Calculated vertical polarized antenna pattern in principal elevation cut at 300 MHz on a 6' ground plane using the NEC-BSC.

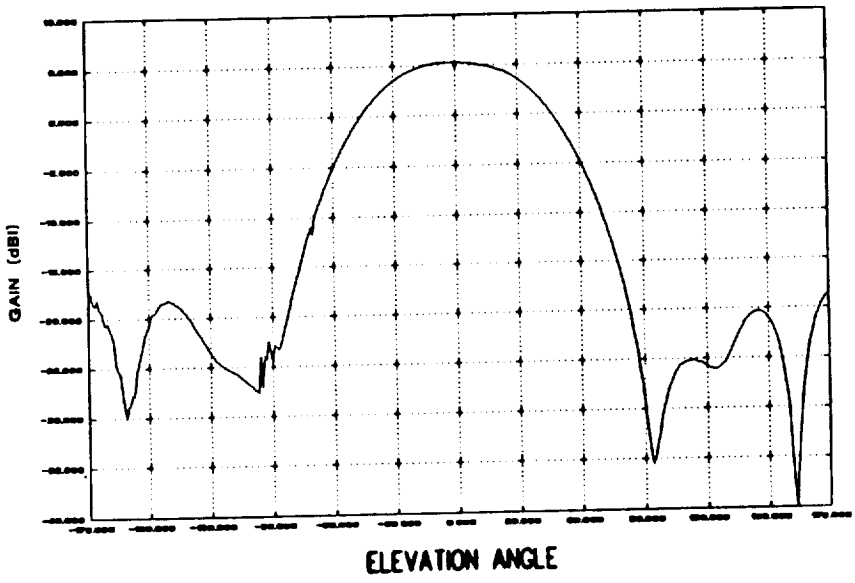

Figure 3.9: Measured vertical polarized antenna pattern in principal elevation cut at 300 MHz on a 6' ground plane. (Pattern supplied by Naval Air Test Center.)

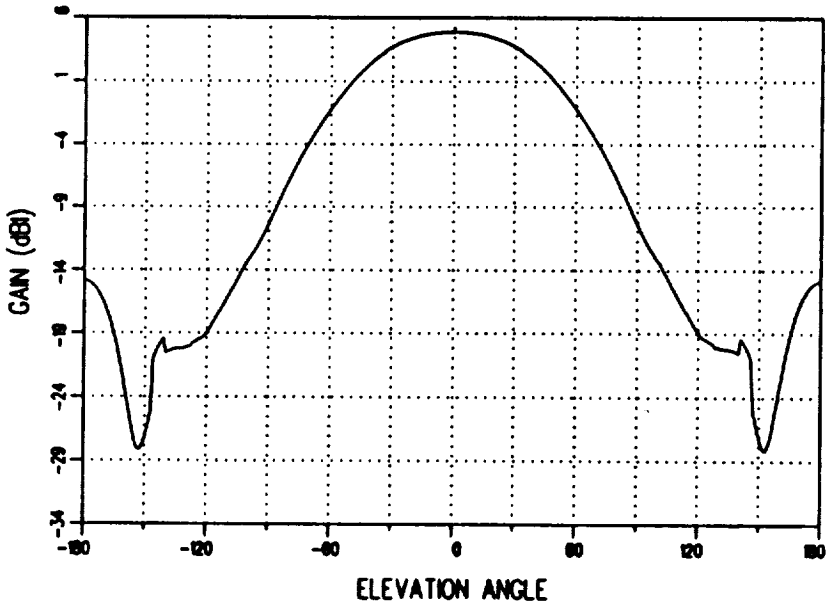

Figure 3.10: Calculated horizontal polarized antenna pattern in principal elevation cut at 300 MHz on a 6' ground plane using the NEC-BSC.

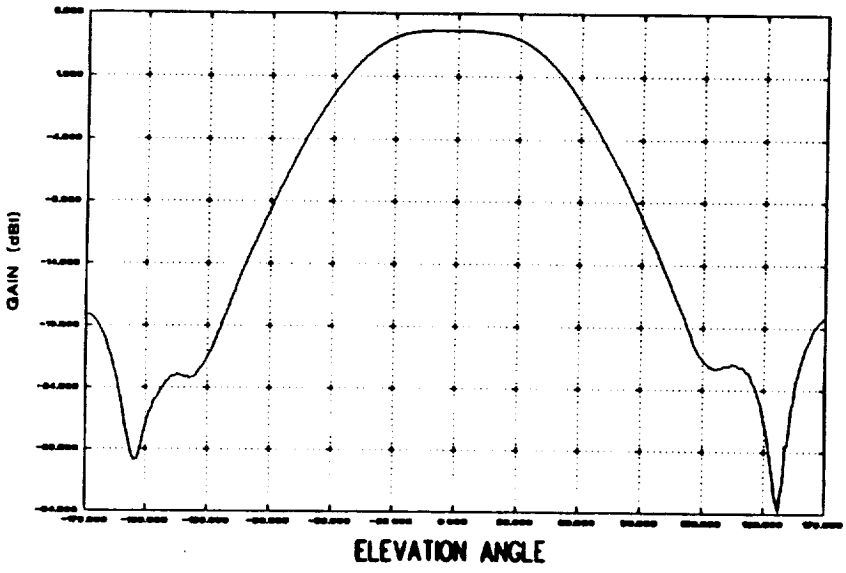

Figure 3.11: Measured horizontal polarized antenna pattern in principal elevation cut at 300 MHz on a 6' ground plane. (Pattern supplied by Naval Air Test Center.)

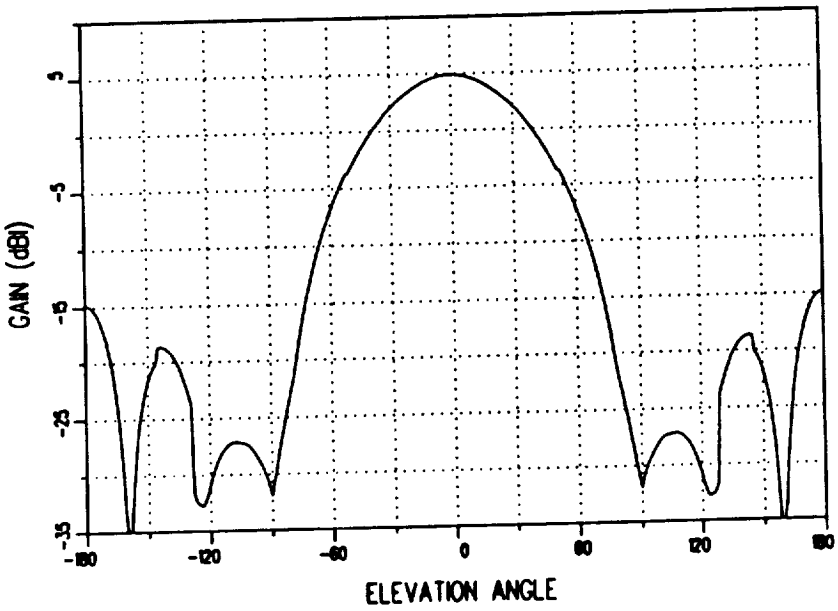

Figure 3.12: Calculated vertical polarized antenna pattern in elevation cut along one of the dipoles at 300 MHz on a 6' ground plane using the NEC-BSC.

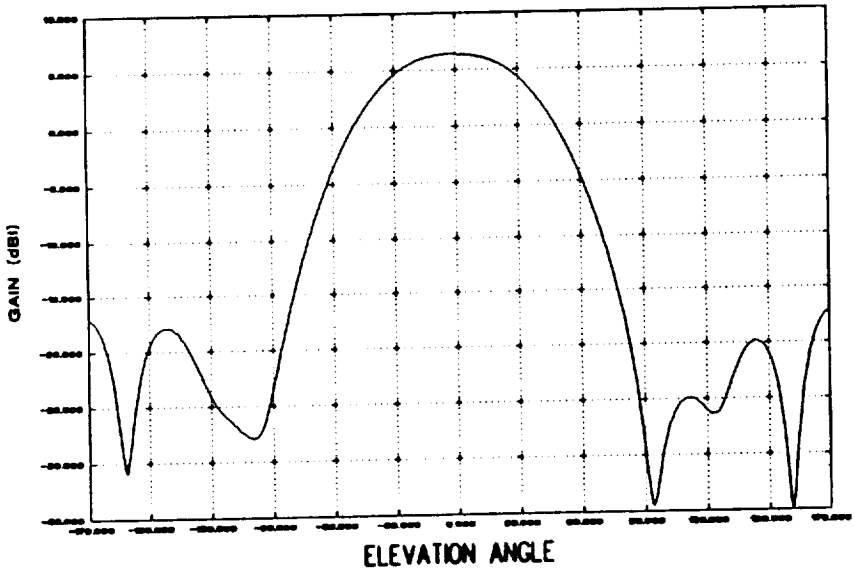

Figure 3.13: Measured vertical polarized antenna pattern in elevation cut along one of the dipoles at 300 MHz on a 6' ground plane. (Pattern supplied by Naval Air Test Center.)

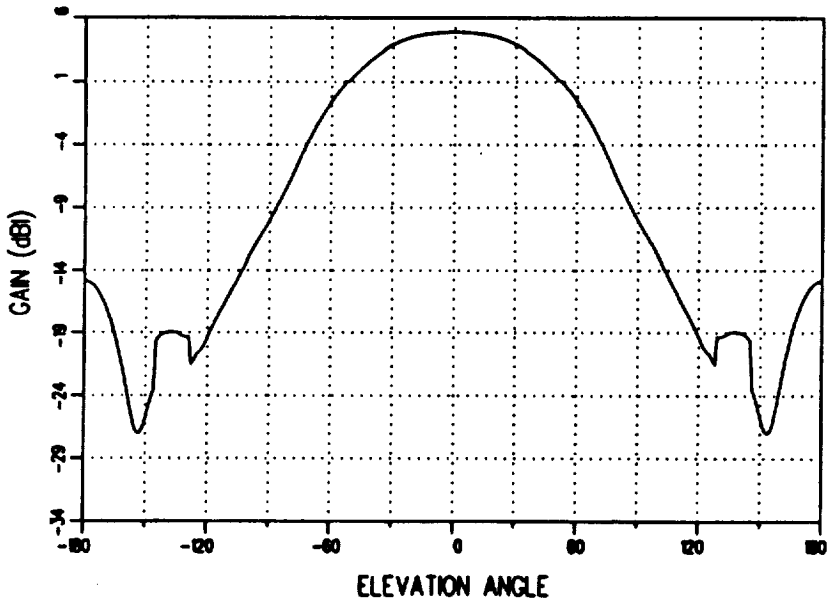

Figure 3.14: Calculated horizontal polarized antenna pattern in elevation cut along one of the dipoles at 300 MHz on a 6' ground plane using the NEC-BSC.

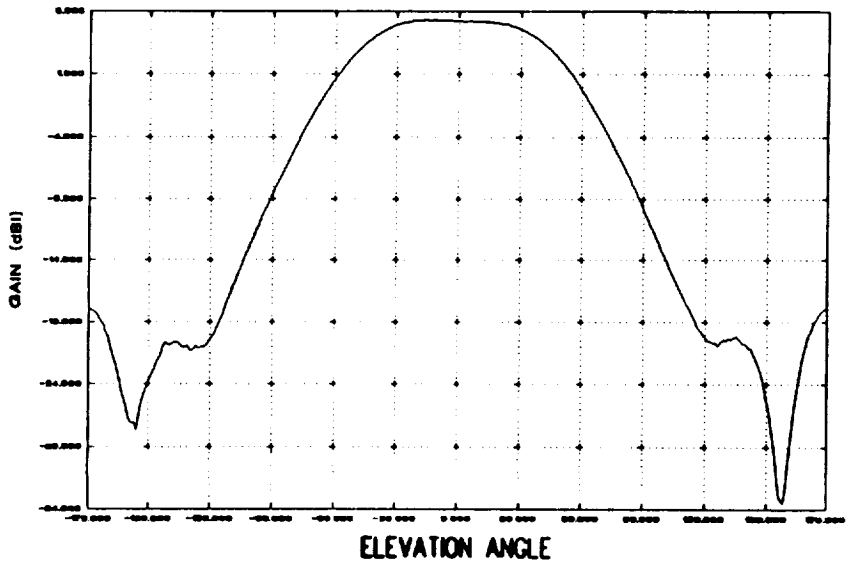

Figure 3.15: Measured horizontal polarized antenna pattern in elevation cut along one of the dipoles at 300 MHz on a 6' ground plane. (Pattern supplied by Naval Air Test Center.)

3.4 Exact Eigenvalue Solution Results

In the majority of the cases investigated, the crossed dipole antenna is positioned near the surface of a cylinder which is used to represent the aircraft fuselage. In order to ensure that the NEC-BSC correctly calculates the fields for this situation, the NEC-BSC calculated radiation patterns for an infinitesimal crossed dipole positioned near the surface of an infinite cylinder can be compared to the radiation patterns determined from the exact eigenvalue solution [7]. For this problem, the dipoles had to be oriented axially and circumferentially to the cylinder due to the eigenfunction solution. In the actual situation, the dipoles are rotated 45°. The NEC-BSC calculated results for the right hand and left hand polarizations in the plane of the crossed dipole antenna shown in Figure 3.16 can be compared to the results determined from the exact eigenvalue solution shown in Figure 3.17. Also, the NEC-BSC calculated results for the right hand and left hand polarizations in a conic cut of 45° about the axis of the infinite cylinder is shown in Figure 3.18. It can be compared to the results determined from the exact eigenvalue solution shown in Figure 3.19. Again there is good agreement between the calculated results using NEC-BSC and the calculated results using the exact eigenvalue solution for both the right hand and left hand polarizations in each of the elevation pattern cuts studied.

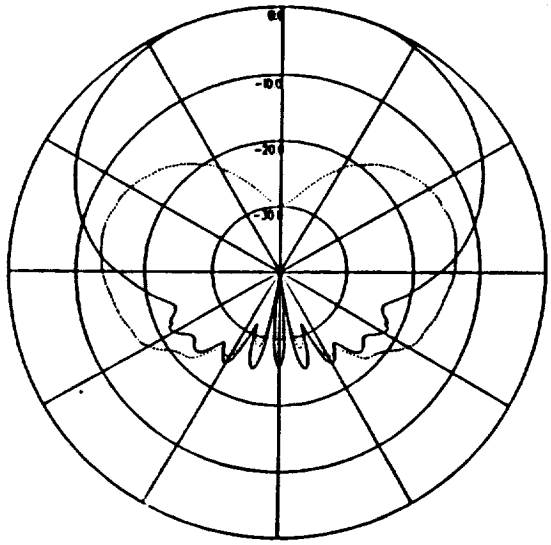

Figure 3.16: Calculated right hand (solid line) and left hand (dashed line) polarized antenna patterns in the plane of infinitesimal crossed dipole antenna positioned near an infinite cylinder using NEC-BSC.

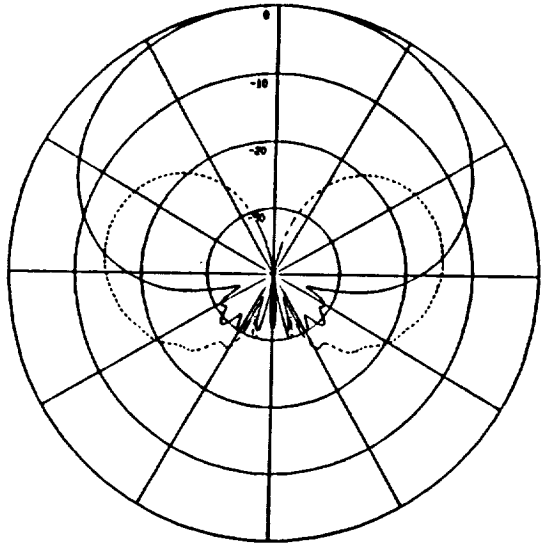

Figure 3.17: Calculated right hand (solid line) and left hand (dashed line) polarized antenna patterns in the plane of infinitesimal crossed dipole antenna positioned near an infinite cylinder using exact eigenvalue solution.

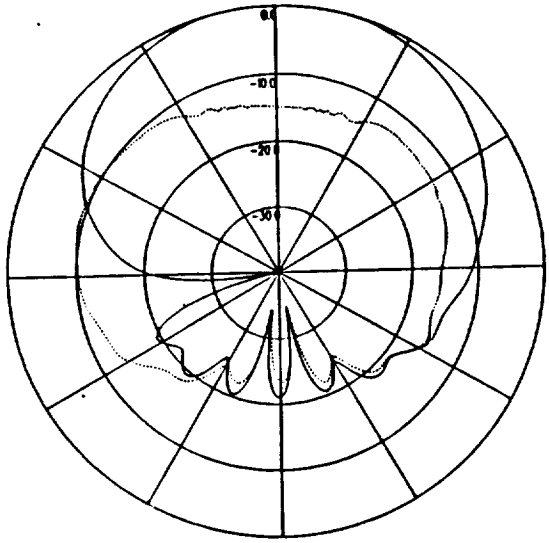

Figure 3.18: Calculated right hand (solid line) and left hand (dashed line) polarized antenna patterns in a conic cut of 45° about the axis of the cylinder for an infinitesimal crossed dipole antenna positioned near an infinite cylinder using NEC-BSC.

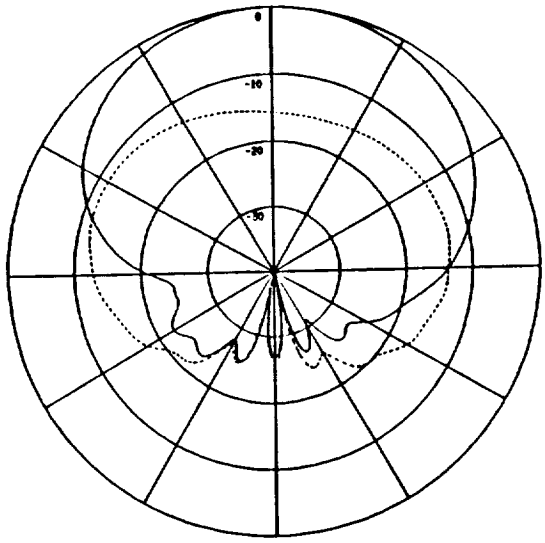

Figure 3.19: Calculated right hand (solid line) and left hand (dashed line) polarized antenna patterns in a conic cut of 45° about the axis of the cylinder for an infinitesimal crossed dipole antenna positioned near an infinite cylinder using exact eigenvalue solution.

Chapter 4

Aircraft Model Validation

Naval Air Test Center has supplied extensive model measurements independently conducted by Boeing on a 1/17 scale model and Lockheed on a 1/10 scale model. In order to validate the aircraft model used in the NEC-BSC code, the calculated patterns in the roll plane, the azimuth plane, the elevation plane and conical pattern planes from 10° to 30° above the horizon have been compared to measured results provided by Boeing and Lockheed. To study the effect of the aircraft model on the calculated patterns, three aircraft models have been used for the antenna location in the Boeing report. The difference between the three aircraft models involves the way the aircraft fuselage is represented. The first case uses a cylinder to represent the fuselage, the second case uses a composite ellipsoid, and the third case uses a cone frustum. The calculations have been compared to the measured patterns in order to determine which aircraft model gives the best representation of the actual P-3C aircraft. To test the stability of the computer aircraft representation, a model for the inner engine has been added to see the effect on the radiation patterns. Comparing these results with the patterns obtained from the aircraft model without the engine determines whether the model for the engine needs to be included in the aircraft model. Also, the calculated patterns for two additional antenna locations have been compared to the measured patterns provided by Lockheed and Boeing in order to ensure that the aircraft computer model is valid for a variety of antenna locations. The results found during these comparisons are discussed below.

4.1 Pattern Coordinate System Definition

The remainder of the report contains radiation patterns in the roll plane, the azimuth plane, the elevation plane and the conical cuts from 10° to 30° above the horizon for various antenna locations on the P-3C aircraft. In order to interpret these results, one must first know what the pattern coordinate systems are relative to the aircraft. The spherical coordinate system relative to the aircraft which is used in this report is given in Figure 4.1. The pattern coordinate system for each of the various radiation patterns relative to the aircraft is illustrated in Figure 4.2. These pattern coordinate systems are used throughout the remainder of the report. The sole exceptions are the measured and calculated elevation patterns for the antenna location studied by Lockheed in Section 4.6 . In these elevation plane patterns, the nose of the aircraft is to the right in the radiation pattern and the tail to the left, which is the exact opposite of the elevation plane patterns for all of the other cases.

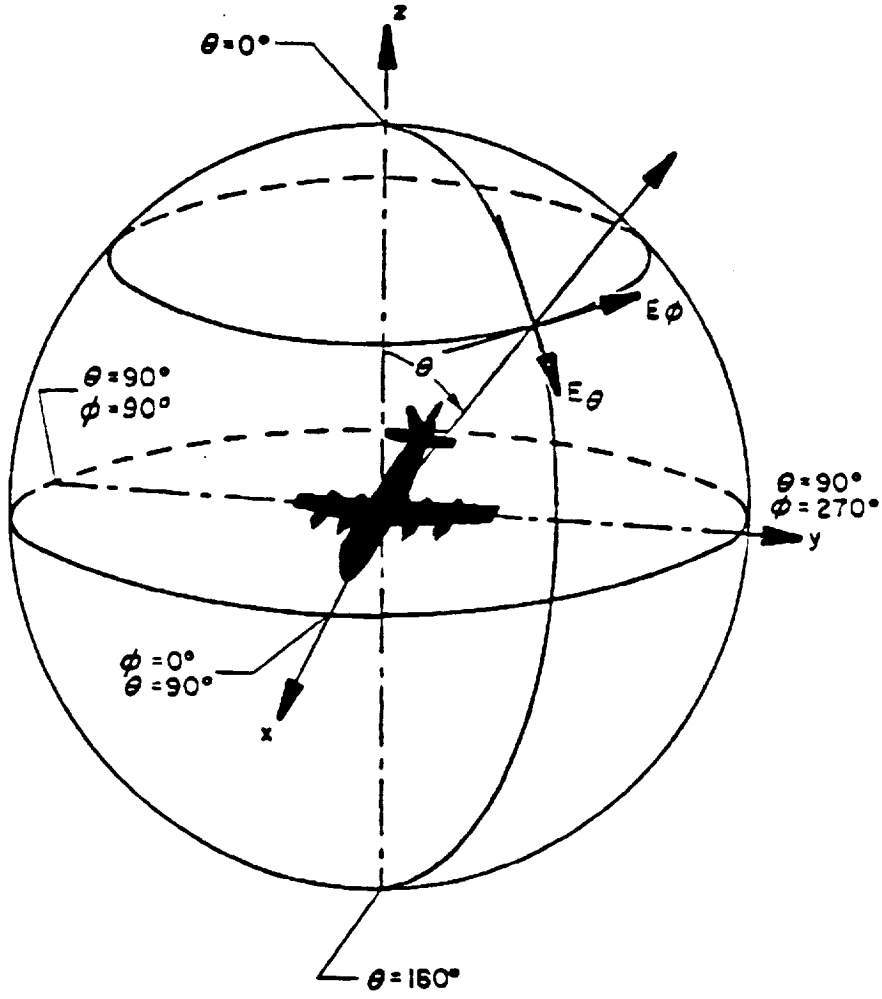

Figure 4.1: Spherical coordinate system relative to the aircraft which is used in the remainder of the report.

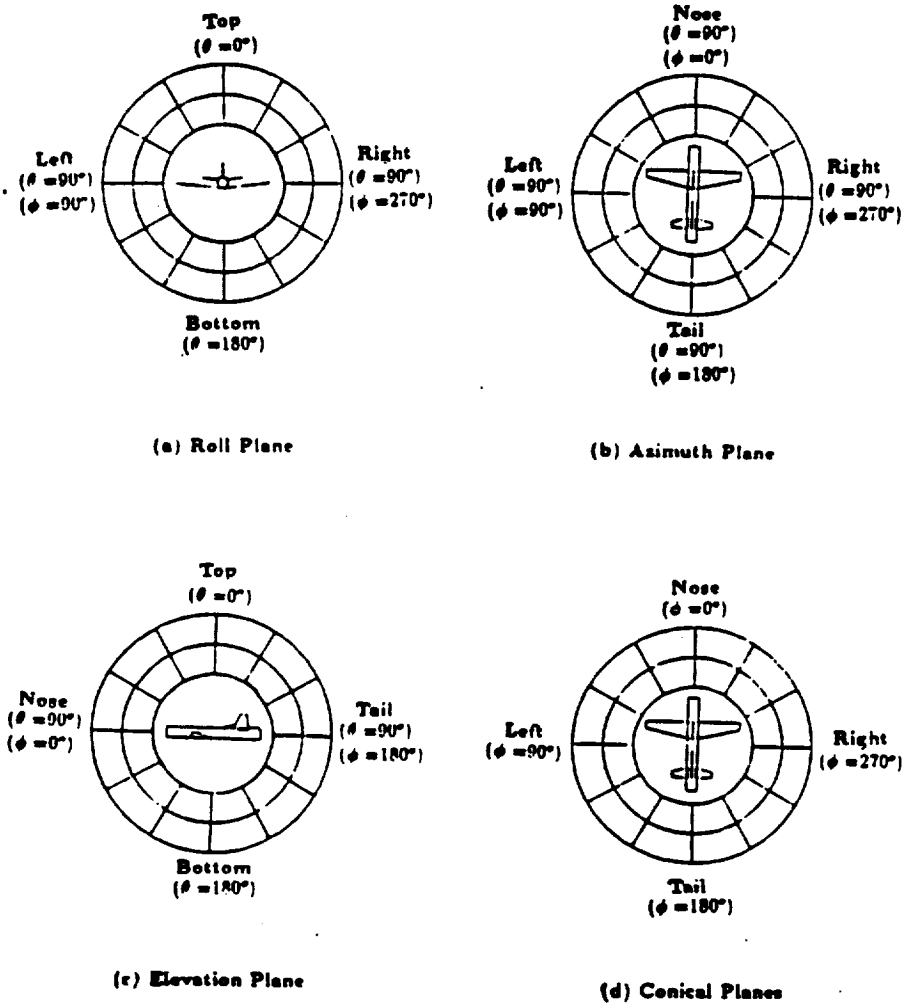

Figure 4.2: Pattern coordinate systems relative to the aircraft for (a) roll plane, (b) azimuth plane, (c) elevation plane, and (d) conical planes.

4.2 Boeing Location with Cylindrical Fuselage

The results computed in this section have been compared to the measured results provided by Boeing [8]. The antenna is located as illustrated in Figure 4.3, which also shows the computer model used to generate the results. The calculated results at 300 MHz are compared with measurements for the roll plane in Figures 4.4 and 4.5, for the azimuth plane in Figures 4.6 and 4.7, for the elevation plane in Figures 4.8 and 4.9, for the conical plane 10° above the horizon in Figures 4.10 and 4.11, for the conical plane 20° above the horizon in Figures 4.12 and 4.13, and for the conical plane 30° above the horizon in Figures 4.14 and 4.15 all for right hand polarization. The cross polarized fields are compared for the roll plane in Figures 4.16 and 4.17, for the azimuth plane in Figures 4.18 and 4.19, for the elevation plane in Figures 4.20 and 4.21, for the conical plane 10° above the horizon in Figures 4.22 and 4.23, for the conical plane 20° above the horizon in Figures 4.24 and 4.25, and for the conical plane 30° above the horizon in Figures 4.26 and 4.27 all for left hand polarization.

Notice that the roll plane results for right hand polarization compare very well throughout the complete pattern. Comparing the calculated and measured azimuth plane results shows that there is good agreement in the region 45° from the nose of the aircraft to the tail of the aircraft. However, as the pattern approaches the nose of the aircraft, the calculated levels increase to as much as 5 dB higher than the measured levels. Comparing the elevation plane results shows that in the region directly above the aircraft (i.e., over 30° above the horizon) the radiation patterns agree very well. However, as the pattern approaches the horizon near the tail, the calculated pattern reaches levels which are as much as 5–8 dB higher than the measured results.

These higher levels near the nose and tail of the aircraft on the horizon have been investigated extensively and are most likely due to the fact that the plate - cylinder interactions which have been simulated using the imaging technique explained in Section 2.2 are only approximations. When the exact plate - cylinder interactions are implemented in the code, the differences between the measured and calculated results are anticipated to be reduced. Comparing the conical pattern planes, however, shows that as

the pattern cut is taken above the horizon there is very good agreement between the patterns.

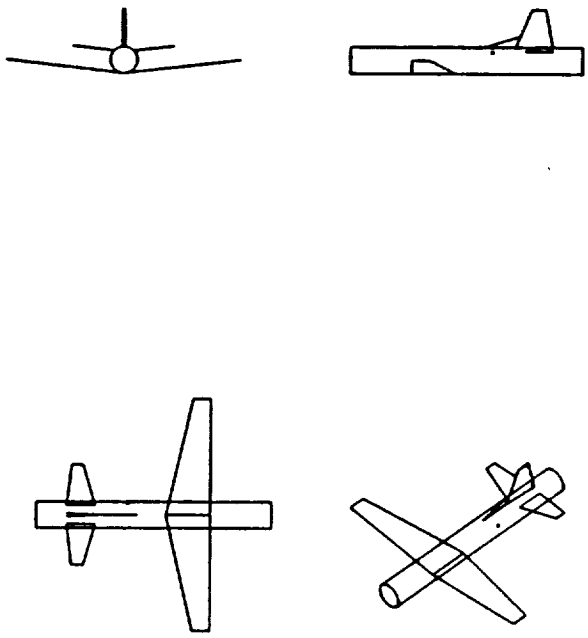

Figure 4.3: Geometry of the cylindrical model of the P-3C aircraft used in the NEC-BSC code showing the location of the antenna.

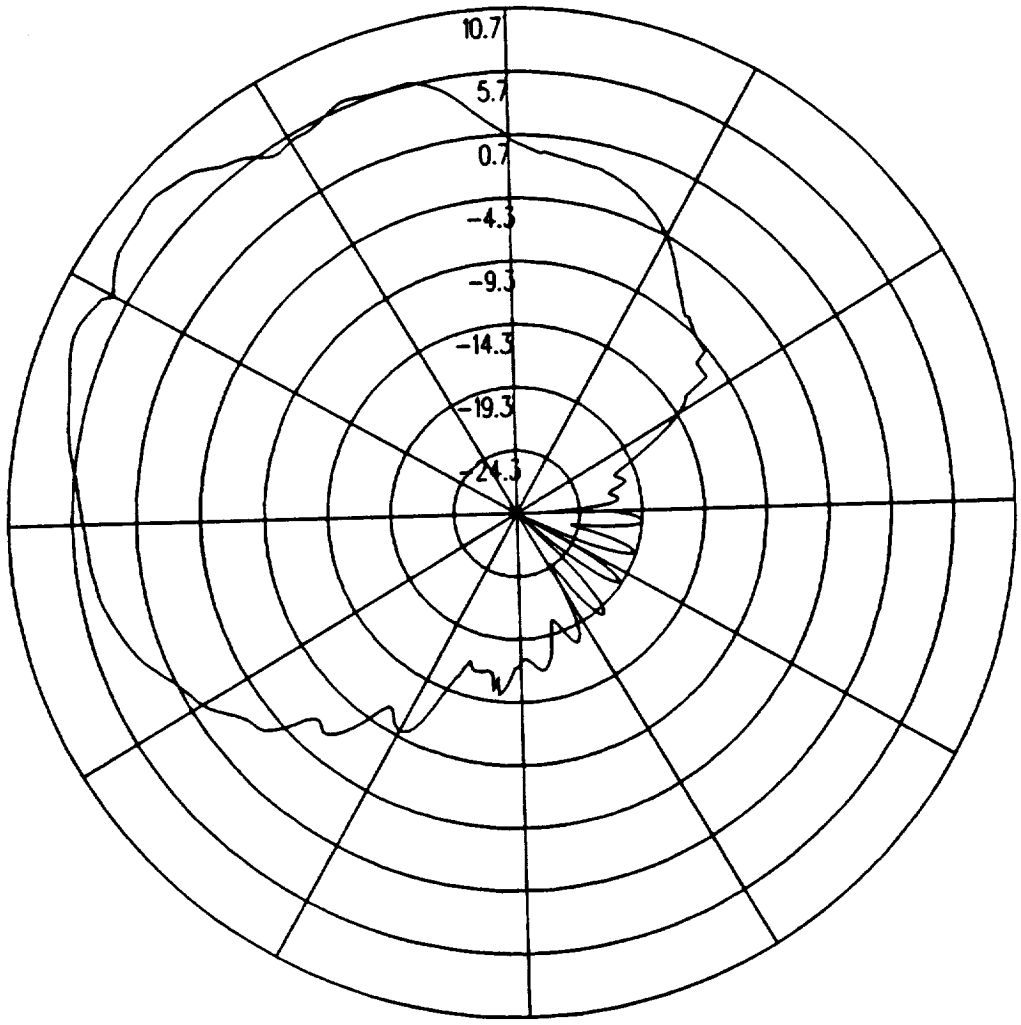

Figure 4.4: UTD calculated roll plane pattern for batwing antenna on a P-3C for right hand circular polarization at 300 MHz.

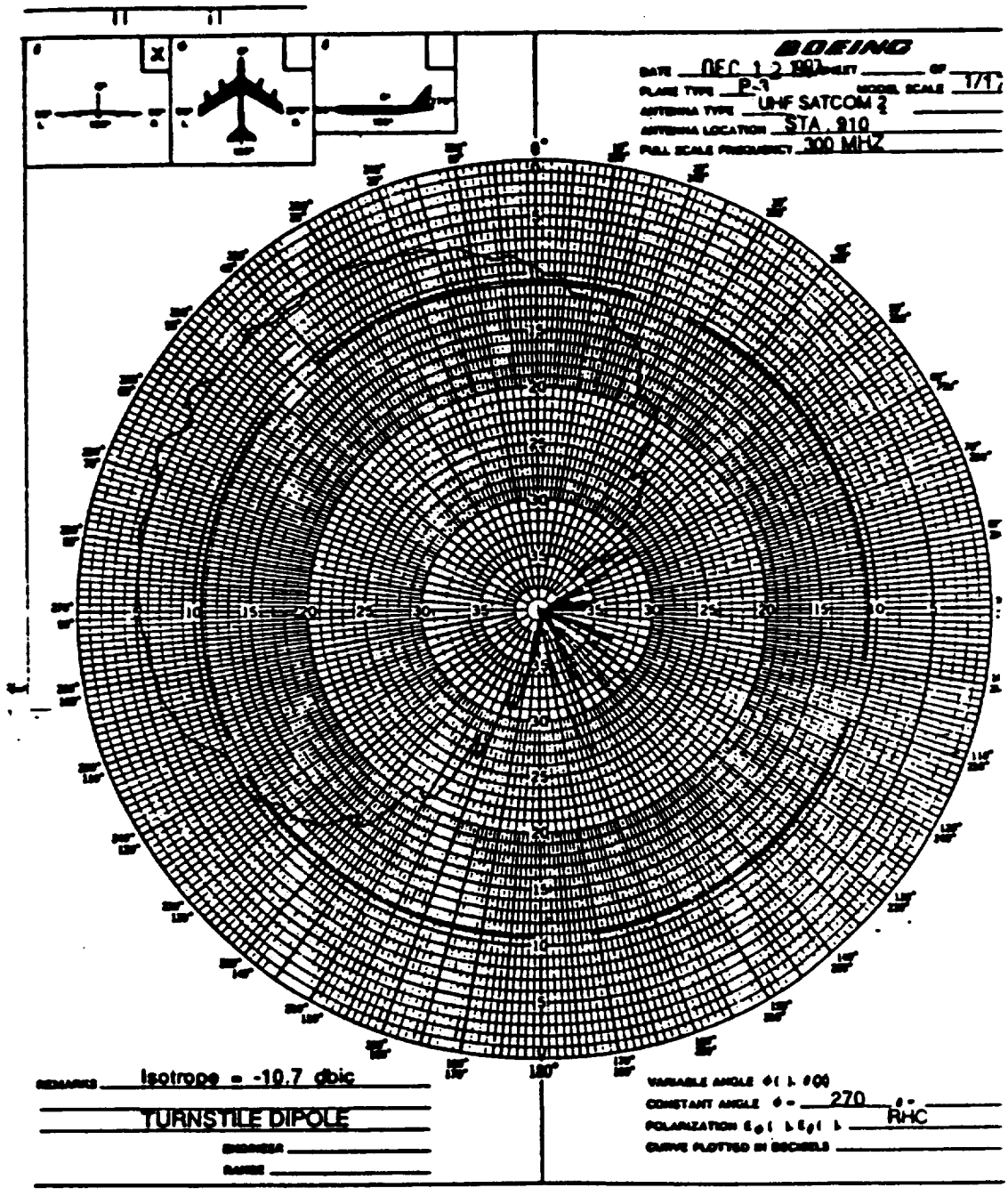

Figure 4.5: Boeing's measured roll plane pattern for batwing antenna on a P-3C for right hand circular polarization at 300 MHz.

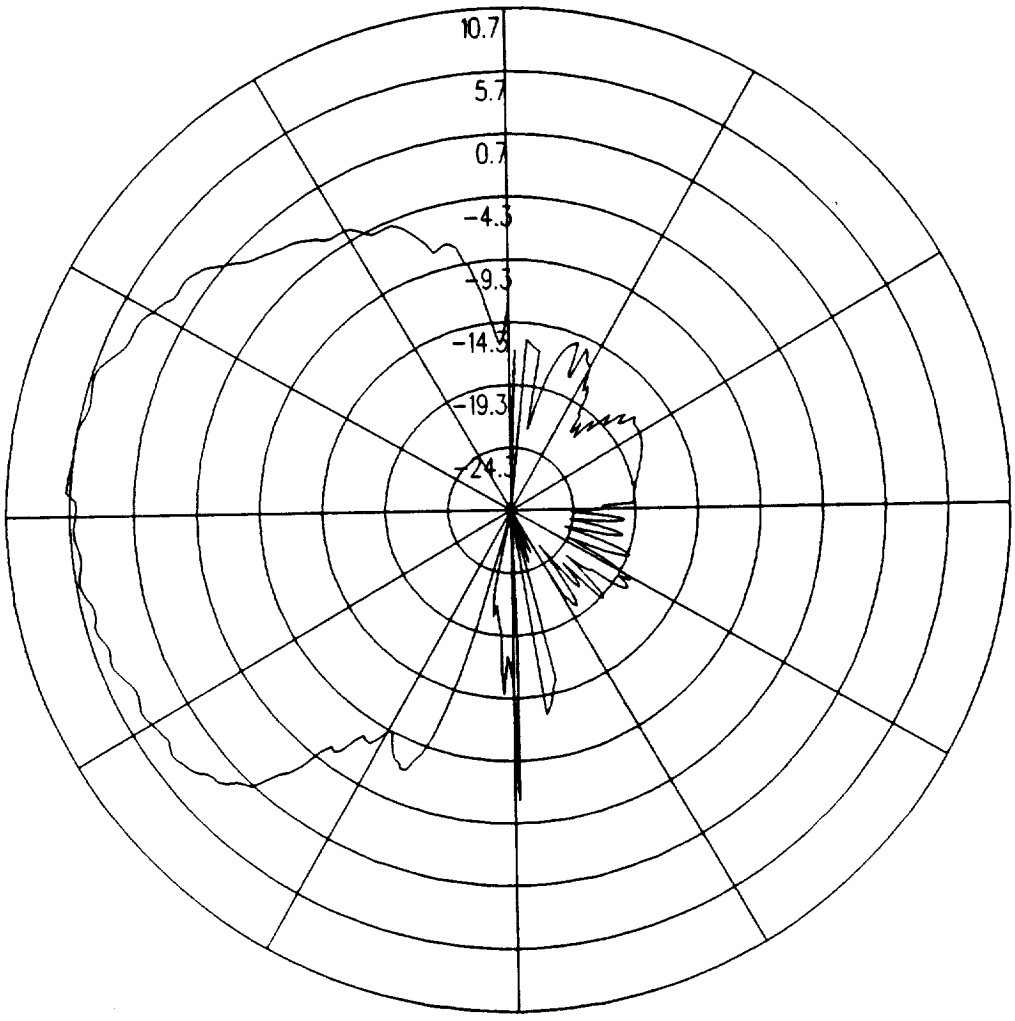

Figure 4.6: UTD calculated azimuth plane pattern for batwing antenna on a P-3C for right hand circular polarization at 300 MHz.

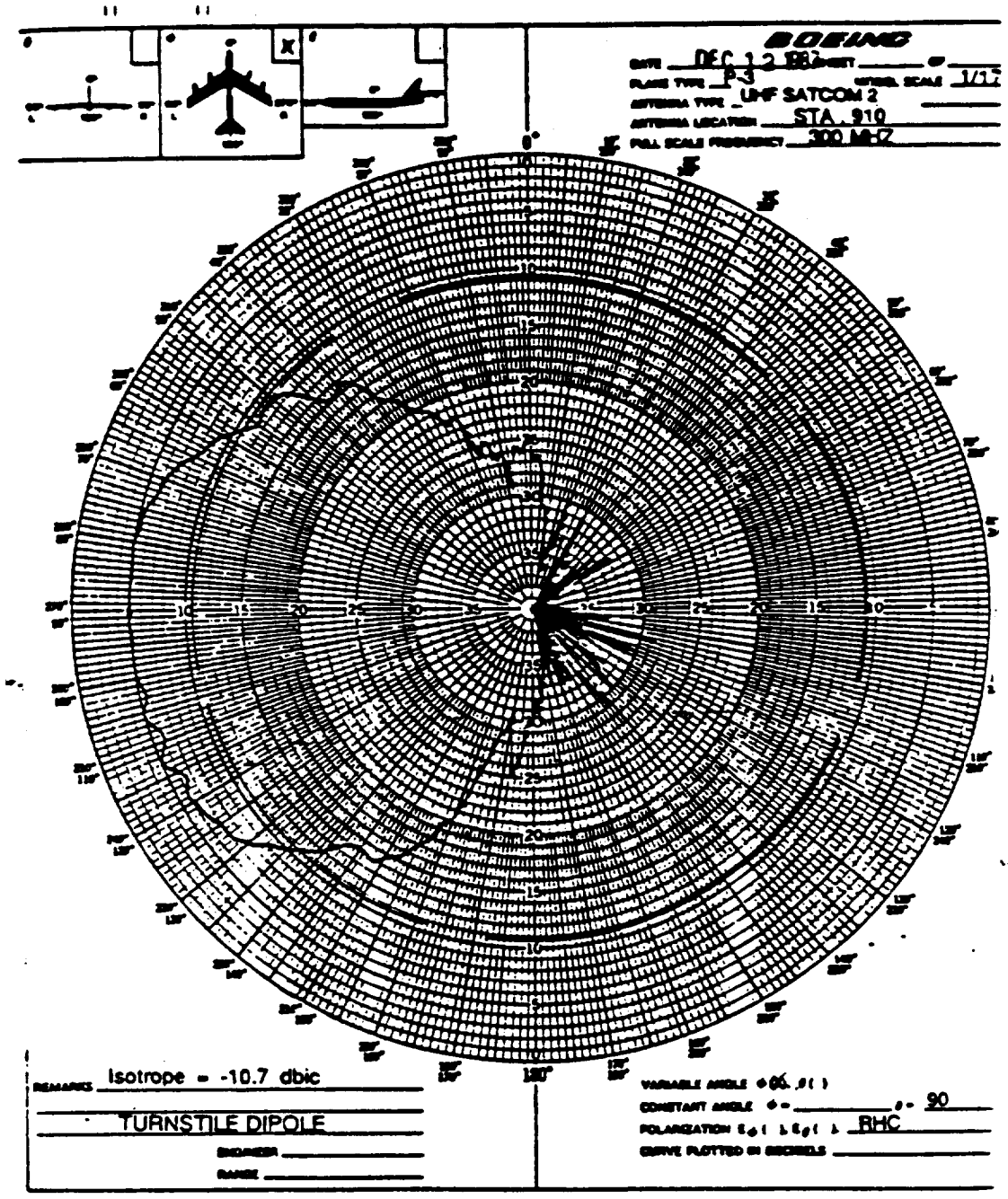

Figure 4.7: Boeing's measured azimuth plane pattern for batwing antenna on a P-3C for right hand circular polarization at 300 MHz.

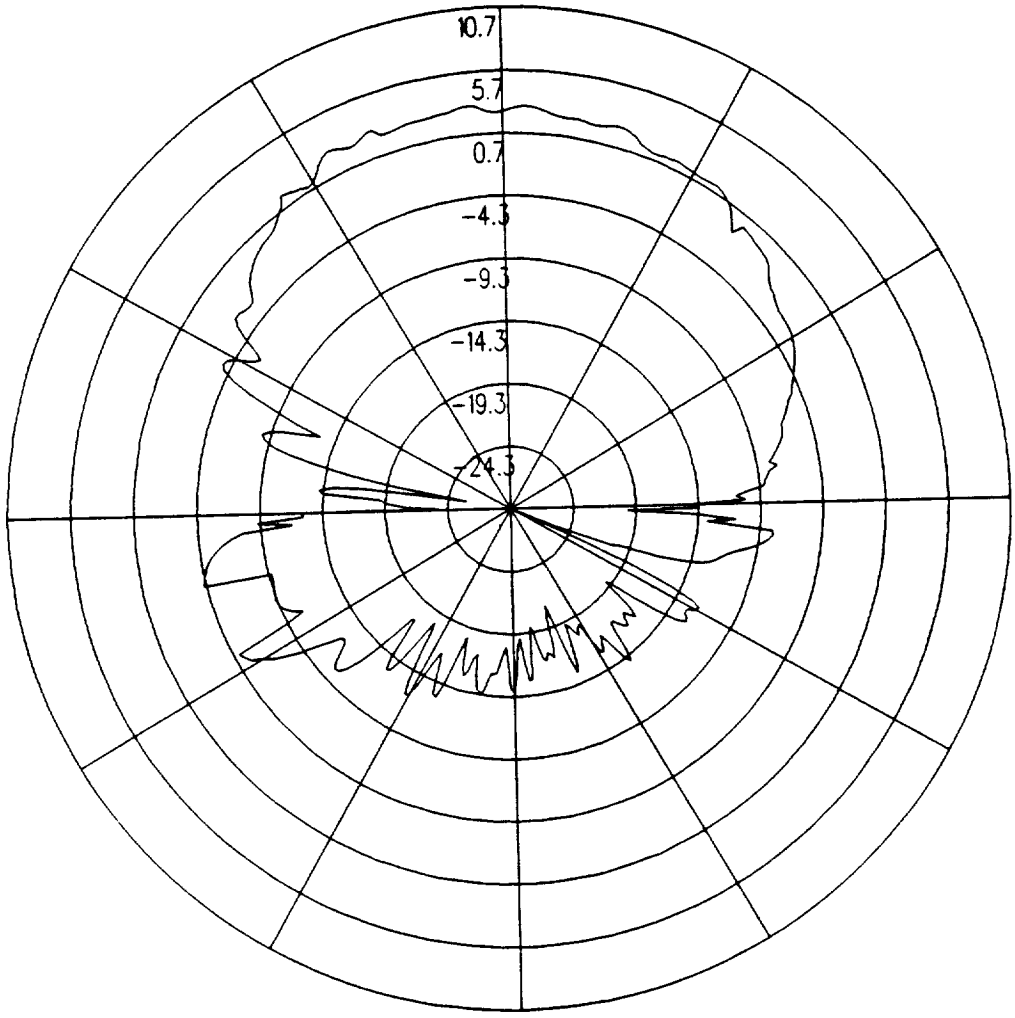

Figure 4.8: UTD calculated elevation plane pattern for batwing antenna on a P-3C for right hand circular polarization at 300 MHz.

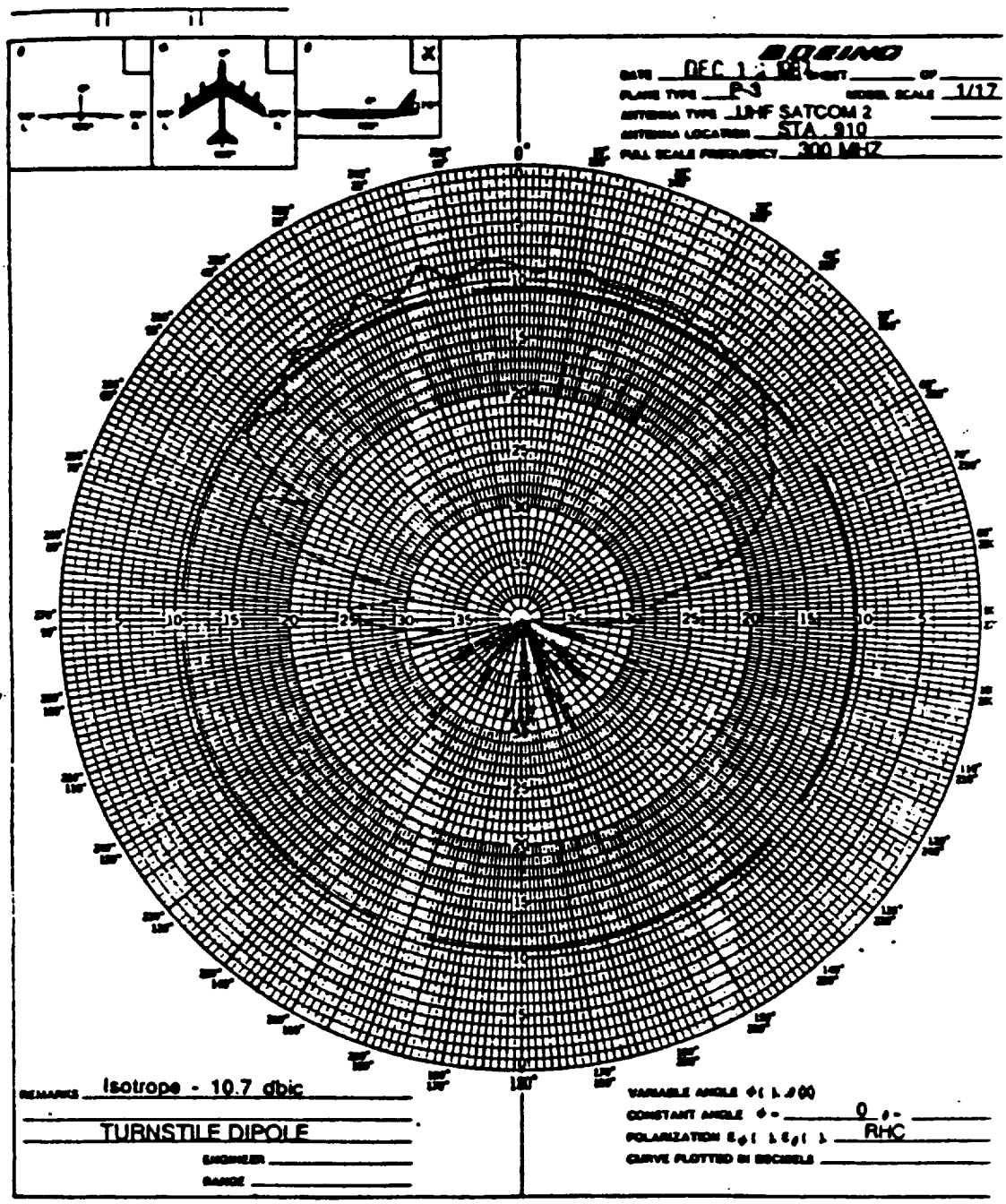

Figure 4.9: Boeing's measured elevation plane pattern for batwing antenna on a P-3C for right hand circular polarization at 300 MHz.

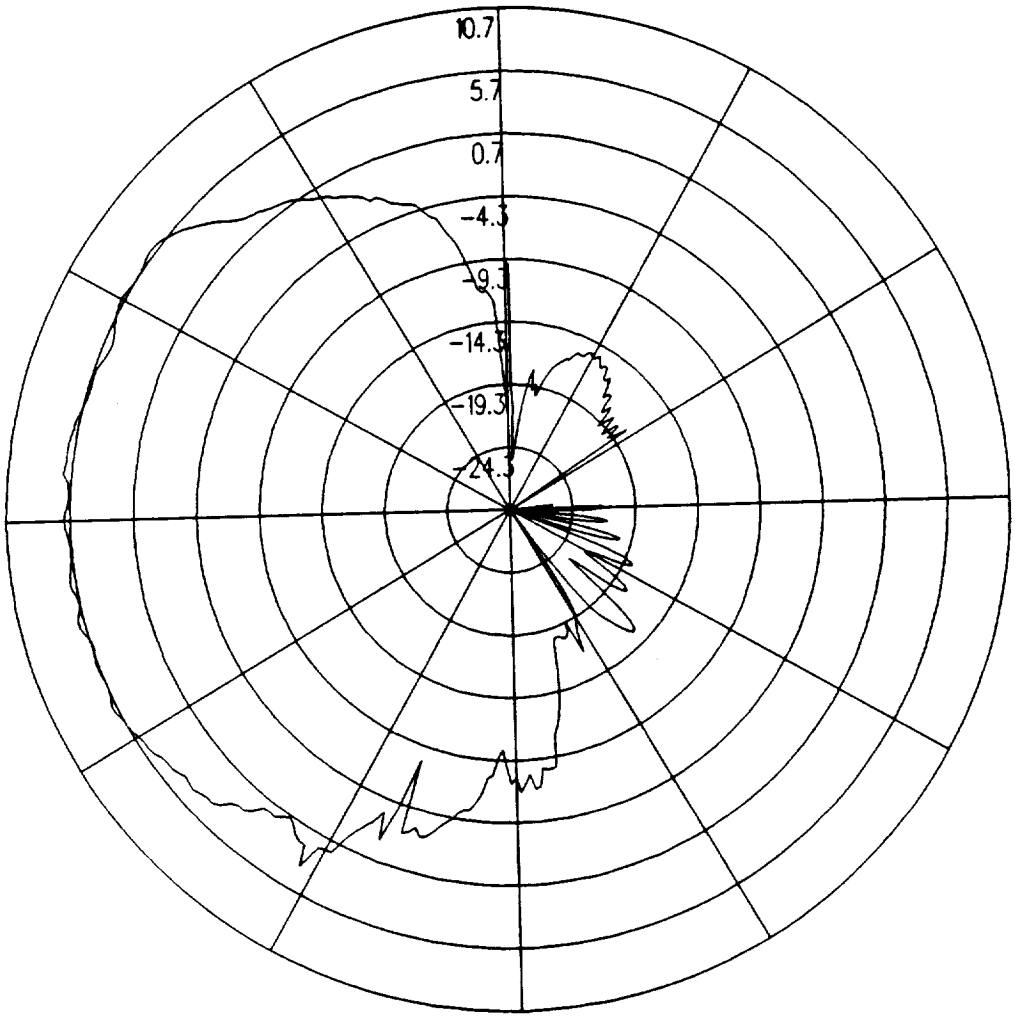

Figure 4.10: UTD calculated conical plane pattern 10° above the horizon for batwing antenna on a P-3C for right hand circular polarization at 300 MHz.

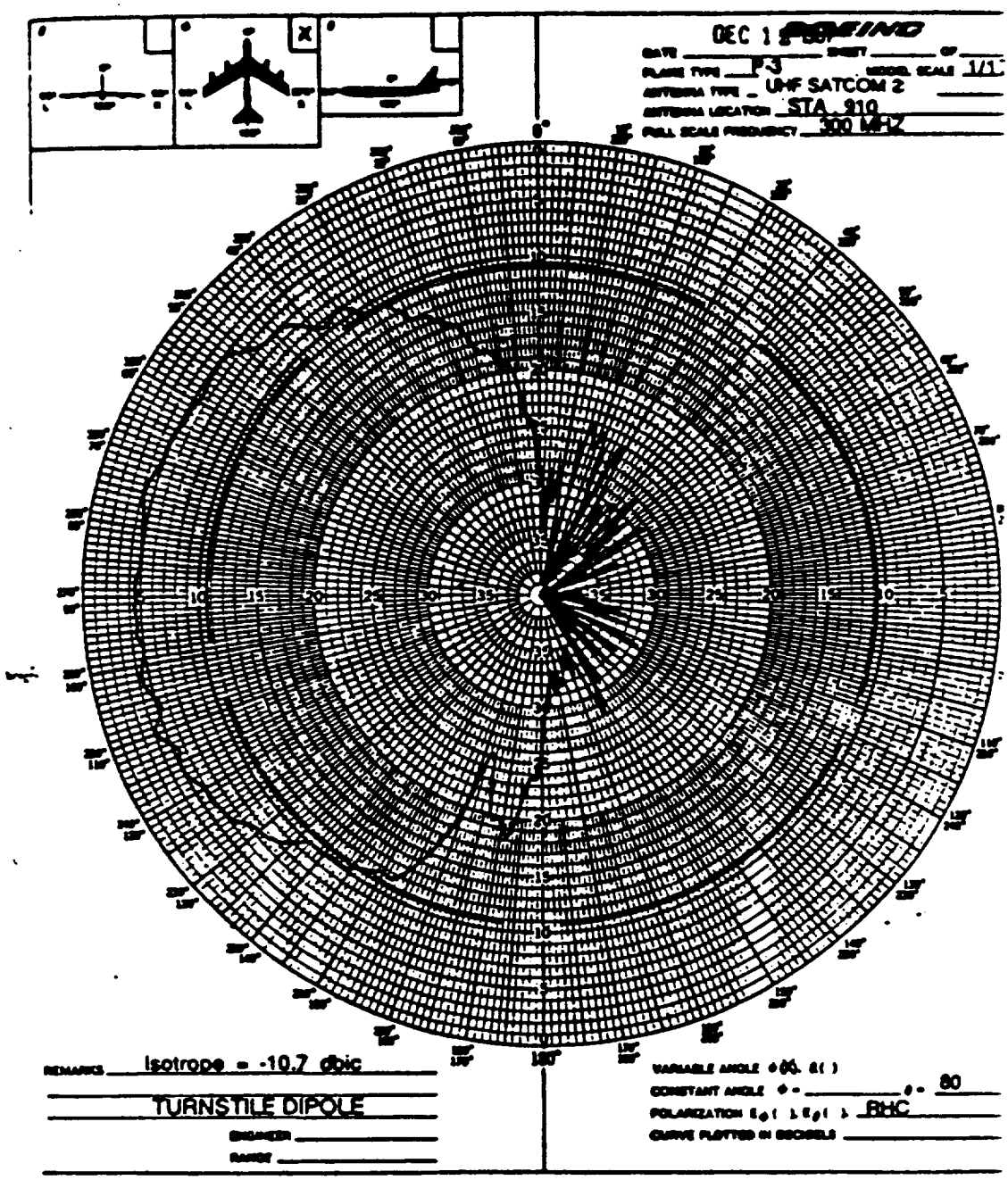

Figure 4.11: Boeing's measured conical plane pattern 10° above the horizon for batwing antenna on a P-3C for right hand circular polarization at 300 MHz.

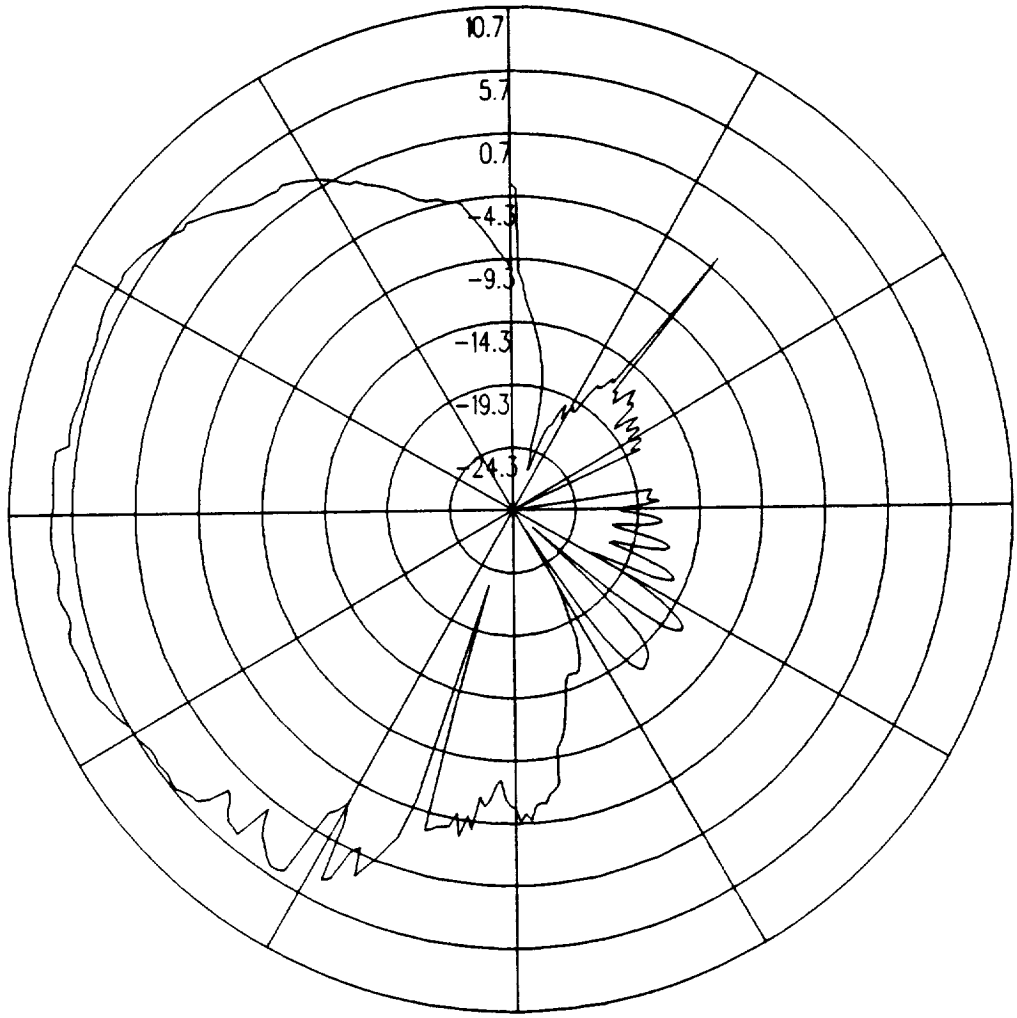

Figure 4.12: UTD calculated conical plane pattern 20° above the horizon for batwing antenna on a P-3C for right hand circular polarization at 300 MHz.

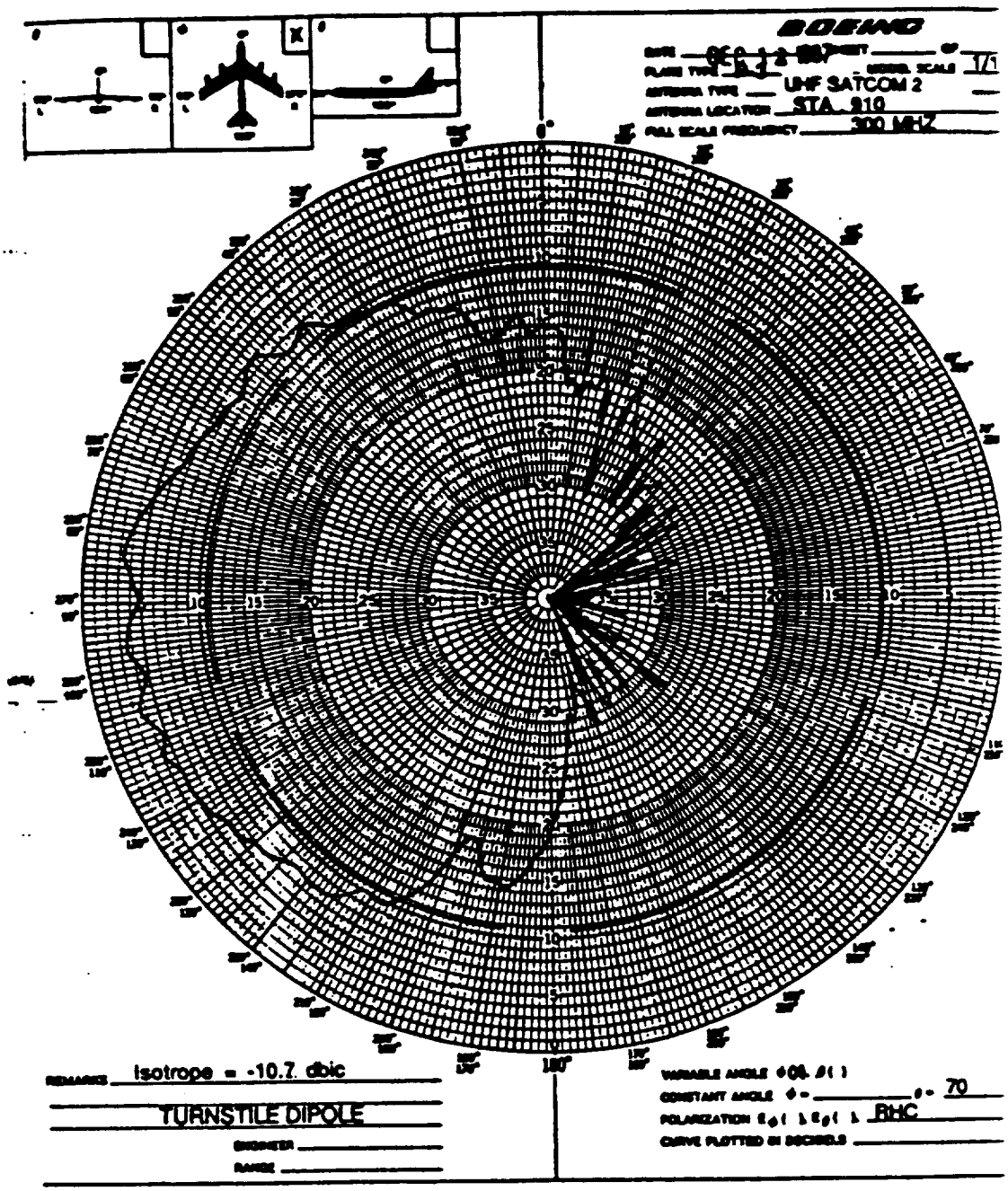

Figure 4.13: Boeing's measured conical plane pattern 20° above the horizon for batwing antenna on a P-3C for right hand circular polarization at 300 MHz.

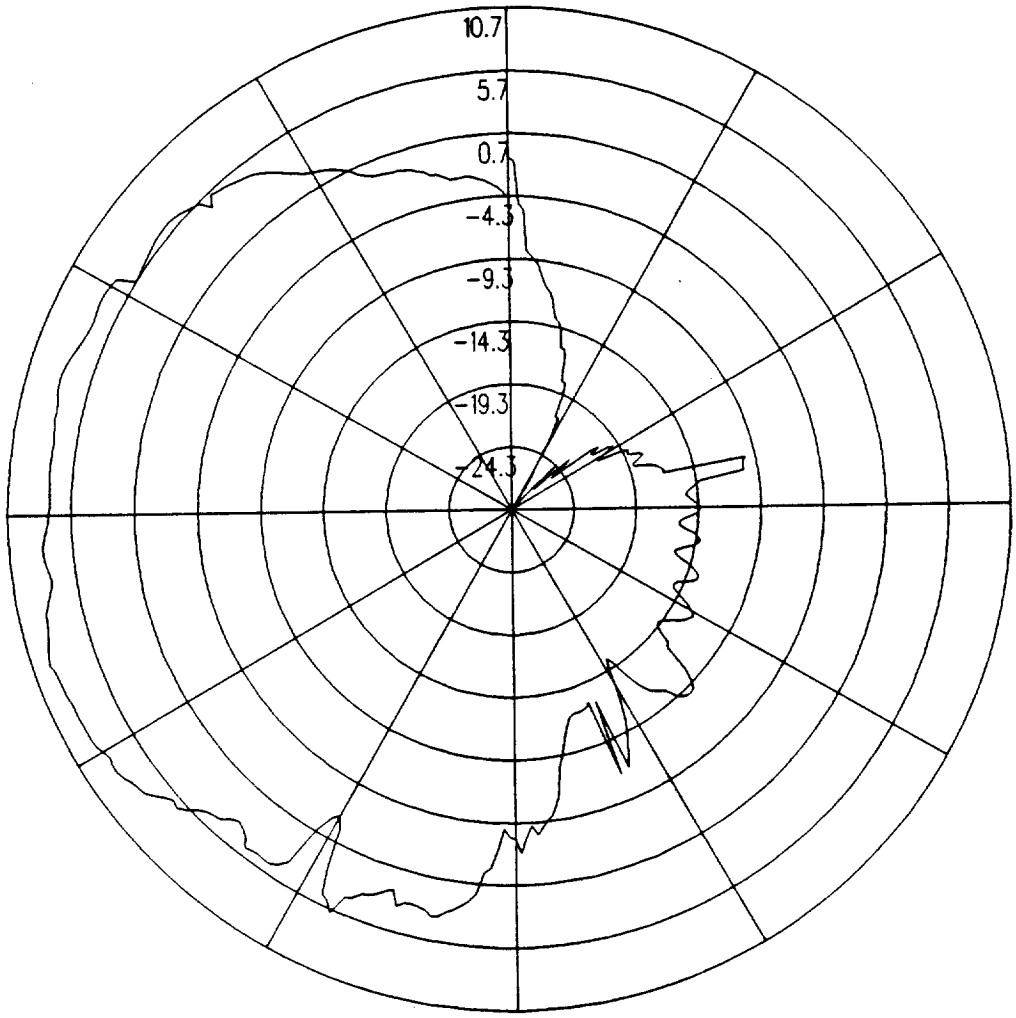

Figure 4.14: UTD calculated conical plane pattern 30° above the horizon for batwing antenna on a P-3C for right hand circular polarization at 300 MHz.

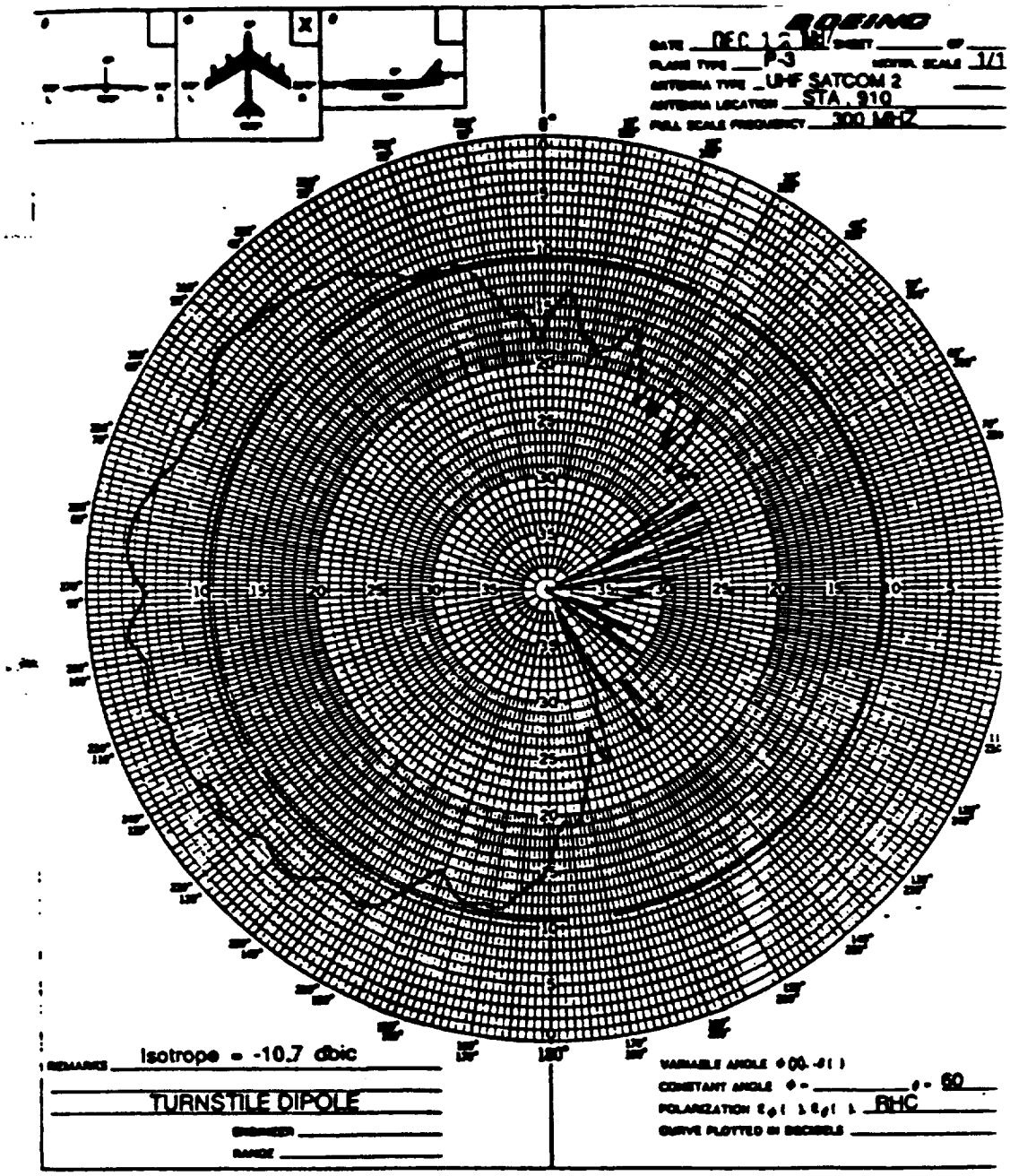

Figure 4.15: Boeing's measured conical plane pattern 30° above the horizon for batwing antenna on a P-3C for right hand circular polarization at 300 MHz.

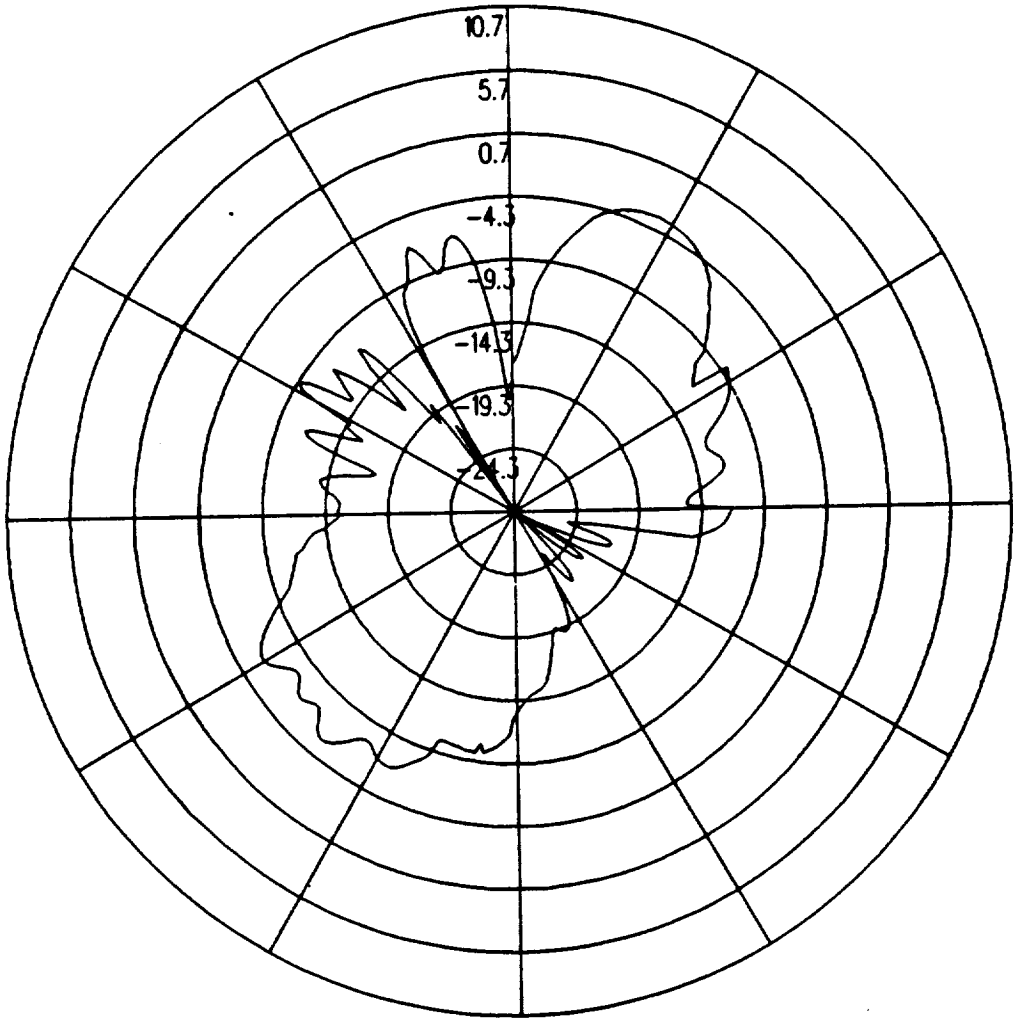

Figure 4.16: UTD calculated roll plane pattern for batwing antenna on a P-3C for left hand circular polarization at 300 MHz.

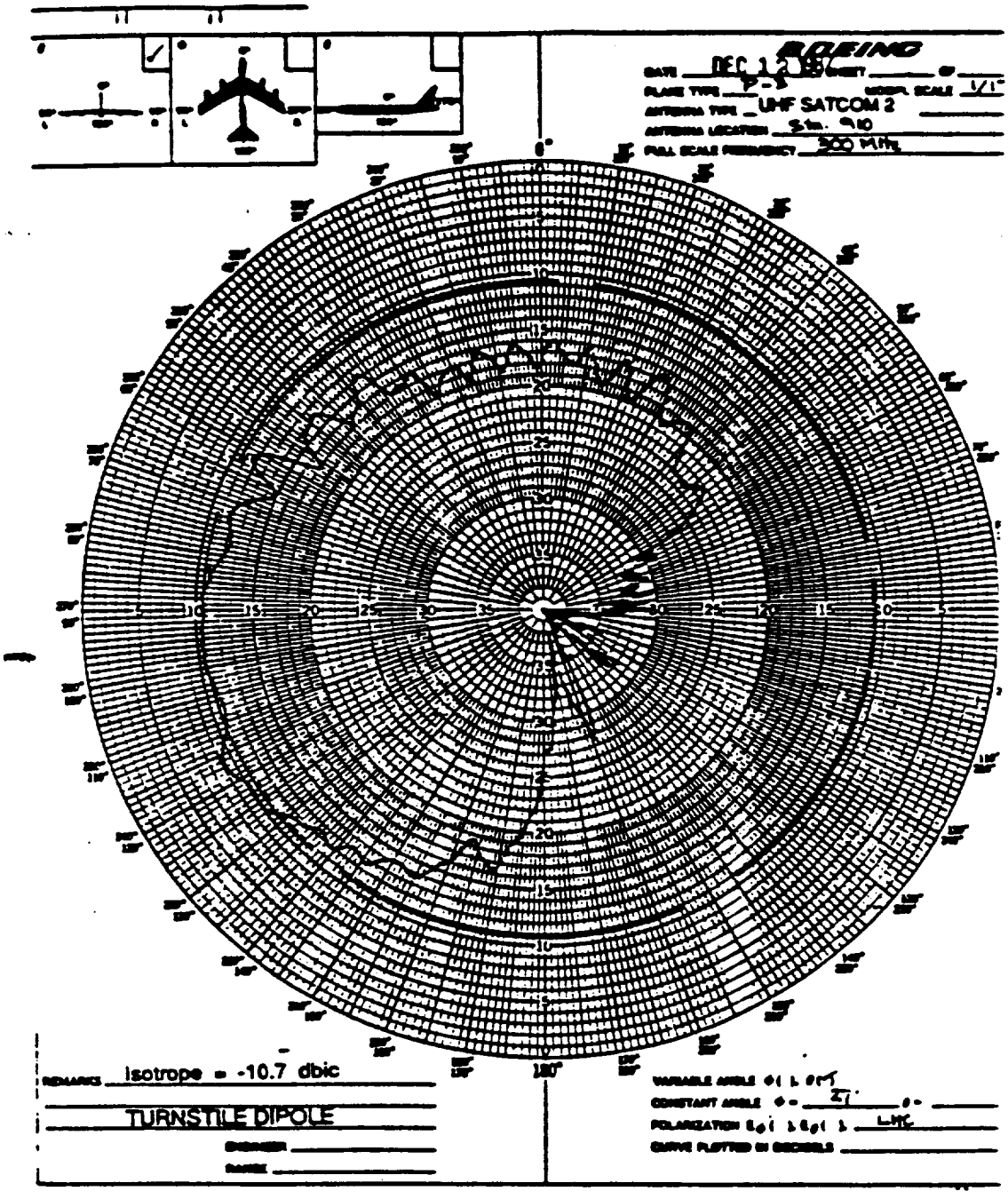

Figure 4.17: Boeing's measured roll plane pattern for batwing antenna on a P-3C for left hand circular polarization at 300 MHz.

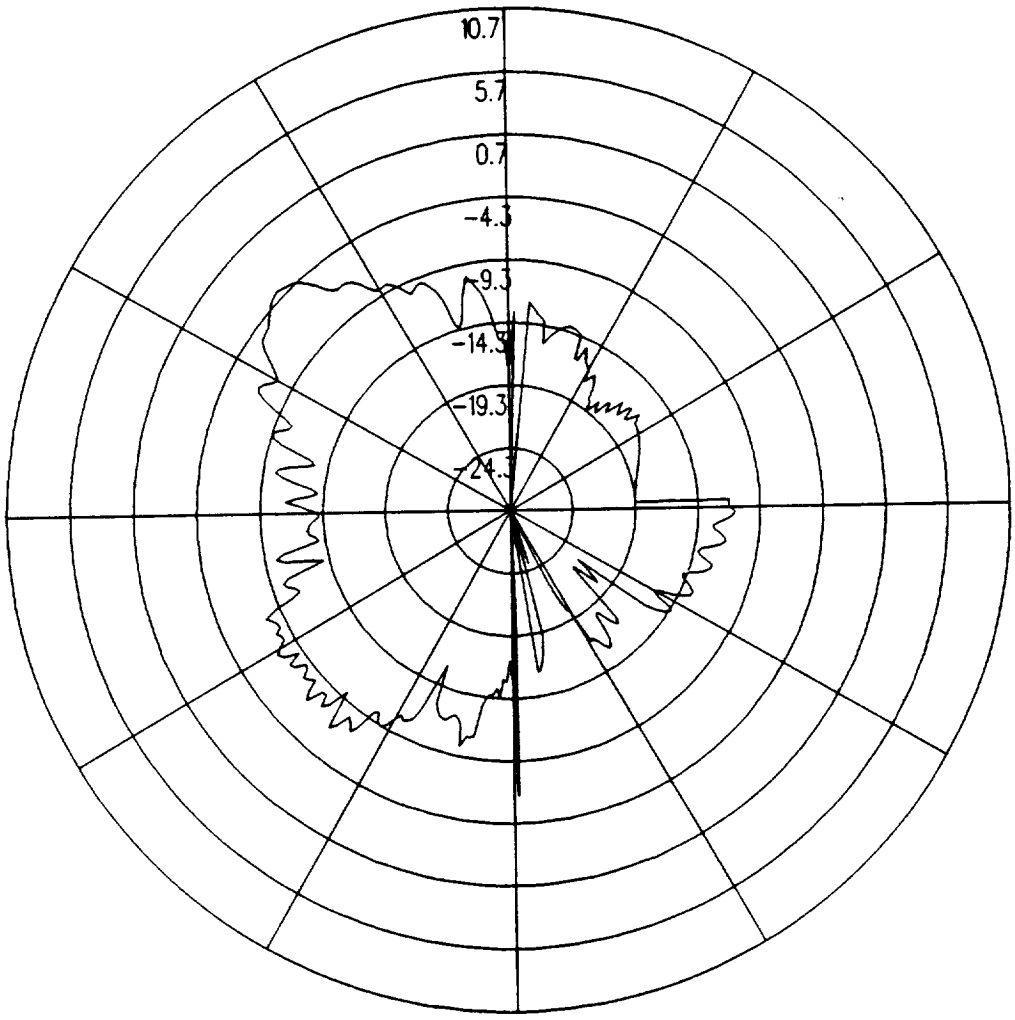

Figure 4.18: UTD calculated azimuth plane pattern for batwing antenna on a P-3C for left hand circular polarization at 300 MHz.

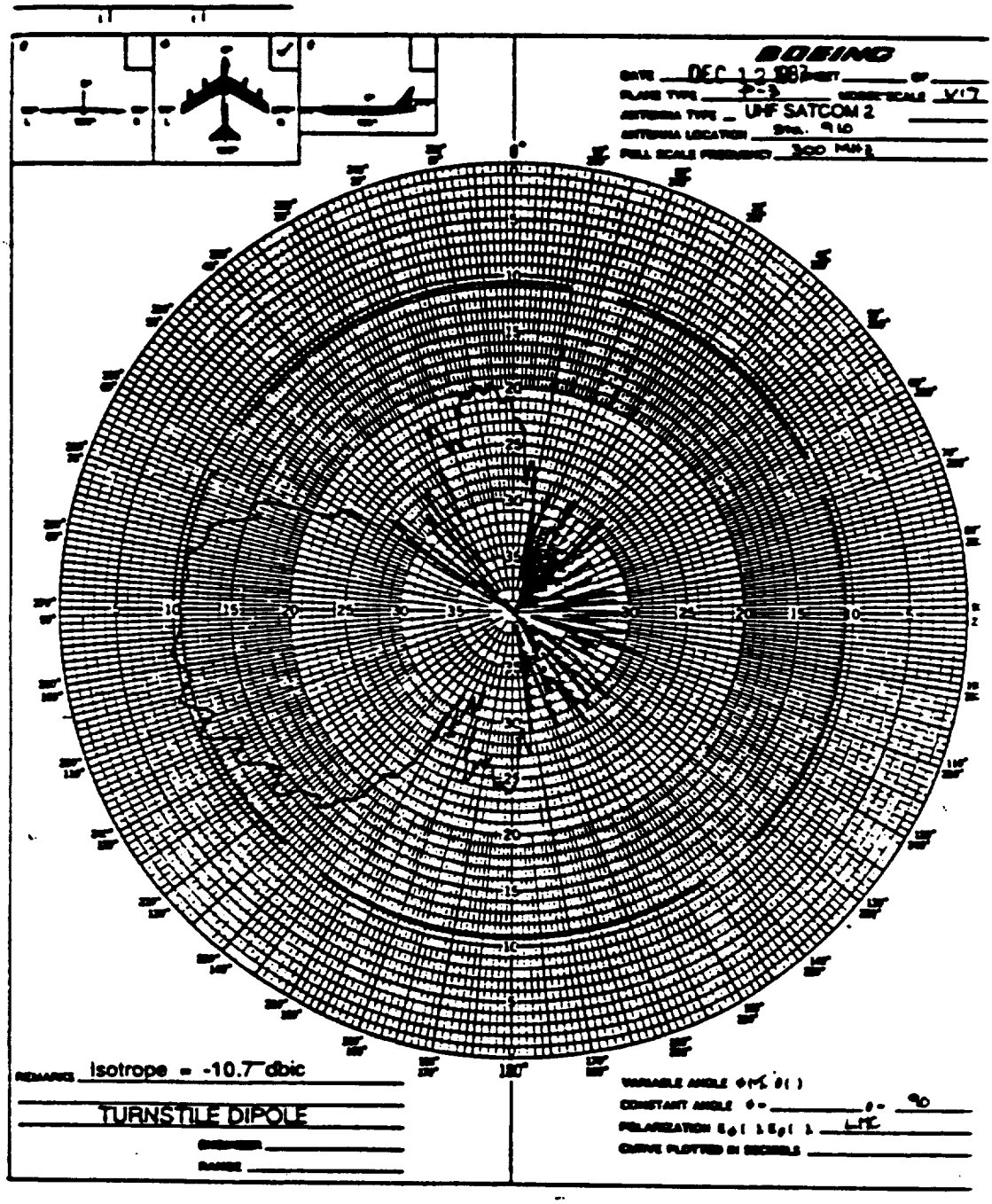

Figure 4.19: Boeing's measured azimuth plane pattern for batwing antenna on a P-3C for left hand circular polarization at 300 MHz.

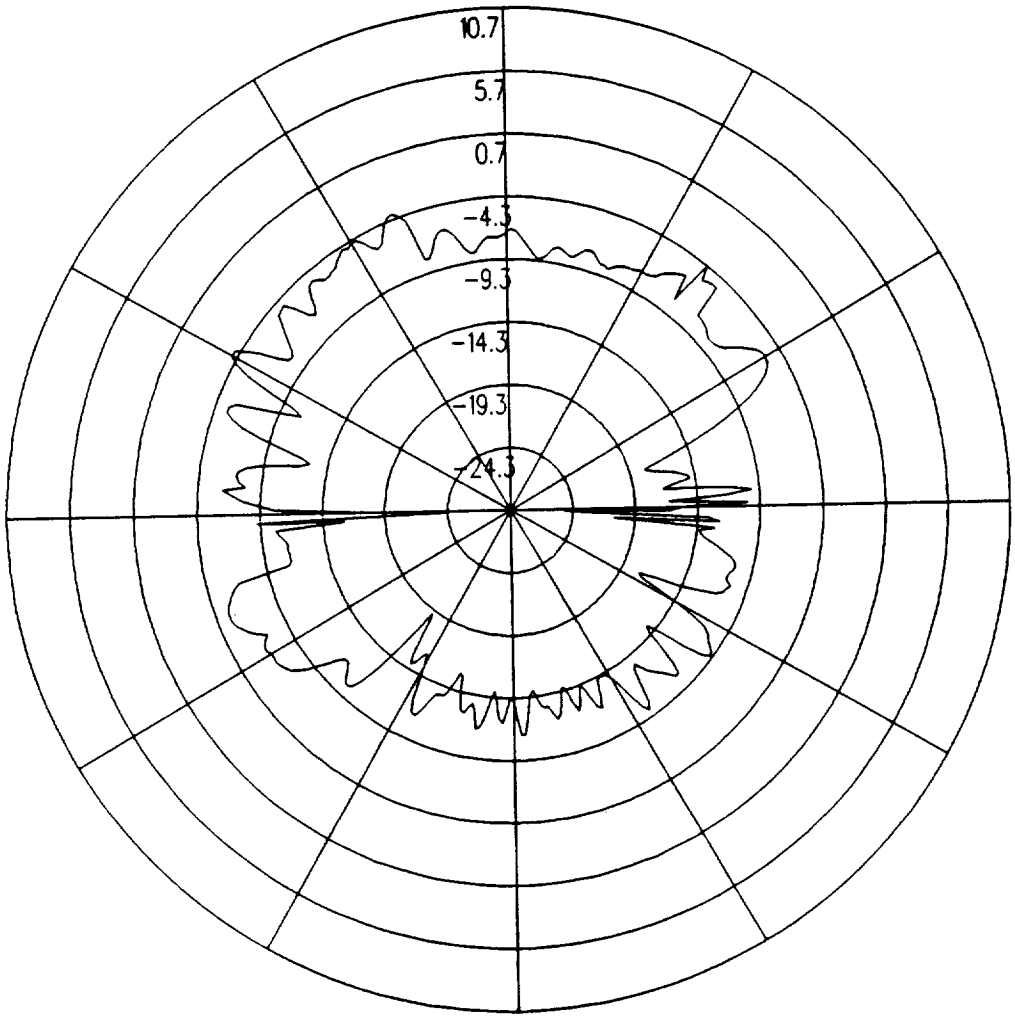

Figure 4.20: UTD calculated elevation plane pattern for batwing antenna on a P-3C for left hand circular polarization at 300 MHz.

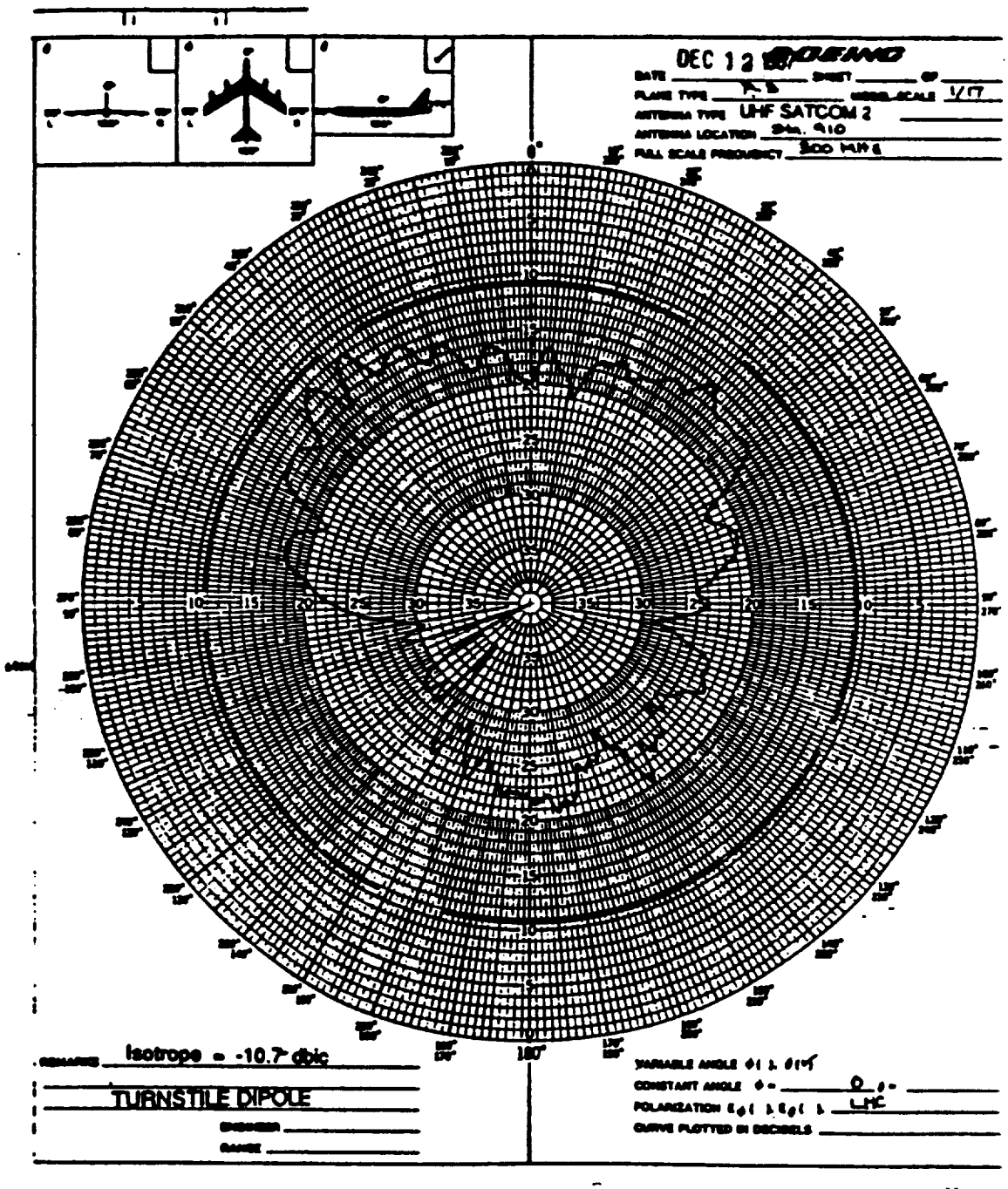

Figure 4.21: Boeing's measured elevation plane pattern for batwing antenna on a P-3C for left hand circular polarization at 300 MHz.

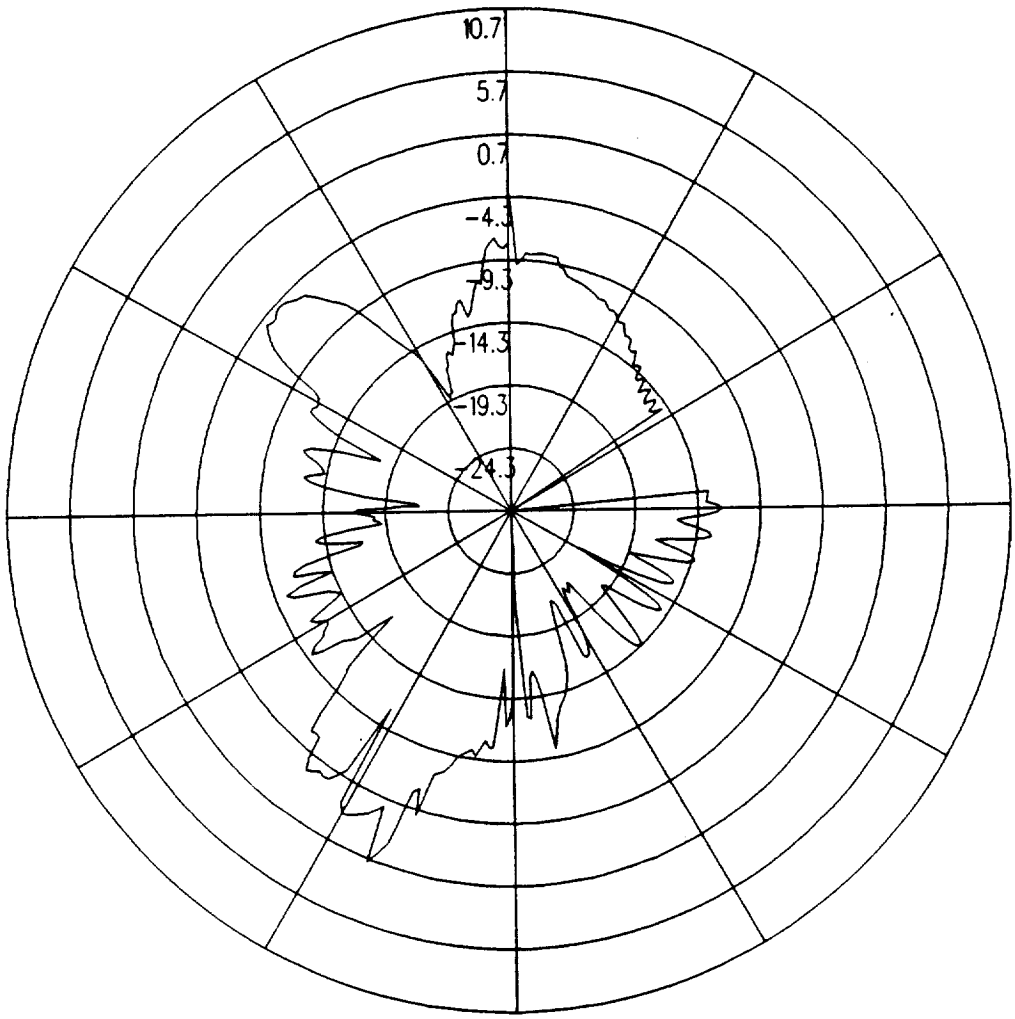

Figure 4.22: UTD calculated conical plane pattern 10° above the horizon for batwing antenna on a P-3C for left hand circular polarization at 300 MHz.

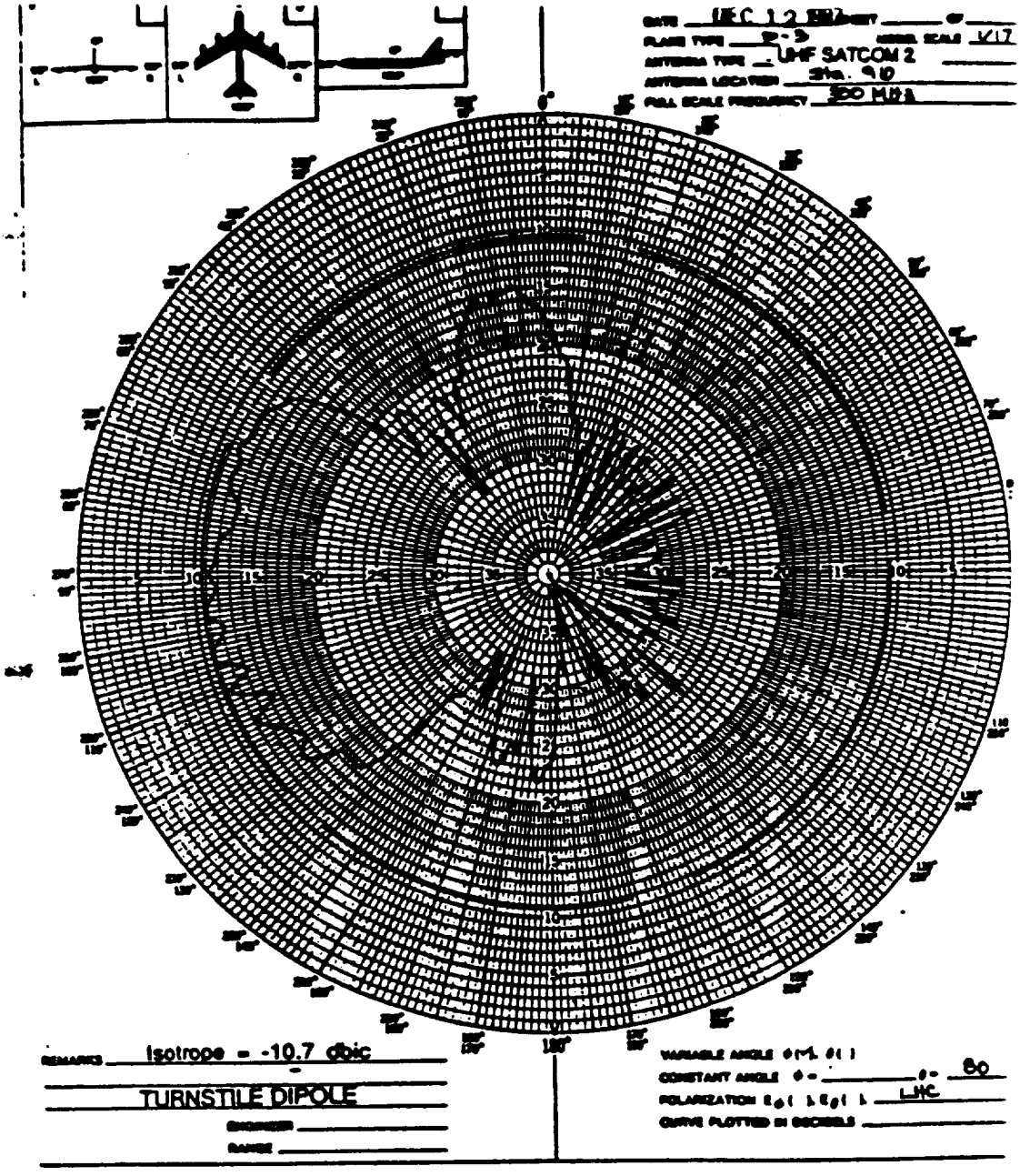

Figure 4.23: Boeing's measured conical plane pattern 10° above the horizon for batwing antenna on a P-3C for left hand circular polarization at 300 MHz.

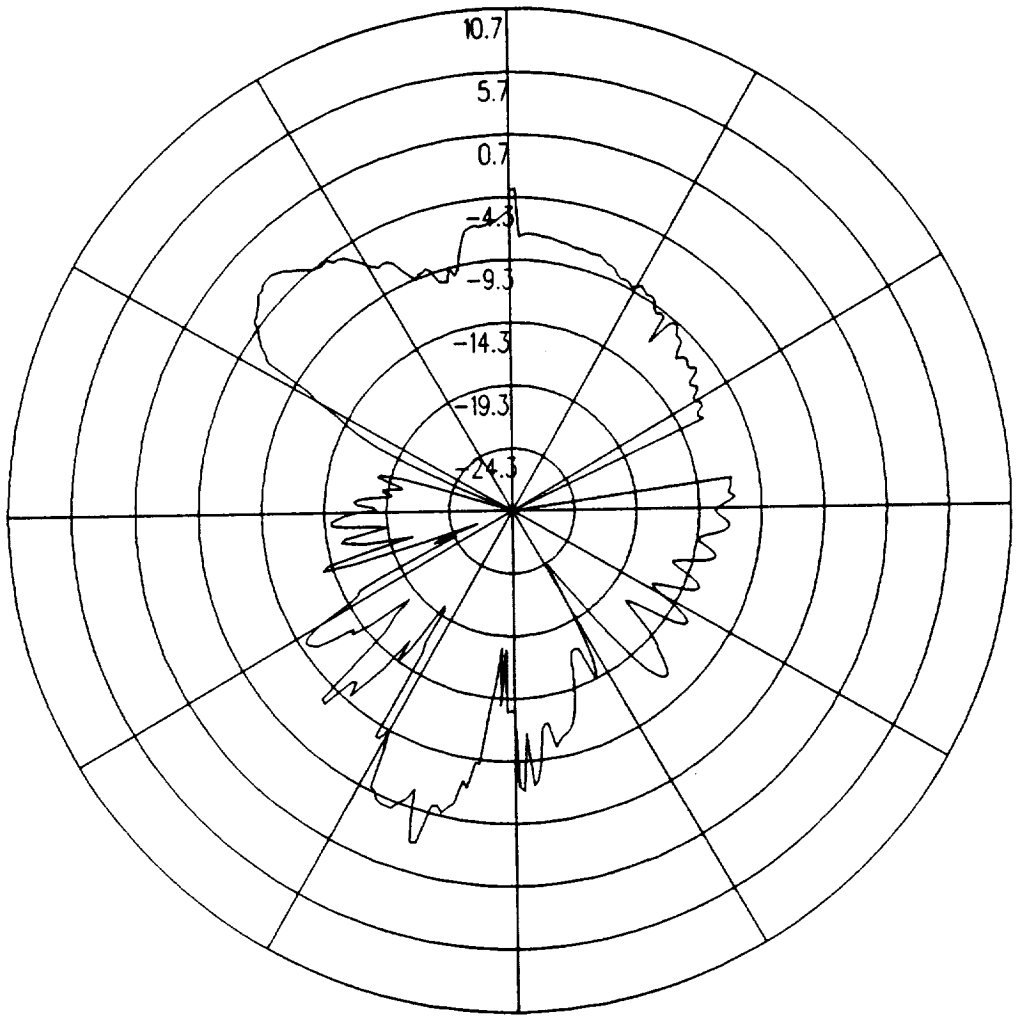

Figure 4.24: UTD calculated conical plane pattern 20° above the horizon for batwing antenna on a P-3C for left hand circular polarization at 300 MHz.

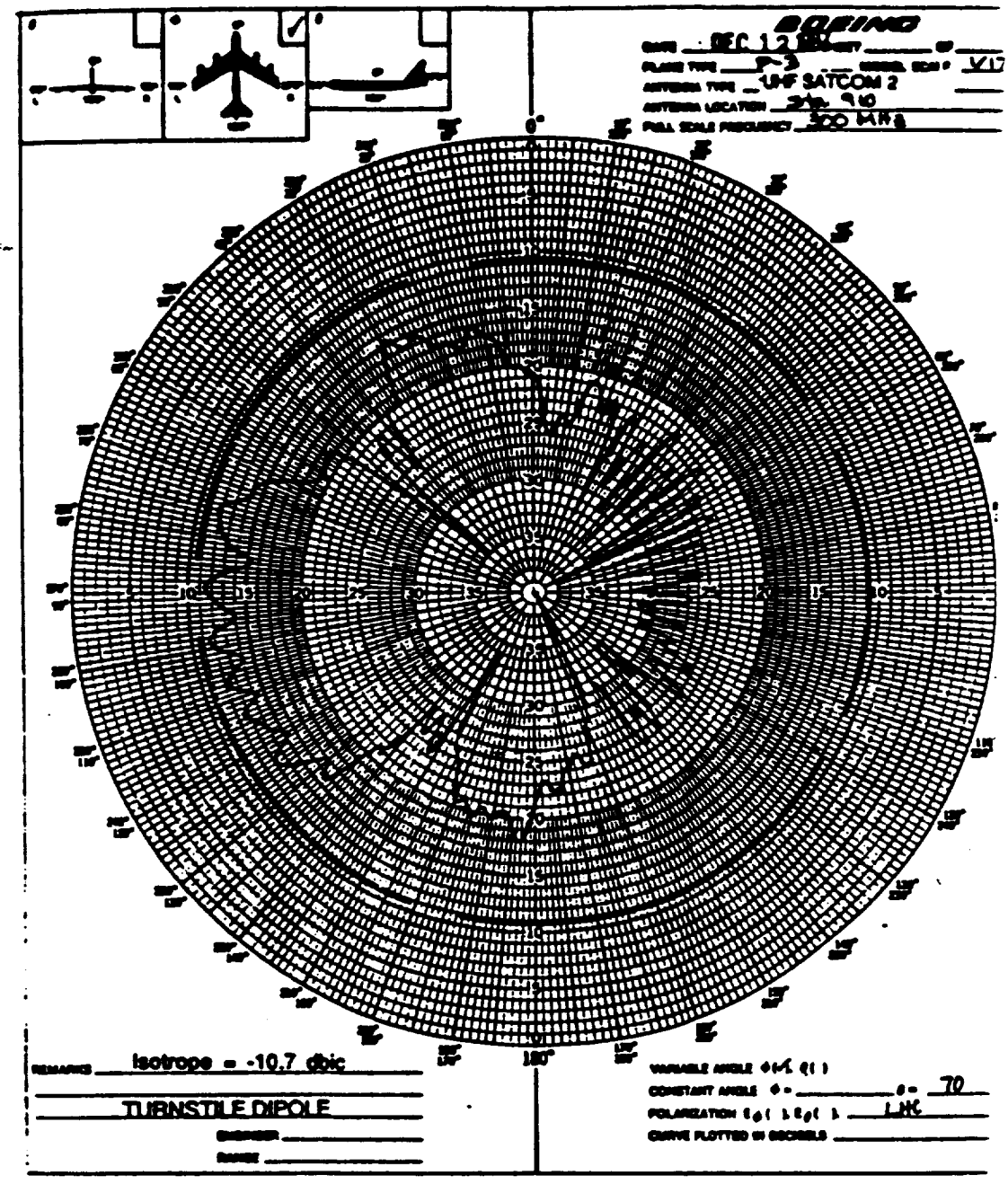

Figure 4.25: Boeing's measured conical plane pattern 20° above the horizon for batwing antenna on a P-3C for left hand circular polarization at 300 MHz.

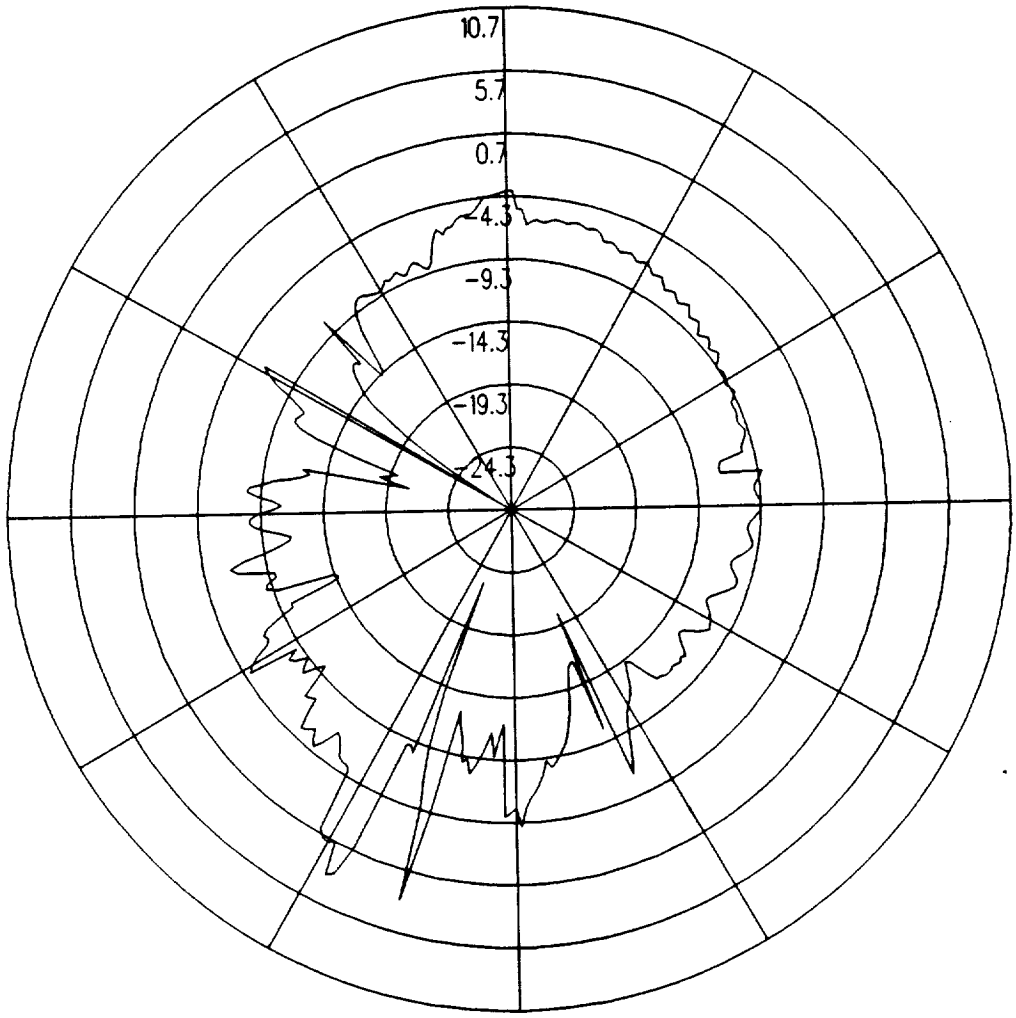

Figure 4.26: UTD calculated conical plane pattern 30° above the horizon for batwing antenna on a P-3C for left hand circular polarization at 300 MHz.

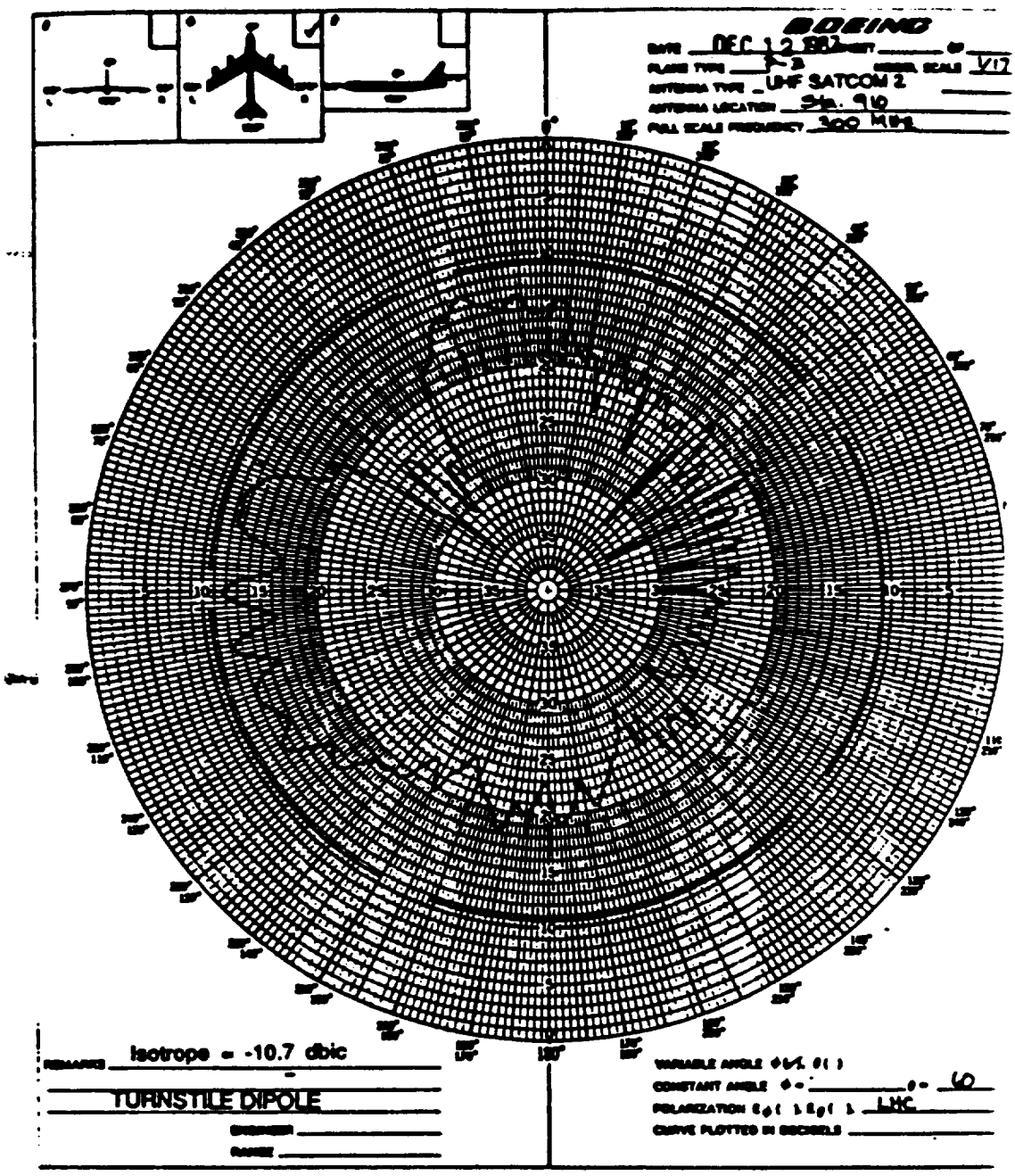

Figure 4.27: Boeing's measured conical plane pattern 30° above the horizon for batwing antenna on a P-3C for left hand circular polarization at 300 MHz.

4.3 Boeing Location with Composite Ellipsoid Fuselage

The results computed in this section using the composite ellipsoid aircraft model have been compared to the calculated results from the previous section as well as the measured results provided by Boeing. The antenna is located as illustrated in Figure 4.28, which also shows the computer model used to generate the results. The calculated results at 300 MHz are shown for the roll plane in Figure 4.29, for the azimuth plane in Figure 4.30, for the elevation plane in Figure 4.31, for the conical plane 10° above the horizon in Figure 4.32, for the conical plane 20° above the horizon in Figure 4.33, and for the conical plane 30° above the horizon in Figure 4.34 all for right hand polarization. These calculated results can be compared with the calculated and measured results found in the previous section in Figure 4.4 through Figure 4.15. The cross polarized fields are shown for the roll plane in Figure 4.35, for the azimuth plane in Figure 4.36, for the elevation plane in Figure 4.37, for the conical plane 10° above the horizon in Figure 4.38, for the conical plane 20° above the horizon in Figure 4.39, and for the conical plane 30° above the horizon in Figure 4.40 all for left hand polarization. These calculated results also can be compared with the calculated and measured results found in the previous section in Figure 4.16 through Figure 4.27.

The roll plane results for the composite ellipsoid model compare very well throughout the complete pattern with the results for the cylindrical model and the measured Boeing results. Comparing the azimuth plane results for the composite ellipsoid model to the results for the cylindrical model shows that the calculated patterns for the ellipsoid model are 5–10 dB higher near the nose and 10–15 dB higher near the tail than for the cylindrical model. Therefore, the calculated levels for the composite ellipsoid model are approximately 10–15 dB higher near the nose and as much as 15 dB higher near the tail than Boeing's measured results. In the main region of the pattern, the levels for the composite ellipsoid model are 3–5 dB below the levels for the cylindrical model and Boeing's measured levels. Comparing the elevation plane results for the composite ellipsoid model to the results for the cylindrical model shows that there is good agreement for the back half of the aircraft. However in the region on the horizon near the

nose of the aircraft, the levels for the composite ellipsoid model are approximately 10 dB higher than the levels calculated for the cylindrical model and Boeing's measured levels. Comparing the conical pattern planes, however, shows that as the pattern cut is taken above the horizon there is very good agreement between the patterns for the composite ellipsoid model, the cylindrical model, and Boeing's scale model.

These lower levels in the main region of the azimuth plane for the composite ellipsoid model can be explained in part by the fact that the radius of curvature of the composite ellipsoid at the location of the antenna is smaller than the radius of curvature of the cylinder at the corresponding location. Also, creeping waves which are calculated for the cylindrical aircraft model are not calculated for the composite ellipsoid aircraft model. This lack of creeping waves can also account for the lower levels seen in the main region of the azimuth plane. This comparison shows that the composite ellipsoid aircraft model has the same problem as the cylindrical aircraft model with high levels on the horizon near the nose and the tail. In addition, this model has a problem in the azimuth plane as described above. Therefore, the cylindrical aircraft model is a better representation for the actual P-3C aircraft than the composite ellipsoid aircraft model.

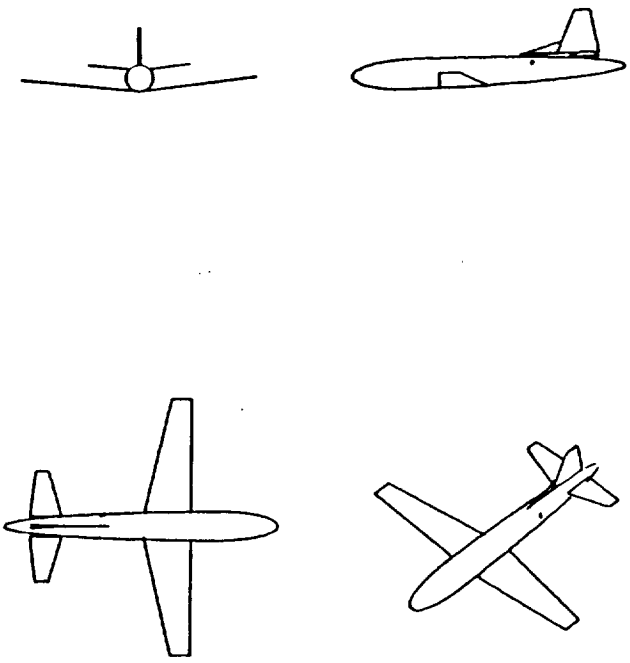

Figure 4.28: Geometry of the composite ellipsoid model of the P-3C aircraft used in the NEC-BSC code showing the location of the antenna.

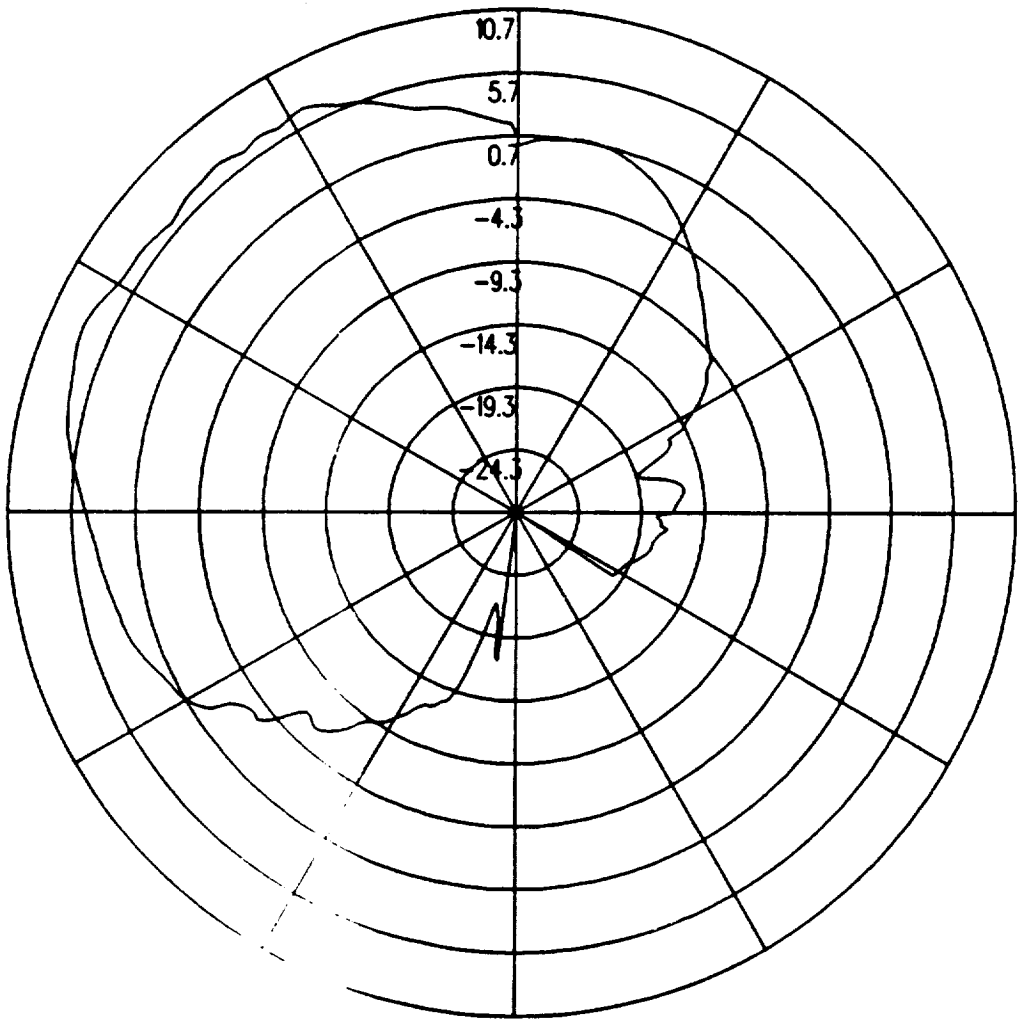

Figure 4.29: UTD calculated roll plane pattern for batwing antenna on a P-3C for right hand circular polarization at 300 MHz. (Composite Ellipsoid Aircraft Model)

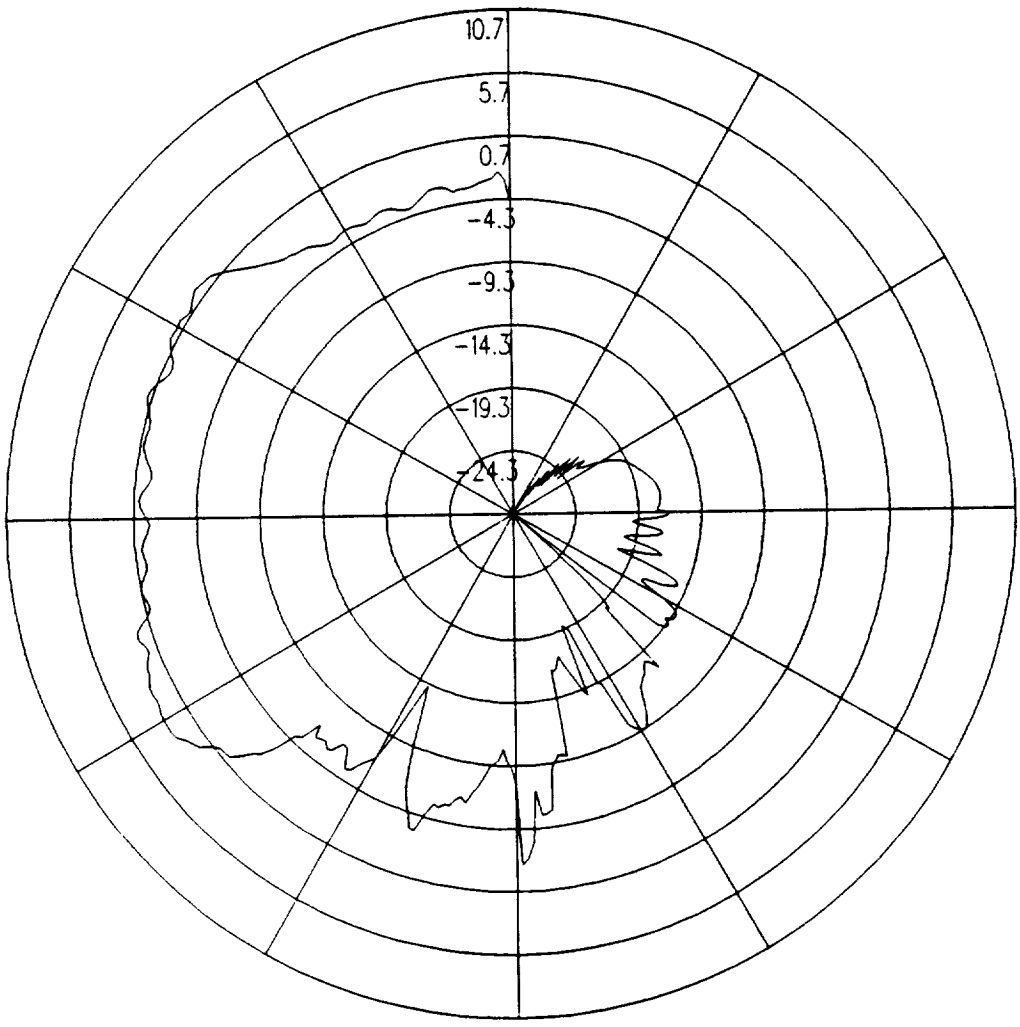

Figure 4.30: UTD calculated azimuth plane pattern for batwing antenna on a P-3C for right hand circular polarization at 300 MHz. (Composite Ellipsoid Aircraft Model)

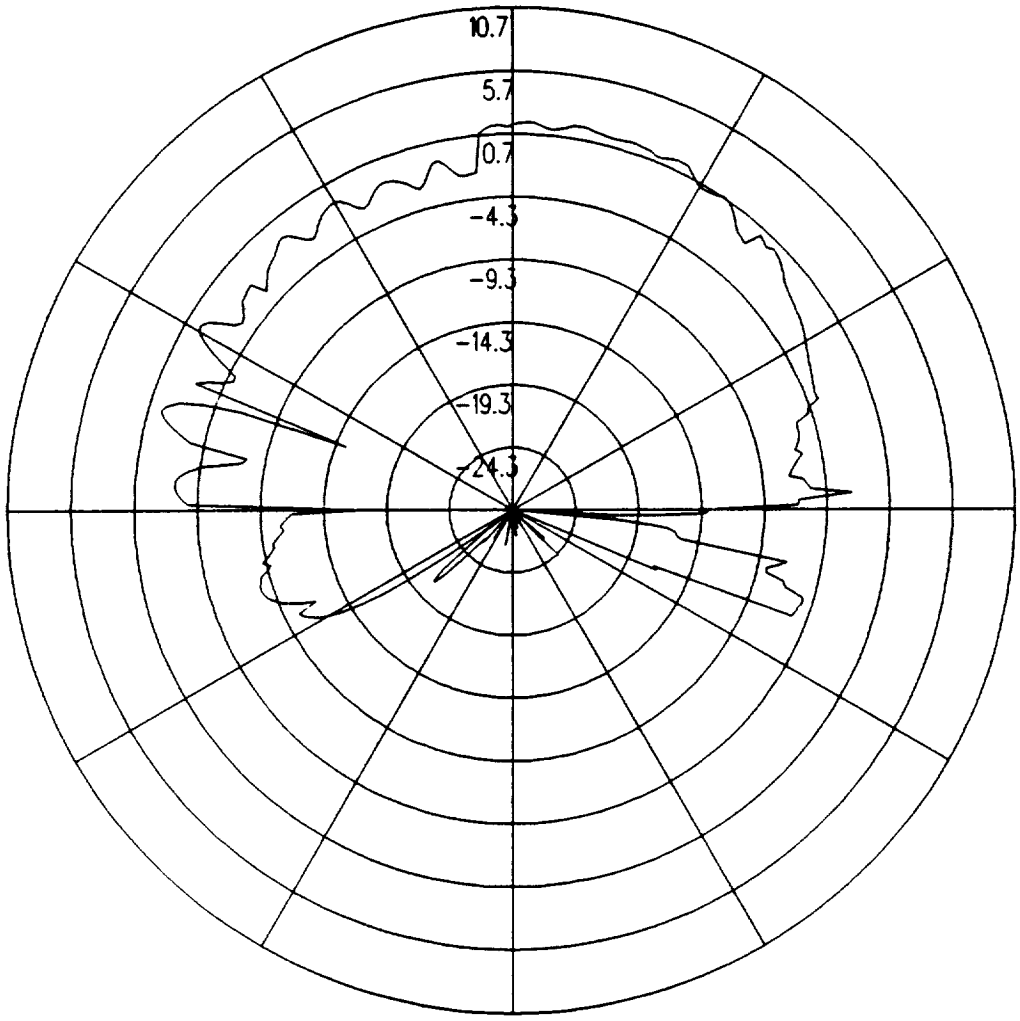

Figure 4.31: UTD calculated elevation plane pattern for batwing antenna on a P-3C for right hand circular polarization at 300 MHz. (Composite Ellipsoid Aircraft Model)

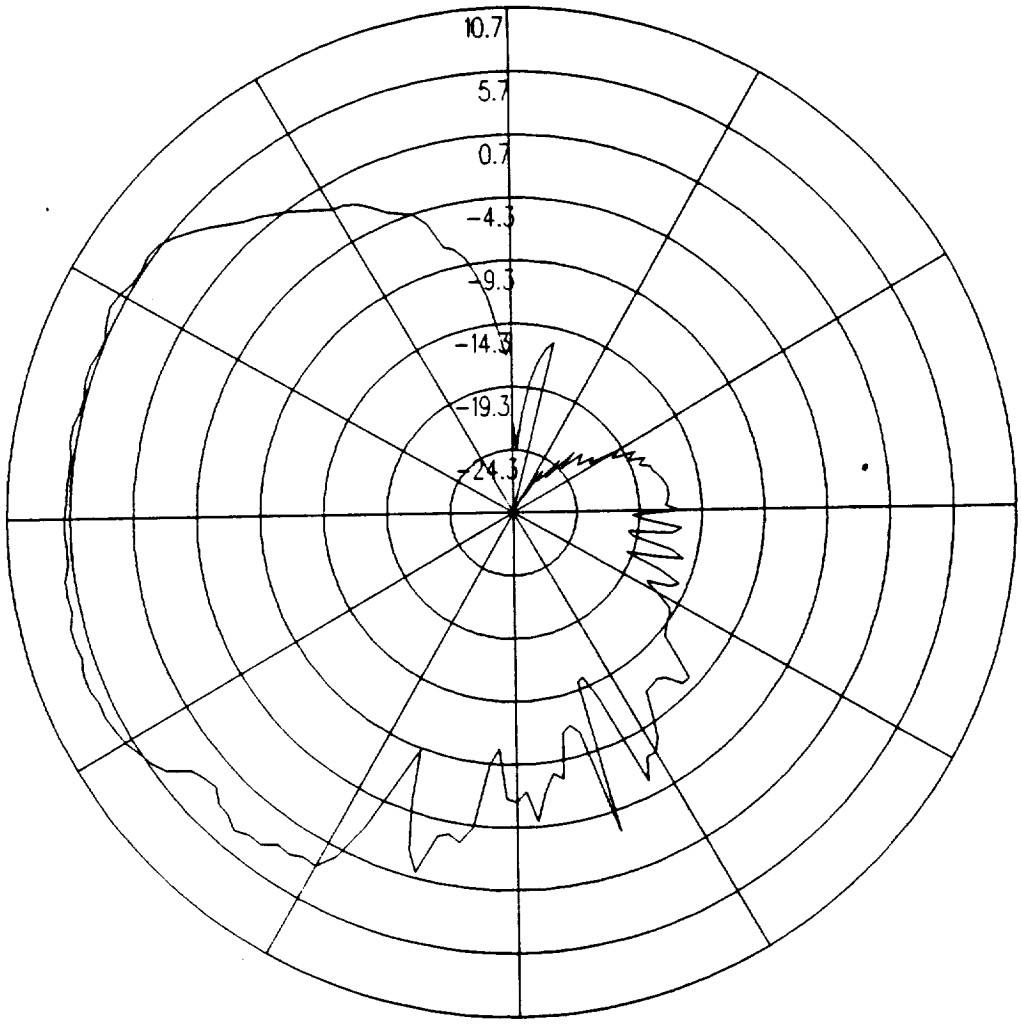

Figure 4.32: UTD calculated conical plane pattern 10° above the horizon for batwing antenna on a P-3C for right hand circular polarization at 300 MHz.(Composite Ellipsoid Aircraft Model)

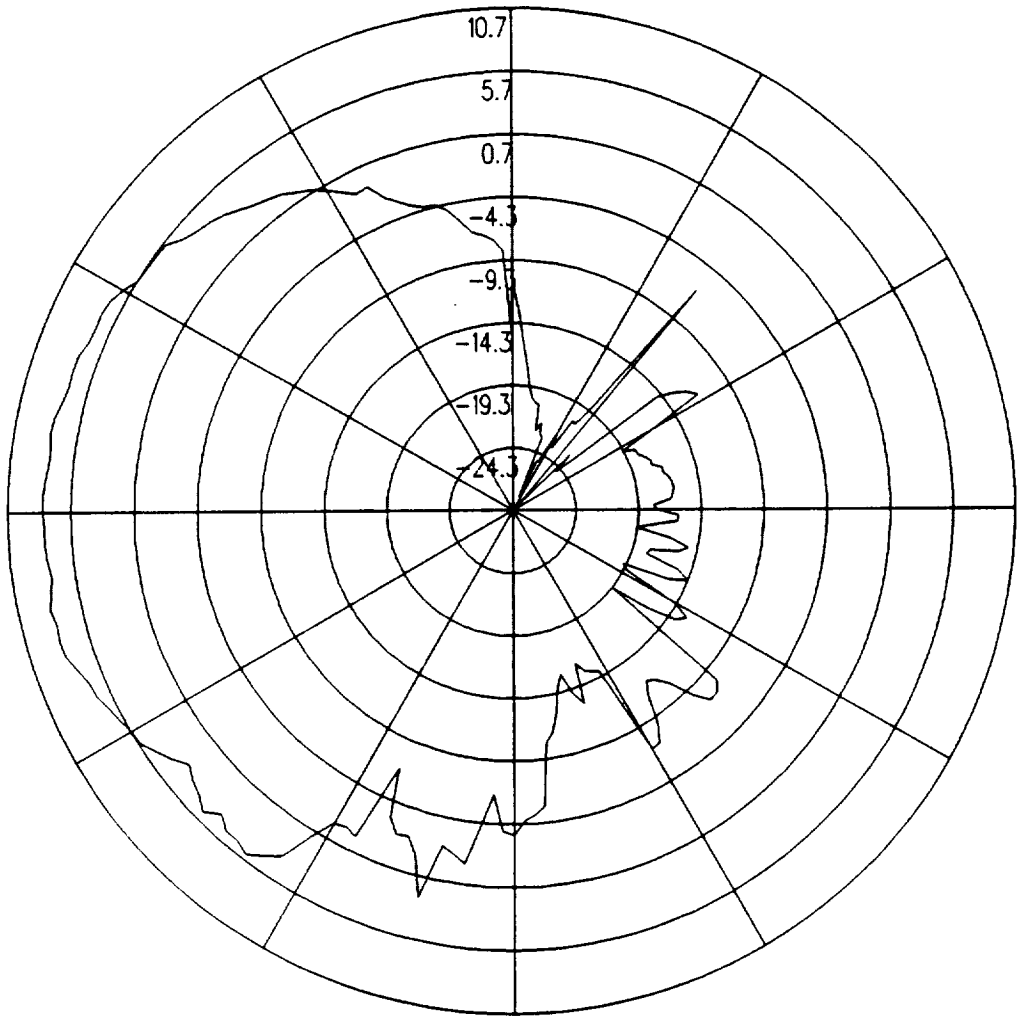

Figure 4.33: UTD calculated conical plane pattern 20° above the horizon for batwing antenna on a P-3C for right hand circular polarization at 300 MHz.(Composite Ellipsoid Aircraft Model)

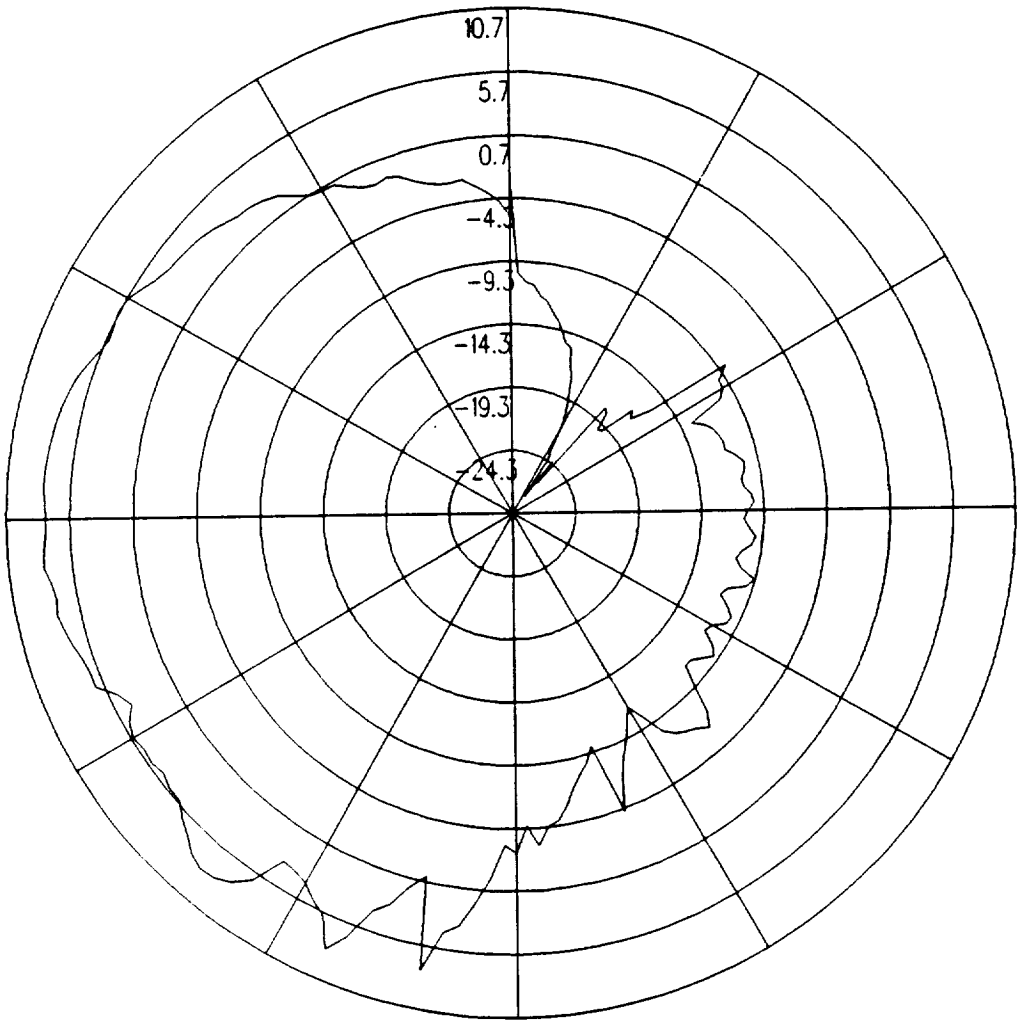

Figure 4.34: UTD calculated conical plane pattern 30° above the horizon for batwing antenna on a P-3C for right hand circular polarization at 300 MHz.(Composite Ellipsoid Aircraft Model)

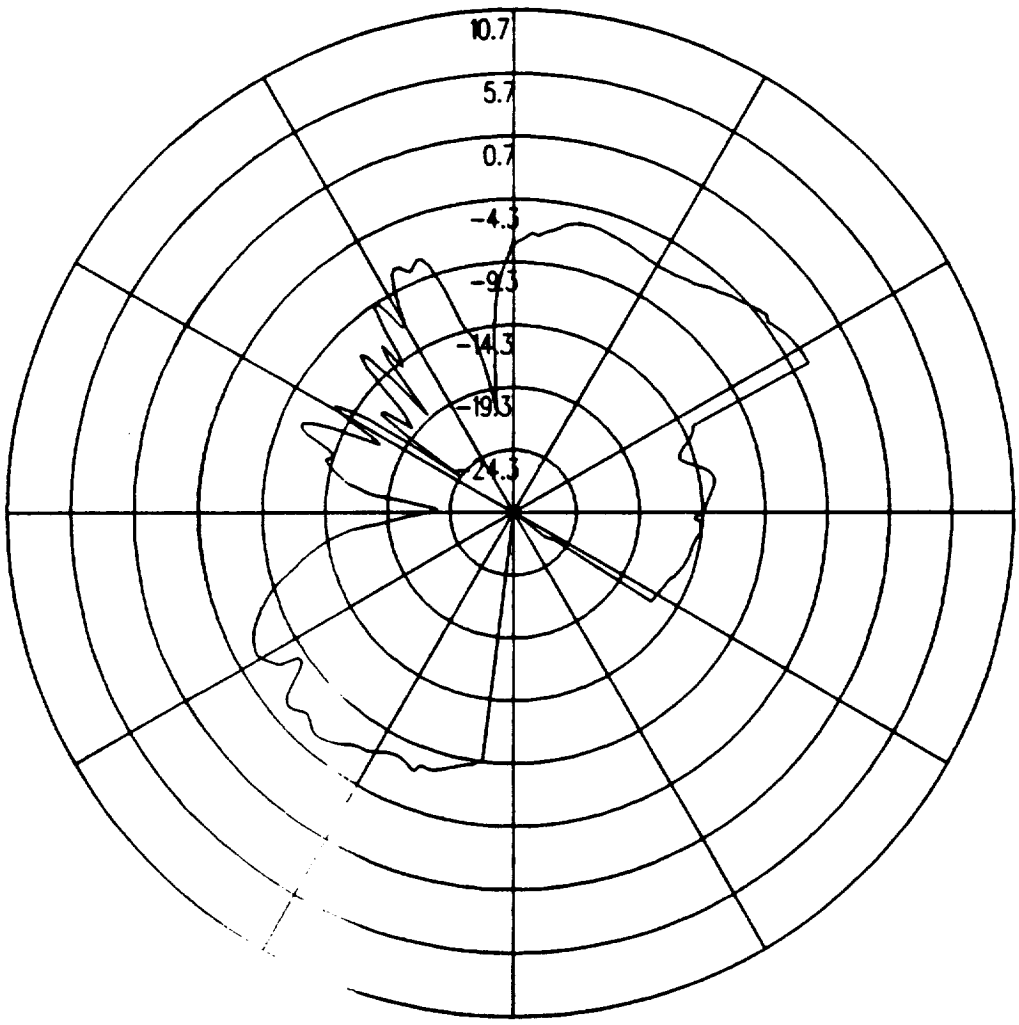

Figure 4.35: UTD calculated roll plane pattern for batwing antenna on a P-3C for left hand circular polarization at 300 MHz. (Composite Ellipsoid Aircraft Model)

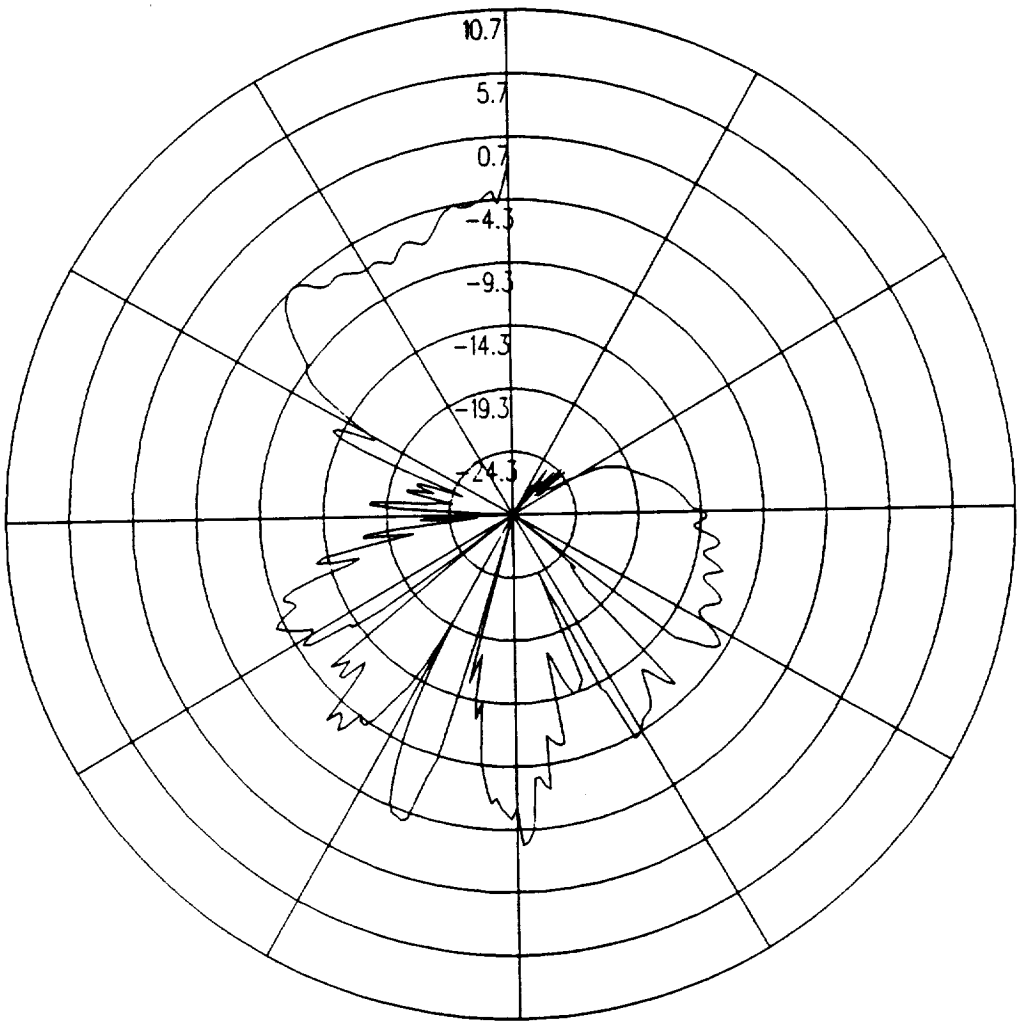

Figure 4.36: UTD calculated azimuth plane pattern for batwing antenna on a P-3C for left hand circular polarization at 300 MHz. (Composite Ellipsoid Aircraft Model)

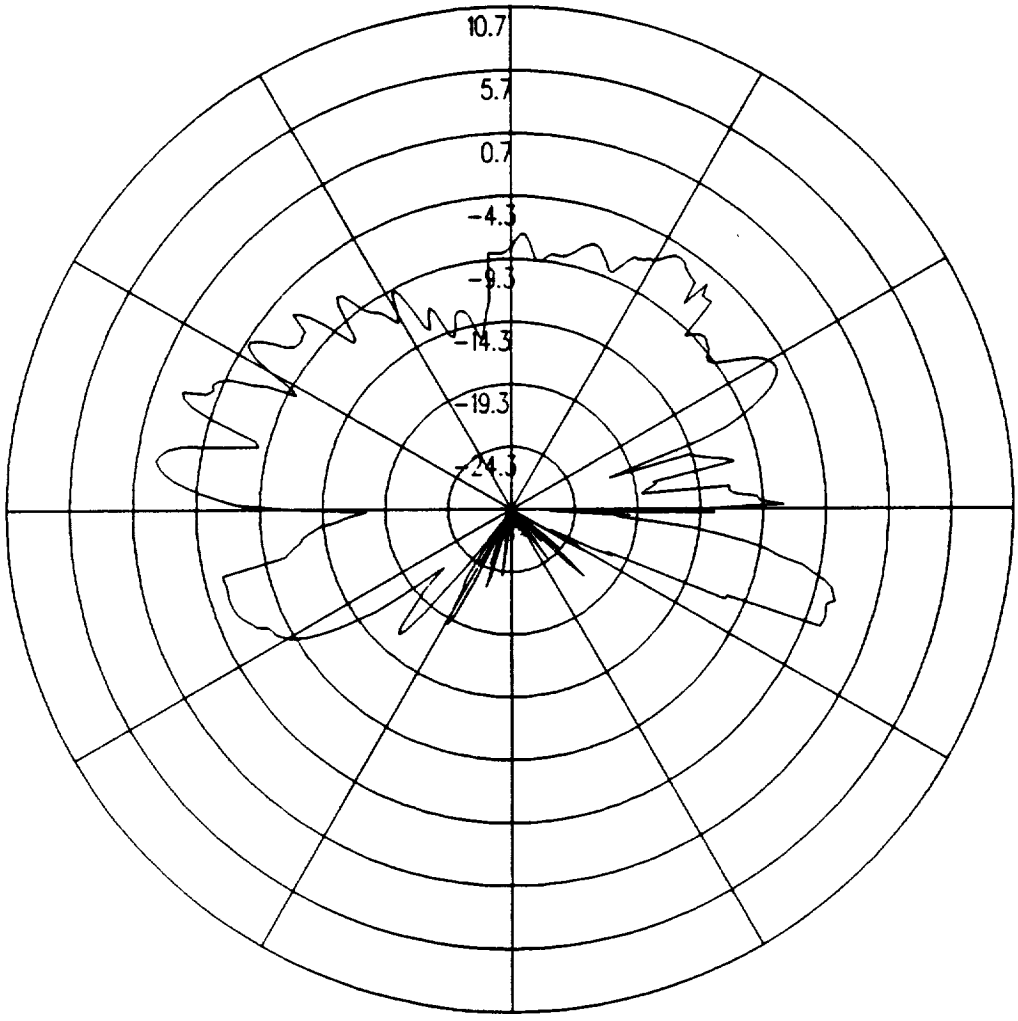

Figure 4.37: UTD calculated elevation plane pattern for batwing antenna on a P-3C for left hand circular polarization at 300 MHz. (Composite Ellipsoid Aircraft Model)

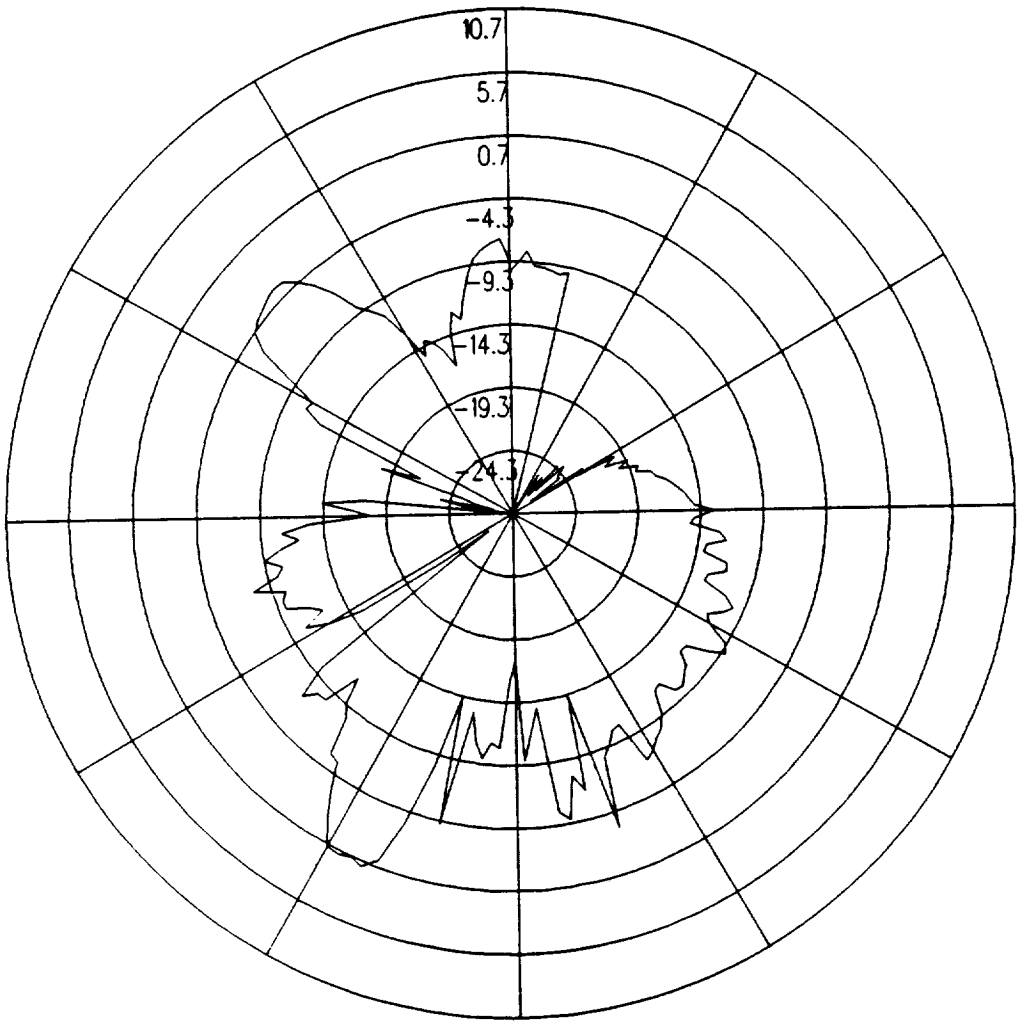

Figure 4.38: UTD calculated conical plane pattern 10° above the horizon for batwing antenna on a P-3C for left hand circular polarization at 300 MHz.(Composite Ellipsoid Aircraft Model)

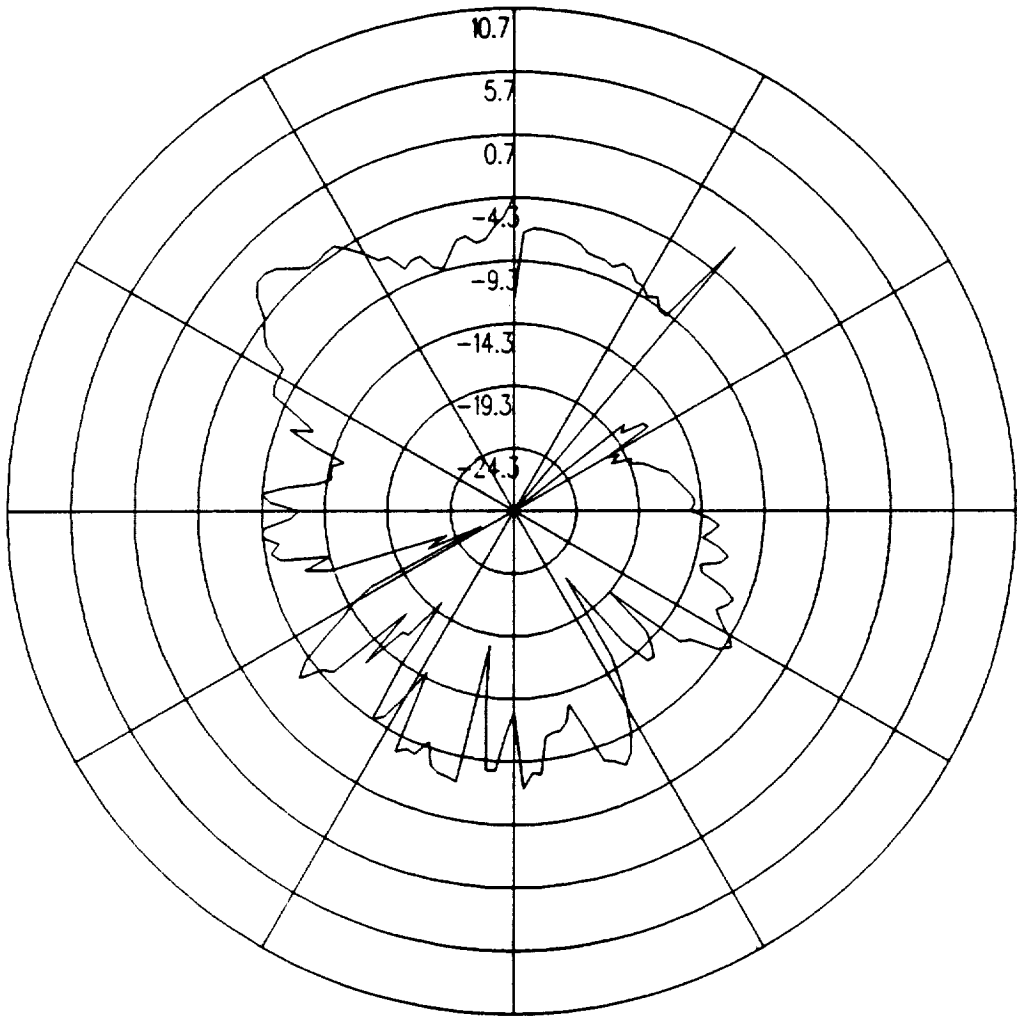

Figure 4.39: UTD calculated conical plane pattern 20° above the horizon for batwing antenna on a P-3C for left hand circular polarization at 300 MHz.(Composite Ellipsoid Aircraft Model)

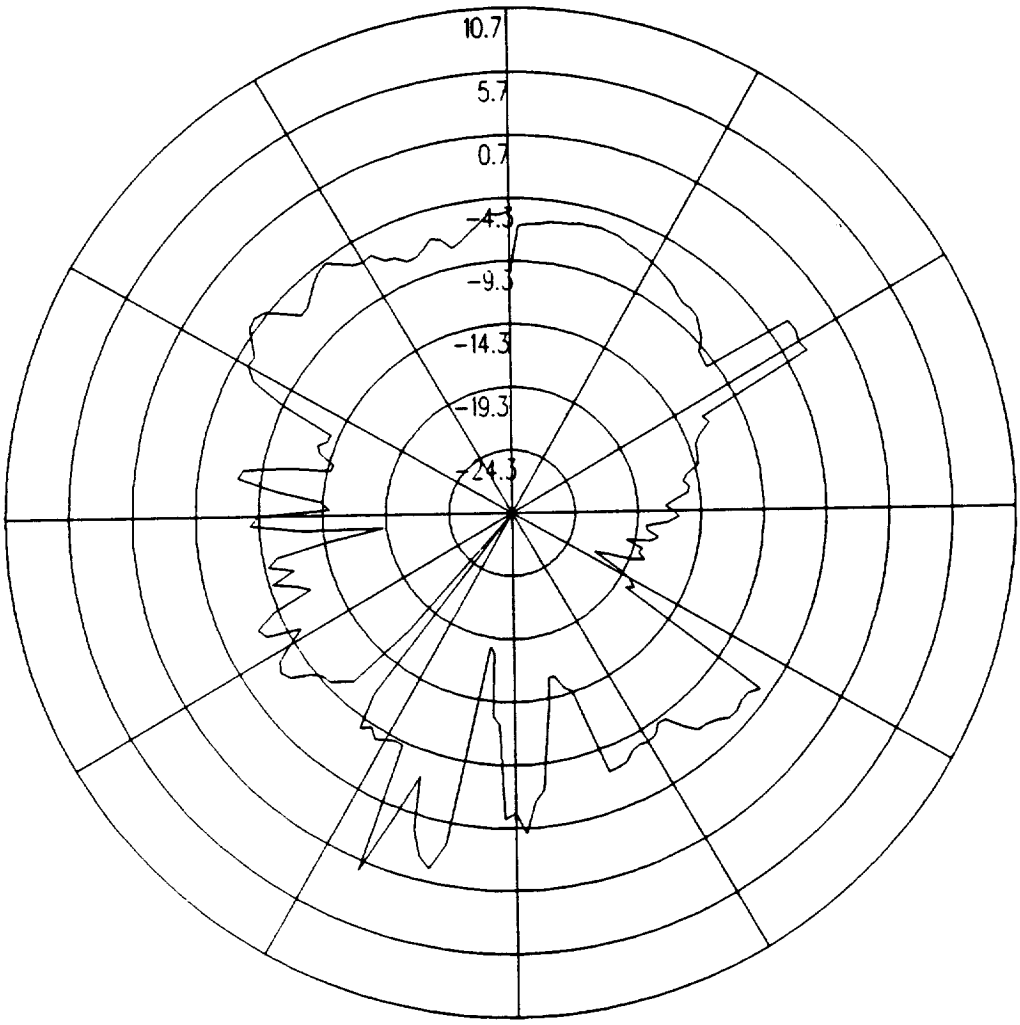

Figure 4.40: UTD calculated conical plane pattern 30° above the horizon for batwing antenna on a P-3C for left hand circular polarization at 300 MHz.(Composite Ellipsoid Aircraft Model)

4.4 Boeing Location with Cone Frustum Fuselage

The results computed in this section using the cone frustum aircraft model have been compared to the calculated results in Section 4.2 as well as the measured results provided by Boeing. The antenna is located as illustrated in Figure 4.41, which also shows the computer model used to generate the results. The calculated results at 300 MHz are shown for the roll plane in Figure 4.42, for the azimuth plane in Figure 4.43, for the elevation plane in Figure 4.44, for the conical plane 10° above the horizon in Figure 4.45, for the conical plane 20° above the horizon in Figure 4.46, and for the conical plane 30° above the horizon in Figure 4.47 all for right hand polarization. These calculated results can be compared with the calculated and measured results in Section 4.2 shown in Figure 4.4 through Figure 4.15. The cross polarized fields are shown for the roll plane in Figure 4.48, for the azimuth plane in Figure 4.49, for the elevation plane in Figure 4.50, for the conical plane 10° above the horizon in Figure 4.51, for the conical plane 20° above the horizon in Figure 4.52, and for the conical plane 30° above the horizon in Figure 4.53 all for left hand polarization. These calculated results also can be compared with the calculated and measured results found in Section 4.2 in Figure 4.16 through Figure 4.27.

Comparing the radiation patterns for the cone frustum aircraft model to the patterns for the cylindrical aircraft model in the azimuth plane, the elevation plane, and the conical planes above the horizon shows that there is good agreement between the two models for each of these pattern cuts except for near the nose of the aircraft where the calculated patterns for the cone frustum model are as much as 10 dB higher than for the original cylindrical model. Another exception is in the roll plane where the pattern for the cone frustum model has a broader main beam than the pattern for the cylindrical model and the measured pattern provided by Boeing. This comparison shows that the cone frustum aircraft model has even greater problem with high levels on the horizon near the nose and the tail as the cylindrical aircraft model. In addition, this model has a problem in the roll plane as described above. Therefore, the cylindrical aircraft model is a better representation for the actual P-3C aircraft than the cone frustum aircraft model.

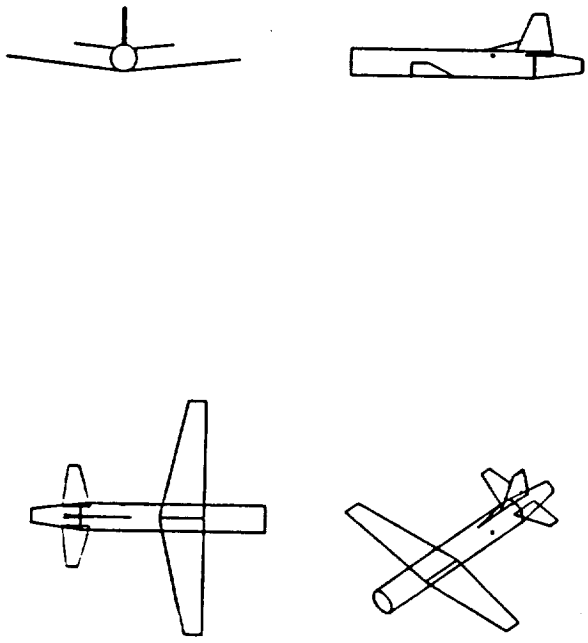

Figure 4.41: Geometry of the cone frustum model of the P-3C aircraft used in the NEC-BSC code showing the location of the antenna.

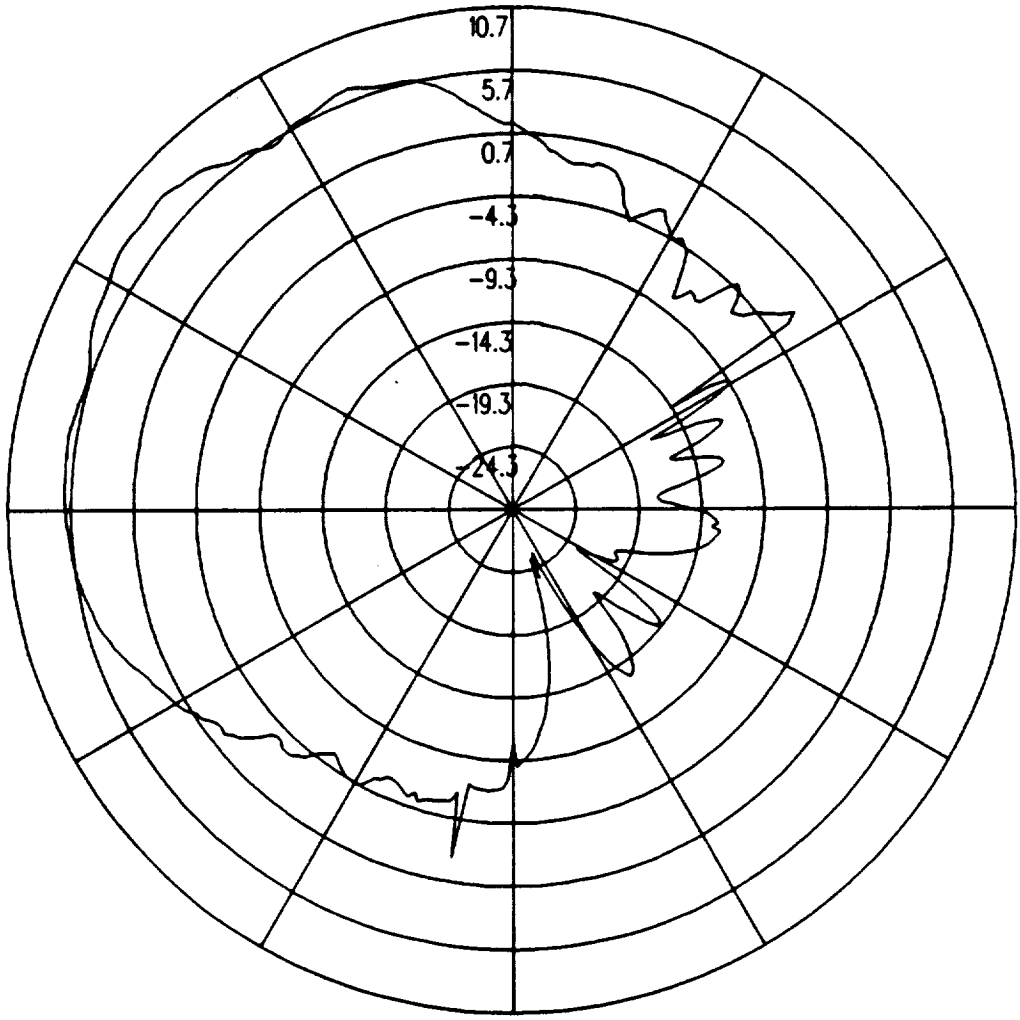

Figure 4.42: UTD calculated roll plane pattern for batwing antenna on a P-3C for right hand circular polarization at 300 MHz. (Cone Frustum Aircraft Model)

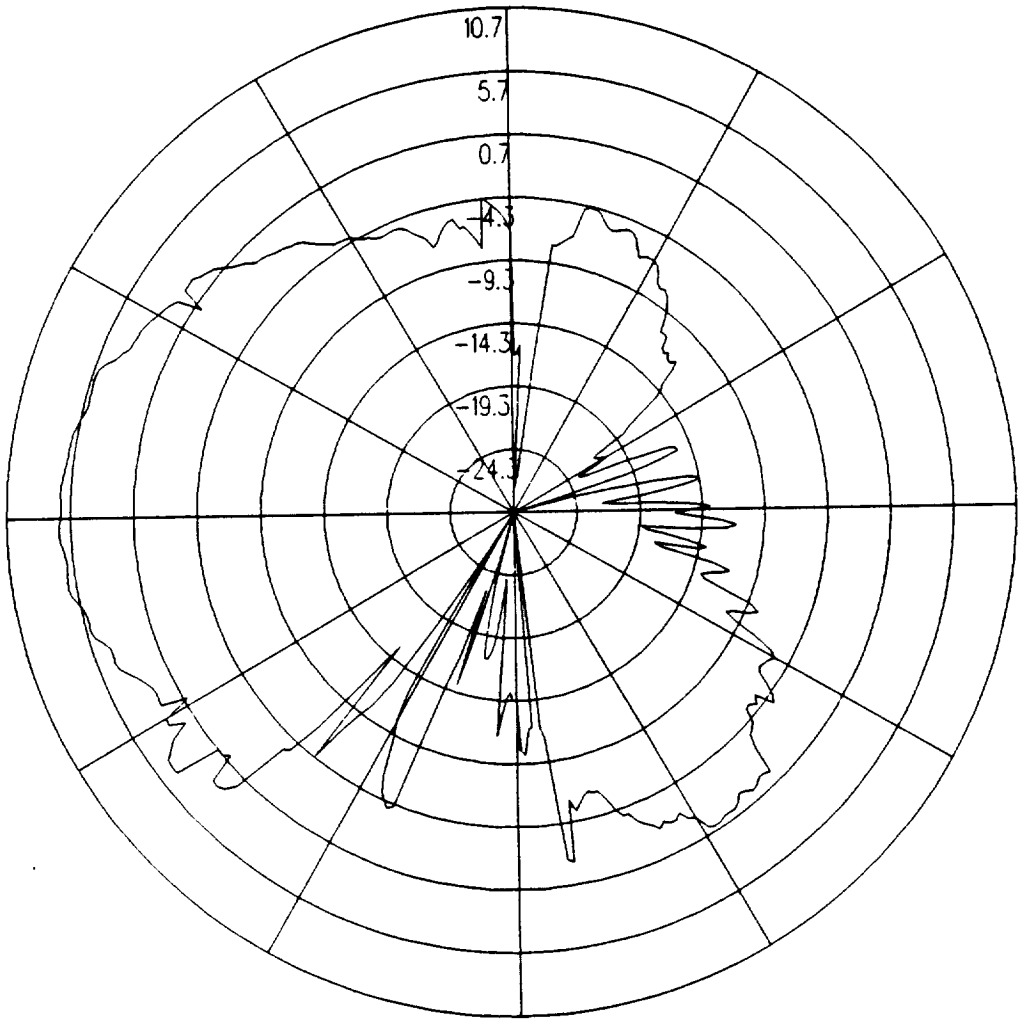

Figure 4.43: UTD calculated azimuth plane pattern for batwing antenna on a P-3C for right hand circular polarization at 300 MHz. (Cone Frustum Aircraft Model)

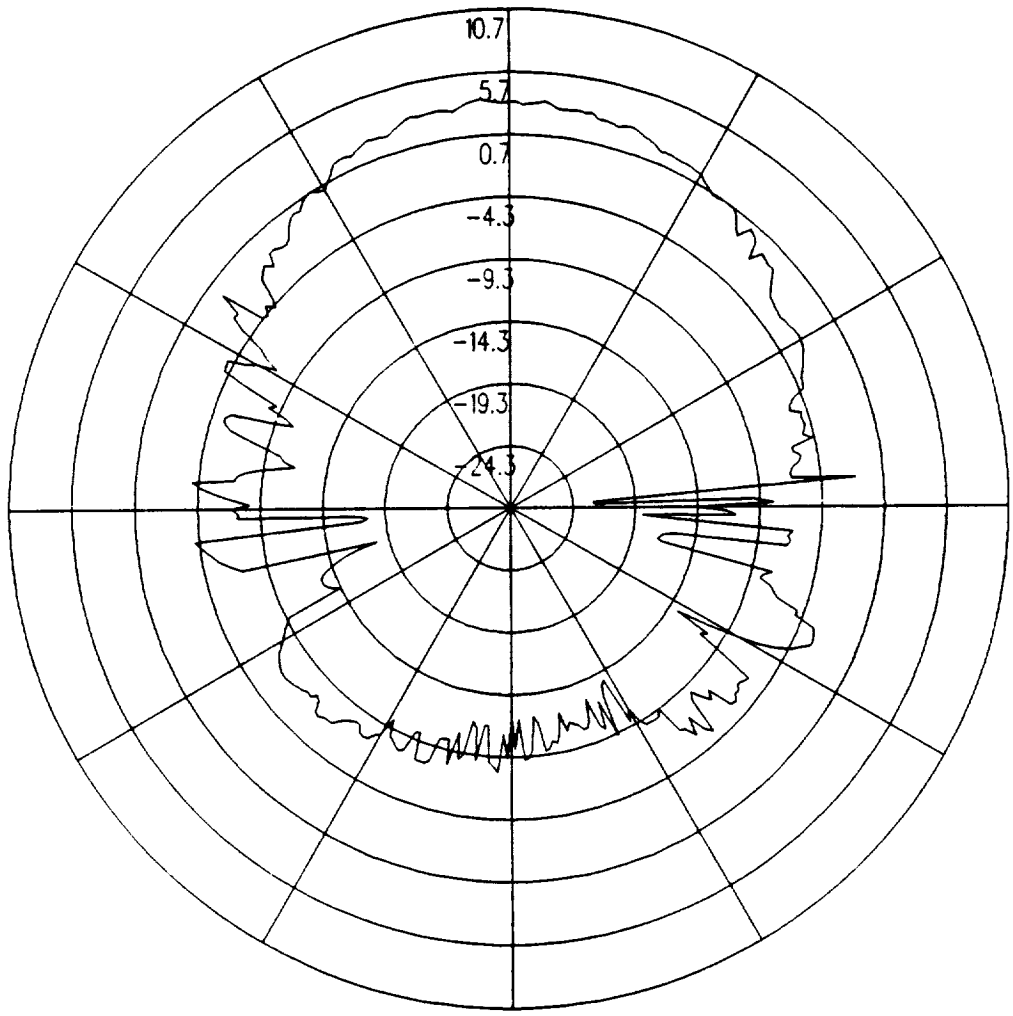

Figure 4.44: UTD calculated elevation plane pattern for batwing antenna on a P-3C for right hand circular polarization at 300 MHz. (Cone Frustum Aircraft Model)

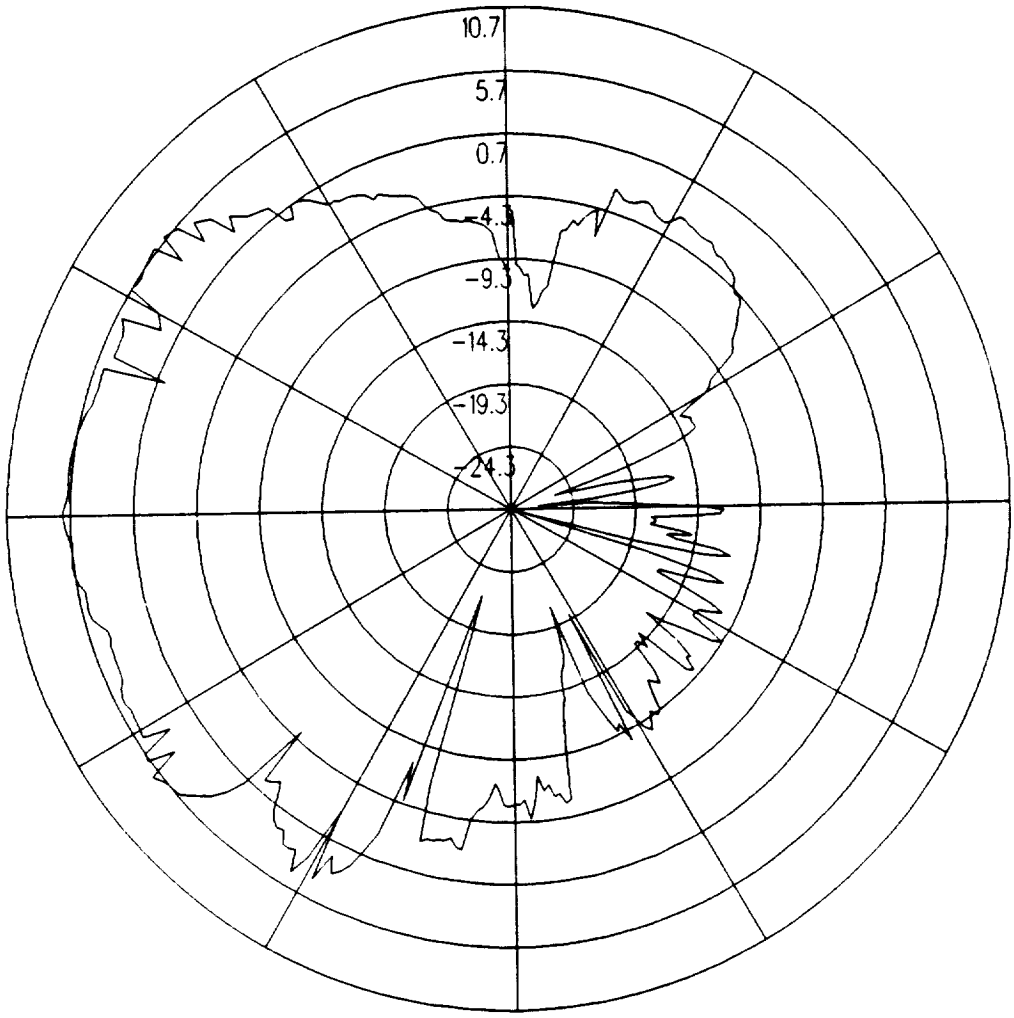

Figure 4.45: UTD calculated conical plane pattern 10° above the horizon for batwing antenna on a P-3C for right hand circular polarization at 300 MHz.(Cone Frustum Aircraft Model)

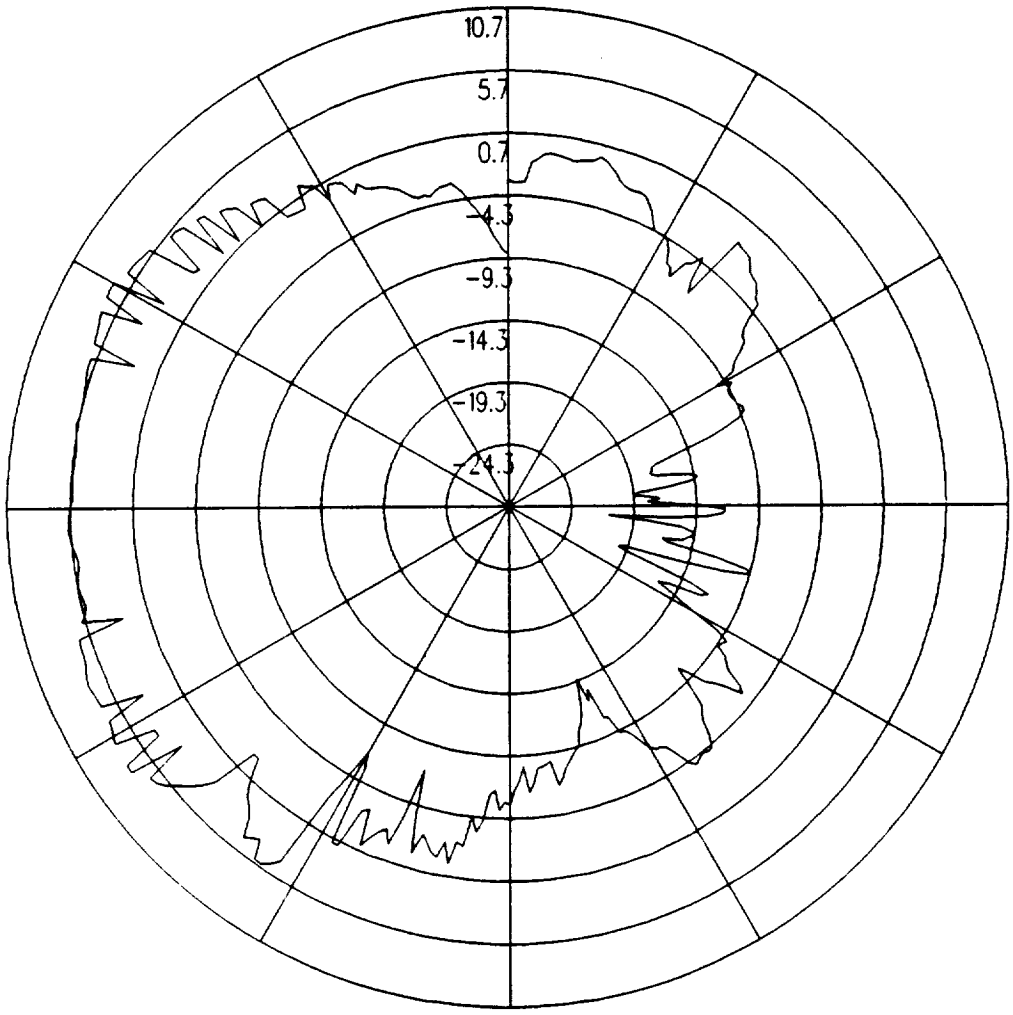

Figure 4.46: UTD calculated conical plane pattern 20° above the horizon for batwing antenna on a P-3C for right hand circular polarization at 300 MHz.(Cone Frustum Aircraft Model)

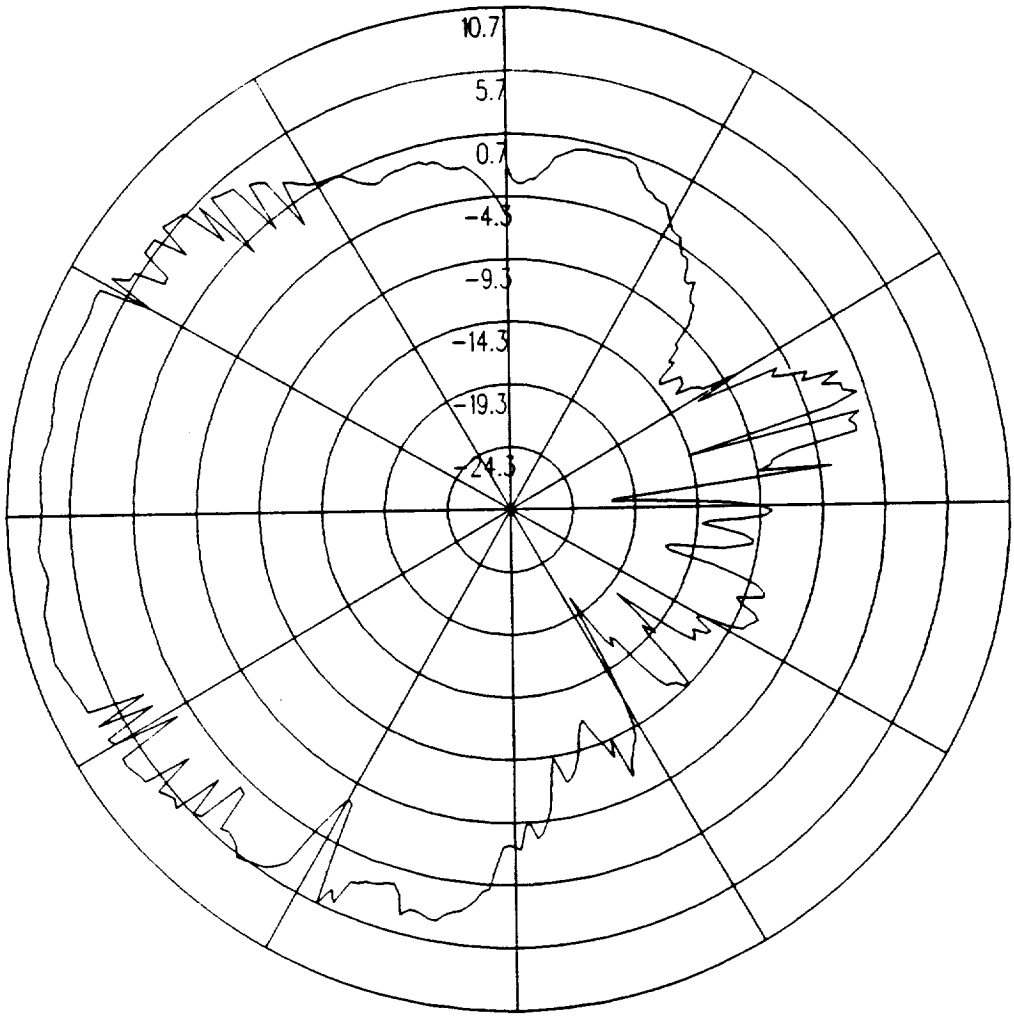

Figure 4.47: UTD calculated conical plane pattern 30° above the horizon for batwing antenna on a P-3C for right hand circular polarization at 300 MHz.(Cone Frustum Aircraft Model)

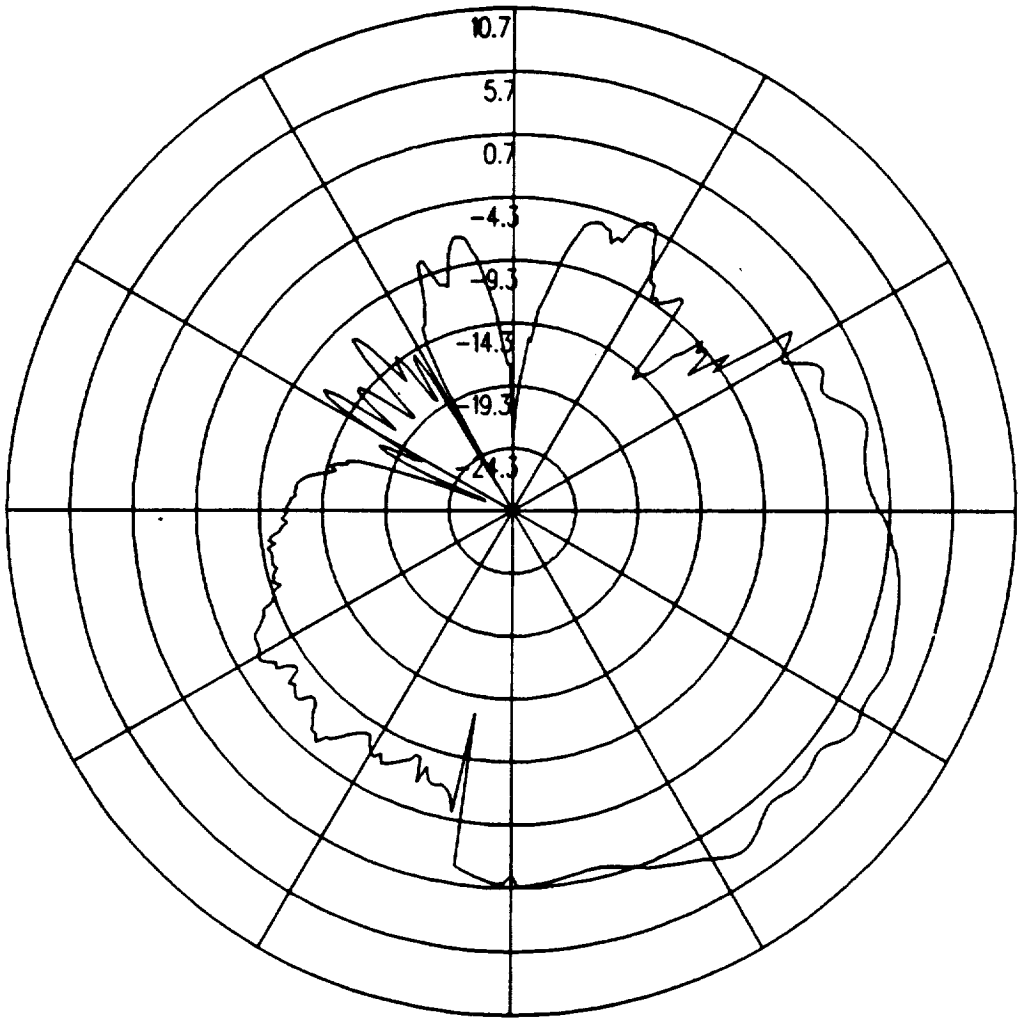

Figure 4.48: UTD calculated roll plane pattern for batwing antenna on a P-3C for left hand circular polarization at 300 MHz. (Cone Frustum Aircraft Model)

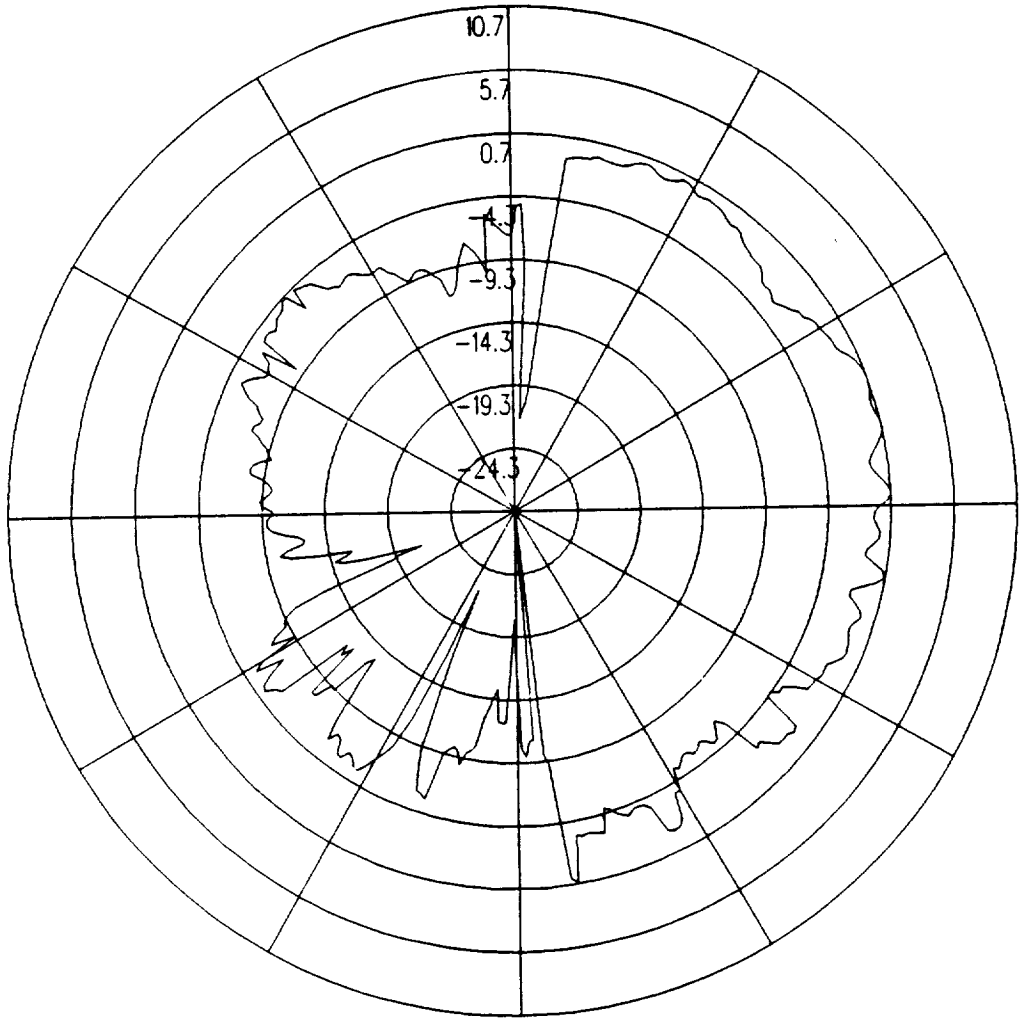

Figure 4.49: UTD calculated azimuth plane pattern for batwing antenna on a P-3C for left hand circular polarization at 300 MHz. (Cone Frustum Aircraft Model)

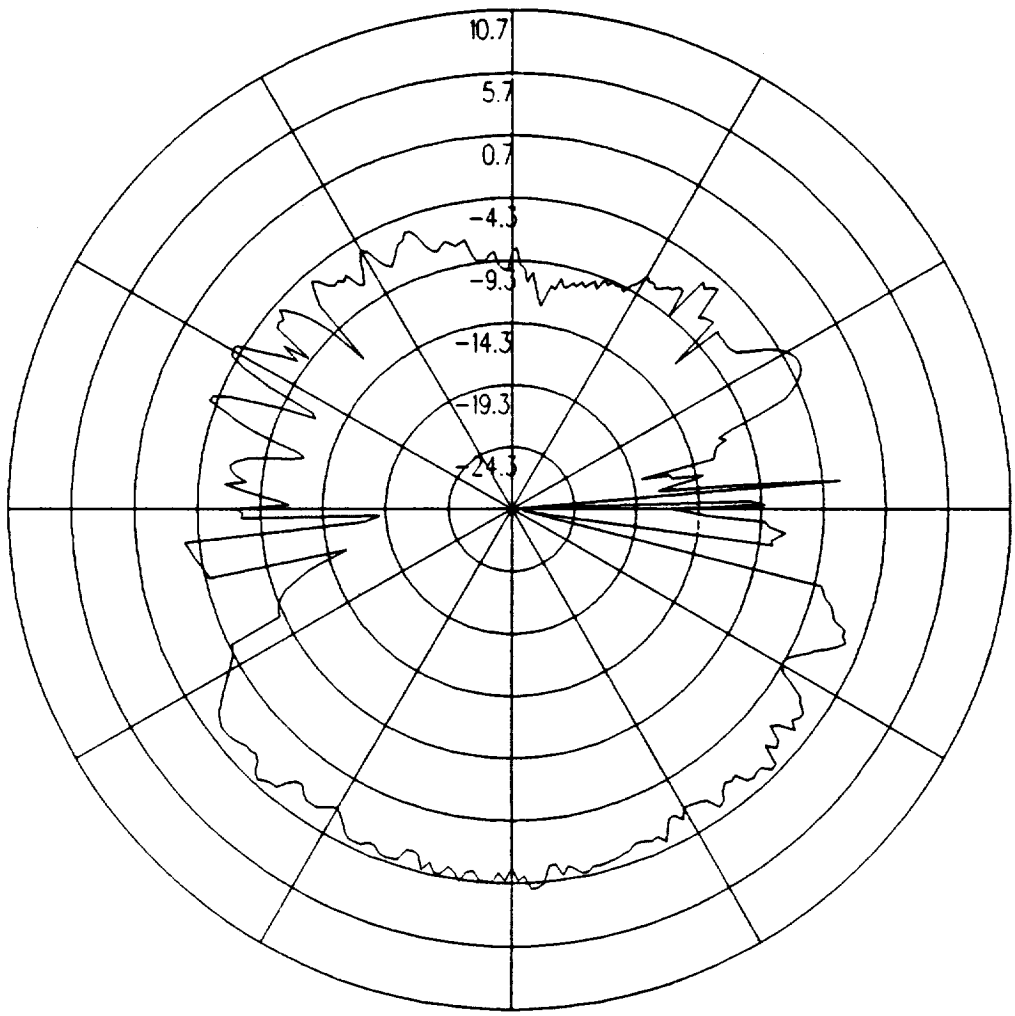

Figure 4.50: UTD calculated elevation plane pattern for batwing antenna on a P-3C for left hand circular polarization at 300 MHz. (Cone Frustum Aircraft Model)

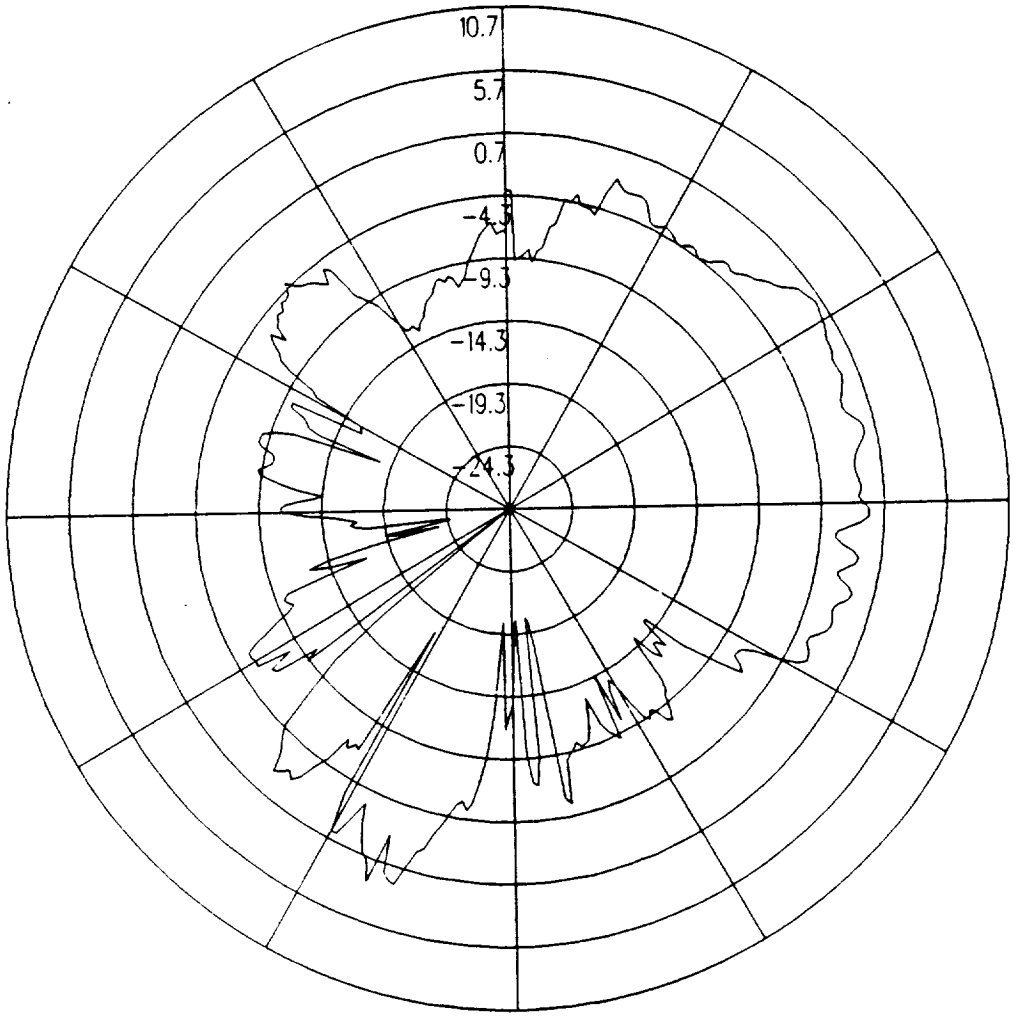

Figure 4.51: UTD calculated conical plane pattern 10° above the horizon for batwing antenna on a P-3C for left hand circular polarization at 300 MHz.(Cone Frustum Aircraft Model)

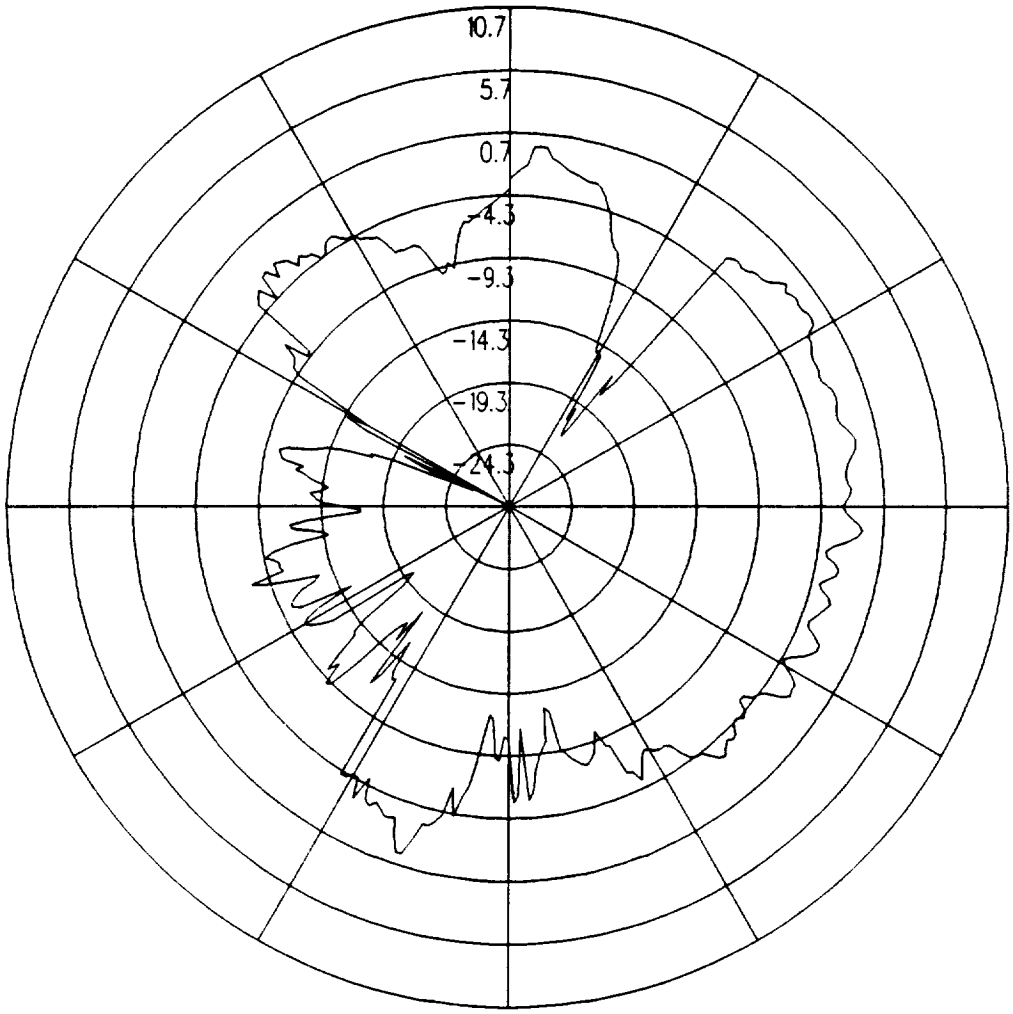

Figure 4.52: UTD calculated conical plane pattern 20° above the horizon for batwing antenna on a P-3C for left hand circular polarization at 300 MHz.(Cone Frustum Aircraft Model)

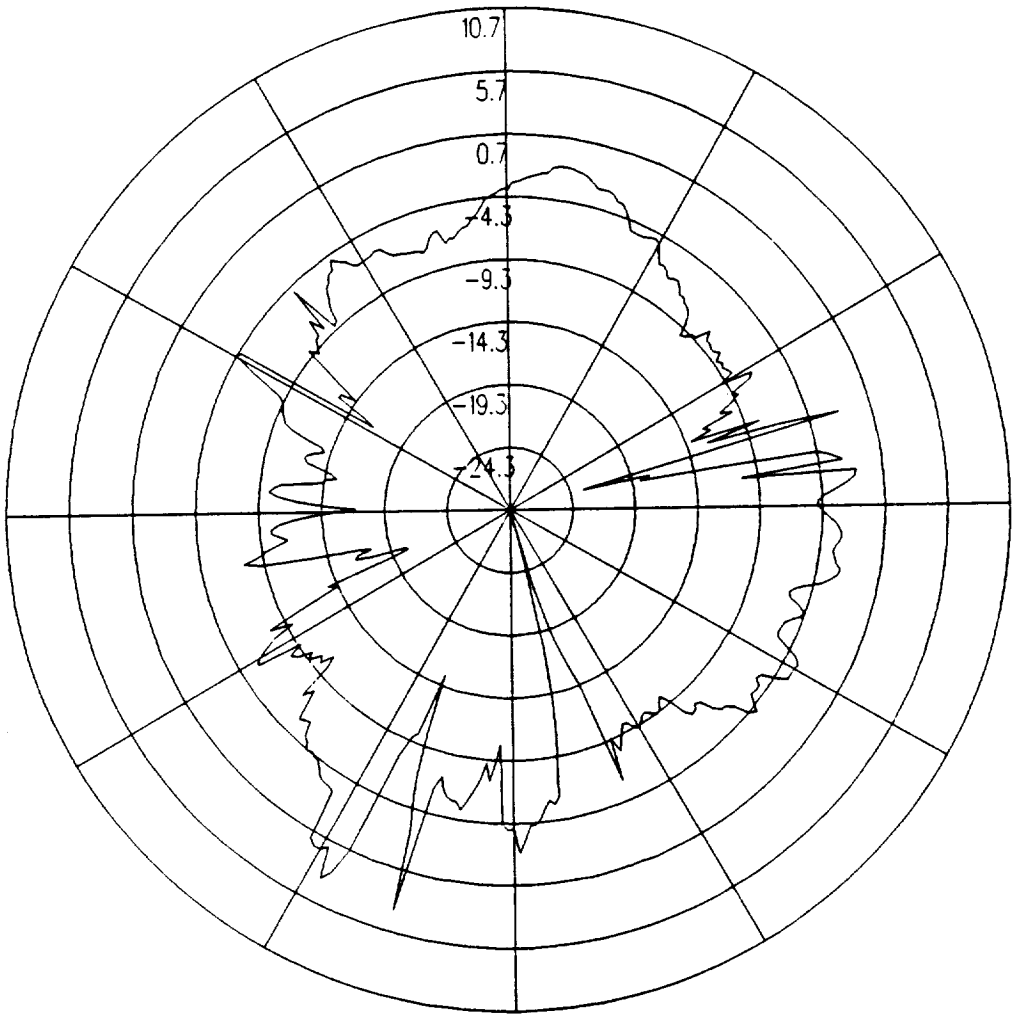

Figure 4.53: UTD calculated conical plane pattern 30° above the horizon for batwing antenna on a P-3C for left hand circular polarization at 300 MHz.(Cone Frustum Aircraft Model)

4.5 Boeing Location with Cylindrical Fuselage and Inner Engine Model Included

To test the stability of the aircraft model, the presence of the aircraft engines on the model had to be studied in order to see the effect on the radiation patterns. Because the inner engine will have the greatest impact on the radiation patterns due to its proximity to the antenna, only the inner engine on the side on which the antenna is located has been included in the aircraft model. The results computed in this section using the aircraft model which includes the inner engine can be compared to the calculated results in Section 4.2 . The antenna is located as illustrated in Figure 4.54, which also shows the computer model used to generate the results. The calculated results at 300 MHz are shown for the roll plane in Figure 4.55, for the azimuth plane in Figure 4.56, for the elevation plane in Figure 4.57, for the conical plane 10° above the horizon in Figure 4.58, for the conical plane 20° above the horizon in Figure 4.59, and for the conical plane 30° above the horizon in Figure 4.60 all for right hand polarization. These calculated results can be compared with the calculated results in Section 4.2 shown in Figure 4.4 through Figure 4.15. The cross polarized fields are shown for the roll plane in Figure 4.61, for the azimuth plane in Figure 4.62, for the elevation plane in Figure 4.63, for the conical plane 10° above the horizon in Figure 4.64, for the conical plane 20° above the horizon in Figure 4.65, and for the conical plane 30° above the horizon in Figure 4.66 all for left hand polarization. These calculated results also can be compared with the calculated results found in Section 4.2 in Figure 4.16 through Figure 4.27.

Comparing the radiation patterns for the aircraft model which includes the inner engine to the patterns for the aircraft model without the engine in the roll plane, the azimuth plane, the elevation plane, and the conical planes above the horizon shows that there is excellent agreement between the two models for each of these pattern cuts taken. The only region where the patterns do not match identically is near the nose of the aircraft in the azimuth plane where the presence of the engine causes there to be spikes in the pattern levels which differ from the model without the engine by 2–5 dB. These spikes are produced because the cylinder to cylinder terms are not present in the code. The approximation discussed in Section 2.2 does not help because it still requires plate to cylinder interactions in this case.

Because the presence of the inner engine on the aircraft model has minimal effect on the radiation patterns, the engine models will not be included in the remainder of the tests in order to reduce the amount of computer time required to run each test.

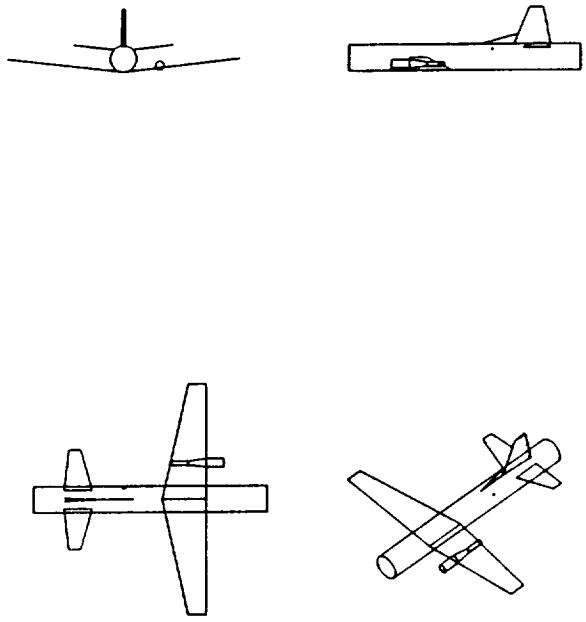

Figure 4.54: Geometry of the model which includes the inner engine of the P-3C aircraft used in the NEC-BSC code showing the location of the antenna.

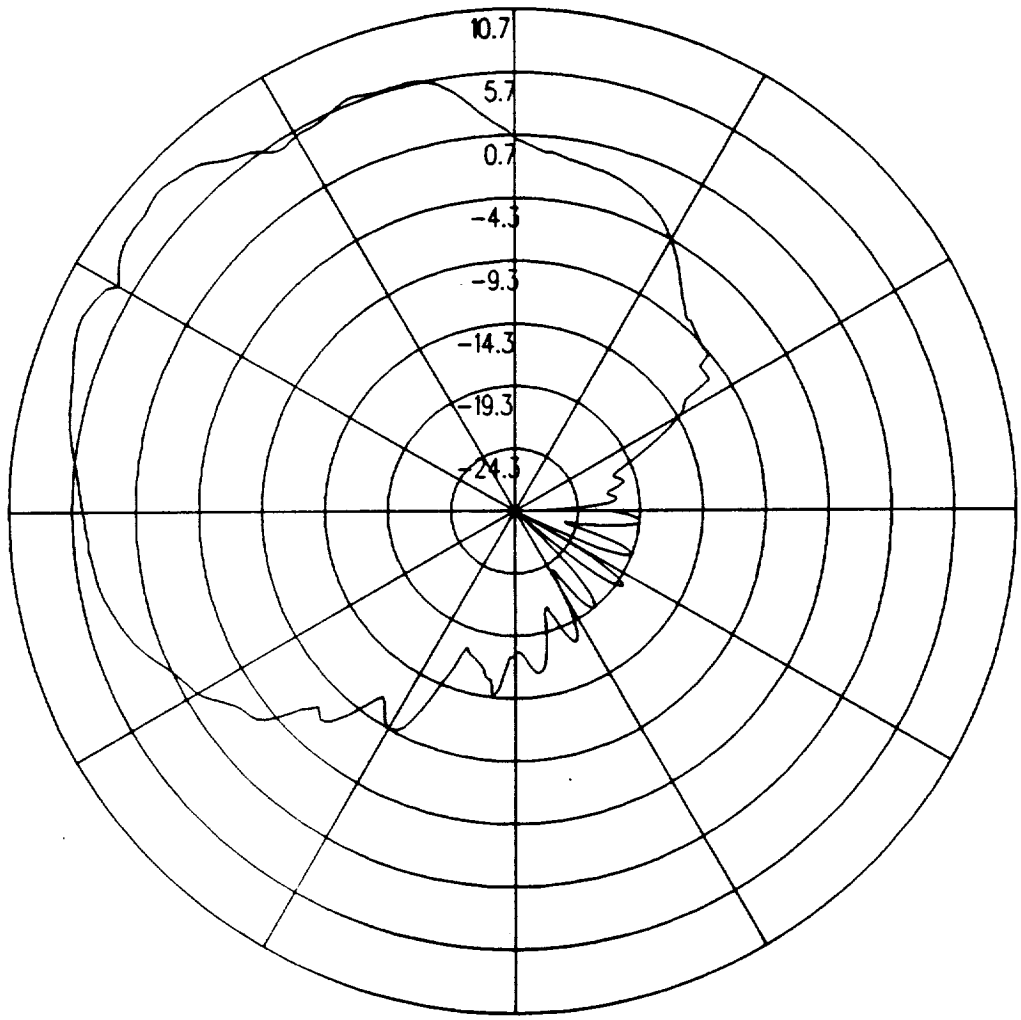

Figure 4.55: UTD calculated roll plane pattern for batwing antenna on a P-3C for right hand circular polarization at 300 MHz. (Aircraft Model with Inner Engine)

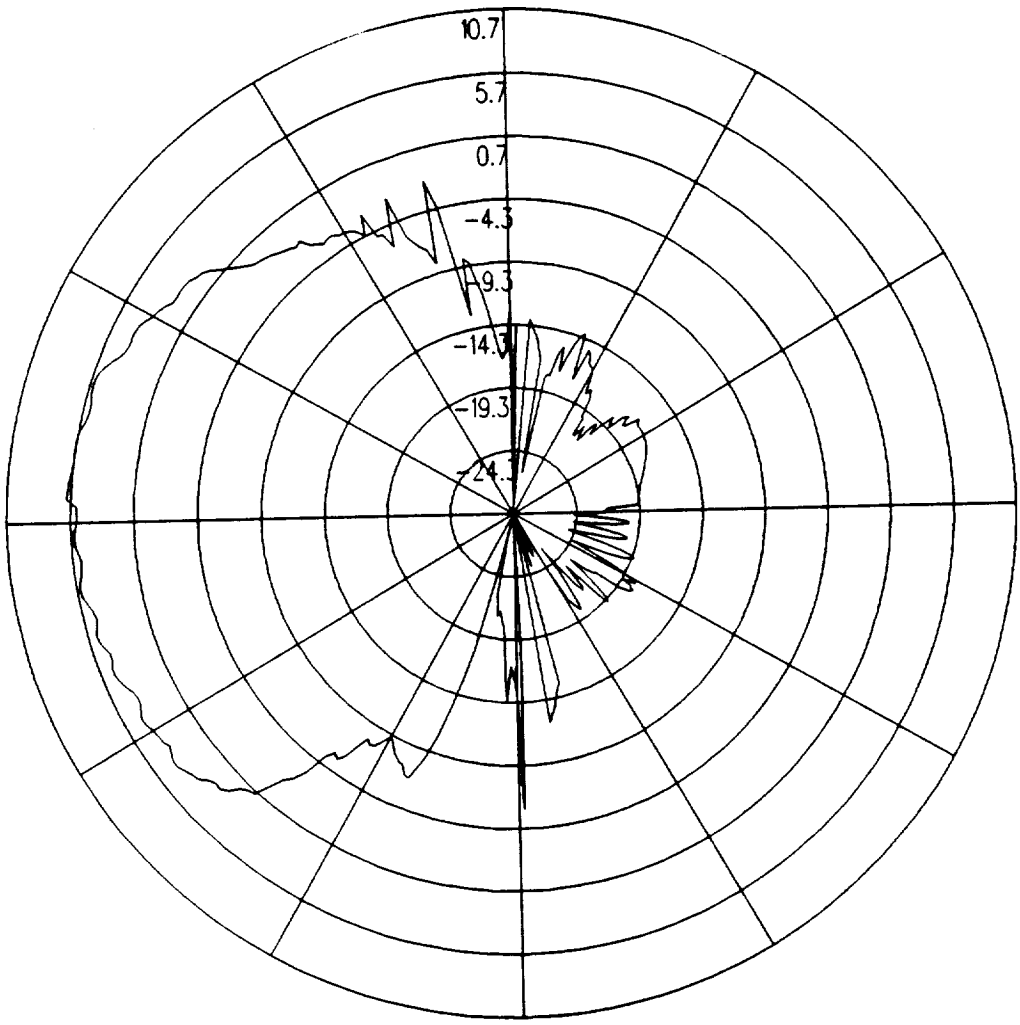

Figure 4.56: UTD calculated azimuth plane pattern for batwing antenna on a P-3C for right hand circular polarization at 300 MHz. (Aircraft Model with Inner Engine)

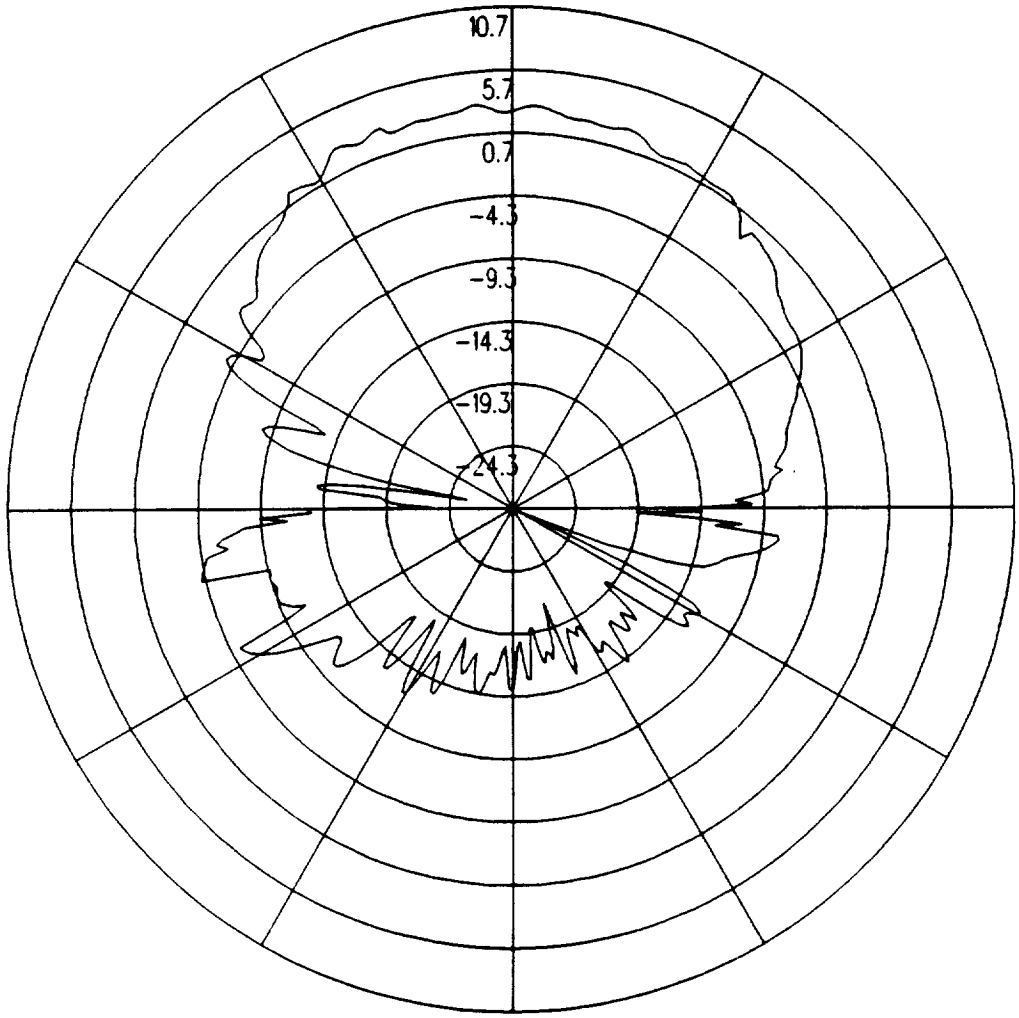

Figure 4.57: UTD calculated elevation plane pattern for batwing antenna on a P-3C for right hand circular polarization at 300 MHz. (Aircraft Model with Inner Engine)

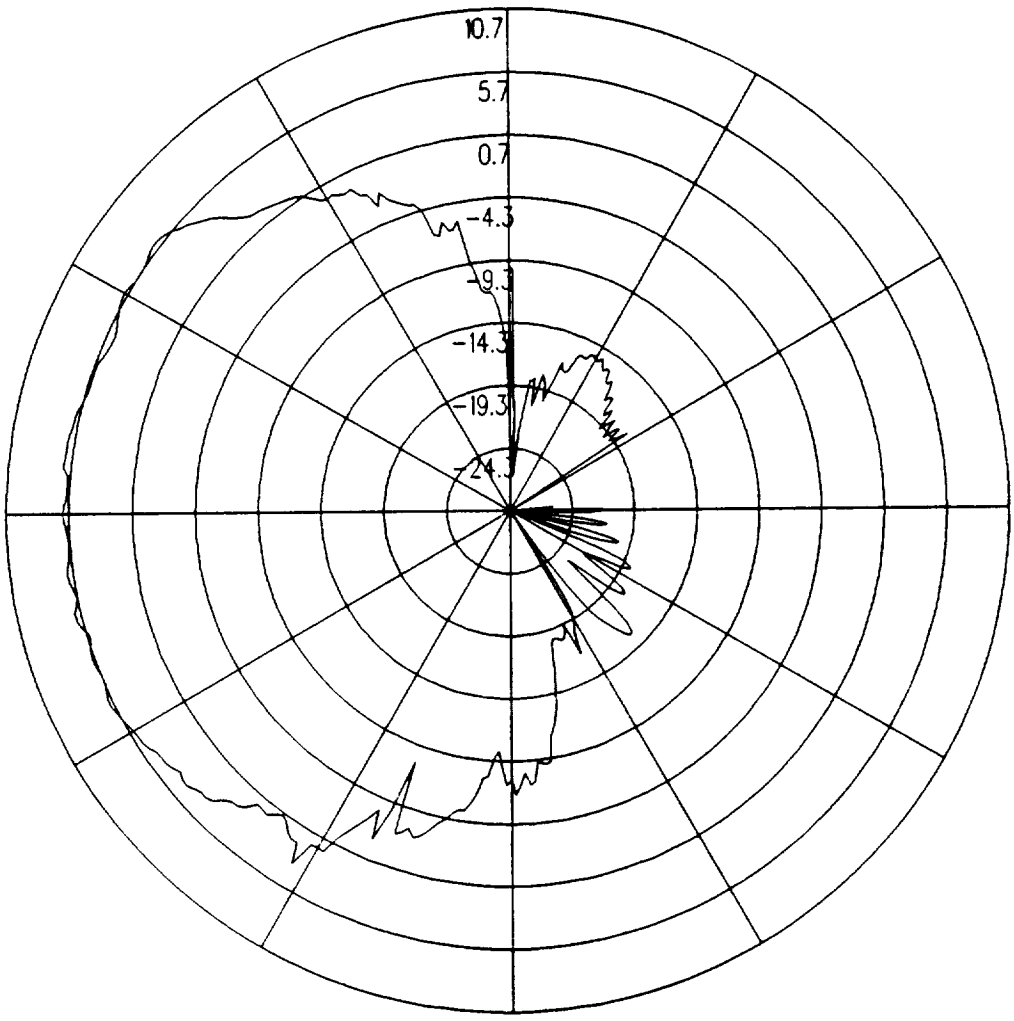

Figure 4.58: UTD calculated conical plane pattern 10° above the horizon for batwing antenna on a P-3C for right hand circular polarization at 300 MHz.(Aircraft Model with Inner Engine)

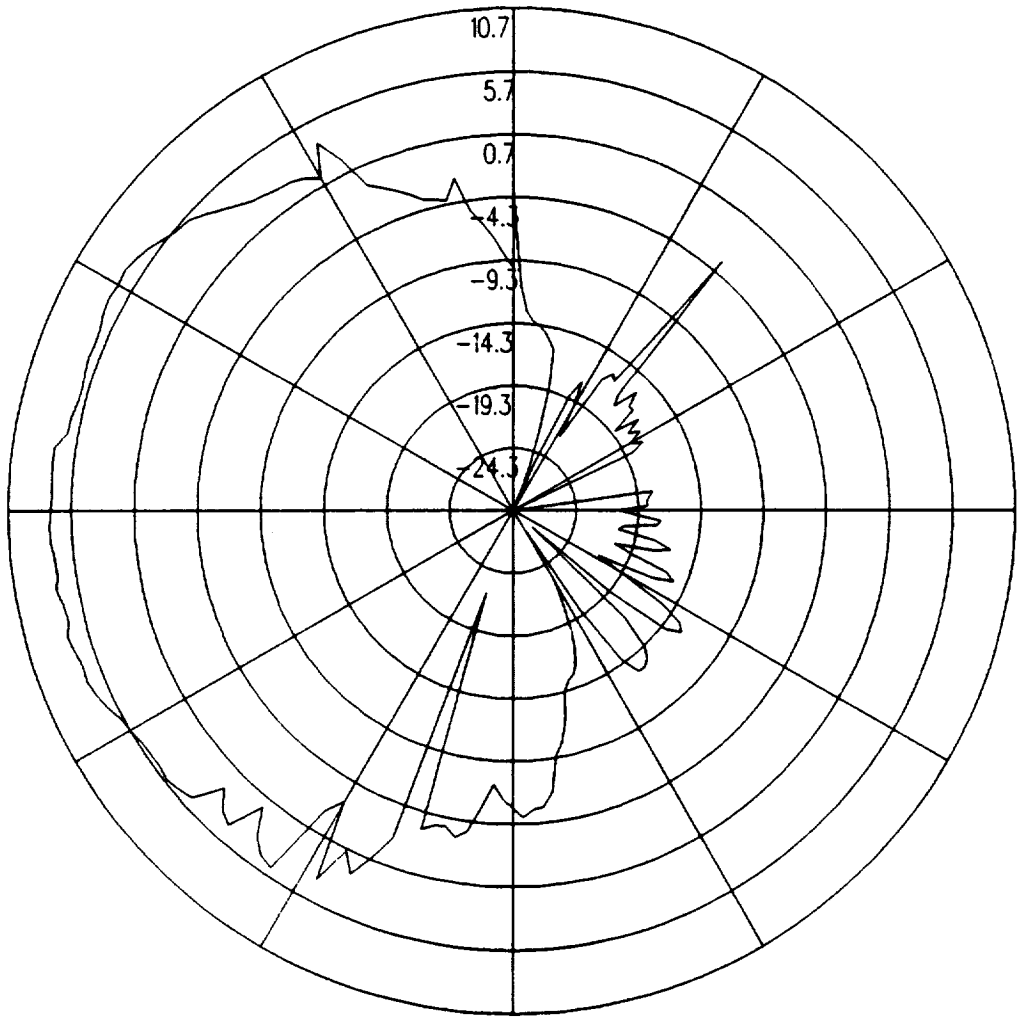

Figure 4.59: UTD calculated conical plane pattern 20° above the horizon for batwing antenna on a P-3C for right hand circular polarization at 300 MHz.(Aircraft Model with Inner Engine)

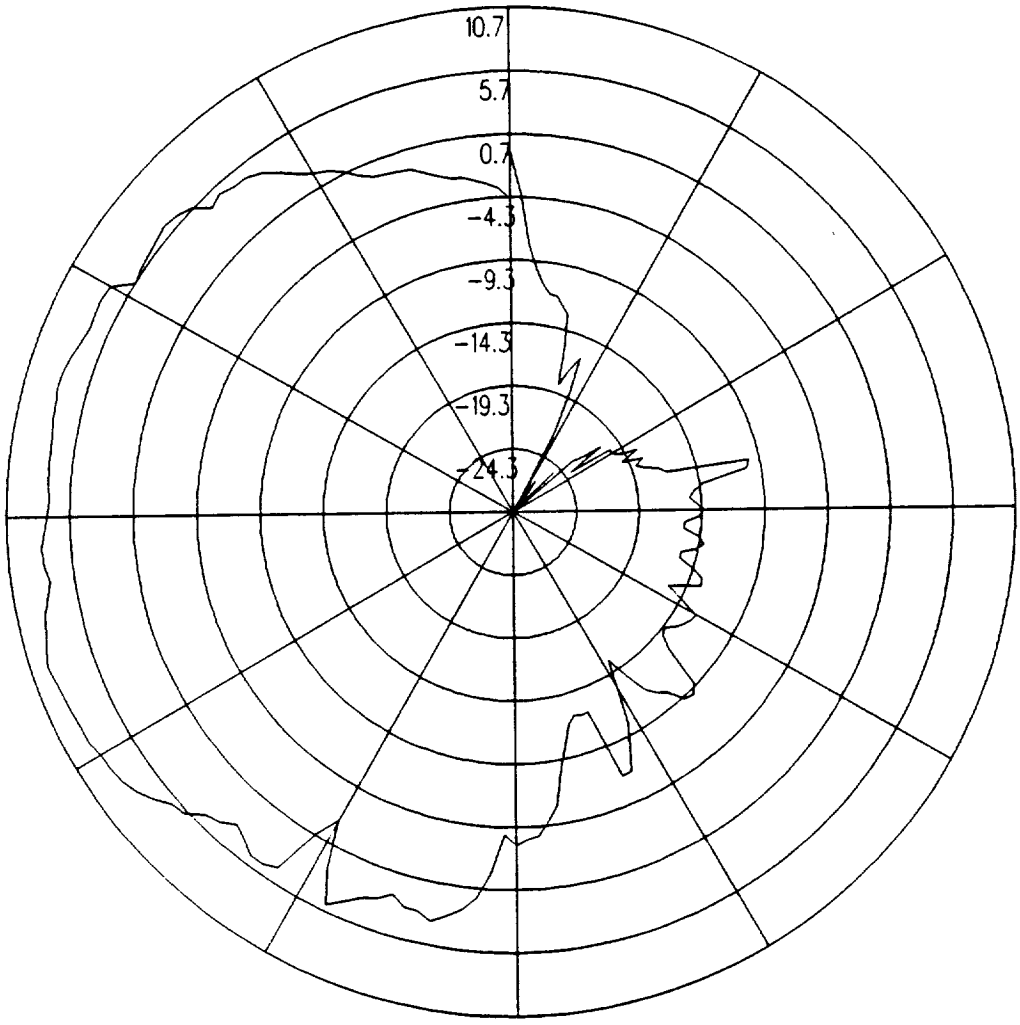

Figure 4.60: UTD calculated conical plane pattern 30° above the horizon for batwing antenna on a P-3C for right hand circular polarization at 300 MHz.(Aircraft Model with Inner Engine)

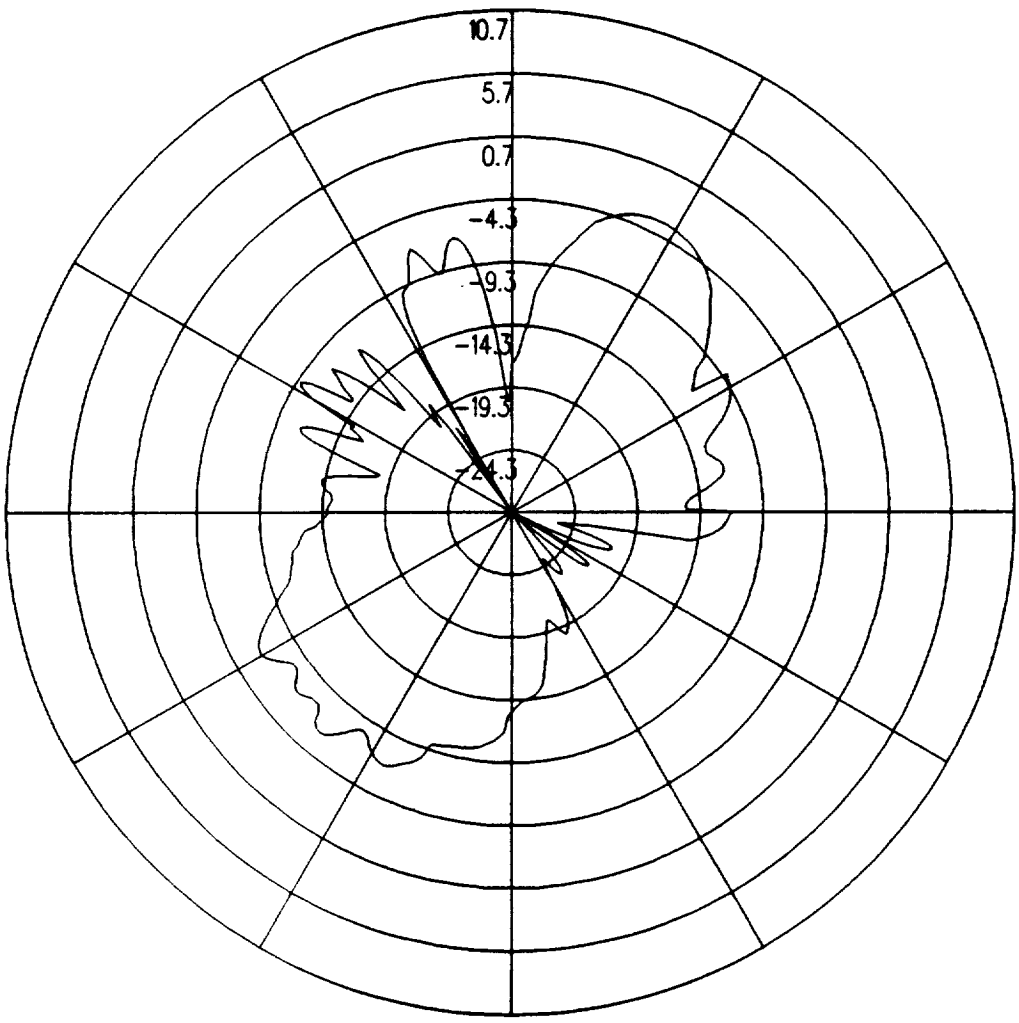

Figure 4.61: UTD calculated roll plane pattern for batwing antenna on a P-3C for left hand circular polarization at 300 MHz. (Aircraft Model with Inner Engine)

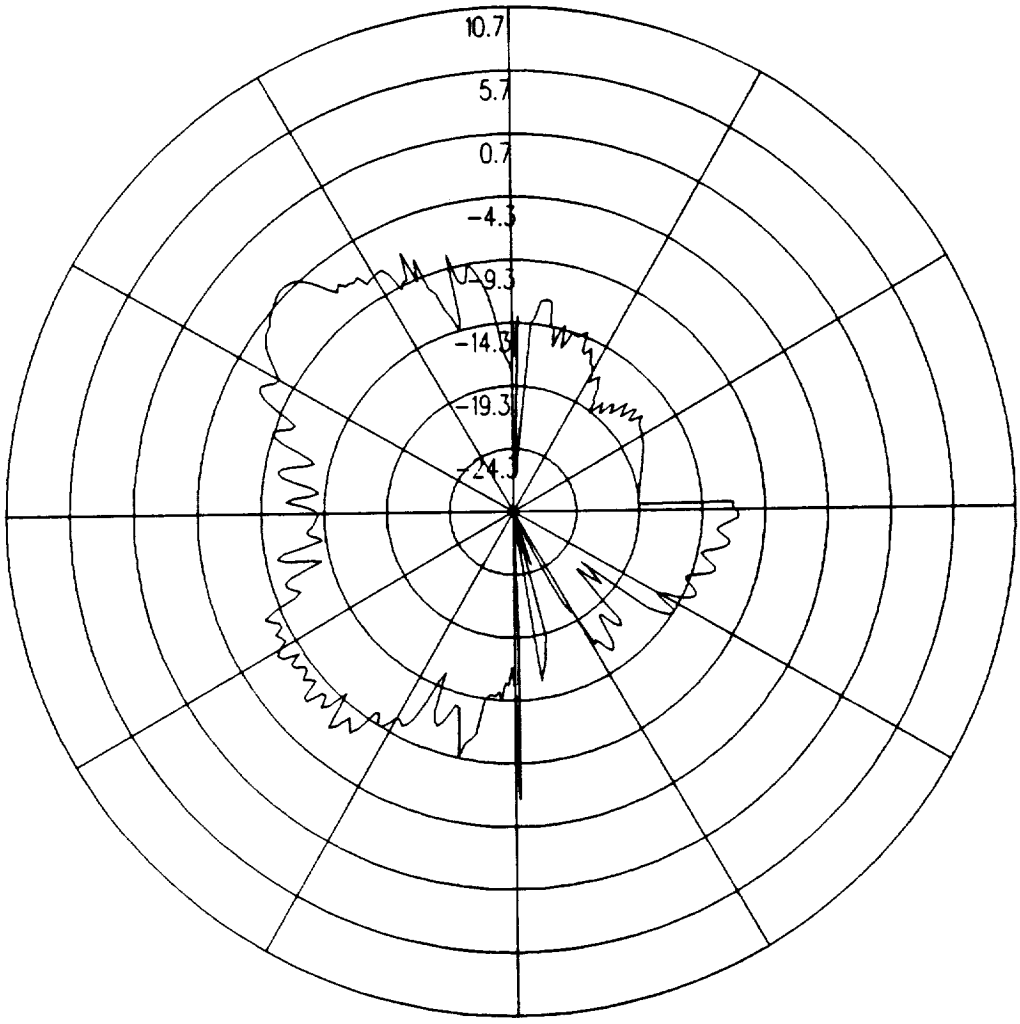

Figure 4.62: UTD calculated azimuth plane pattern for batwing antenna on a P-3C for left hand circular polarization at 300 MHz. (Aircraft Model with Inner Engine)

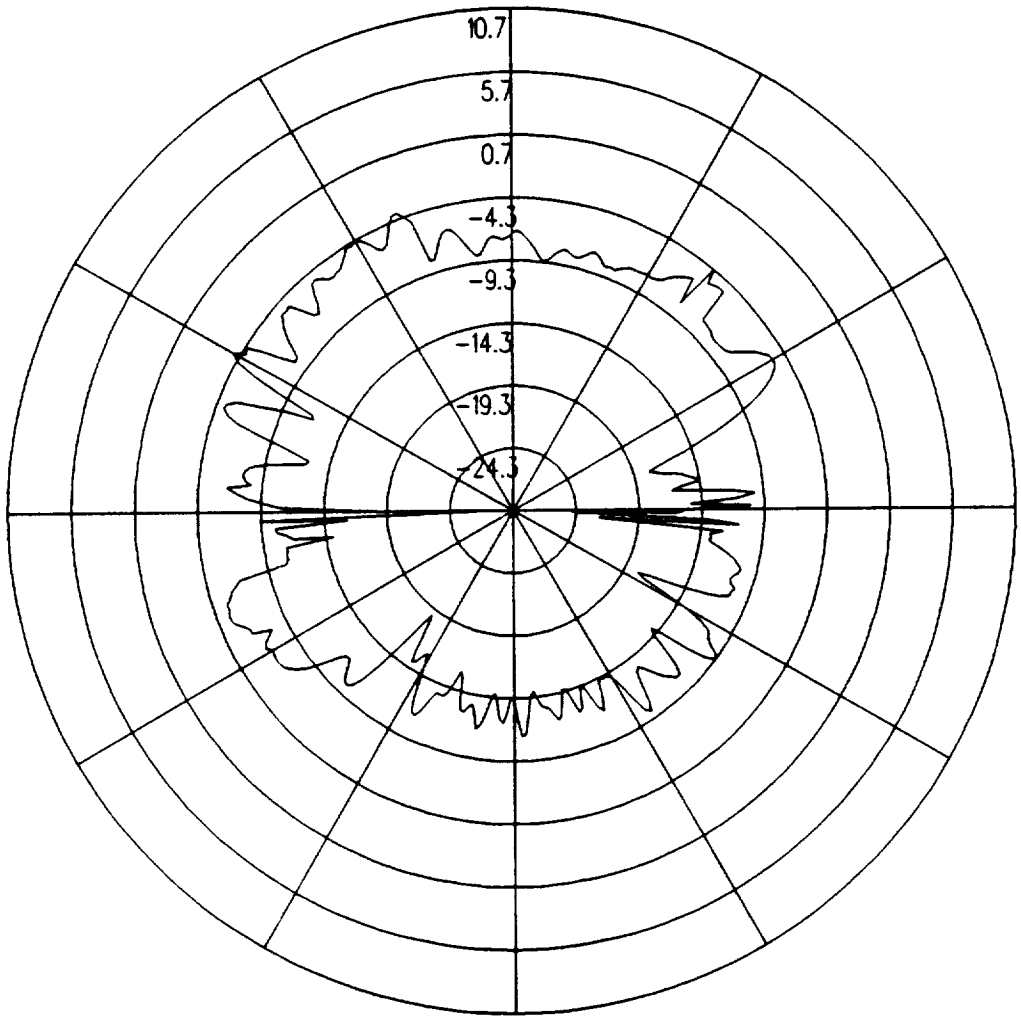

Figure 4.63: UTD calculated elevation plane pattern for batwing antenna on a P-3C for left hand circular polarization at 300 MHz. (Aircraft Model with Inner Engine)

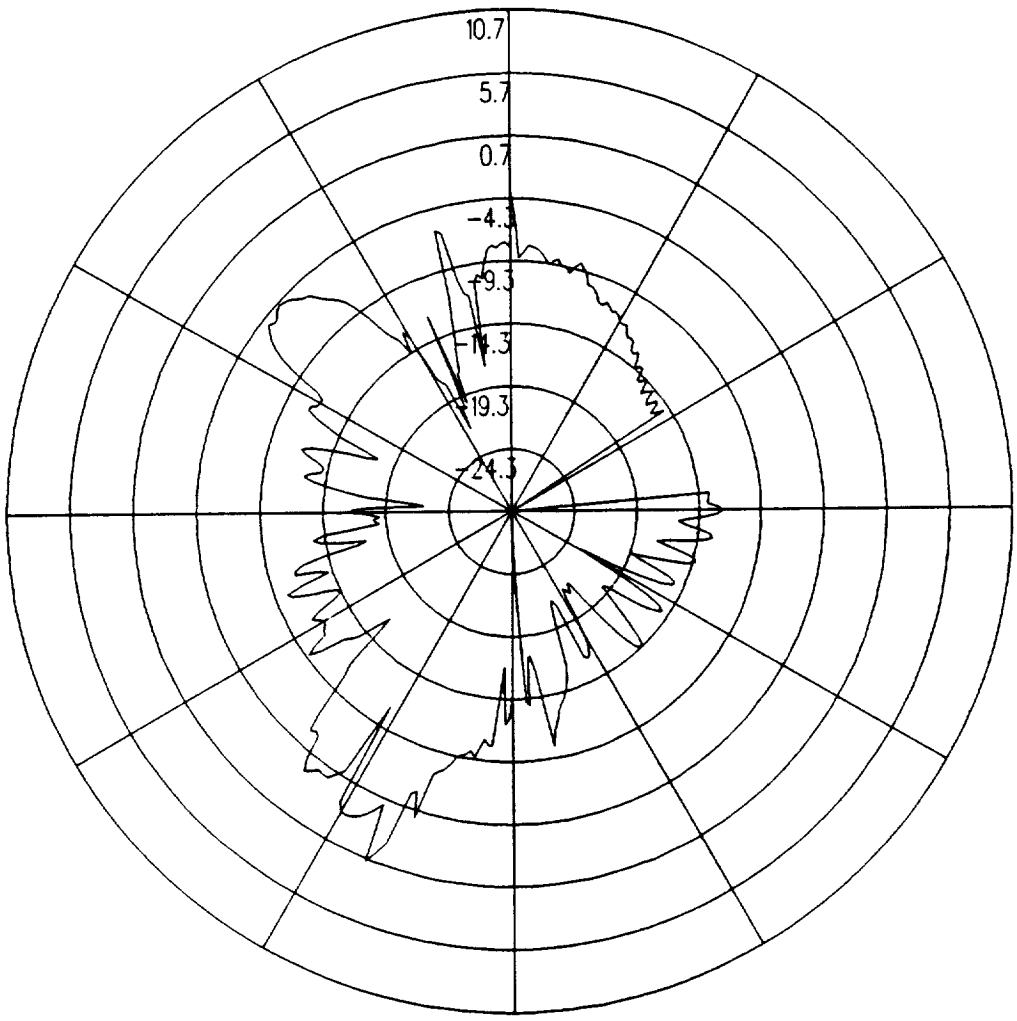

Figure 4.64: UTD calculated conical plane pattern 10° above the horizon for batwing antenna on a P-3C for left hand circular polarization at 300 MHz.(Aircraft Model with Inner Engine)

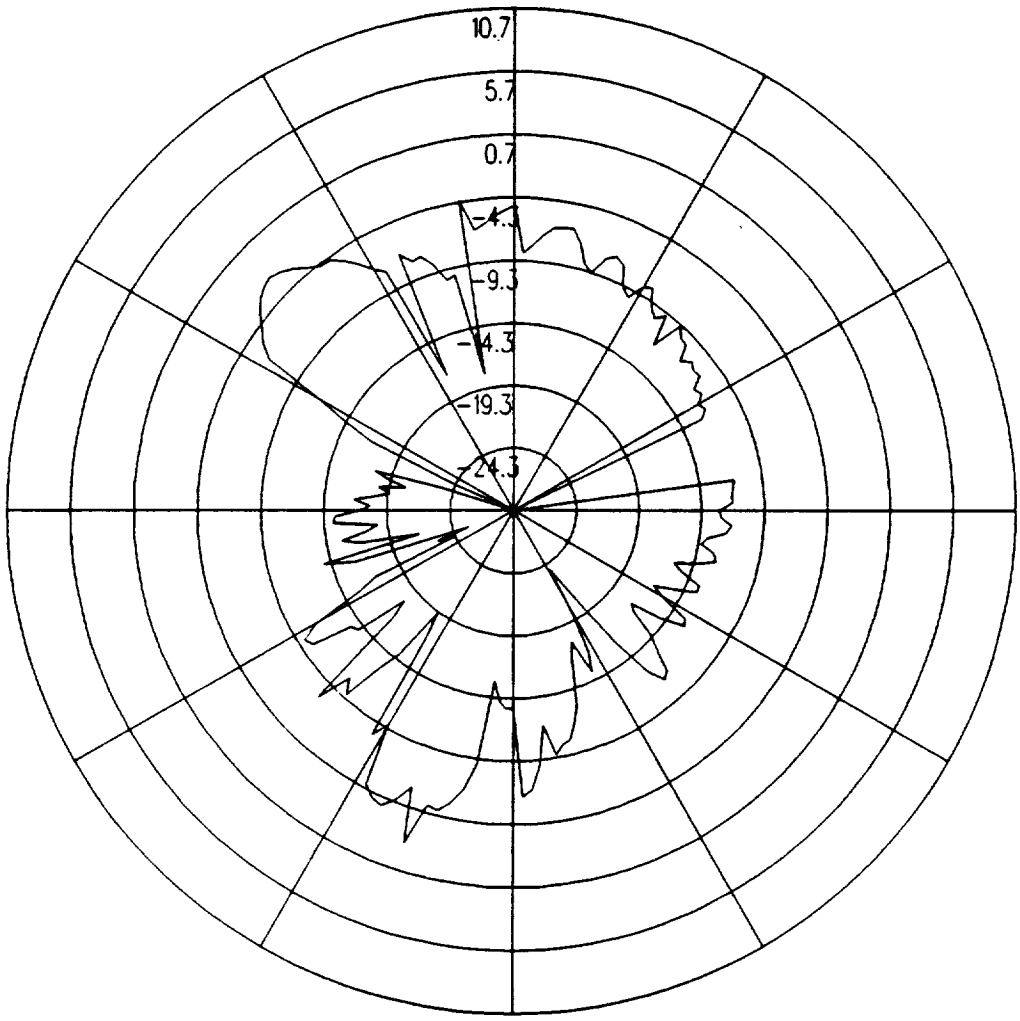

Figure 4.65: UTD calculated conical plane pattern 20° above the horizon for batwing antenna on a P-3C for left hand circular polarization at 300 MHz.(Aircraft Model with Inner Engine)

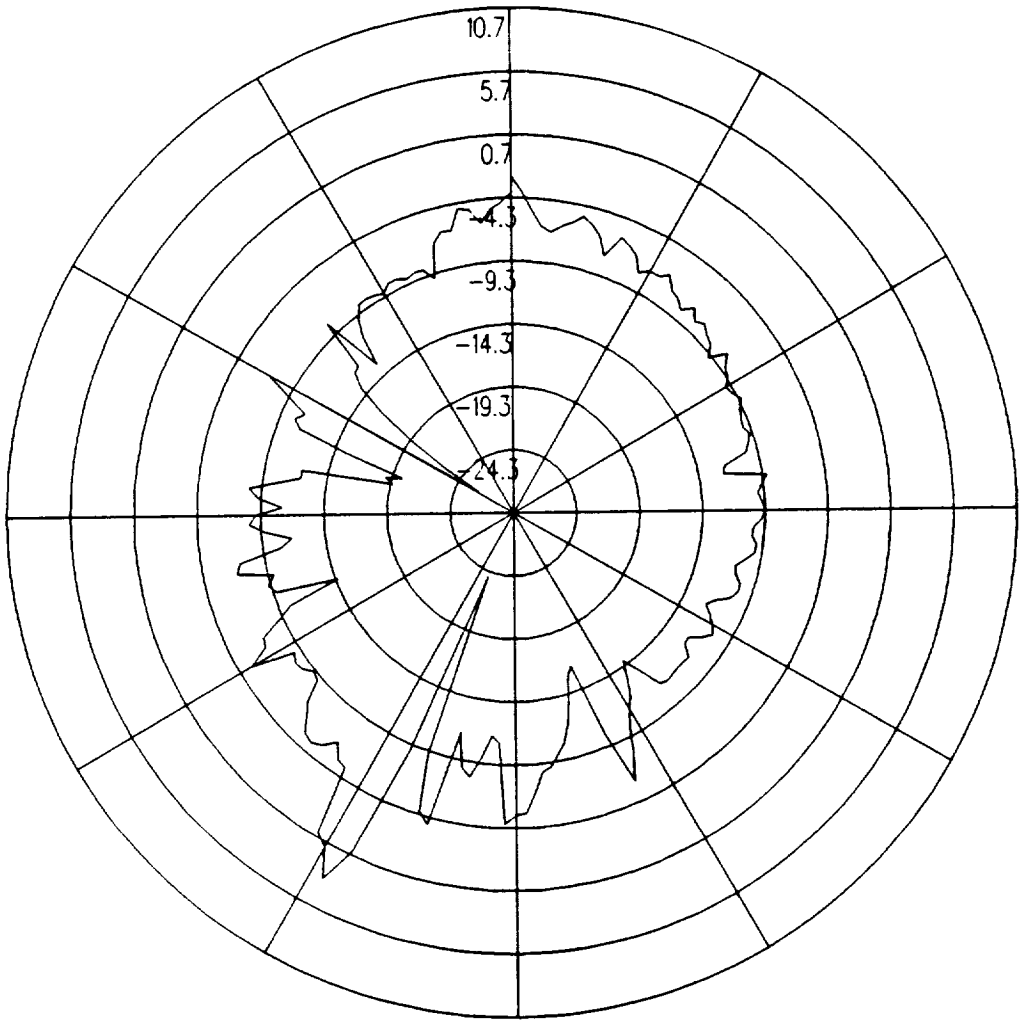

Figure 4.66: UTD calculated conical plane pattern 30° above the horizon for batwing antenna on a P-3C for left hand circular polarization at 300 MHz.(Aircraft Model with Inner Engine)

4.6 Lockheed Location

Another antenna study for the DM 1501341 Batwing antenna on a P-3C aircraft has been provided by Lockheed [9] in which measured results are obtained for the antenna located at an alternative location on the P-3C aircraft. In this section, radiation patterns for the antenna positioned at this alternative location have been calculated and compared to the measured results provided by Lockheed in order to ensure that the aircraft model is also valid for this antenna location. The antenna is located as illustrated in Figure 4.67, which also shows the computer model used to generate the results. The calculated results at 300 MHz are compared with measurements for the roll plane in Figures 4.68 and 4.69, for the azimuth plane in Figures 4.70 and 4.71, for the elevation plane in Figures 4.72 and 4.73, for the conical plane 10° above the horizon in Figures 4.74 and 4.75, for the conical plane 20° above the horizon in Figures 4.76 and 4.77, and for the conical plane 30° above the horizon in Figures 4.78 and 4.79 all for right hand polarization. The cross polarized fields are compared for the roll plane in Figures 4.80 and 4.81, for the azimuth plane in Figures 4.82 and 4.83, for the elevation plane in Figures 4.84 and 4.85, for the conical plane 10° above the horizon in Figures 4.86 and 4.87, for the conical plane 20° above the horizon in Figures 4.88 and 4.89, and for the conical plane 30° above the horizon in Figures 4.90 and 4.91 all for left hand polarization.

Again notice that the roll plane results for right hand polarization compare very well throughout the complete pattern. Comparing the calculated and measured azimuth plane results shows that the pattern levels are in good agreement except for the region near the nose of the aircraft where the calculated levels increase to as much as 5 dB higher than Lockheed's measured levels. This is the same trend which has been seen when comparing the computed results with the Boeing results in Section 4.2. Comparing the elevation plane results shows that in the region directly above the aircraft (i.e., over 15° above the horizon) and near the tail of aircraft the radiation patterns agree very well. However, near the nose of the aircraft the calculated pattern level is approximately 3–5 dB higher than Lockheed's measured level. Again this is the same trend which has been seen in the Boeing results. Comparing the conical pattern planes, however, shows that as the pattern cut is taken above the horizon there is very good agreement between the calculated and measured patterns.

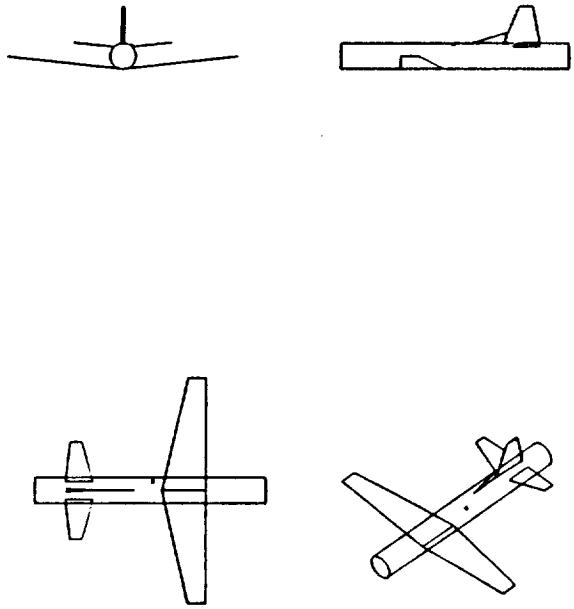

Figure 4.67: Geometry of the cylindrical model of the P-3C aircraft used in the NEC-BSC code showing the location of the antenna.

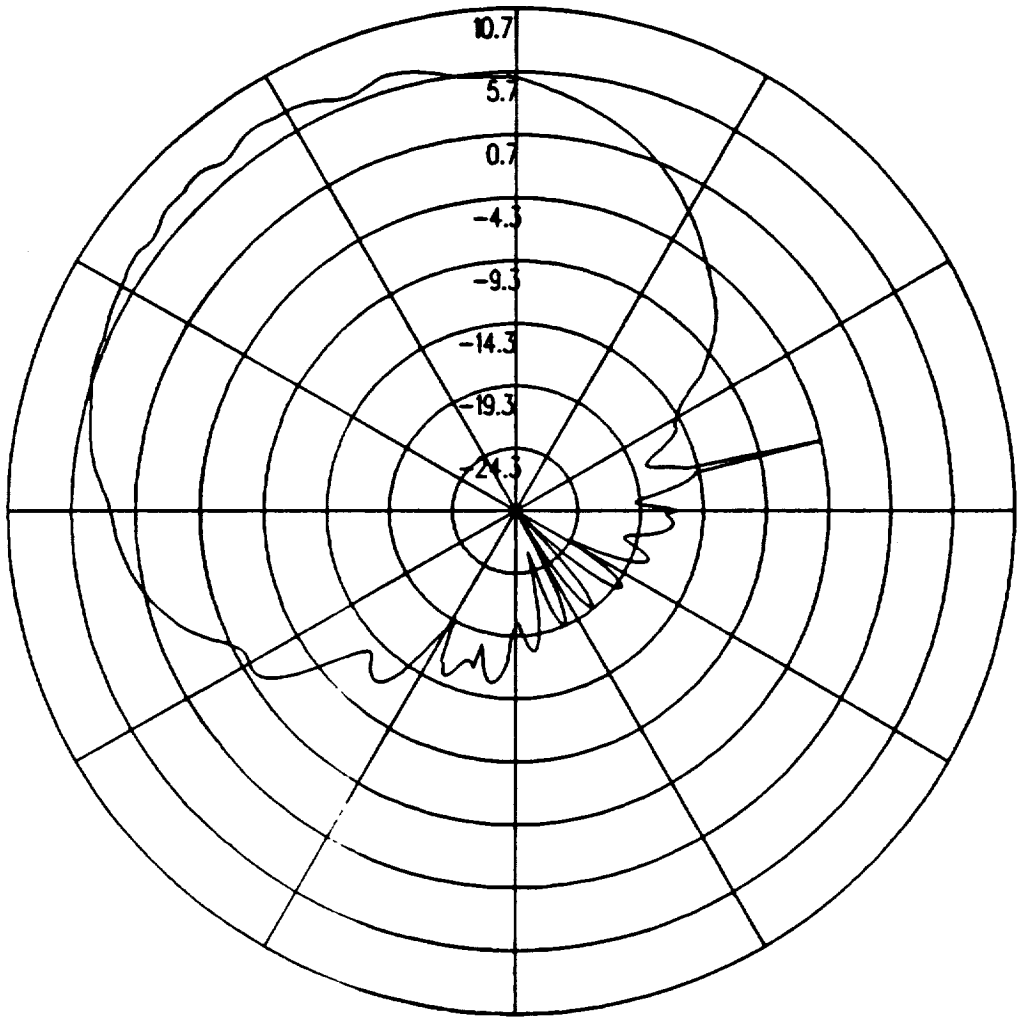

Figure 4.68: UTD calculated roll plane pattern for batwing antenna on a P-3C for right hand circular polarization at 300 MHz. (Lockheed Antenna Location)

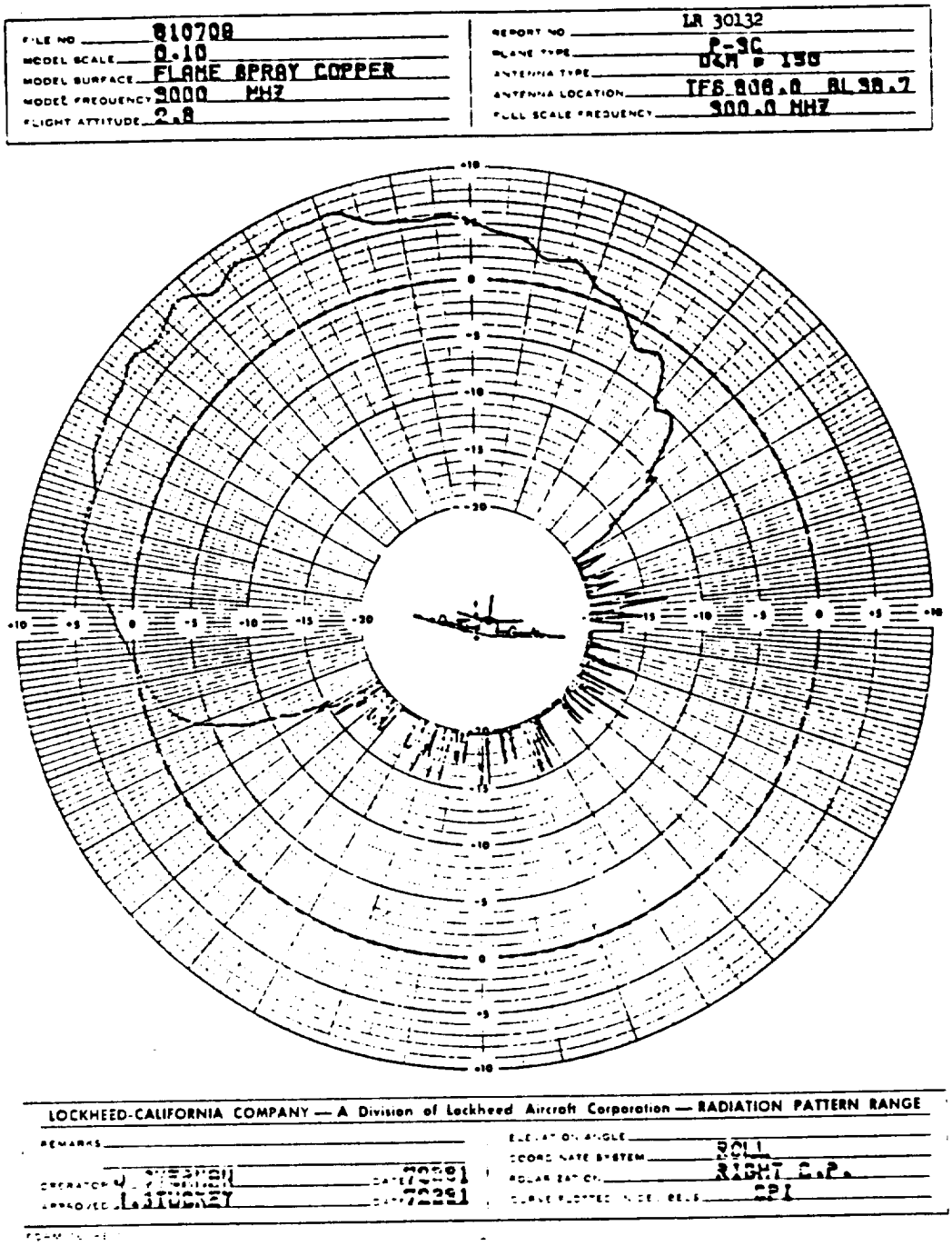

Figure 4.69: Lockheed's measured roll plane pattern for batwing antenna on a P-3C for right hand circular polarization at 300 MHz.

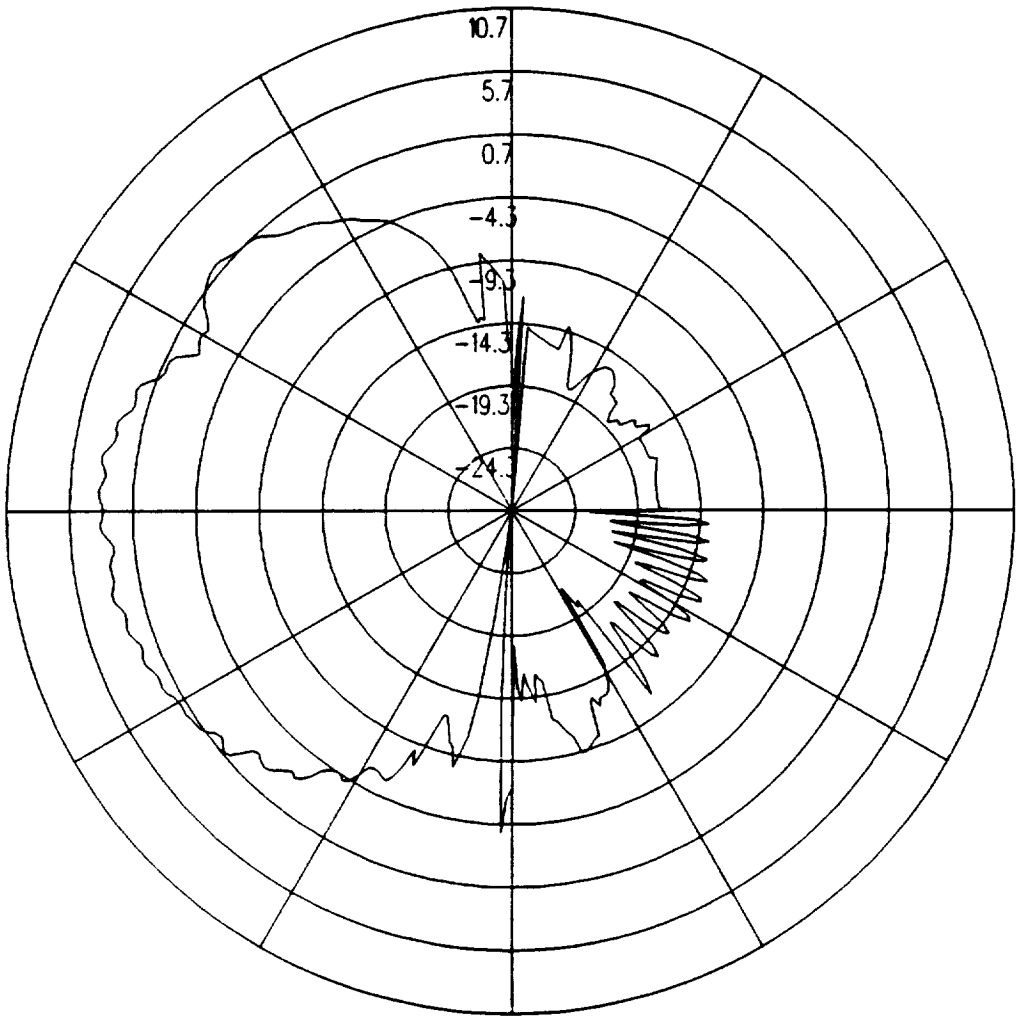

Figure 4.70: UTD calculated azimuth plane pattern for batwing antenna on a P-3C for right hand circular polarization at 300 MHz. (Lockheed Antenna Location)

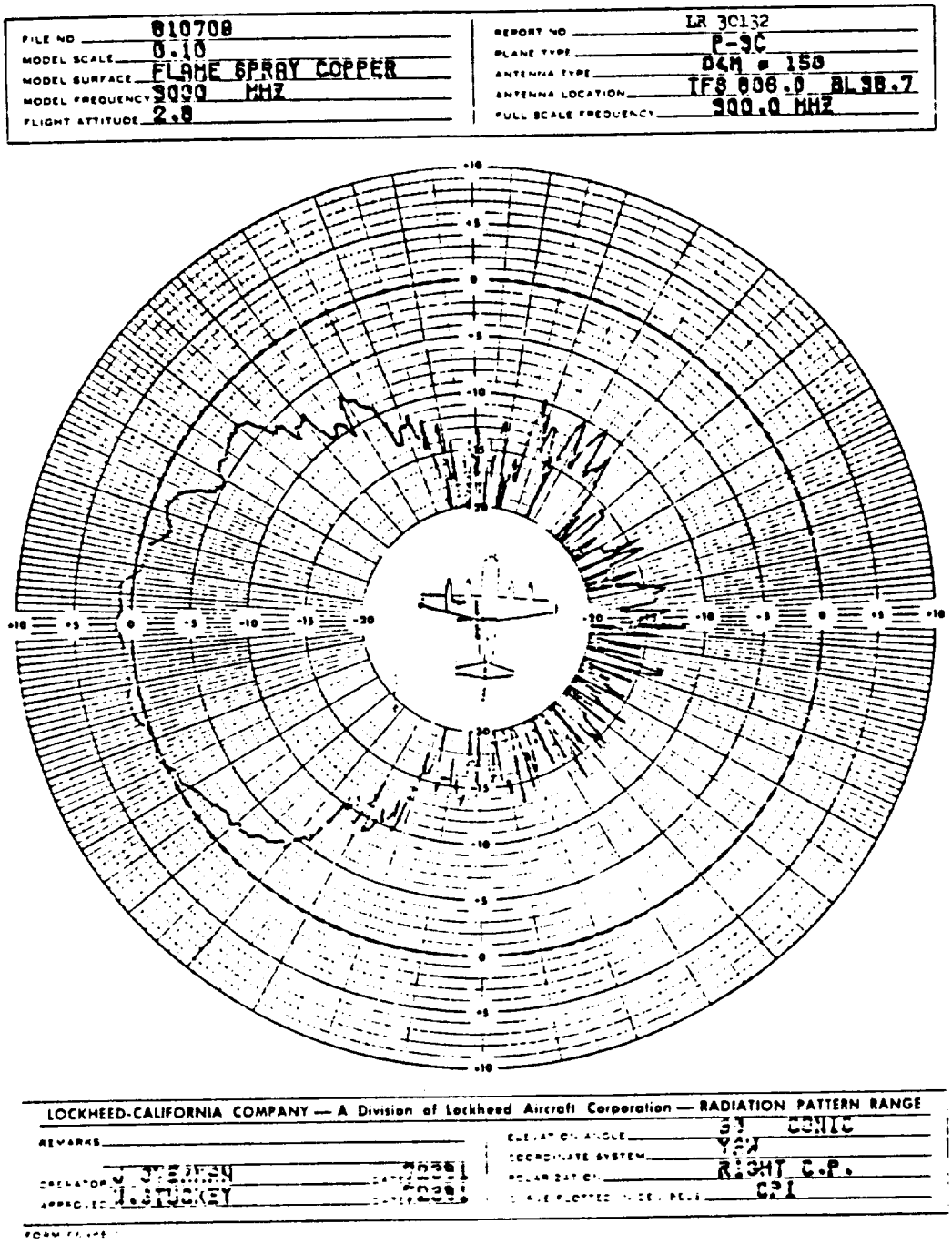

Figure 4.71: Lockheed's measured azimuth plane pattern for batwing antenna on a P-3C for right hand circular polarization at 300 MHz.

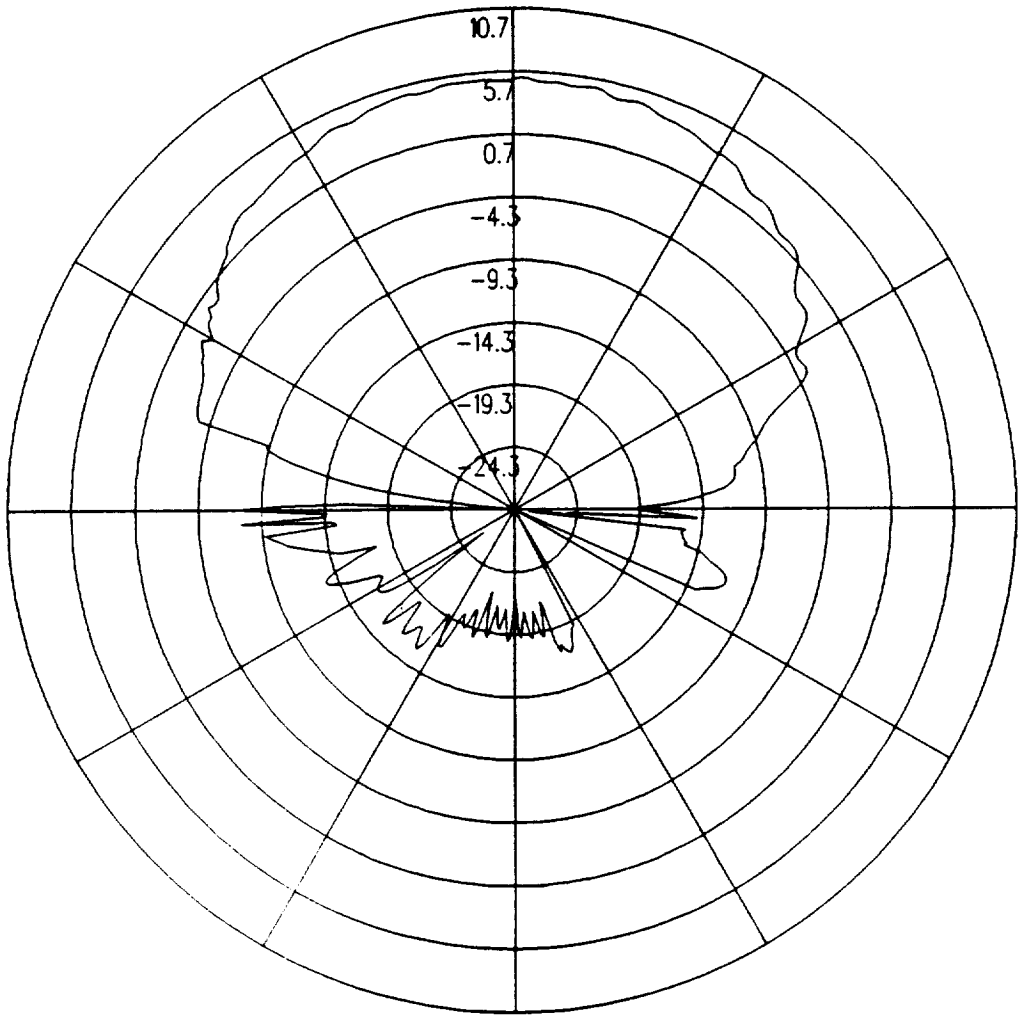

Figure 4.72: UTD calculated elevation plane pattern for batwing antenna on a P-3C for right hand circular polarization at 300 MHz. (Note that the nose is to the right and the tail to the left in this pattern.) (Lockheed Antenna Location)

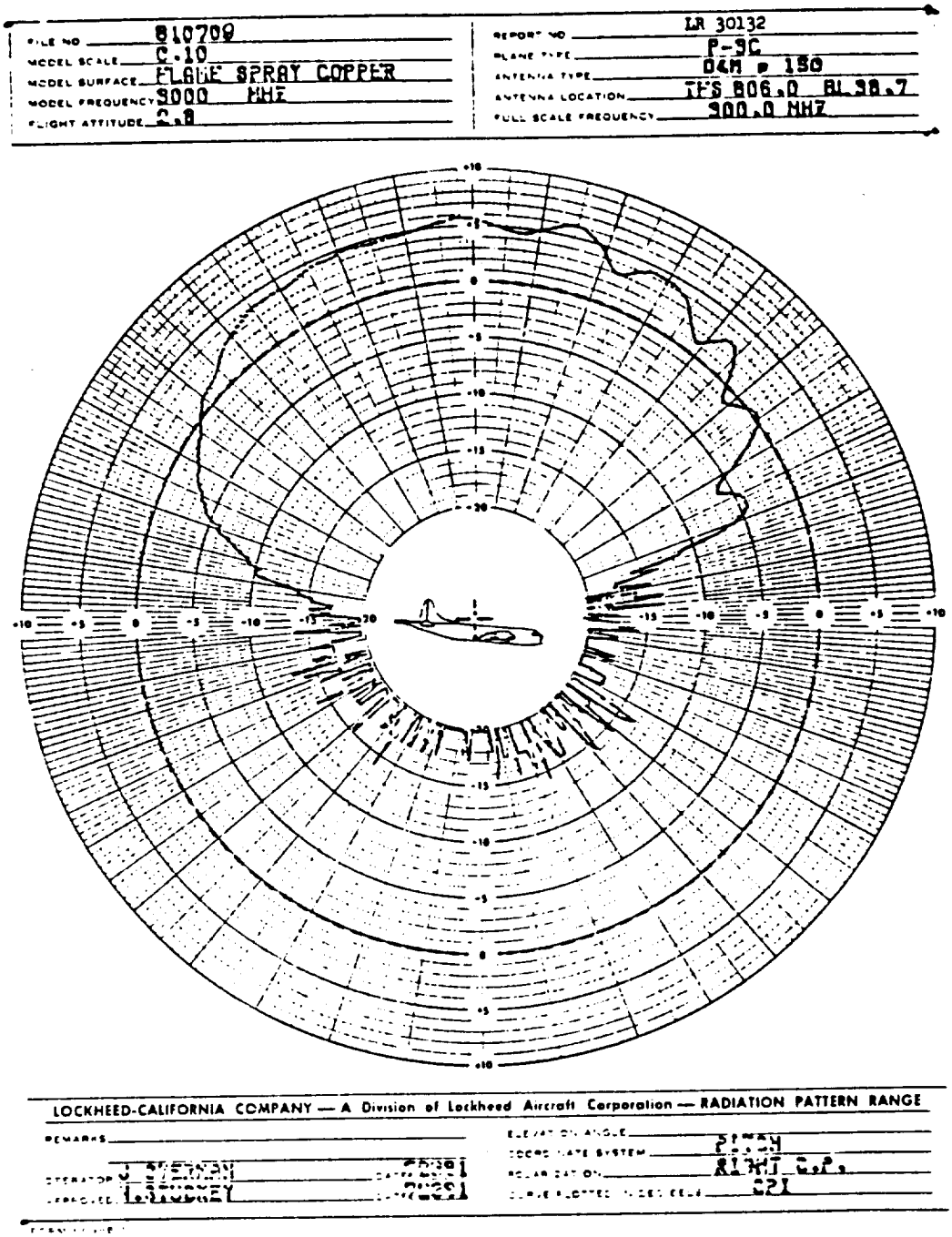

Figure 4.73: Lockheed's measured elevation plane pattern for batwing antenna on a P-3C for right hand circular polarization at 300 MHz.(Note that the nose is to the right and the tail to the left in this pattern.)

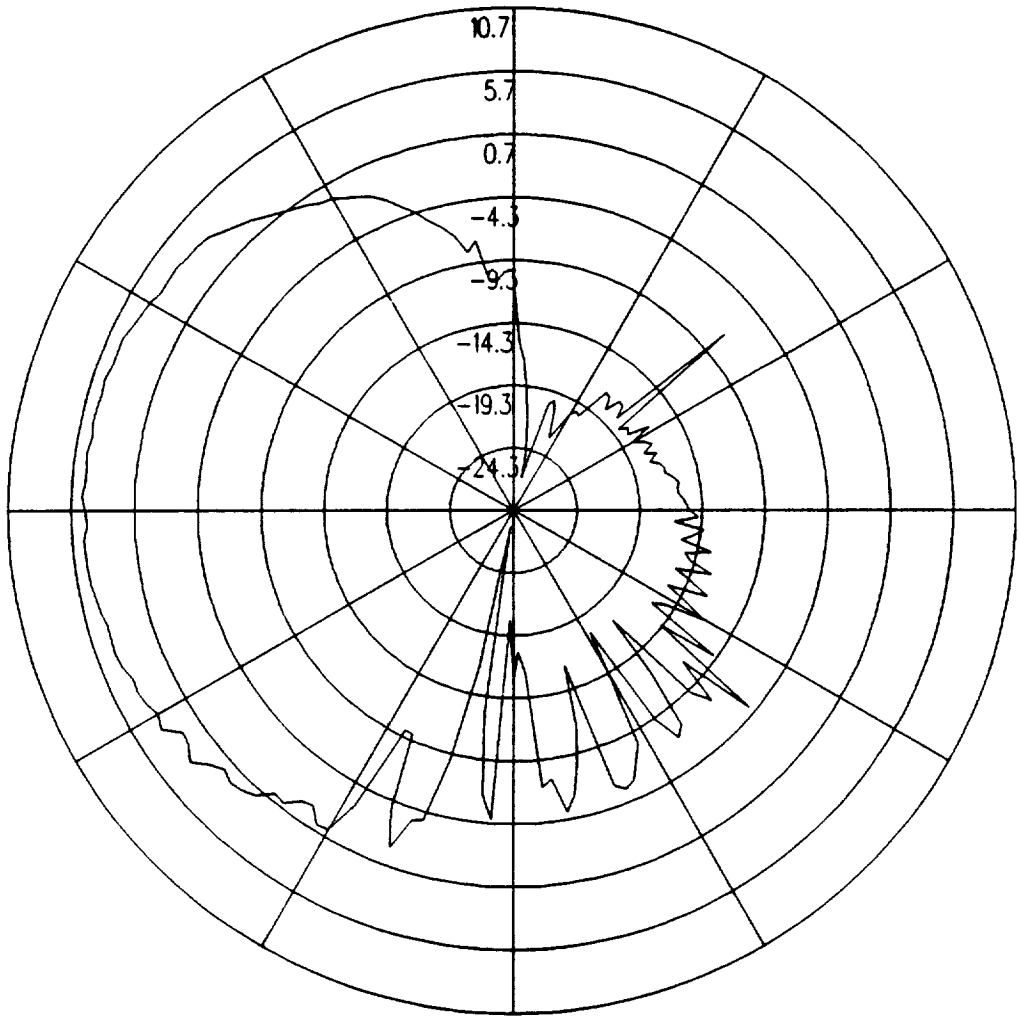

Figure 4.74: UTD calculated conical plane pattern 10° above the horizon for batwing antenna on a P-3C for right hand circular polarization at 300 MHz.(Lockheed Antenna Location)

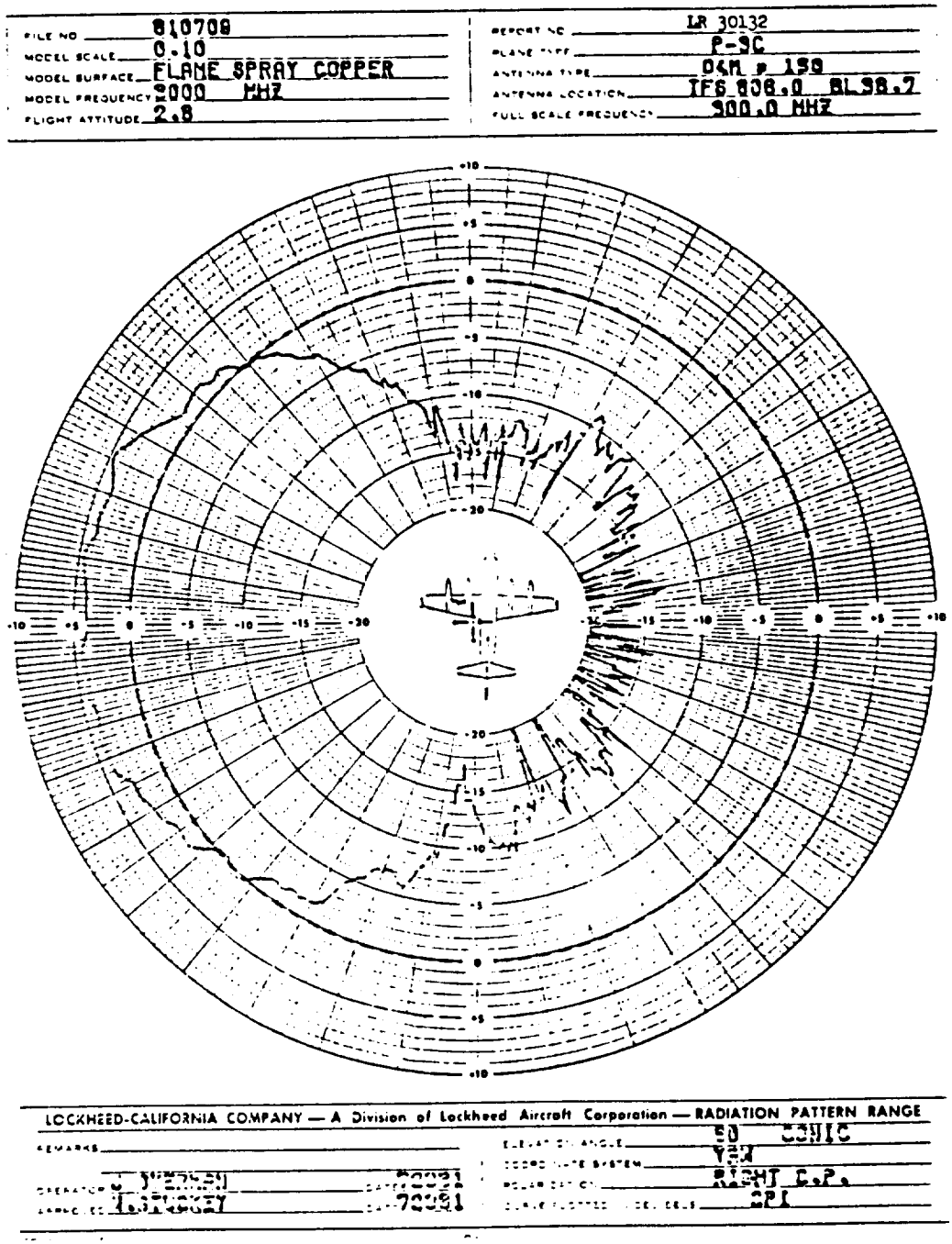

Figure 4.75: Lockheed's measured conical plane pattern 10° above the horizon for batwing antenna on a P-3C for right hand circular polarization at 300 MHz.

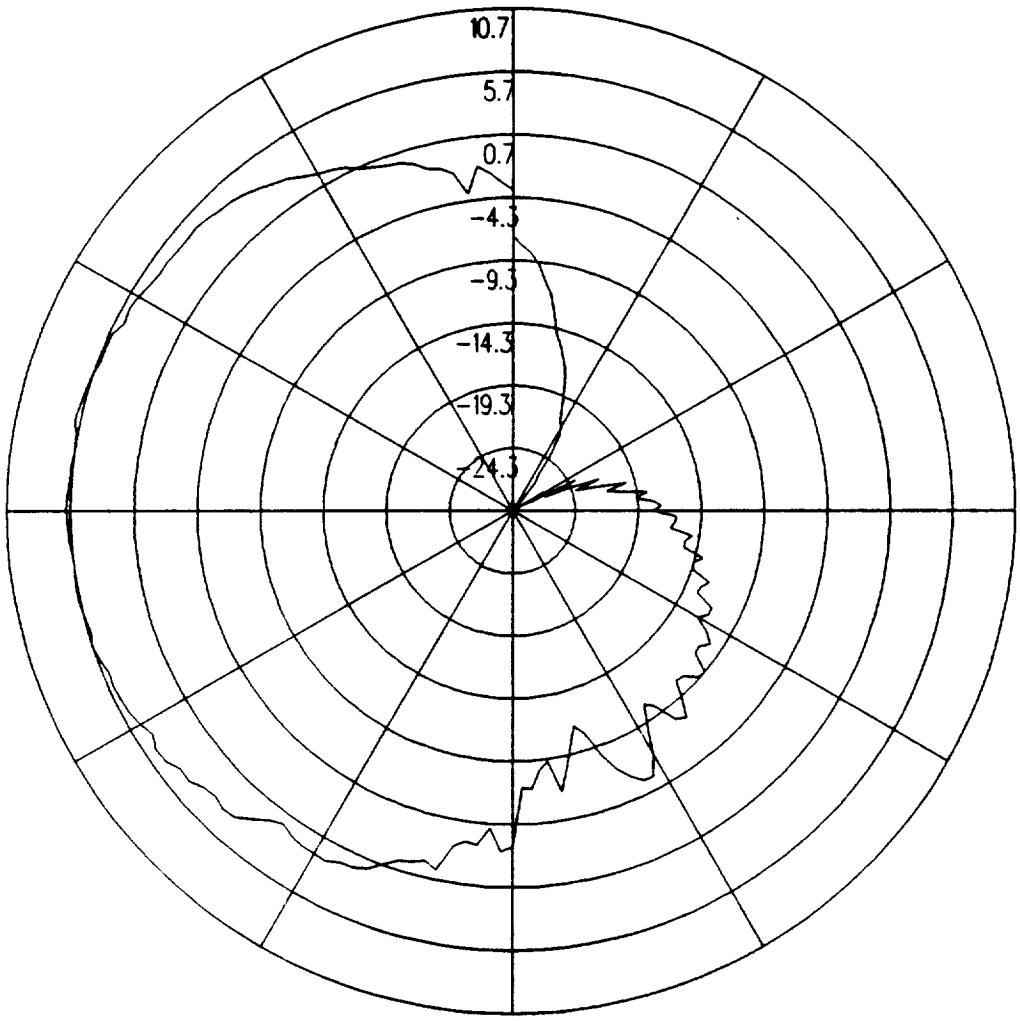

Figure 4.76: UTD calculated conical plane pattern 20° above the horizon for batwing antenna on a P-3C for right hand circular polarization at 300 MHz.(Lockheed Antenna Location)

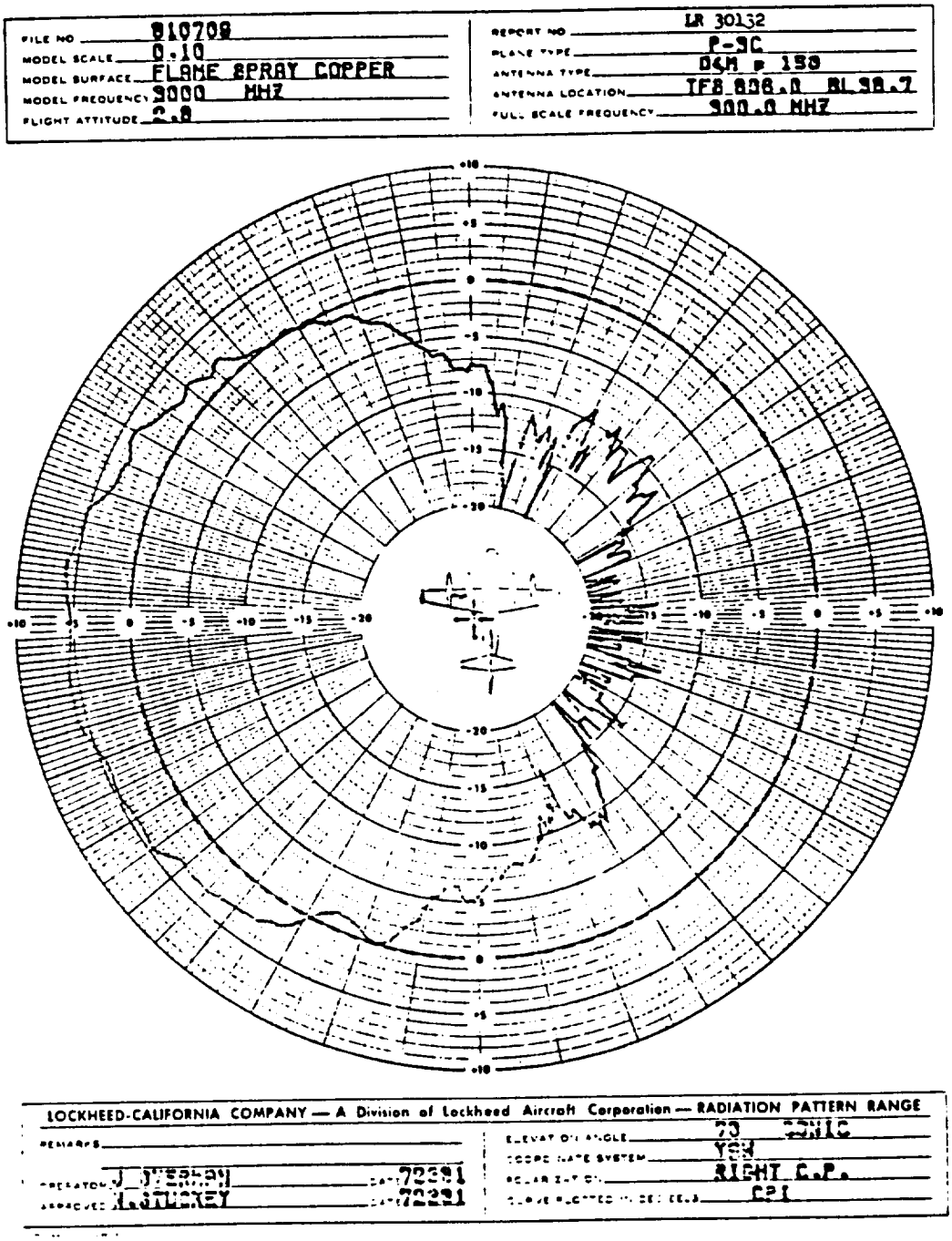

Figure 4.77: Lockheed's measured conical plane pattern 20° above the horizon for batwing antenna on a P-3C for right hand circular polarization at 300 MHz.

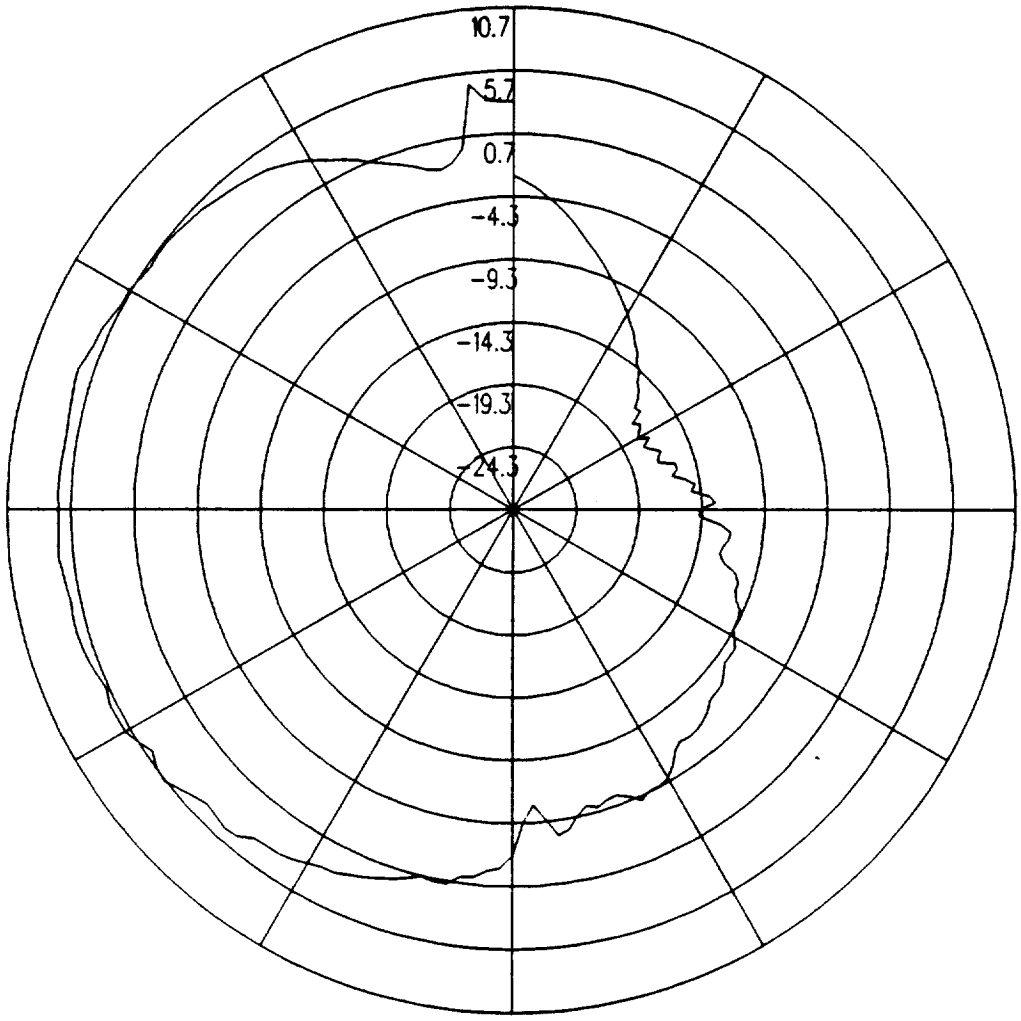

Figure 4.78: UTD calculated conical plane pattern 30° above the horizon for batwing antenna on a P-3C for right hand circular polarization at 300 MHz.(Lockheed Antenna Location)

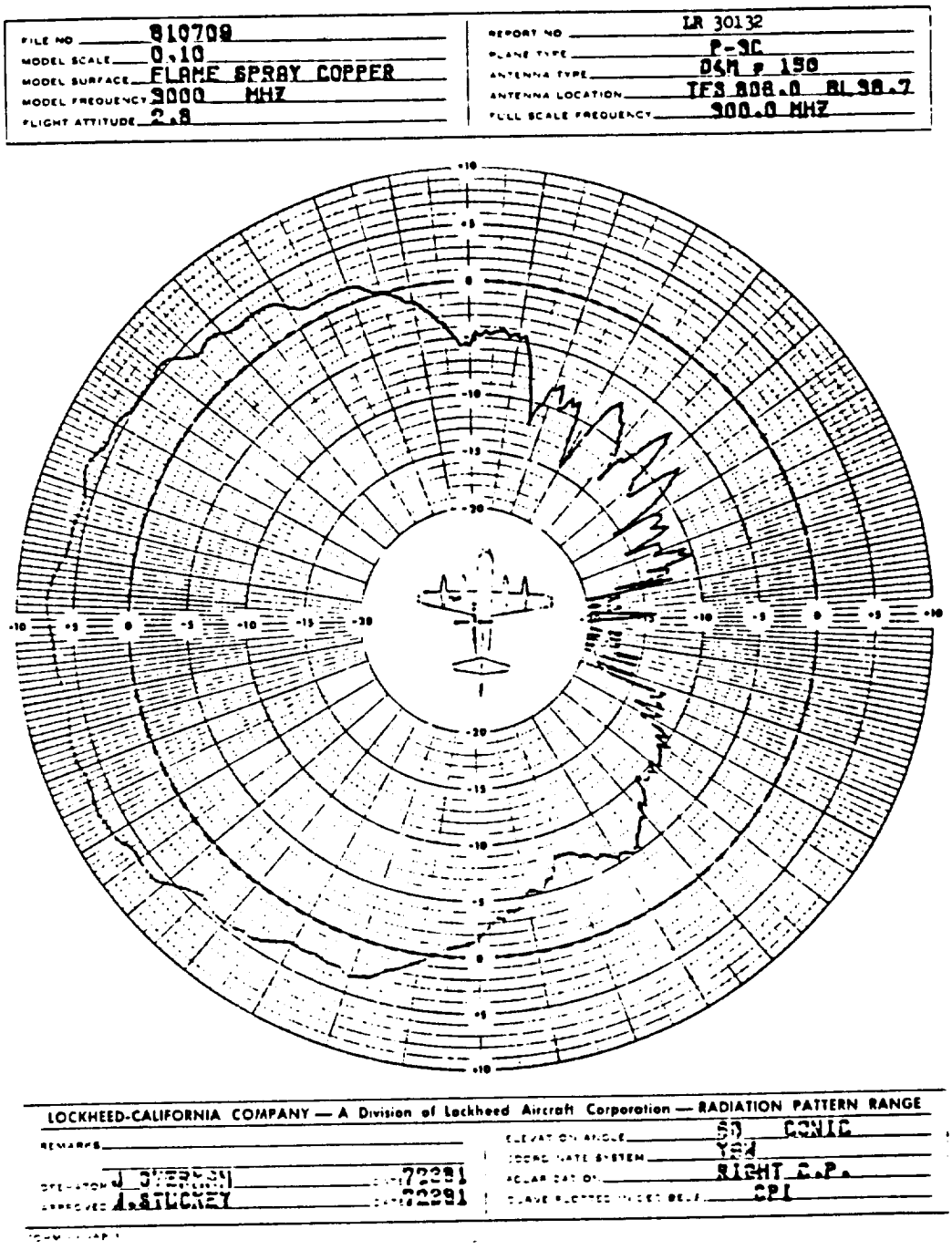

Figure 4.79: Lockheed's measured conical plane pattern 30° above the horizon for batwing antenna on a P-3C for right hand circular polarization at 300 MHz.

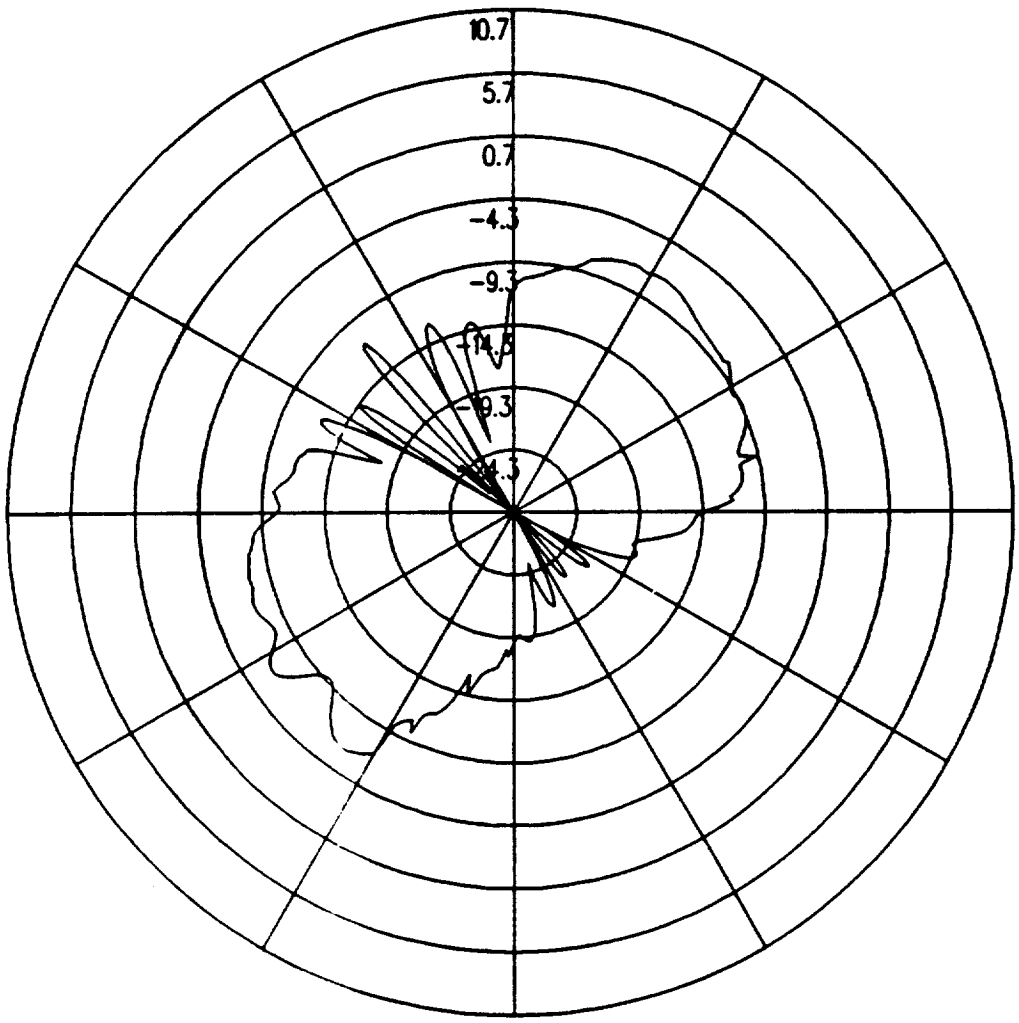

Figure 4.80: UTD calculated roll plane pattern for batwing antenna on a P-3C for left hand circular polarization at 300 MHz. (Lockheed Antenna Location)

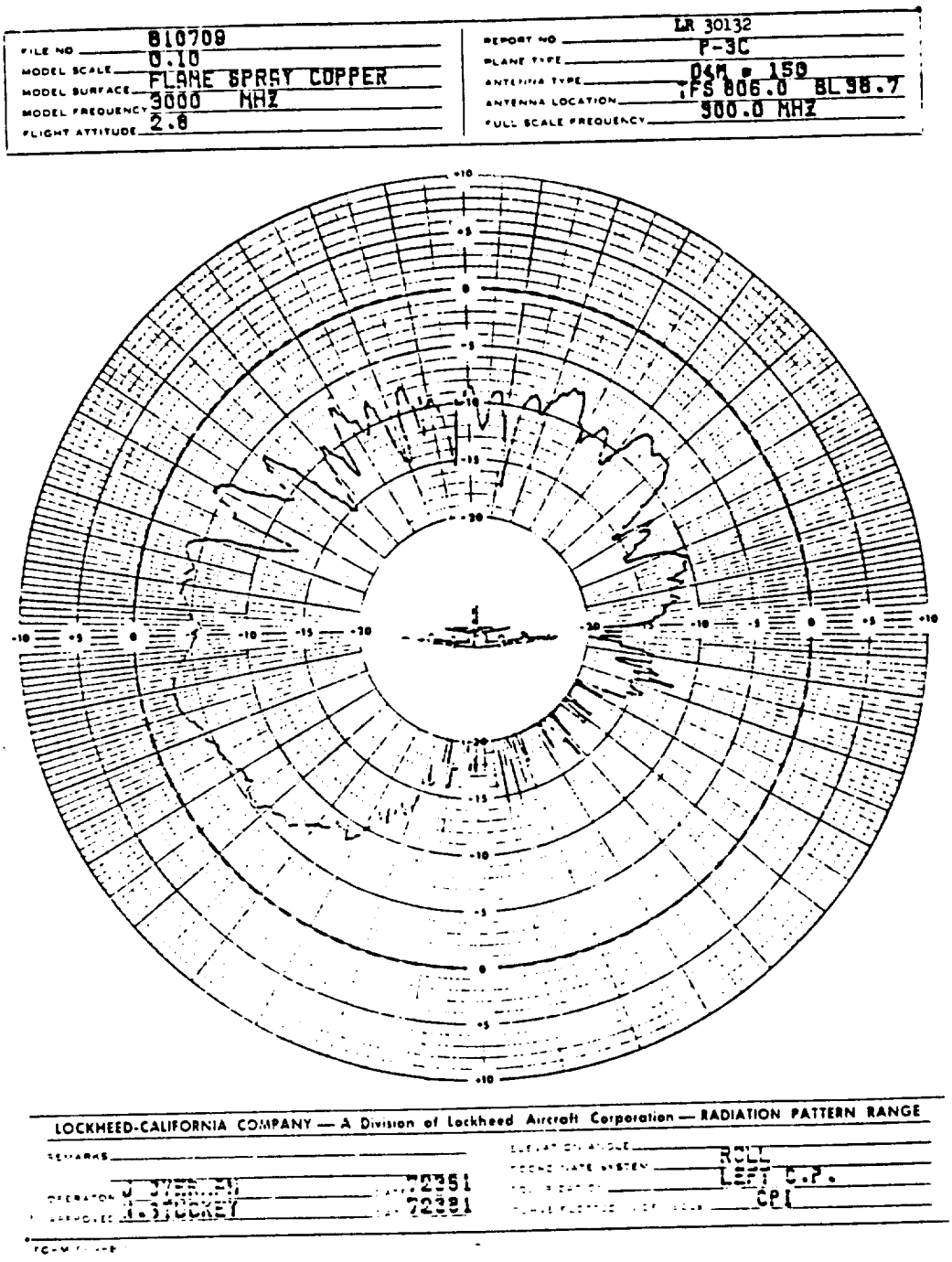

Figure 4.81: Lockheed's measured roll plane pattern for batwing antenna on a P-3C for left hand circular polarization at 300 MHz.

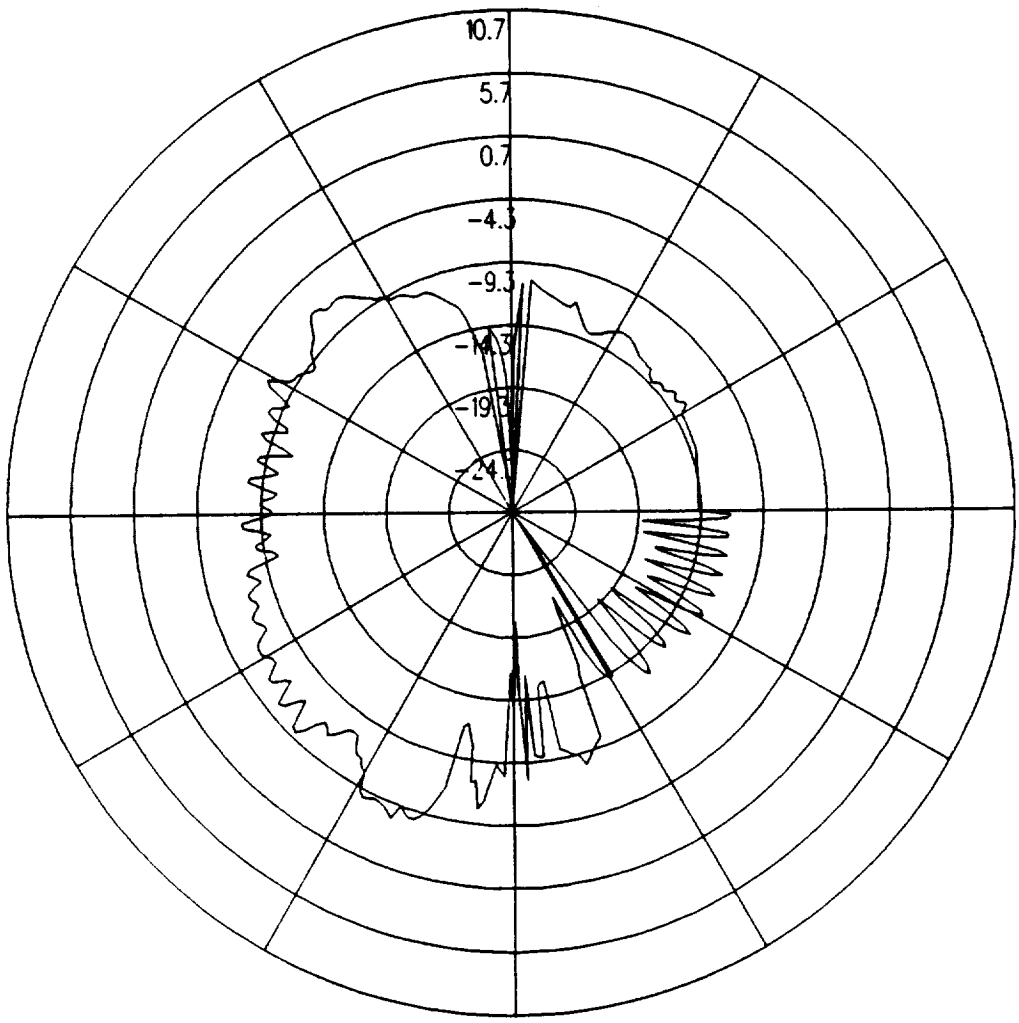

Figure 4.82: UTD calculated azimuth plane pattern for batwing antenna on a P-3C for left hand circular polarization at 300 MHz. (Lockheed Antenna Location)

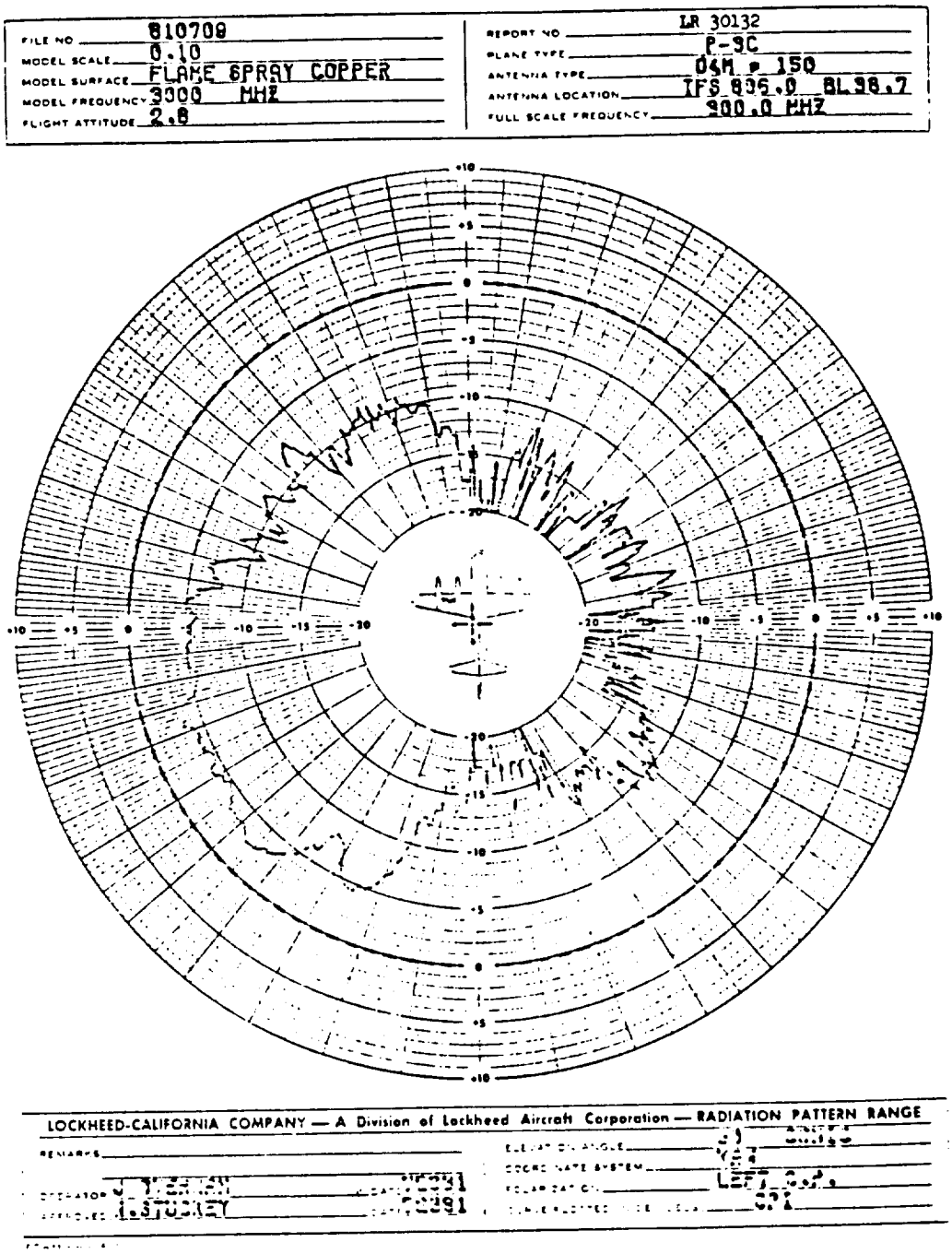

Figure 4.83: Lockheed's measured azimuth plane pattern for batwing antenna on a P-3C for left hand circular polarization at 300 MHz.

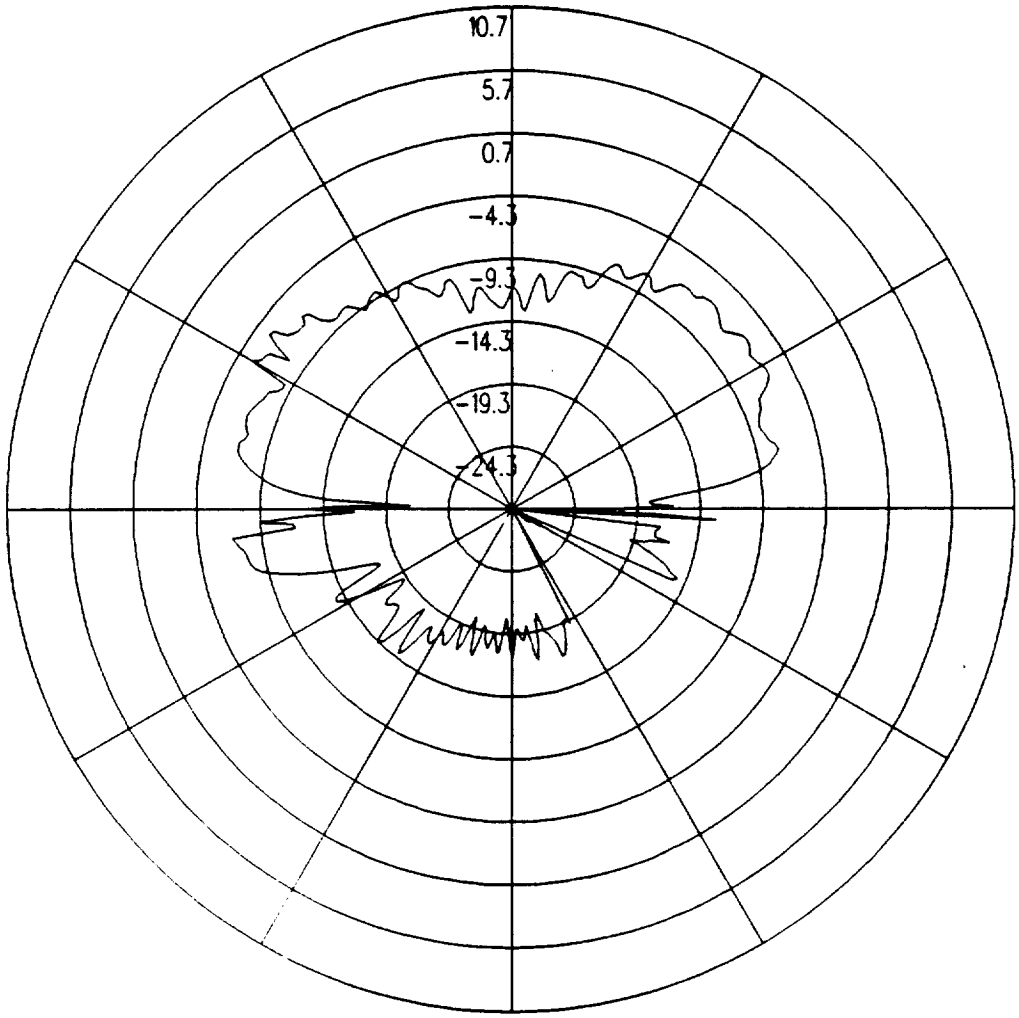

Figure 4.84: UTD calculated elevation plane pattern for batwing antenna on a P-3C for left hand circular polarization at 300 MHz. (Note that the nose is to the right and the tail to the left in this pattern.) (Lockheed Antenna Location)

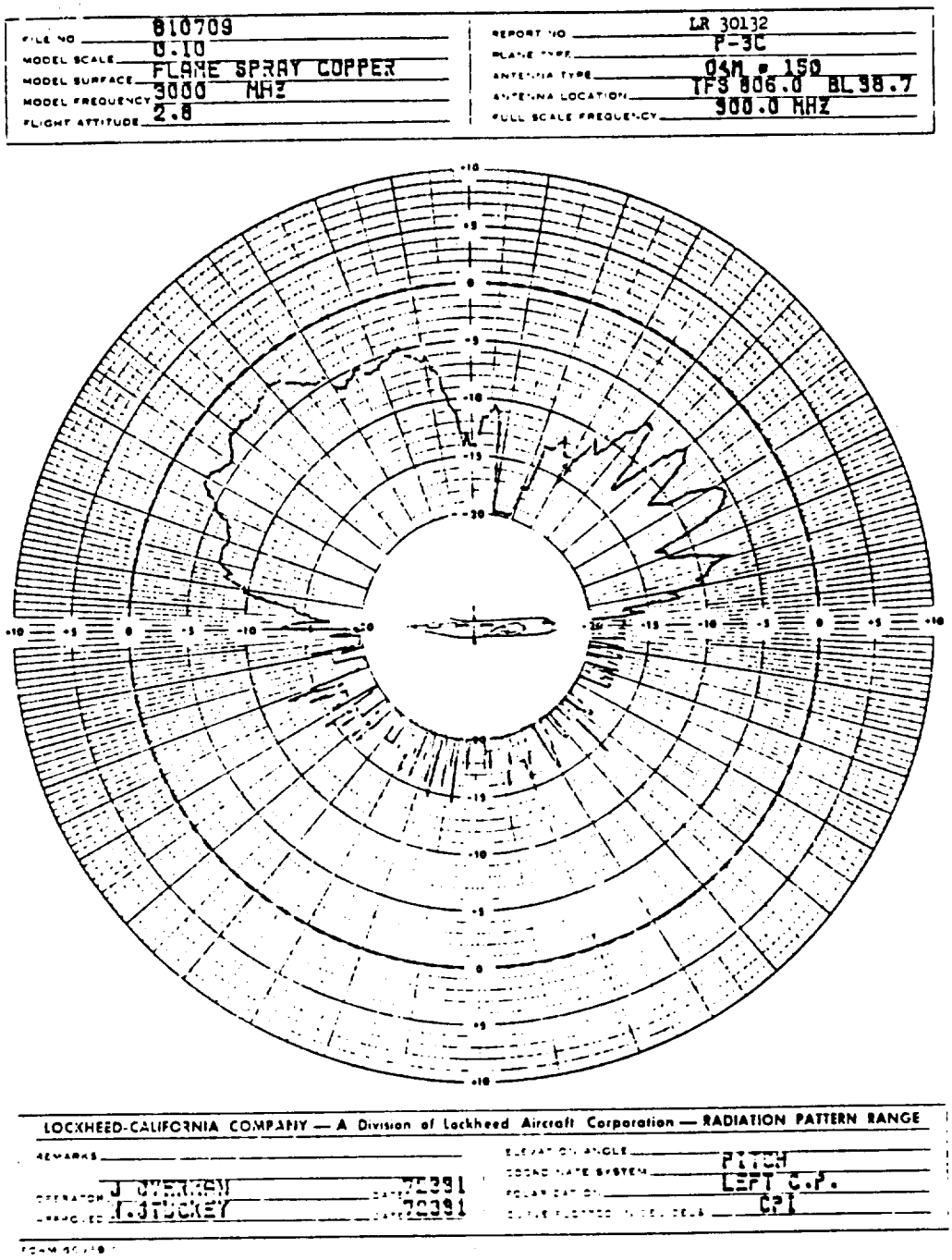

Figure 4.85: Lockheed's measured elevation plane pattern for batwing antenna on a P-3C for left hand circular polarization at 300 MHz. (Note that the nose is to the right and the tail to the left in this pattern.)

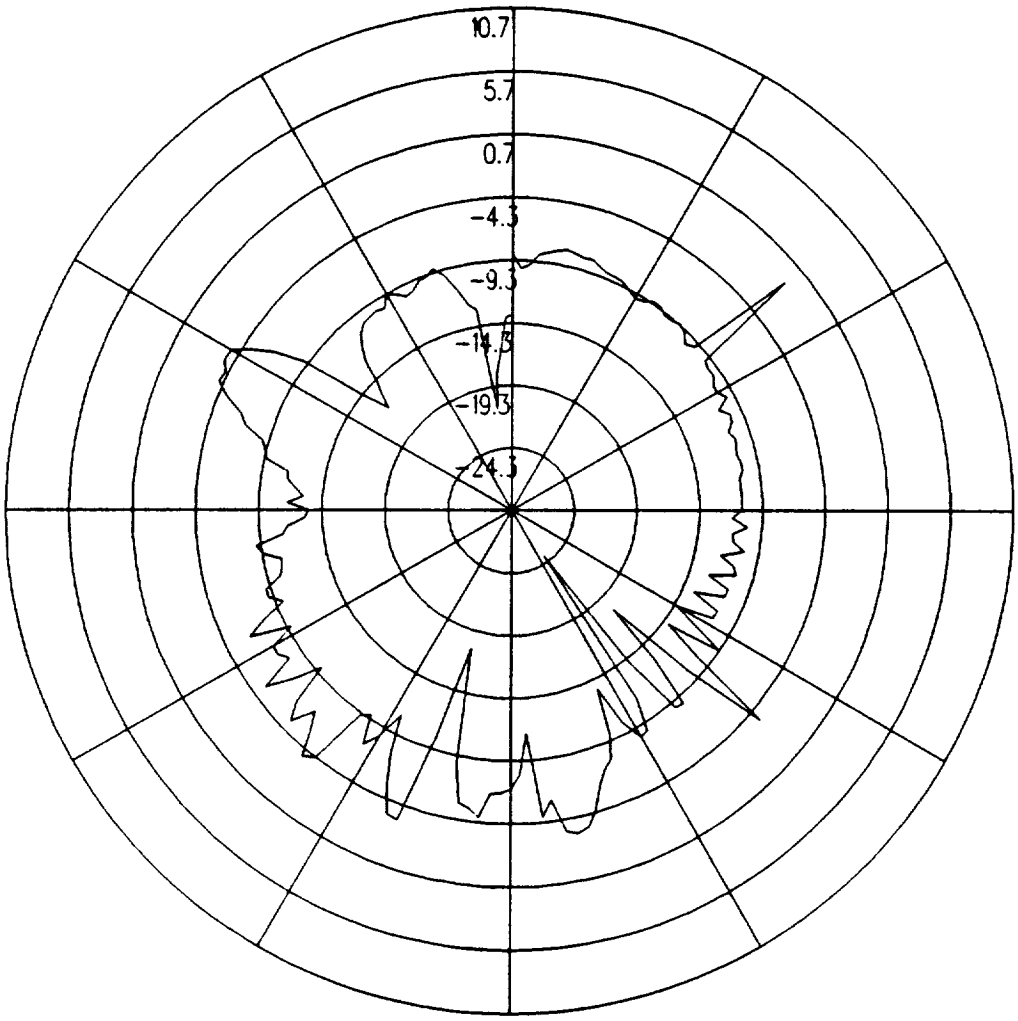

Figure 4.86: UTD calculated conical plane pattern 10° above the horizon for batwing antenna on a P-3C for left hand circular polarization at 300 MHz.(Lockheed Antenna Location)

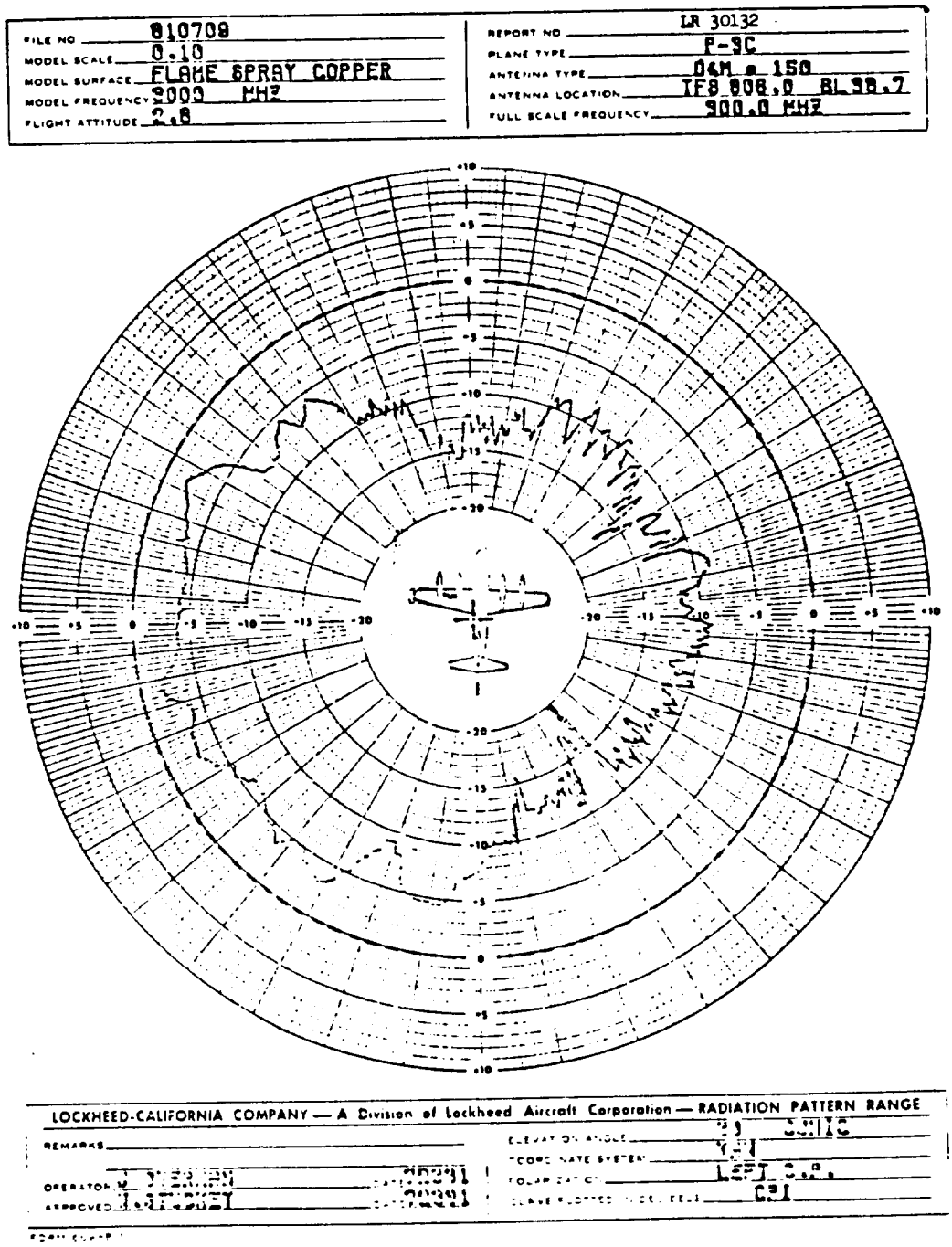

Figure 4.87: Lockheed's measured conical plane pattern 10° above the horizon for batwing antenna on a P-3C for left hand circular polarization at 300 MHz.

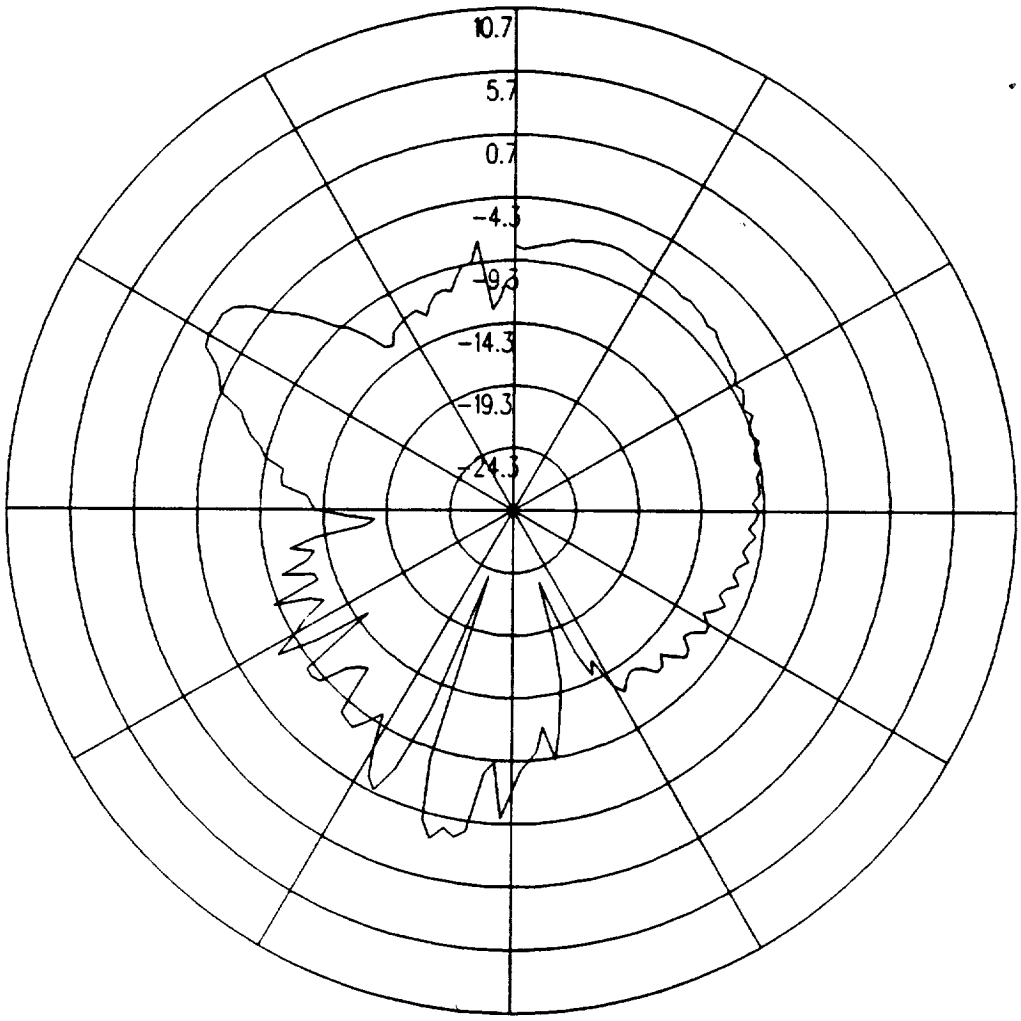

Figure 4.88: UTD calculated conical plane pattern 20° above the horizon for batwing antenna on a P-3C for left hand circular polarization at 300 MHz.(Lockheed Antenna Location)

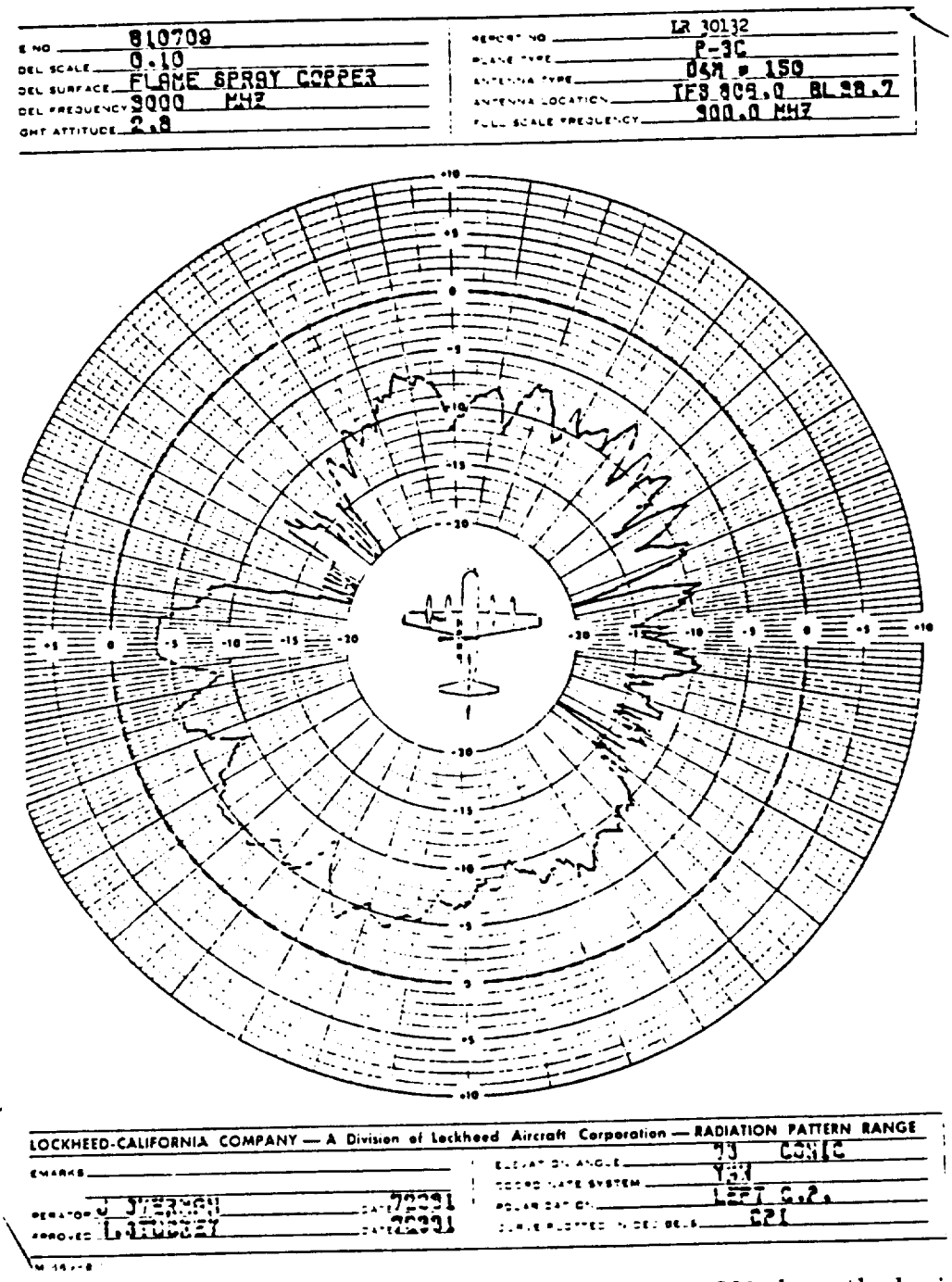

Figure 4.89: Lockheed's measured conical plane pattern 20° above the horizon for batwing antenna on a P-3C for left hand circular polarization at 300 MHz.

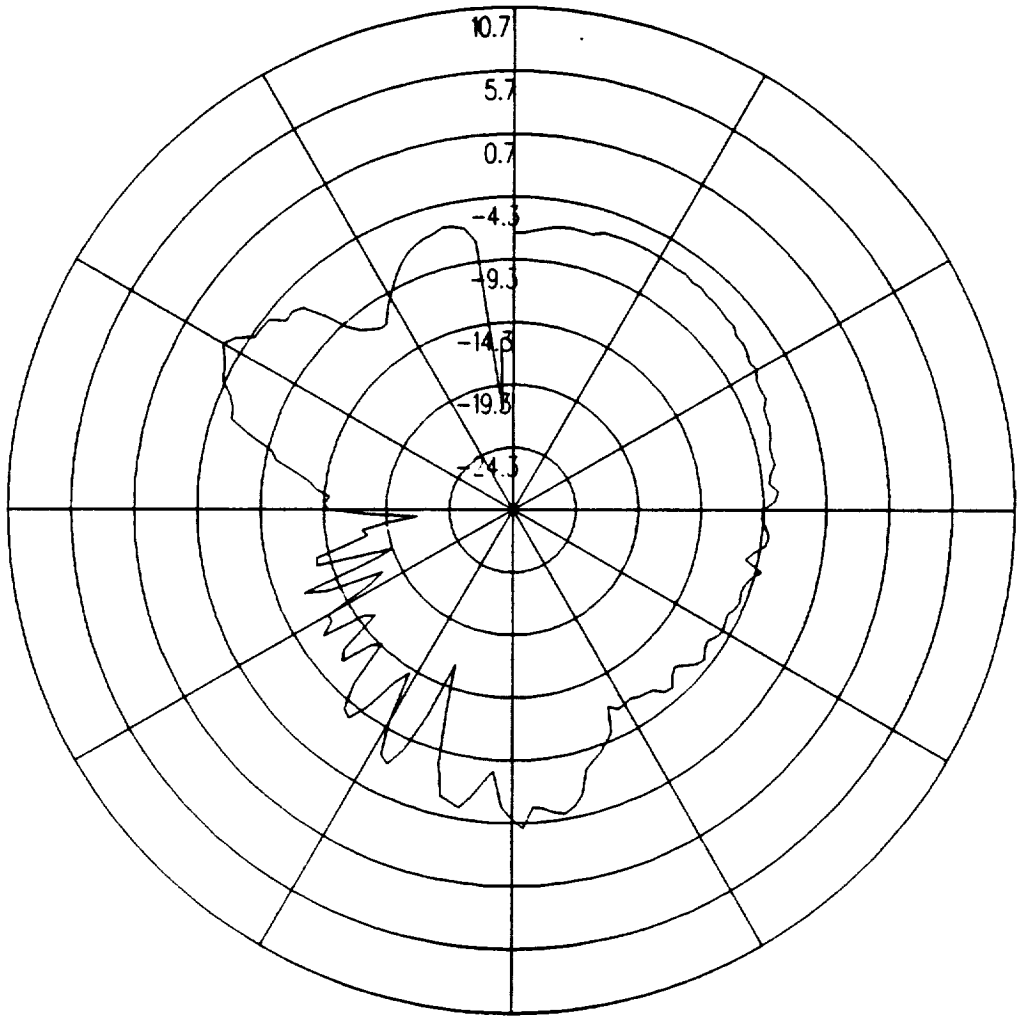

Figure 4.90: UTD calculated conical plane pattern 30° above the horizon for batwing antenna on a P-3C for left hand circular polarization at 300 MHz.(Lockheed Antenna Location)

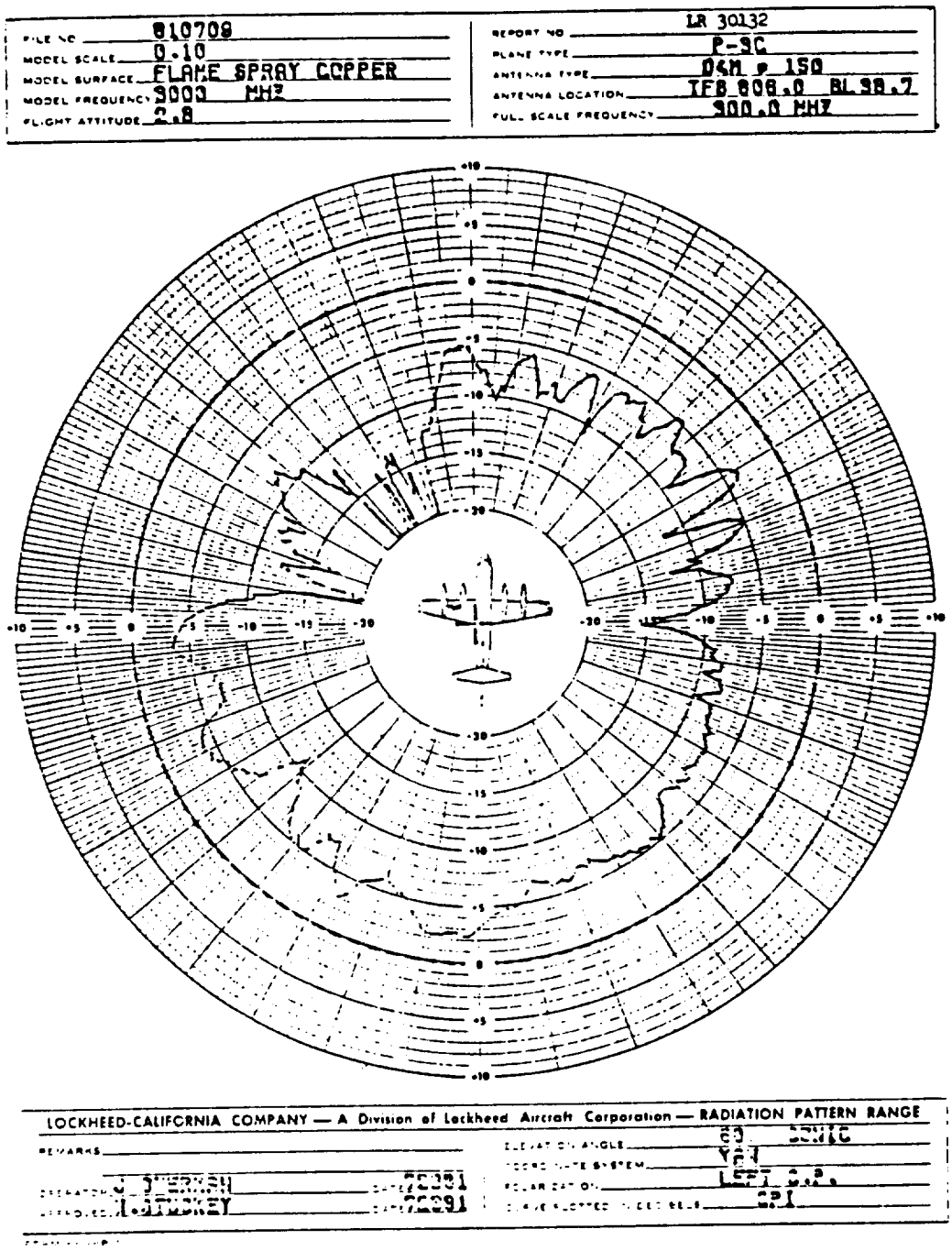

Figure 4.91: Lockheed's measured conical plane pattern 30° above the horizon for batwing antenna on a P-3C for left hand circular polarization at 300 MHz.

4.7 Alternative Boeing Location

In the Boeing report [8], an alternate location for the DM 1501341 Batwing antenna is evaluated but not used in the final configuration. In this section, radiation patterns for the antenna positioned at this alternative location have been calculated. These results can be compared to the measured results provided by Boeing in order to ensure that the aircraft model is also valid for this antenna location. The antenna is located as illustrated in Figure 4.92, which also shows the computer model used to generate the results. The calculated results at 300 MHz are compared with measurements for the roll plane in Figures 4.93 and 4.94, for the azimuth plane in Figures 4.95 and 4.96, for the elevation plane in Figures 4.97 and 4.98, for the conical plane 10° above the horizon in Figures 4.99 and 4.100, for the conical plane 20° above the horizon in Figures 4.101 and 4.102, and for the conical plane 30° above the horizon in Figures 4.103 and 4.104 all for right hand polarization. The cross polarized fields are compared for the roll plane in Figures 4.105 and 4.106, for the azimuth plane in Figures 4.107 and 4.108, for the elevation plane in Figures 4.109 and 4.110, for the conical plane 10° above the horizon in Figures 4.111 and 4.112, for the conical plane 20° above the horizon in Figures 4.113 and 4.114, and for the conical plane 30° above the horizon in Figures 4.115 and 4.116 all for left hand polarization.

Notice that for this antenna location, the roll plane results for right hand polarization also compare very well throughout the complete pattern. Comparing the calculated and measured azimuth plane results also shows that there is very good agreement between the calculated and measured results. Comparing the calculated and measured elevation plane results shows that in the main region of the pattern and near the nose of the aircraft there is very good agreement. However, near the tail of the aircraft (i.e., up to 30° above the horizon) the calculated level is approximately 5–8 dB higher than Boeing's measured level. Again this is the same trend which has been seen in the previous results. Comparing the conical pattern planes, however, shows that as the pattern cut is taken above the horizon there is very good agreement between the calculated and measured patterns.

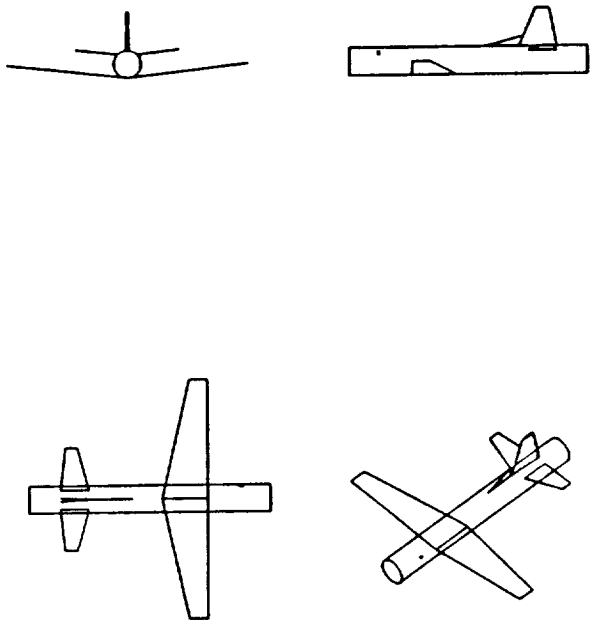

Figure 4.92: Geometry of the cylindrical model of the P-3C aircraft used in the NEC-BSC code showing the location of the antenna.

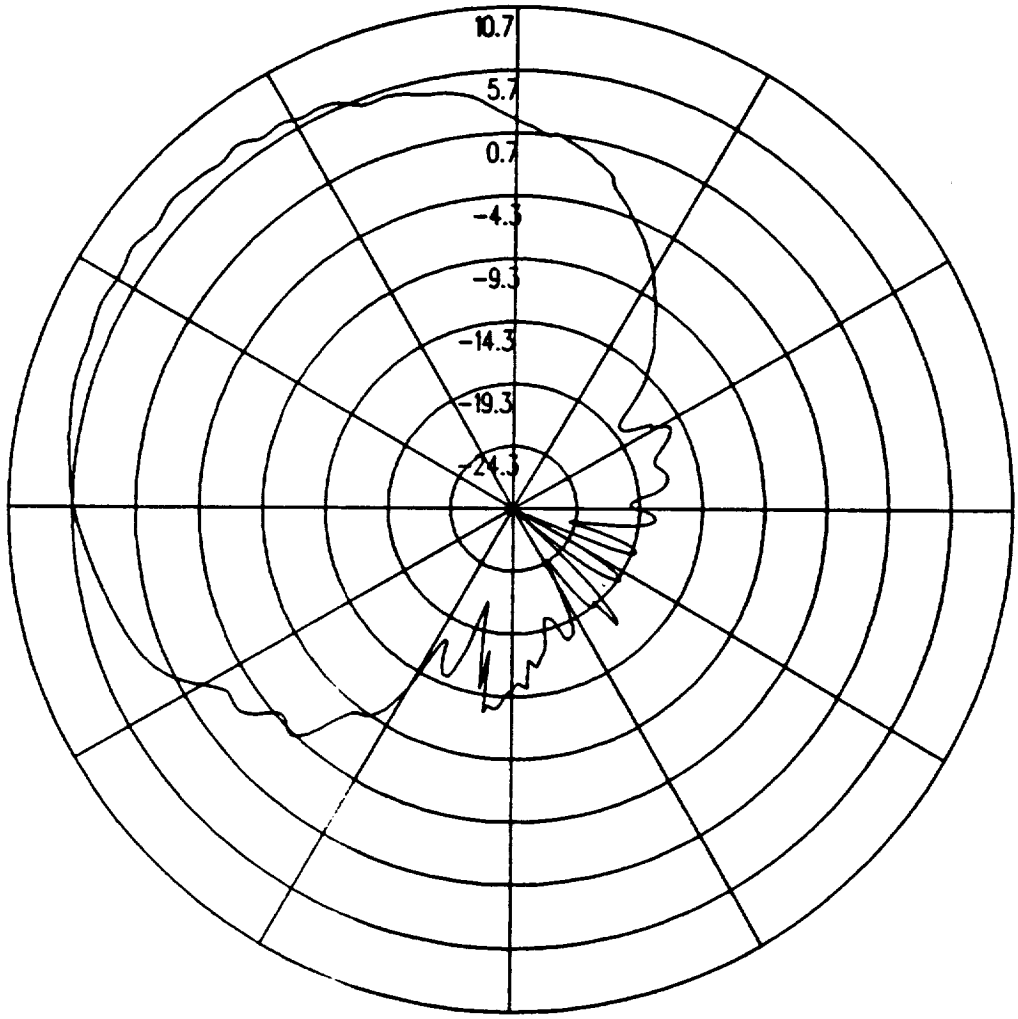

Figure 4.93: UTD calculated roll plane pattern for batwing antenna on a P-3C for right hand circular polarization at 300 MHz. (Alternative Boeing Antenna Location)

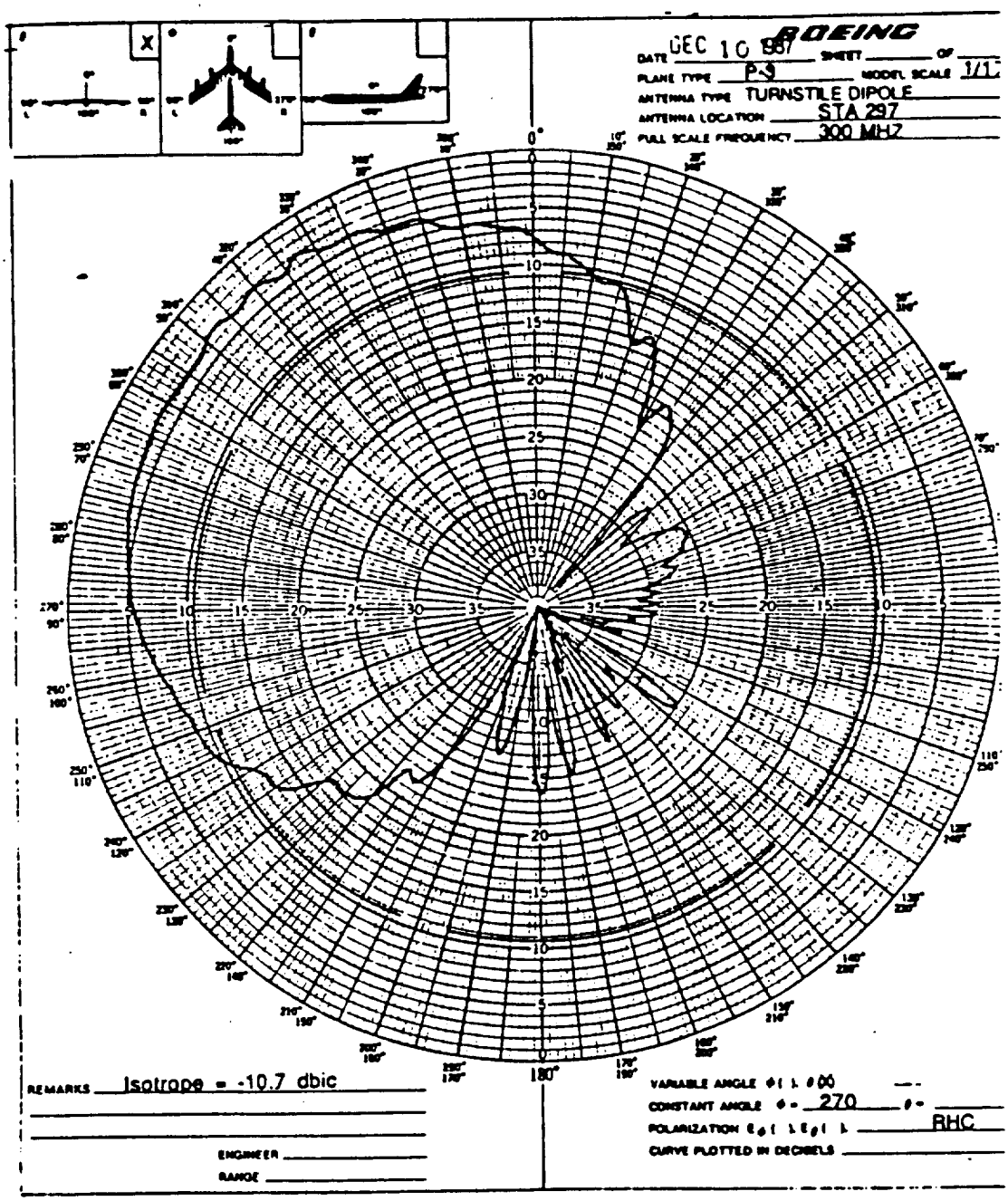

Figure 4.94: Boeing's measured roll plane pattern for batwing antenna on a P-3C for right hand circular polarization at 300 MHz.

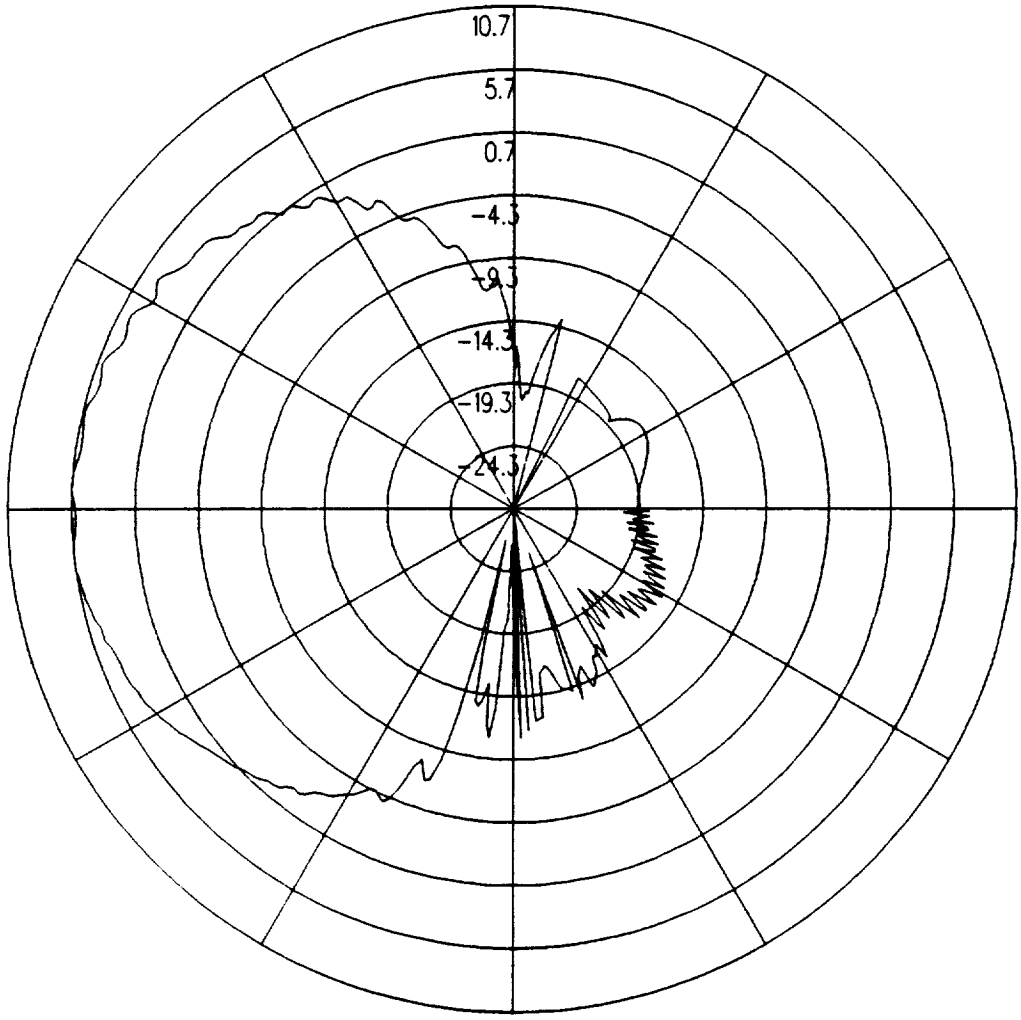

Figure 4.95: UTD calculated azimuth plane pattern for batwing antenna on a P-3C for right hand circular polarization at 300 MHz. (Alternative Boeing Antenna Location)

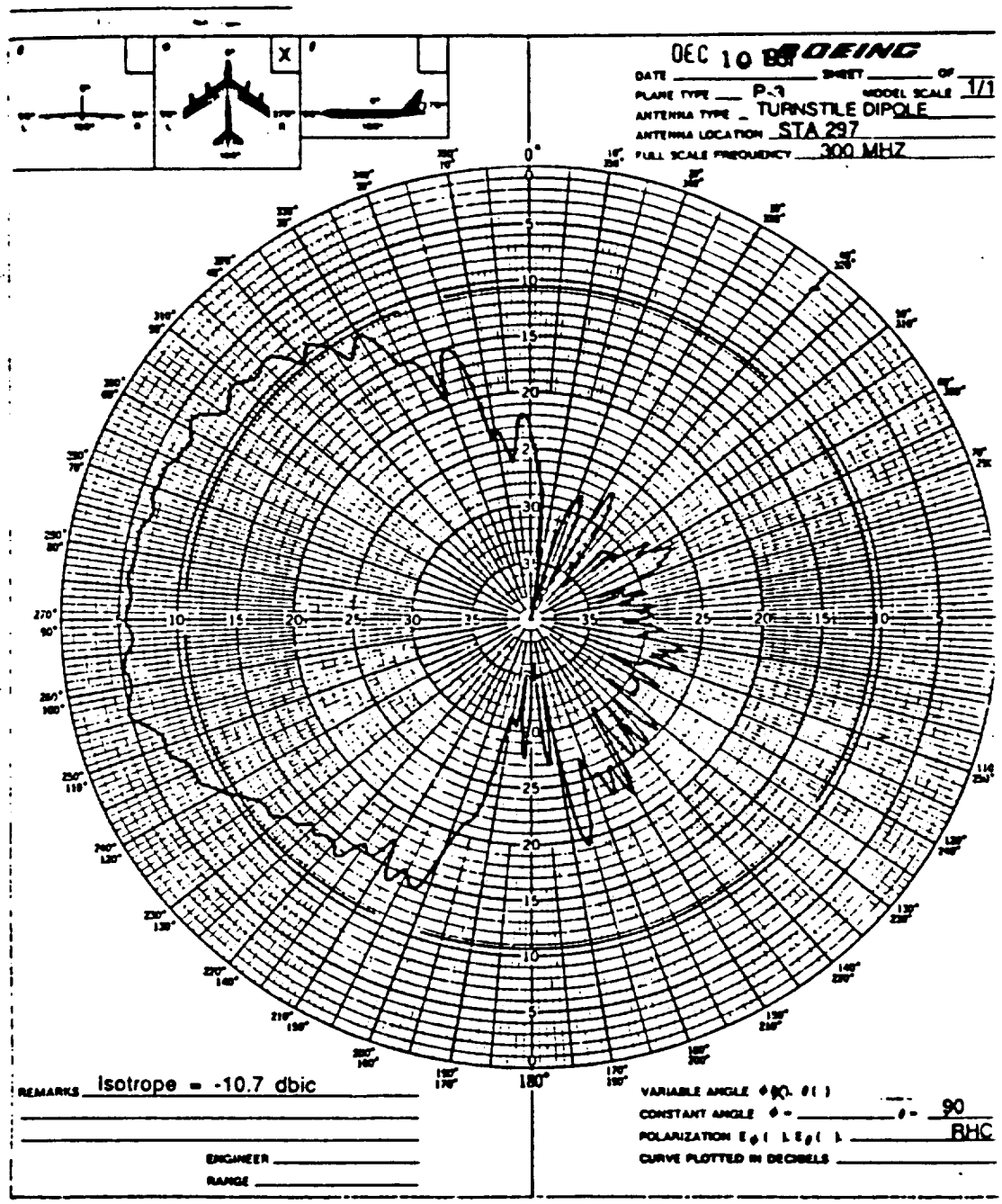

Figure 4.96: Boeing's measured azimuth plane pattern for batwing antenna on a P-3C for right hand circular polarization at 300 MHz.

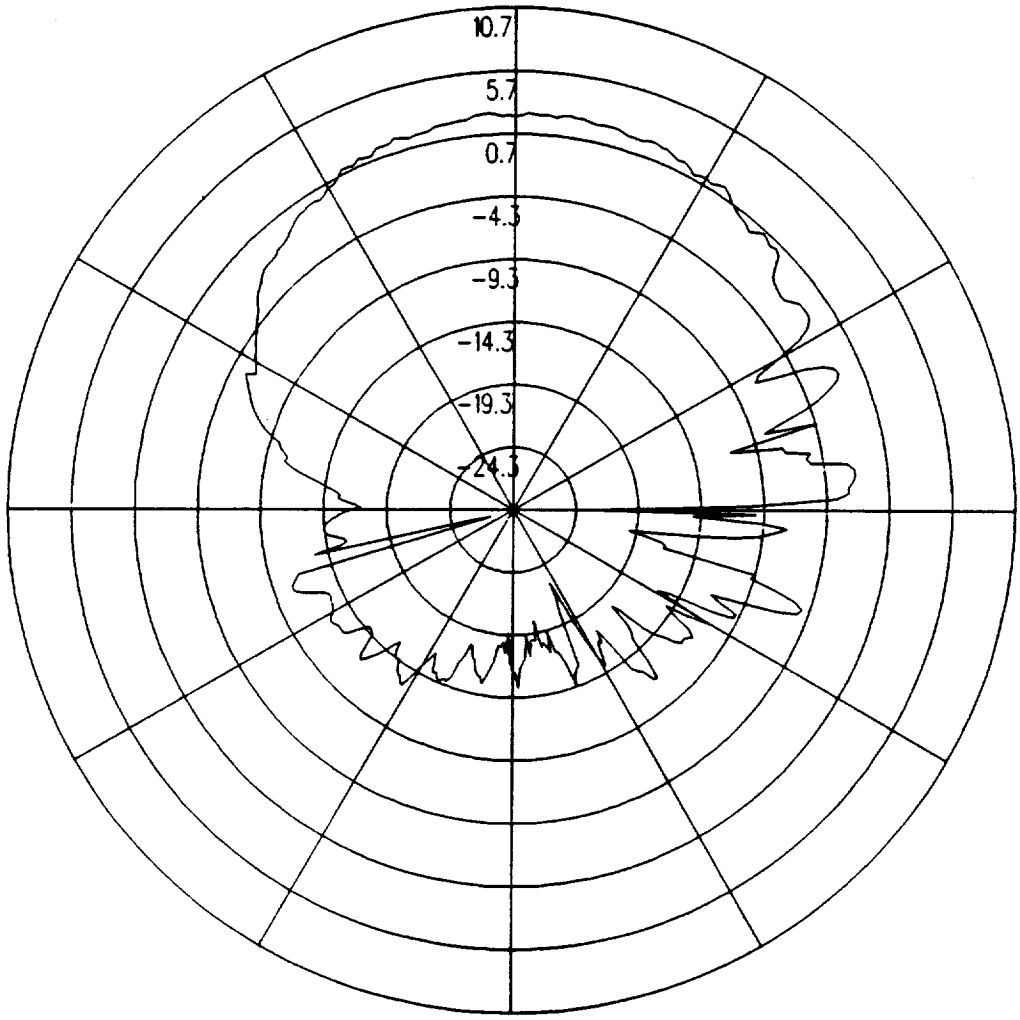

Figure 4.97: UTD calculated elevation plane pattern for batwing antenna on a P-3C for right hand circular polarization at 300 MHz. (Alternative Boeing Antenna Location)

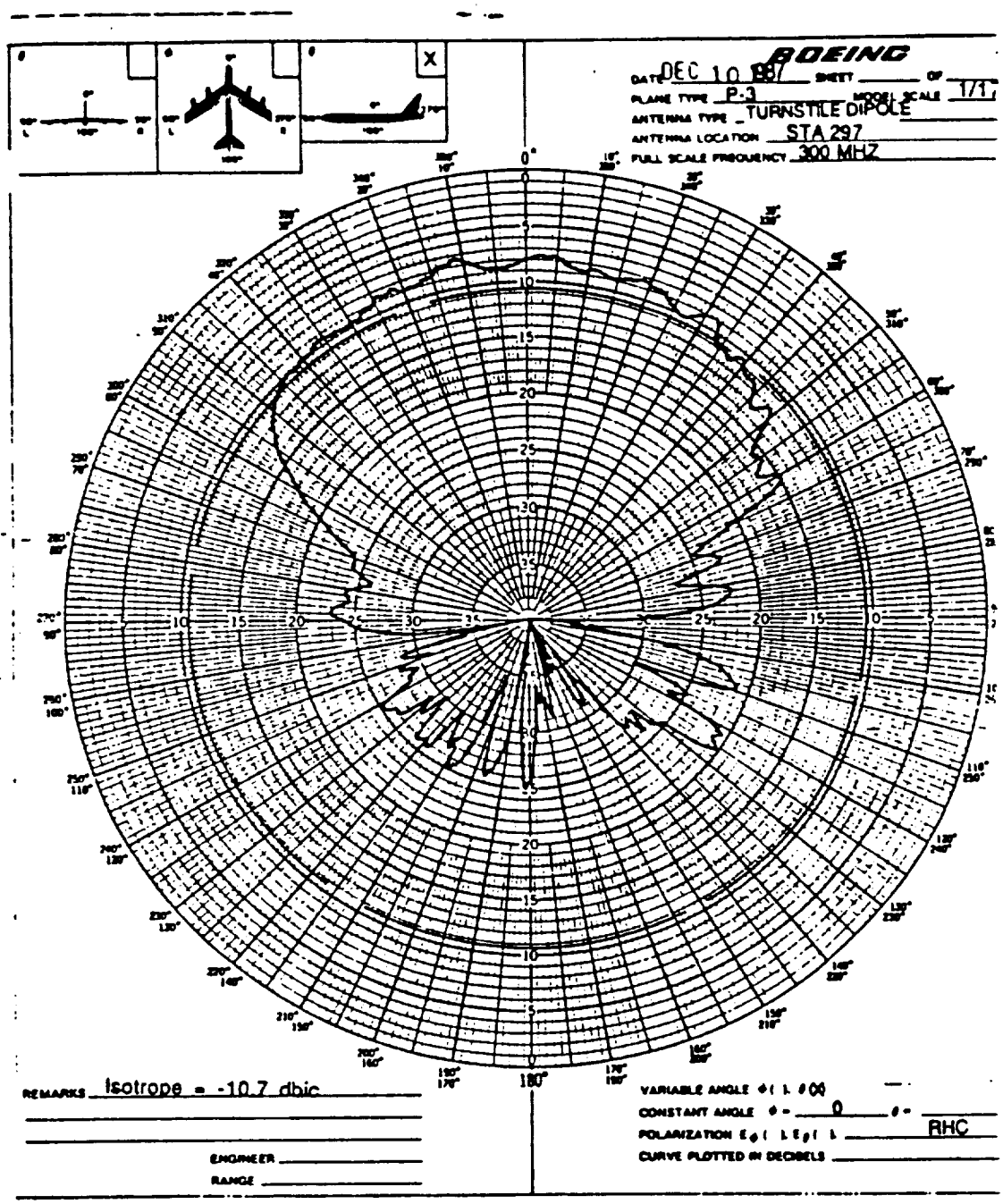

Figure 4.98: Boeing's measured elevation plane pattern for batwing antenna on a P-3C for right hand circular polarization at 300 MHz.

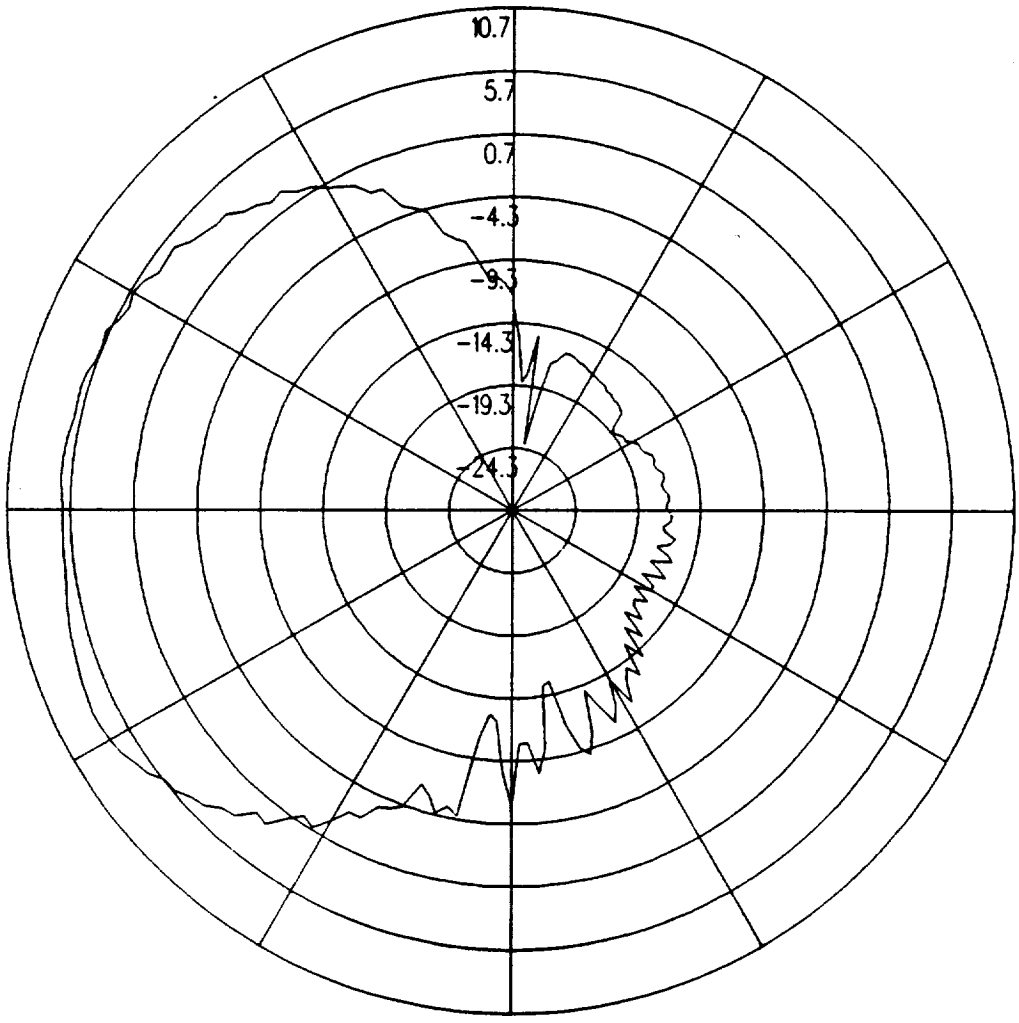

Figure 4.99: UTD calculated conical plane pattern 10° above the horizon for batwing antenna on a P-3C for right hand circular polarization at 300 MHz.(Alternative Boeing Antenna Location)

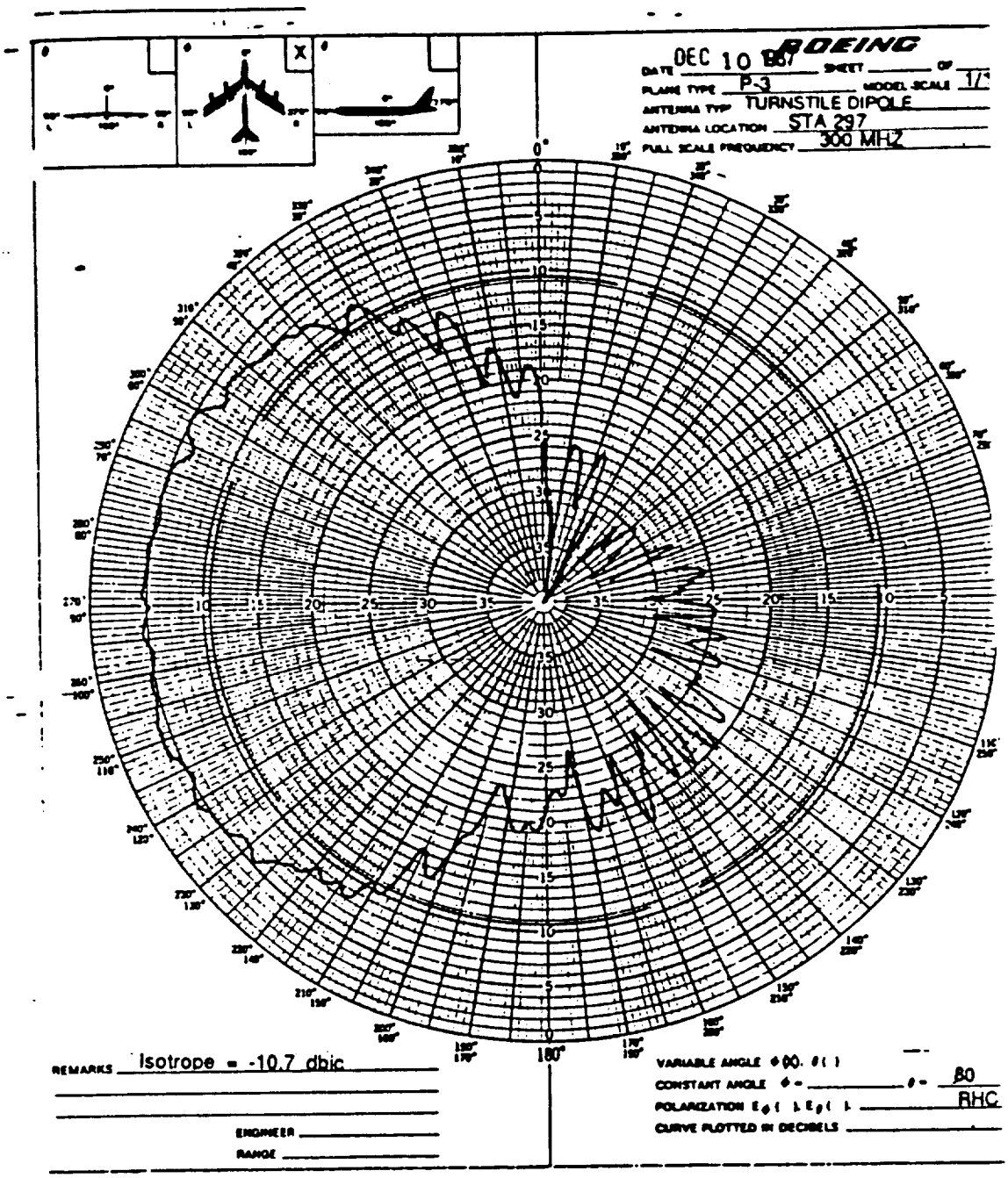

Figure 4.100: Boeing's measured conical plane pattern 10° above the horizon for batwing antenna on a P-3C for right hand circular polarization at 300 MHz.

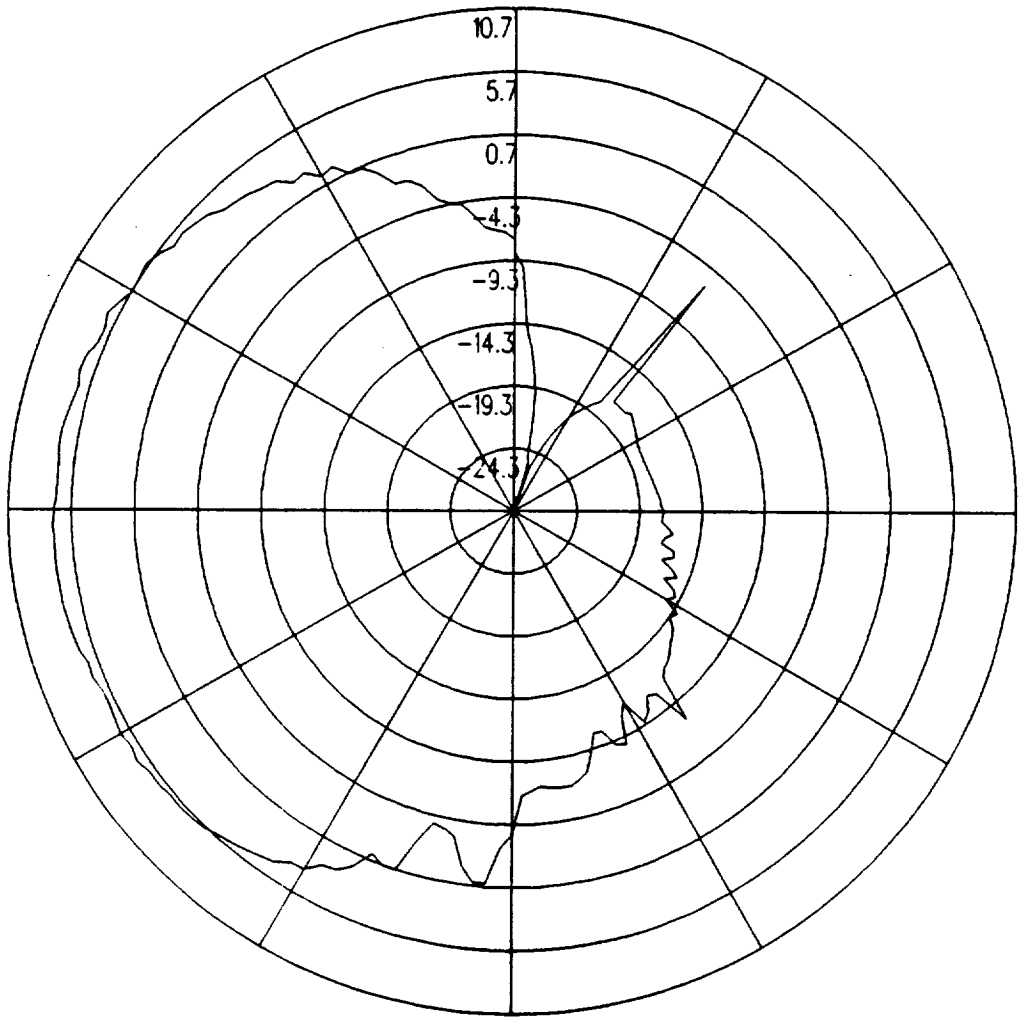

Figure 4.101: UTD calculated conical plane pattern 20° above the horizon for batwing antenna on a P-3C for right hand circular polarization at 300 MHz.(Alternative Boeing Antenna Location)

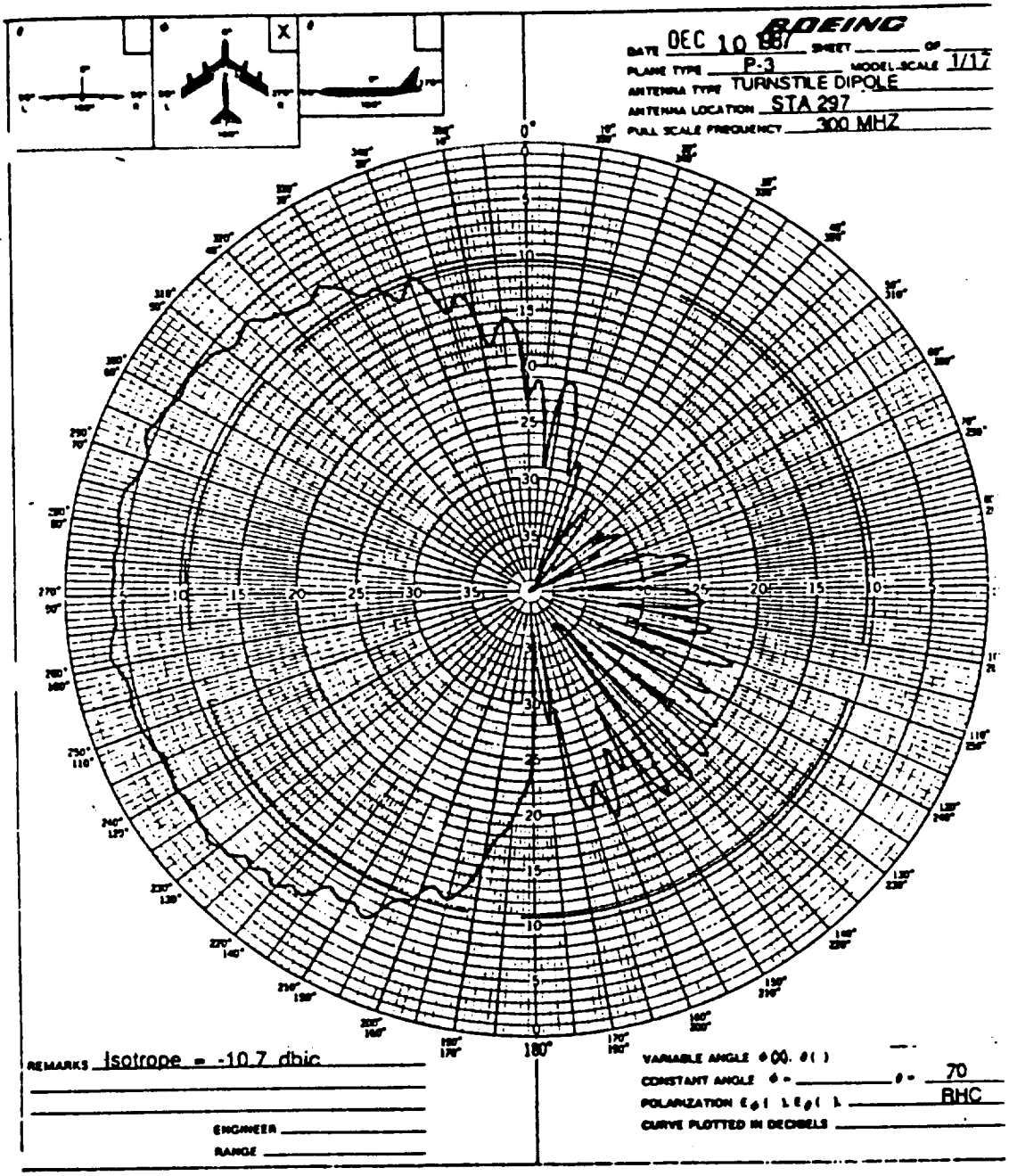

Figure 4.102: Boeing's measured conical plane pattern 20° above the horizon for batwing antenna on a P-3C for right hand circular polarization at 300 MHz.

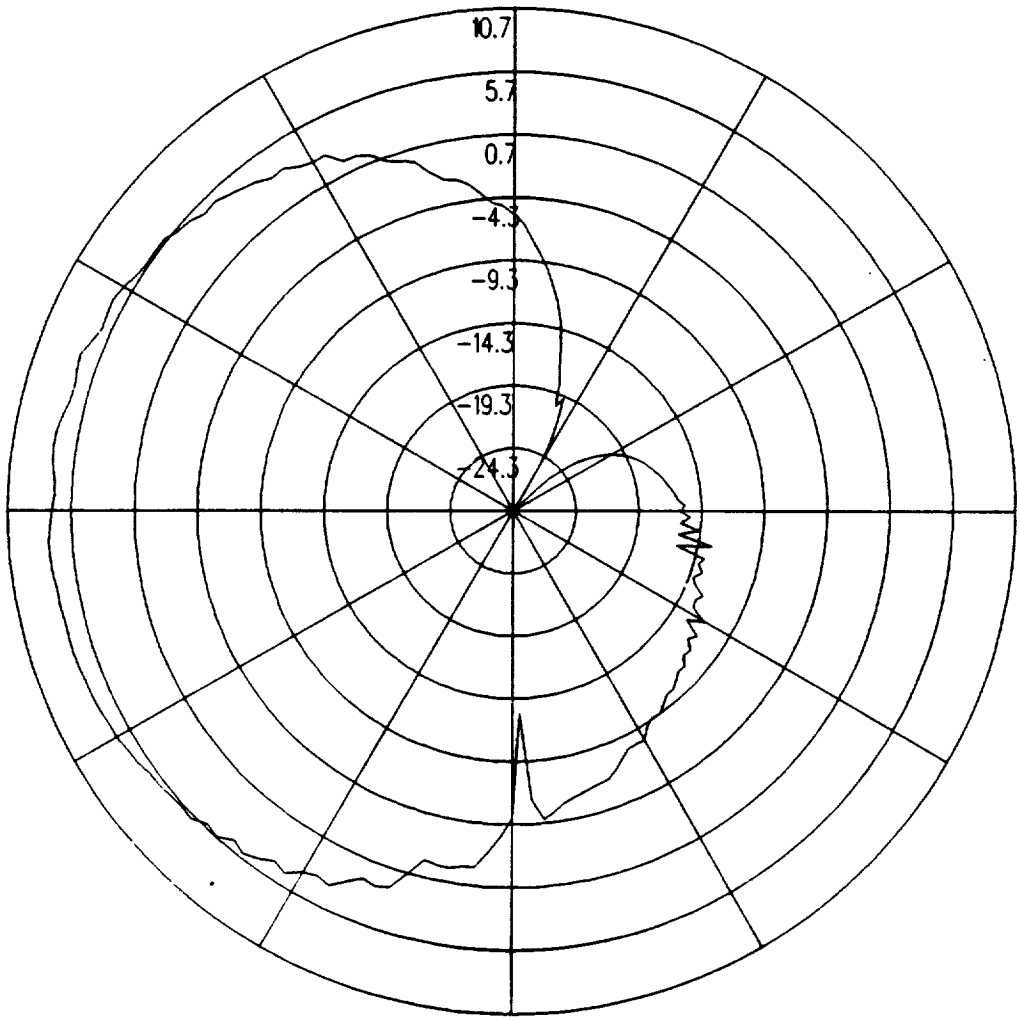

Figure 4.103: UTD calculated conical plane pattern 30° above the horizon for batwing antenna on a P-3C for right hand circular polarization at 300 MHz.(Alternative Boeing Antenna Location)

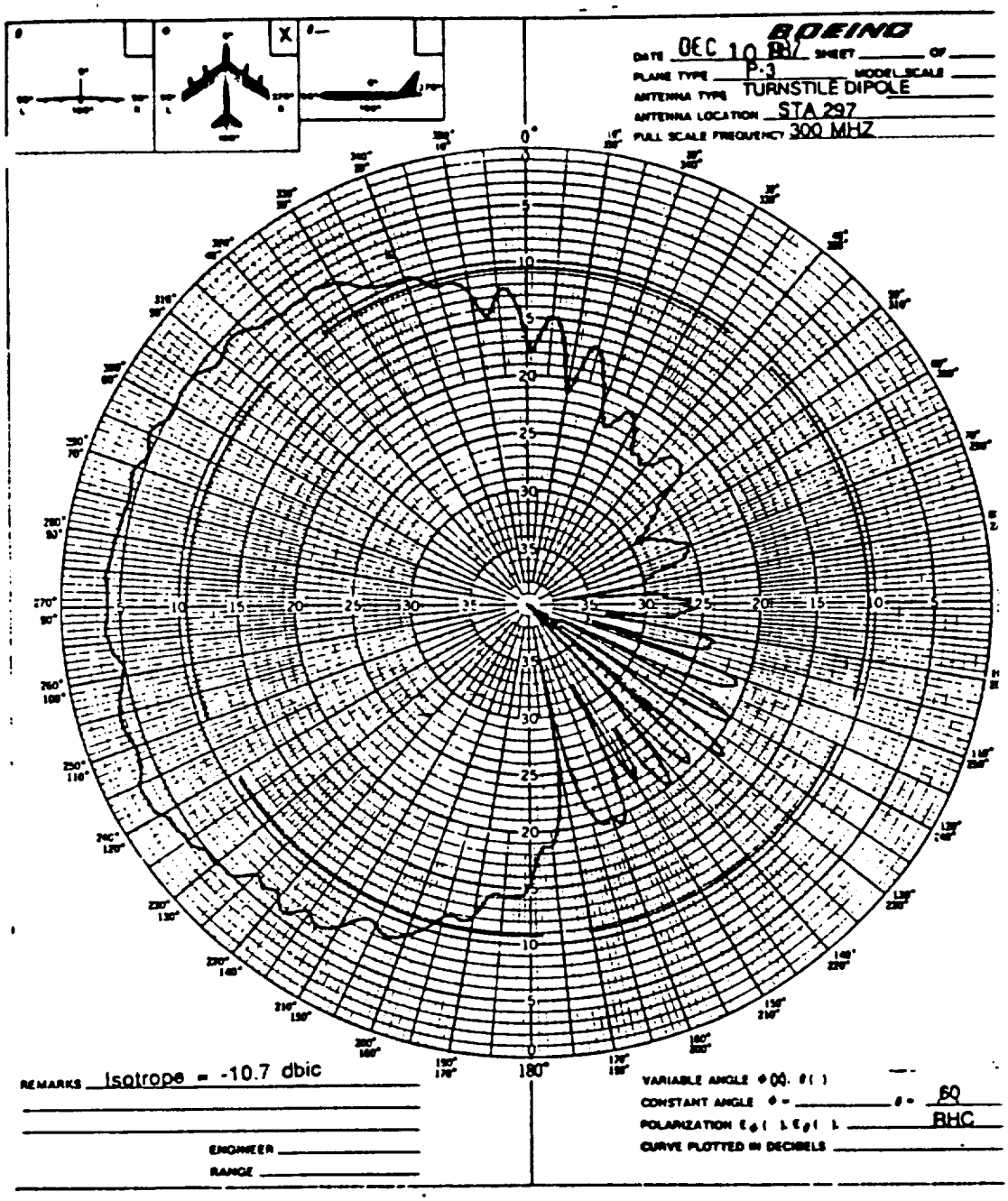

Figure 4.104: Boeing's measured conical plane pattern 30° above the horizon for batwing antenna on a P-3C for right hand circular polarization at 300 MHz.

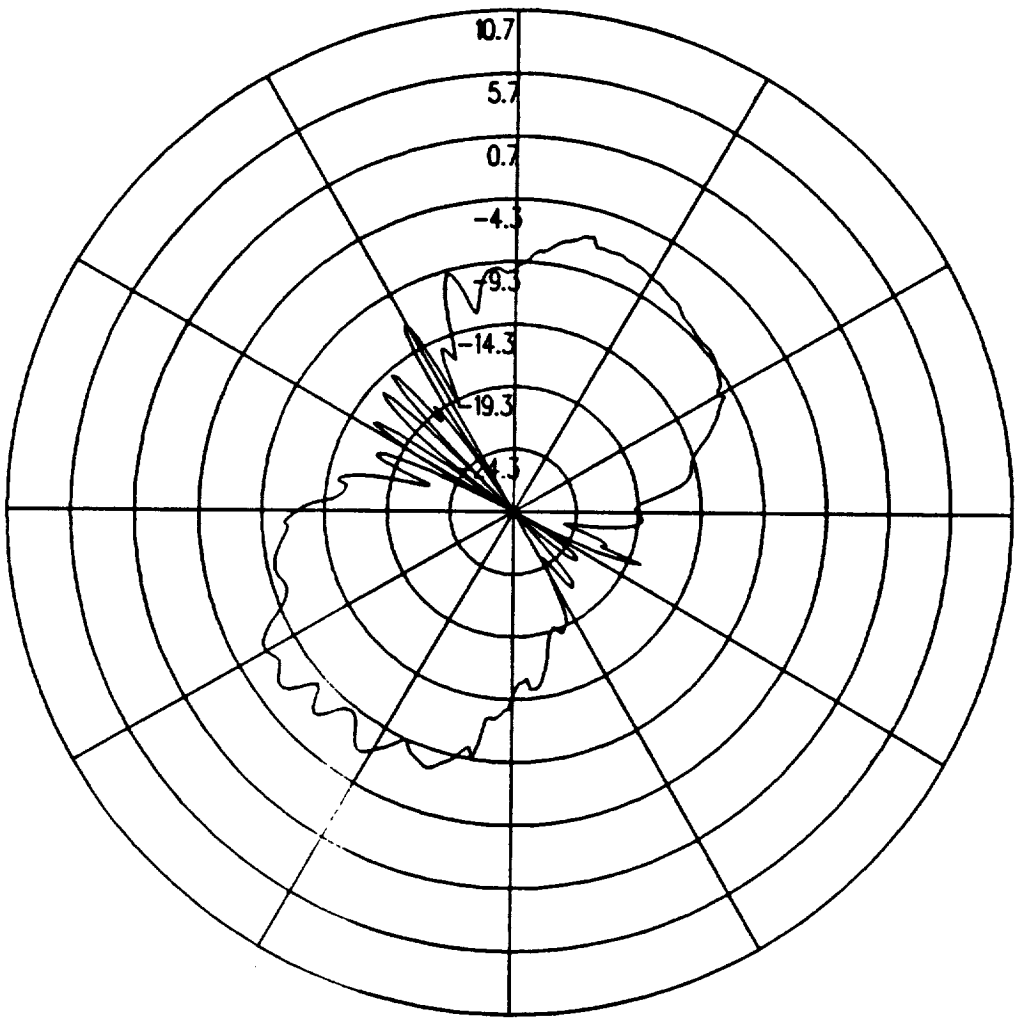

Figure 4.105: UTD calculated roll plane pattern for batwing antenna on a P-3C for left hand circular polarization at 300 MHz. (Alternative Boeing Antenna Location)

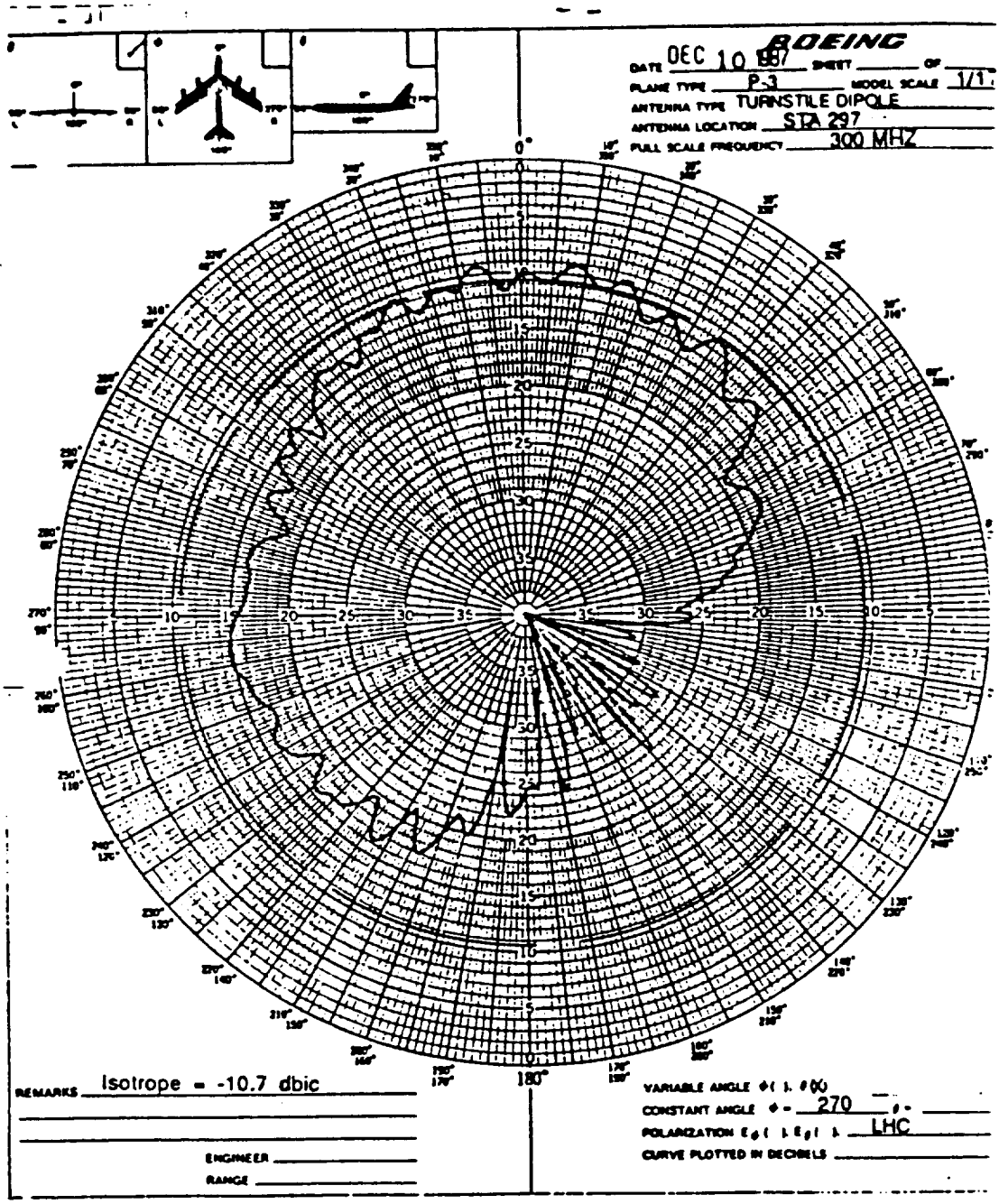

Figure 4.106: Boeing's measured roll plane pattern for batwing antenna on a P-3C for left hand circular polarization at 300 MHz.

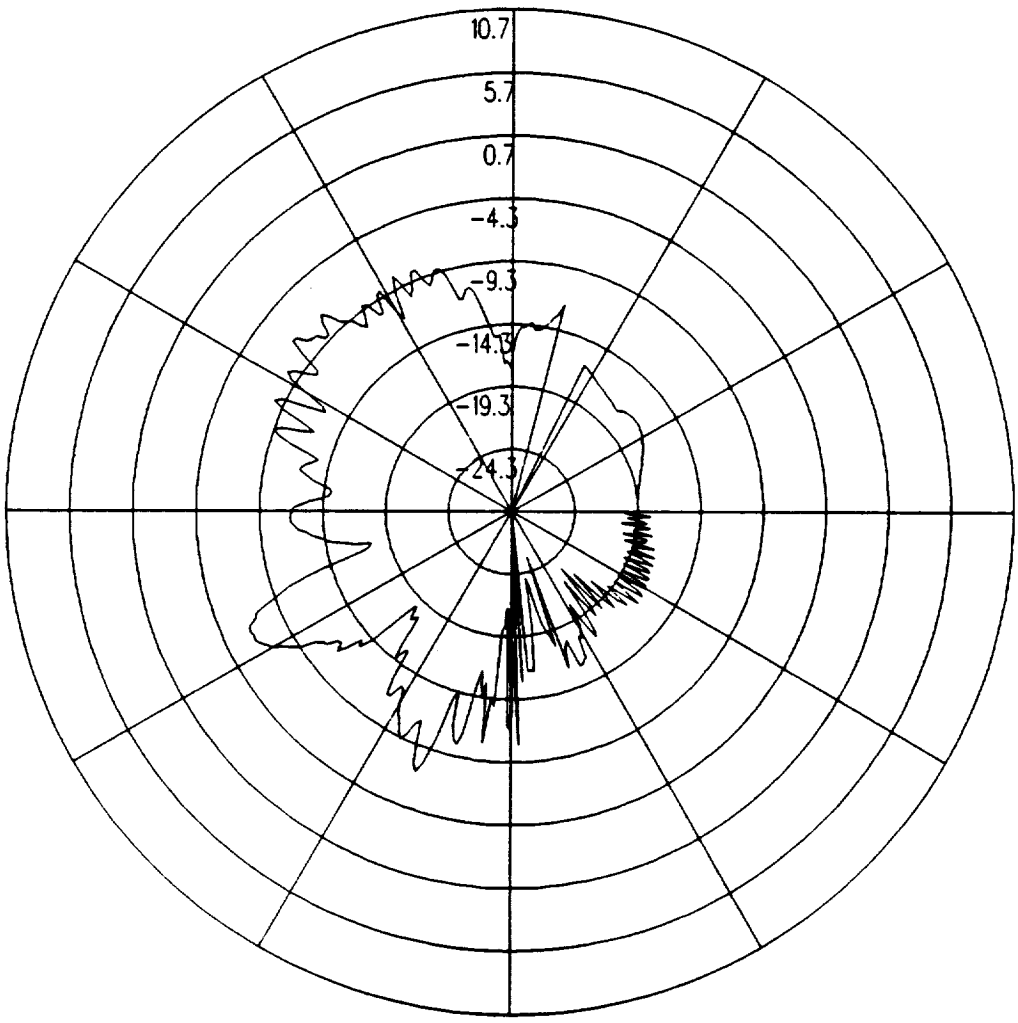

Figure 4.107: UTD calculated azimuth plane pattern for batwing antenna on a P-3C for left hand circular polarization at 300 MHz. (Alternative Boeing Antenna Location)

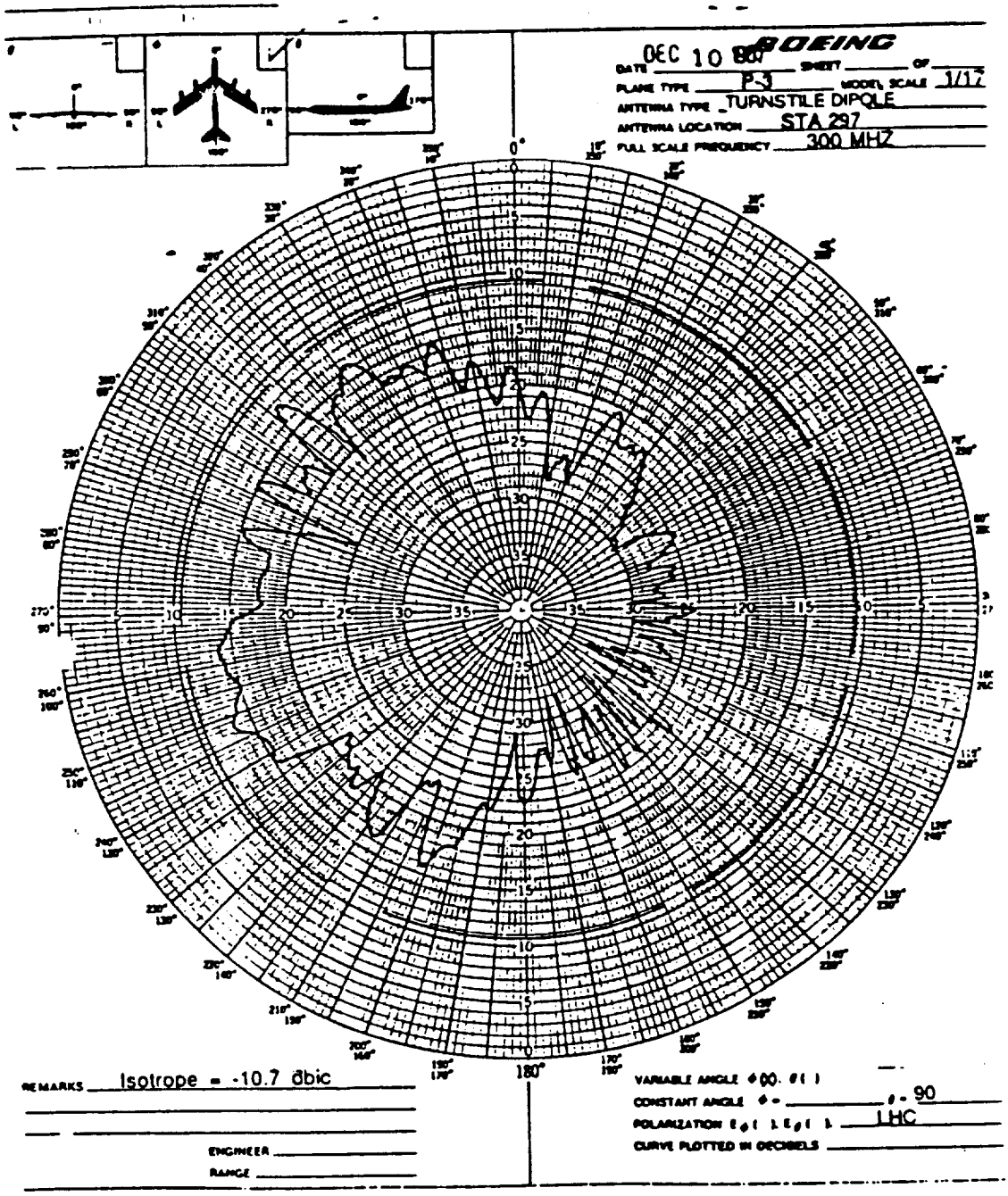

Figure 4.108: Boeing's measured azimuth plane pattern for batwing antenna on a P-3C for left hand circular polarization at 300 MHz.

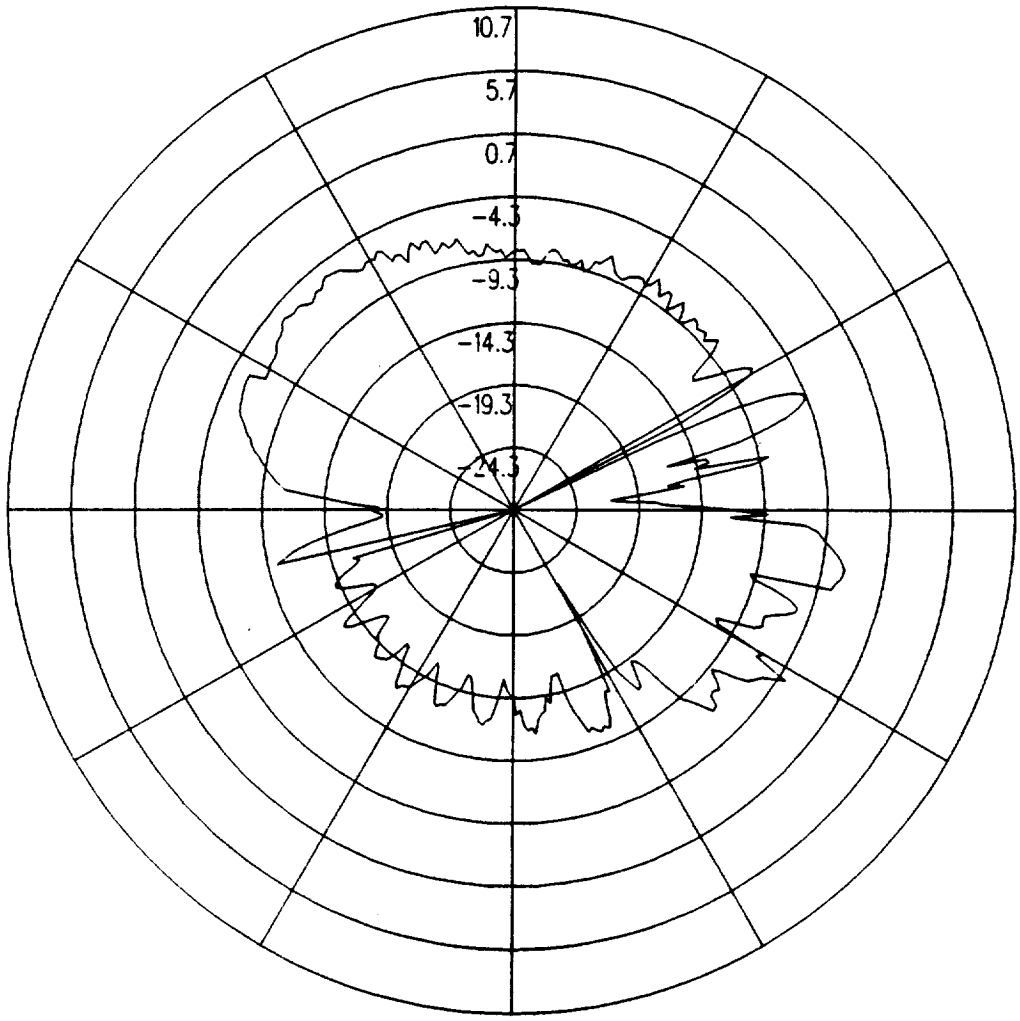

Figure 4.109: UTD calculated elevation plane pattern for batwing antenna on a P-3C for left hand circular polarization at 300 MHz. (Alternative Boeing Antenna Location)

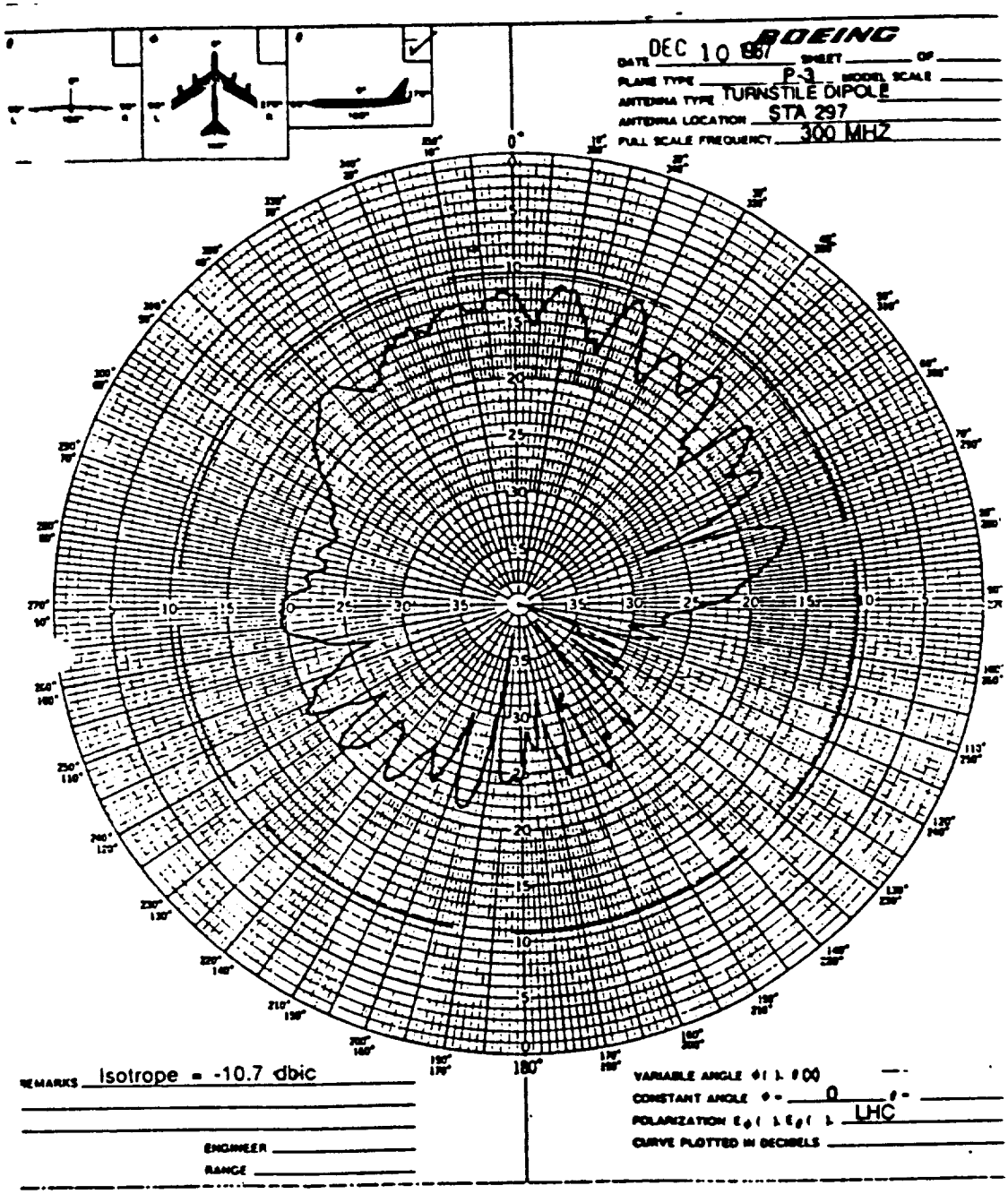

Figure 4.110: Boeing's measured elevation plane pattern for batwing antenna on a P-3C for left hand circular polarization at 300 MHz.

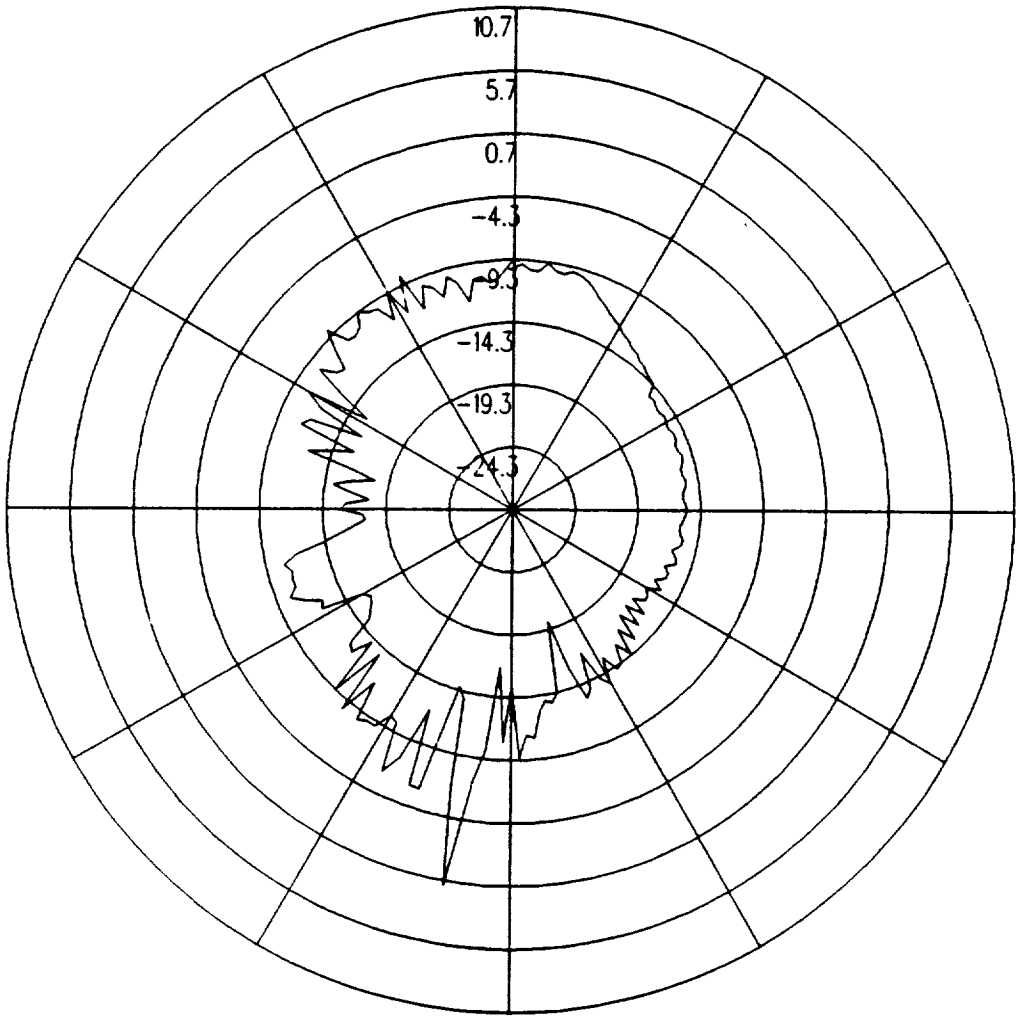

Figure 4.111: UTD calculated conical plane pattern 10° above the horizon for batwing antenna on a P-3C for left hand circular polarization at 300 MHz.(Alternative Boeing Antenna Location)

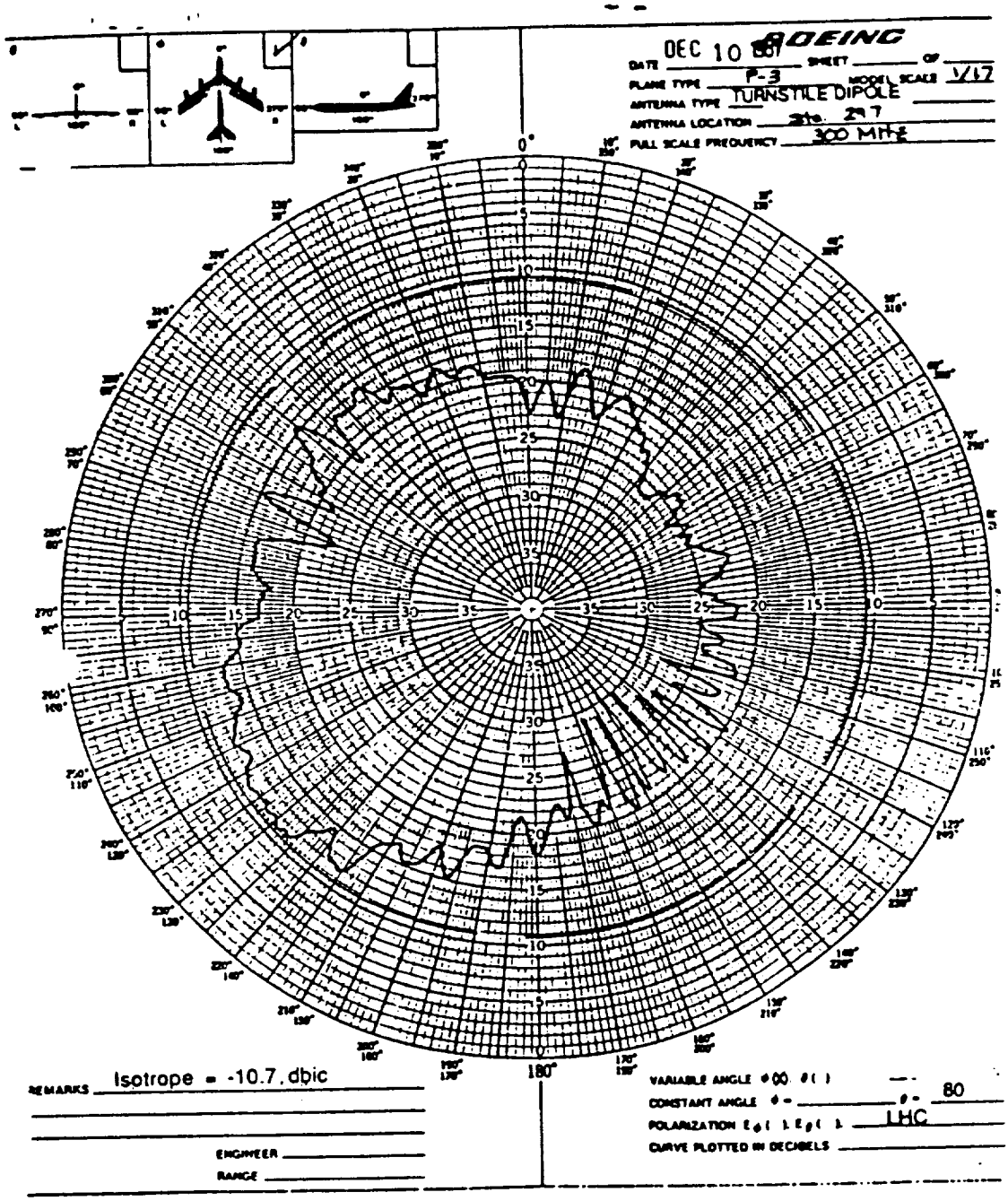

Figure 4.112: Boeing's measured conical plane pattern 10° above the horizon for batwing antenna on a P-3C for left hand circular polarization at 300 MHz.

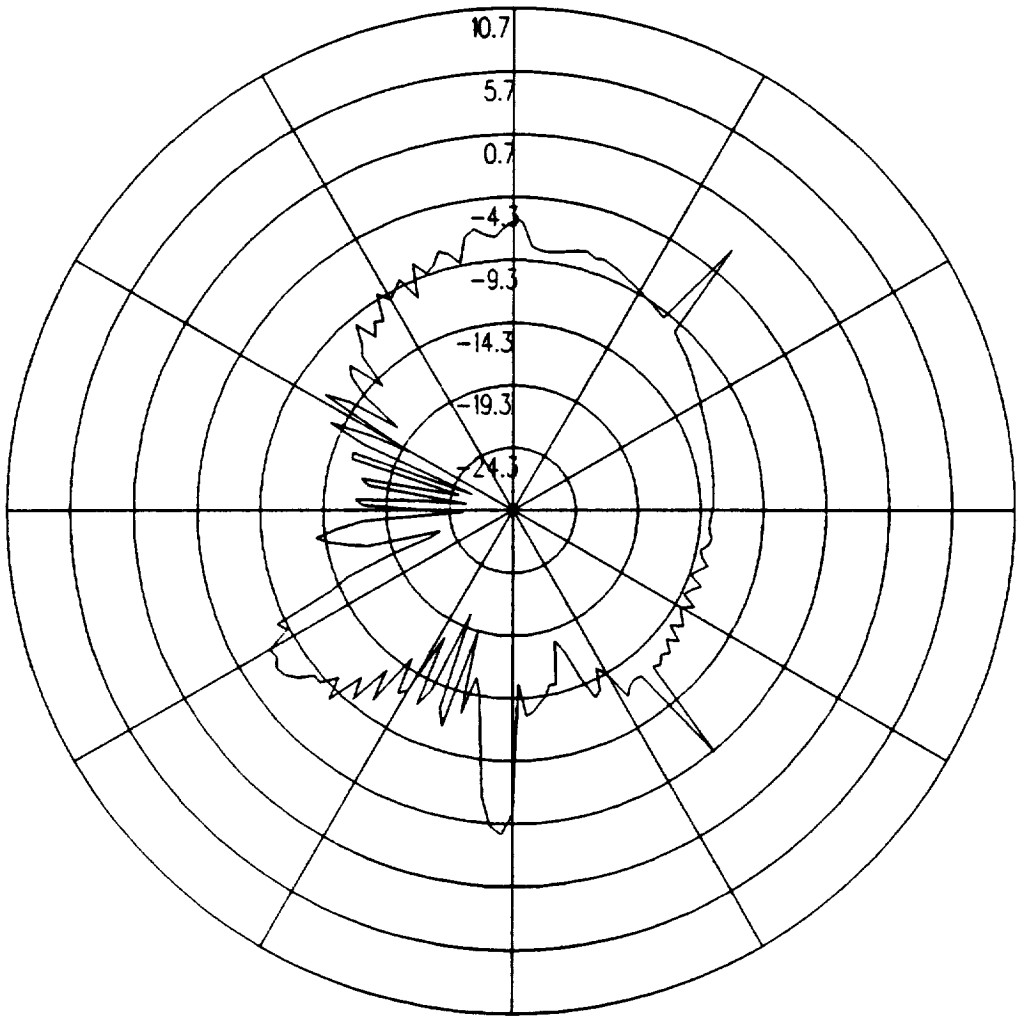

Figure 4.113: UTD calculated conical plane pattern 20° above the horizon for batwing antenna on a P-3C for left hand circular polarization at 300 MHz.(Alternative Boeing Antenna Location)

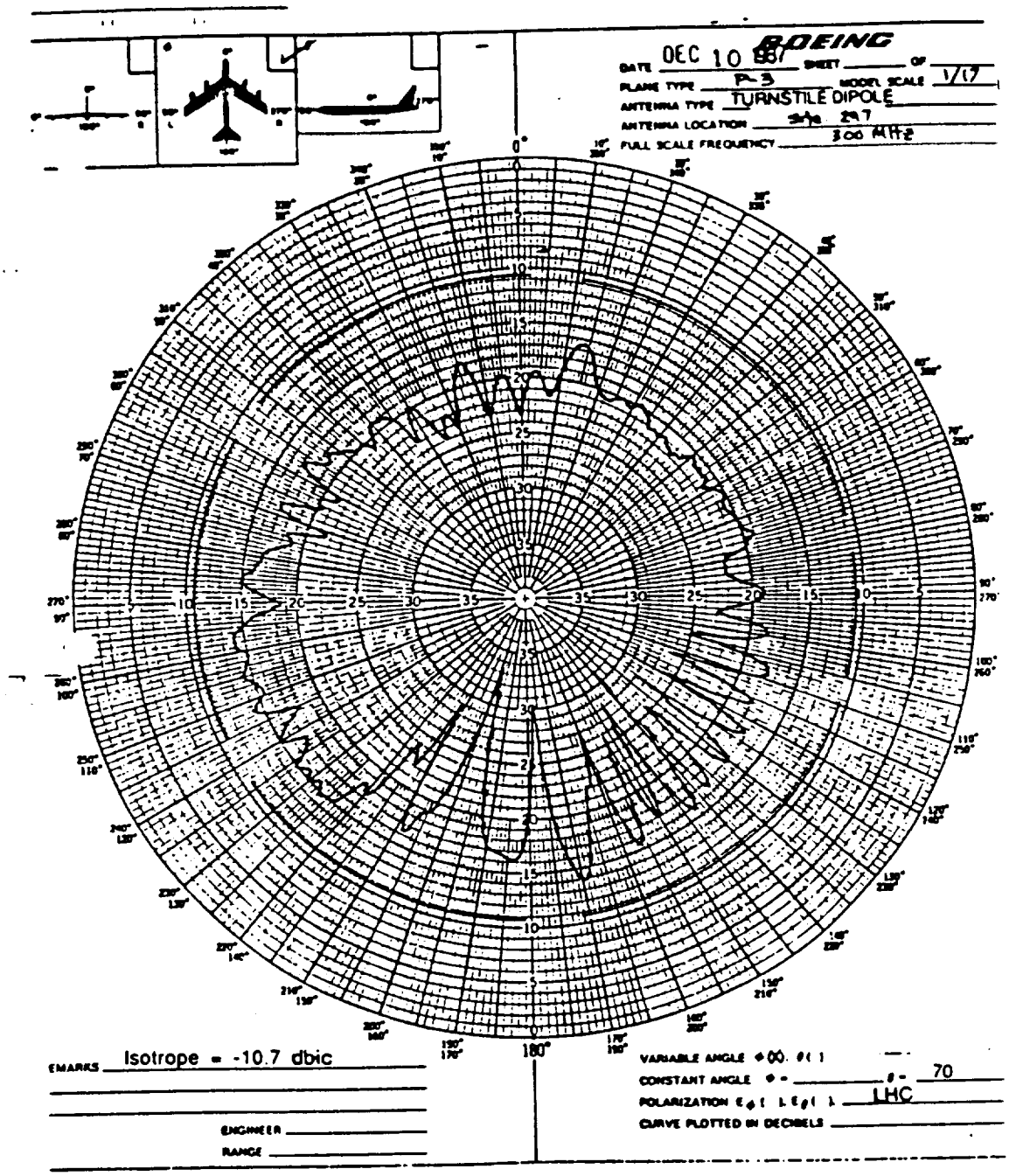

Figure 4.114: Boeing's measured conical plane pattern 20° above the horizon for batwing antenna on a P-3C for left hand circular polarization at 300 MHz.

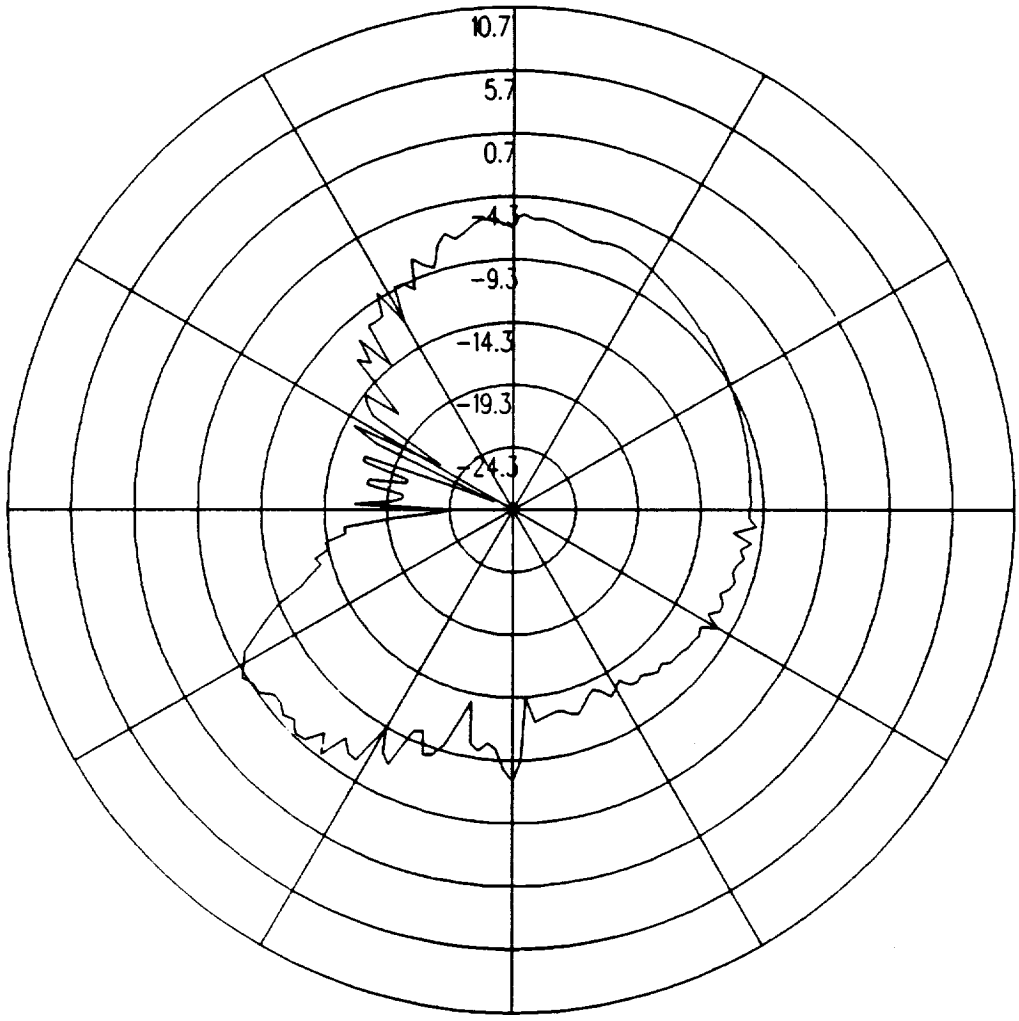

Figure 4.115: UTD calculated conical plane pattern 30° above the horizon for batwing antenna on a P-3C for left hand circular polarization at 300 MHz.(Alternative Boeing Antenna Location)

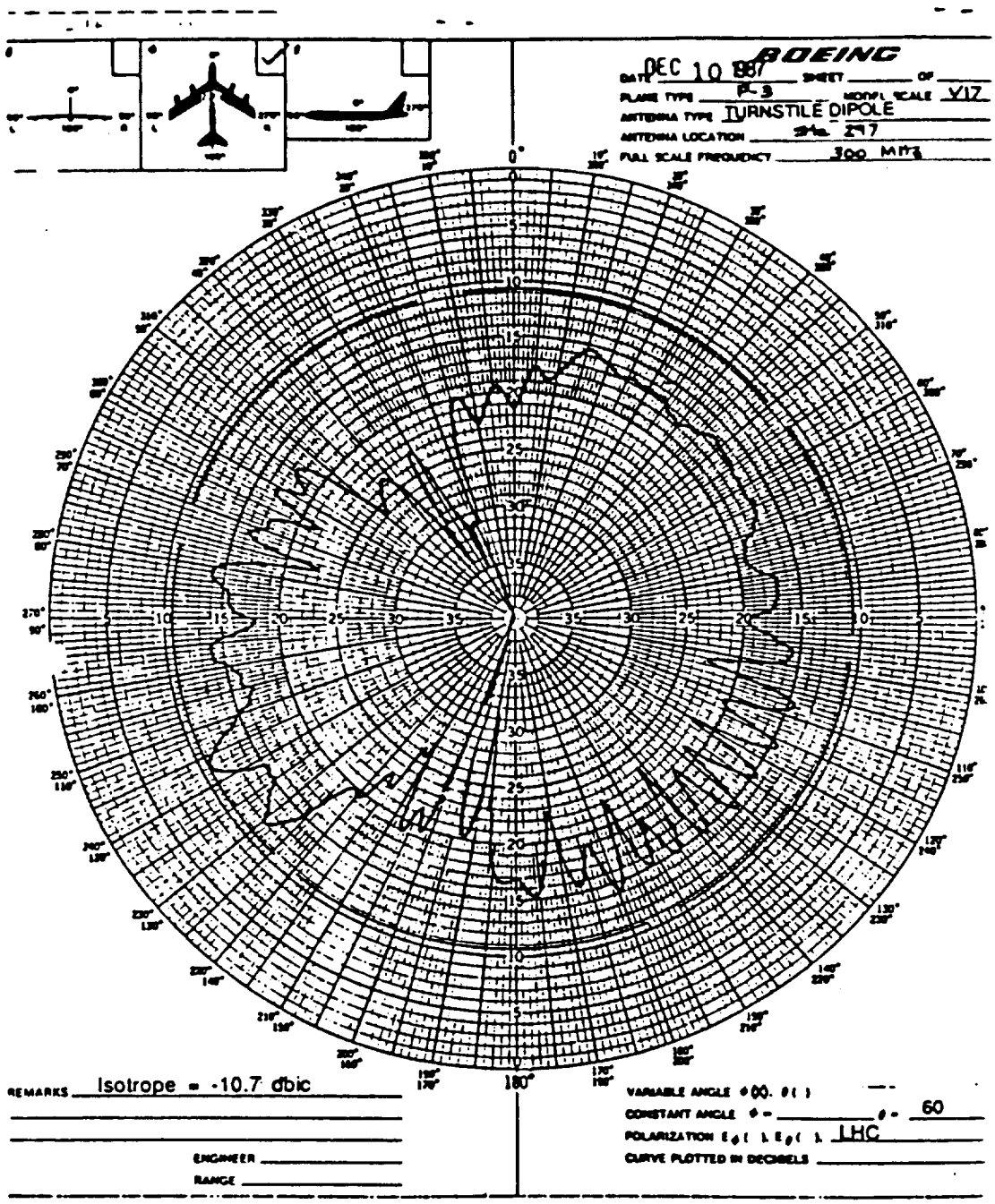

Figure 4.116: Boeing's measured conical plane pattern 30° above the horizon for batwing antenna on a P-3C for left hand circular polarization at 300 MHz.

4.8 Aircraft Model Conclusions

The first three sections of this chapter have studied three different computer models of the P-3C. By comparing the calculated data with measured patterns from Boeing, it is shown that the cylindrical aircraft model gives the closest agreement. This is true even though the cone frustum and ellipsoid model visually resemble the actual P-3C aircraft better. The reason that the cylindrical aircraft model represents the actual aircraft the best is that the most important characteristic of the aircraft is the cylindrical fuselage and the subsequent interactions between the fuselage and the wings and stabilizers. The cylindrical aircraft model most accurately models the actual fuselage and the subsequent interactions, therefore, this is why the cylindrical aircraft model is used throughout the remainder of this report except as noted below. It has also been shown that the presence of the aircraft engine has minimal effect on the radiation patterns and, therefore, does not need to be included in the aircraft model. Finally, the calculated patterns for the two additional antenna locations studied in the previous two sections have been compared to the measured patterns in order to ensure that the aircraft model is valid for a variety of antenna locations. Therefore, the cylindrical aircraft model has been used in the remainder of the cases studied with the exception of the two tests where the antenna is placed on the nose of the aircraft. The composite ellipsoid aircraft model's elliptical nose is critical in the radiation patterns in these cases.

Overall, the NEC-BSC calculated radiation patterns showed good agreement with the measured radiation patterns for the various antenna locations throughout the majority of the patterns. The sole exception is that the calculated levels near the nose and tail in the horizon of the aircraft are higher by as much as 5–8 dB than the measured levels provided by Boeing and Lockheed. These higher levels near the nose and tail of the aircraft on the horizon have been investigated extensively and are most likely due to the fact that the plate - cylinder interactions which have been simulated using the imaging technique explained in Section 2.2 are only approximations. When the exact plate - cylinder interactions are implemented in the code, the differences between the measured and calculated results are anticipated to be reduced.

Chapter 5

Antenna Location Study

In this chapter, radiation patterns in the roll plane, the azimuth plane, the elevation plane, and conical pattern planes from 10° to 30° above the horizon have been calculated for eleven alternative antenna locations given in addition to the two given in the previous chapter. The antenna model used in these studies is the same model used to represent the DM 1501341 Batwing antenna as in the previous chapters. Each section in this chapter contains the radiation patterns for one of the alternative antenna locations studied.

5.1 Test Location 1

The antenna is located as illustrated in Figure 5.1, which also shows the computer model used to generate the results. The calculated results at 300 MHz are shown for the roll plane in Figure 5.2, for the azimuth plane in Figure 5.3, for the elevation plane in Figure 5.4, for the conical plane 10° above the horizon in Figure 5.5, for the conical plane 20° above the horizon in Figure 5.6, and for the conical plane 30° above the horizon in Figure 5.7 all for right hand polarization. The cross polarized fields are shown for the roll plane in Figure 5.8, for the azimuth plane in Figure 5.9, for the elevation plane in Figure 5.10, for the conical plane 10° above the horizon in Figure 5.11, for the conical plane 20° above the horizon in Figure 5.12, and for the conical plane 30° above the horizon in Figure 5.13 all for left hand polarization.

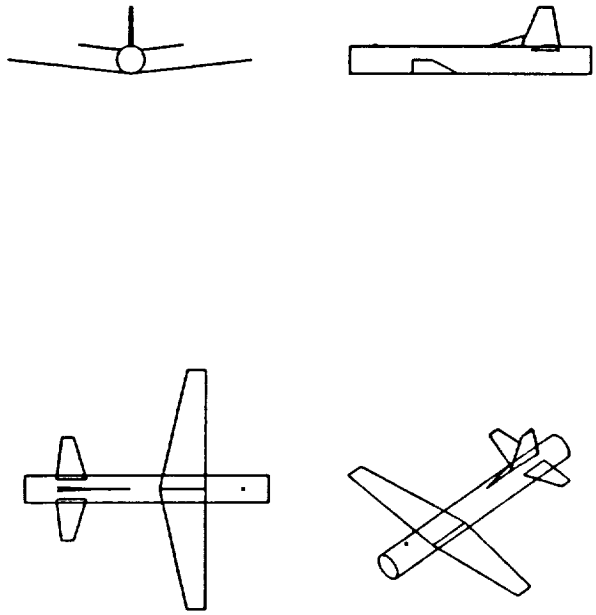

Figure 5.1: Geometry of the model of the P-3C aircraft used in the NEC-BSC code showing the location of the antenna.

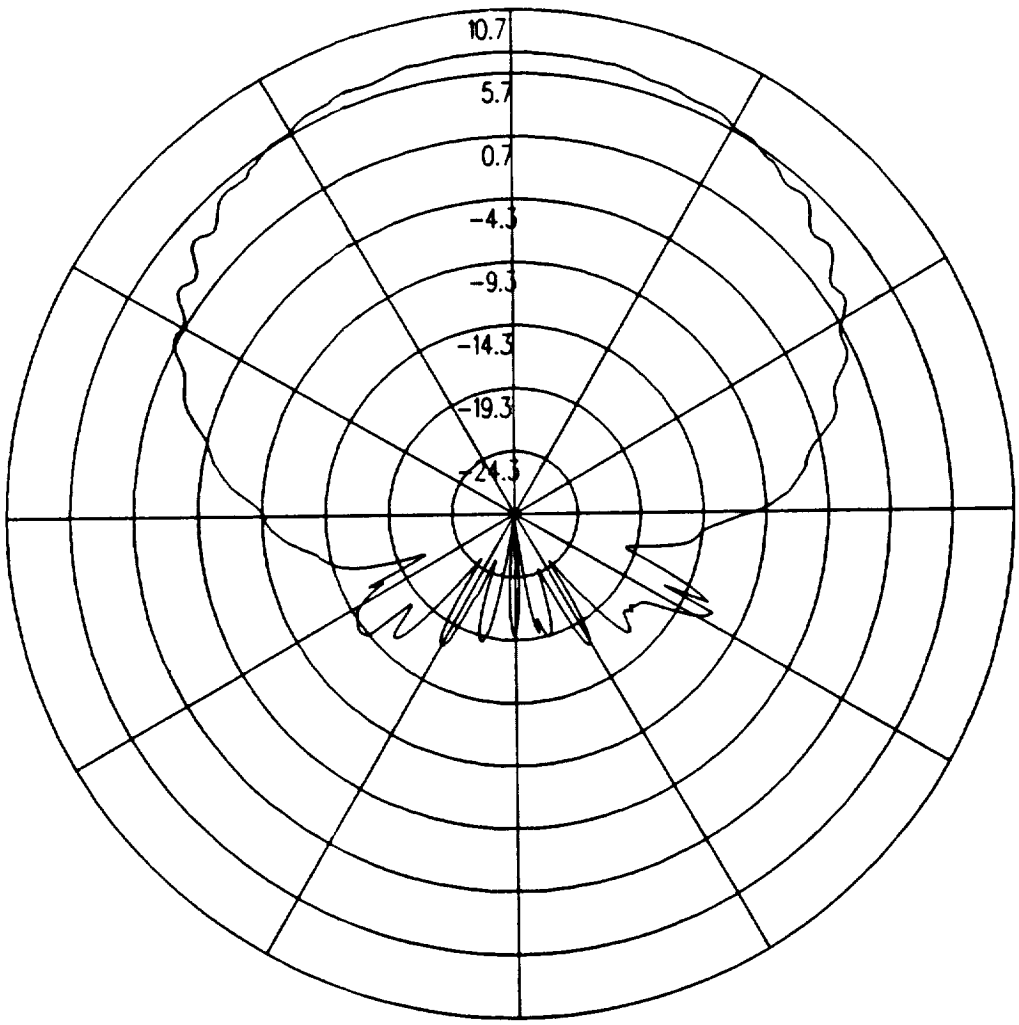

Figure 5.2: UTD calculated roll plane pattern for batwing antenna on a P-3C for right hand circular polarization at 300 MHz. (Test Location 1)

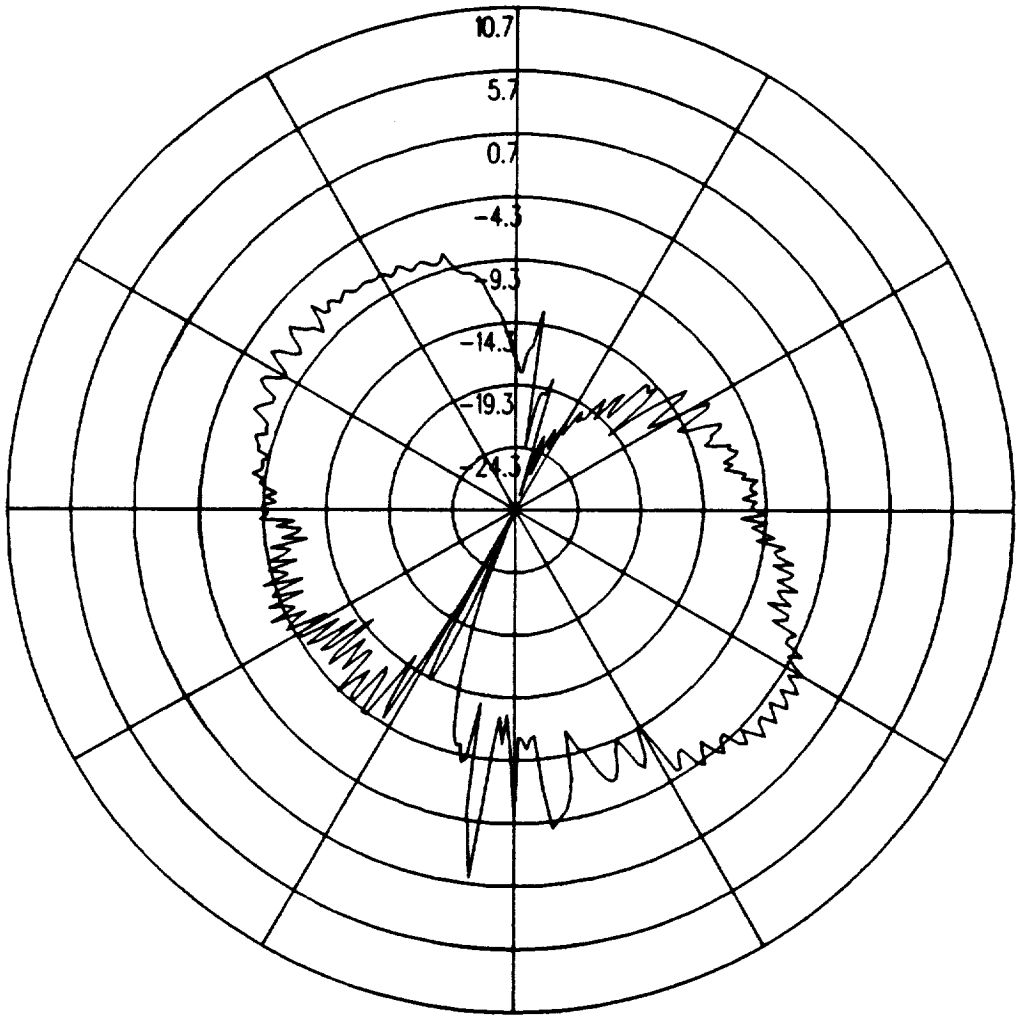

Figure 5.3: UTD calculated azimuth plane pattern for batwing antenna on a P-3C for right hand circular polarization at 300 MHz. (Test Location 1)

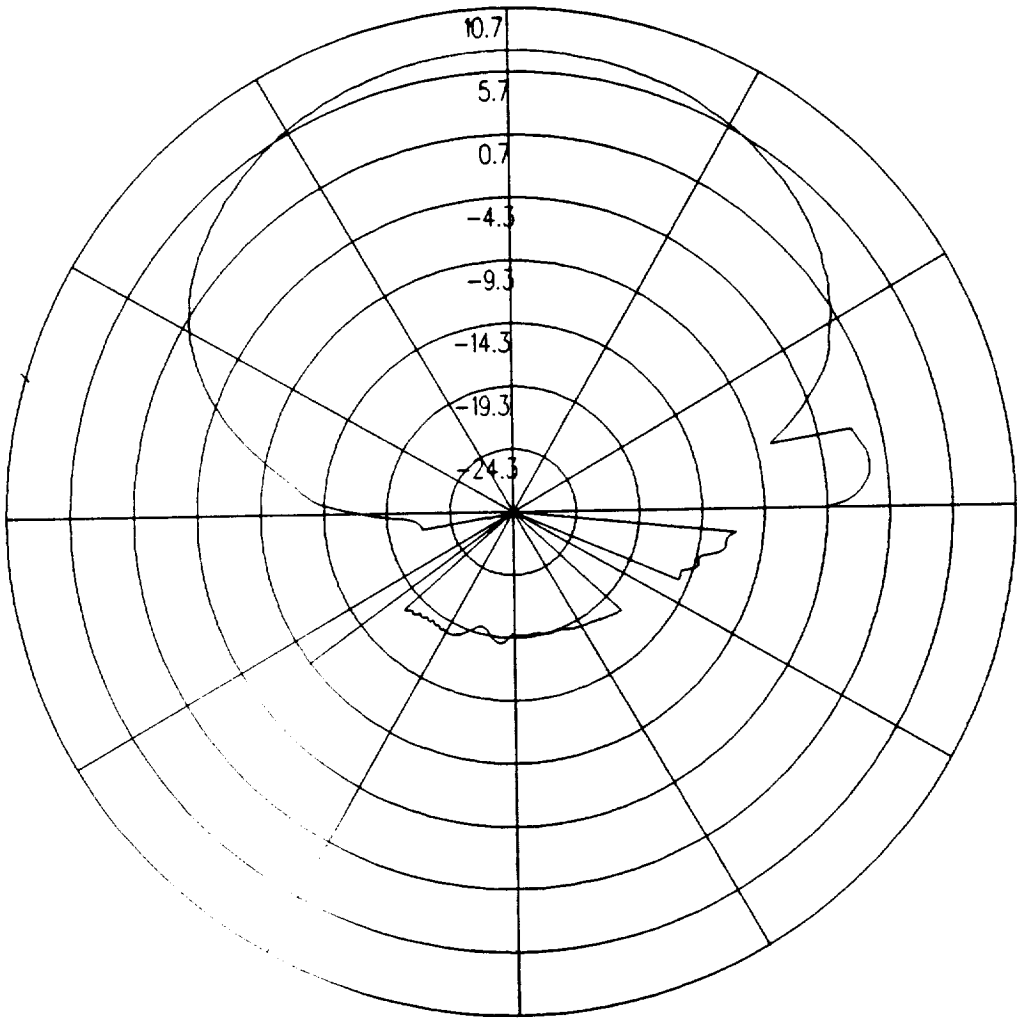

Figure 5.4: UTD calculated elevation plane pattern for batwing antenna on a P-3C for right hand circular polarization at 300 MHz. (Test Location 1)

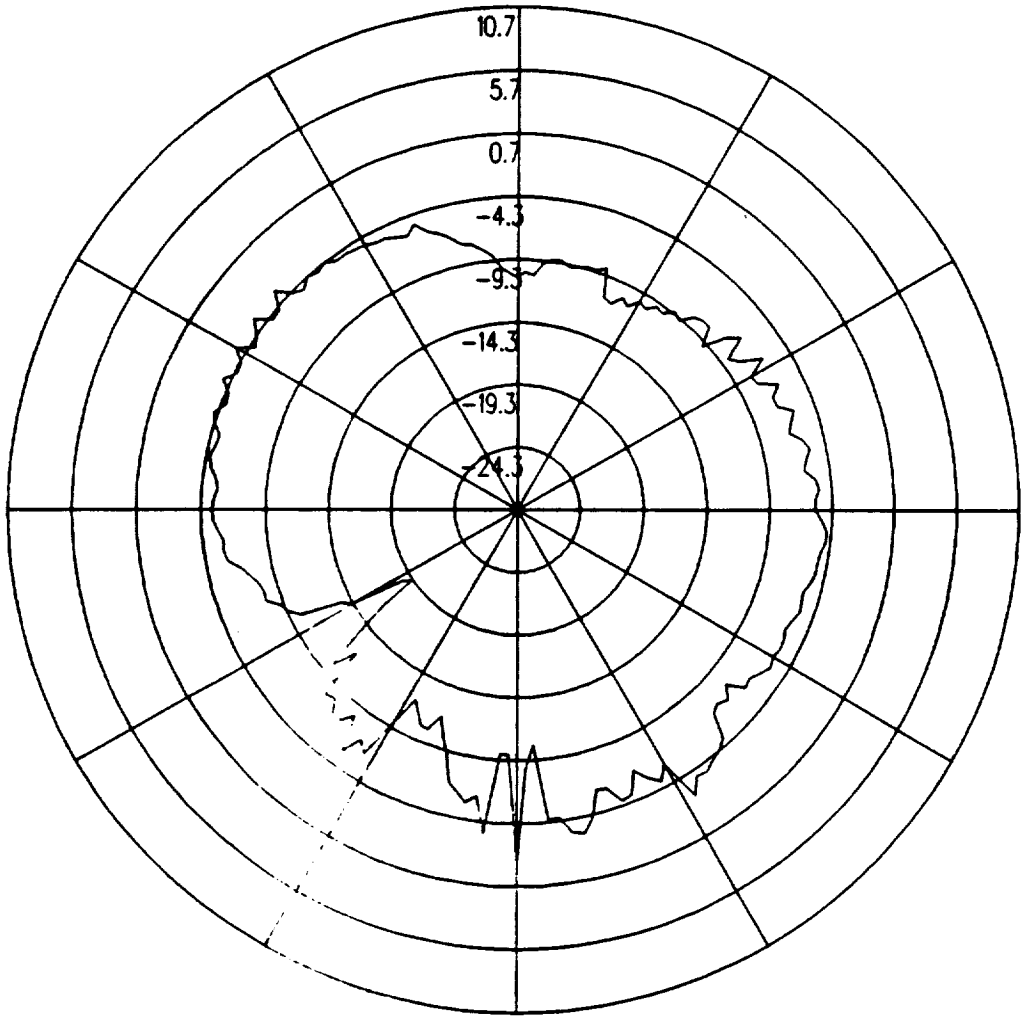

Figure 5.5: UTD calculated conical plane pattern 10° above the horizon for batwing antenna on a P-3C for right hand circular polarization at 300 MHz.(Test Location 1)

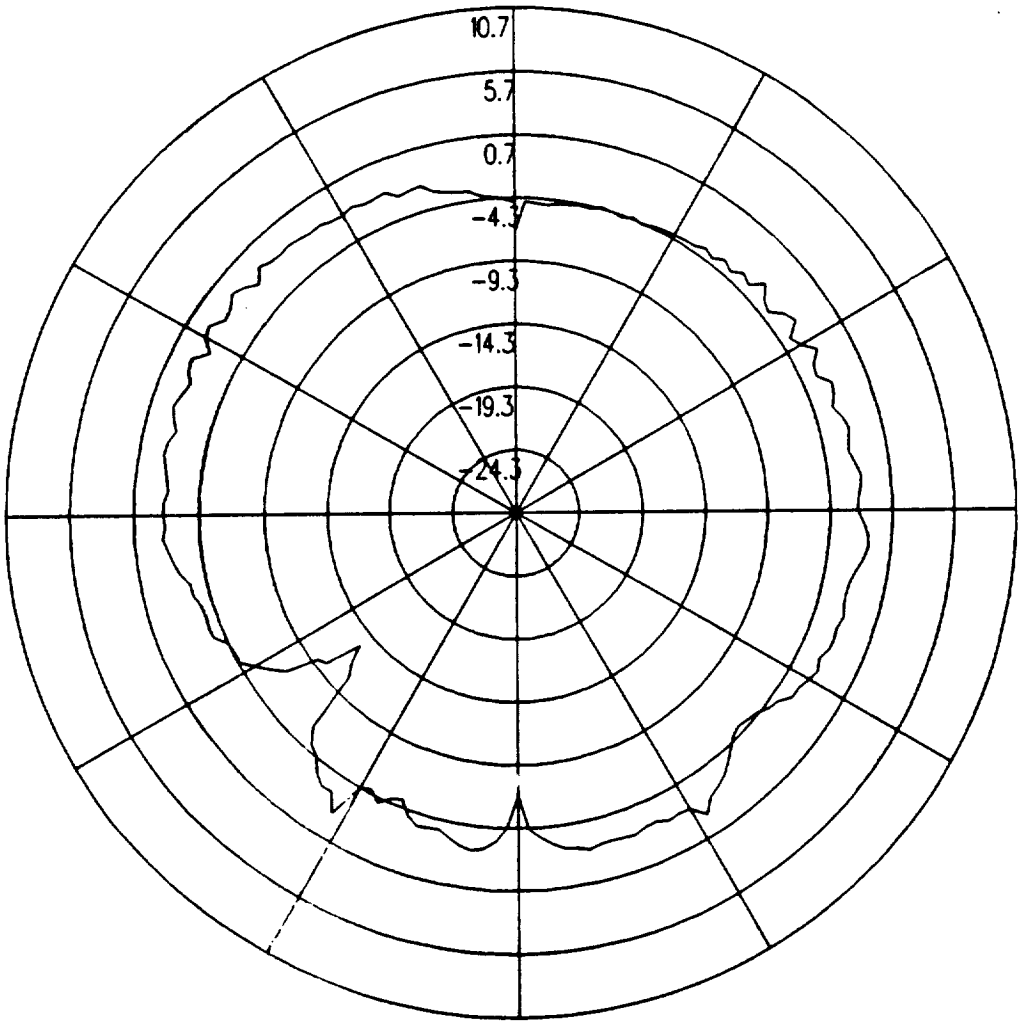

Figure 5.6: UTD calculated conical plane pattern 20° above the horizon for batwing antenna on a P-3C for right hand circular polarization at 300 MHz.(Test Location 1)

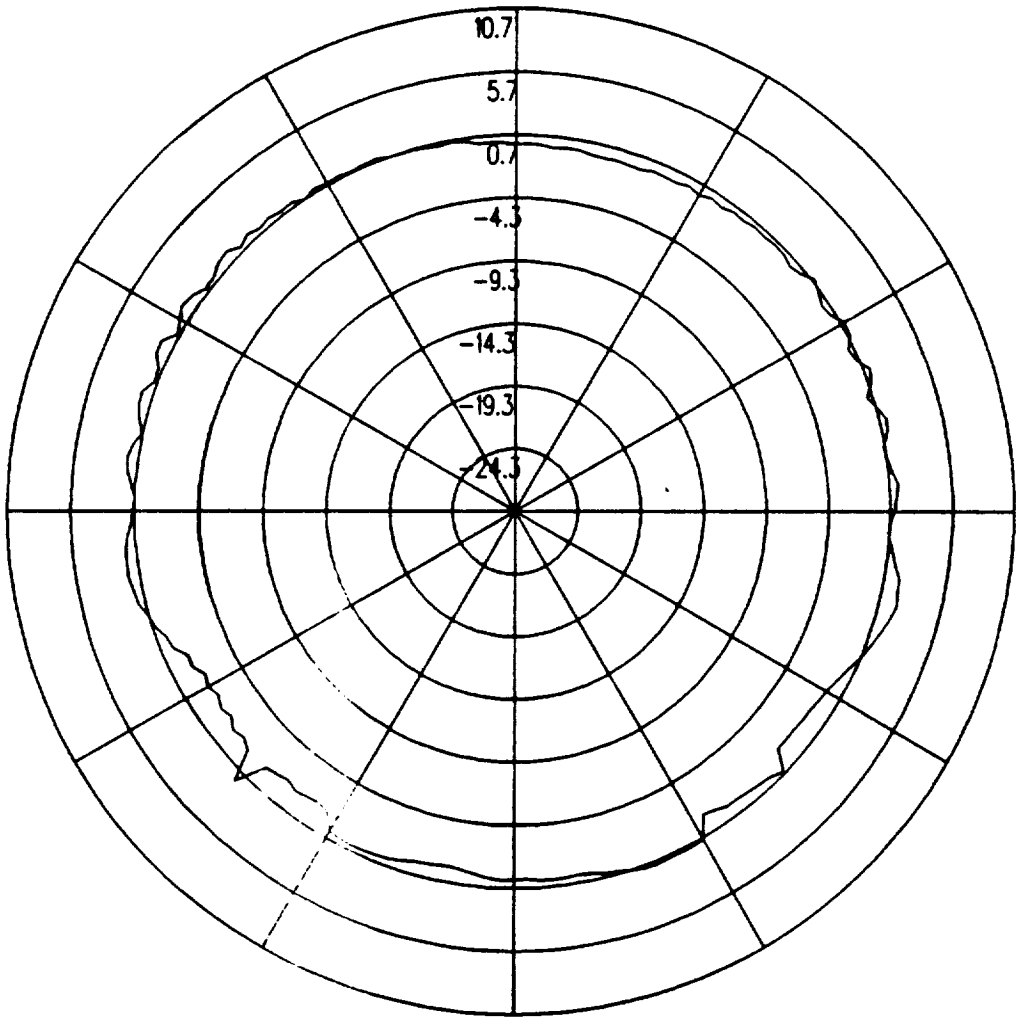

Figure 5.7: UTD calculated conical plane pattern 30° above the horizon for batwing antenna on a P-3C for right hand circular polarization at 300 MHz.(Test Location 1)

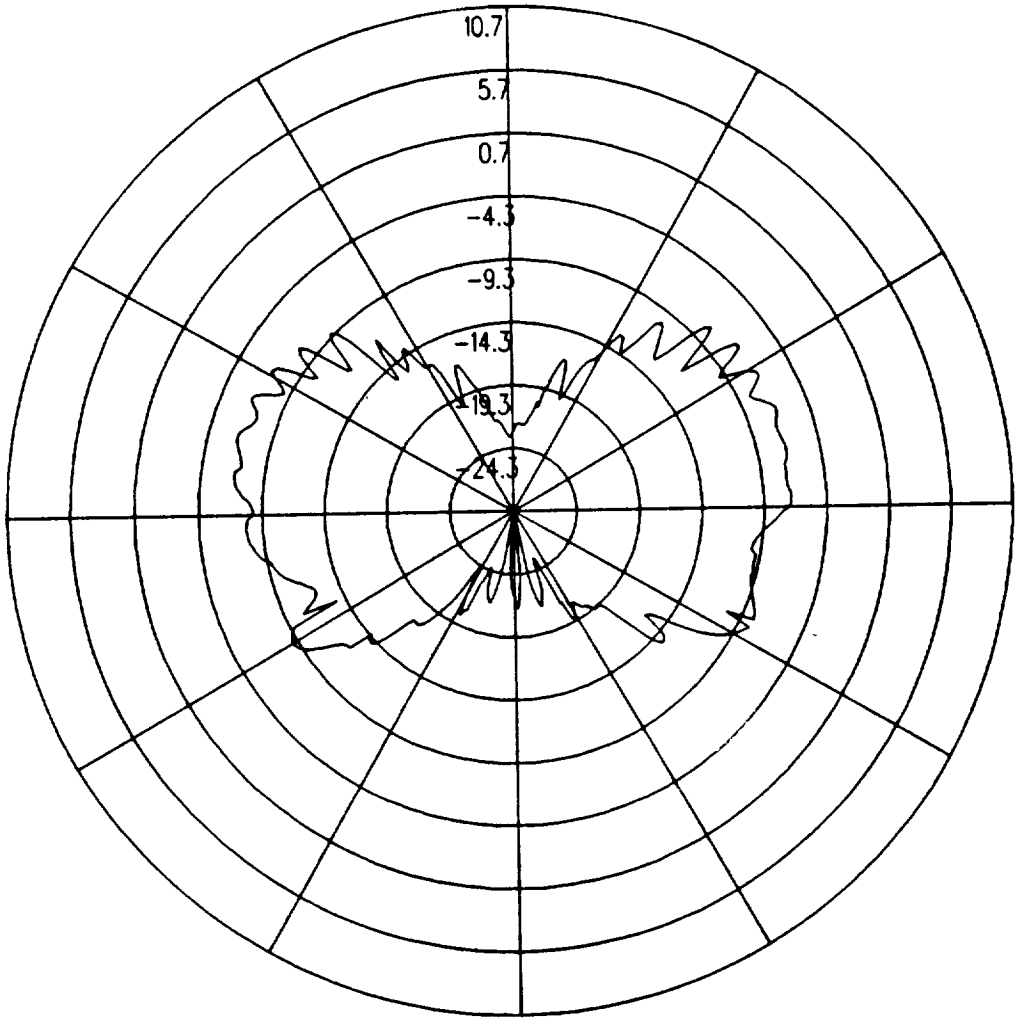

Figure 5.8: UTD calculated roll plane pattern for batwing antenna on a P-3C for left hand circular polarization at 300 MHz. (Test Location 1)

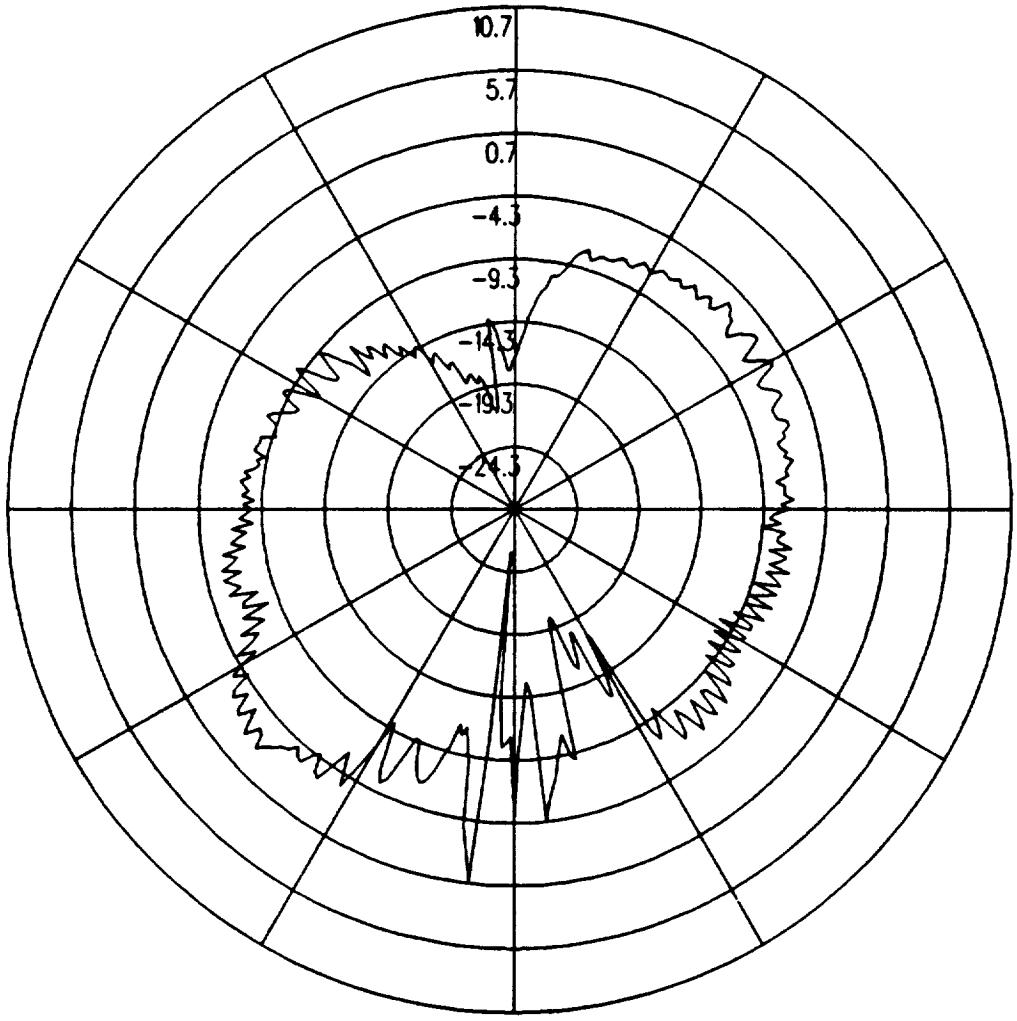

Figure 5.9: UTD calculated azimuth plane pattern for batwing antenna on a P-3C for left hand circular polarization at 300 MHz. (Test Location 1)

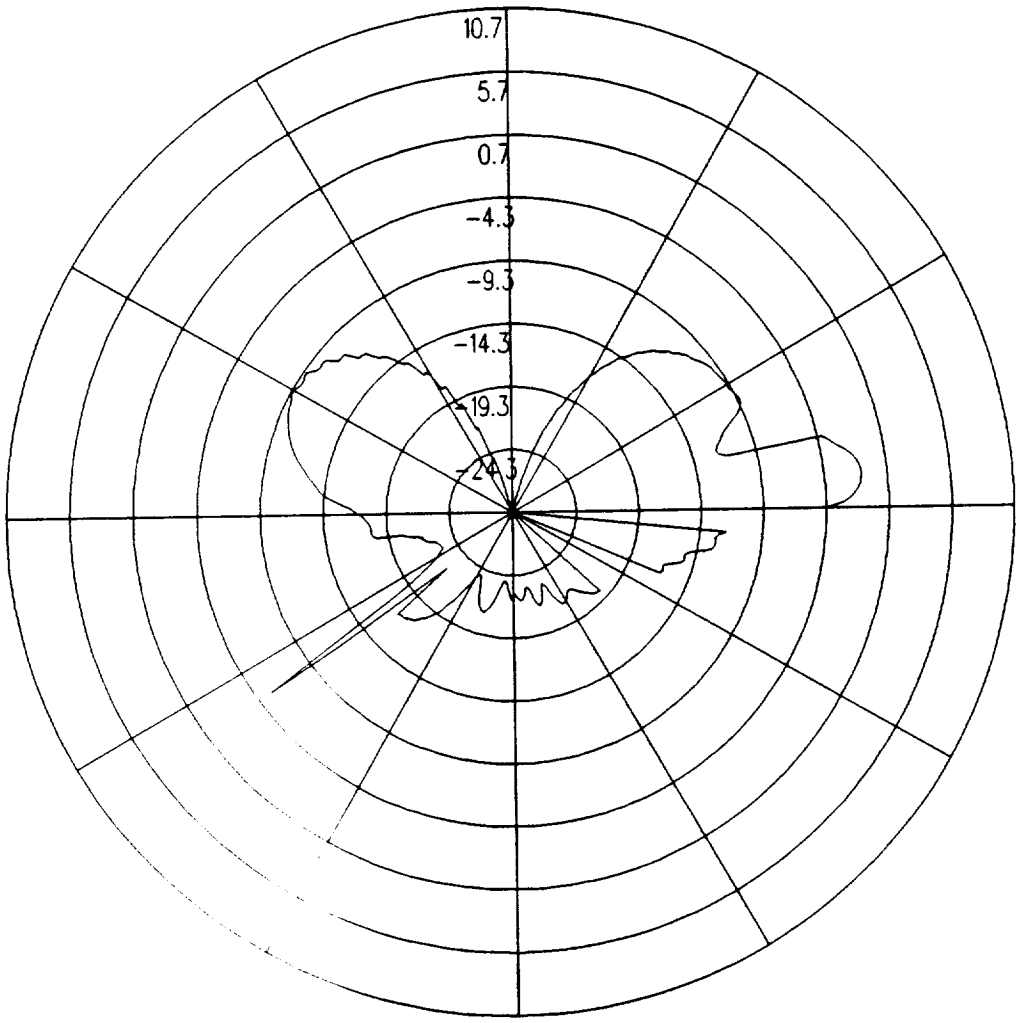

Figure 5.10: UTD calculated elevation plane pattern for batwing antenna on a P-3C for left hand circular polarization at 300 MHz. (Test Location 1)

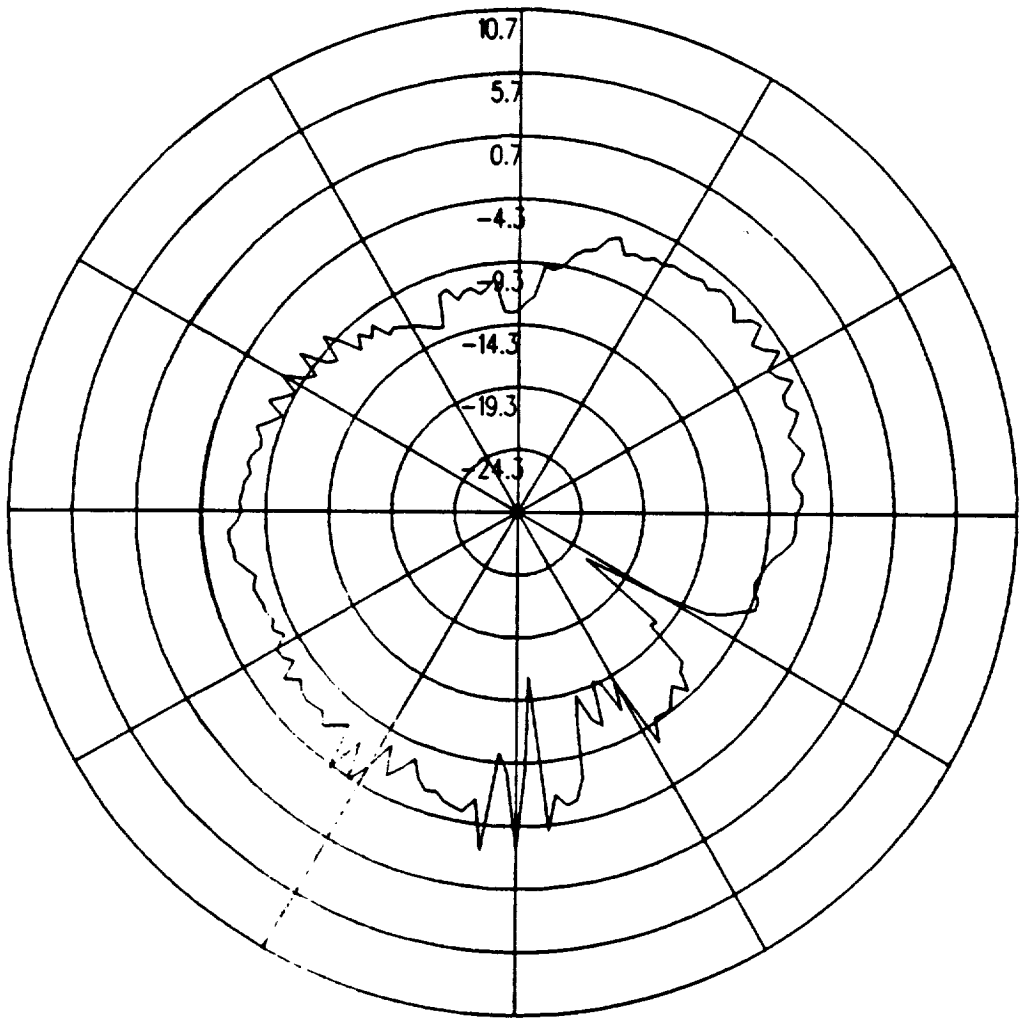

Figure 5.11: UTD calculated conical plane pattern 10° above the horizon for batwing antenna on a P-3C for left hand circular polarization at 300 MHz.(Test Location 1)

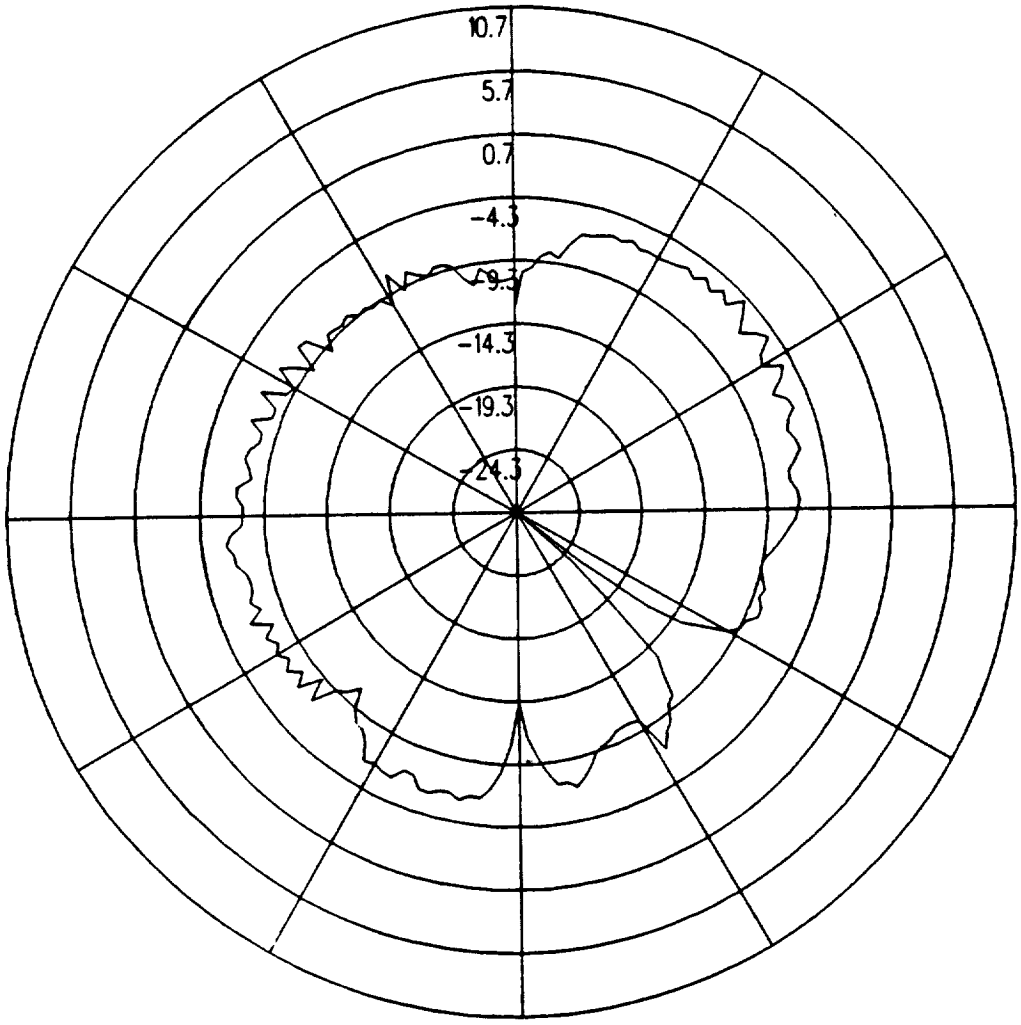

Figure 5.12: UTD calculated conical plane pattern 20° above the horizon for batwing antenna on a P-3C for left hand circular polarization at 300 MHz.(Test Location 1)

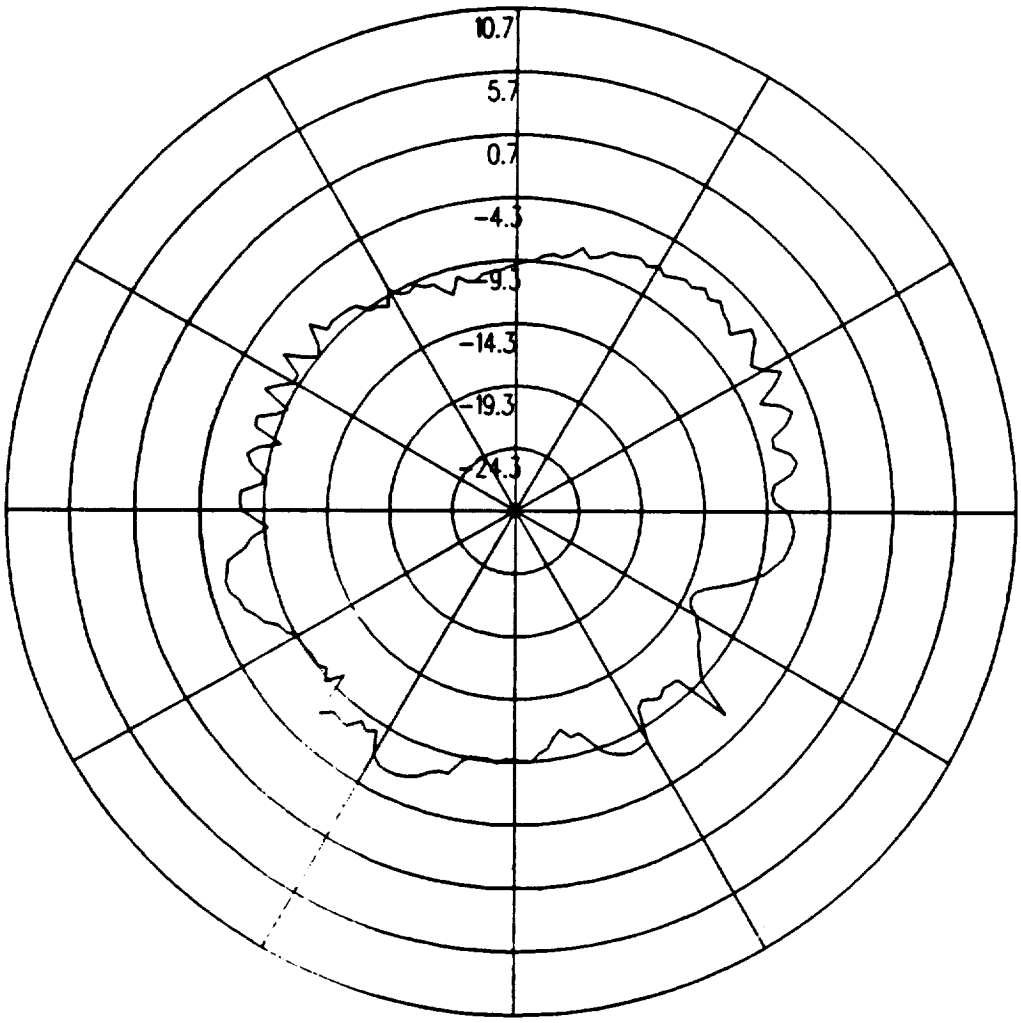

Figure 5.13: UTD calculated conical plane pattern 30° above the horizon for batwing antenna on a P-3C for left hand circular polarization at 300 MHz.(Test Location 1)

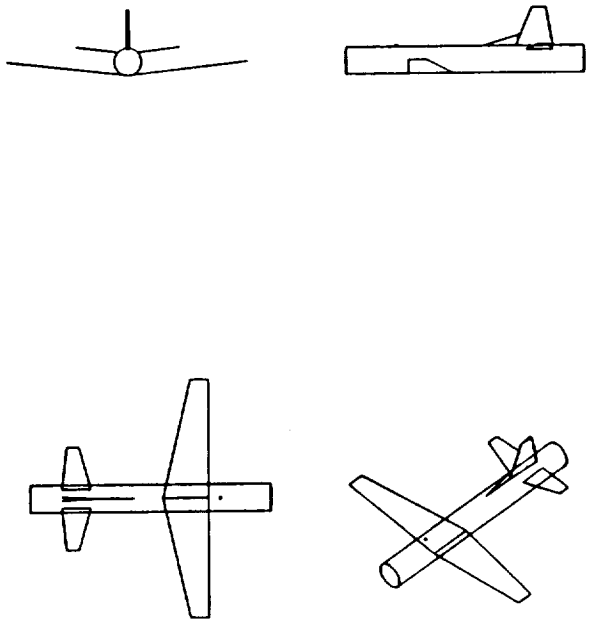

Figure 5.14: Geometry of the model of the P-3C aircraft used in the NEC-BSC code showing the location of the antenna.

5.2 Test Location 2

The antenna is located as illustrated in Figure 5.14, which also shows the computer model used to generate the results. The calculated results at 300 MHz are shown for the roll plane in Figure 5.15, for the azimuth plane in Figure 5.16, for the elevation plane in Figure 5.17, for the conical plane 10° above the horizon in Figure 5.18, for the conical plane 20° above the horizon in Figure 5.19, and for the conical plane 30° above the horizon in Figure 5.20 all for right hand polarization. The cross polarized fields are shown for the roll plane in Figure 5.21, for the azimuth plane in Figure 5.22, for the elevation plane in Figure 5.23, for the conical plane 10° above the horizon in Figure 5.24, for the conical plane 20° above the horizon in Figure 5.25, and for the conical plane 30° above the horizon in Figure 5.26 all for left hand polarization.

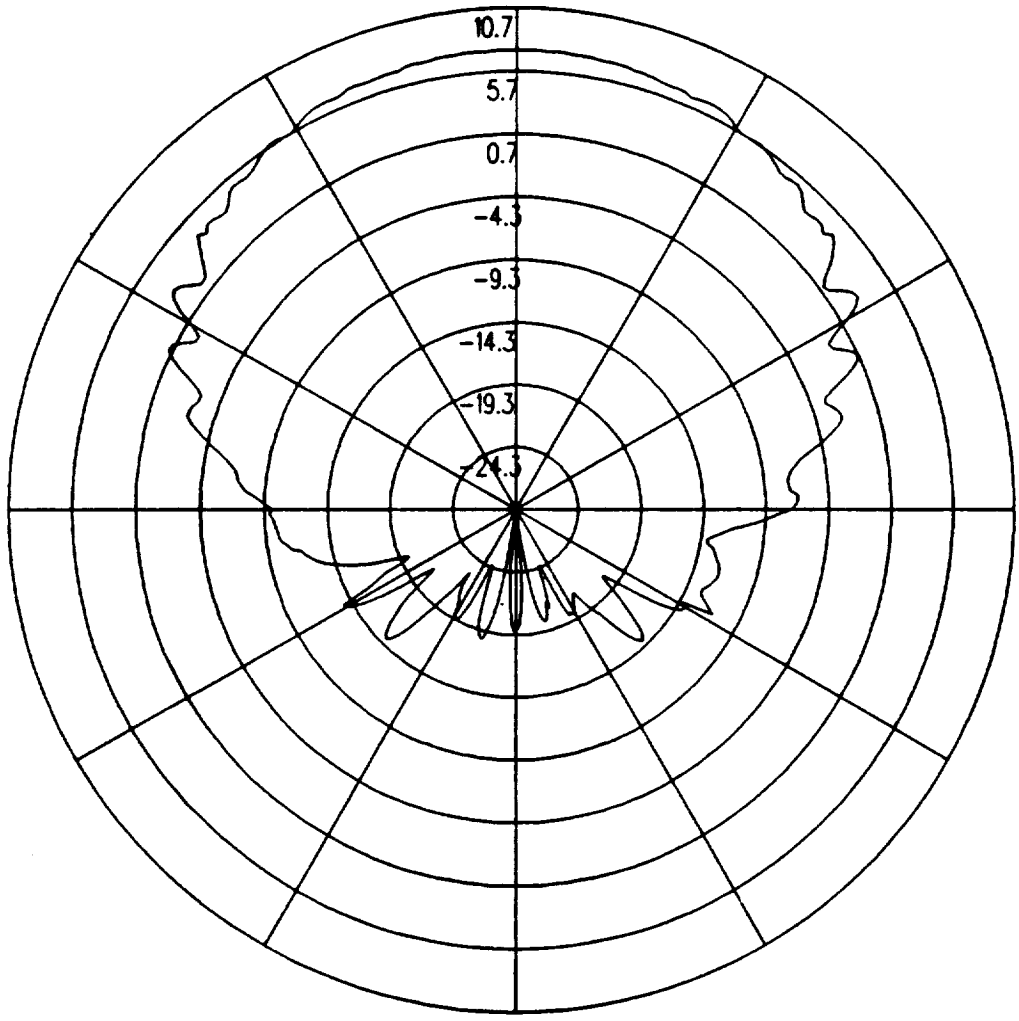

Figure 5.15: UTD calculated roll plane pattern for batwing antenna on a P-3C for right hand circular polarization at 300 MHz. (Test Location 2)

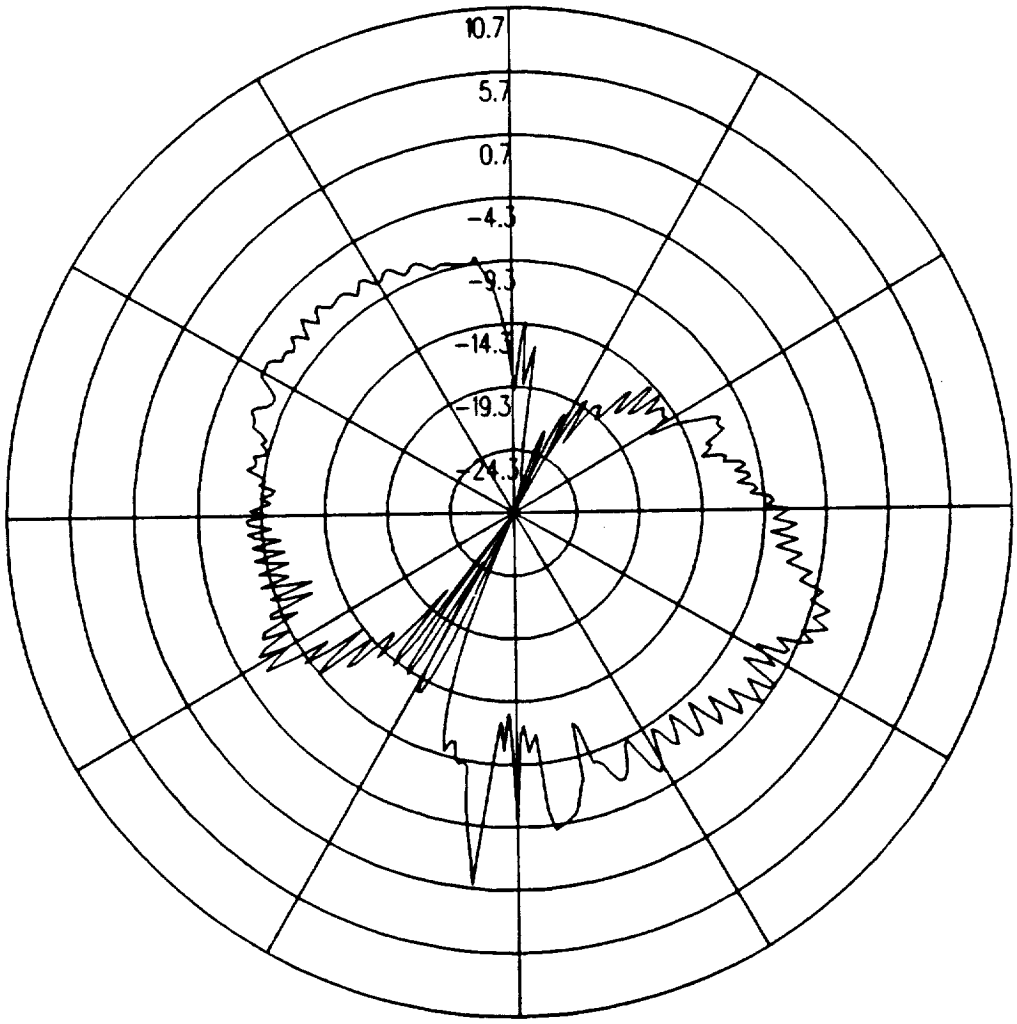

Figure 5.16: UTD calculated azimuth plane pattern for batwing antenna on a P-3C for right hand circular polarization at 300 MHz. (Test Location 2)

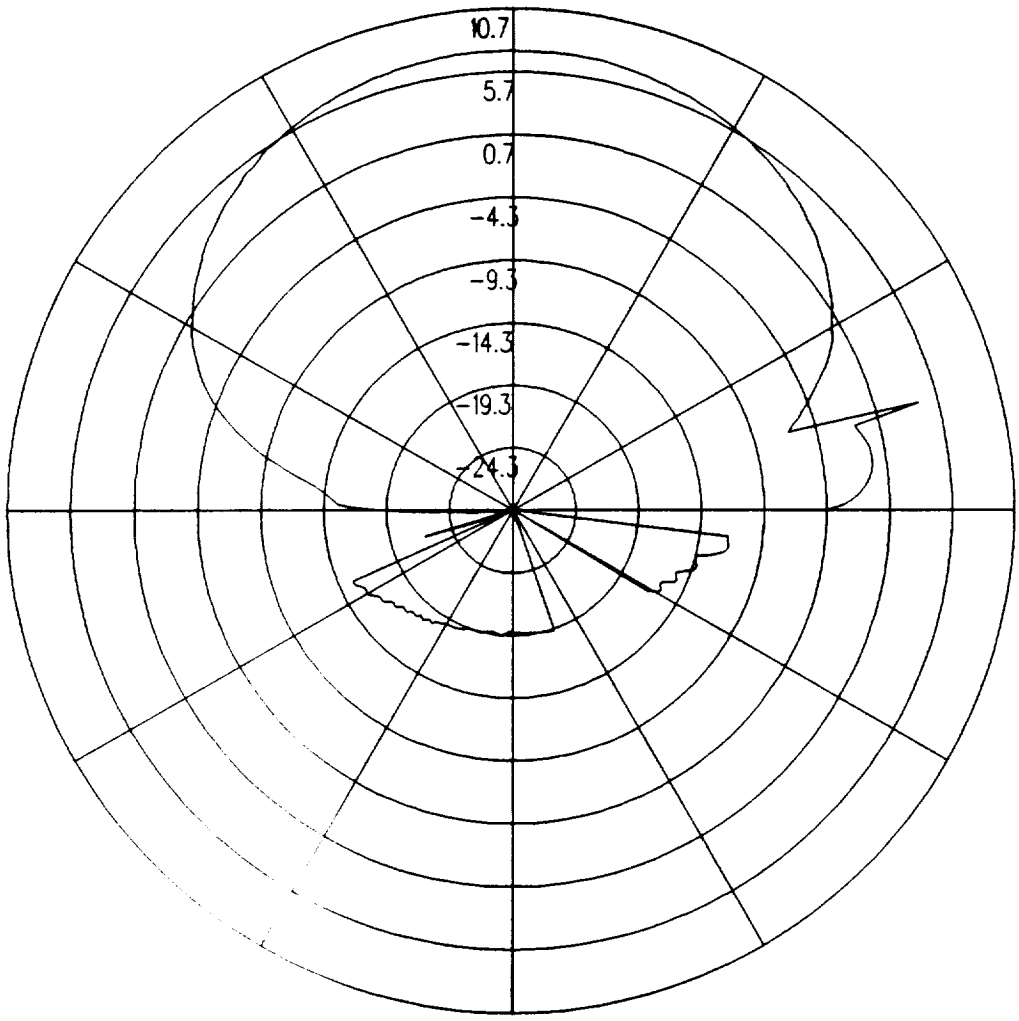

Figure 5.17: UTD calculated elevation plane pattern for batwing antenna on a P-3C for right hand circular polarization at 300 MHz. (Test Location 2)

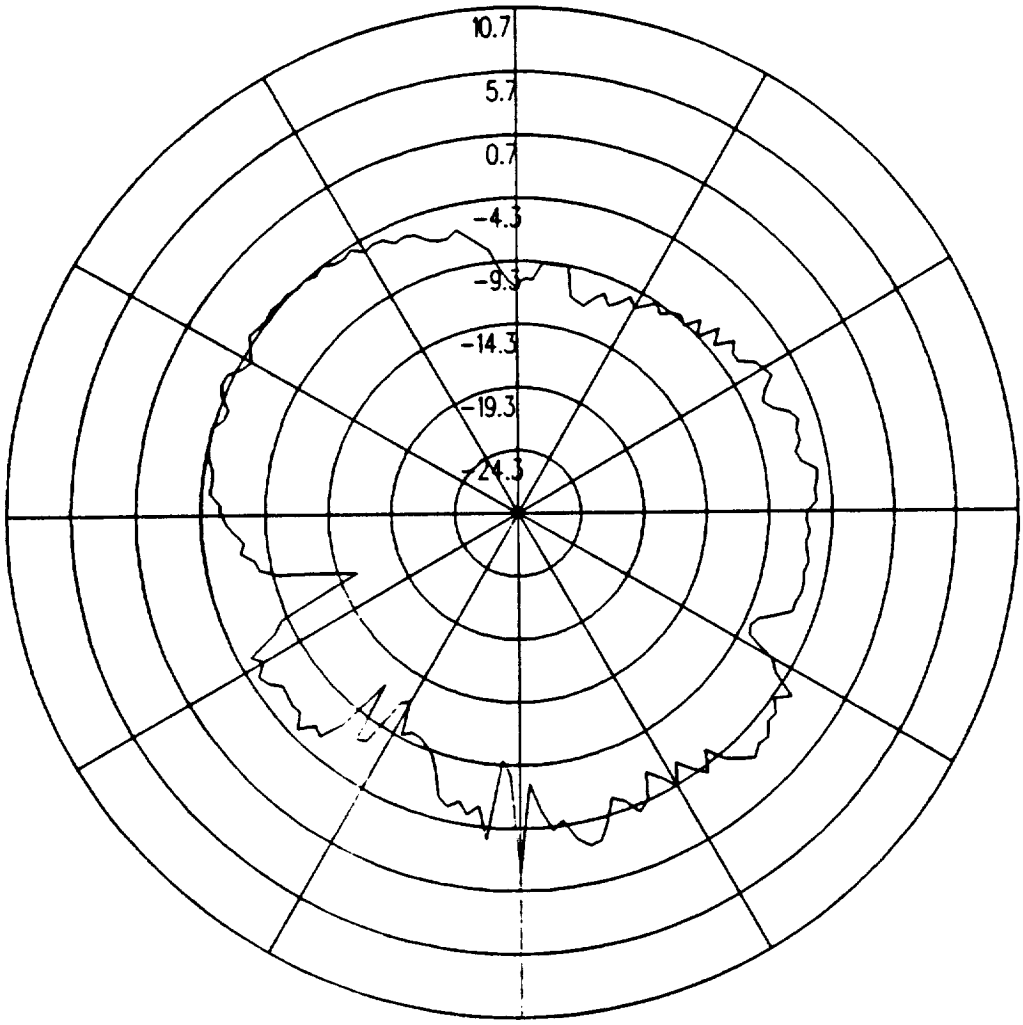

Figure 5.18: UTD calculated conical plane pattern 10° above the horizon for batwing antenna on a P-3C for right hand circular polarization at 300 MHz.(Test Location 2)

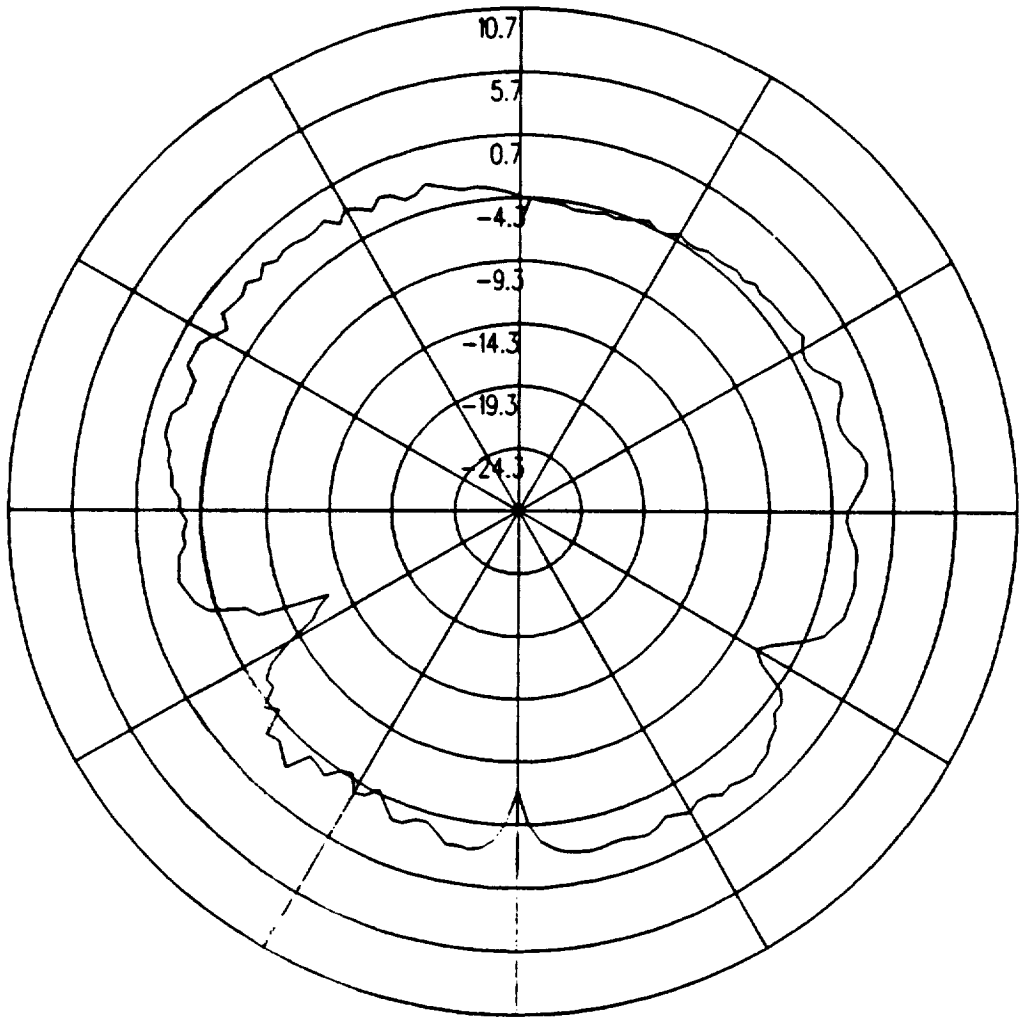

Figure 5.19: UTD calculated conical plane pattern 20° above the horizon for batwing antenna on a P-3C for right hand circular polarization at 300 MHz.(Test Location 2)

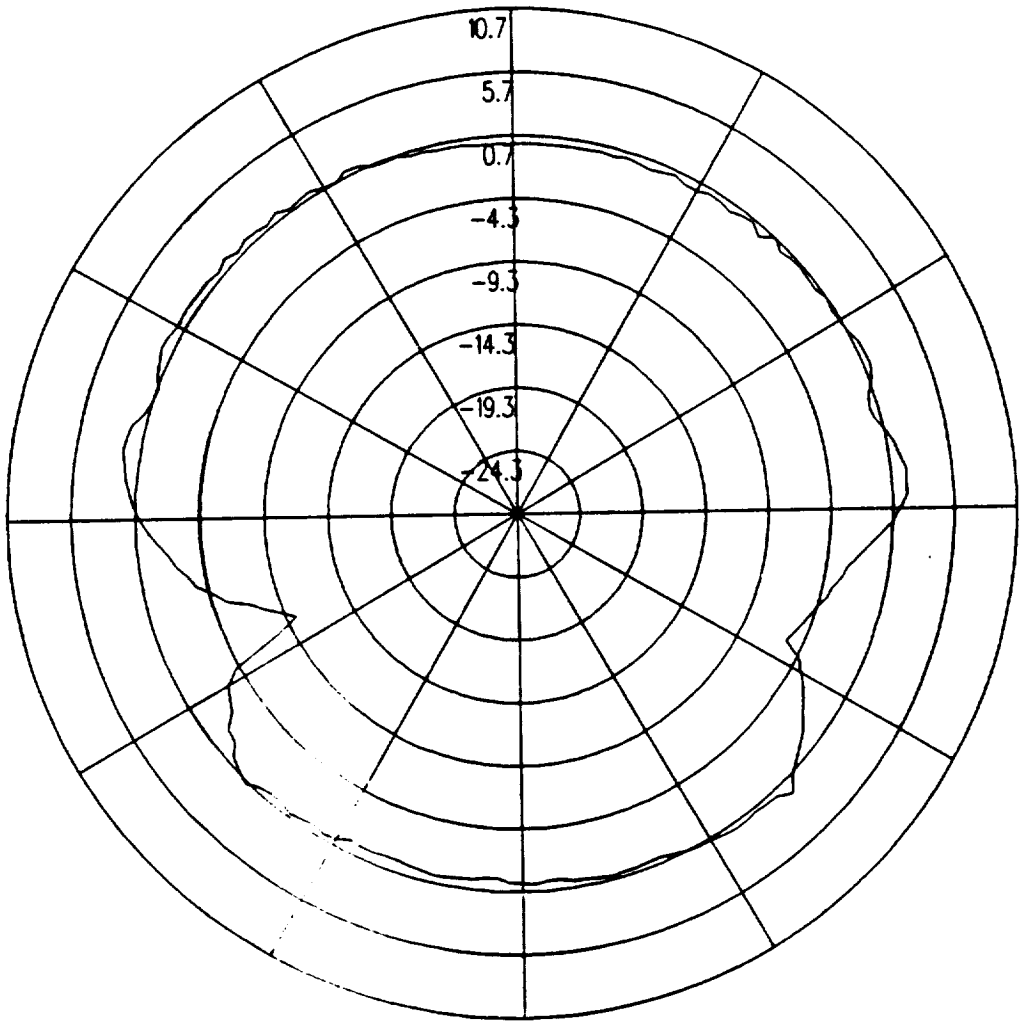

Figure 5.20: UTD calculated conical plane pattern 30° above the horizon for batwing antenna on a P-3C for right hand circular polarization at 300 MHz.(Test Location 2)

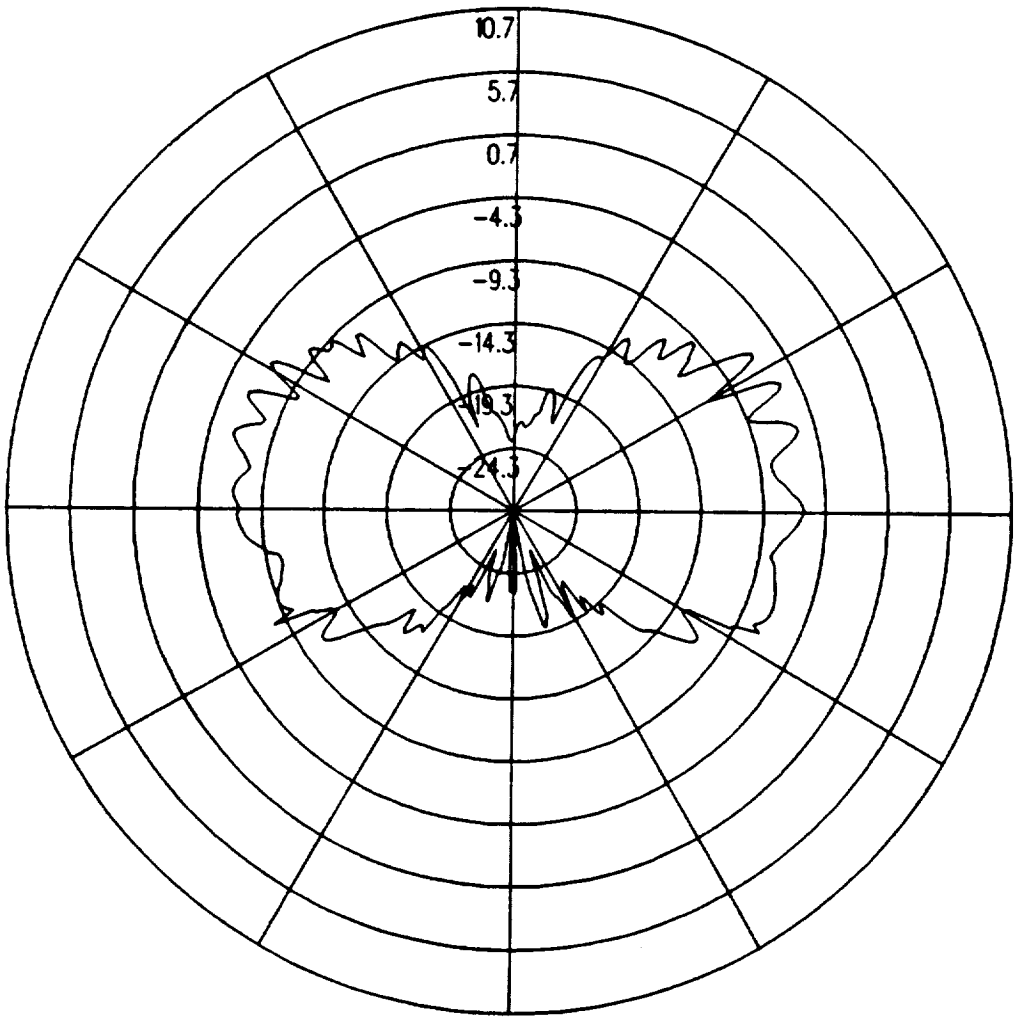

Figure 5.21: UTD calculated roll plane pattern for batwing antenna on a P-3C for left hand circular polarization at 300 MHz. (Test Location 2)

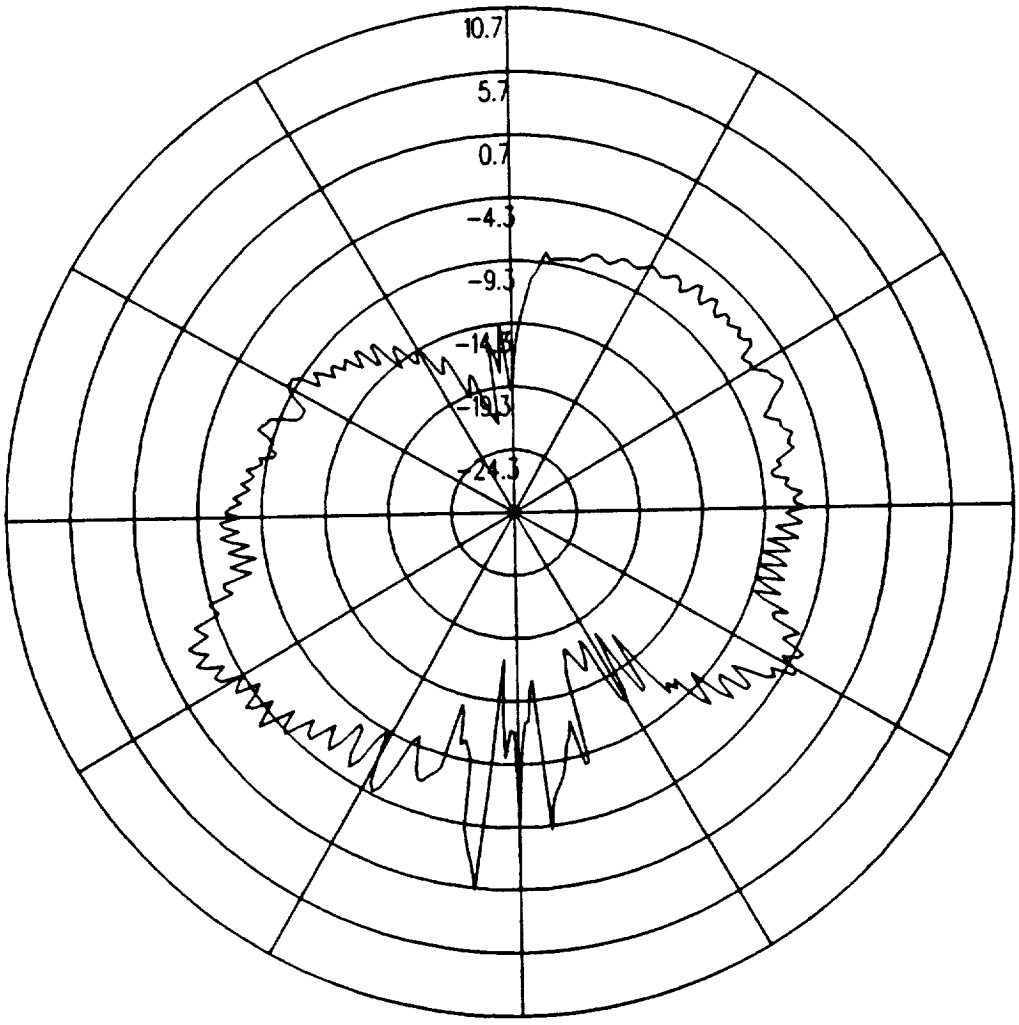

Figure 5.22: UTD calculated azimuth plane pattern for batwing antenna on a P-3C for left hand circular polarization at 300 MHz. (Test Location 2)

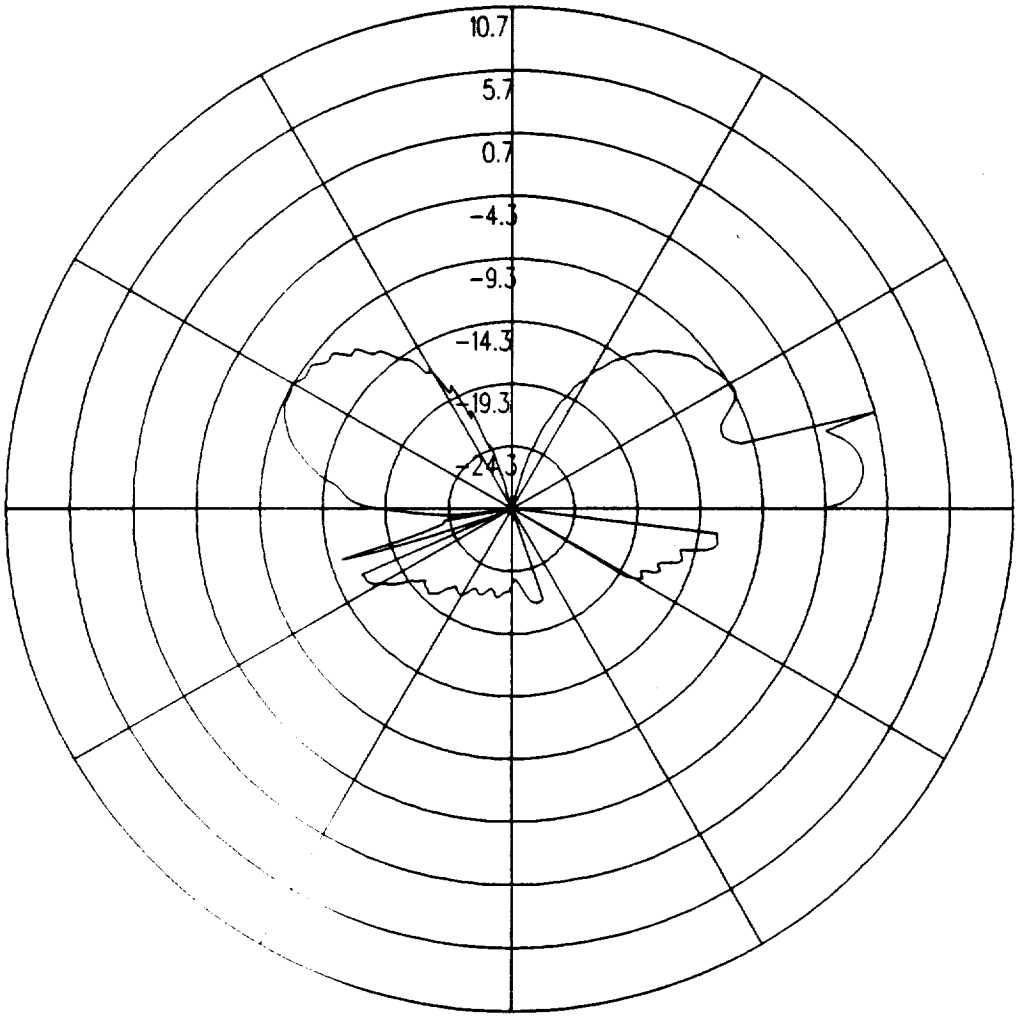

Figure 5.23: UTD calculated elevation plane pattern for batwing antenna on a P-3C for left hand circular polarization at 300 MHz. (Test Location 2)

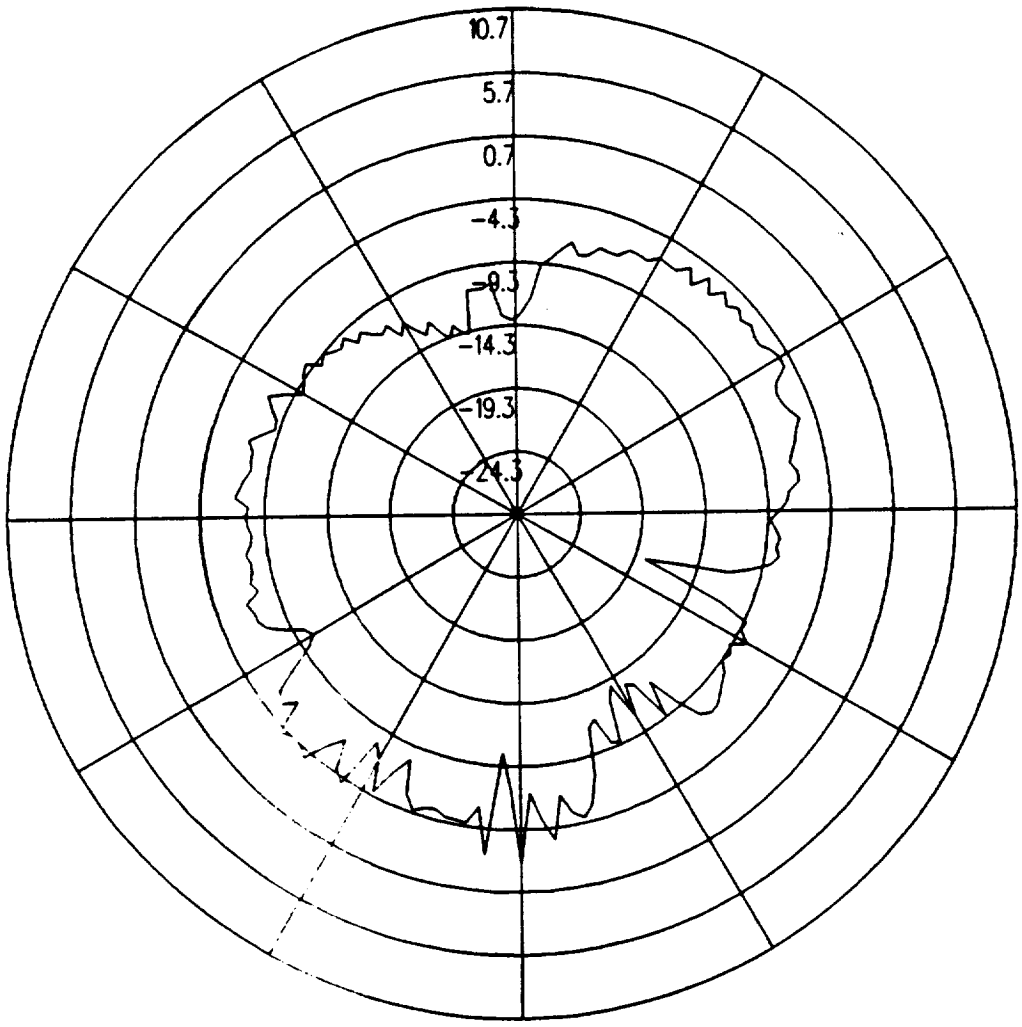

Figure 5.24: UTD calculated conical plane pattern 10° above the horizon for batwing antenna on a P-3C for left hand circular polarization at 300 MHz.(Test Location 2)

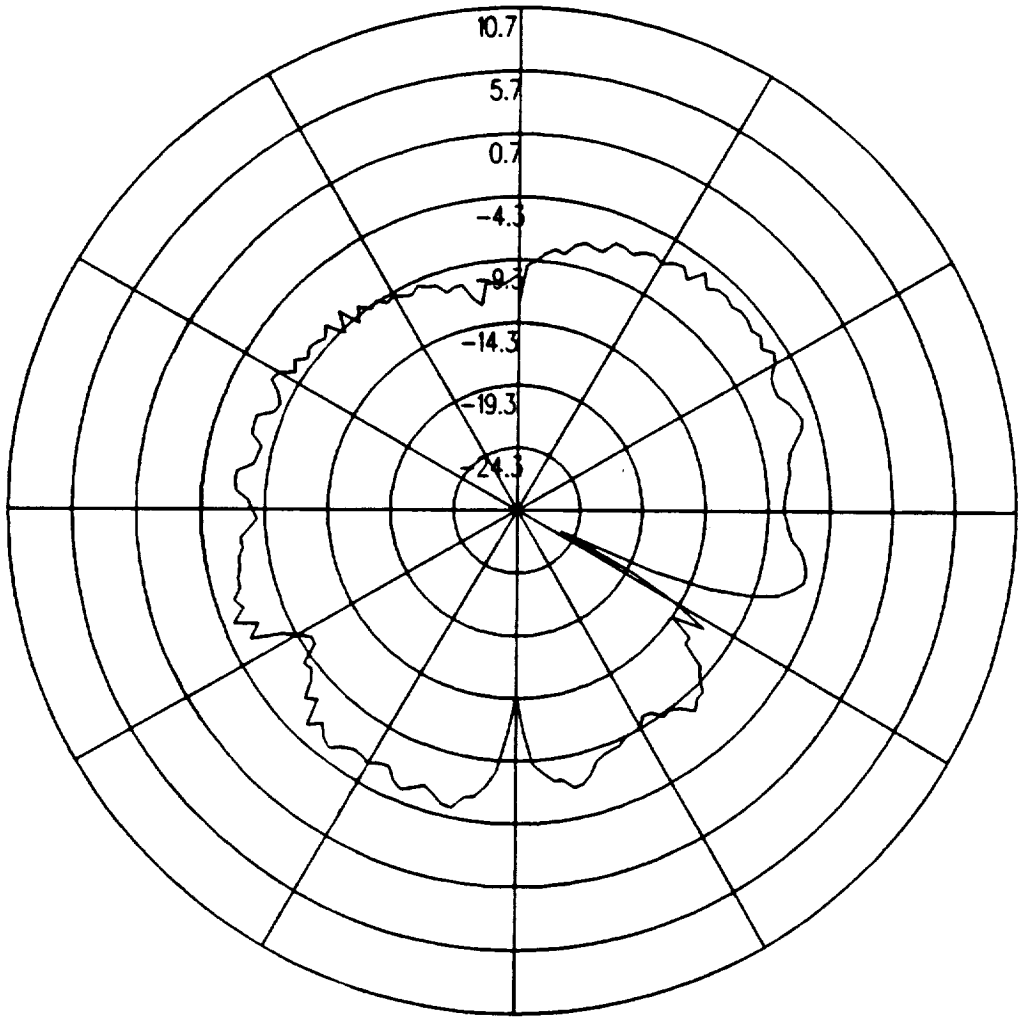

Figure 5.25: UTD calculated conical plane pattern 20° above the horizon for batwing antenna on a P-3C for left hand circular polarization at 300 MHz.(Test Location 2)

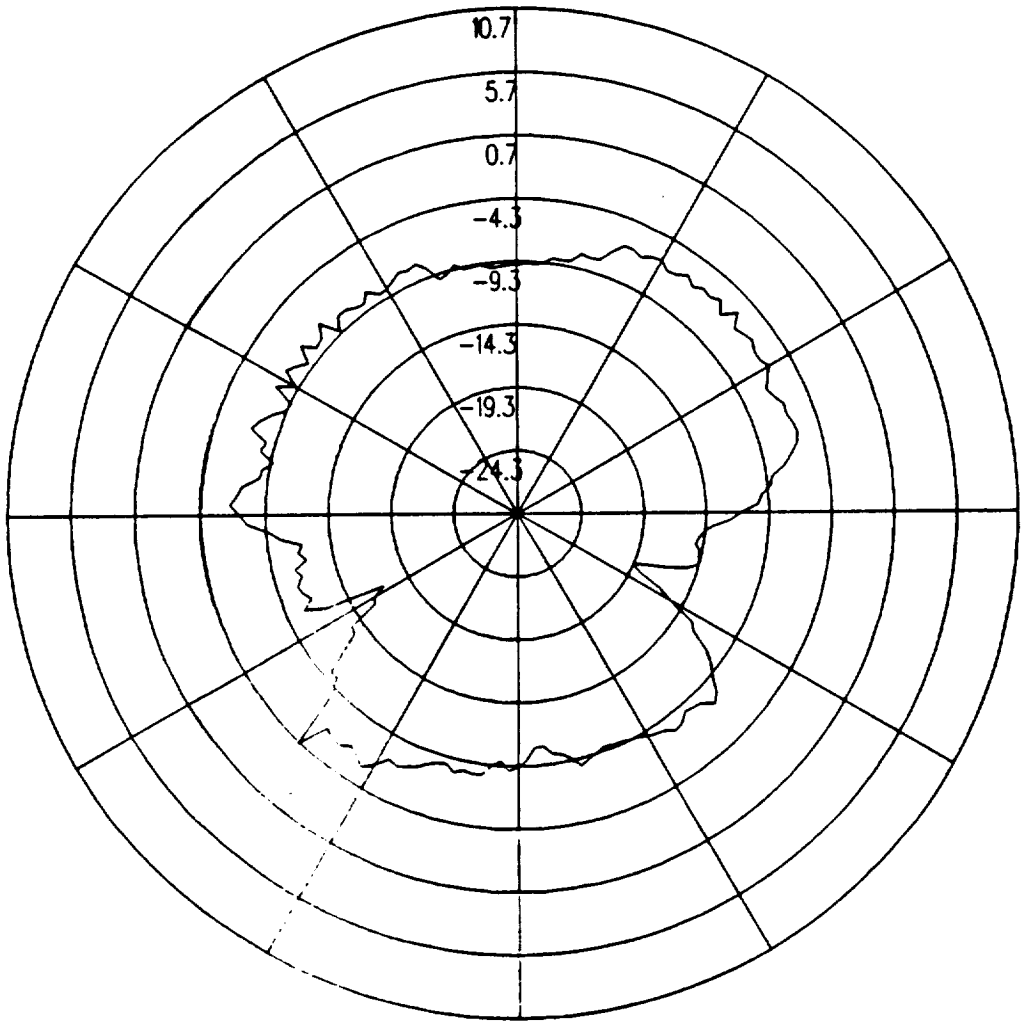

Figure 5.26: UTD calculated conical plane pattern 30° above the horizon for batwing antenna on a P-3C for left hand circular polarization at 300 MHz.(Test Location 2)

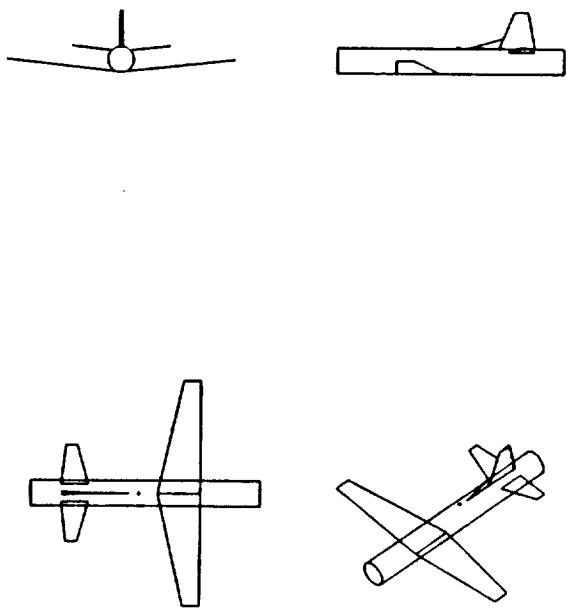

Figure 5.27: Geometry of the model of the P-3C aircraft used in the NEC-BSC code showing the location of the antenna.

5.3 Test Location 3

The antenna is located as illustrated in Figure 5.27, which also shows the computer model used to generate the results. The calculated results at 300 MHz are shown for the roll plane in Figure 5.28, for the azimuth plane in Figure 5.29, for the elevation plane in Figure 5.30, for the conical plane 10° above the horizon in Figure 5.31, for the conical plane 20° above the horizon in Figure 5.32, and for the conical plane 30° above the horizon in Figure 5.33 all for right hand polarization. The cross polarized fields are shown for the roll plane in Figure 5.34, for the azimuth plane in Figure 5.35, for the elevation plane in Figure 5.36, for the conical plane 10° above the horizon in Figure 5.37, for the conical plane 20° above the horizon in Figure 5.38, and for the conical plane 30° above the horizon in Figure 5.39 all for left hand polarization.

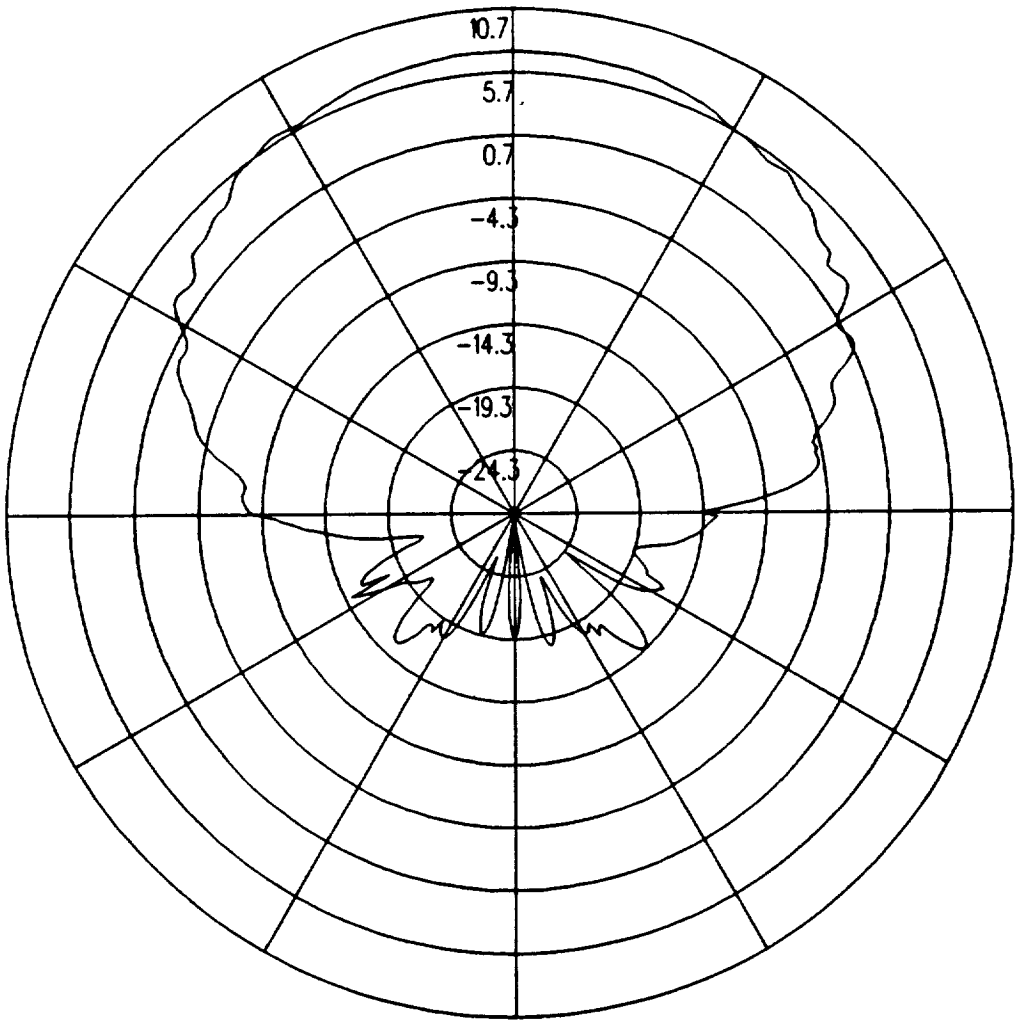

Figure 5.28: UTD calculated roll plane pattern for batwing antenna on a P-3C for right hand circular polarization at 300 MHz. (Test Location 3)

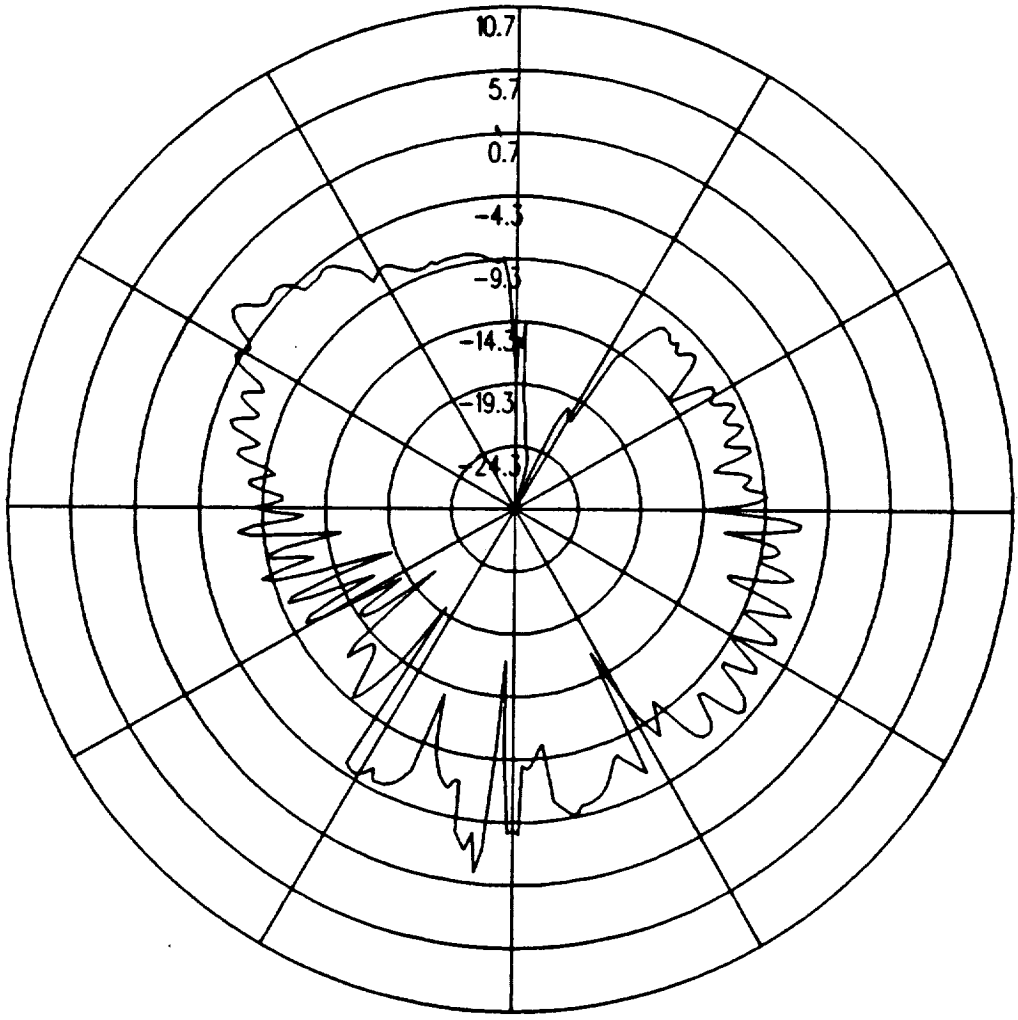

Figure 5.29: UTD calculated azimuth plane pattern for batwing antenna on a P-3C for right hand circular polarization at 300 MHz. (Test Location 3)

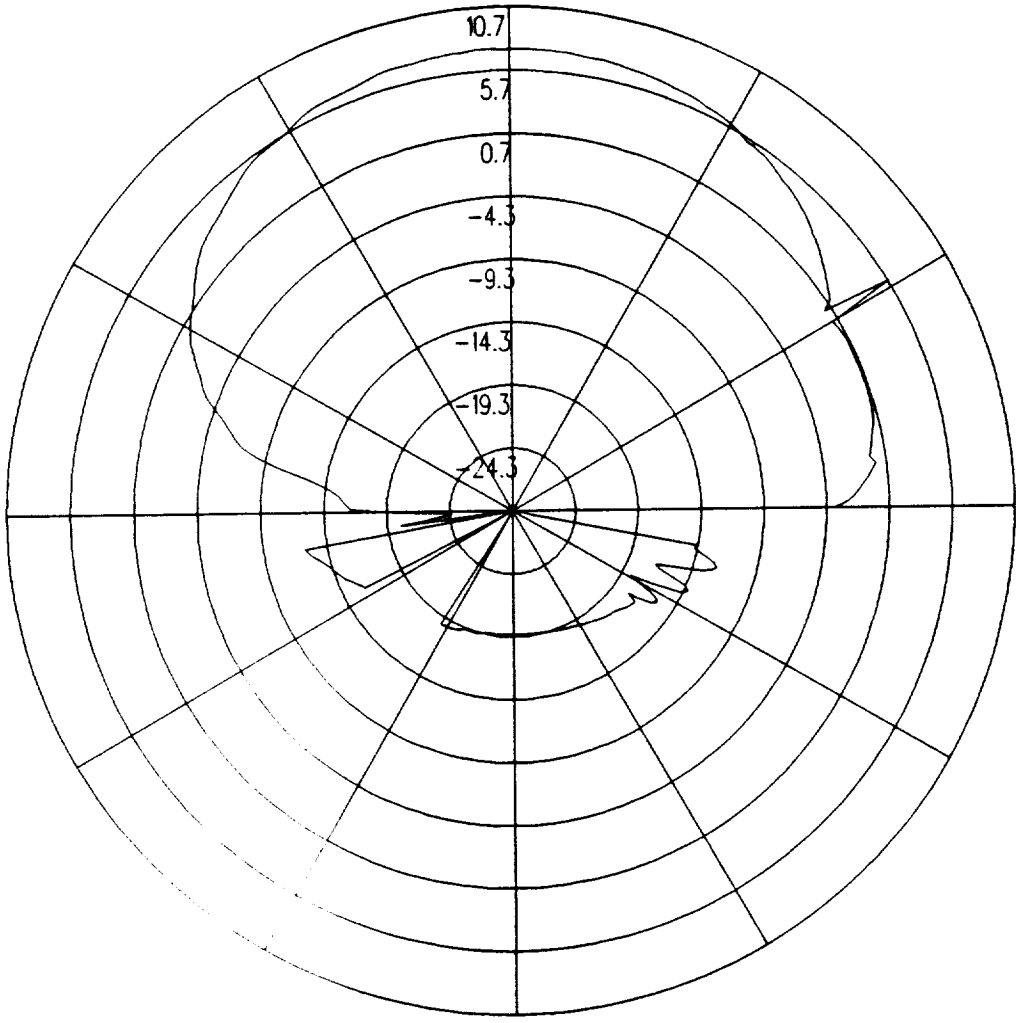

Figure 5.30: UTD calculated elevation plane pattern for batwing antenna on a P-3C for right hand circular polarization at 300 MHz. (Test Location 3)

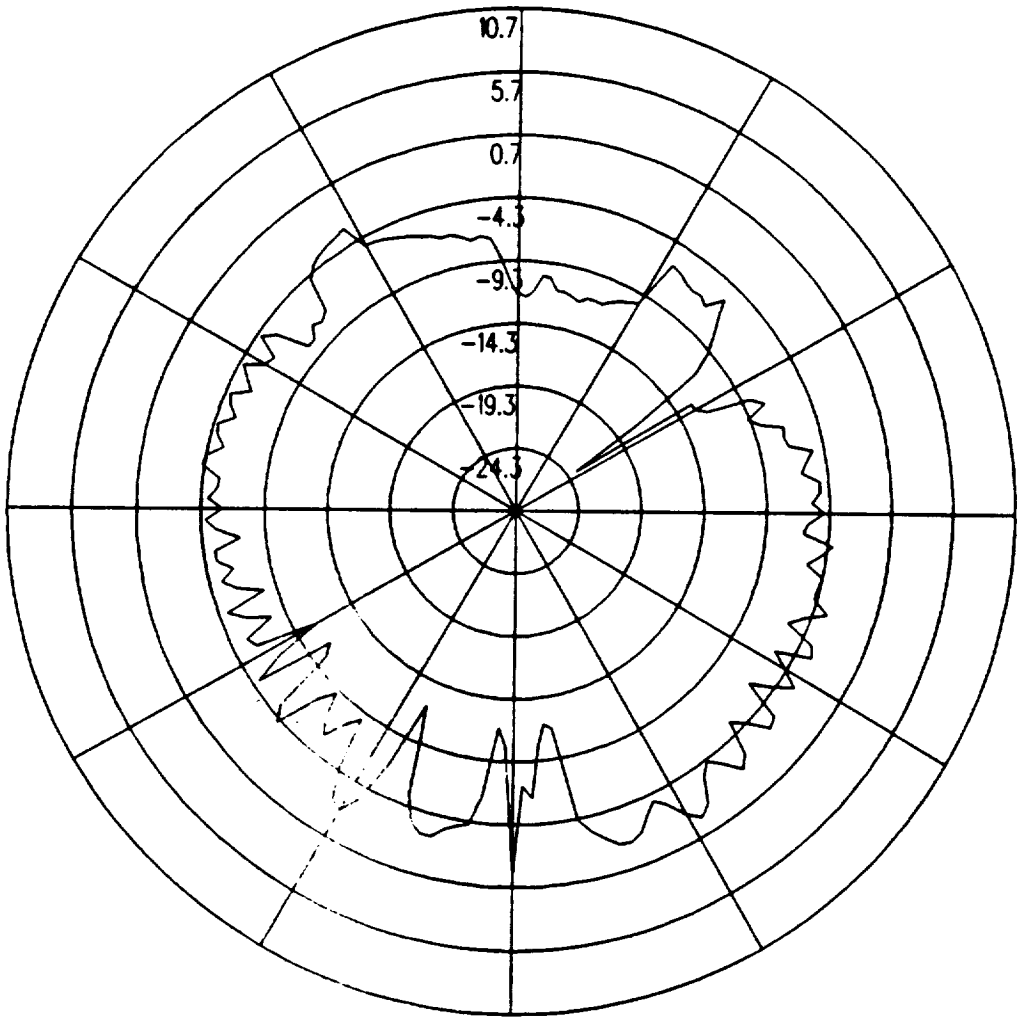

Figure 5.31: UTD calculated conical plane pattern 10° above the horizon for batwing antenna on a P-3C for right hand circular polarization at 300 MHz.(Test Location 3)

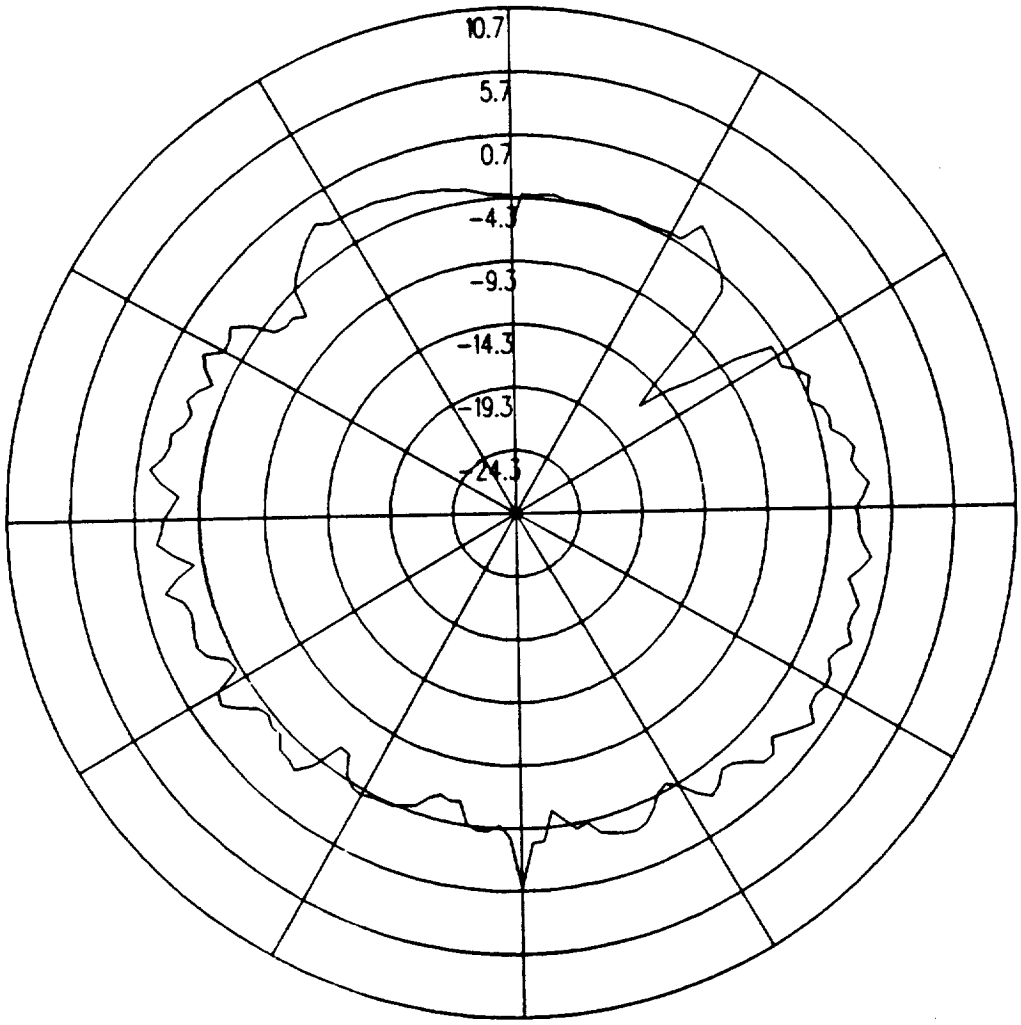

Figure 5.32: UTD calculated conical plane pattern 20° above the horizon for batwing antenna on a P-3C for right hand circular polarization at 300 MHz.(Test Location 3)

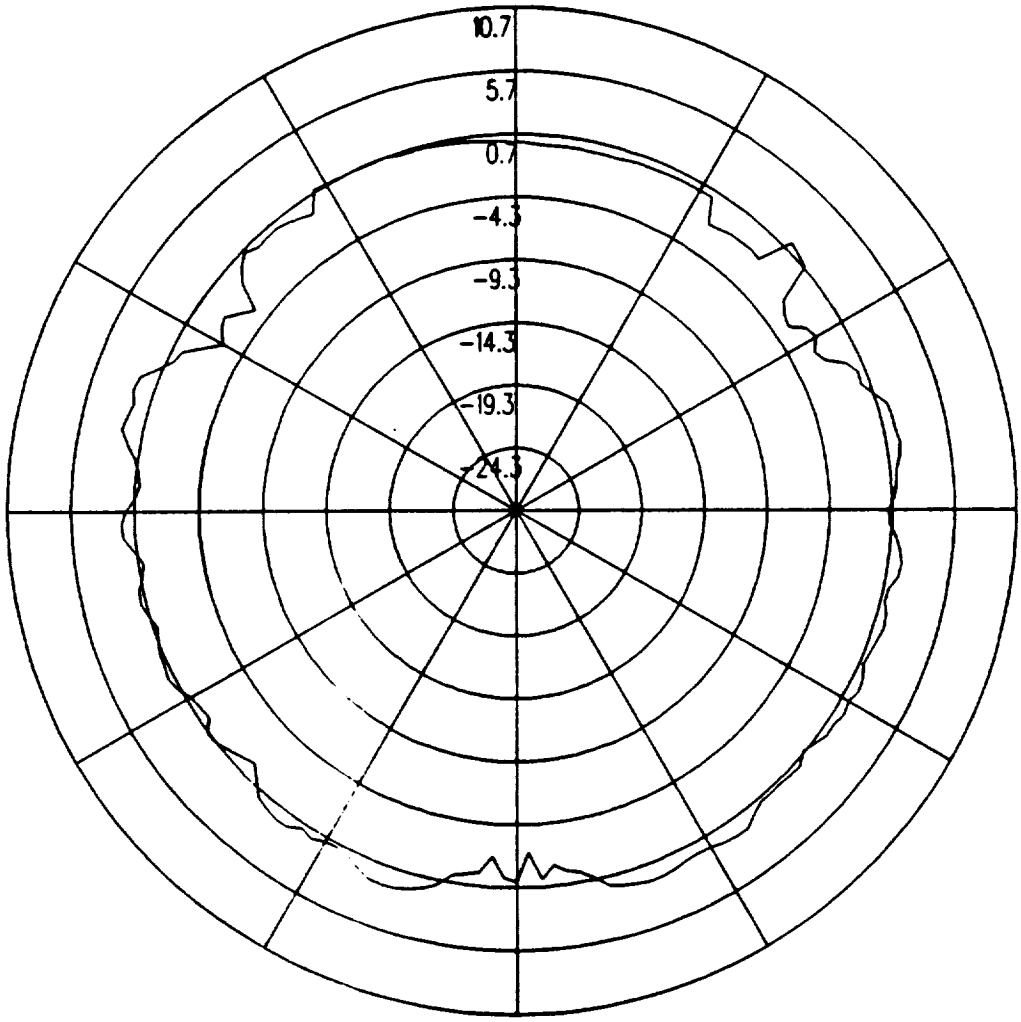

Figure 5.33: UTD calculated conical plane pattern 30° above the horizon for batwing antenna on a P-3C for right hand circular polarization at 300 MHz.(Test Location 3)

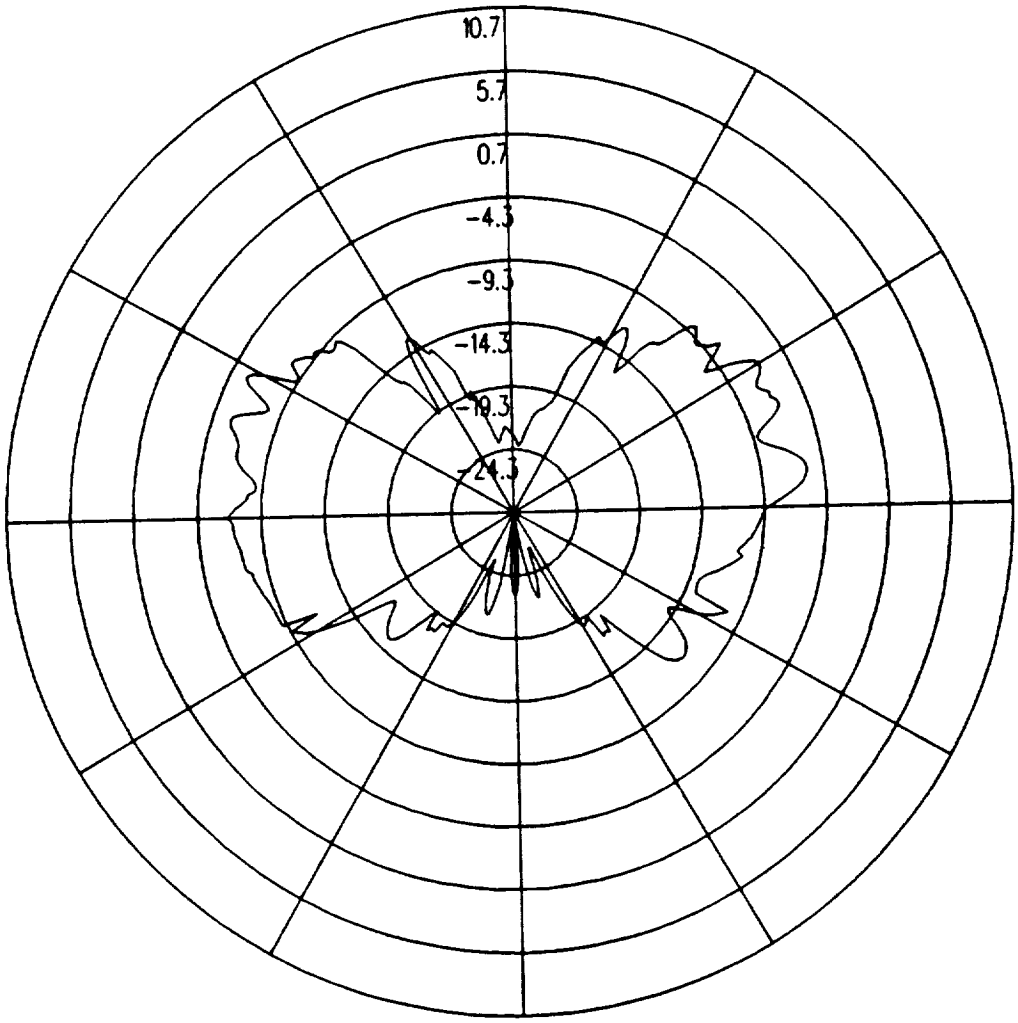

Figure 5.34: UTD calculated roll plane pattern for batwing antenna on a P-3C for left hand circular polarization at 300 MHz. (Test Location 3)

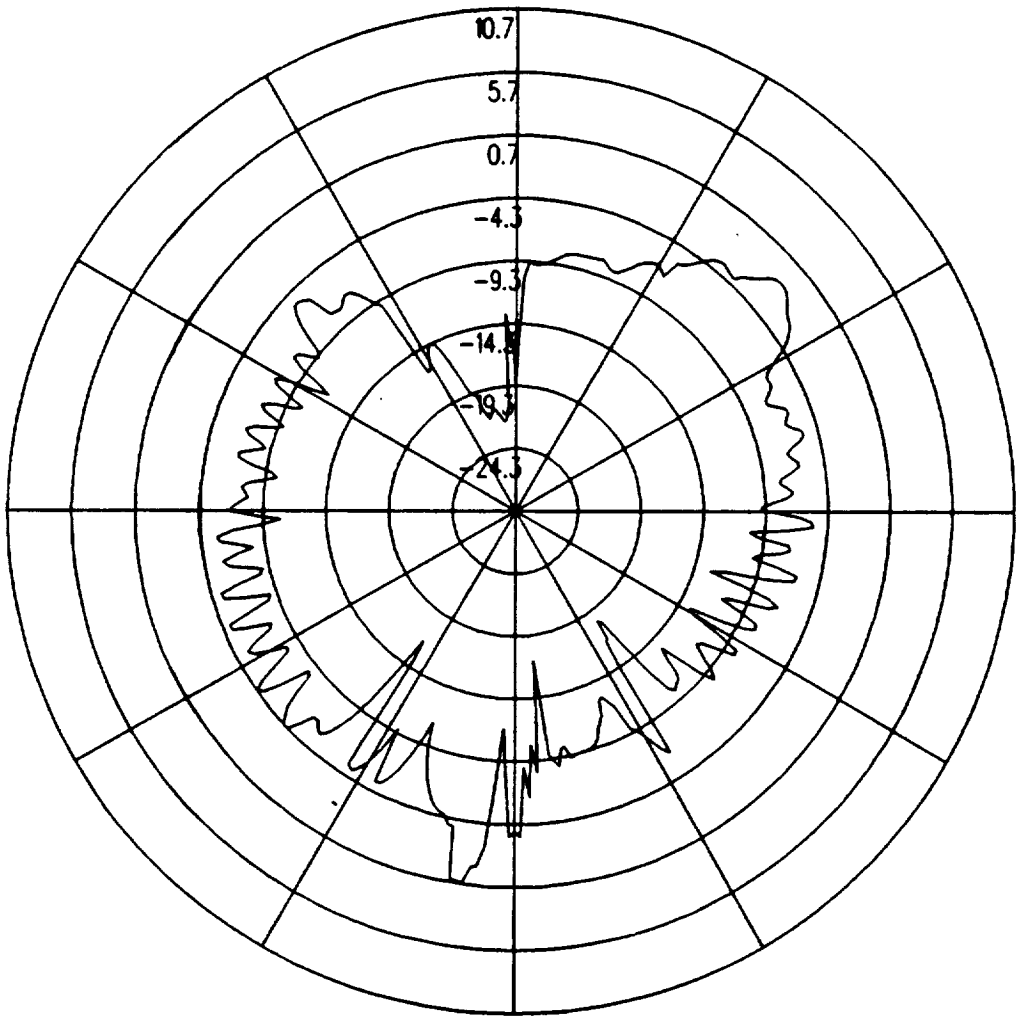

Figure 5.35: UTD calculated azimuth plane pattern for batwing antenna on a P-3C for left hand circular polarization at 300 MHz. (Test Location 3)

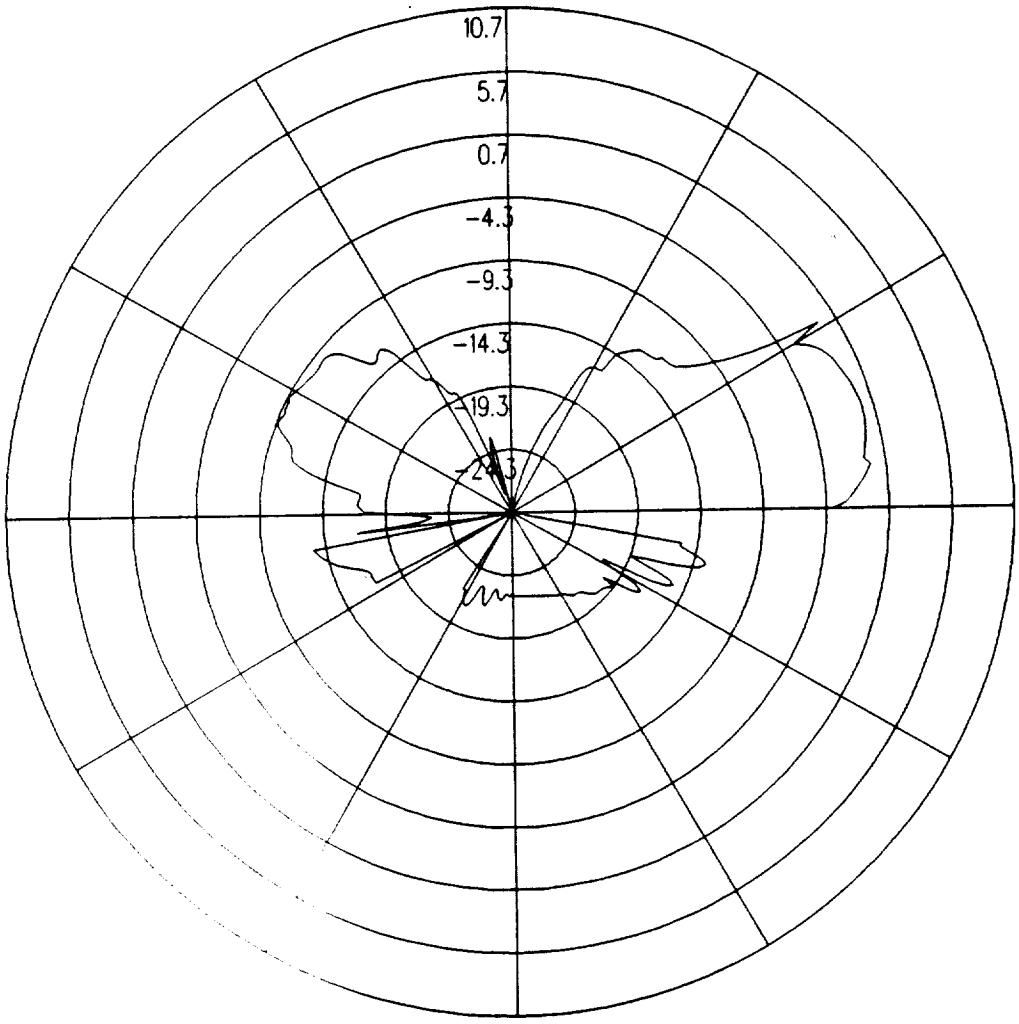

Figure 5.36: UTD calculated elevation plane pattern for batwing antenna on a P-3C for left hand circular polarization at 300 MHz. (Test Location 3)

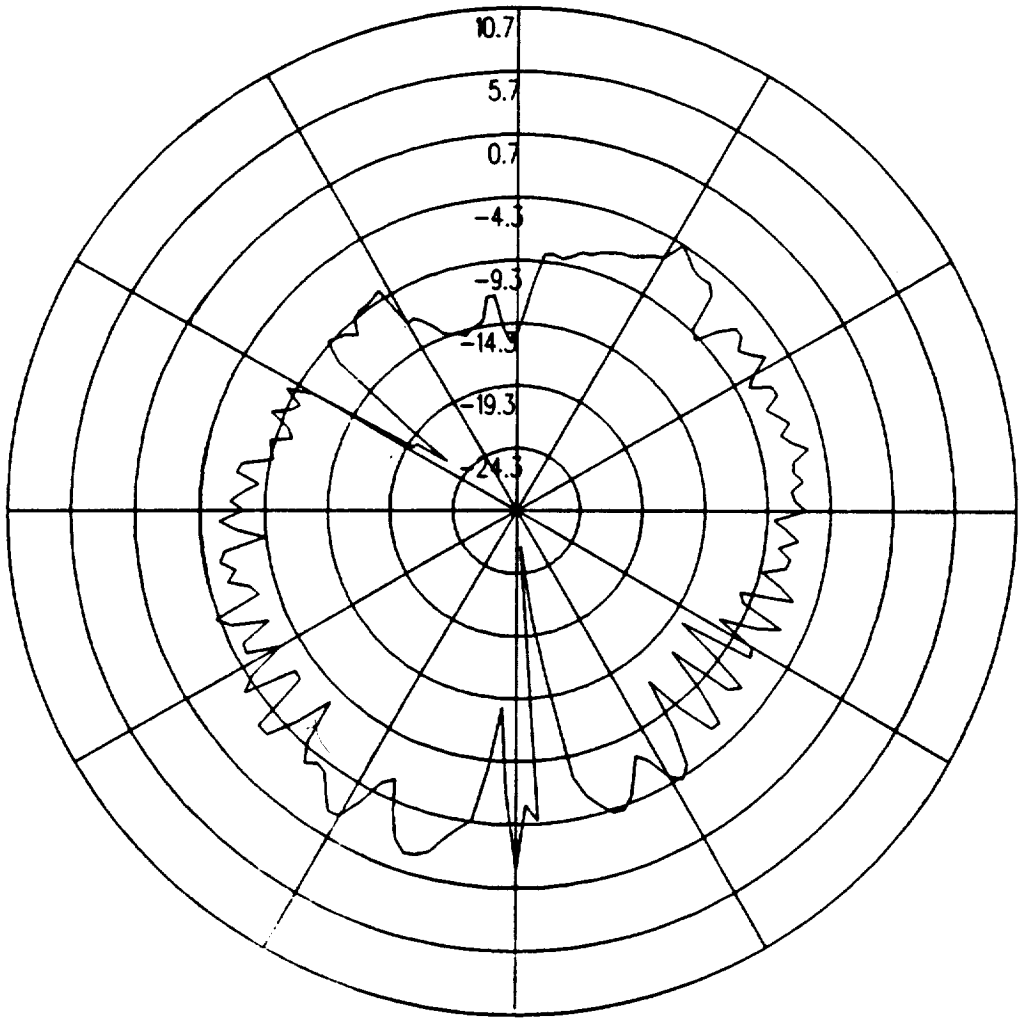

Figure 5.37: UTD calculated conical plane pattern 10° above the horizon for batwing antenna on a P-3C for left hand circular polarization at 300 MHz.(Test Location 3)

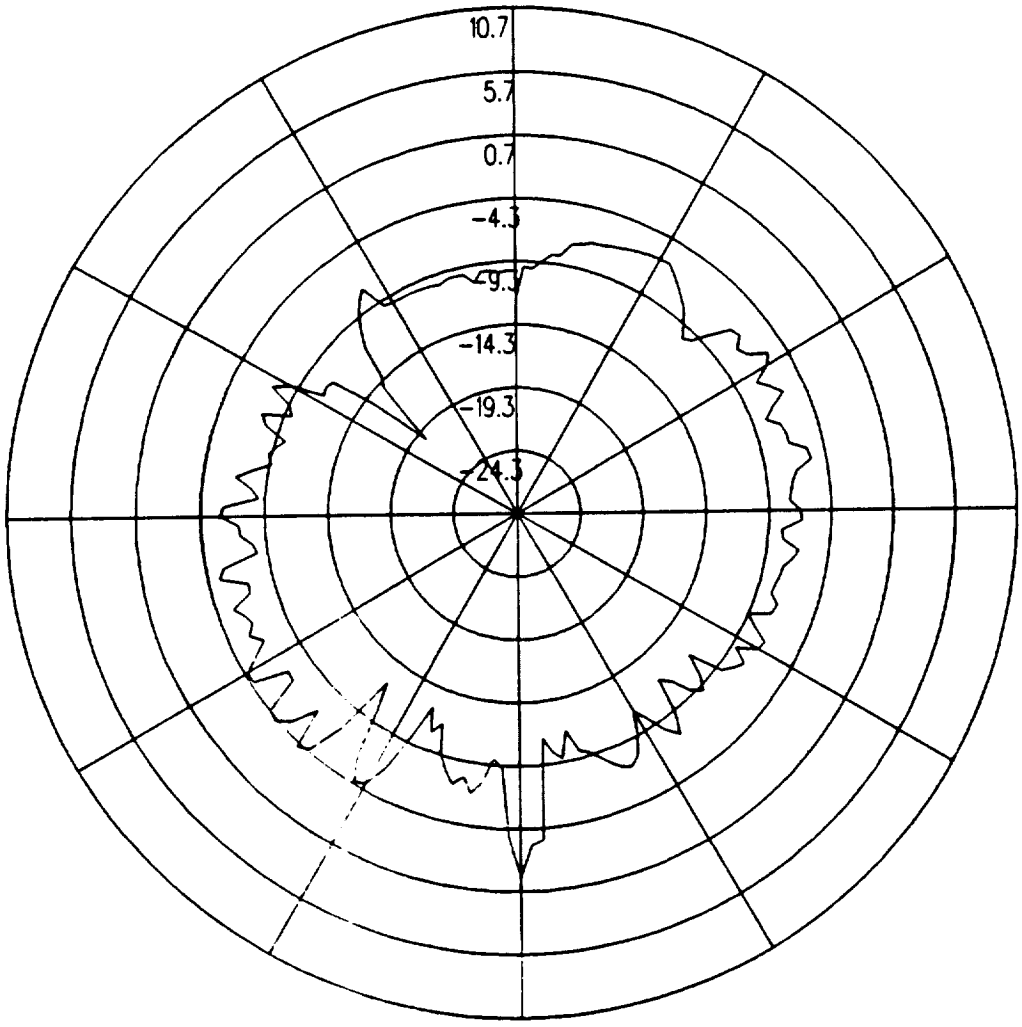

Figure 5.38: UTD calculated conical plane pattern 20° above the horizon for batwing antenna on a P-3C for left hand circular polarization at 300 MHz.(Test Location 3)

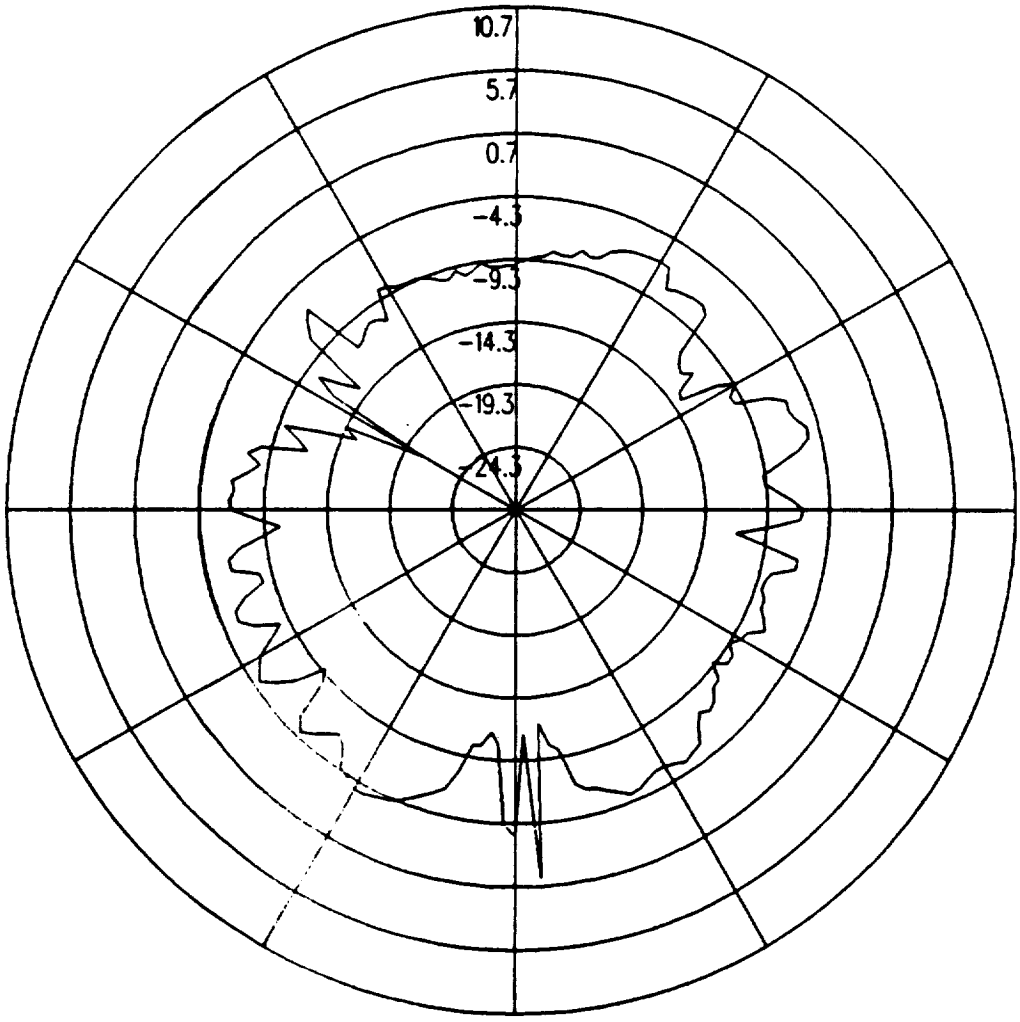

Figure 5.39: UTD calculated conical plane pattern 30° above the horizon for batwing antenna on a P-3C for left hand circular polarization at 300 MHz.(Test Location 3)

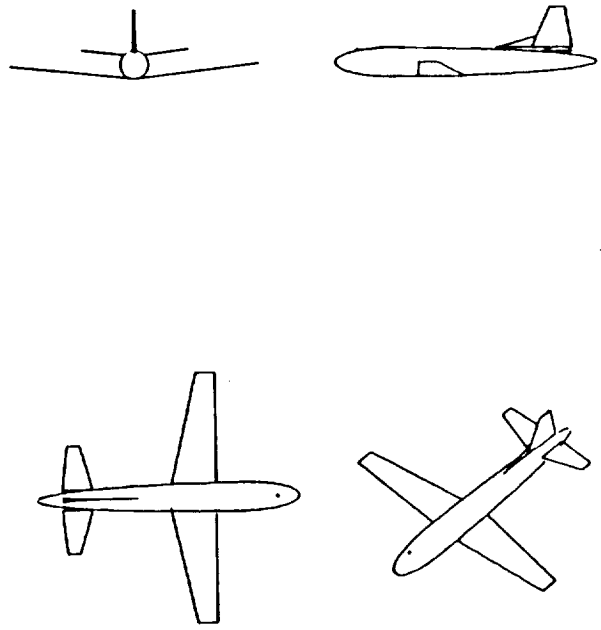

Figure 5.40: Geometry of the model of the P-3C aircraft used in the NEC-BSC code showing the location of the antenna.

5.4 Test Location 4

The antenna is located as illustrated in Figure 5.40, which also shows the computer model used to generate the results. The calculated results at 300 MHz are shown for the roll plane in Figure 5.41, for the azimuth plane in Figure 5.42, for the elevation plane in Figure 5.43, for the conical plane 10° above the horizon in Figure 5.44, for the conical plane 20° above the horizon in Figure 5.45, and for the conical plane 30° above the horizon in Figure 5.46 all for right hand polarization. The cross polarized fields are shown for the roll plane in Figure 5.47, for the azimuth plane in Figure 5.48, for the elevation plane in Figure 5.49, for the conical plane 10° above the horizon in Figure 5.50, for the conical plane 20° above the horizon in Figure 5.51, and for the conical plane 30° above the horizon in Figure 5.52 all for left hand polarization.

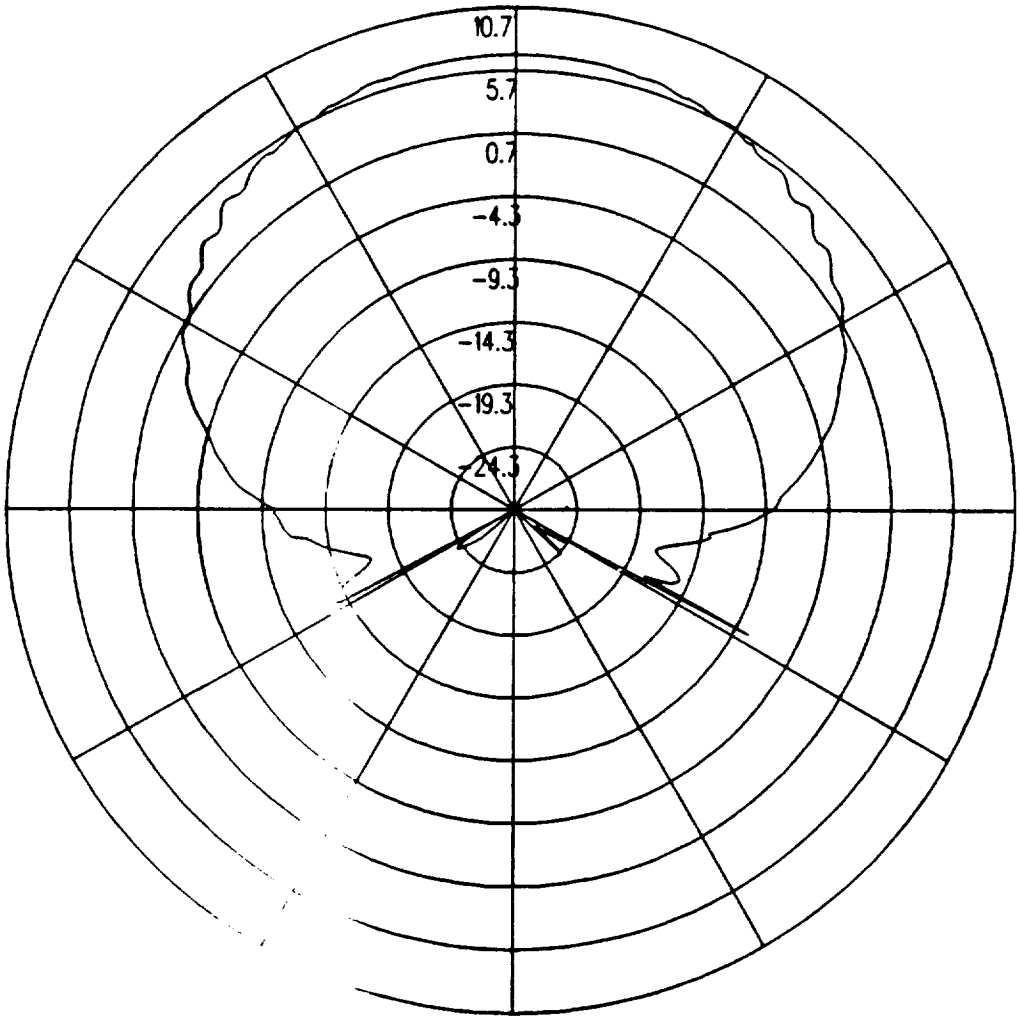

Figure 5.41: UTD calculated roll plane pattern for batwing antenna on a P-3C for right hand circular polarization at 300 MHz. (Test Location 4)

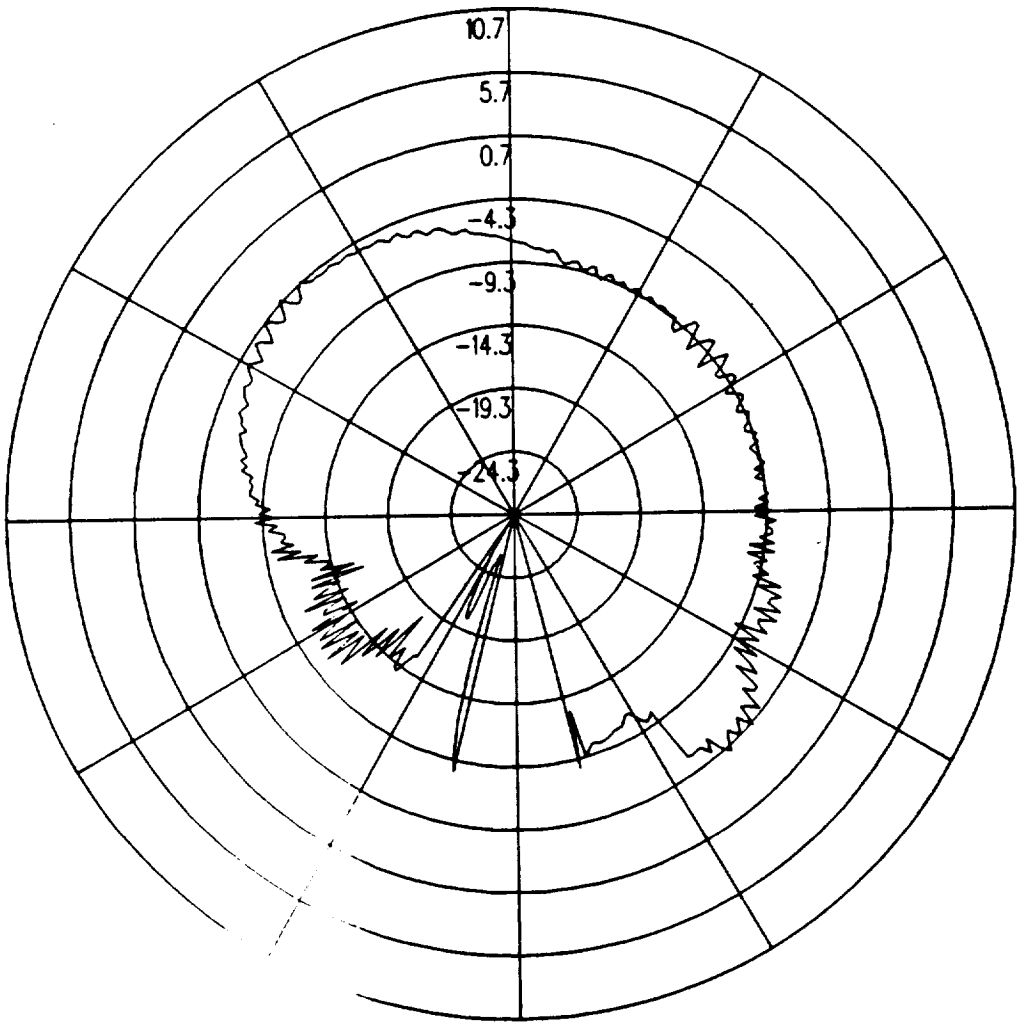

Figure 5.42: UTD calculated azimuth plane pattern for batwing antenna on a P-3C for right hand circular polarization at 300 MHz. (Test Location 4)

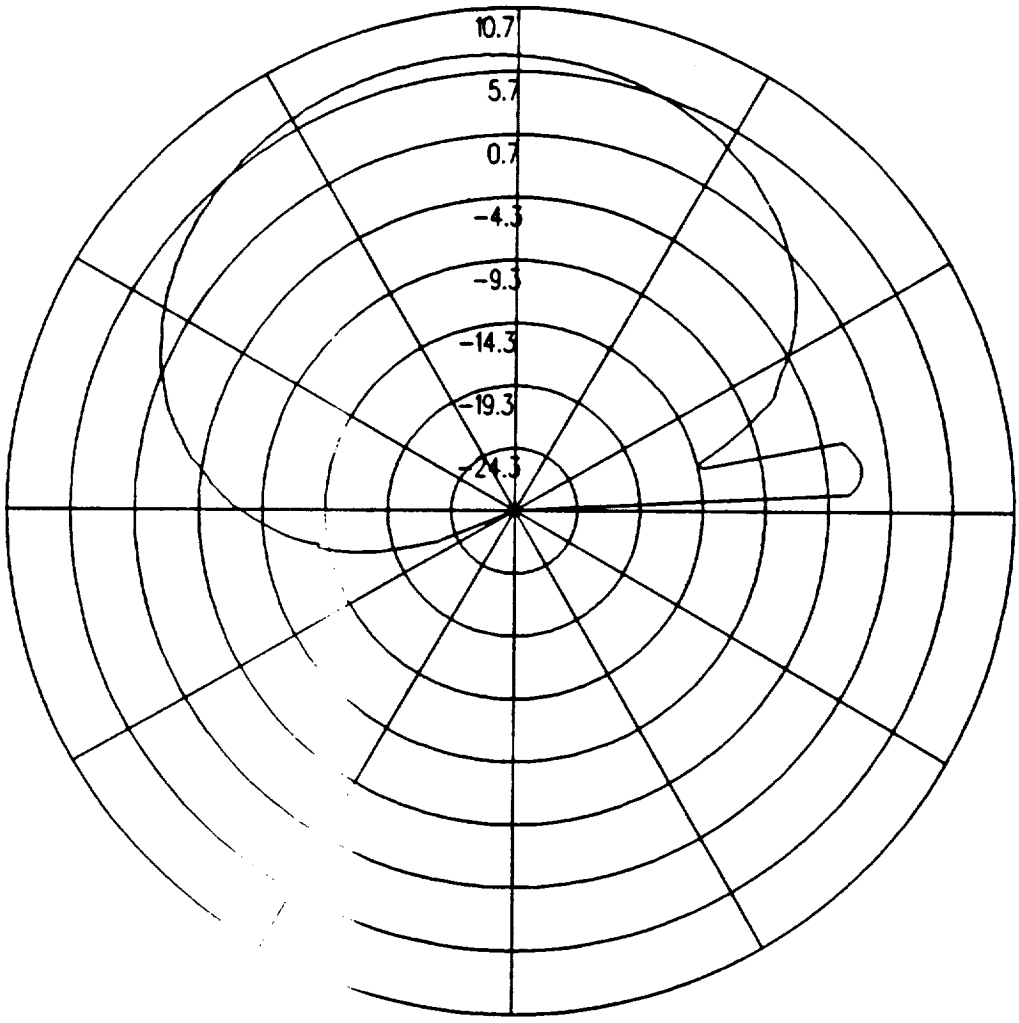

Figure 5.43: UTD calculated elevation plane pattern for batwing antenna on a P-3C for right hand circular polarization at 300 MHz. (Test Location 4)

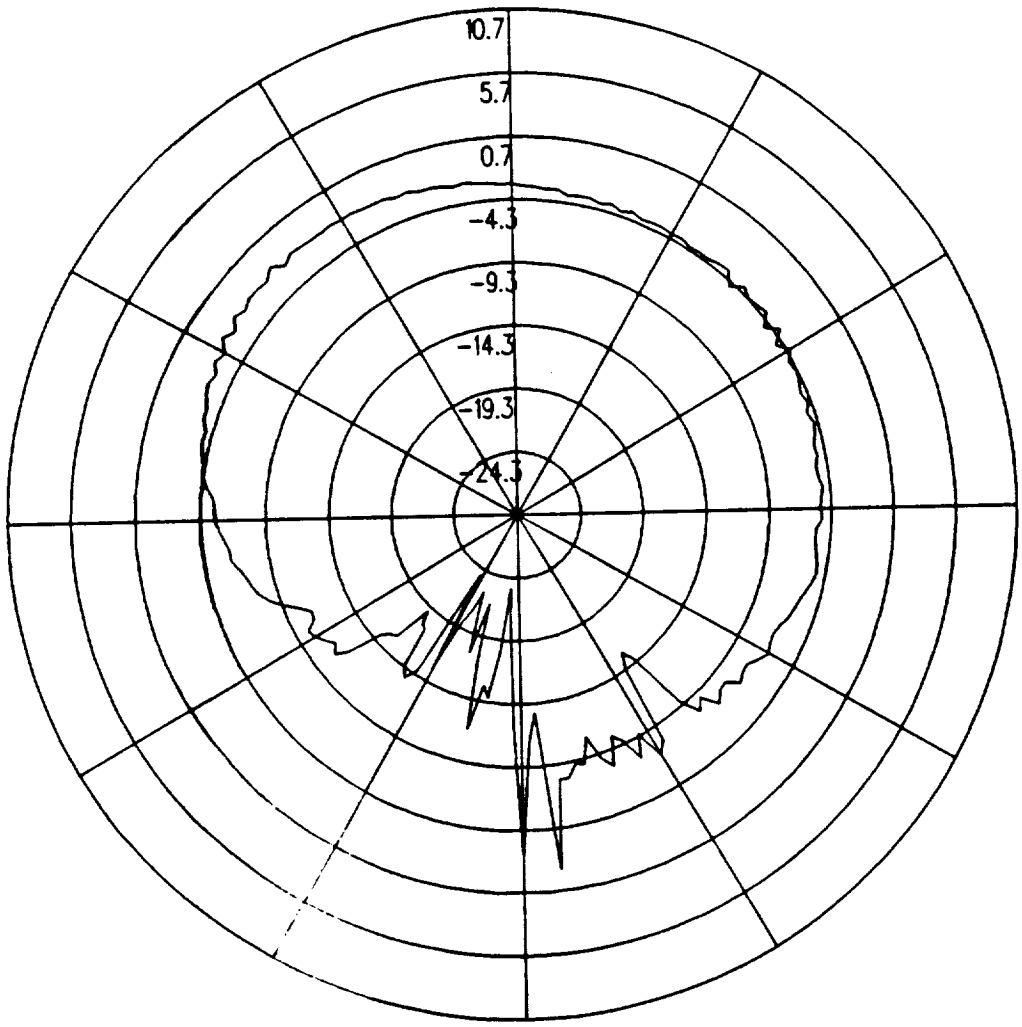

Figure 5.44: UTD calculated conical plane pattern 10° above the horizon for batwing antenna on a P-3C for right hand circular polarization at 300 MHz.(Test Location 4)

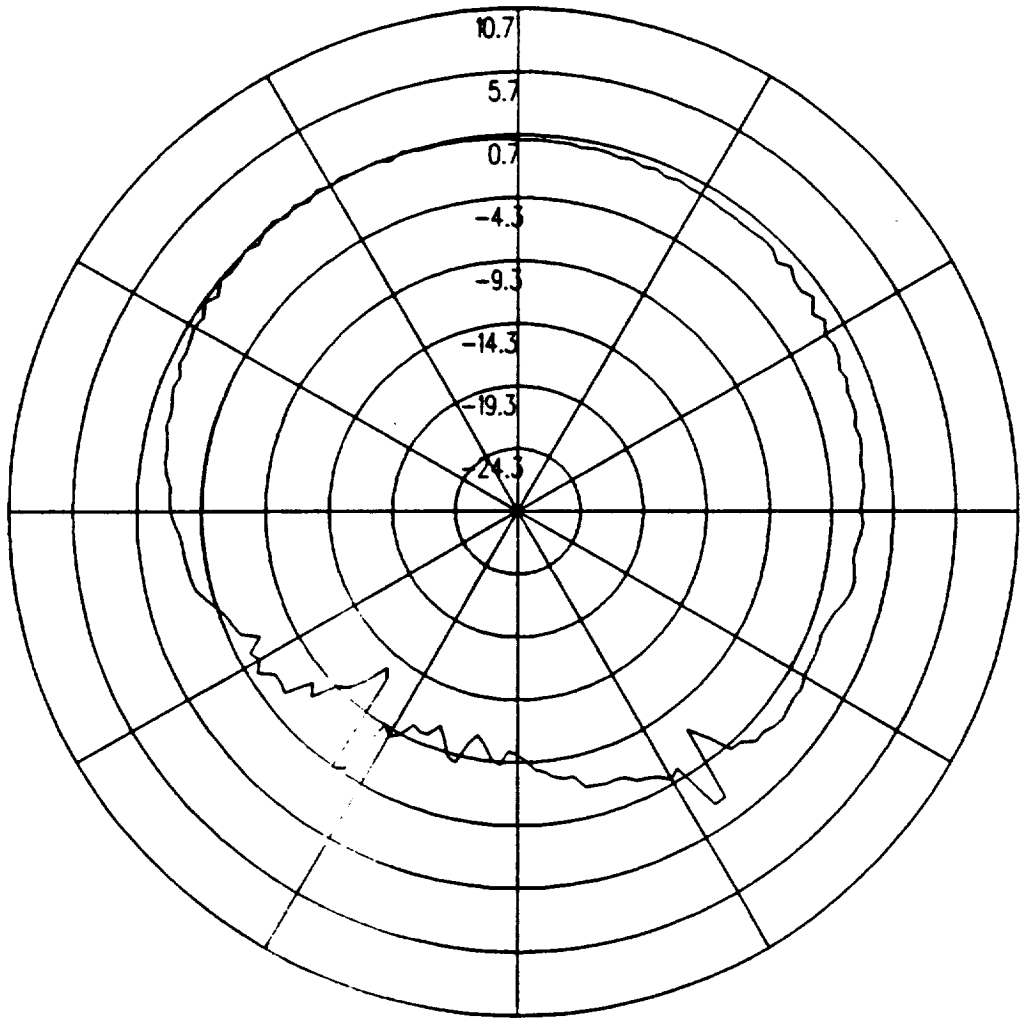

Figure 5.45: UTD calculated conical plane pattern 20° above the horizon for batwing antenna on a P-3C for right hand circular polarization at 300 MHz.(Test Location 4)

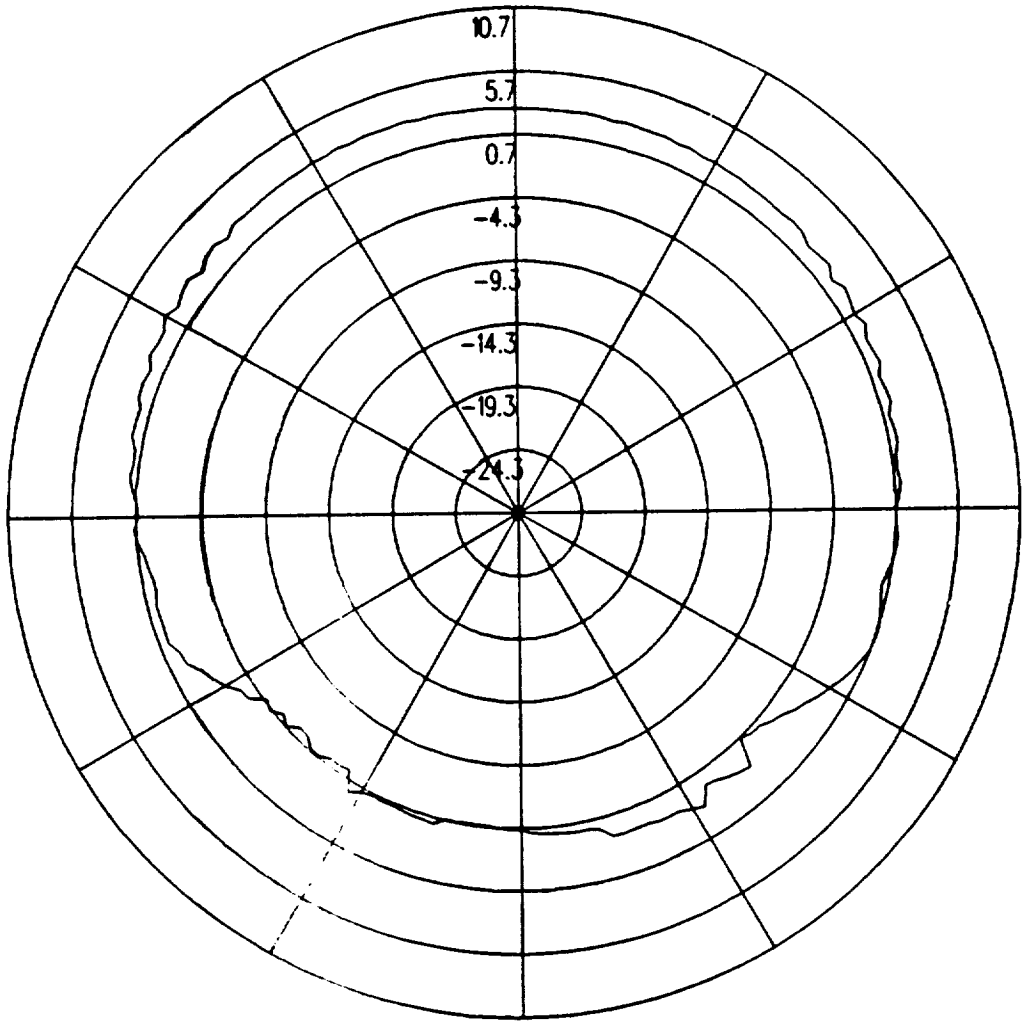

Figure 5.46: UTD calculated conical plane pattern 30° above the horizon for batwing antenna on a P-3C for right hand circular polarization at 300 MHz.(Test Location 4)

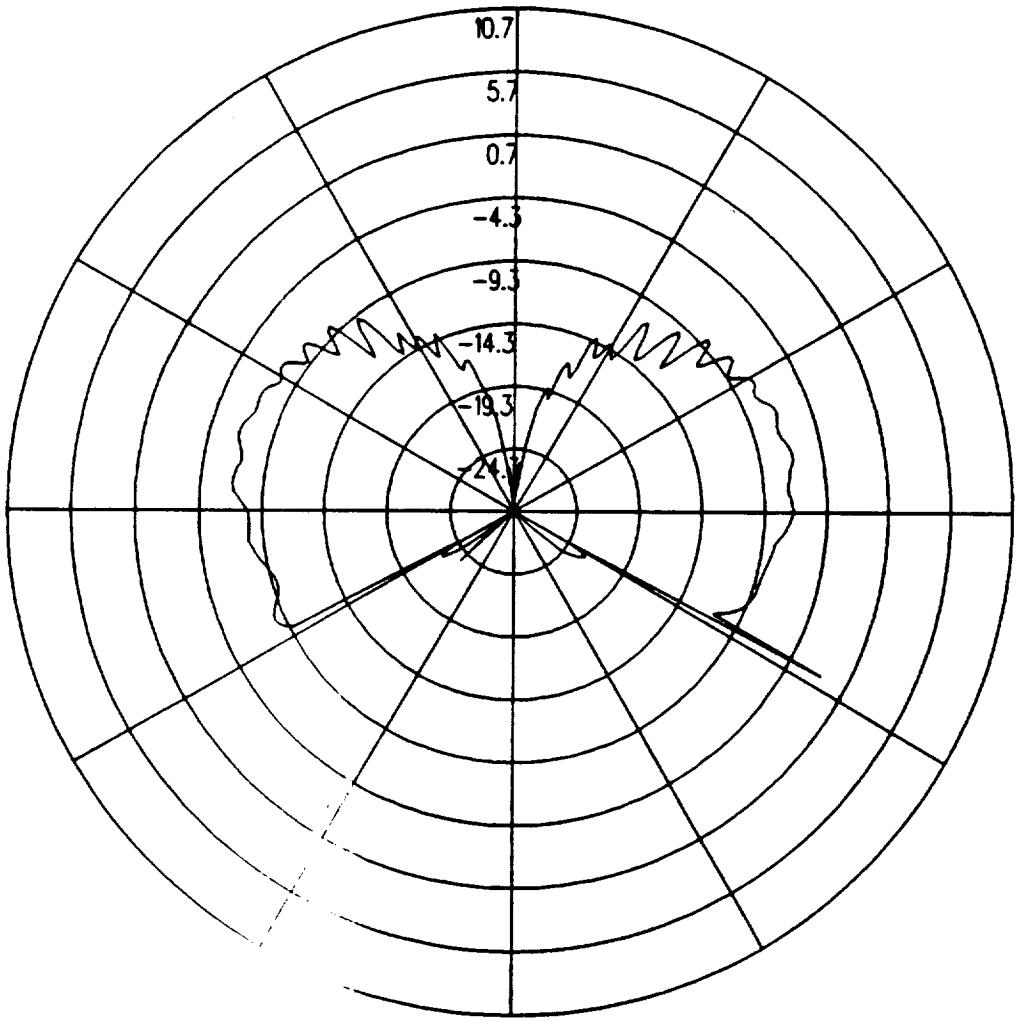

Figure 5.47: UTD calculated roll plane pattern for batwing antenna on a P-3C for left hand circular polarization at 300 MHz. (Test Location 4)

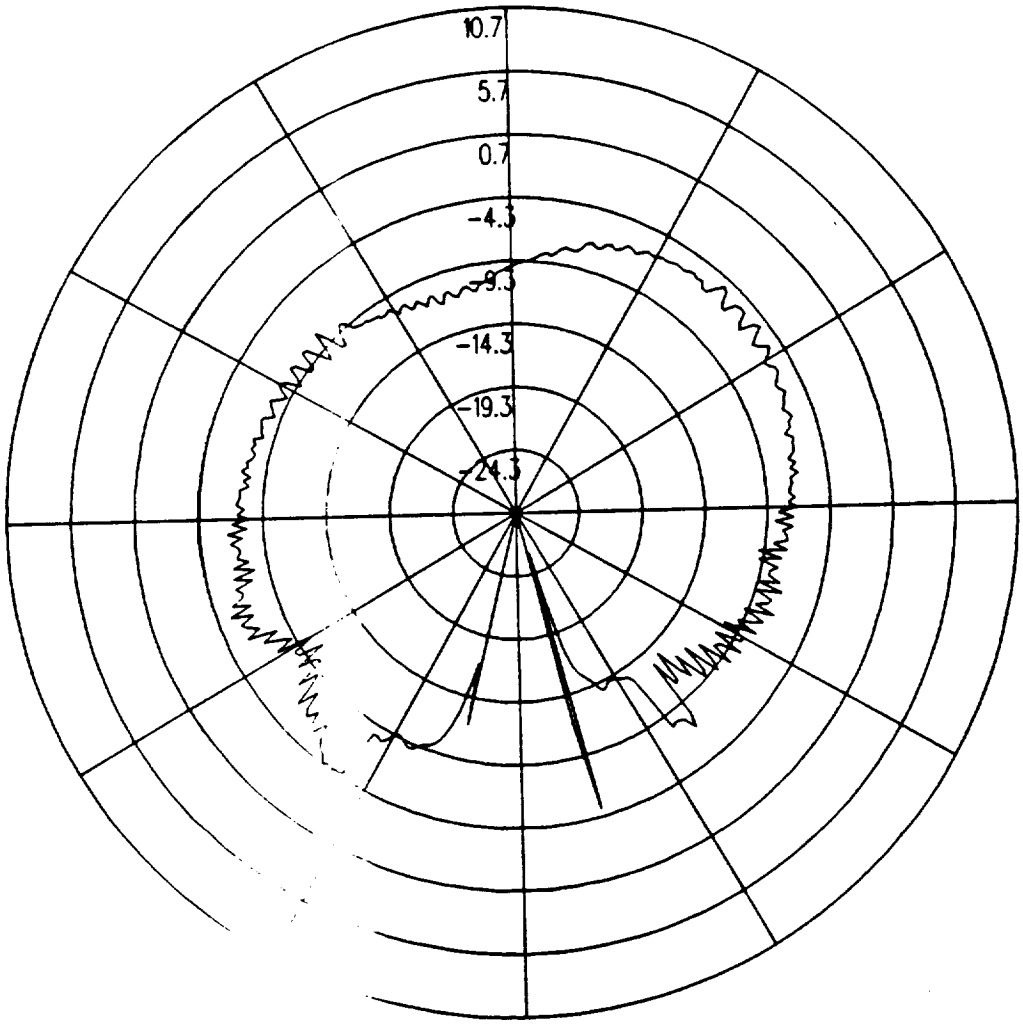

Figure 5.48: UTD calculated azimuth plane pattern for batwing antenna on a P-3C for left hand circular polarization at 300 MHz. (Test Location 4)

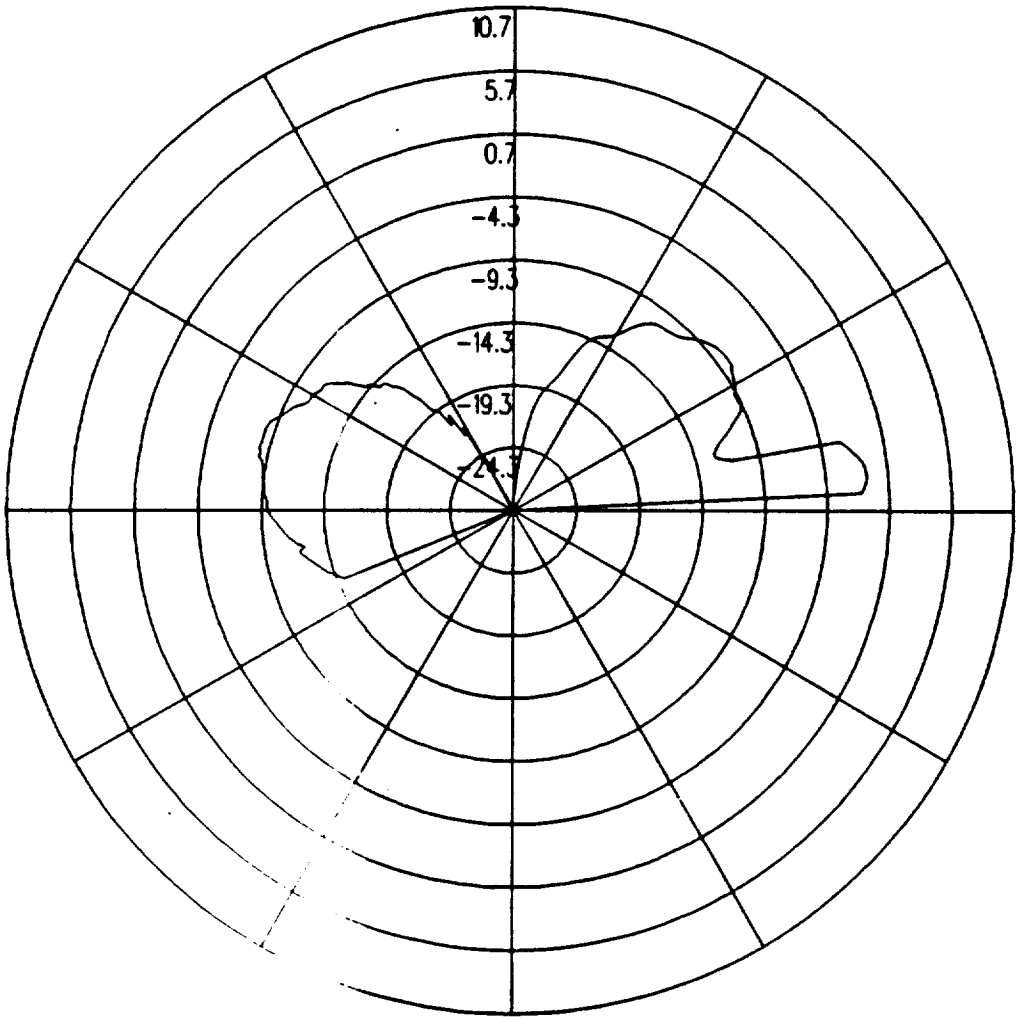

Figure 5.49: UTD calculated elevation plane pattern for batwing antenna on a P-3C for left hand circular polarization at 300 MHz. (Test Location 4)

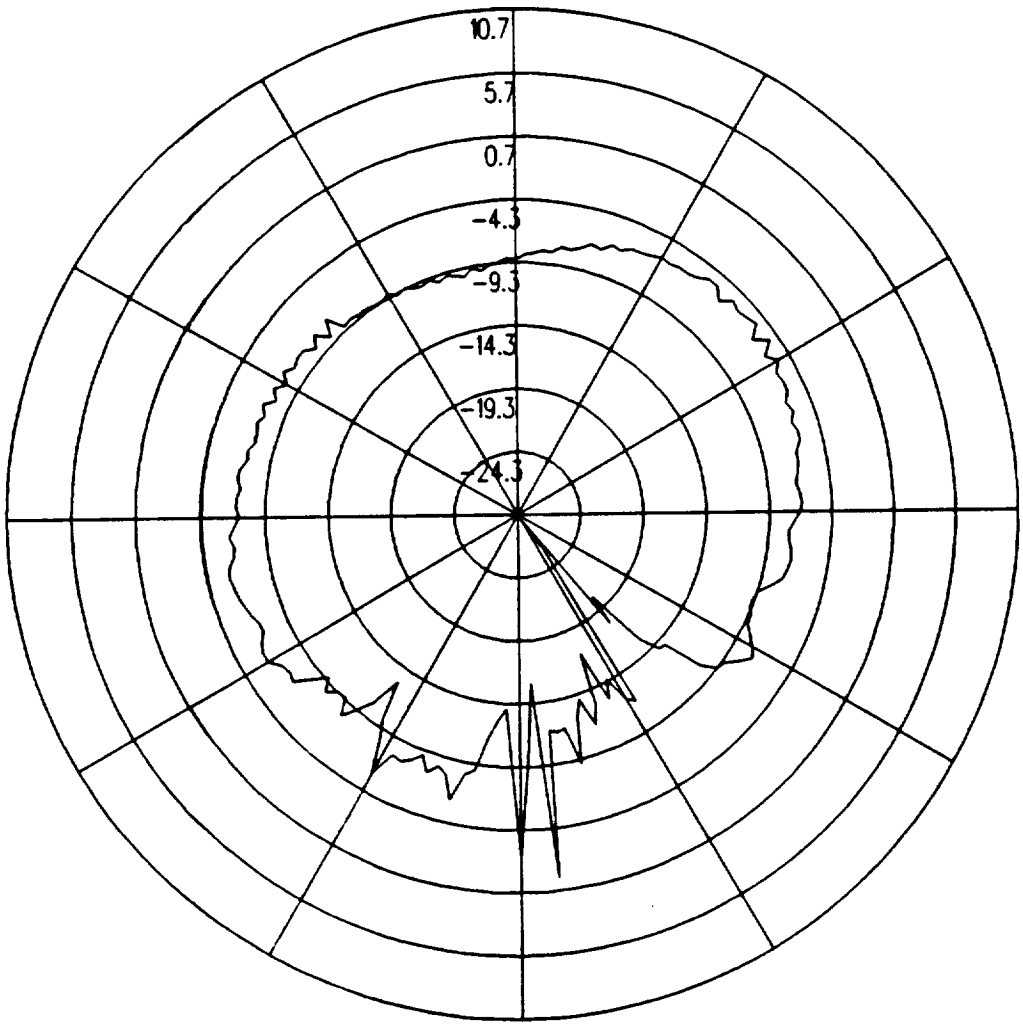

Figure 5.50: UTD calculated conical plane pattern 10° above the horizon for batwing antenna on a P-3C for left hand circular polarization at 300 MHz.(Test Location 4)

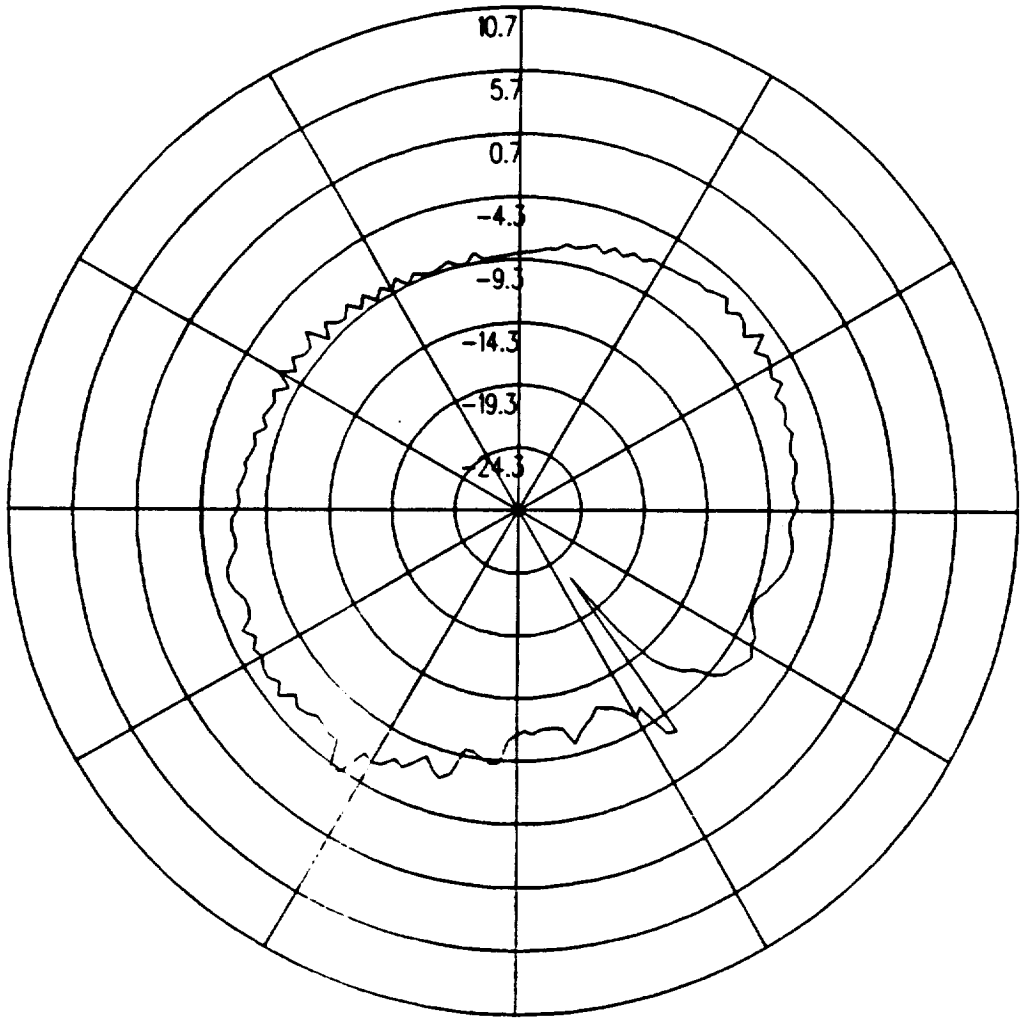

Figure 5.51: UTD calculated conical plane pattern 20° above the horizon for batwing antenna on a P-3C for left hand circular polarization at 300 MHz.(Test Location 4)

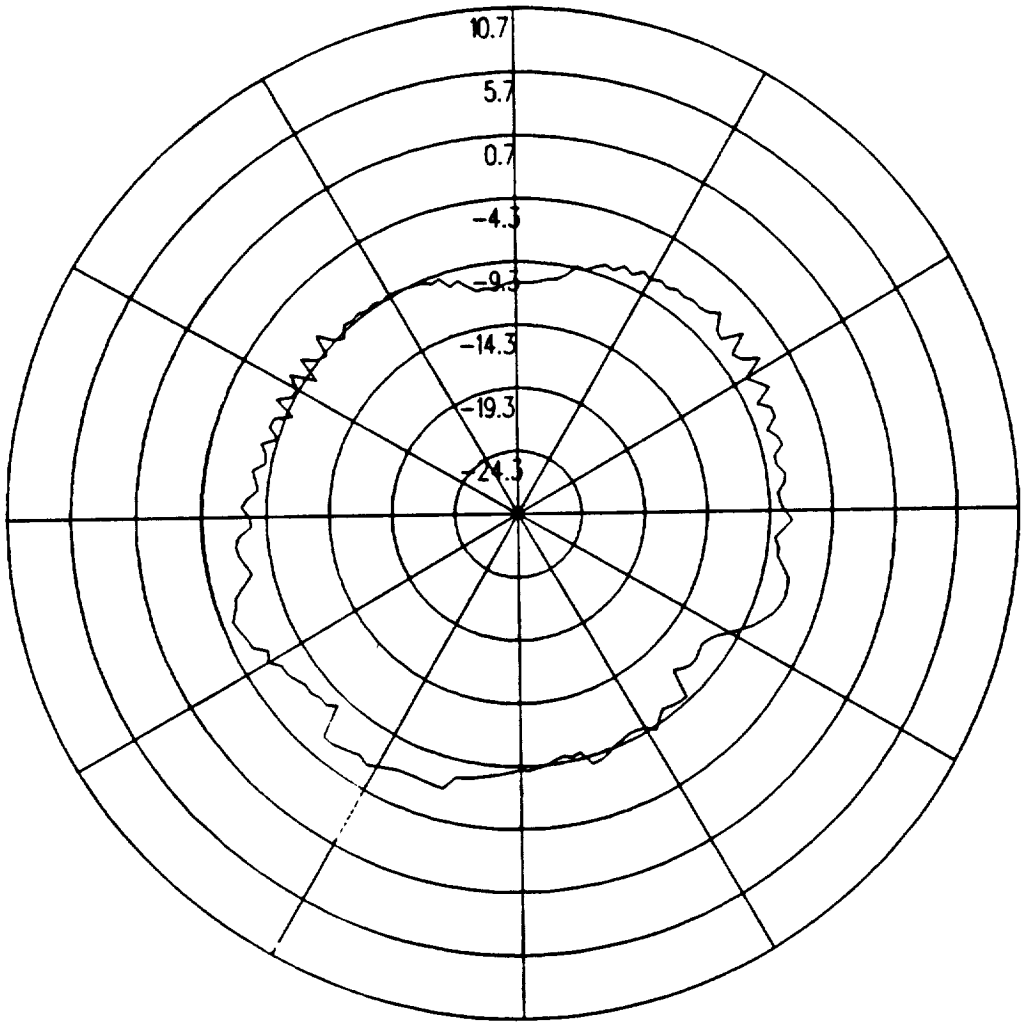

Figure 5.52: UTD calculated conical plane pattern 30° above the horizon for batwing antenna on a P-3C for left hand circular polarization at 300 MHz.(Test Location 4)

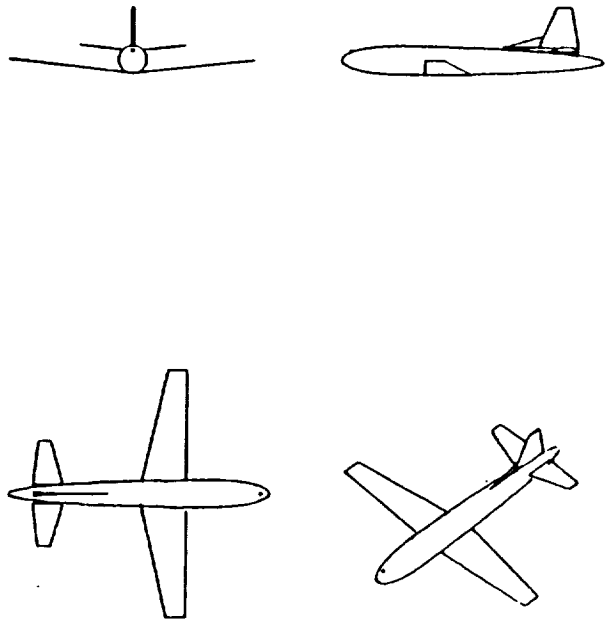

Figure 5.53: Geometry of the model of the P-3C aircraft used in the NEC-BSC code showing the location of the antenna.

5.5 Test Location 5

The antenna is located as illustrated in Figure 5.53, which also shows the computer model used to generate the results. The calculated results at 300 MHz are shown for the roll plane in Figure 5.54, for the azimuth plane in Figure 5.55, for the elevation plane in Figure 5.56, for the conical plane 10° above the horizon in Figure 5.57, for the conical plane 20° above the horizon in Figure 5.58, and for the conical plane 30° above the horizon in Figure 5.59 all for right hand polarization. The cross polarized fields are shown for the roll plane in Figure 5.60, for the azimuth plane in Figure 5.61, for the elevation plane in Figure 5.62, for the conical plane 10° above the horizon in Figure 5.63, for the conical plane 20° above the horizon in Figure 5.64, and for the conical plane 30° above the horizon in Figure 5.65 all for left hand polarization.

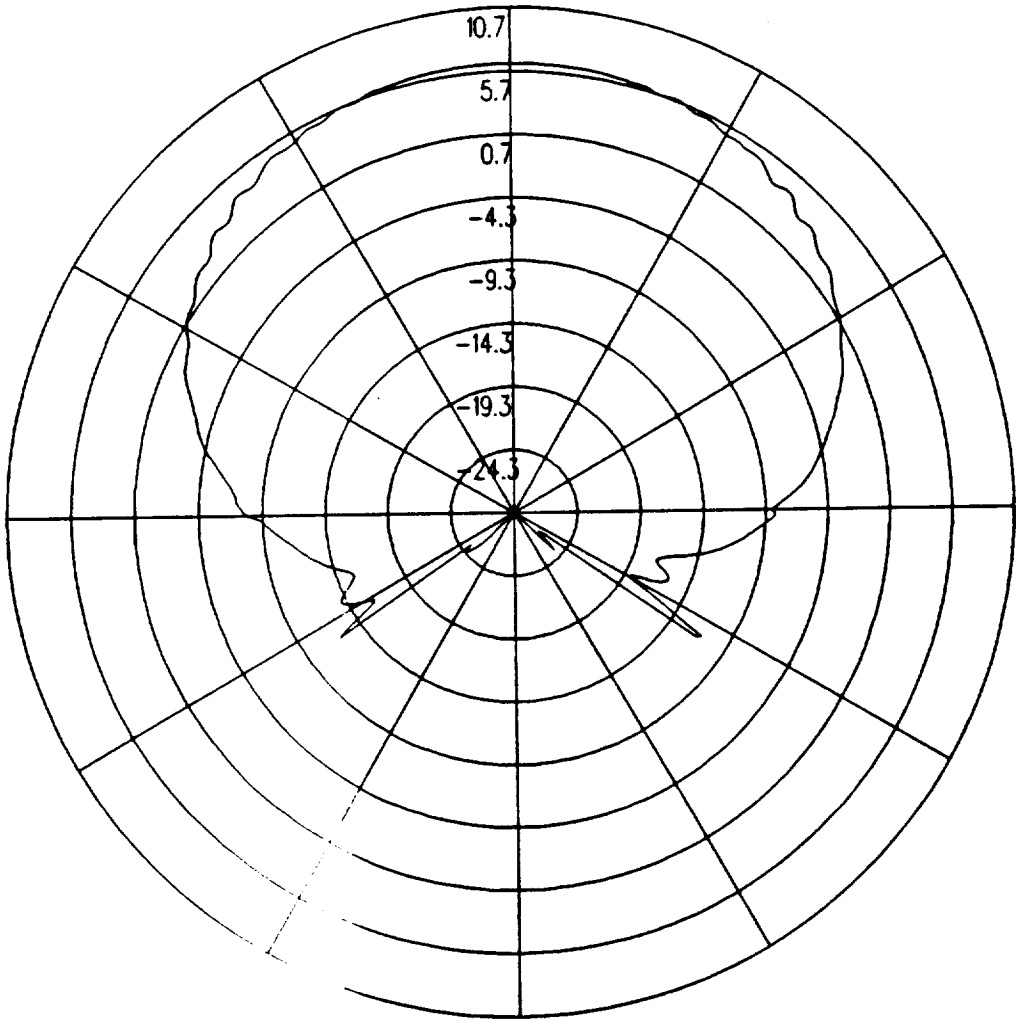

Figure 5.54: UTD calculated roll plane pattern for batwing antenna on a P-3C for right hand circular polarization at 300 MHz. (Test Location 5)

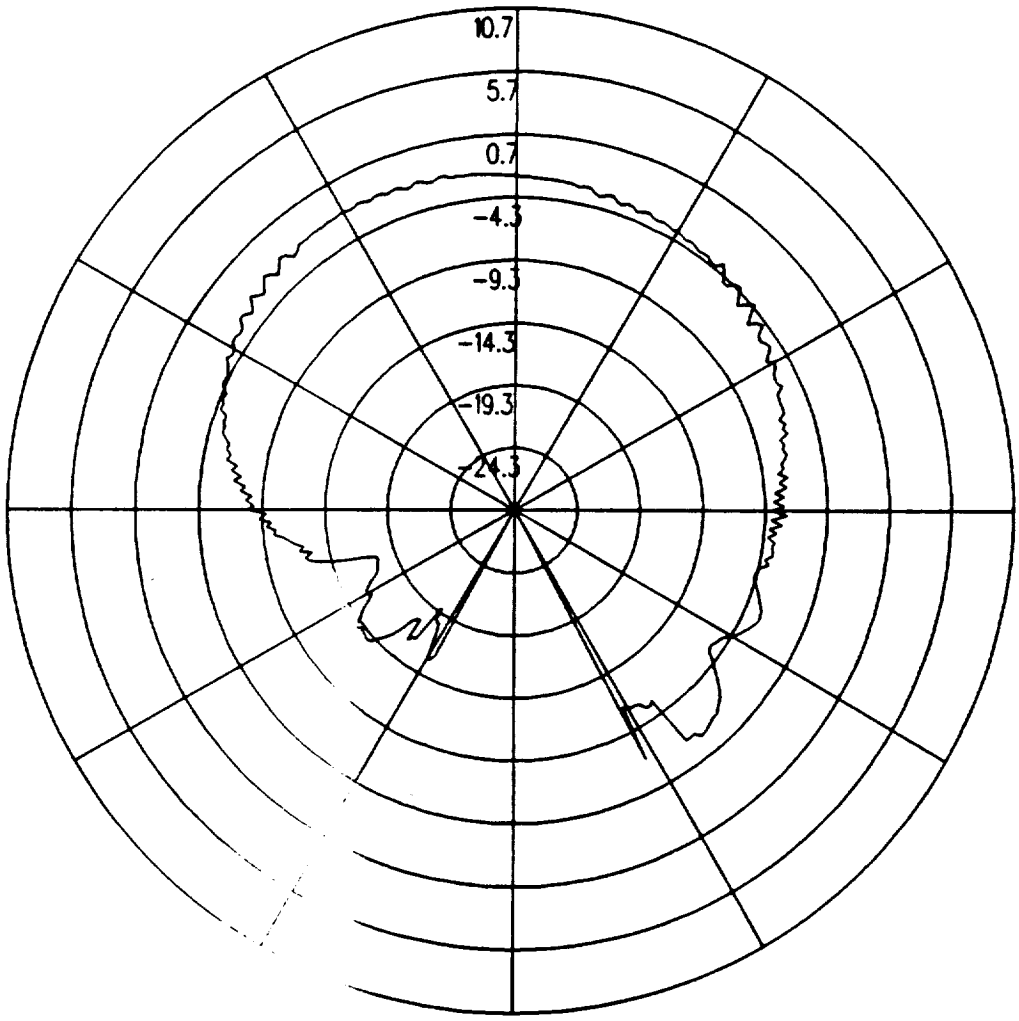

Figure 5.55: UTD calculated azimuth plane pattern for batwing antenna on a P-3C for right hand circular polarization at 300 MHz. (Test Location 5)

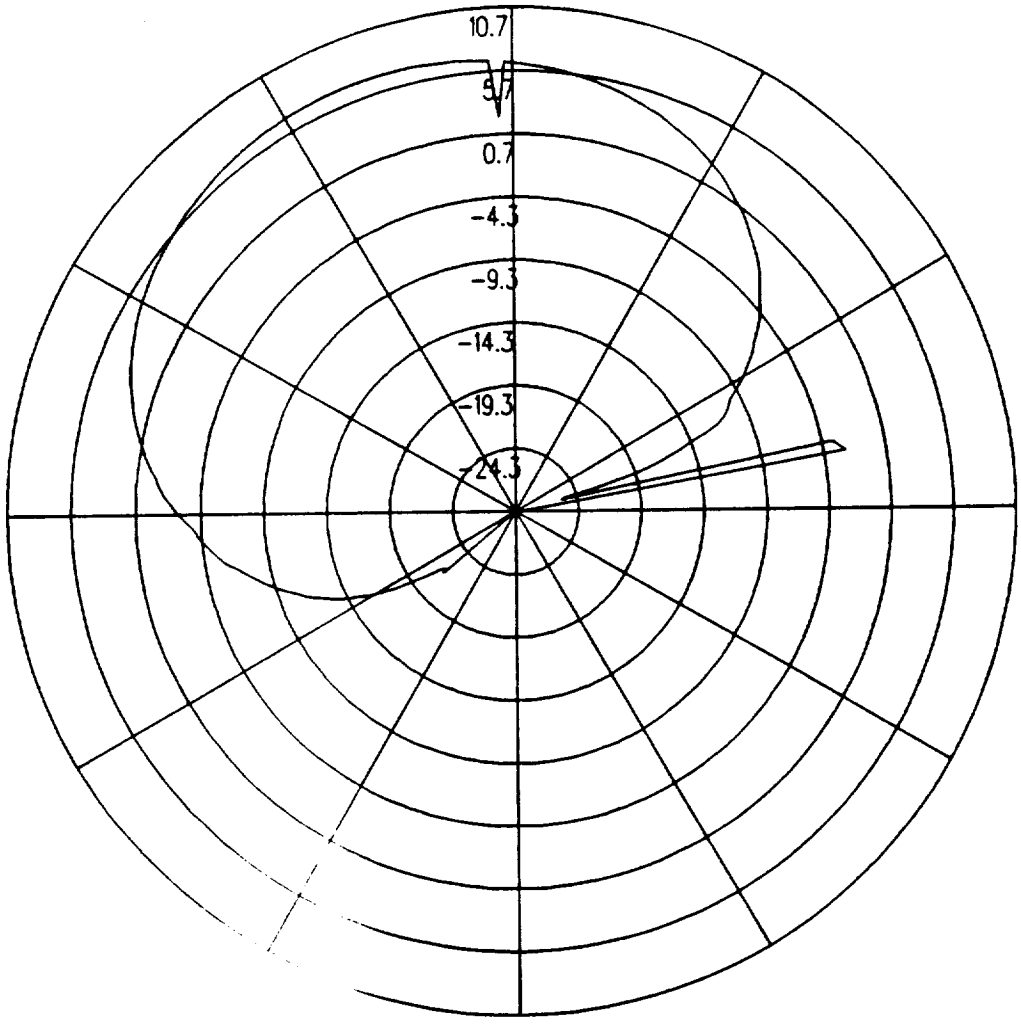

Figure 5.56: UTD calculated elevation plane pattern for batwing antenna on a P-3C for right hand circular polarization at 300 MHz. (Test Location 5)

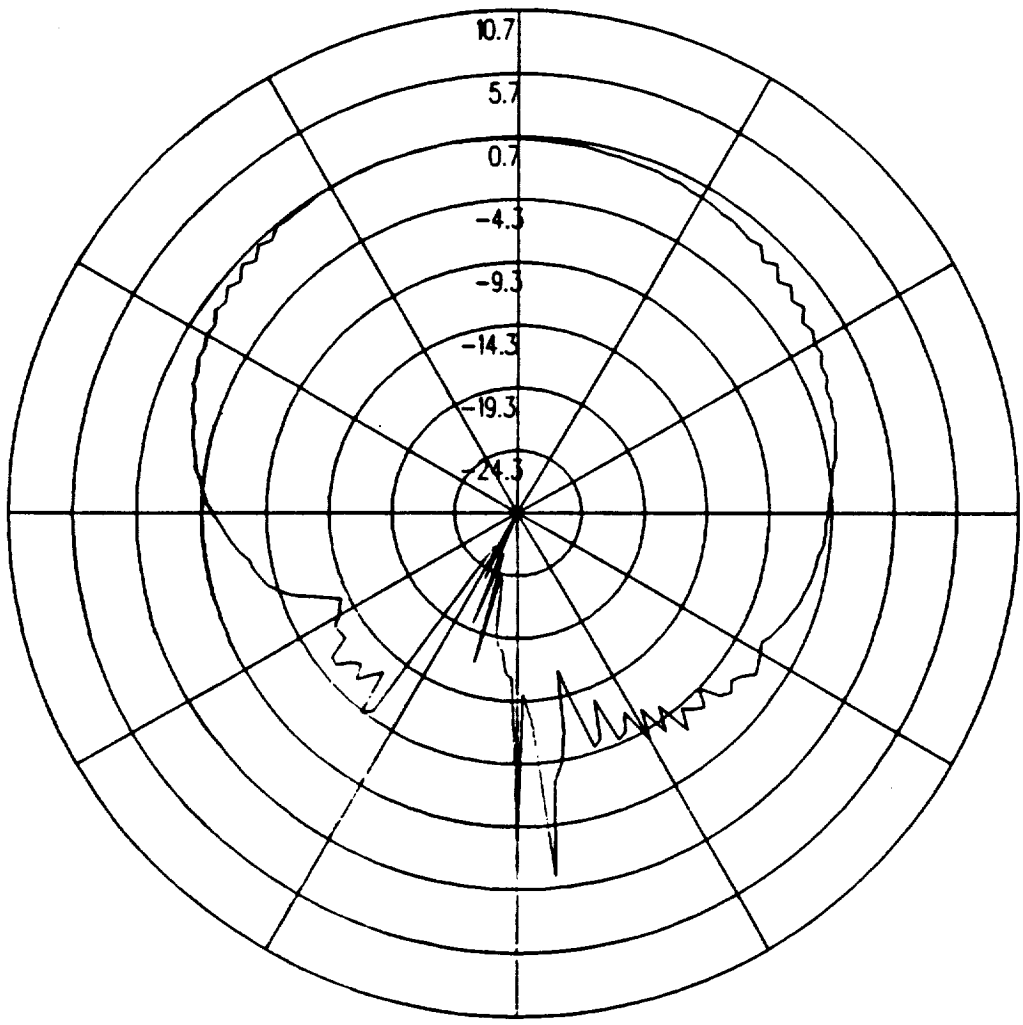

Figure 5.57: UTD calculated conical plane pattern 10° above the horizon for batwing antenna on a P-3C for right hand circular polarization at 300 MHz.(Test Location 5)

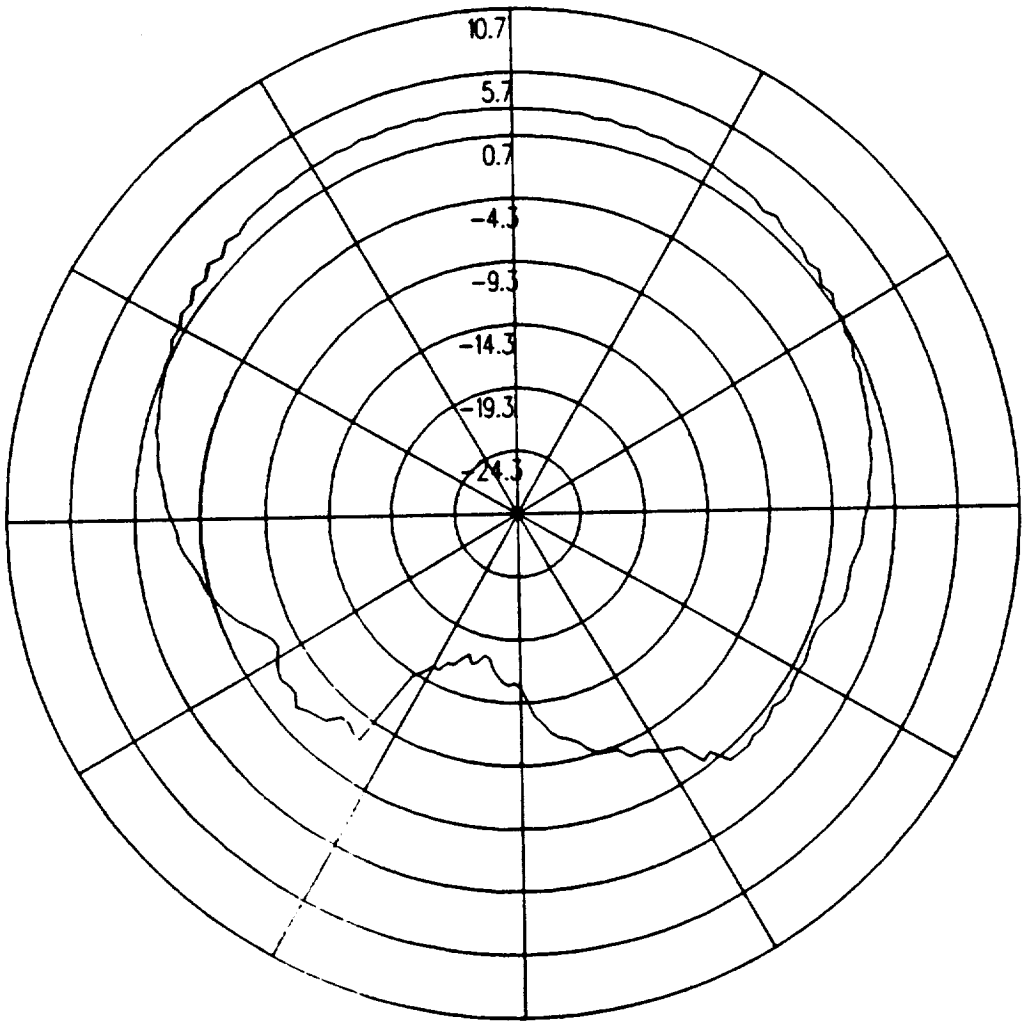

Figure 5.58: UTD calculated conical plane pattern 20° above the horizon for batwing antenna on a P-3C for right hand circular polarization at 300 MHz.(Test Location 5)

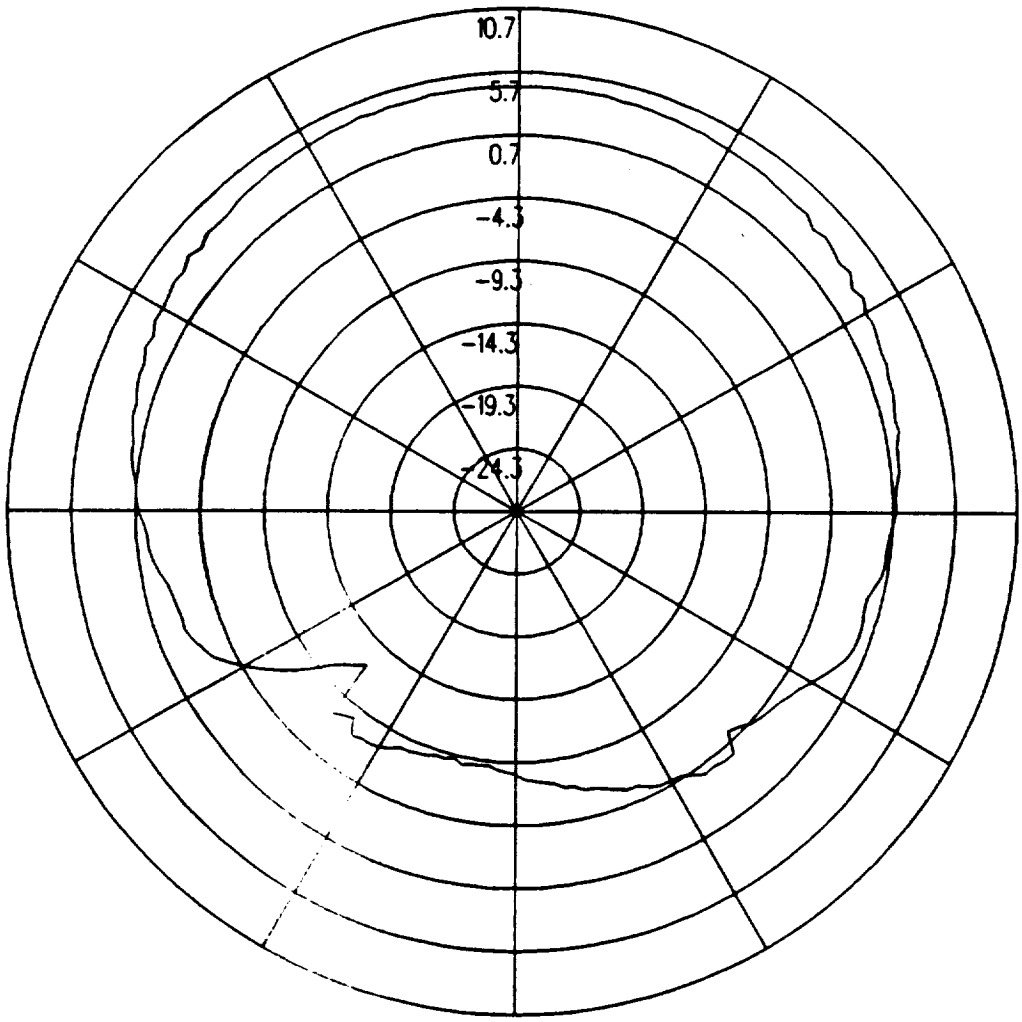

Figure 5.59: UTD calculated conical plane pattern 30° above the horizon for batwing antenna on a P-3C for right hand circular polarization at 300 MHz.(Test Location 5)

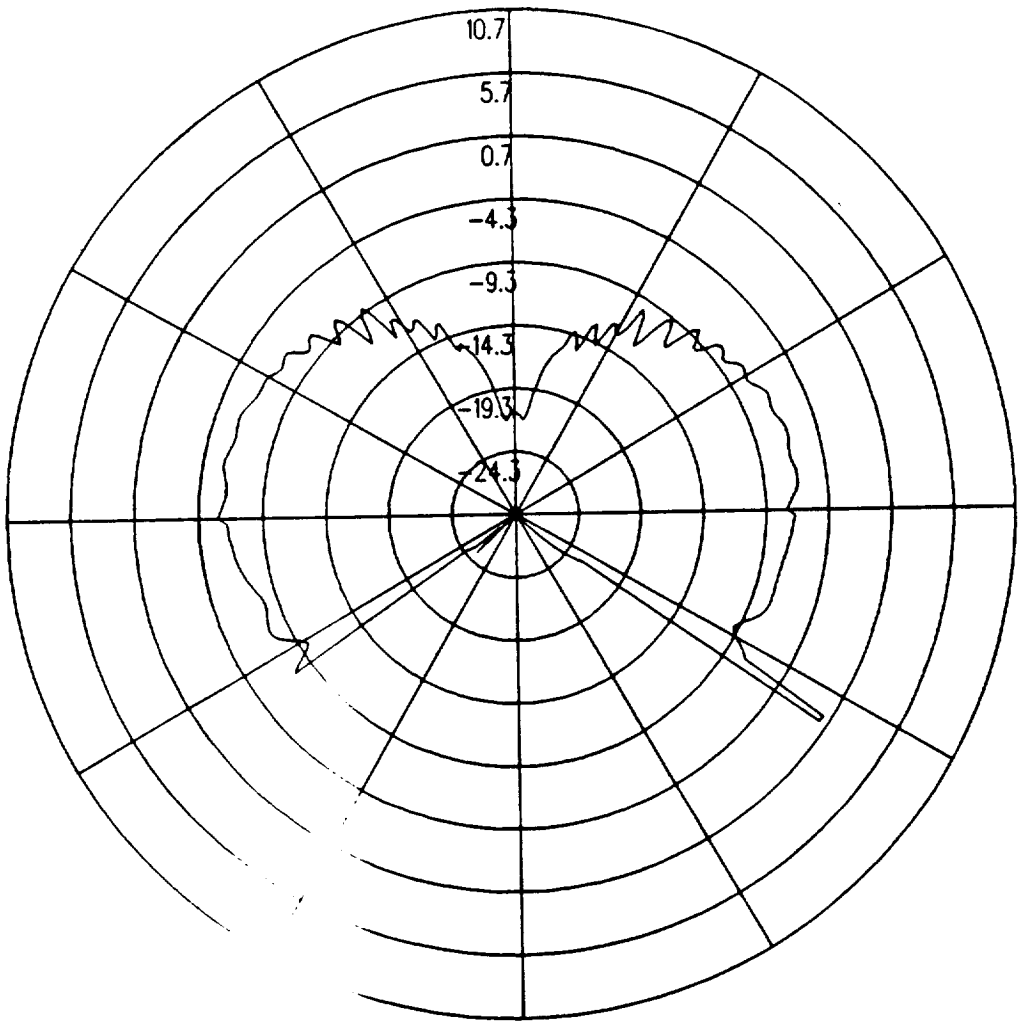

Figure 5.60: UTD calculated roll plane pattern for batwing antenna on a P-3C for left hand circular polarization at 300 MHz. (Test Location 5)

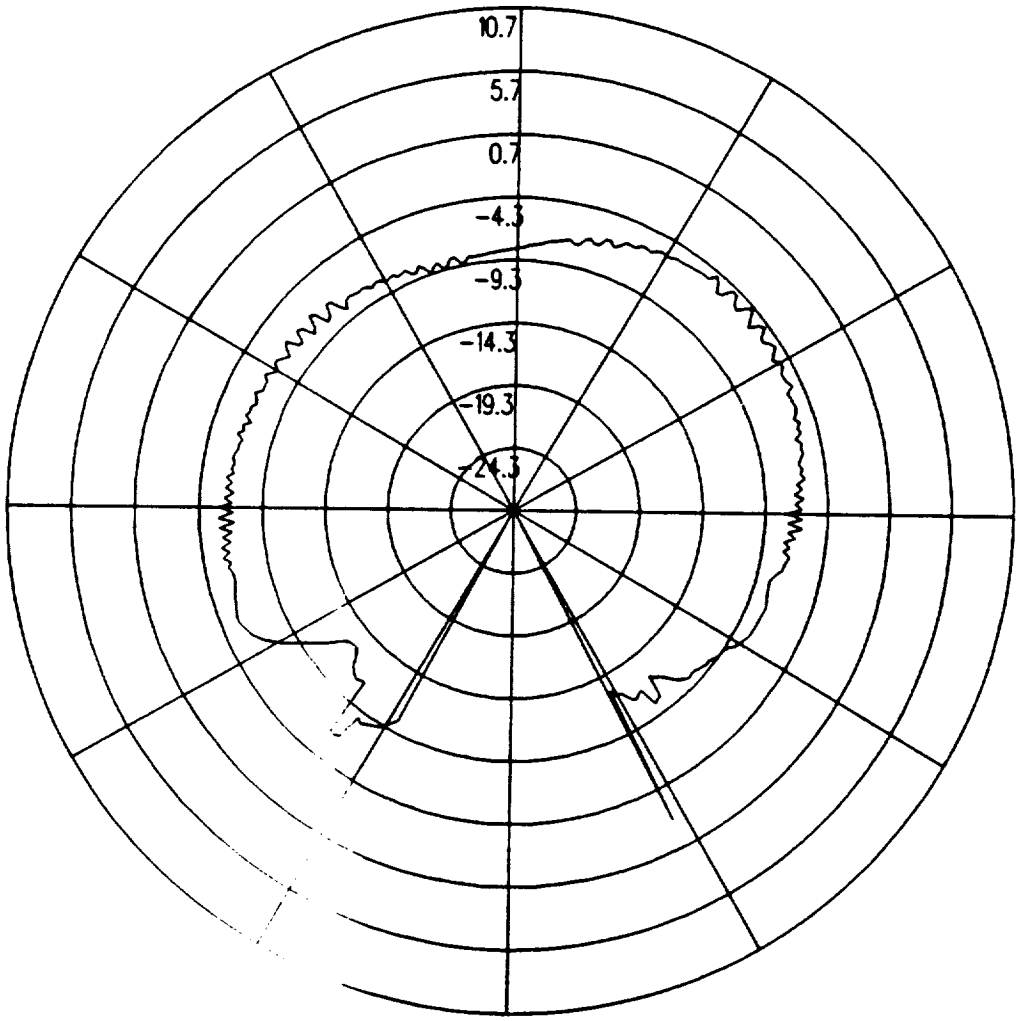

Figure 5.61: UTD calculated azimuth plane pattern for batwing antenna on a P-3C for left hand circular polarization at 300 MHz. (Test Location 5)

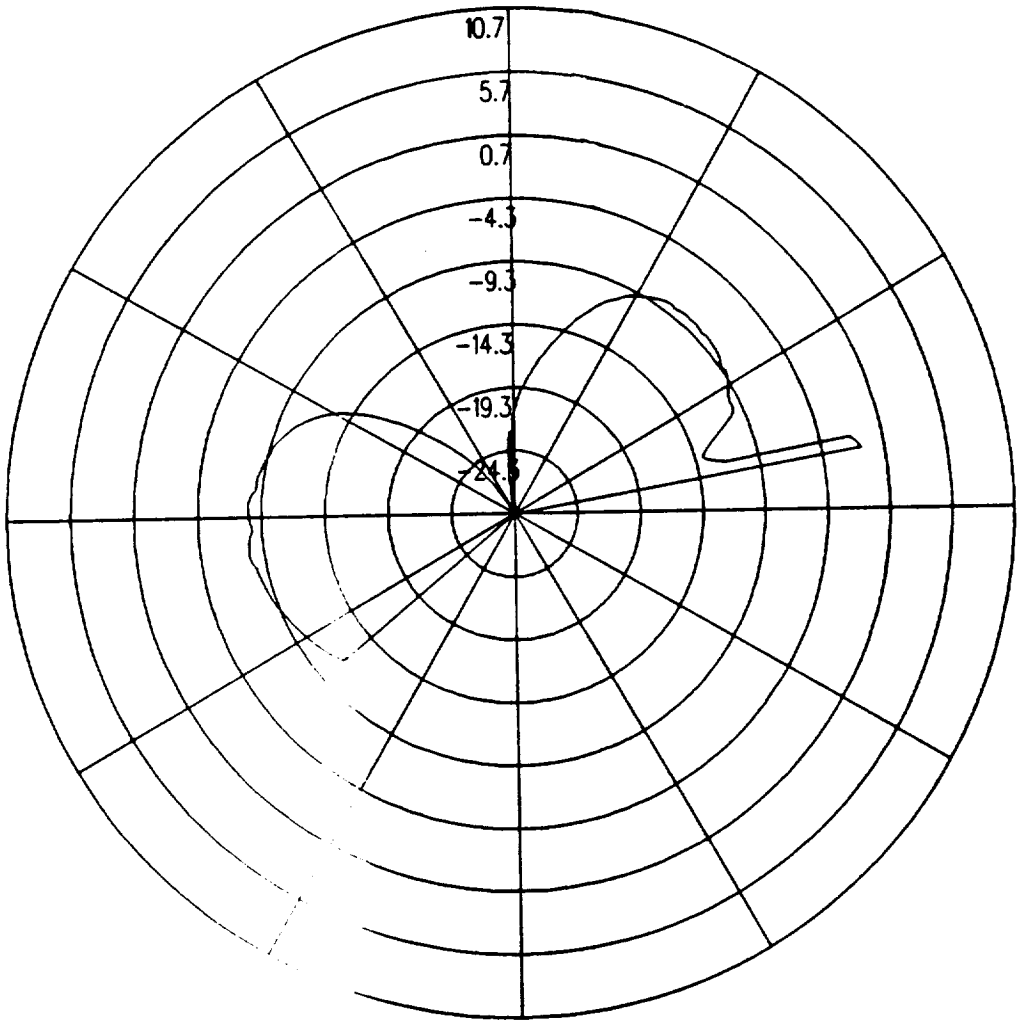

Figure 5.62: UTD calculated elevation plane pattern for batwing antenna on a P-3C for left hand circular polarization at 300 MHz. (Test Location 5)

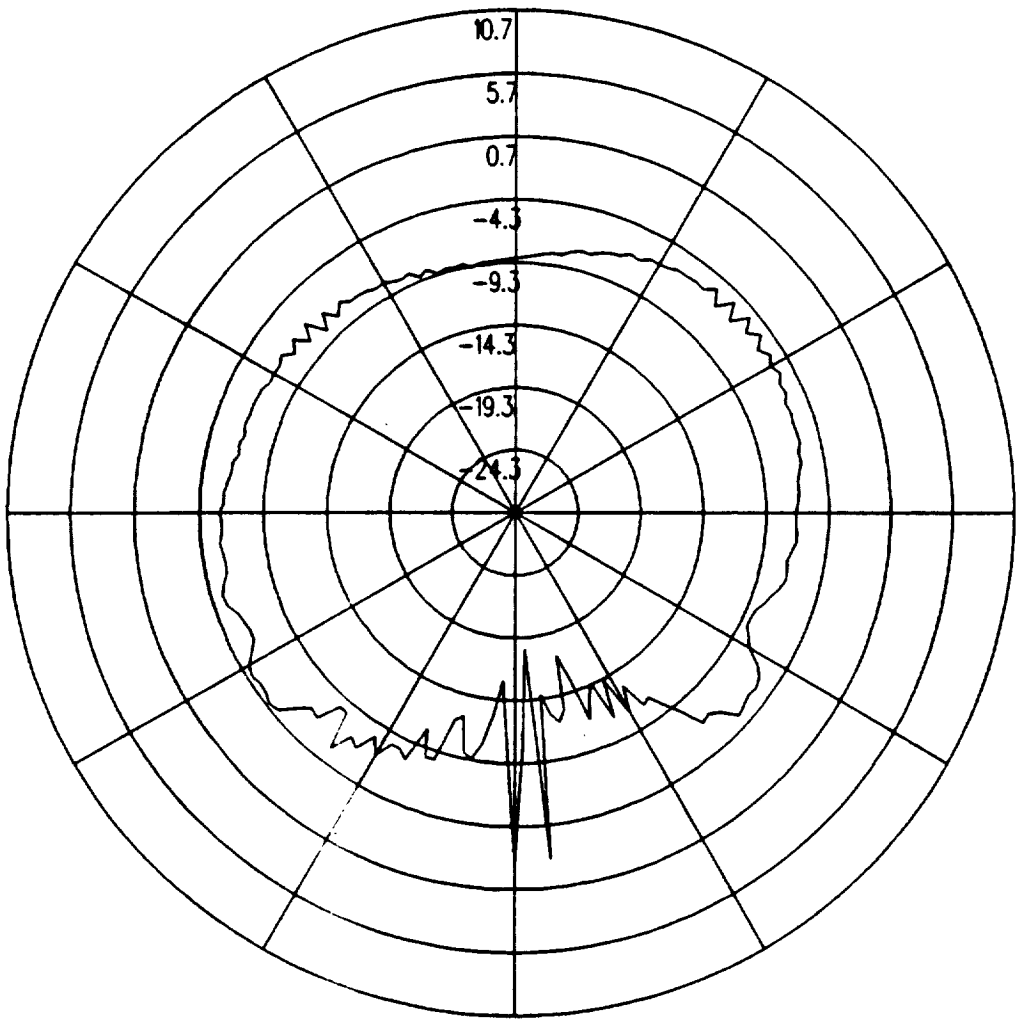

Figure 5.63: UTD calculated conical plane pattern 10° above the horizon for batwing antenna on a P-3C for left hand circular polarization at 300 MHz.(Test Location 5)

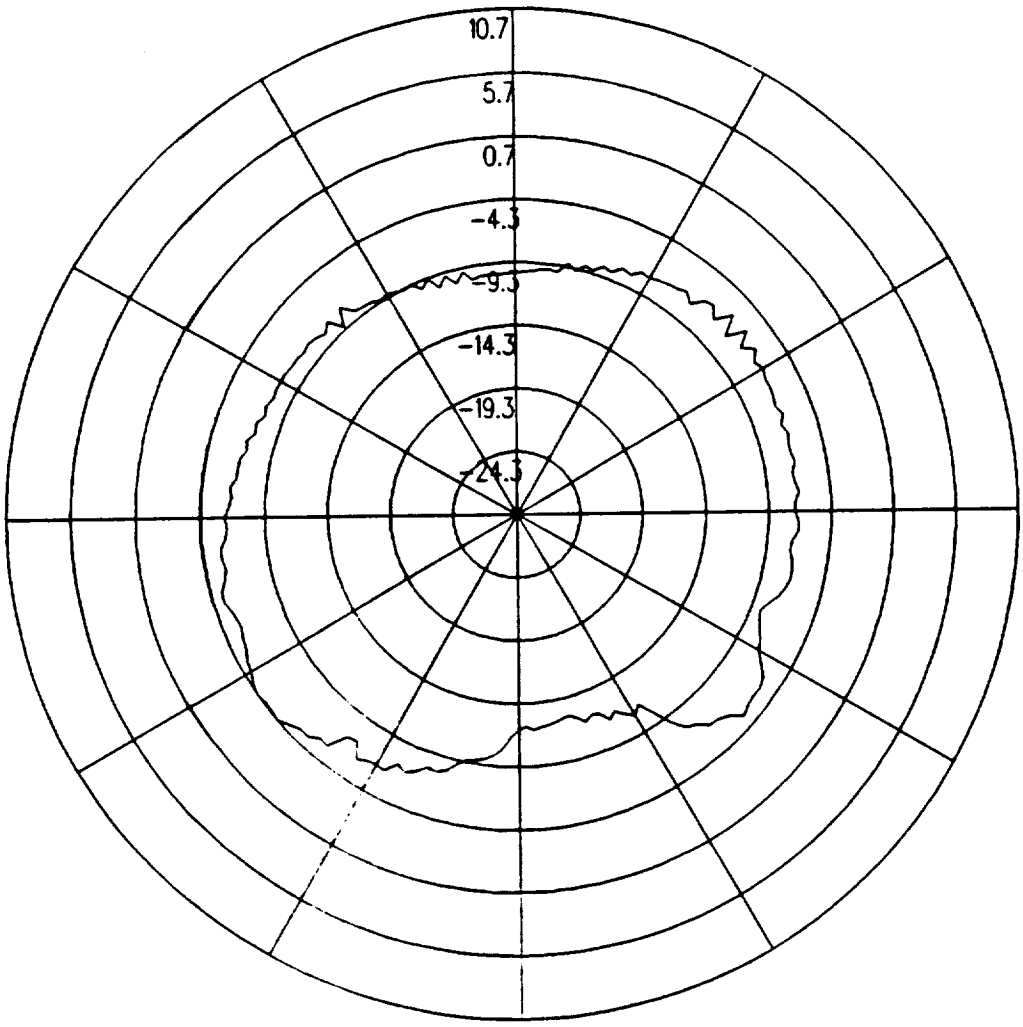

Figure 5.64: UTD calculated conical plane pattern 20° above the horizon for batwing antenna on a P-3C for left hand circular polarization at 300 MHz.(Test Location 5)

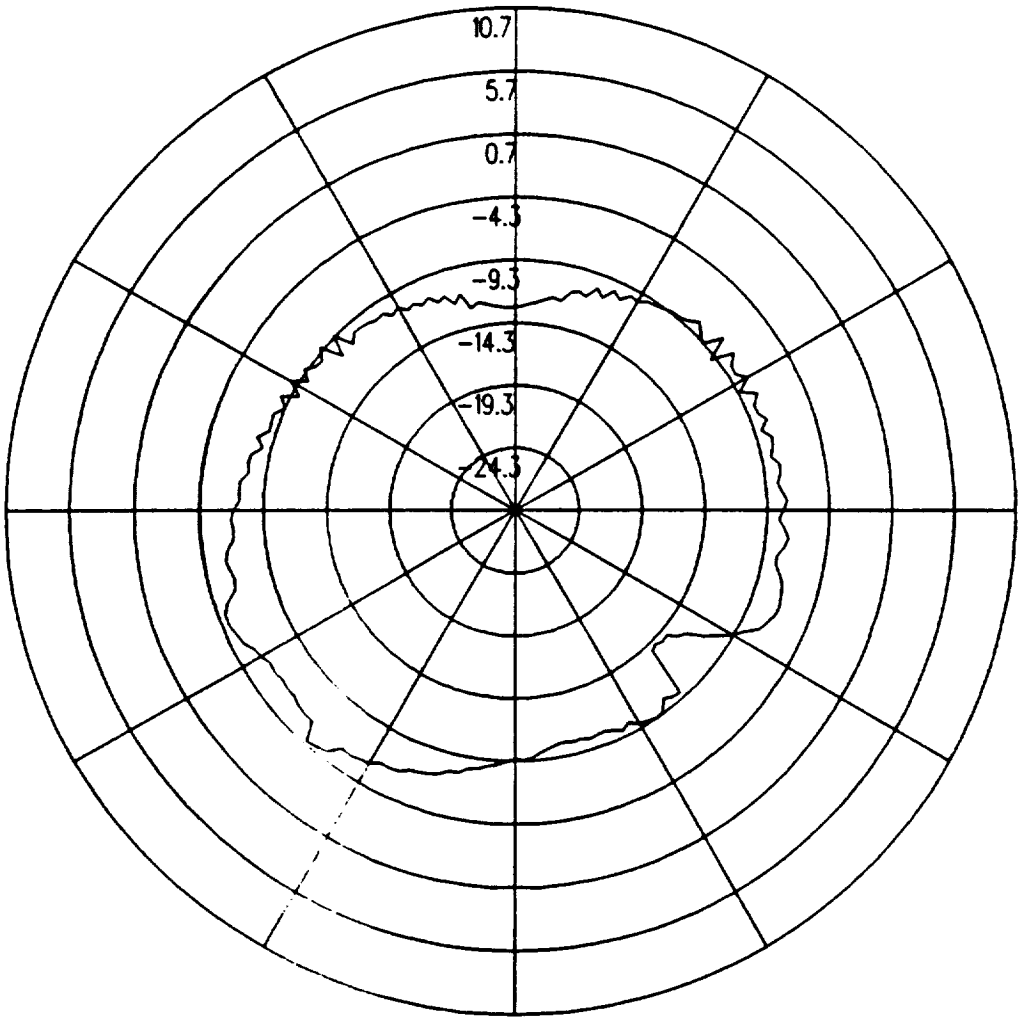

Figure 5.65: UTD calculated conical plane pattern 30° above the horizon for batwing antenna on a P-3C for left hand circular polarization at 300 MHz.(Test Location 5)

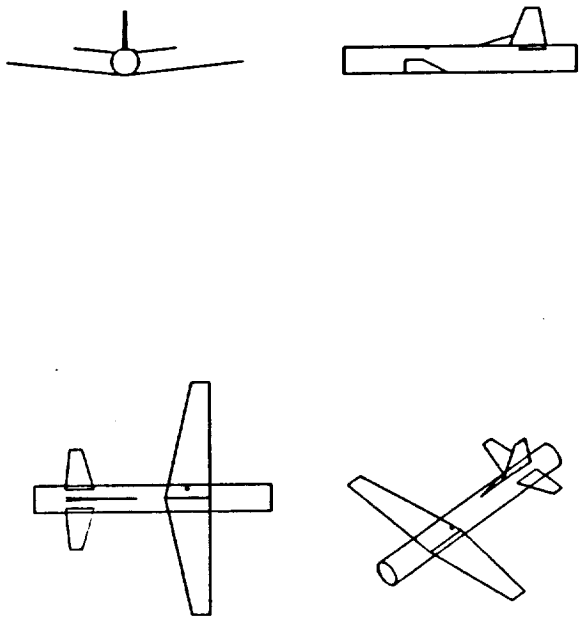

Figure 5.66: Geometry of the model of the P-3C aircraft used in the NEC-BSC code showing the location of the antenna.

5.6 Test Location 6

The antenna is located as illustrated in Figure 5.66, which also shows the computer model used to generate the results. The calculated results at 300 MHz are shown for the roll plane in Figure 5.67, for the azimuth plane in Figure 5.68, for the elevation plane in Figure 5.69, for the conical plane 10° above the horizon in Figure 5.70, for the conical plane 20° above the horizon in Figure 5.71, and for the conical plane 30° above the horizon in Figure 5.72 all for right hand polarization. The cross polarized fields are shown for the roll plane in Figure 5.73, for the azimuth plane in Figure 5.74, for the elevation plane in Figure 5.75, for the conical plane 10° above the horizon in Figure 5.76, for the conical plane 20° above the horizon in Figure 5.77, and for the conical plane 30° above the horizon in Figure 5.78 all for left hand polarization.

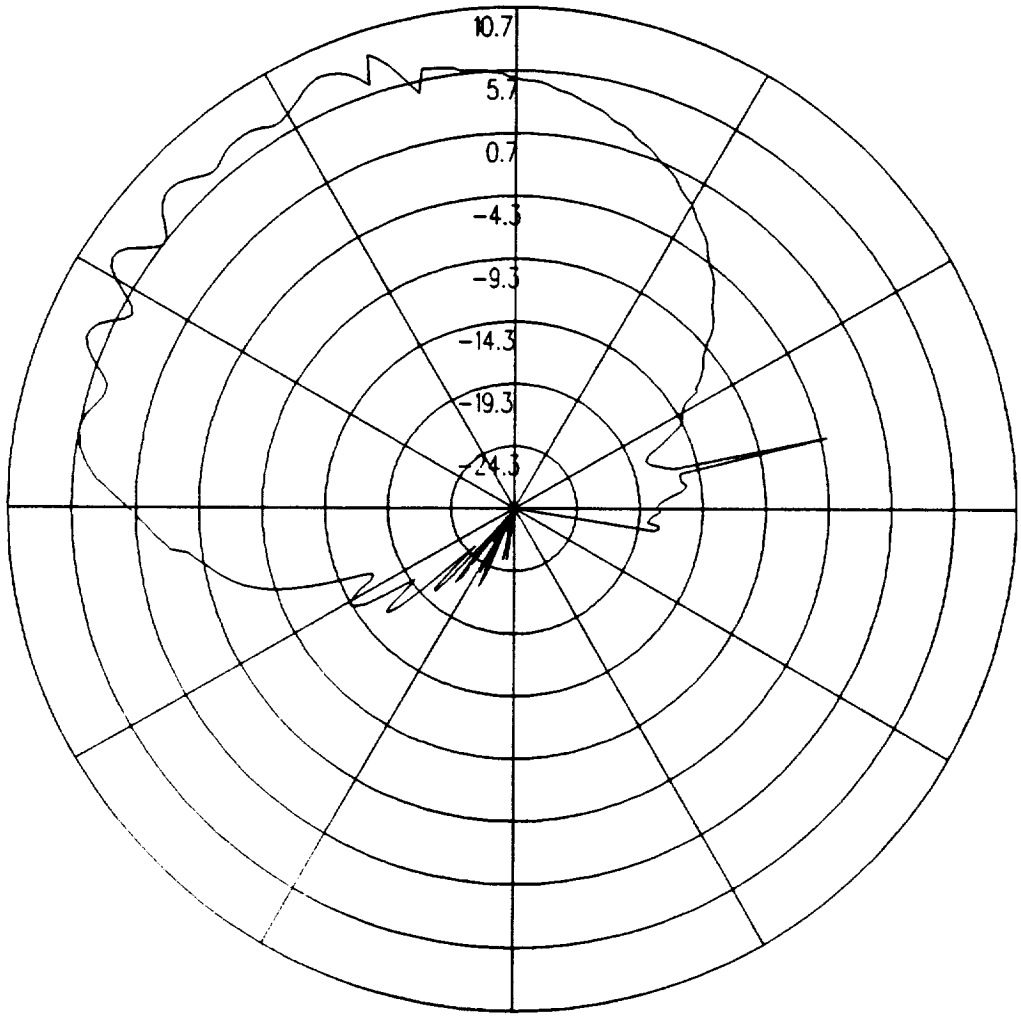

Figure 5.67: UTD calculated roll plane pattern for batwing antenna on a P-3C for right hand circular polarization at 300 MHz. (Test Location 6)

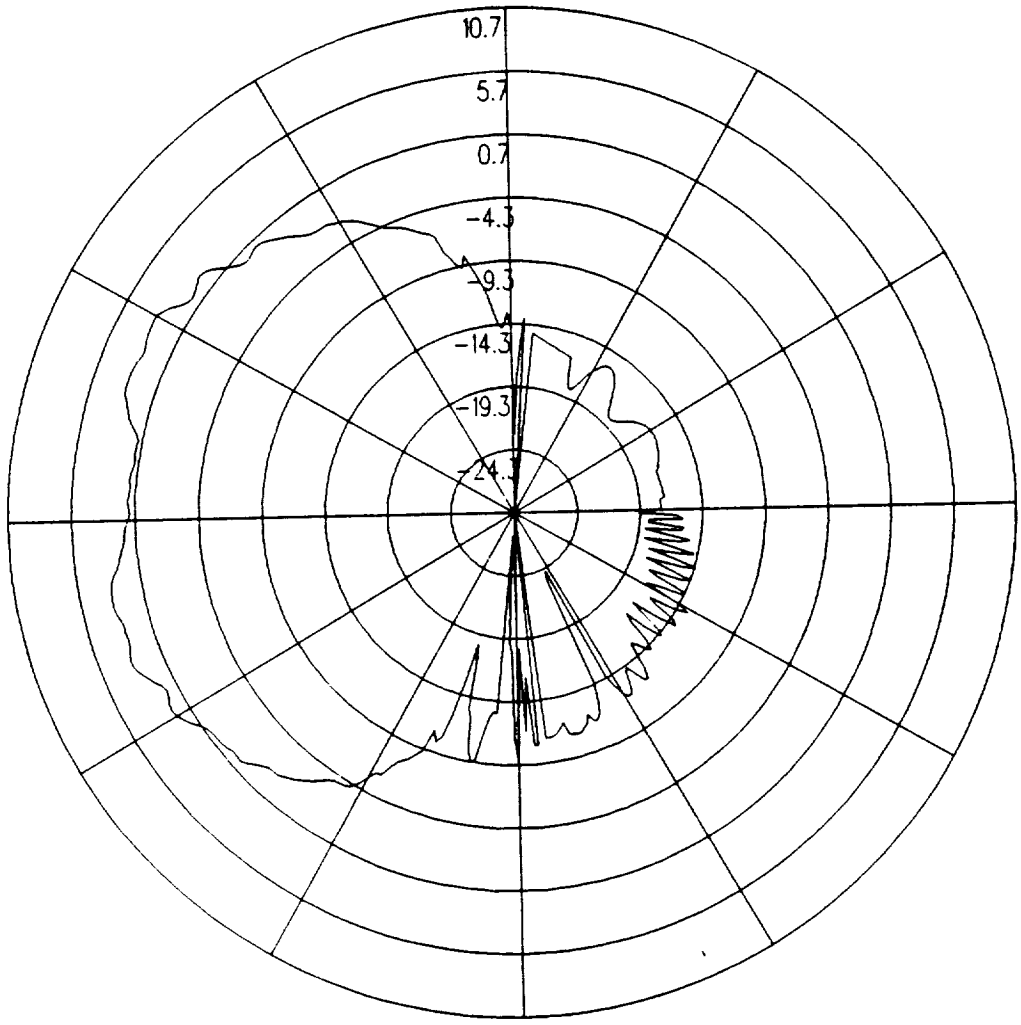

Figure 5.68: UTD calculated azimuth plane pattern for batwing antenna on a P-3C for right hand circular polarization at 300 MHz. (Test Location 6)

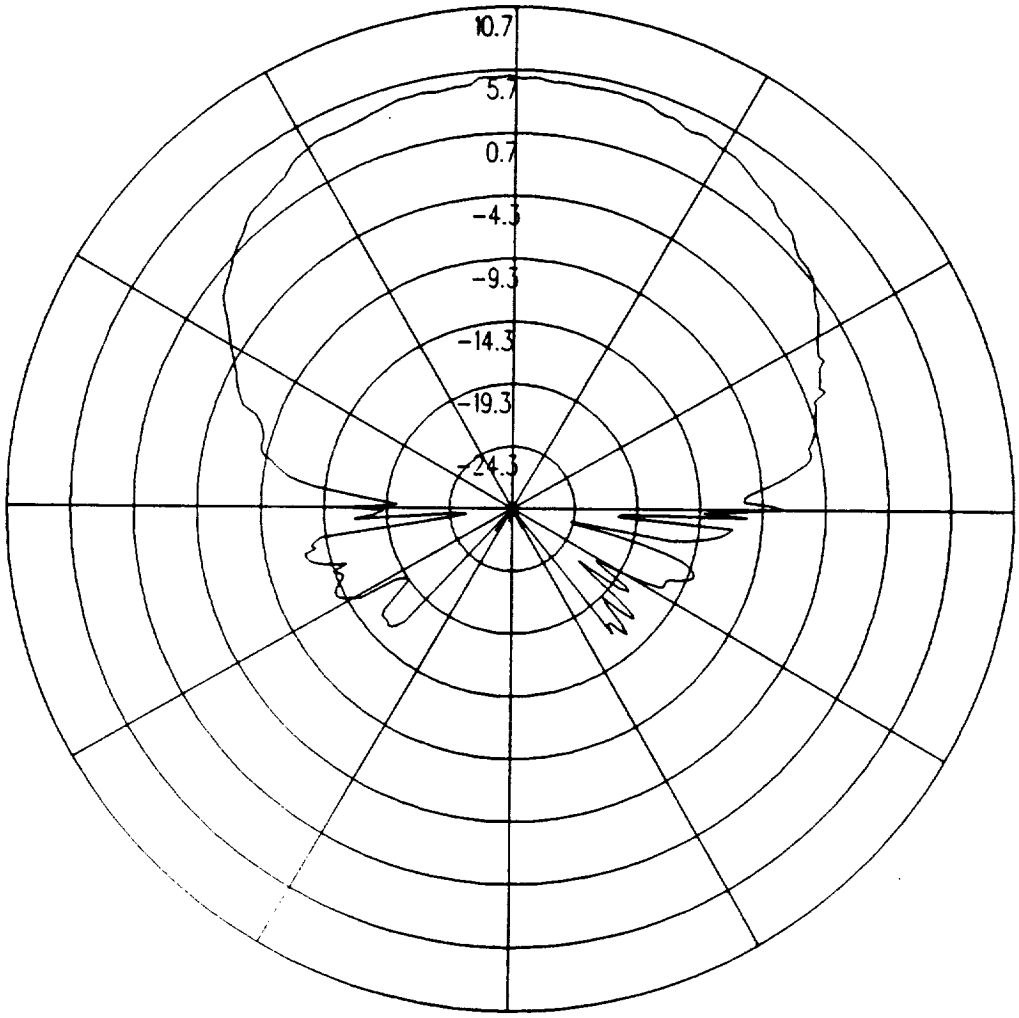

Figure 5.69: UTD calculated elevation plane pattern for batwing antenna on a P-3C for right hand circular polarization at 300 MHz. (Test Location 6)

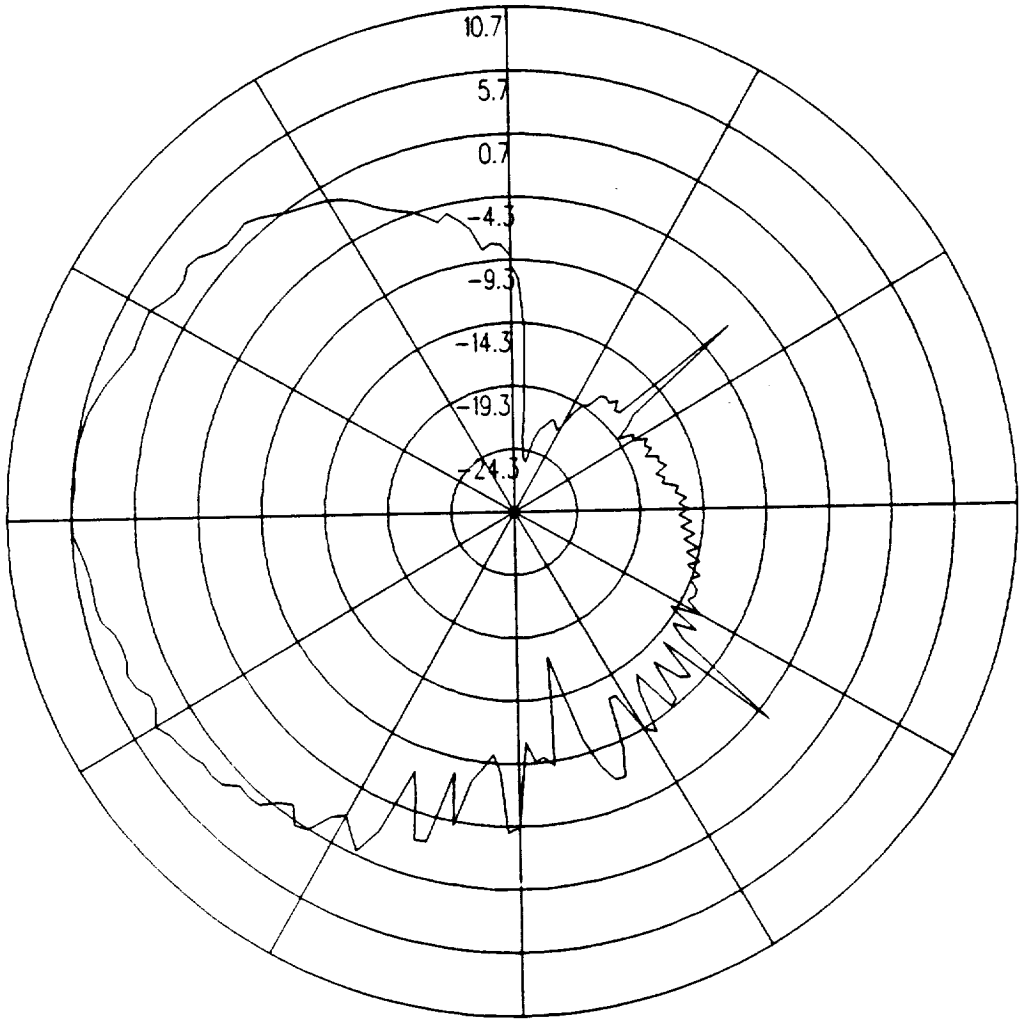

Figure 5.70: UTD calculated conical plane pattern 10° above the horizon for batwing antenna on a P-3C for right hand circular polarization at 300 MHz.(Test Location 6)

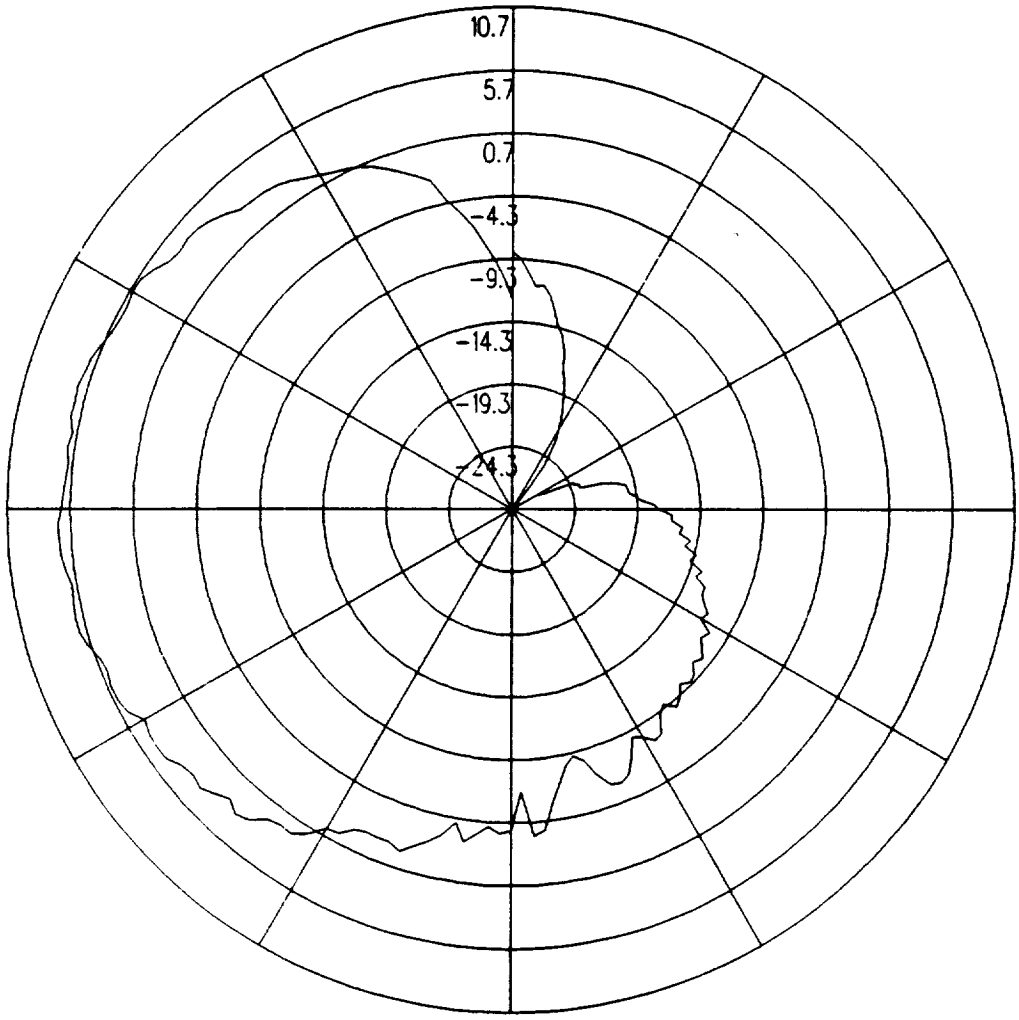

Figure 5.71: UTD calculated conical plane pattern 20° above the horizon for batwing antenna on a P-3C for right hand circular polarization at 300 MHz.(Test Location 6)

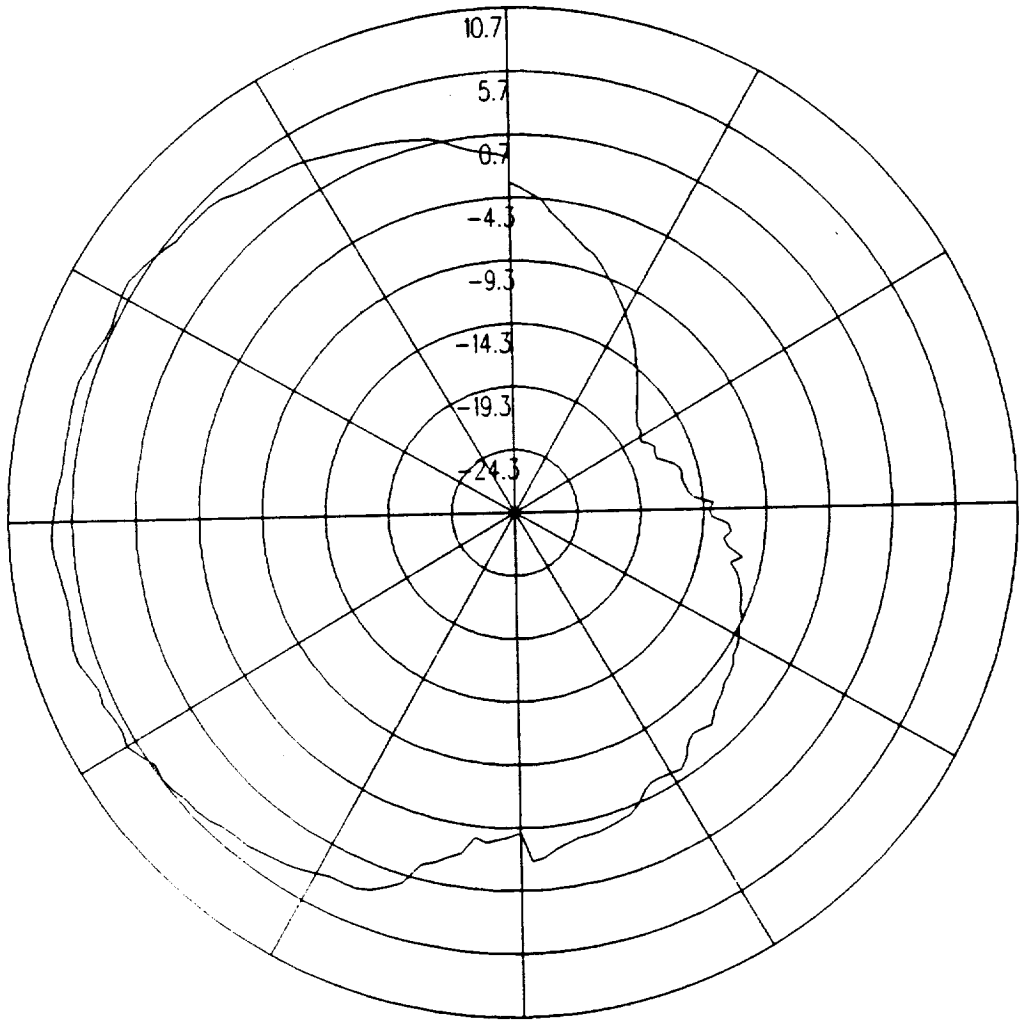

Figure 5.72: UTD calculated conical plane pattern 30° above the horizon for batwing antenna on a P-3C for right hand circular polarization at 300 MHz.(Test Location 6)

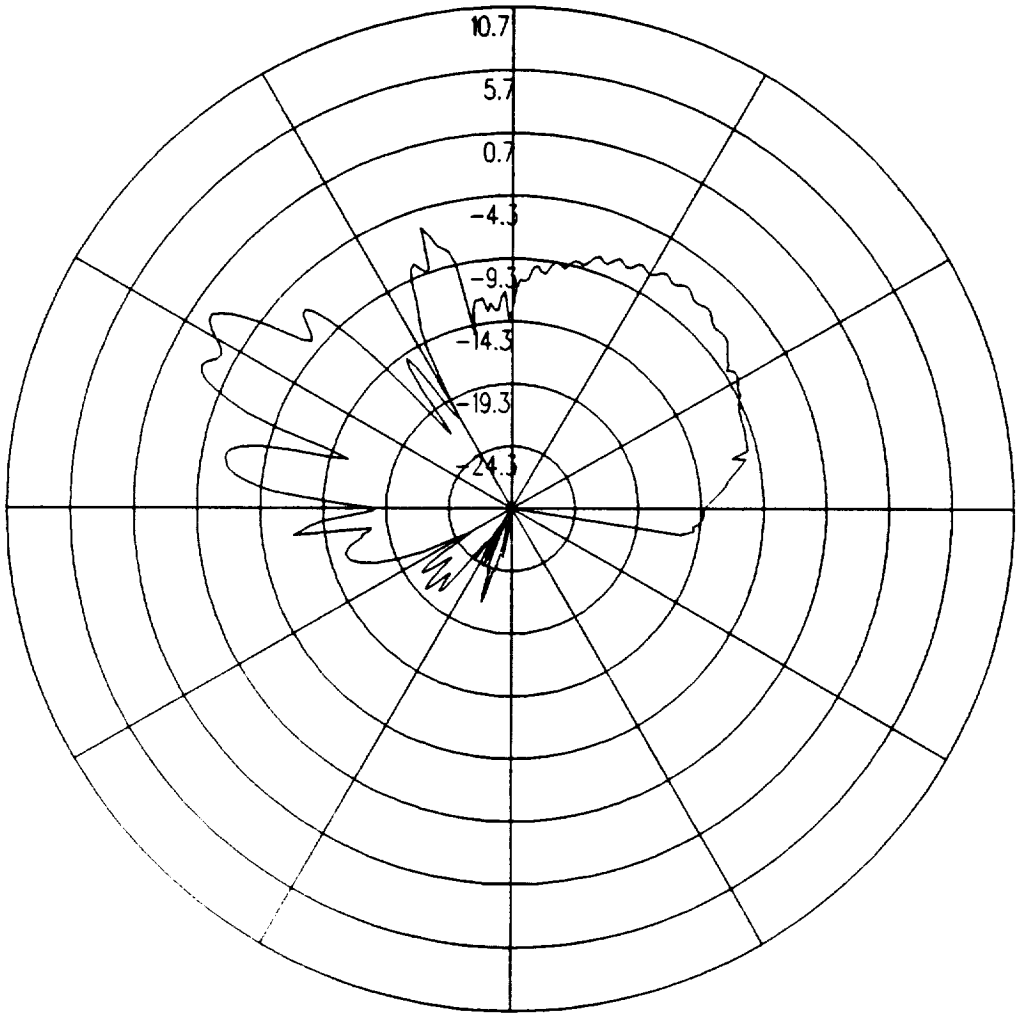

Figure 5.73: UTD calculated roll plane pattern for batwing antenna on a P-3C for left hand circular polarization at 300 MHz. (Test Location 6)

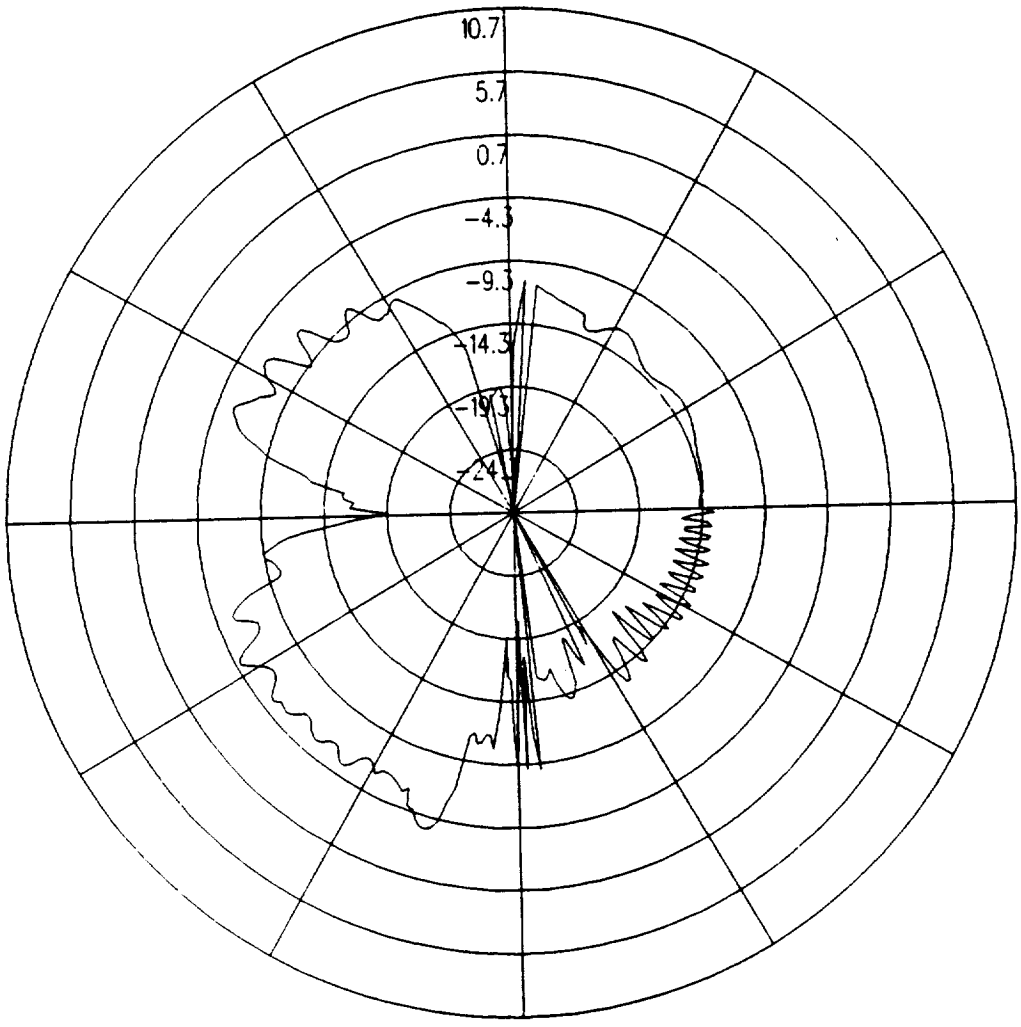

Figure 5.74: UTD calculated azimuth plane pattern for batwing antenna on a P-3C for left hand circular polarization at 300 MHz. (Test Location 6)

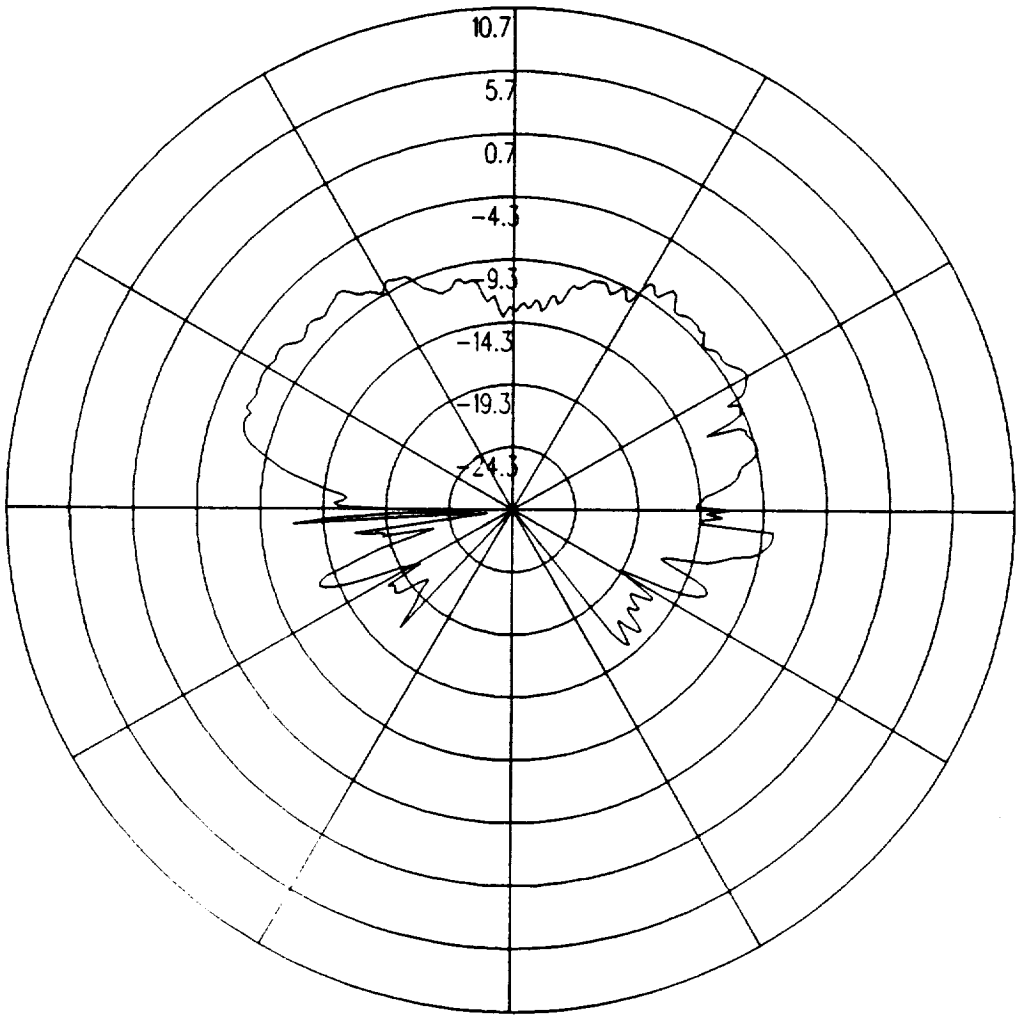

Figure 5.75: UTD calculated elevation plane pattern for batwing antenna on a P-3C for left hand circular polarization at 300 MHz. (Test Location 6)

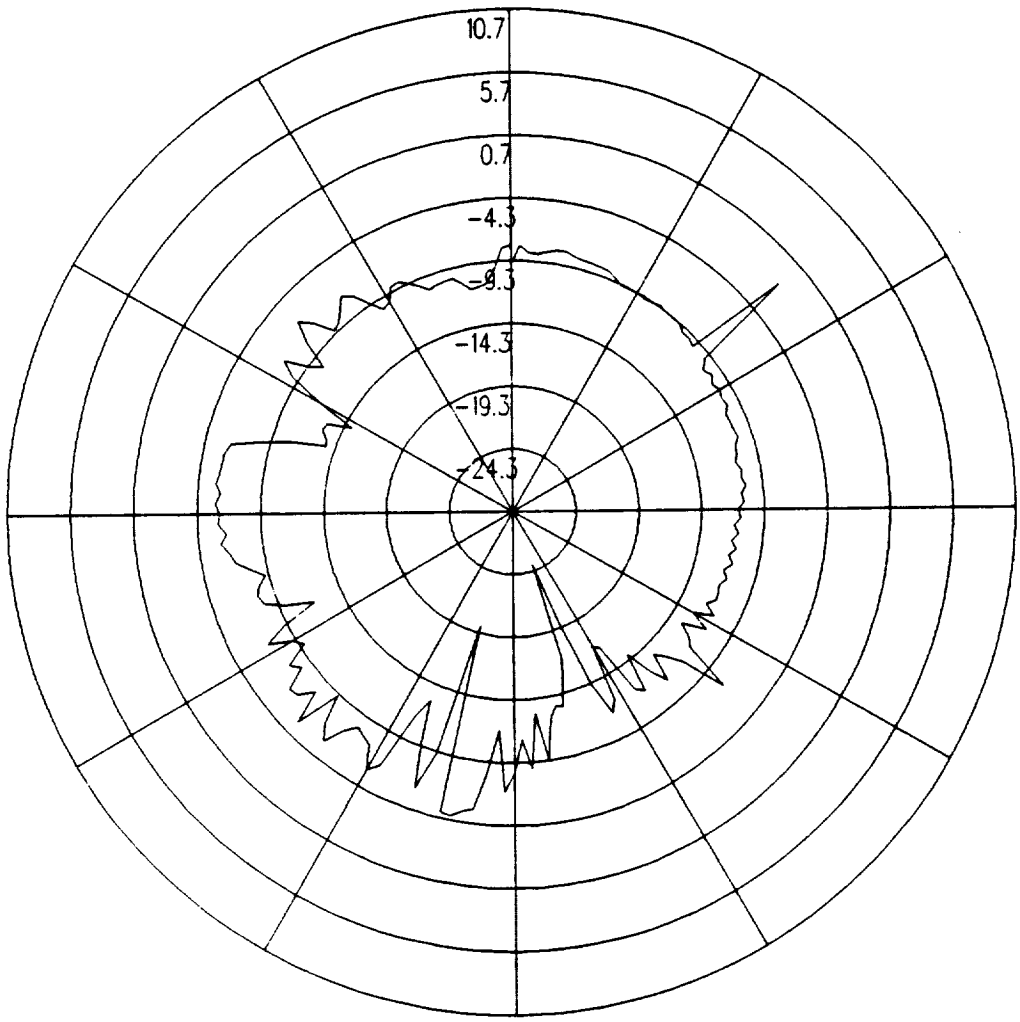

Figure 5.76: UTD calculated conical plane pattern 10° above the horizon for batwing antenna on a P-3C for left hand circular polarization at 300 MHz.(Test Location 6)

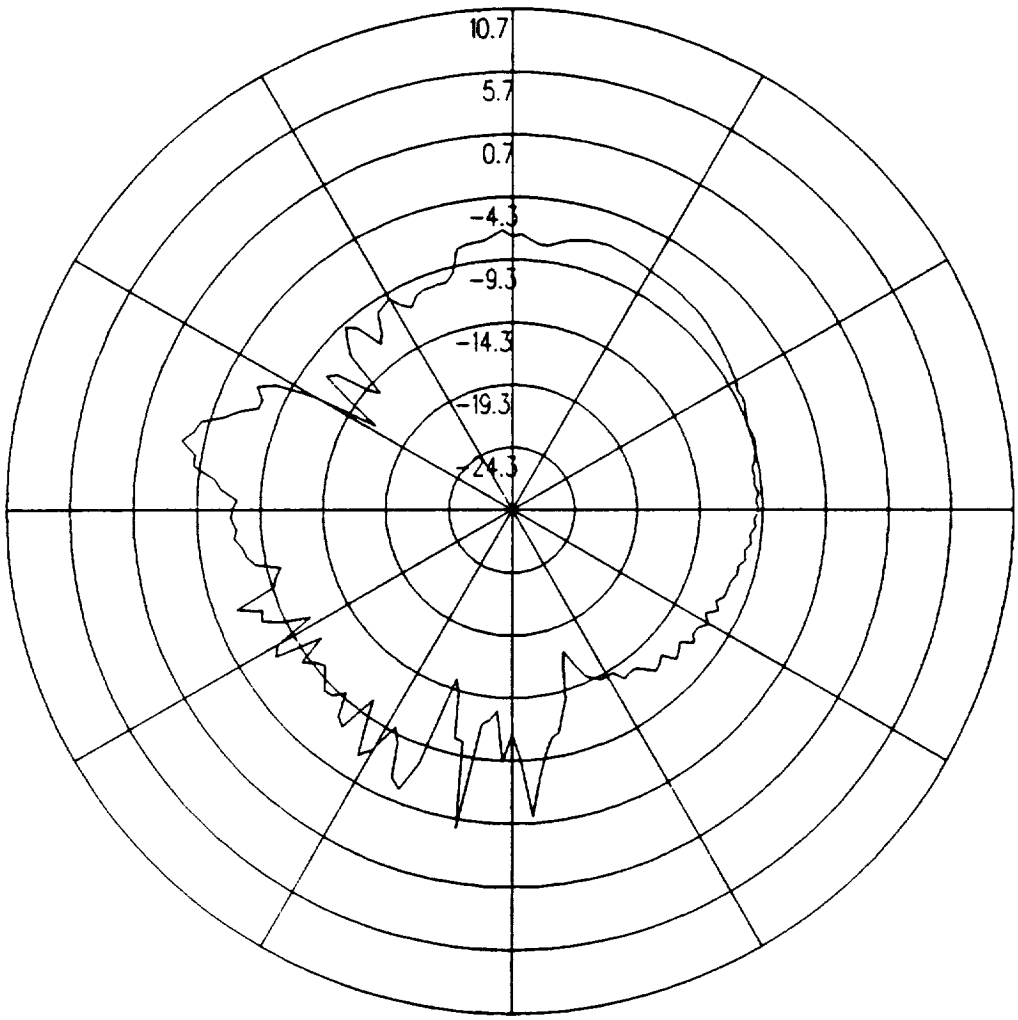

Figure 5.77: UTD calculated conical plane pattern 20° above the horizon for batwing antenna on a P-3C for left hand circular polarization at 300 MHz.(Test Location 6)

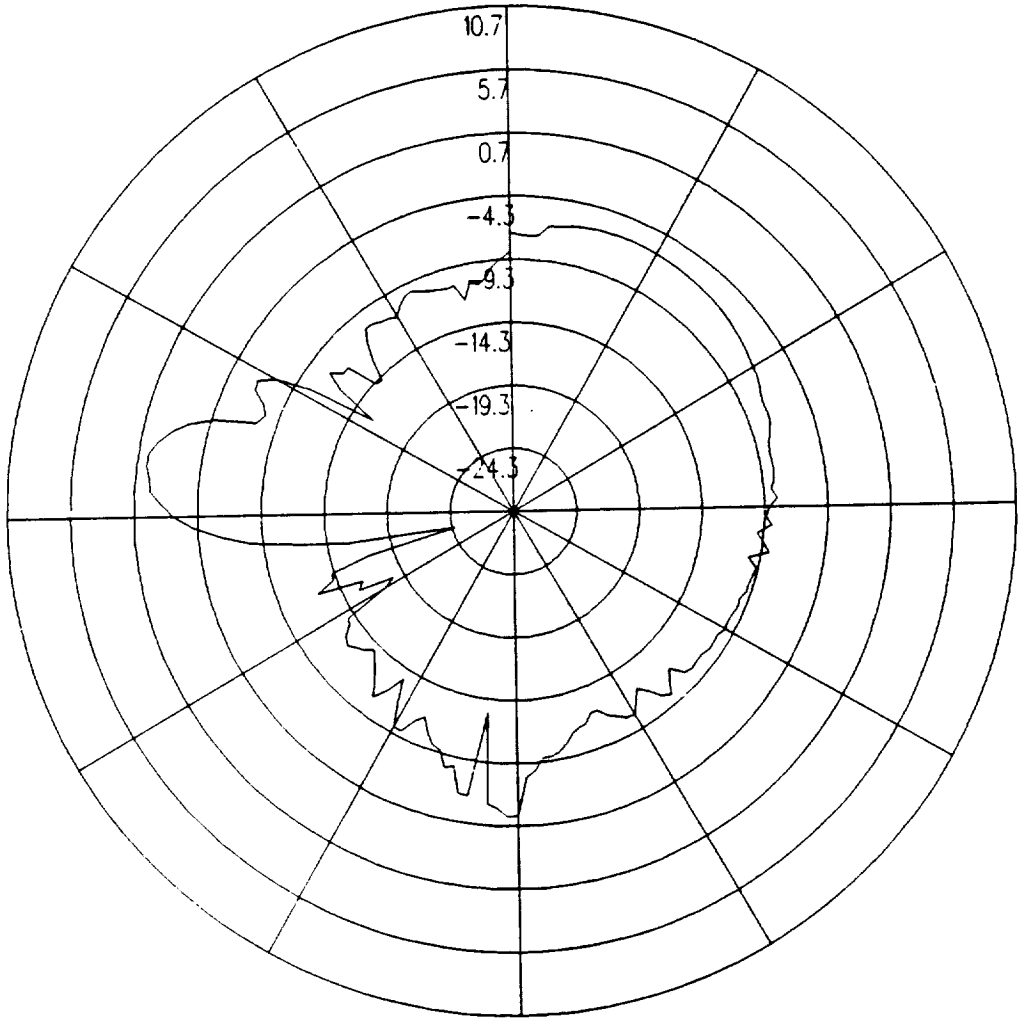

Figure 5.78: UTD calculated conical plane pattern 30° above the horizon for batwing antenna on a P-3C for left hand circular polarization at 300 MHz.(Test Location 6)

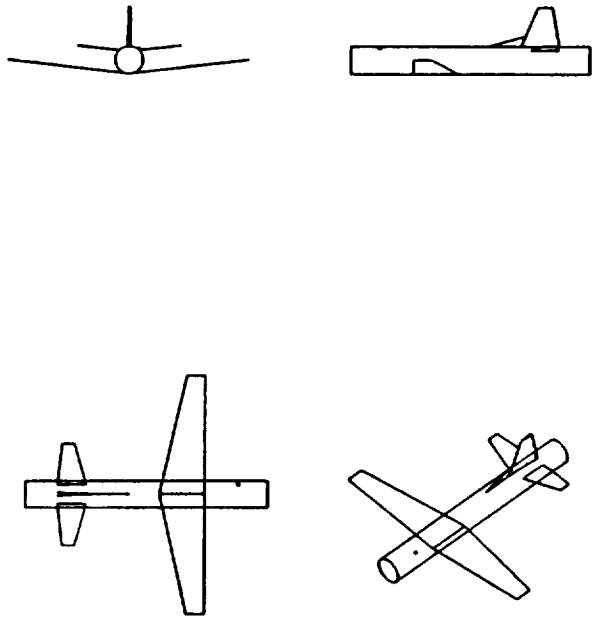

Figure 5.79: Geometry of the model of the P-3C aircraft used in the NEC-BSC code showing the location of the antenna.

5.7 Test Location 7

The antenna is located as illustrated in Figure 5.79, which also shows the computer model used to generate the results. The calculated results at 300 MHz are shown for the roll plane in Figure 5.80, for the azimuth plane in Figure 5.81, for the elevation plane in Figure 5.82, for the conical plane 10° above the horizon in Figure 5.83, for the conical plane 20° above the horizon in Figure 5.84, and for the conical plane 30° above the horizon in Figure 5.85 all for right hand polarization. The cross polarized fields are shown for the roll plane in Figure 5.86, for the azimuth plane in Figure 5.87, for the elevation plane in Figure 5.88, for the conical plane 10° above the horizon in Figure 5.89, for the conical plane 20° above the horizon in Figure 5.90, and for the conical plane 30° above the horizon in Figure 5.91 all for left hand polarization.

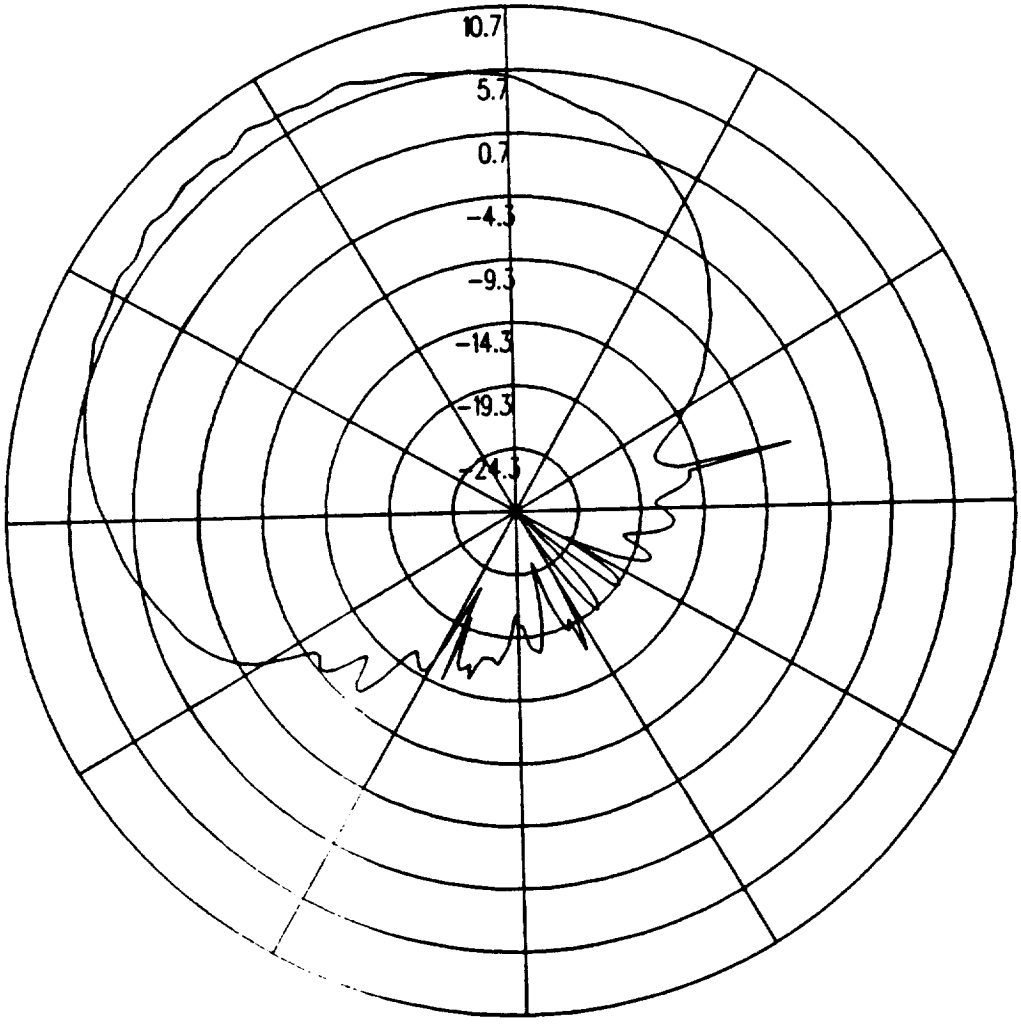

Figure 5.80: UTD calculated roll plane pattern for batwing antenna on a P-3C for right hand circular polarization at 300 MHz. (Test Location 7)

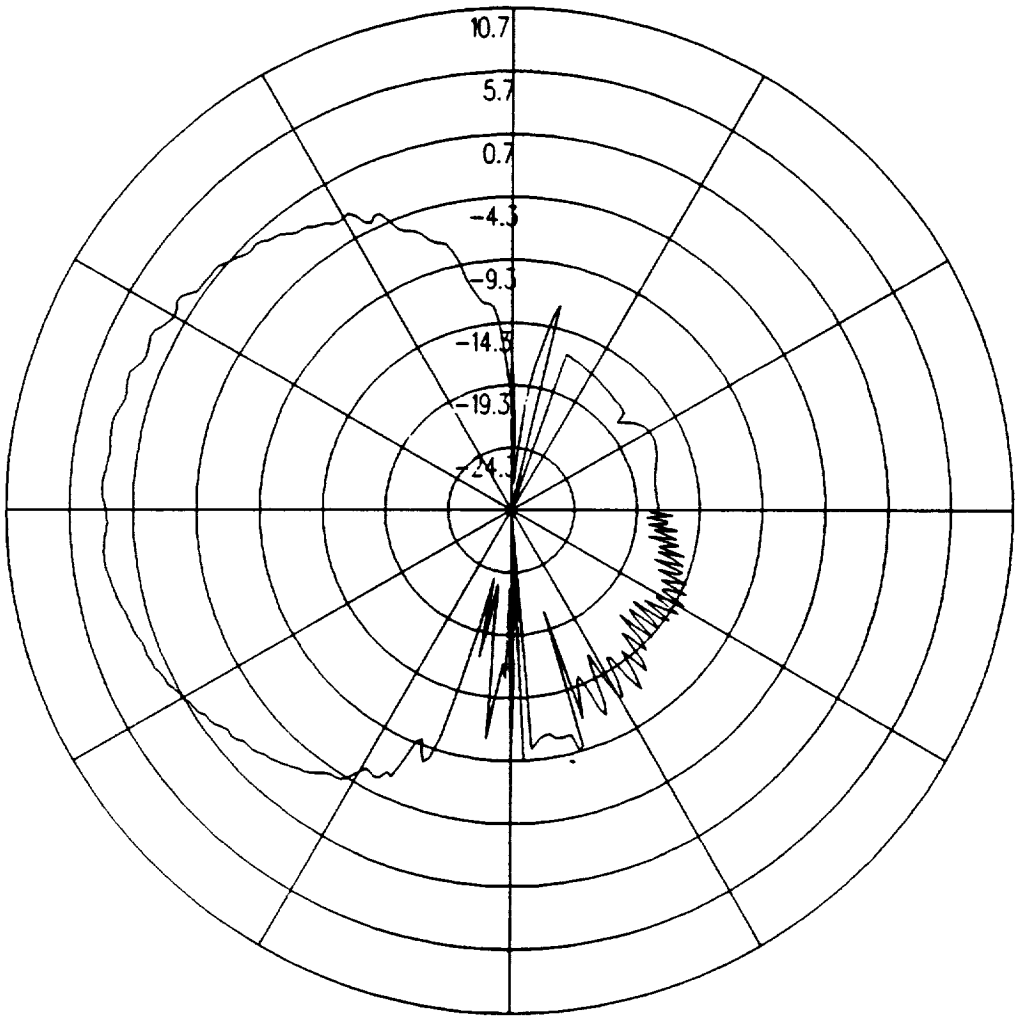

Figure 5.81: UTD calculated azimuth plane pattern for batwing antenna on a P-3C for right hand circular polarization at 300 MHz. (Test Location 7)

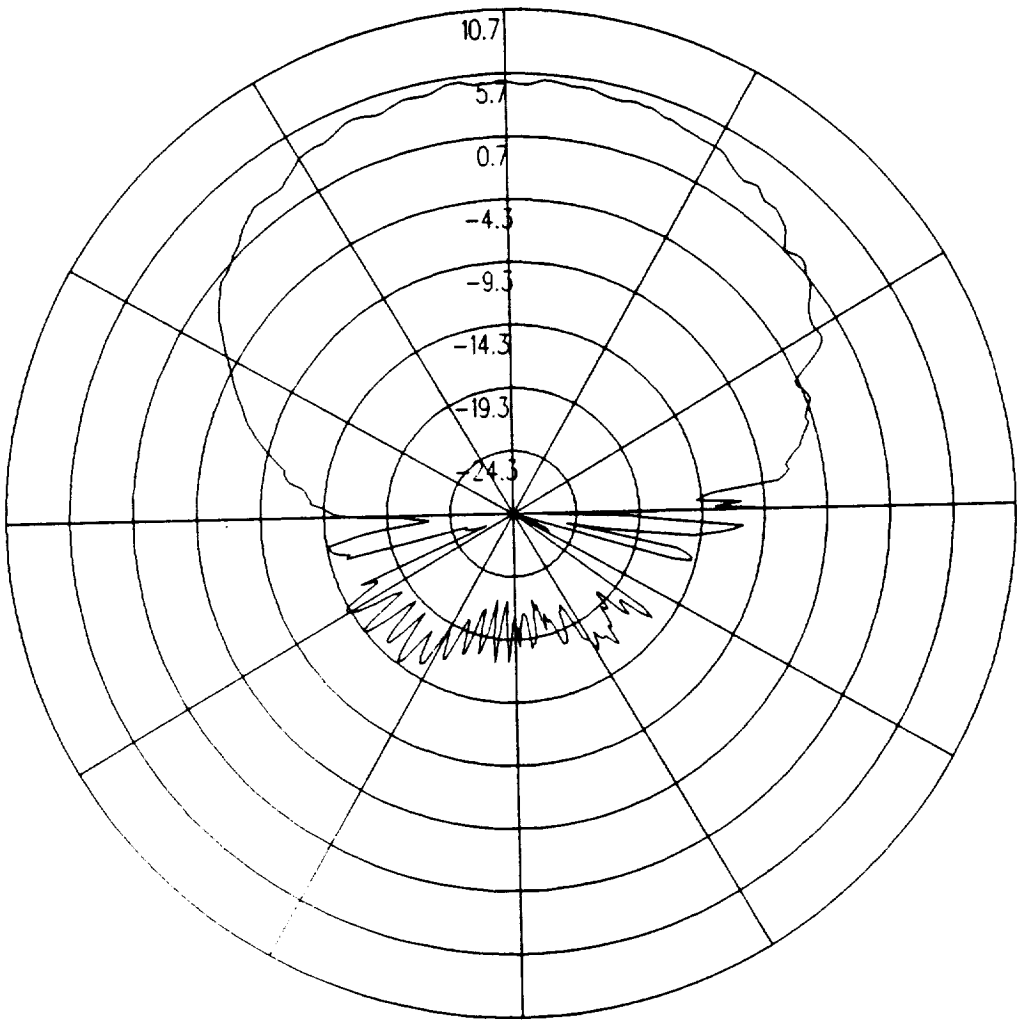

Figure 5.82: UTD calculated elevation plane pattern for batwing antenna on a P-3C for right hand circular polarization at 300 MHz. (Test Location 7)

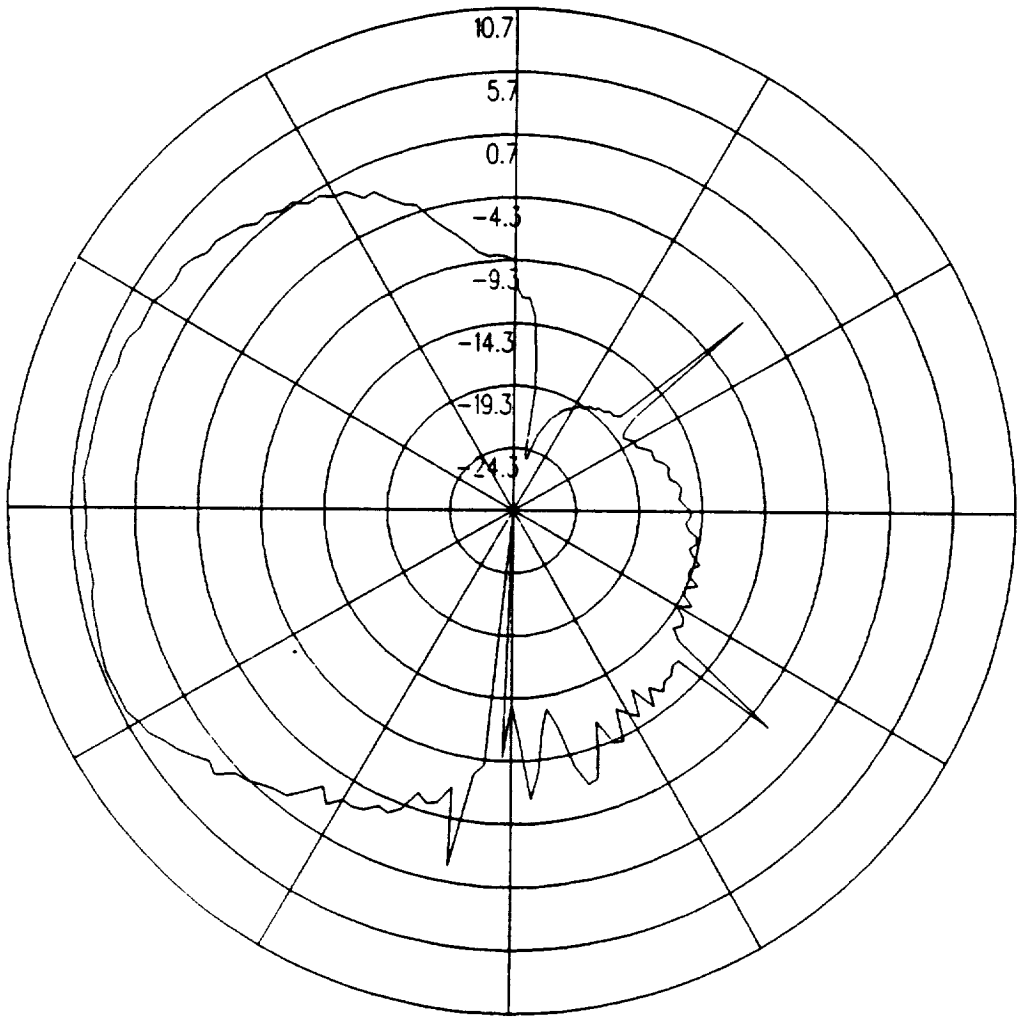

Figure 5.83: UTD calculated conical plane pattern 10° above the horizon for batwing antenna on a P-3C for right hand circular polarization at 300 MHz.(Test Location 7)

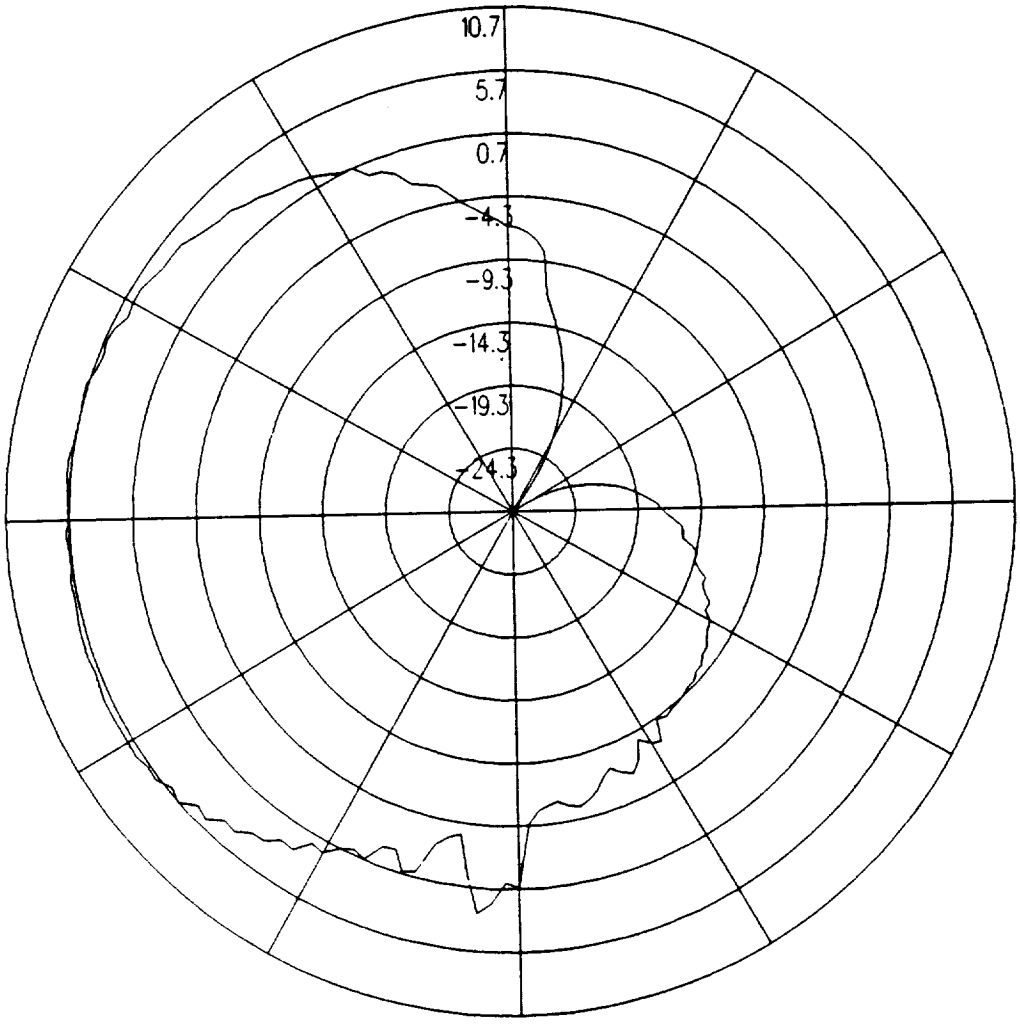

Figure 5.84: UTD calculated conical plane pattern 20° above the horizon for batwing antenna on a P-3C for right hand circular polarization at 300 MHz.(Test Location 7)

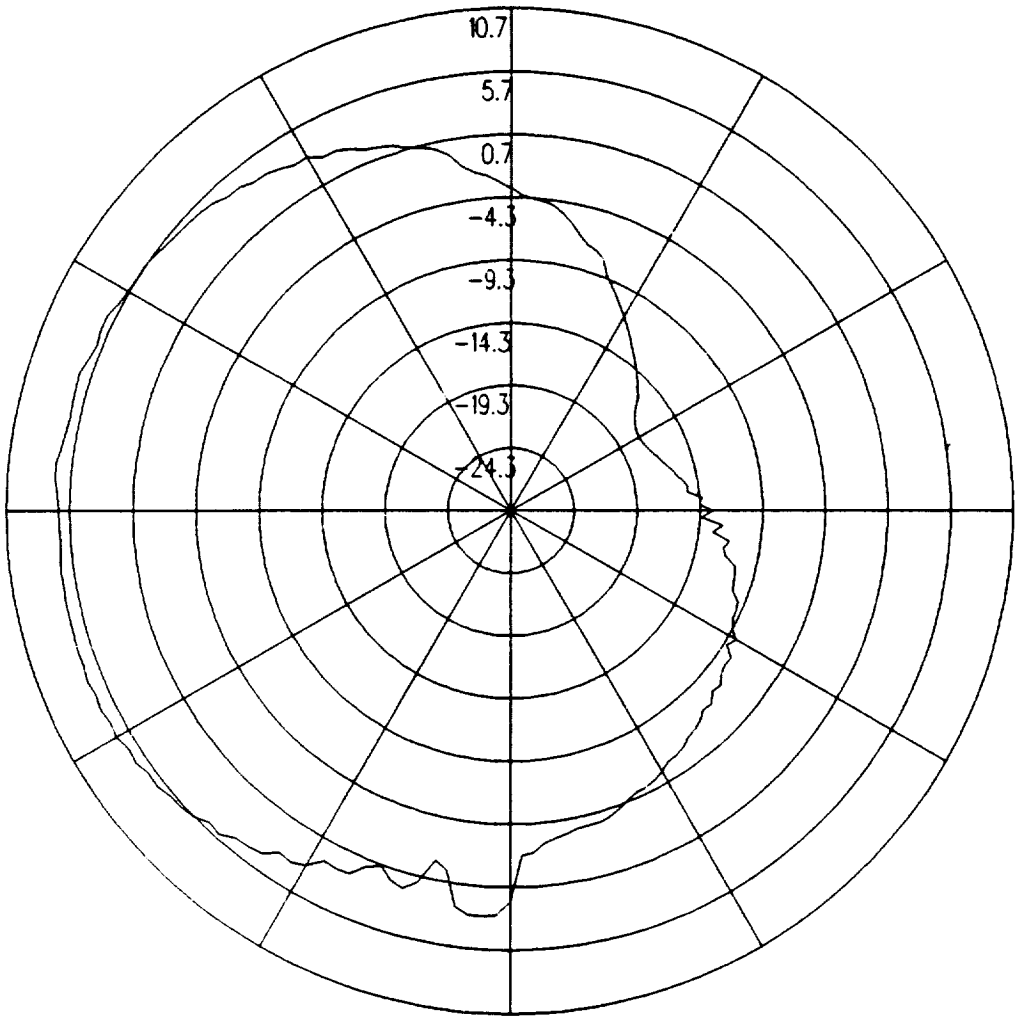

Figure 5.85: UTD calculated conical plane pattern 30° above the horizon for batwing antenna on a P-3C for right hand circular polarization at 300 MHz.(Test Location 7)

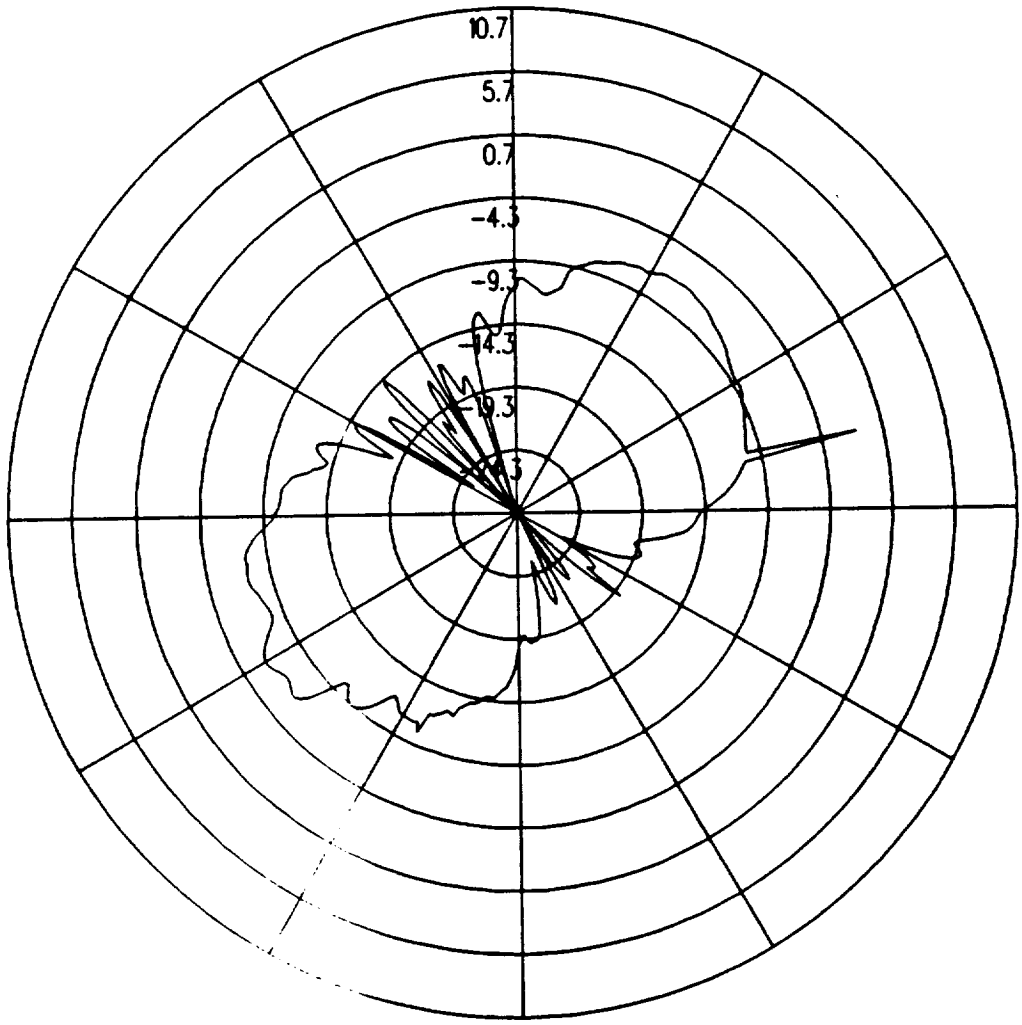

Figure 5.86: UTD calculated roll plane pattern for batwing antenna on a P-3C for left hand circular polarization at 300 MHz. (Test Location 7)

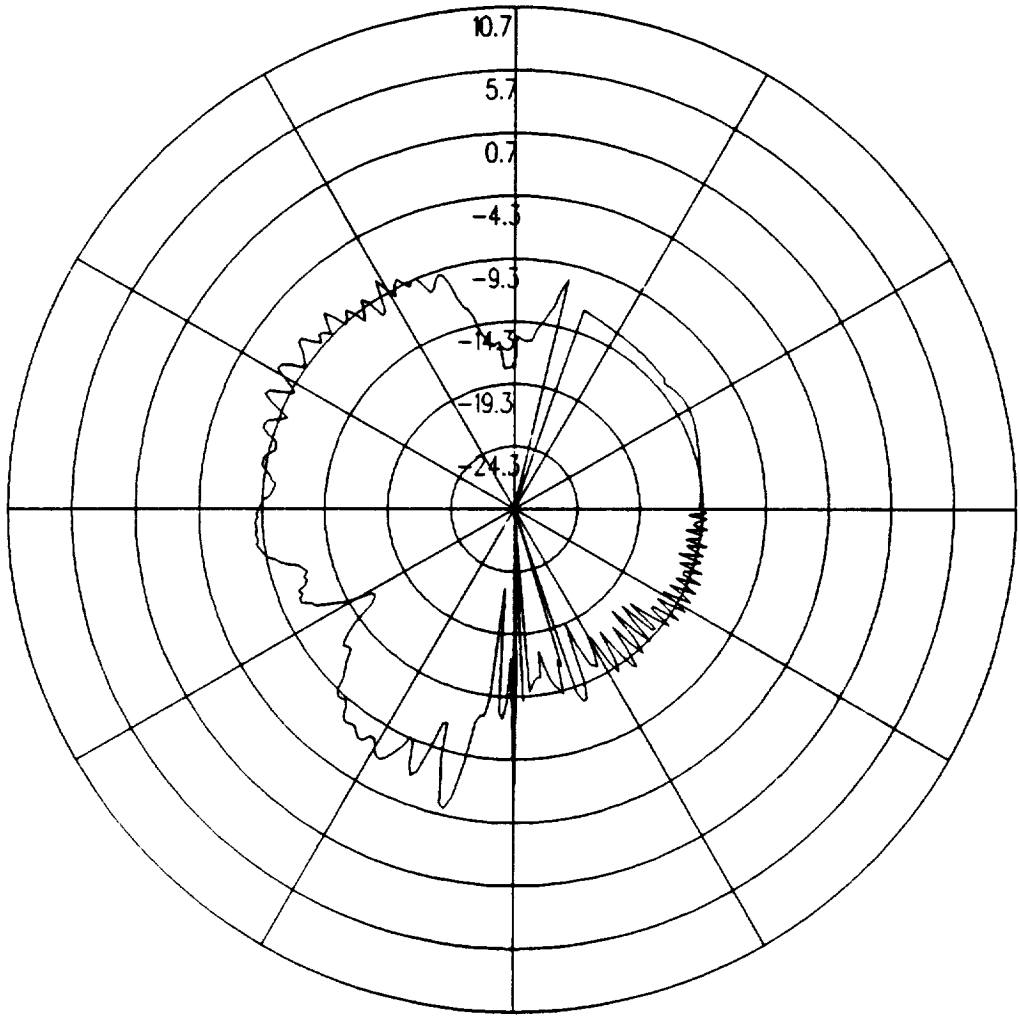

Figure 5.87: UTD calculated azimuth plane pattern for batwing antenna on a P-3C for left hand circular polarization at 300 MHz. (Test Location 7)

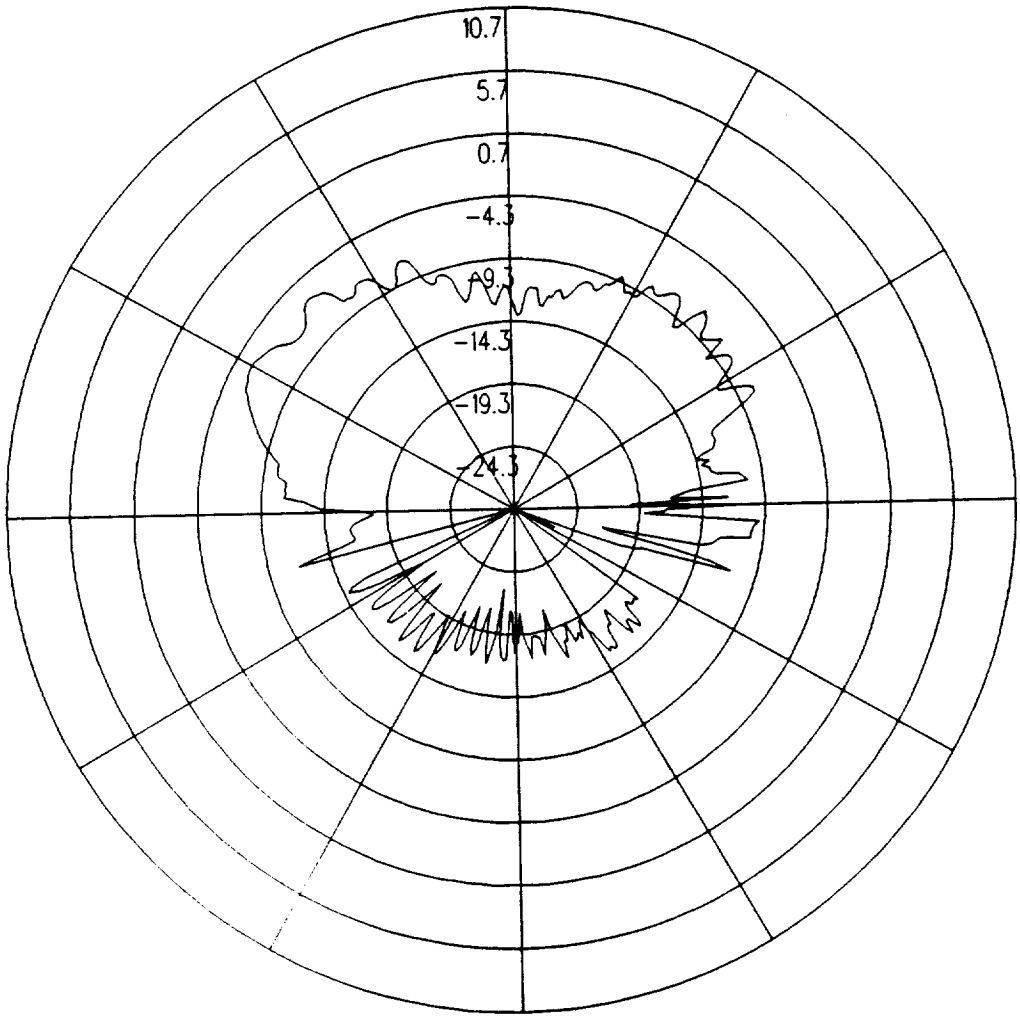

Figure 5.88: UTD calculated elevation plane pattern for batwing antenna on a P-3C for left hand circular polarization at 300 MHz. (Test Location 7)

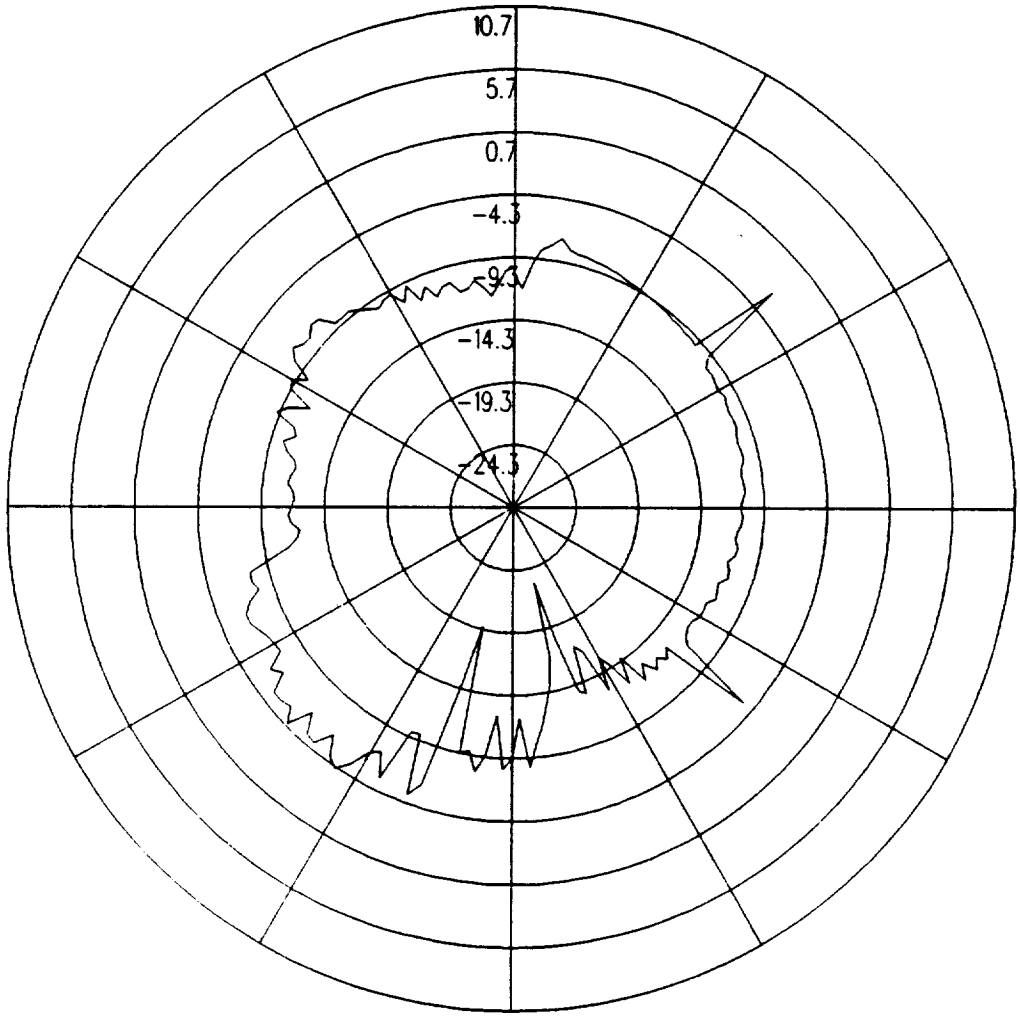

Figure 5.89: UTD calculated conical plane pattern 10° above the horizon for batwing antenna on a P-3C for left hand circular polarization at 300 MHz.(Test Location 7)

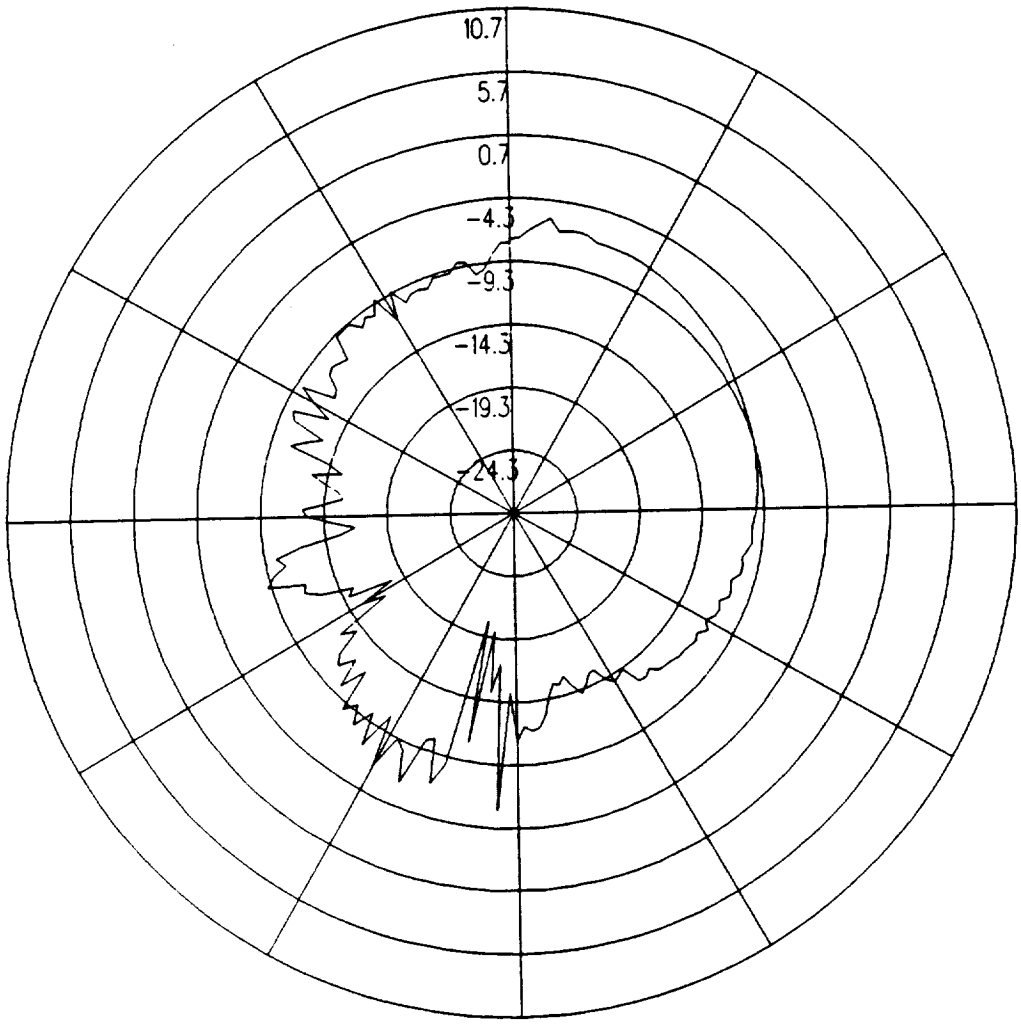

Figure 5.90: UTD calculated conical plane pattern 20° above the horizon for batwing antenna on a P-3C for left hand circular polarization at 300 MHz.(Test Location 7)

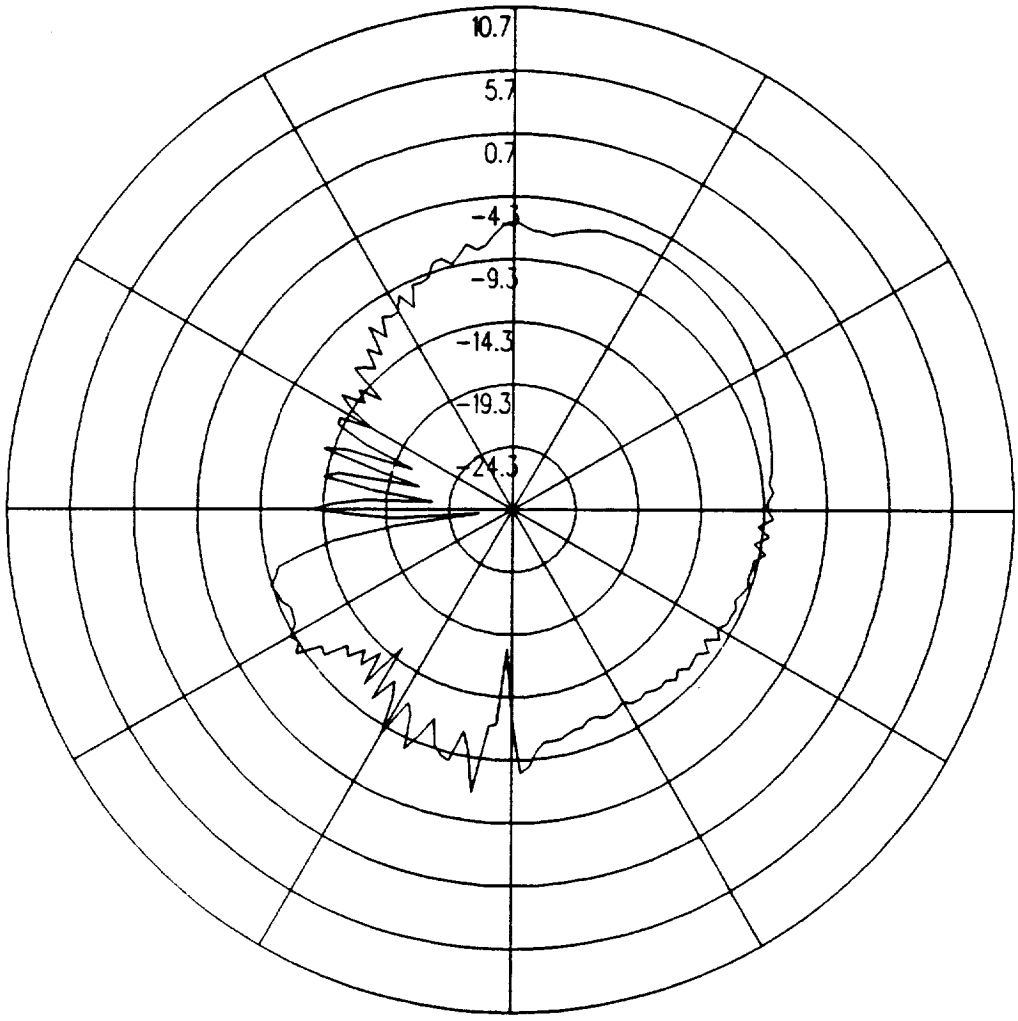

Figure 5.91: UTD calculated conical plane pattern 30° above the horizon for batwing antenna on a P-3C for left hand circular polarization at 300 MHz.(Test Location 7)

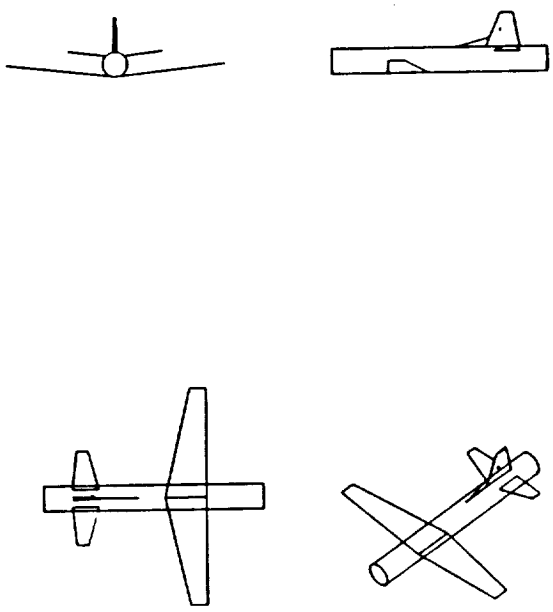

Figure 5.92: Geometry of the model of the P-3C aircraft used in the NEC-BSC code showing the location of the antenna.

5.8 Test Location 8

The antenna is located as illustrated in Figure 5.92, which also shows the computer model used to generate the results. The calculated results at 300 MHz are shown for the roll plane in Figure 5.93, for the azimuth plane in Figure 5.94, for the elevation plane in Figure 5.95, for the conical plane 10° above the horizon in Figure 5.96, for the conical plane 20° above the horizon in Figure 5.97, and for the conical plane 30° above the horizon in Figure 5.98 all for right hand polarization. The cross polarized fields are shown for the roll plane in Figure 5.99, for the azimuth plane in Figure 5.100, for the elevation plane in Figure 5.101, for the conical plane 10° above the horizon in Figure 5.102, for the conical plane 20° above the horizon in Figure 5.103, and for the conical plane 30° above the horizon in Figure 5.104 all for left hand polarization.

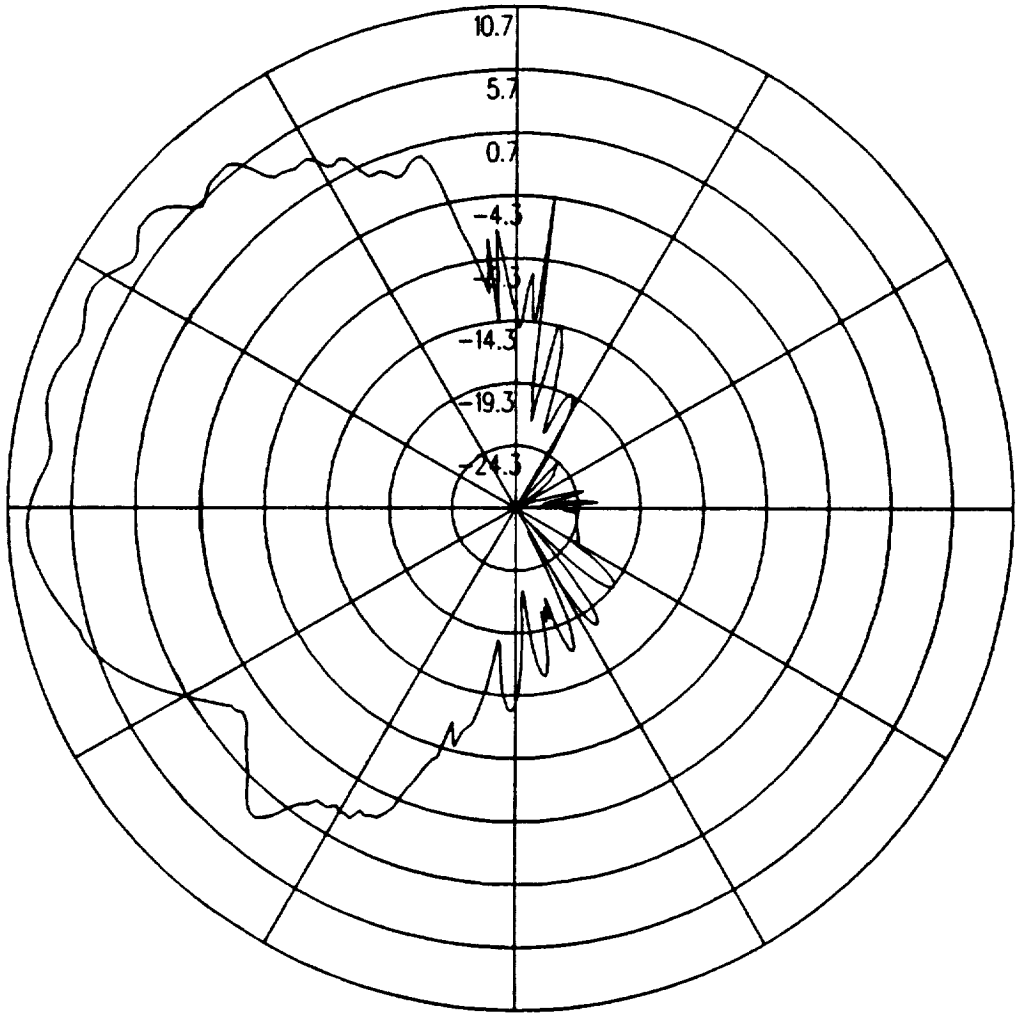

Figure 5.93: UTD calculated roll plane pattern for batwing antenna on a P-3C for right hand circular polarization at 300 MHz. (Test Location 8)

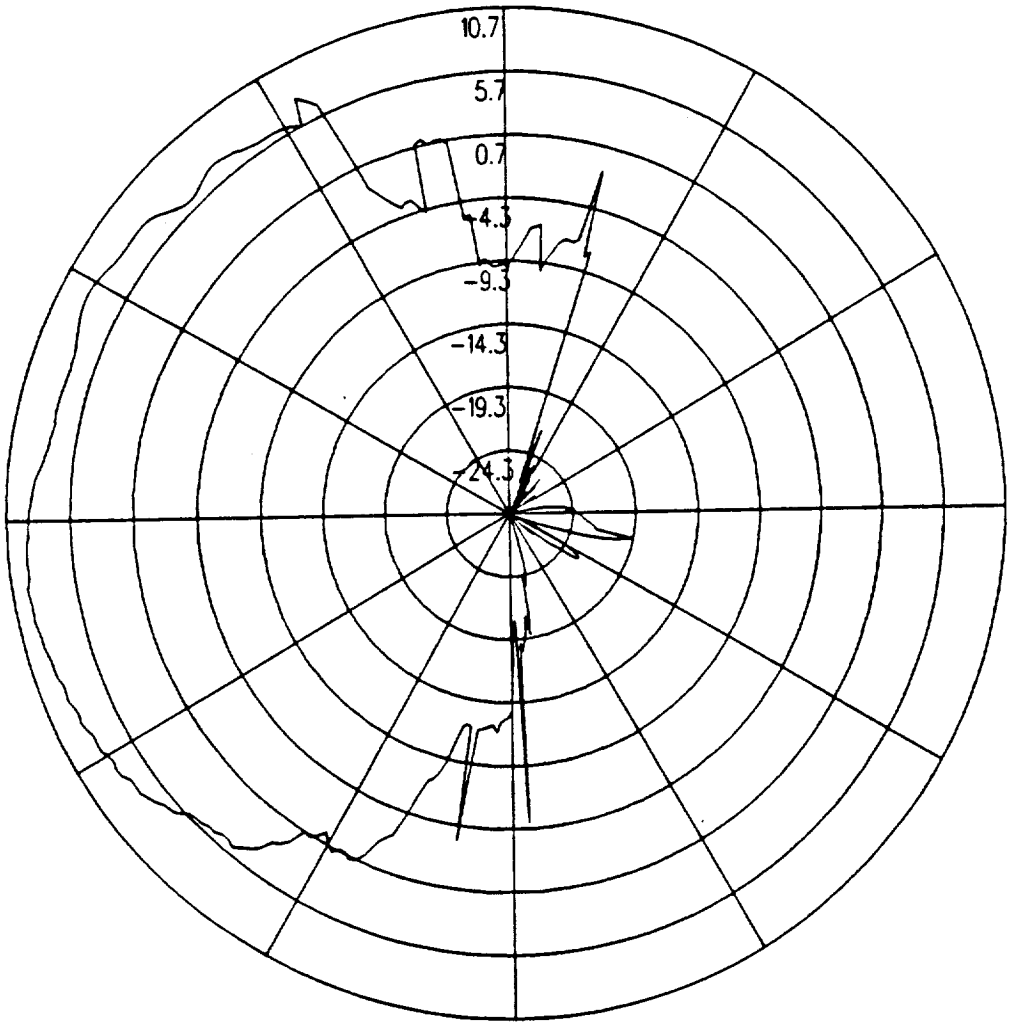

Figure 5.94: UTD calculated azimuth plane pattern for batwing antenna on a P-3C for right hand circular polarization at 300 MHz. (Test Location 8)

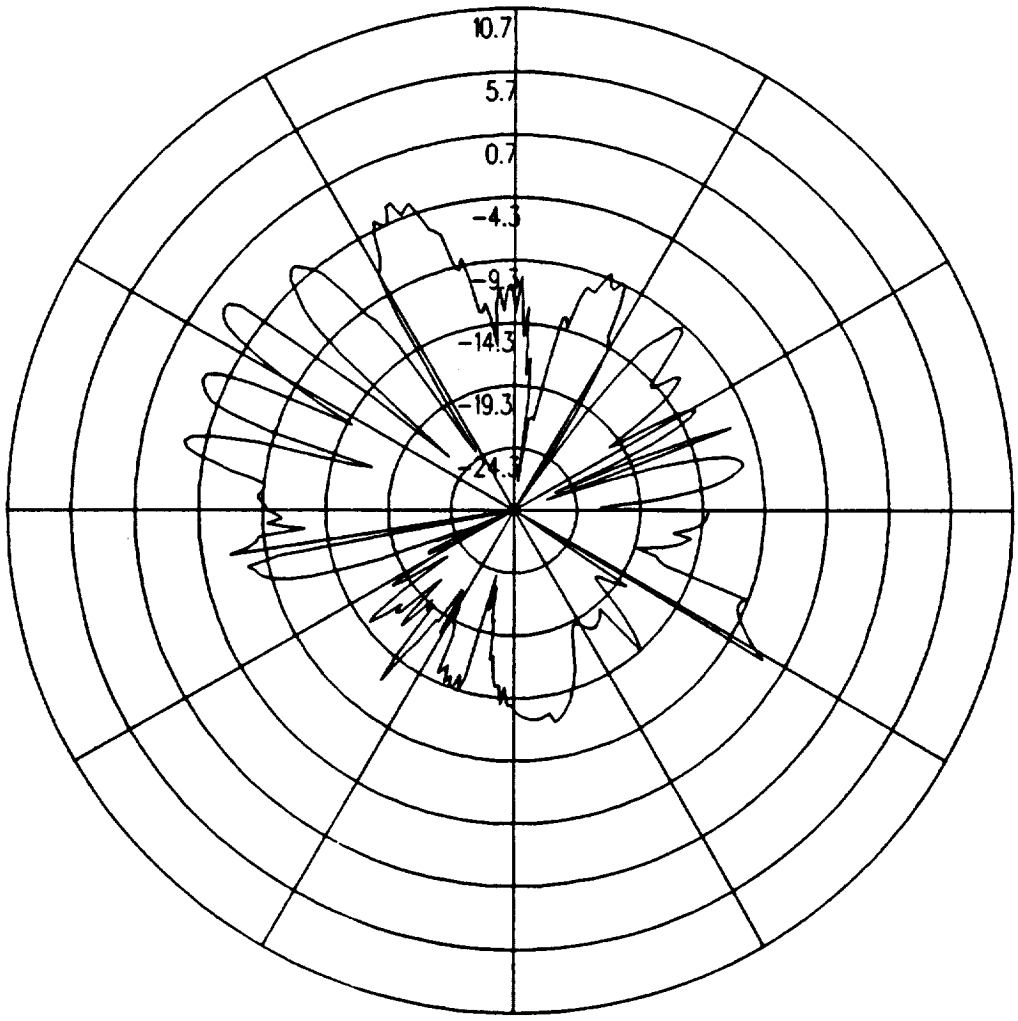

Figure 5.95: UTD calculated elevation plane pattern for batwing antenna on a P-3C for right hand circular polarization at 300 MHz. (Test Location 8)

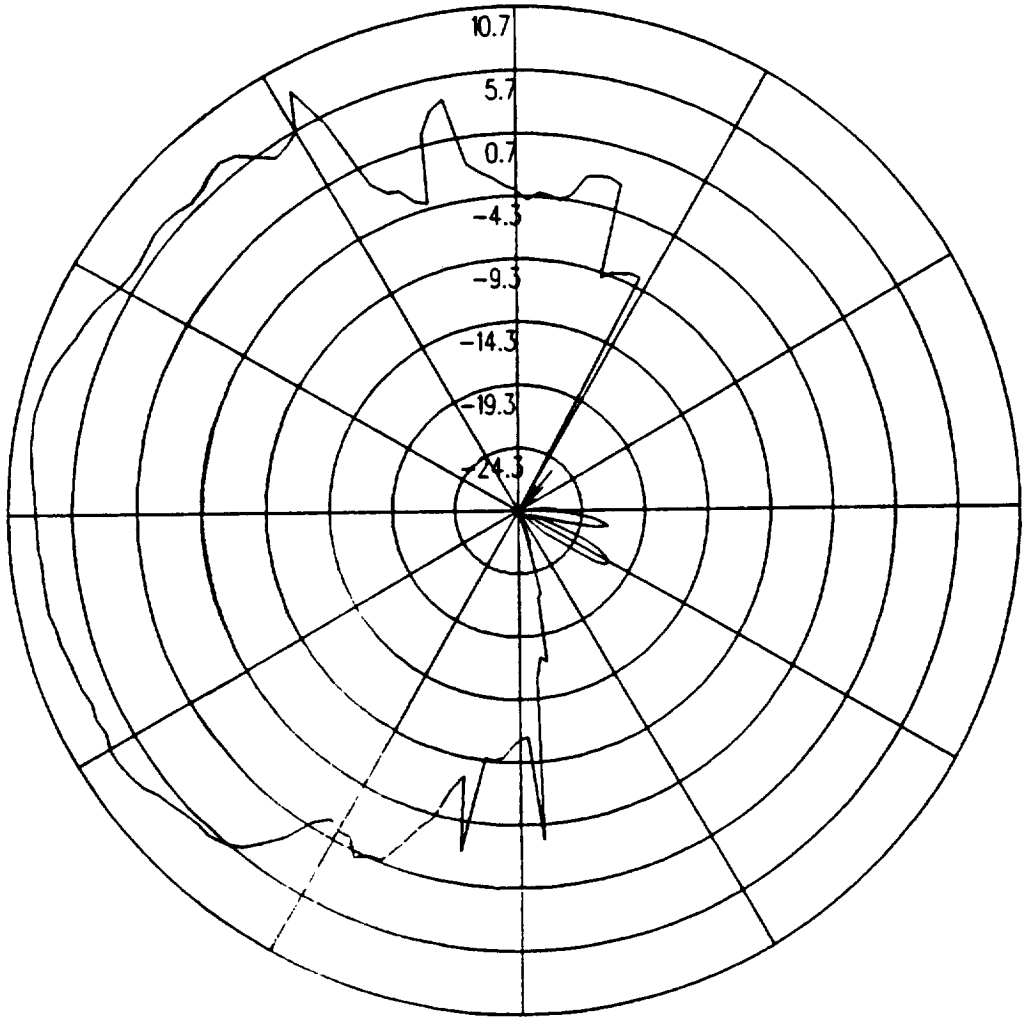

Figure 5.96: UTD calculated conical plane pattern 10° above the horizon for batwing antenna on a P-3C for right hand circular polarization at 300 MHz.(Test Location 8)

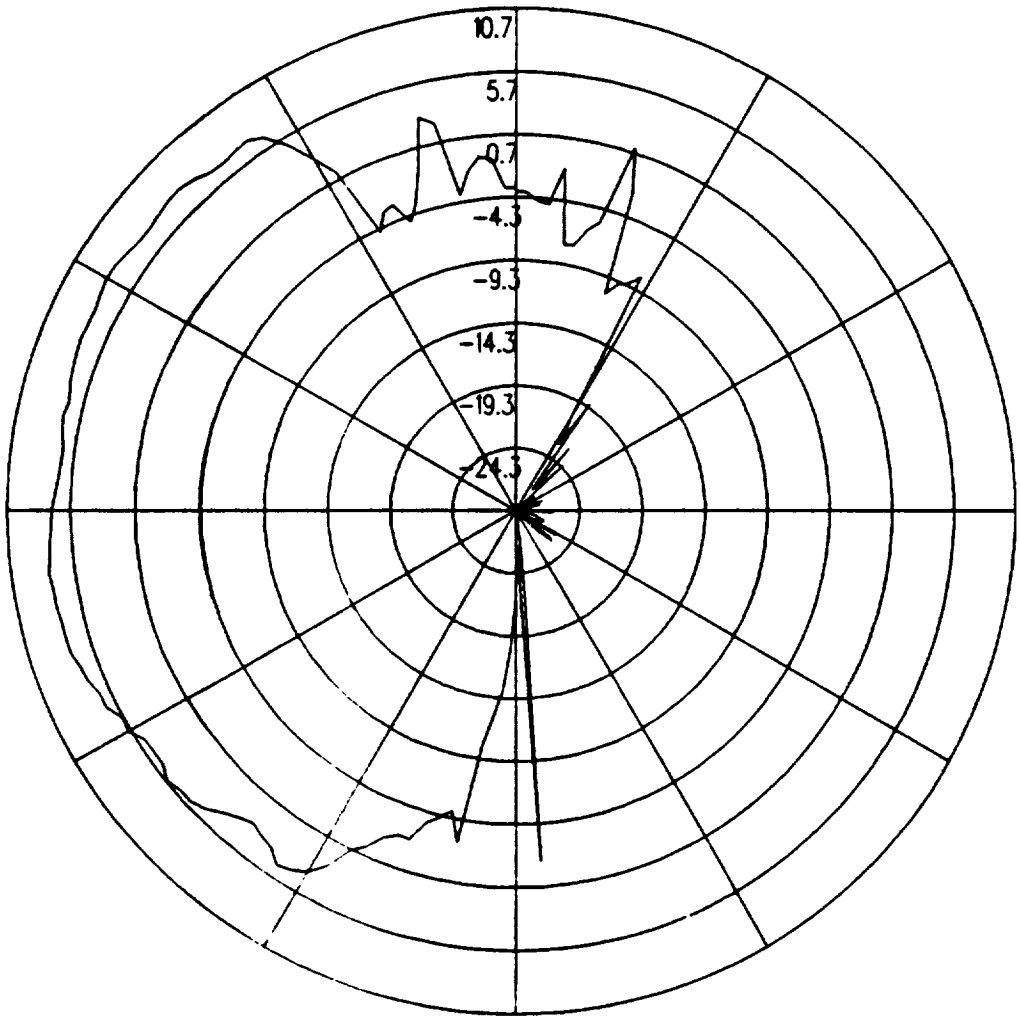

Figure 5.97: UTD calculated conical plane pattern 20° above the horizon for batwing antenna on a P-3C for right hand circular polarization at 300 MHz.(Test Location 8)

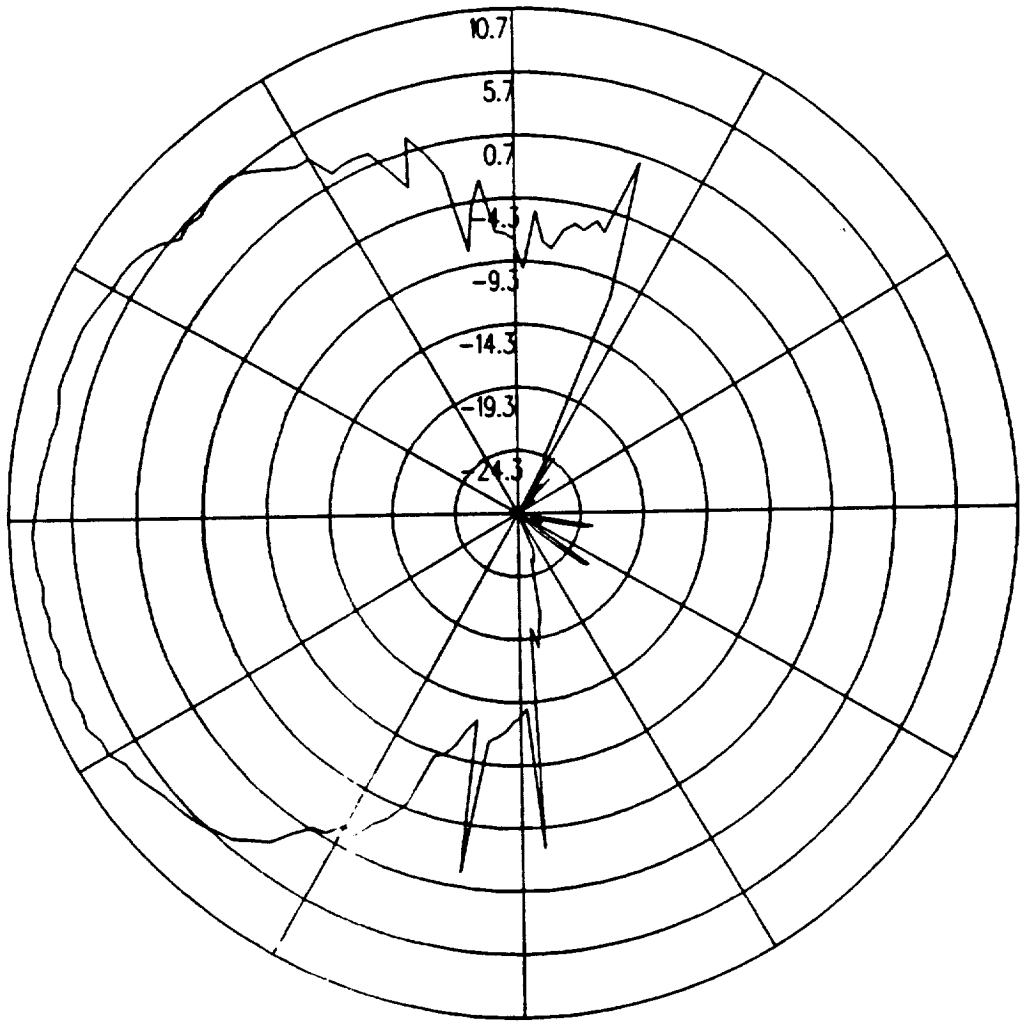

Figure 5.98: UTD calculated conical plane pattern 30° above the horizon for batwing antenna on a P-3C for right hand circular polarization at 300 MHz.(Test Location 8)

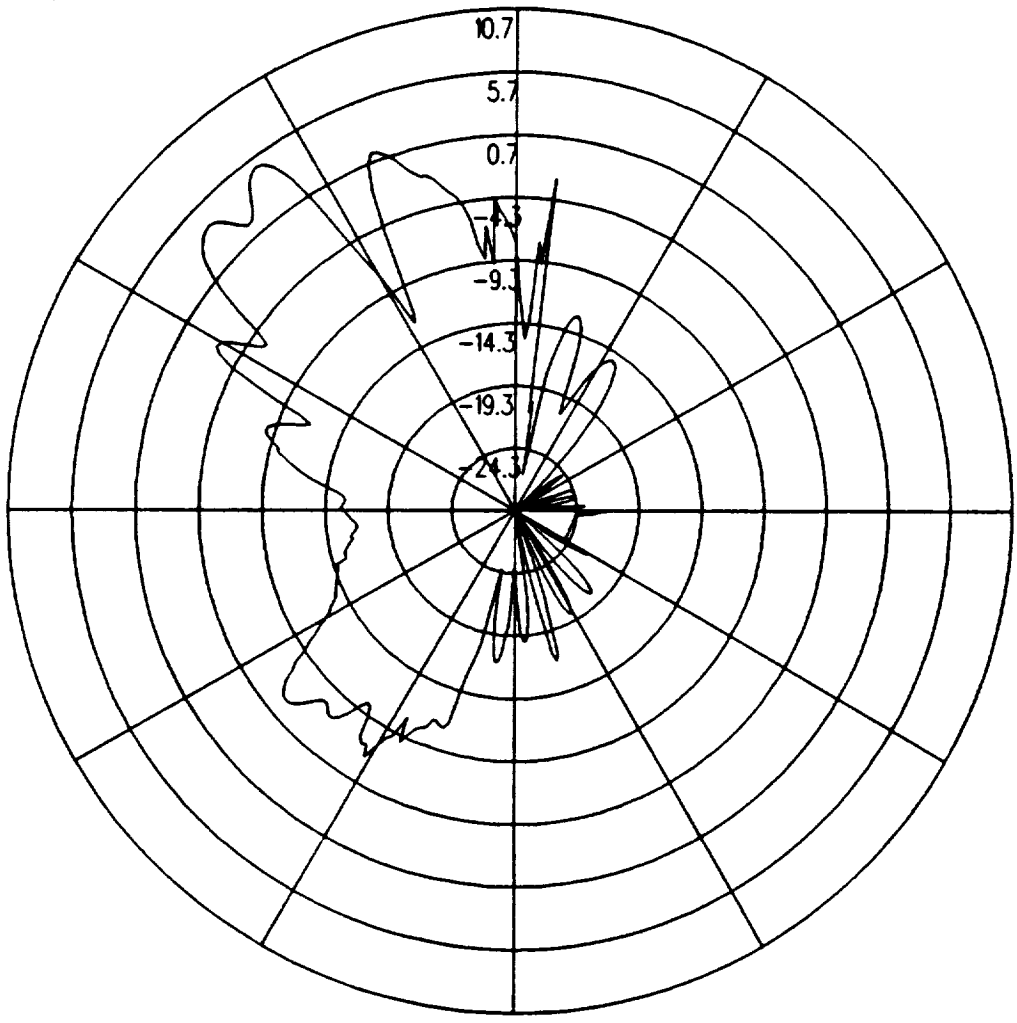

Figure 5.99: UTD calculated roll plane pattern for batwing antenna on a P-3C for left hand circular polarization at 300 MHz. (Test Location 8)

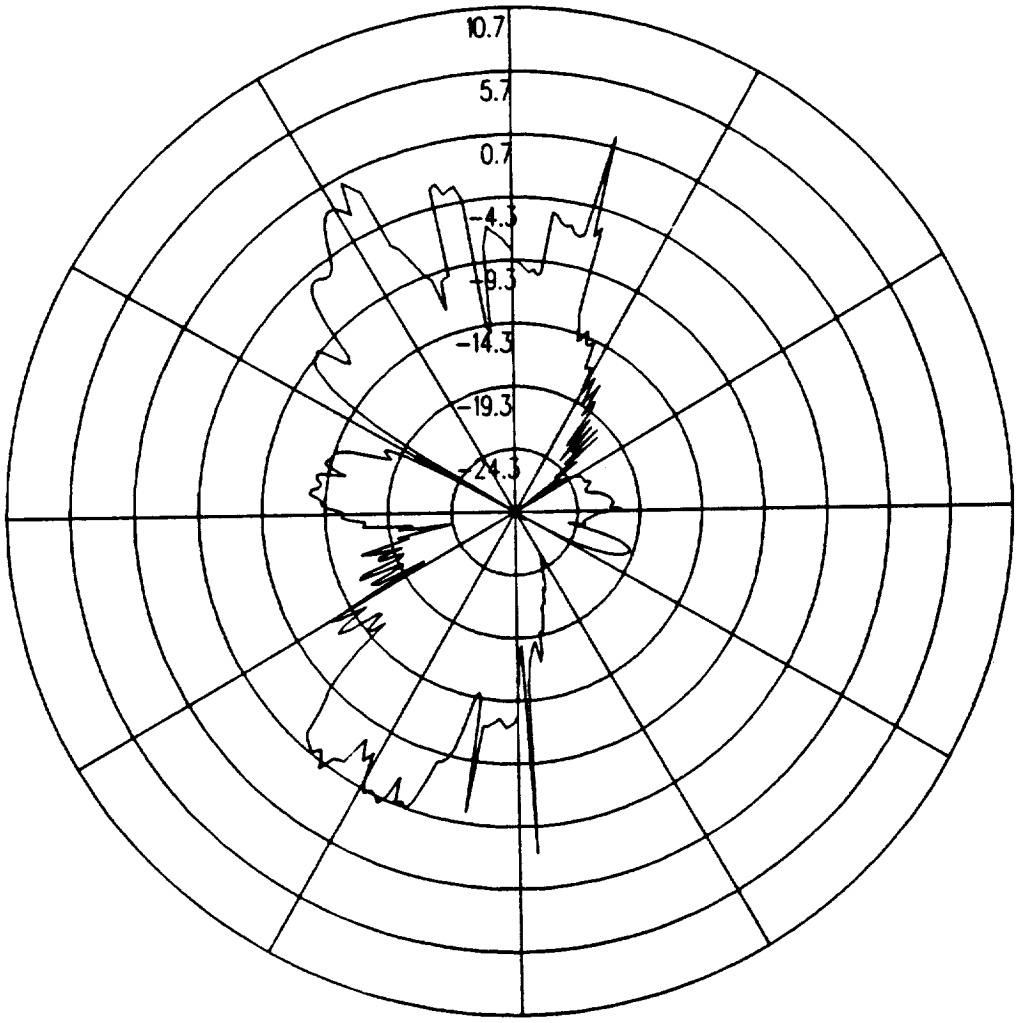

Figure 5.100: UTD calculated azimuth plane pattern for batwing antenna on a P-3C for left hand circular polarization at 300 MHz. (Test Location 8)

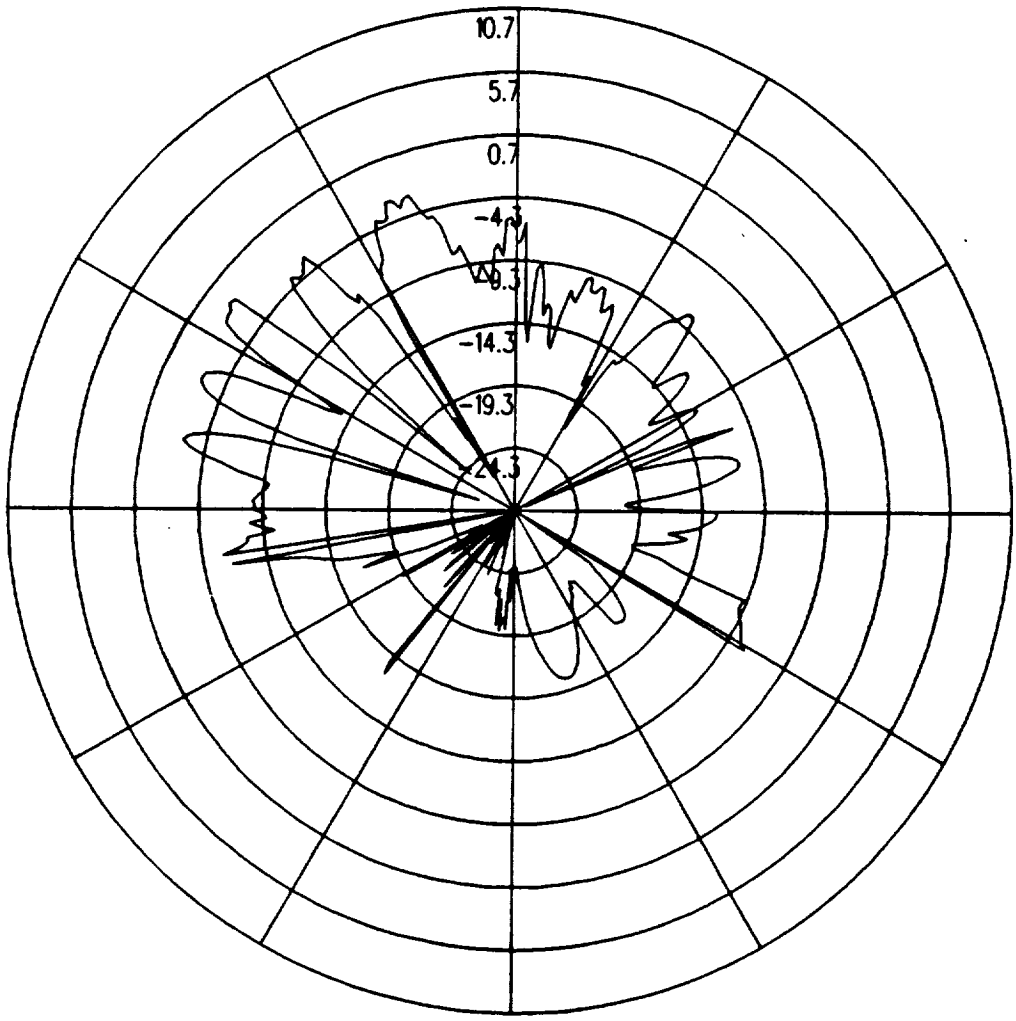

Figure 5.101: UTD calculated elevation plane pattern for batwing antenna on a P-3C for left hand circular polarization at 300 MHz. (Test Location 8)

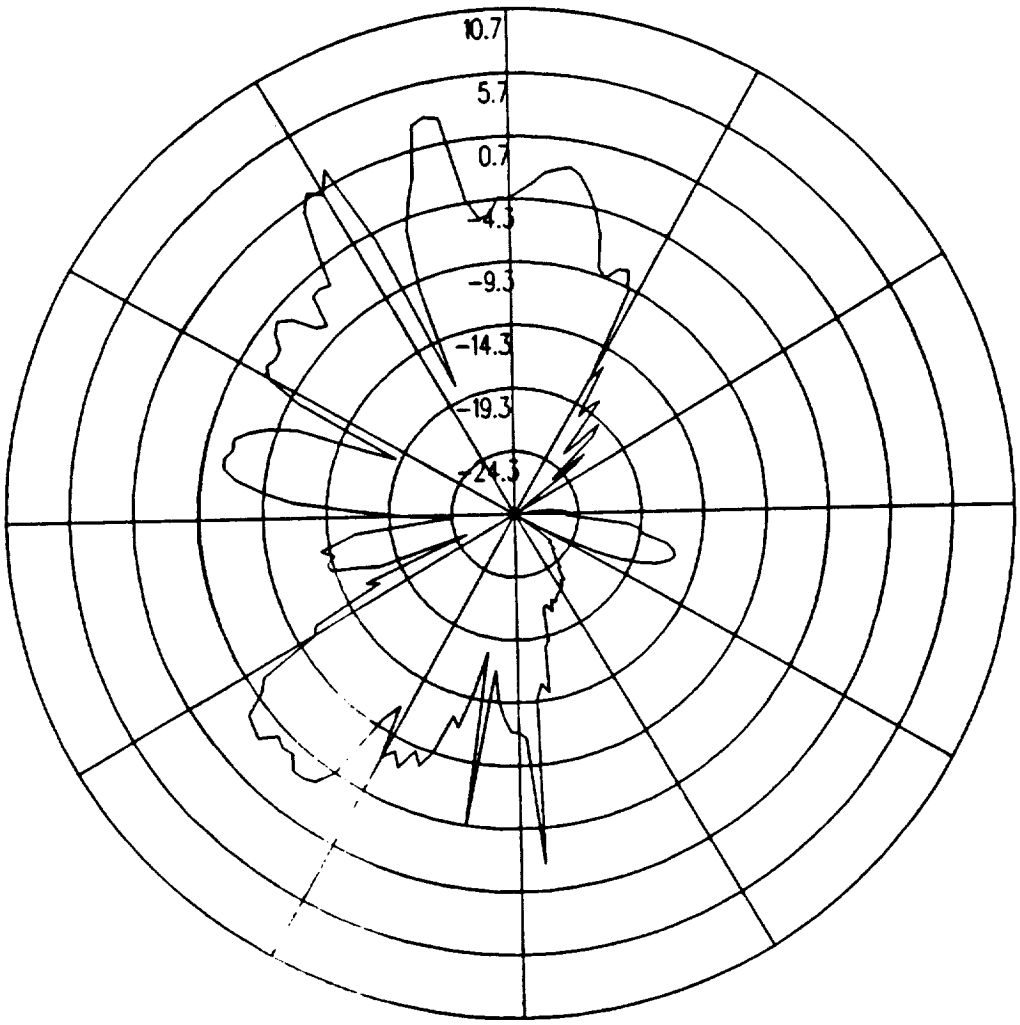

Figure 5.102: UTD calculated conical plane pattern 10° above the horizon for batwing antenna on a P-3C for left hand circular polarization at 300 MHz.(Test Location 8)

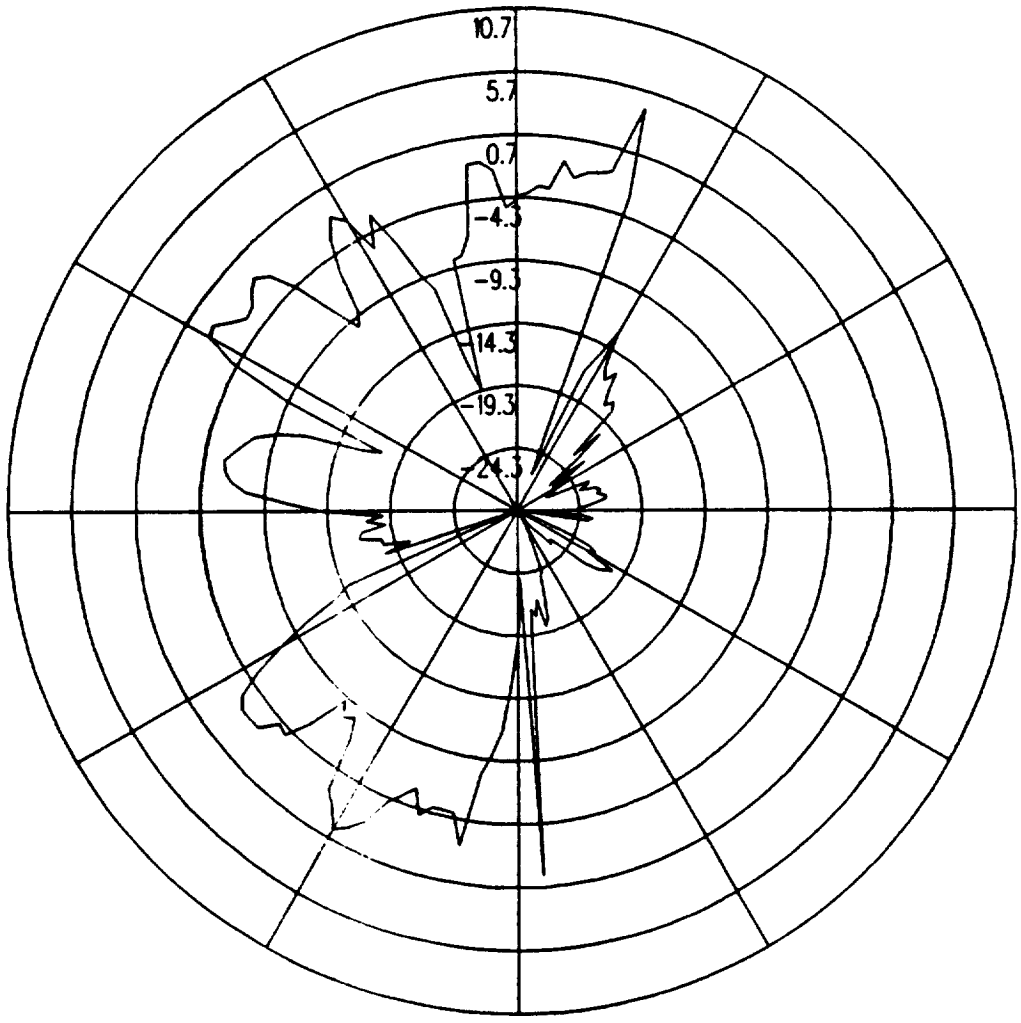

Figure 5.103: UTD calculated conical plane pattern 20° above the horizon for batwing antenna on a P-3C for left hand circular polarization at 300 MHz.(Test Location 8)

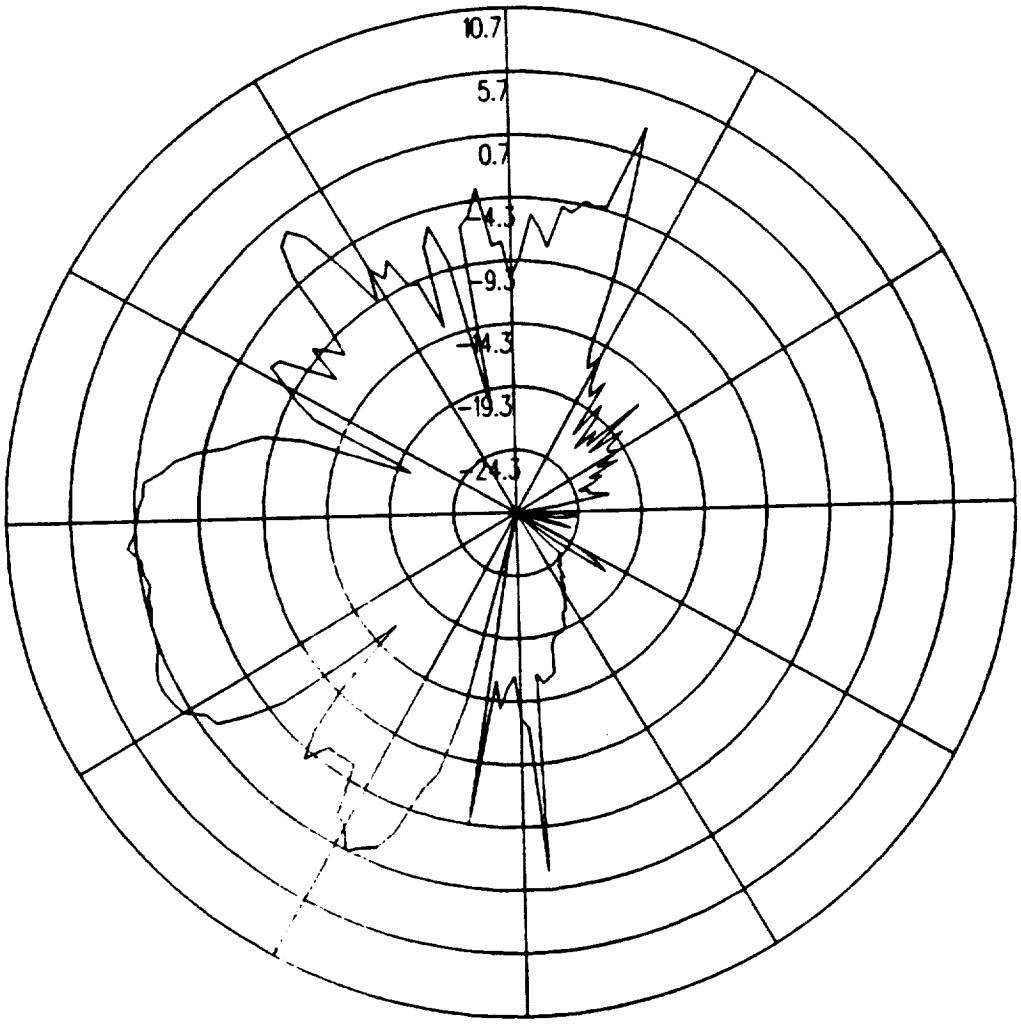

Figure 5.104: UTD calculated conical plane pattern 30° above the horizon for batwing antenna on a P-3C for left hand circular polarization at 300 MHz.(Test Location 8)

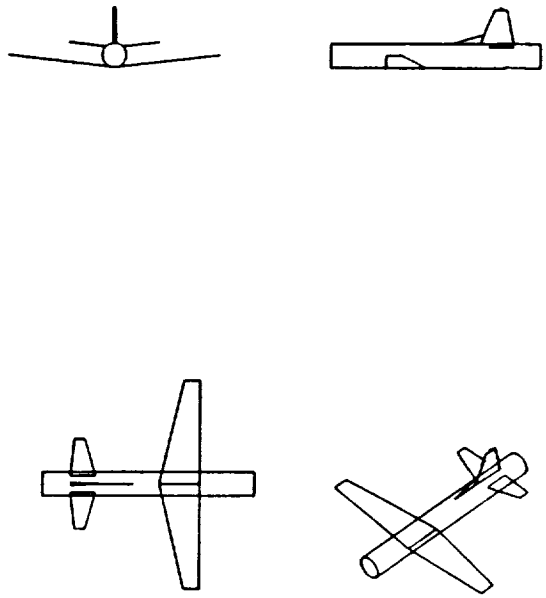

Figure 5.105: Geometry of the model of the P-3C aircraft used in the NEC-BSC code showing the location of the antenna.

5.9 Test Location 9

The antenna is located as illustrated in Figure 5.105, which also shows the computer model used to generate the results. The calculated results at 300 MHz are shown for the roll plane in Figure 5.106, for the azimuth plane in Figure 5.107, for the elevation plane in Figure 5.108, for the conical plane 10° above the horizon in Figure 5.109, for the conical plane 20° above the horizon in Figure 5.110, and for the conical plane 30° above the horizon in Figure 5.111 all for right hand polarization. The cross polarized fields are shown for the roll plane in Figure 5.112, for the azimuth plane in Figure 5.113, for the elevation plane in Figure 5.114, for the conical plane 10° above the horizon in Figure 5.115, for the conical plane 20° above the horizon in Figure 5.116, and for the conical plane 30° above the horizon in Figure 5.117 all for left hand polarization.

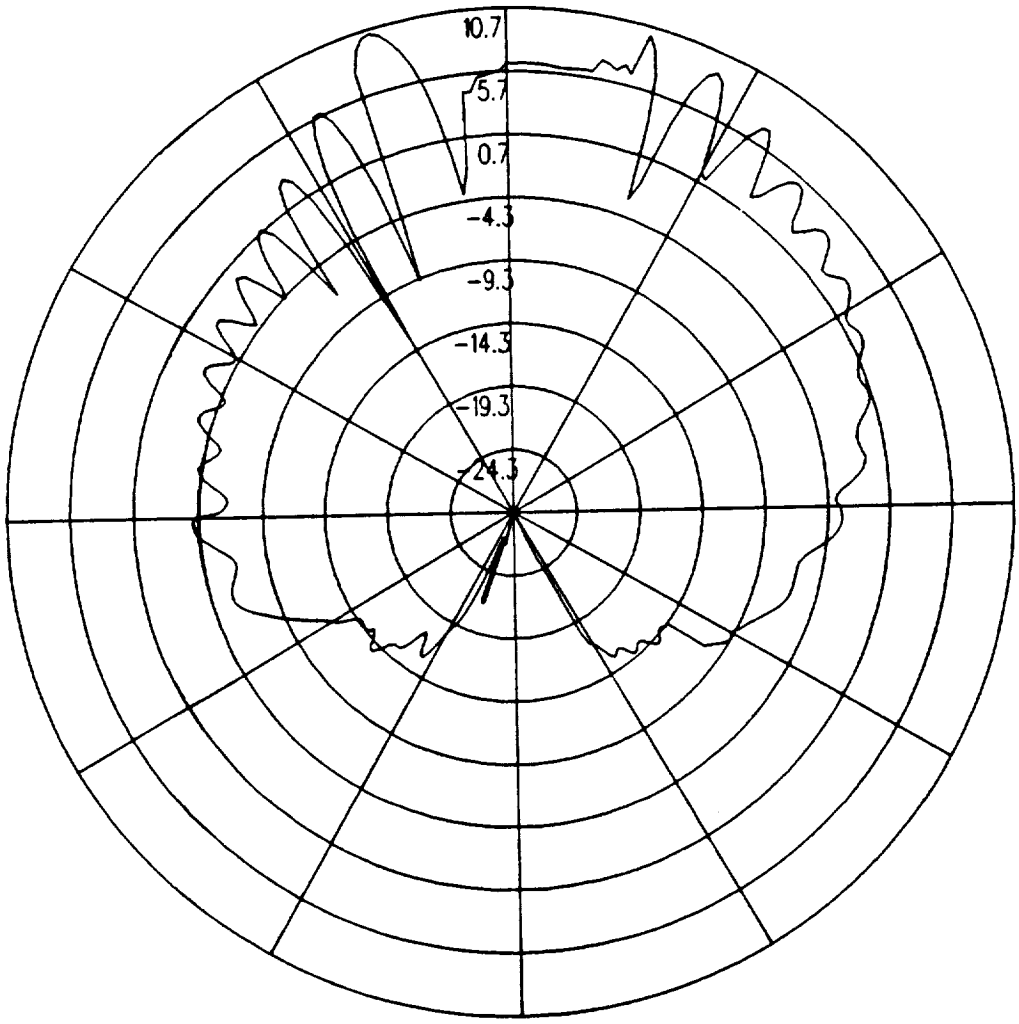

Figure 5.106: UTD calculated roll plane pattern for batwing antenna on a P-3C for right hand circular polarization at 300 MHz. (Test Location 9)

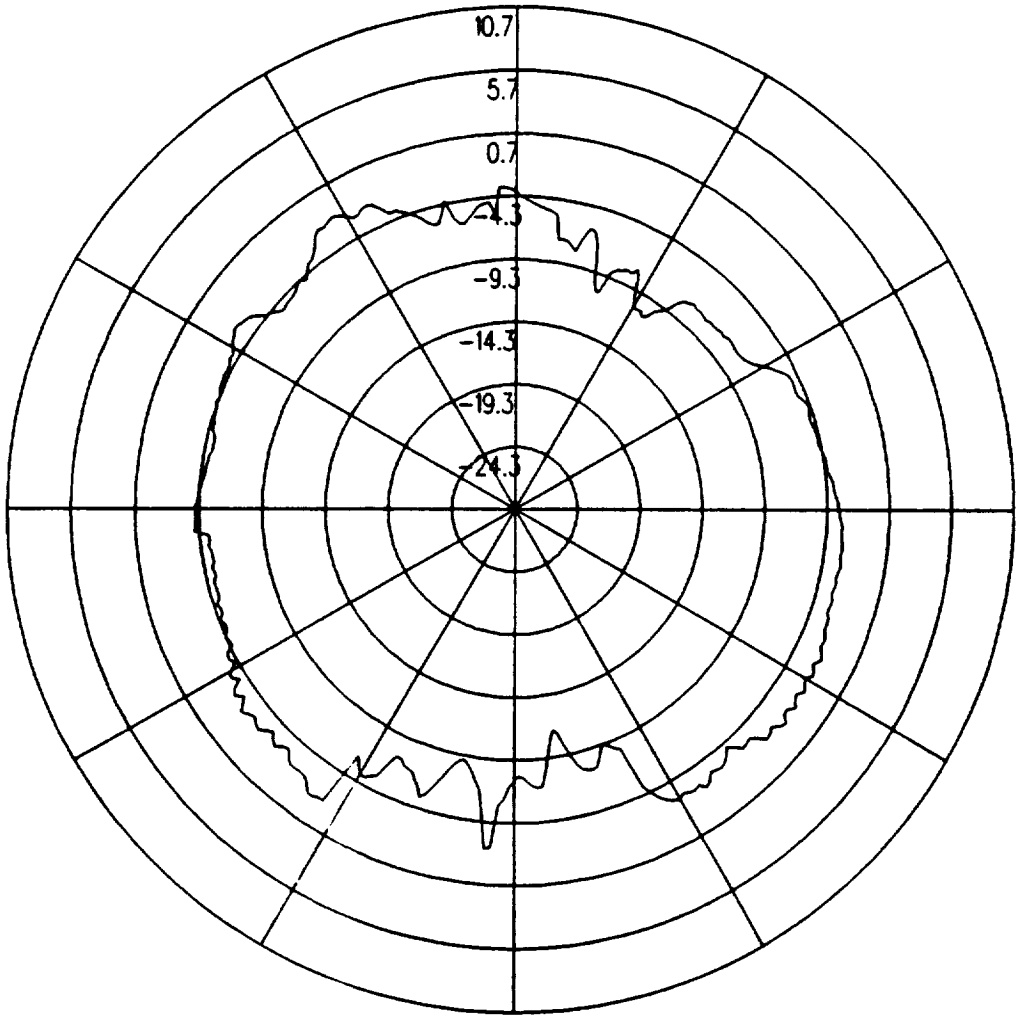

Figure 5.107: UTD calculated azimuth plane pattern for batwing antenna on a P-3C for right hand circular polarization at 300 MHz. (Test Location 9)

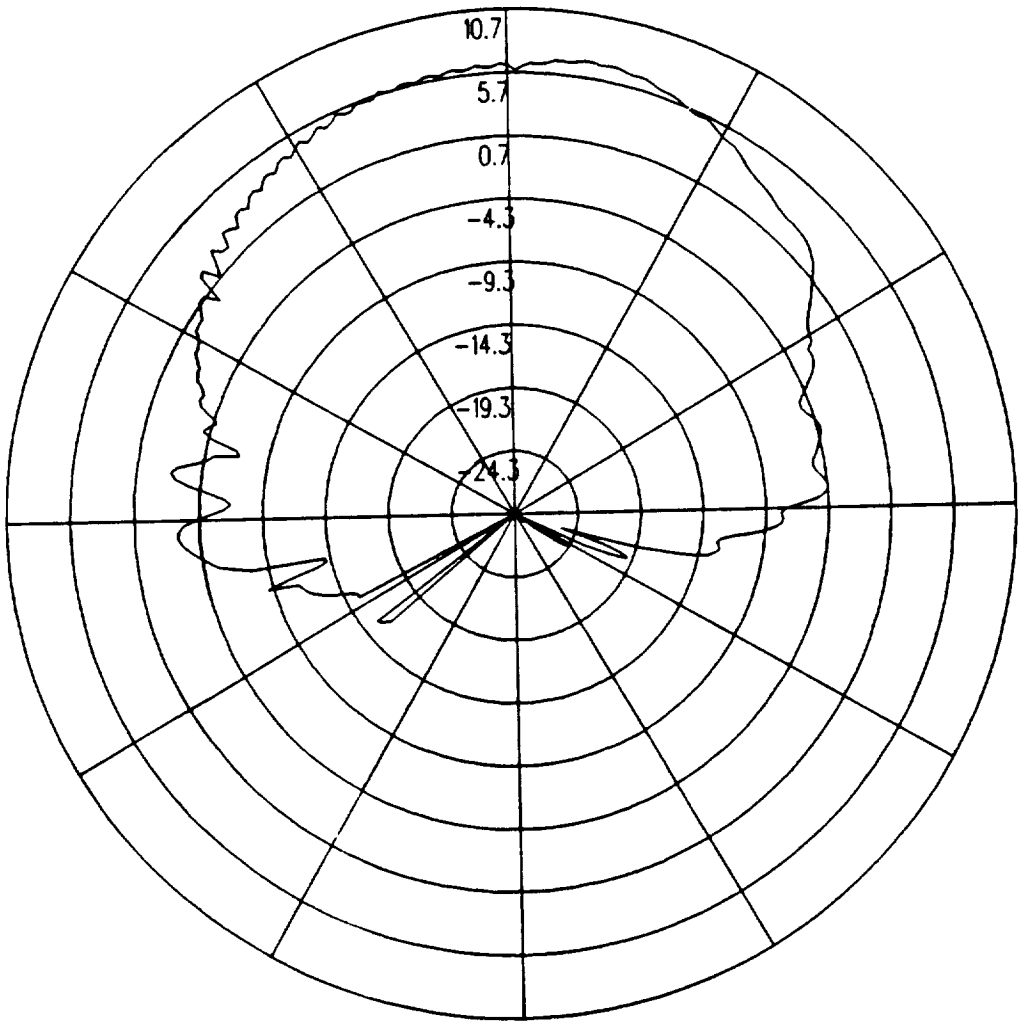

Figure 5.108: UTD calculated elevation plane pattern for batwing antenna on a P-3C for right hand circular polarization at 300 MHz. (Test Location 9)

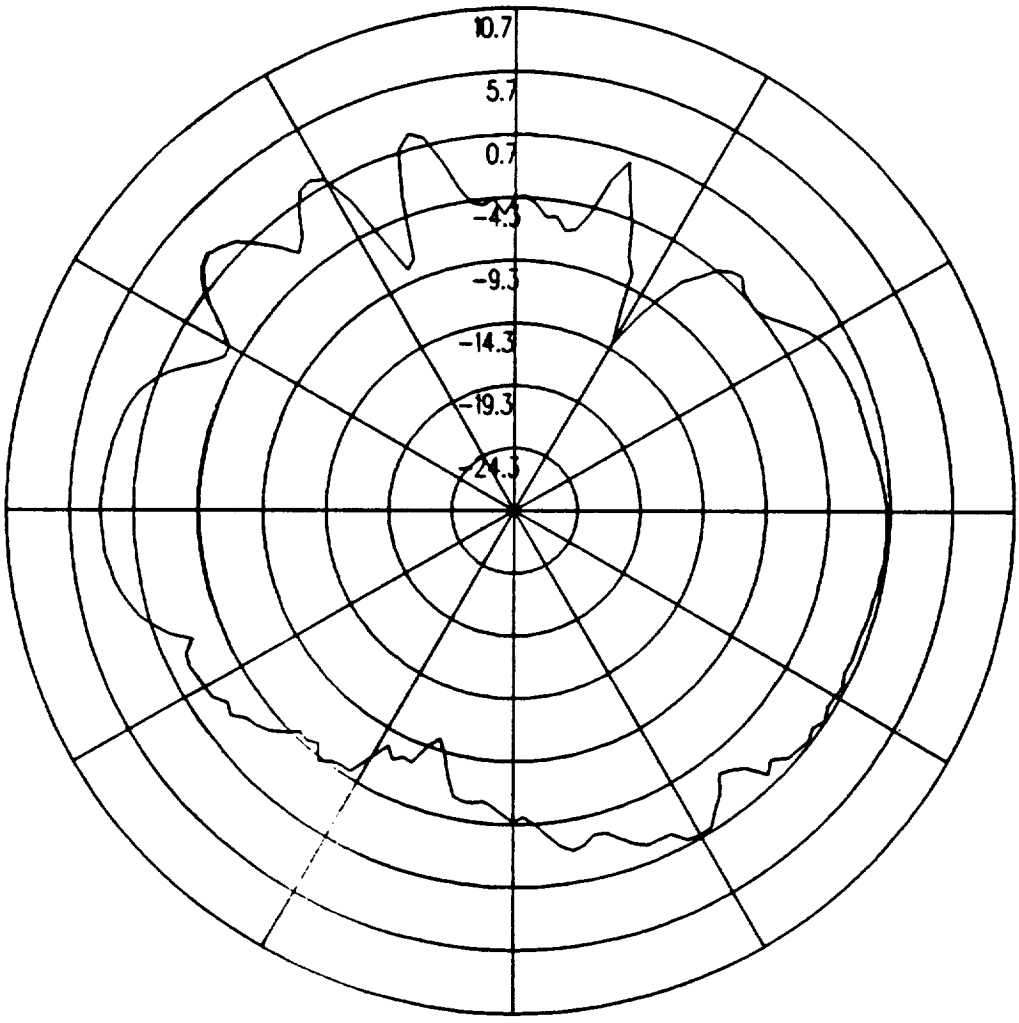

Figure 5.109: UTD calculated conical plane pattern 10° above the horizon for batwing antenna on a P-3C for right hand circular polarization at 300 MHz.(Test Location 9)

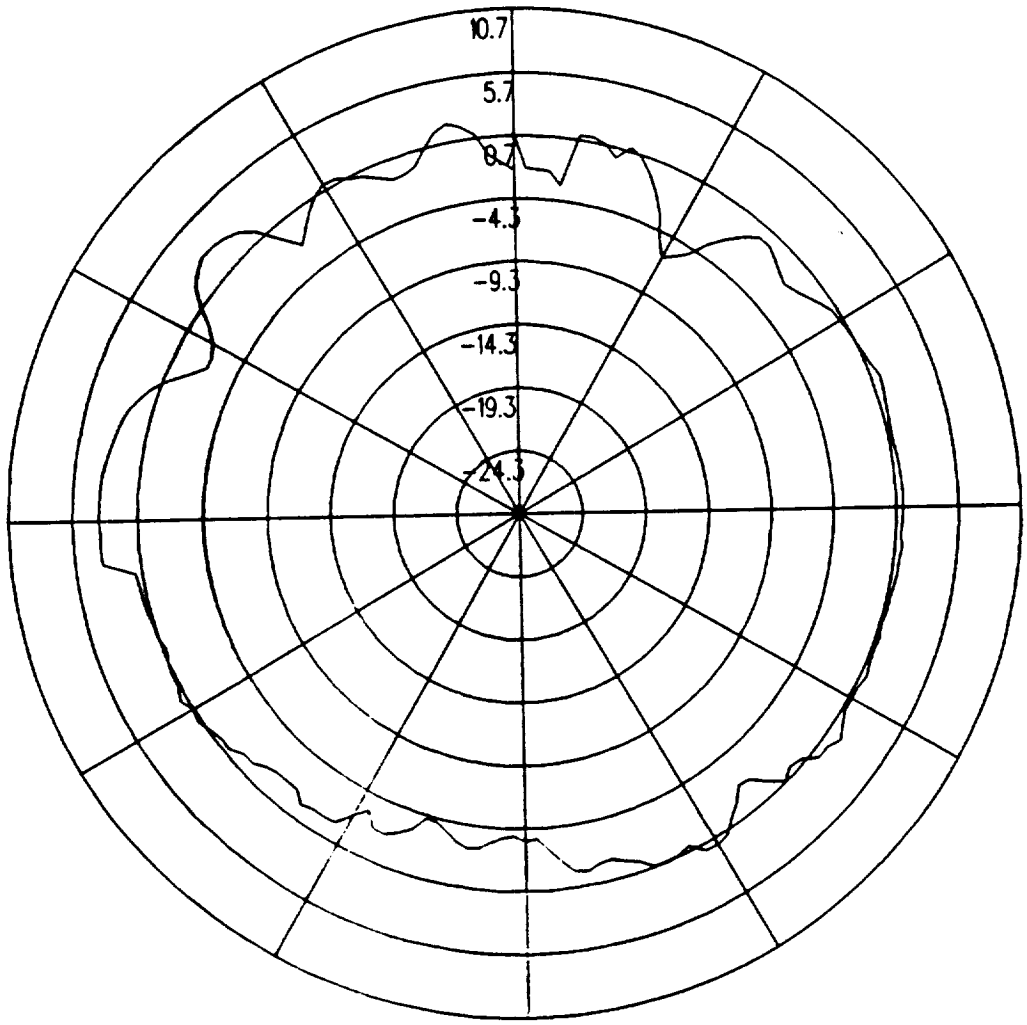

Figure 5.110: UTD calculated conical plane pattern 20° above the horizon for batwing antenna on a P-3C for right hand circular polarization at 300 MHz.(Test Location 9)

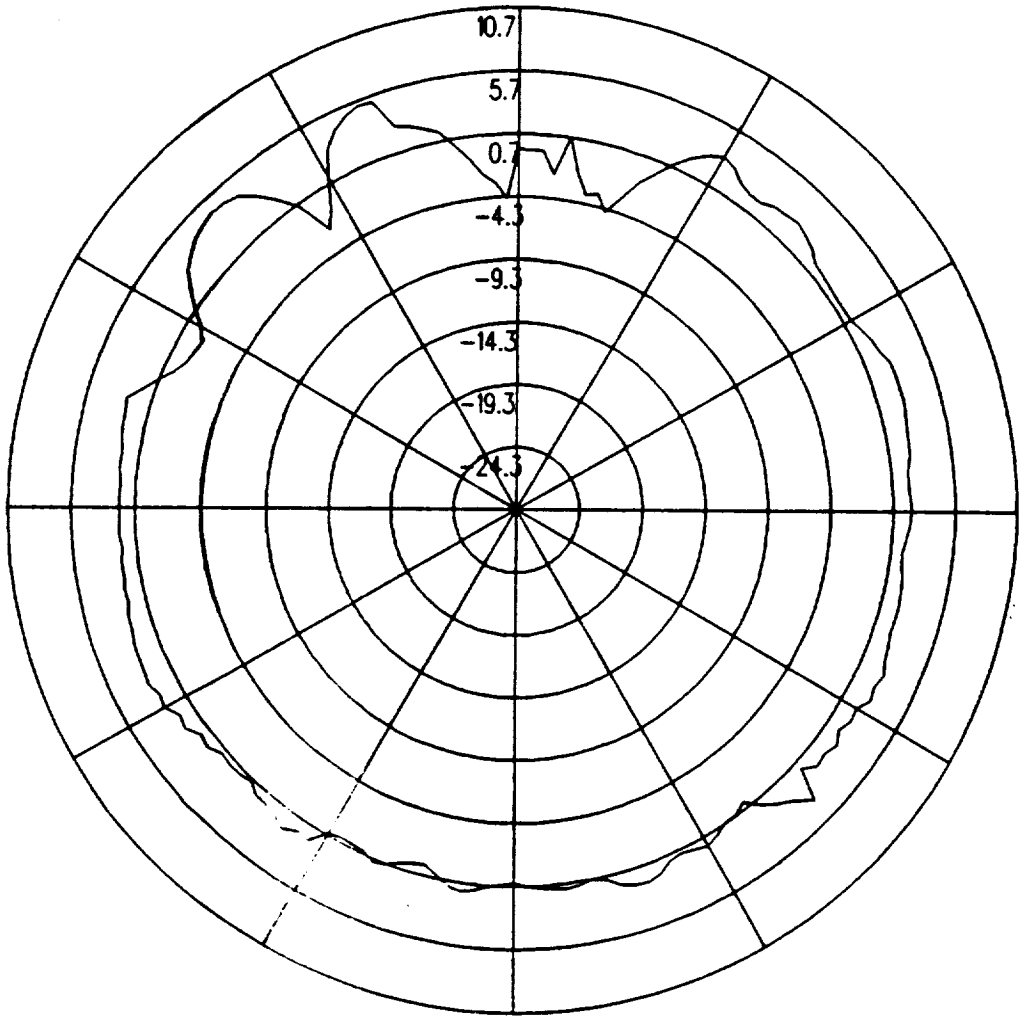

Figure 5.111: UTD calculated conical plane pattern 30° above the horizon for batwing antenna on a P-3C for right hand circular polarization at 300 MHz.(Test Location 9)

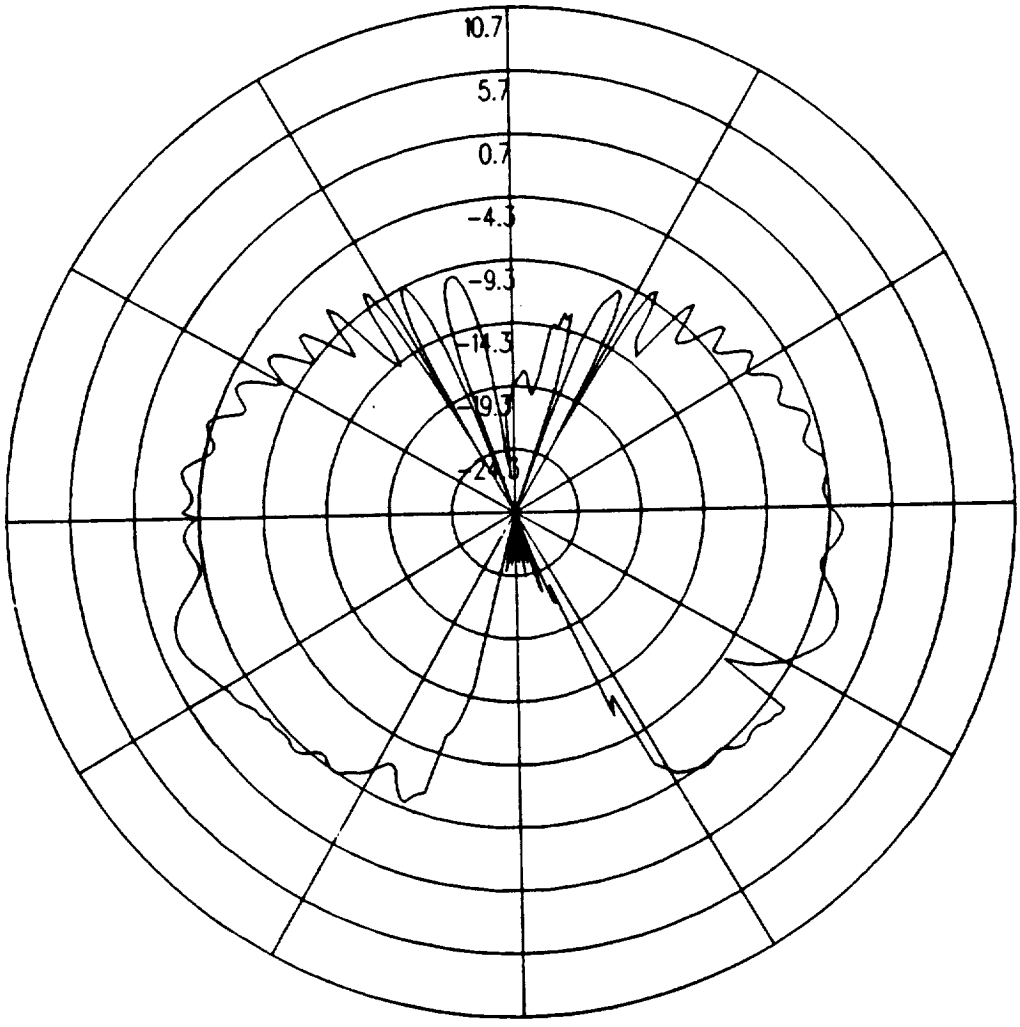

Figure 5.112: UTD calculated roll plane pattern for batwing antenna on a P-3C for left hand circular polarization at 300 MHz. (Test Location 9)

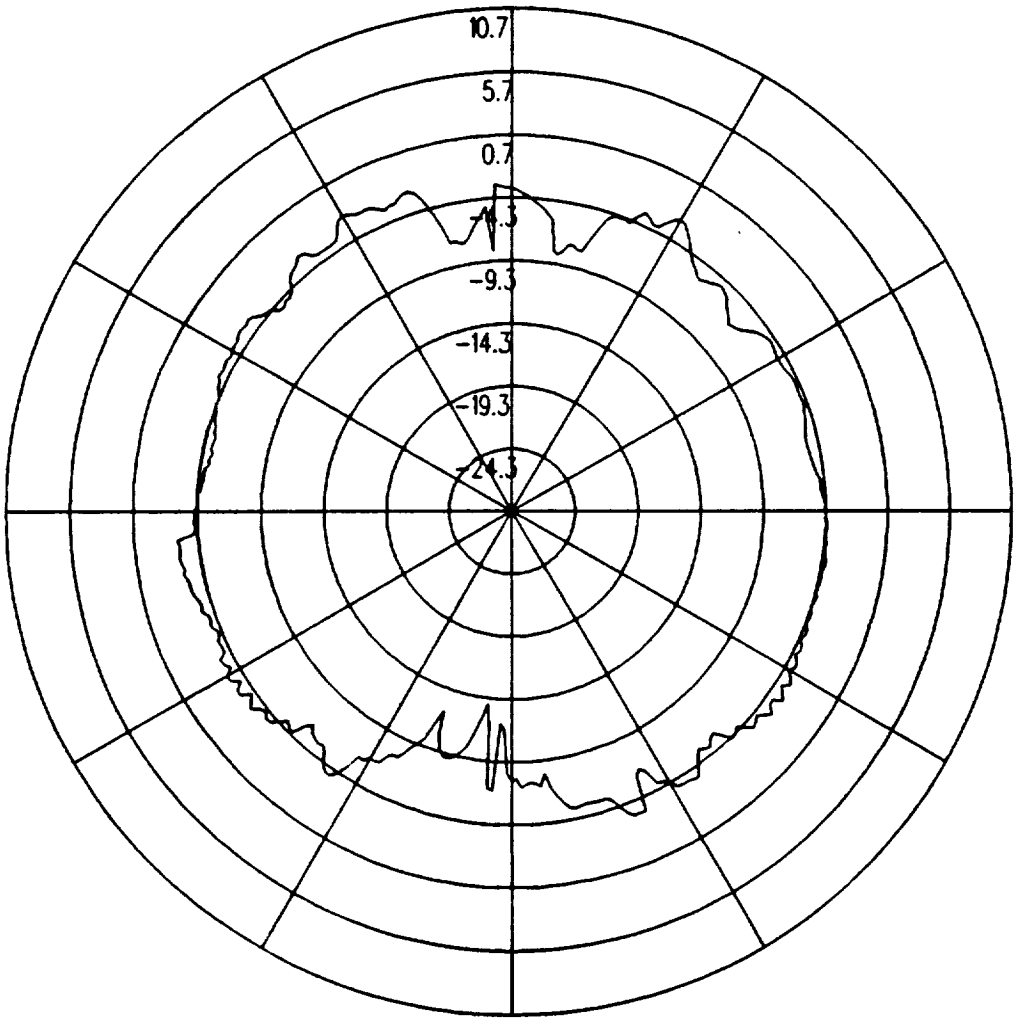

Figure 5.113: UTD calculated azimuth plane pattern for batwing antenna on a P-3C for left hand circular polarization at 300 MHz. (Test Location 9)

C-4

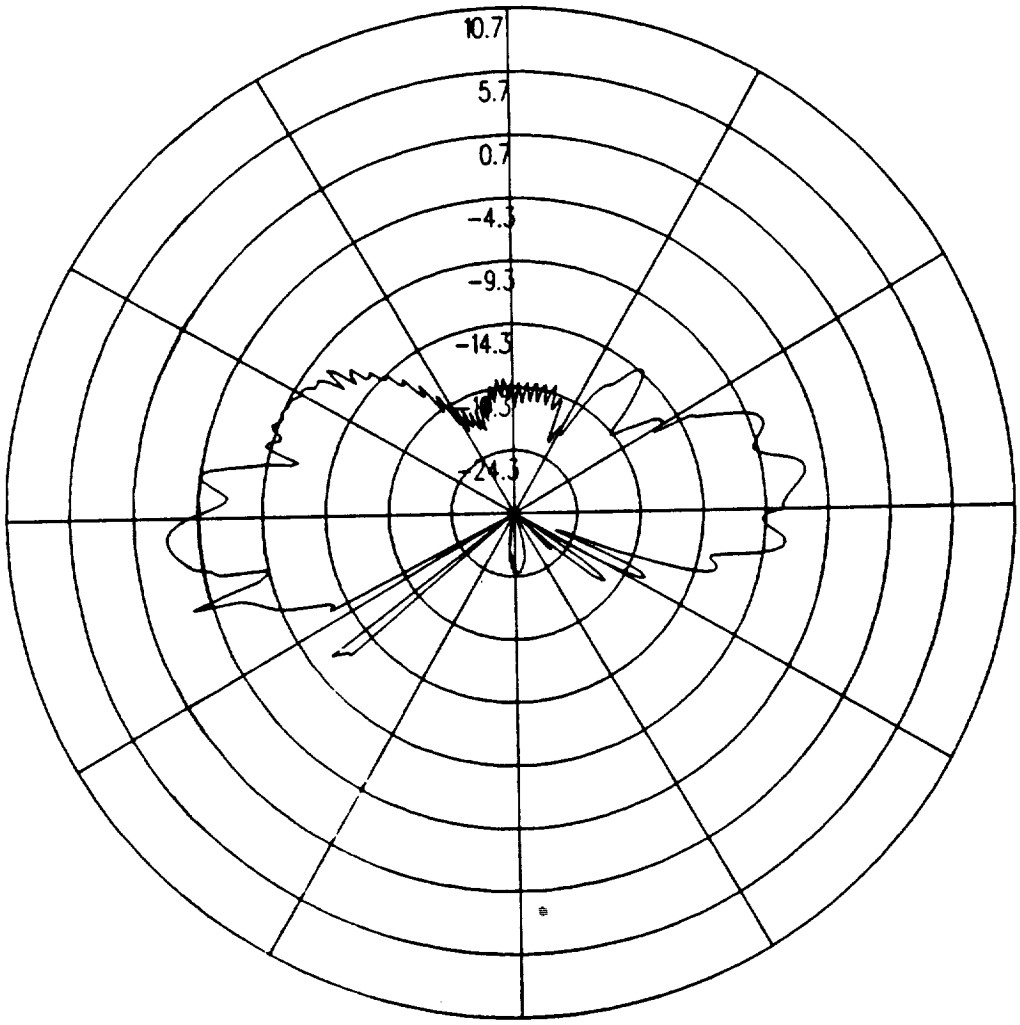

Figure 5.114: UTD calculated elevation plane pattern for batwing antenna on a P-3C for left hand circular polarization at 300 MHz. (Test Location 9)

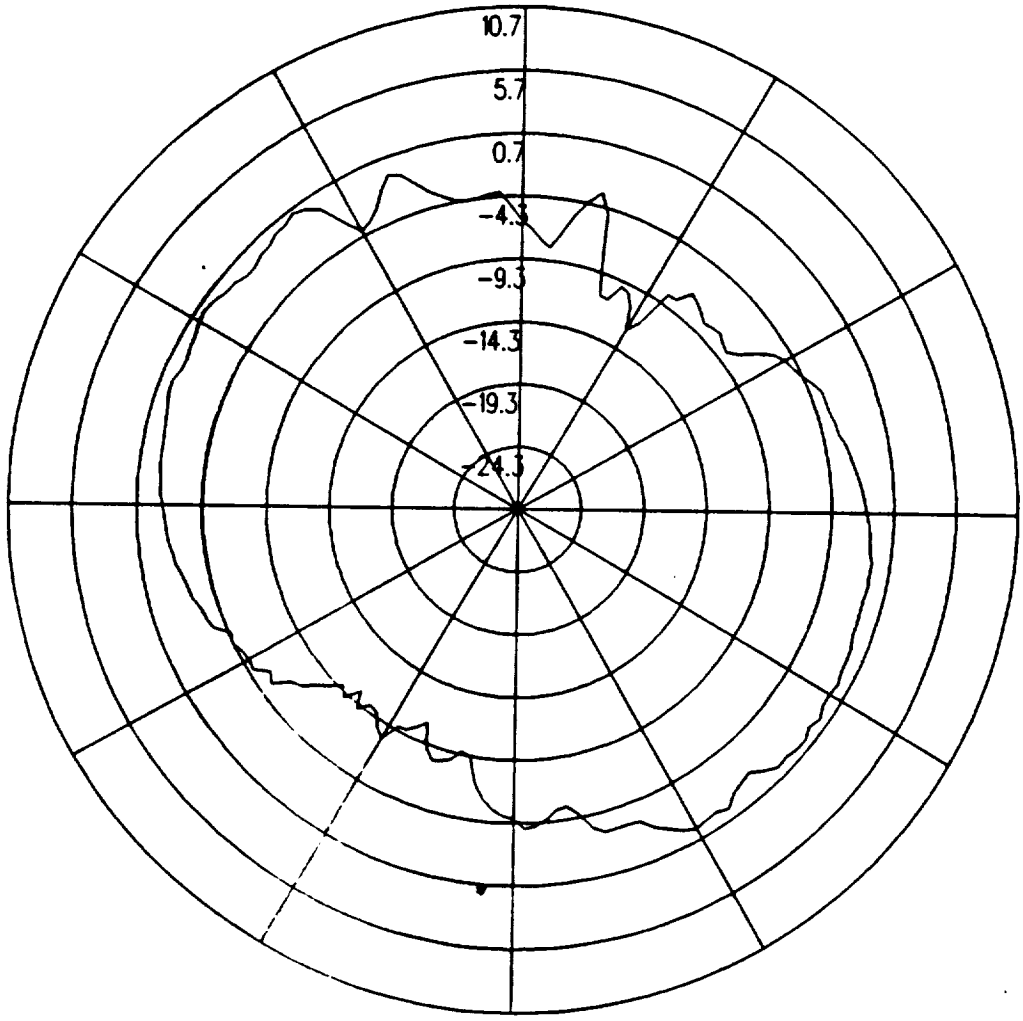

Figure 5.115: UTD calculated conical plane pattern 10° above the horizon for batwing antenna on a P-3C for left hand circular polarization at 300 MHz.(Test Location 9)

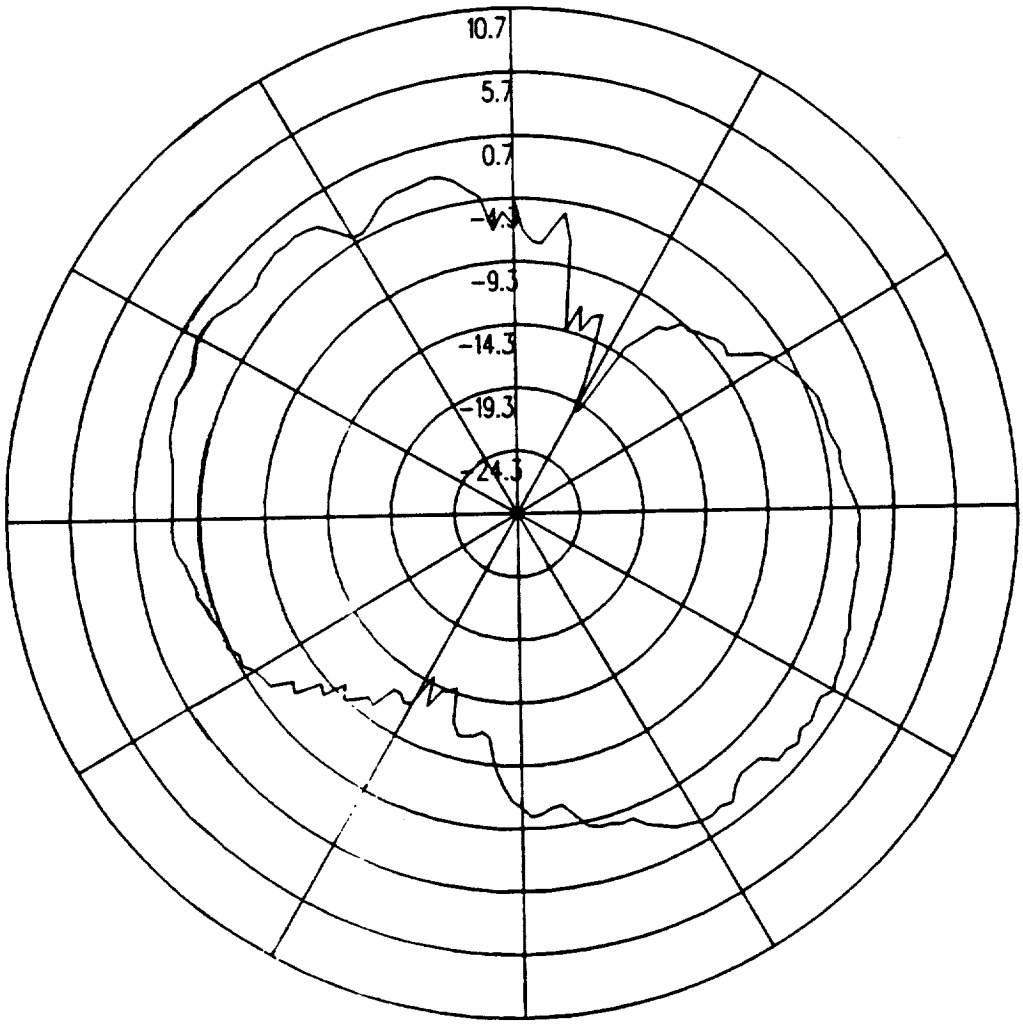

Figure 5.116: UTD calculated conical plane pattern 20° above the horizon for batwing antenna on a P-3C for left hand circular polarization at 300 MHz.(Test Location 9)

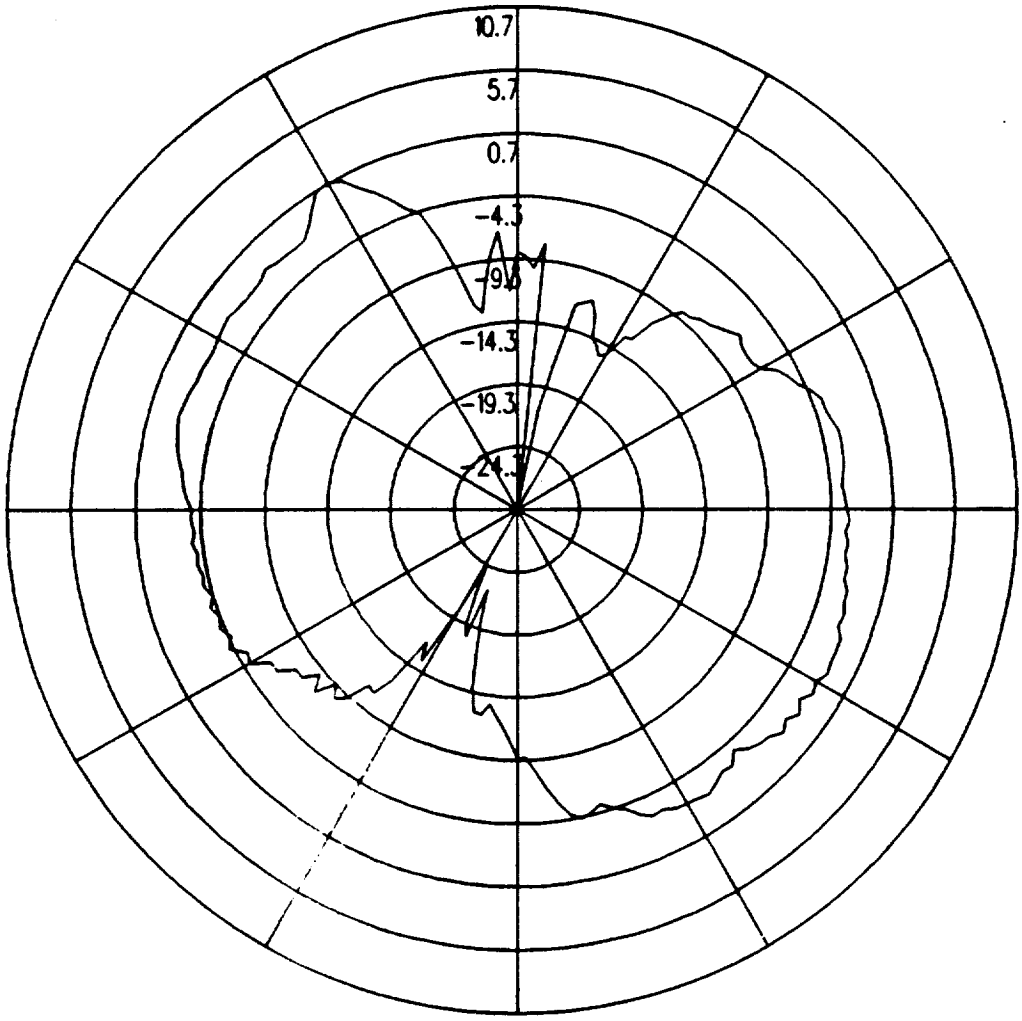

Figure 5.117: UTD calculated conical plane pattern 30° above the horizon for batwing antenna on a P-3C for left hand circular polarization at 300 MHz.(Test Location 9)

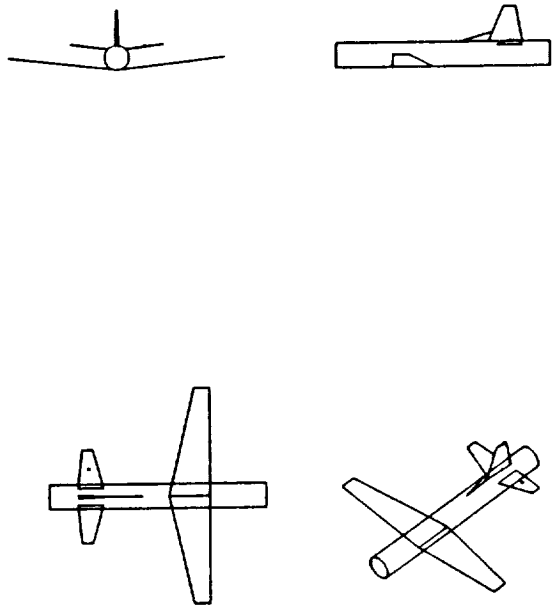

Figure 5.118: Geometry of the model of the P-3C aircraft used in the NEC-BSC code showing the location of the antenna.

5.10 Test Location 10

The antenna is located as illustrated in Figure 5.118, which also shows the computer model used to generate the results. The calculated results at 300 MHz are shown for the roll plane in Figure 5.119, for the azimuth plane in Figure 5.120, for the elevation plane in Figure 5.121, for the conical plane 10° above the horizon in Figure 5.122, for the conical plane 20° above the horizon in Figure 5.123, and for the conical plane 30° above the horizon in Figure 5.124 all for right hand polarization. The cross polarized fields are shown for the roll plane in Figure 5.125, for the azimuth plane in Figure 5.126, for the elevation plane in Figure 5.127, for the conical plane 10° above the horizon in Figure 5.128, for the conical plane 20° above the horizon in Figure 5.129, and for the conical plane 30° above the horizon in Figure 5.130 all for left hand polarization.

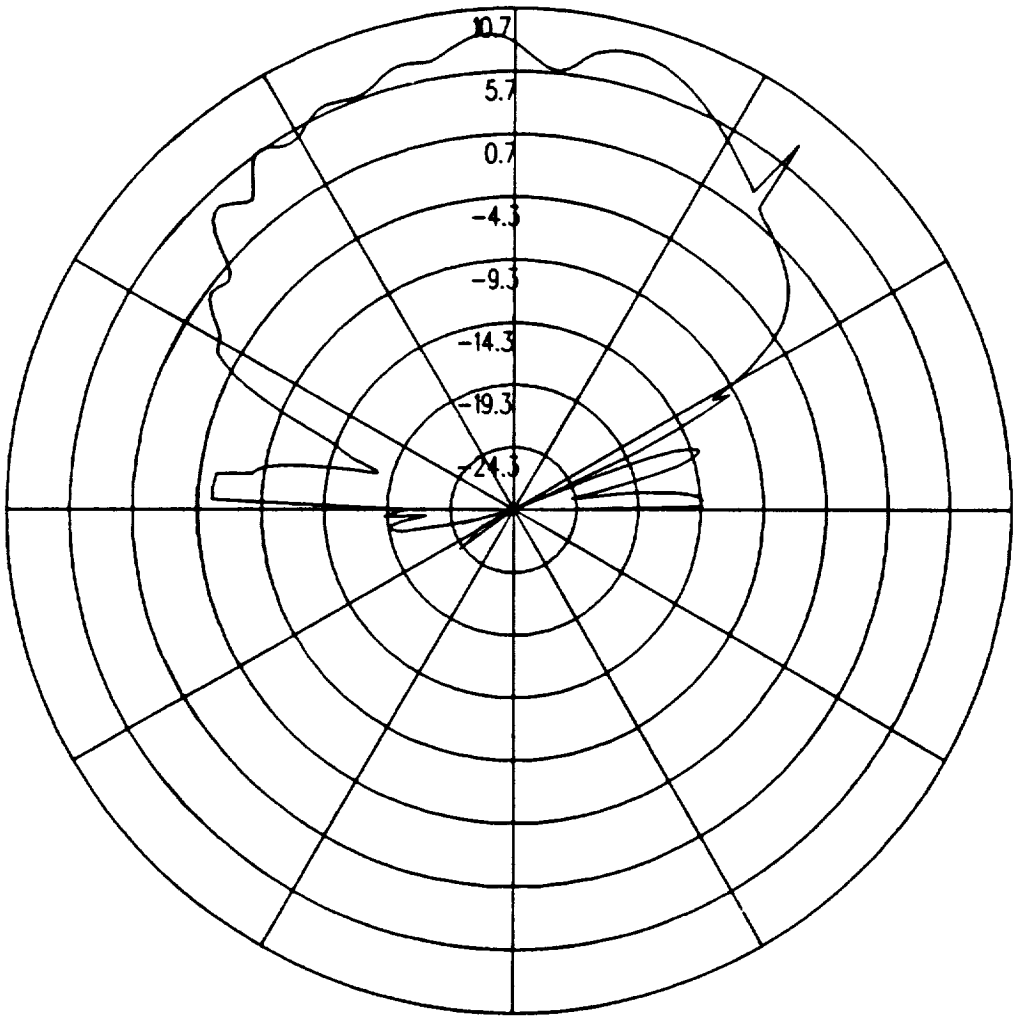

Figure 5.119: UTD calculated roll plane pattern for batwing antenna on a P-3C for right hand circular polarization at 300 MHz. (Test Location 10)

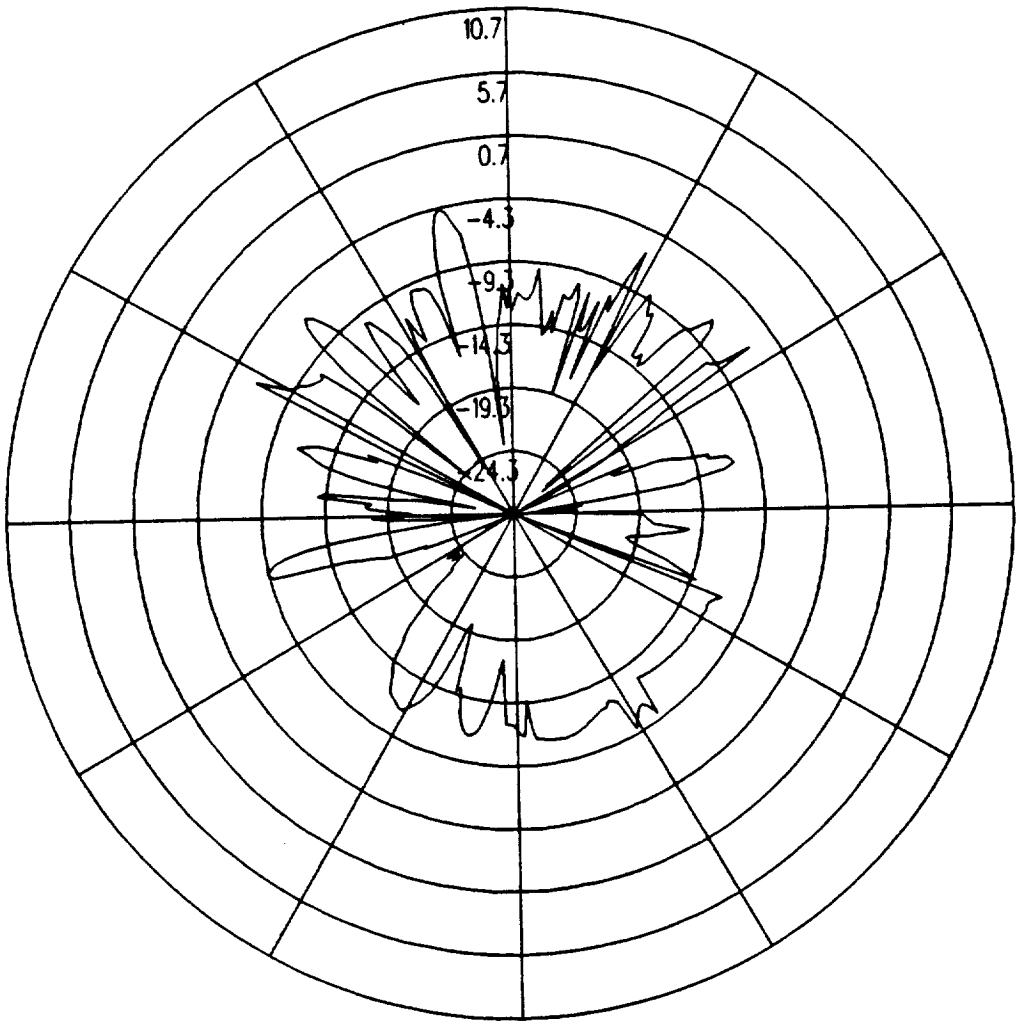

Figure 5.120: UTD calculated azimuth plane pattern for batwing antenna on a P-3C for right hand circular polarization at 300 MHz. (Test Location 10)

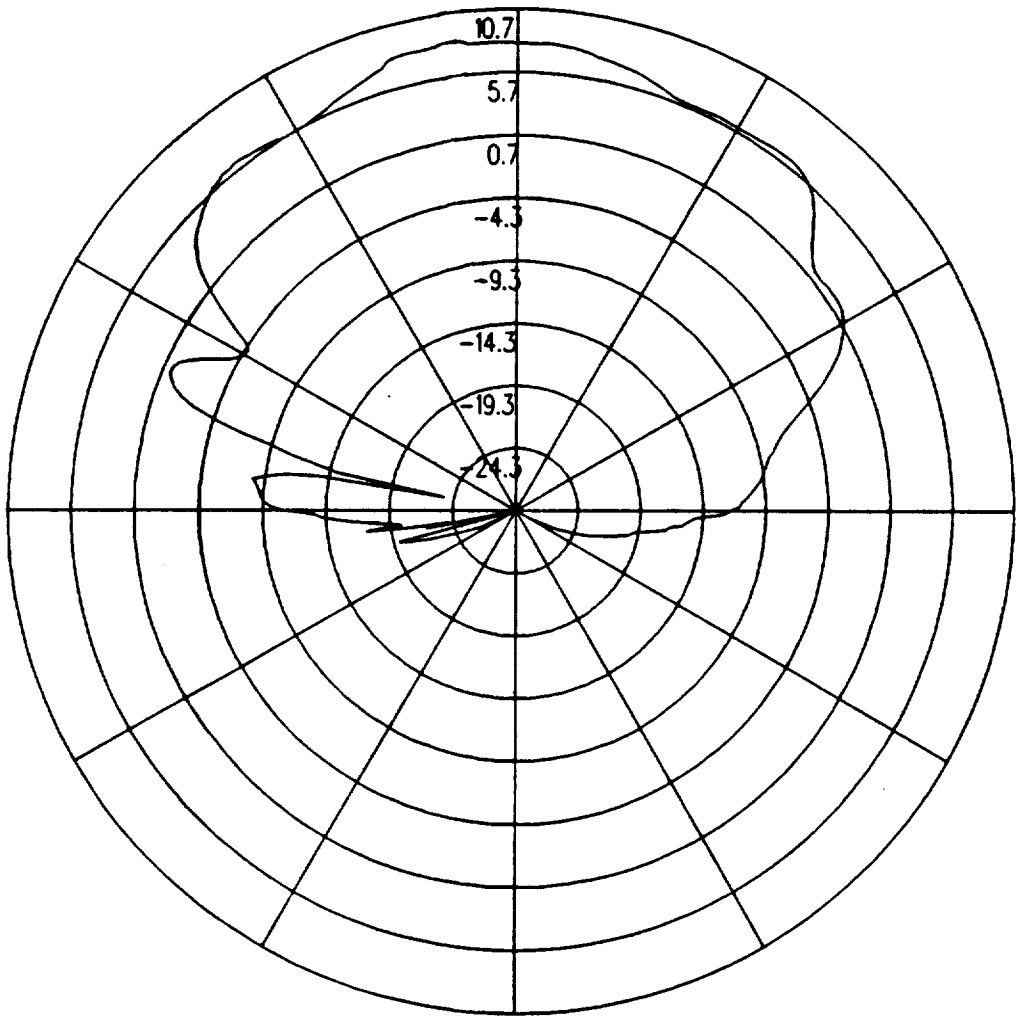

Figure 5.121: UTD calculated elevation plane pattern for batwing antenna on a P-3C for right hand circular polarization at 300 MHz. (Test Location 10)

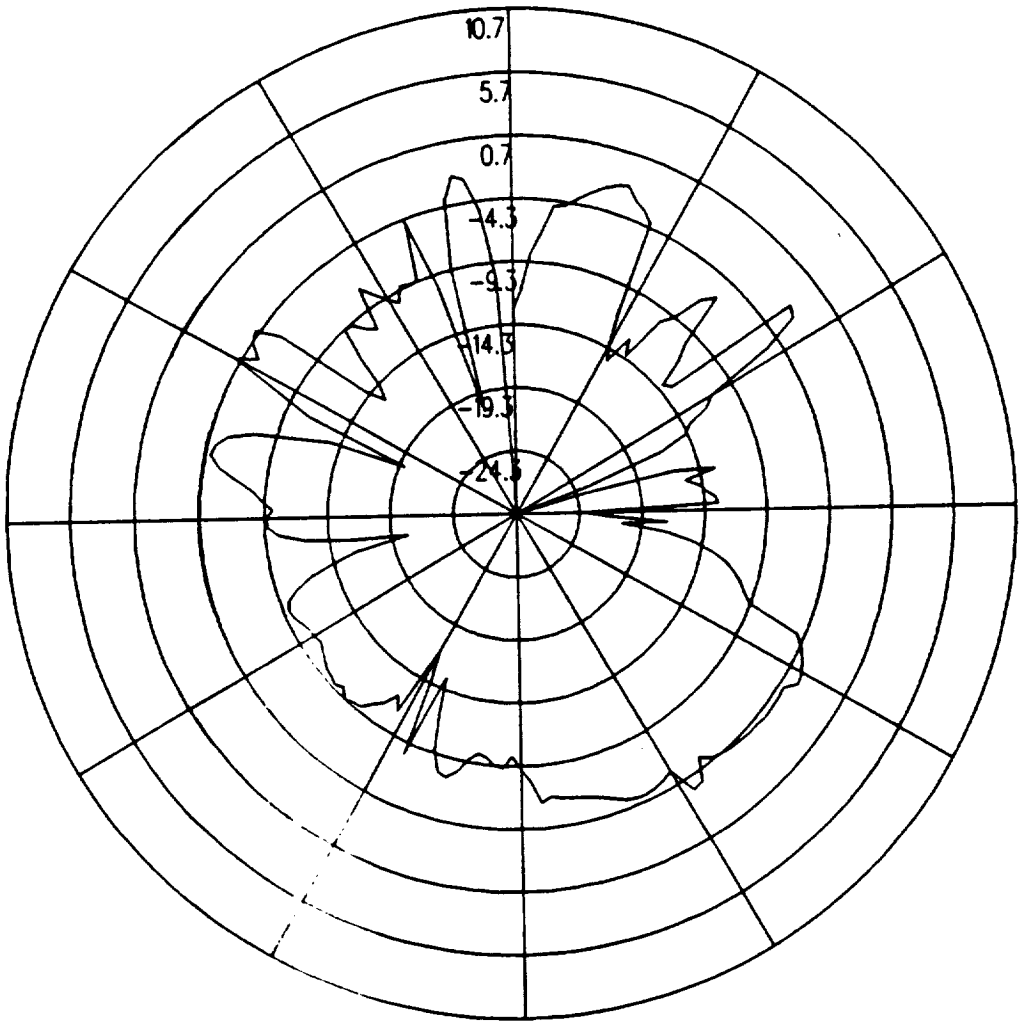

Figure 5.122: UTD calculated conical plane pattern 10° above the horizon for batwing antenna on a P-3C for right hand circular polarization at 300 MHz.(Test Location 10)

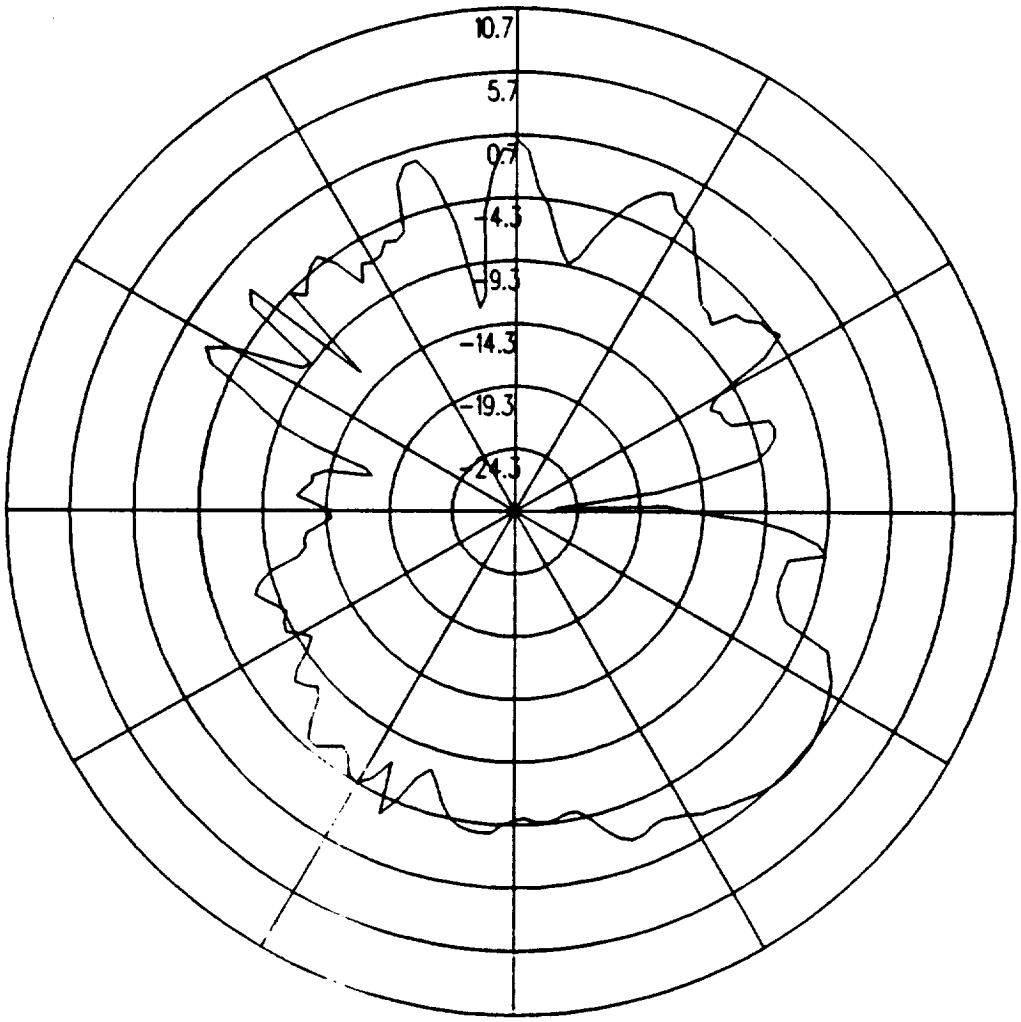

Figure 5.123: UTD calculated conical plane pattern 20° above the horizon for batwing antenna on a P-3C for right hand circular polarization at 300 MHz.(Test Location 10)

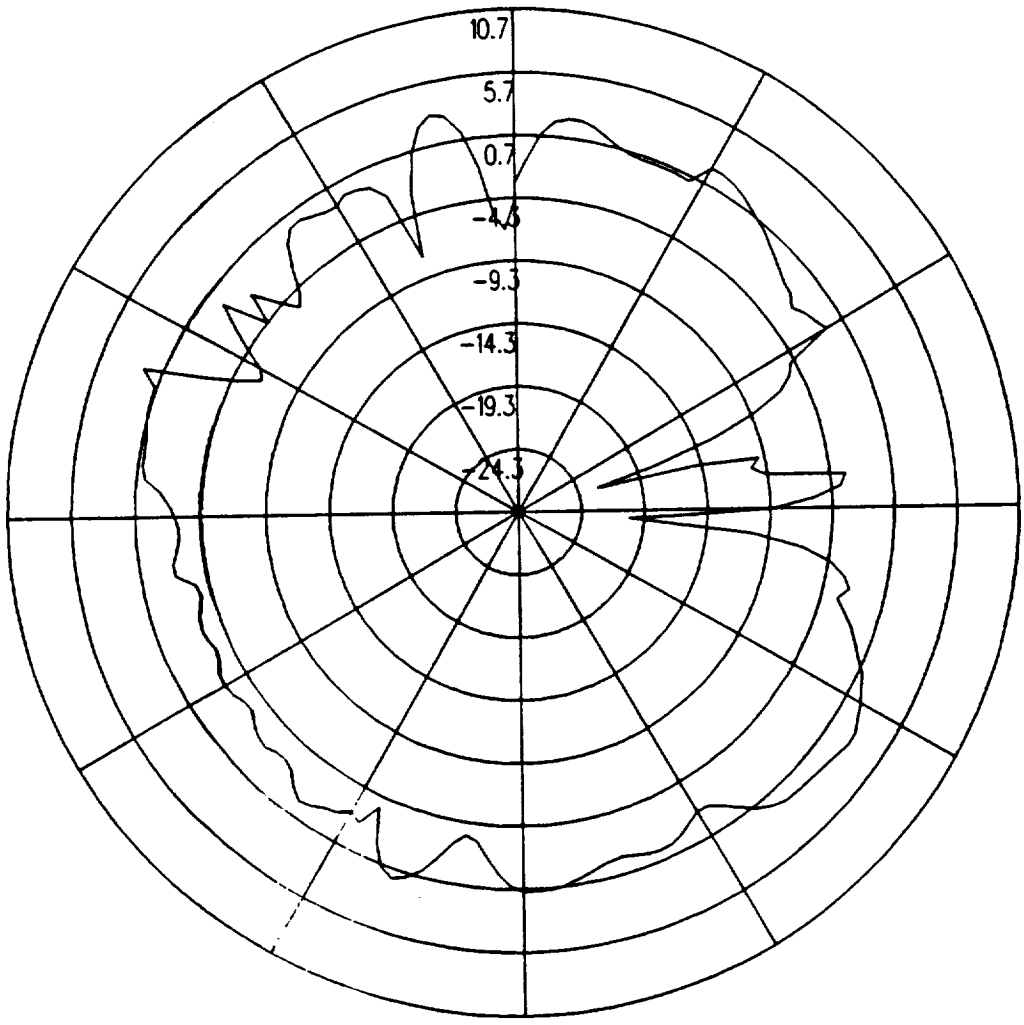

Figure 5.124: UTD calculated conical plane pattern 30° above the horizon for batwing antenna on a P-3C for right hand circular polarization at 300 MHz.(Test Location 10)

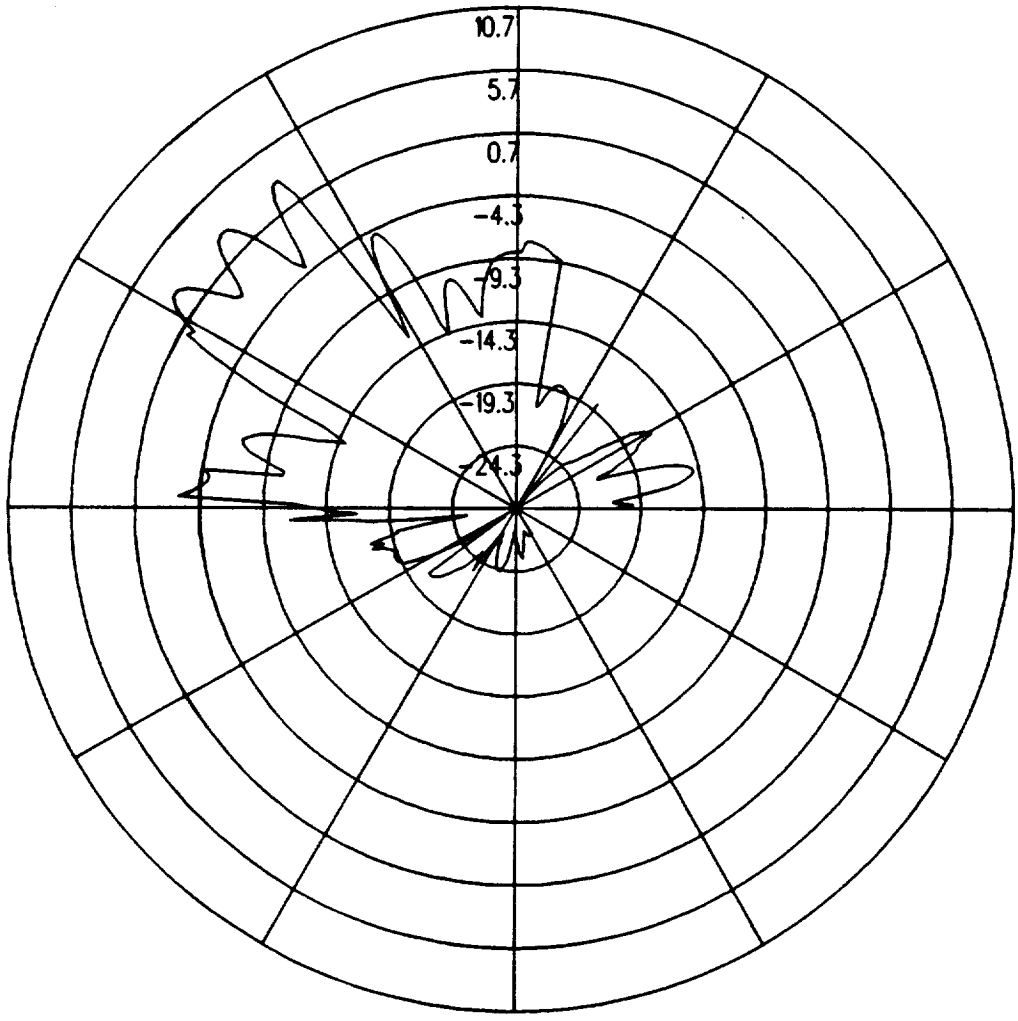

Figure 5.125: UTD calculated roll plane pattern for batwing antenna on a P-3C for left hand circular polarization at 300 MHz. (Test Location 10)

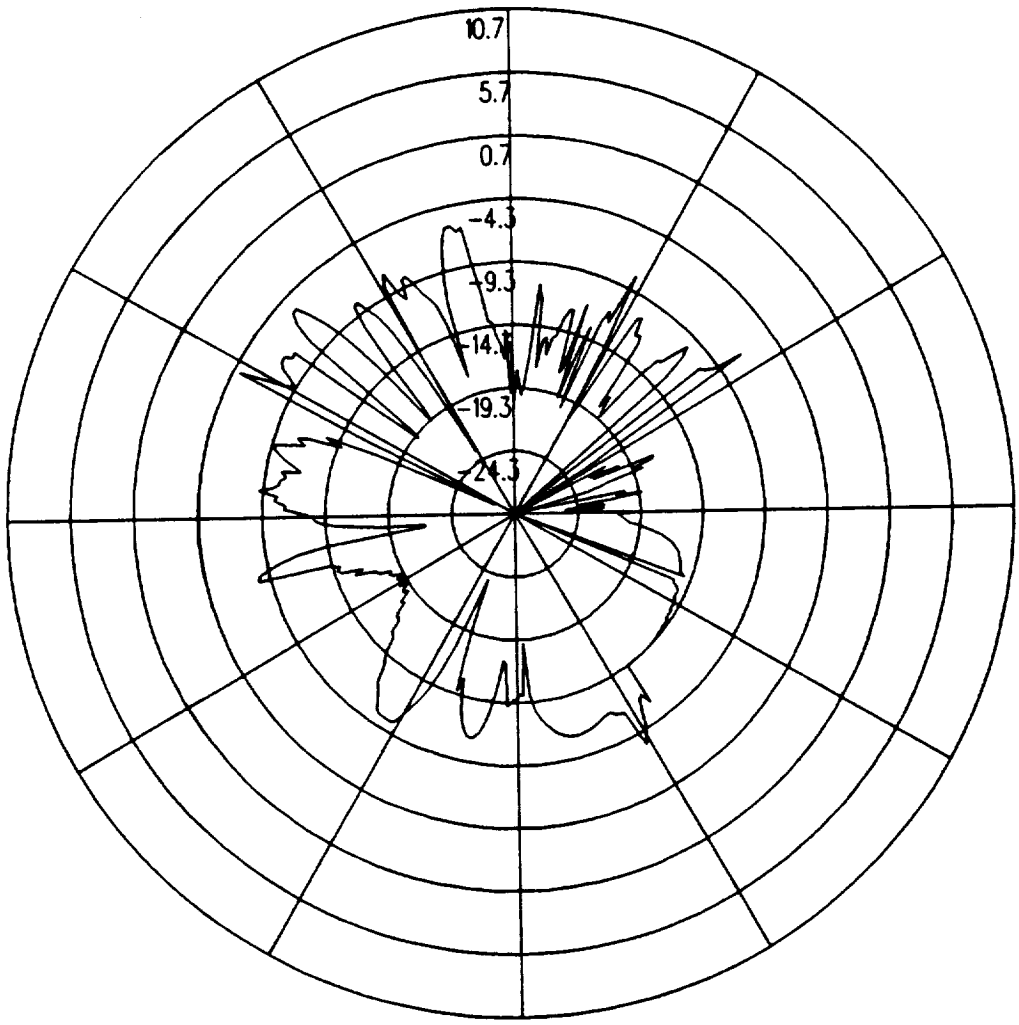

Figure 5.126: UTD calculated azimuth plane pattern for batwing antenna on a P-3C for left hand circular polarization at 300 MHz. (Test Location 10)

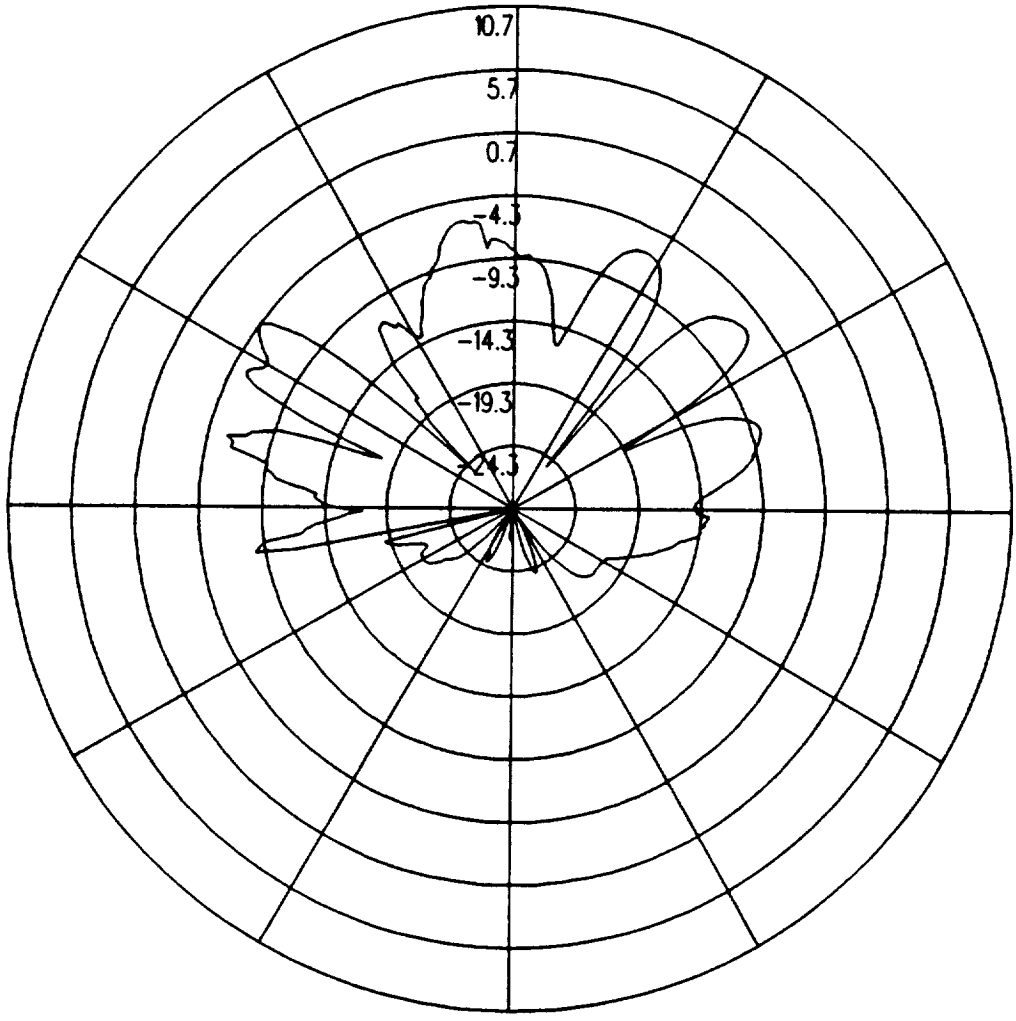

Figure 5.127: UTD calculated elevation plane pattern for batwing antenna on a P-3C for left hand circular polarization at 300 MHz. (Test Location 10)

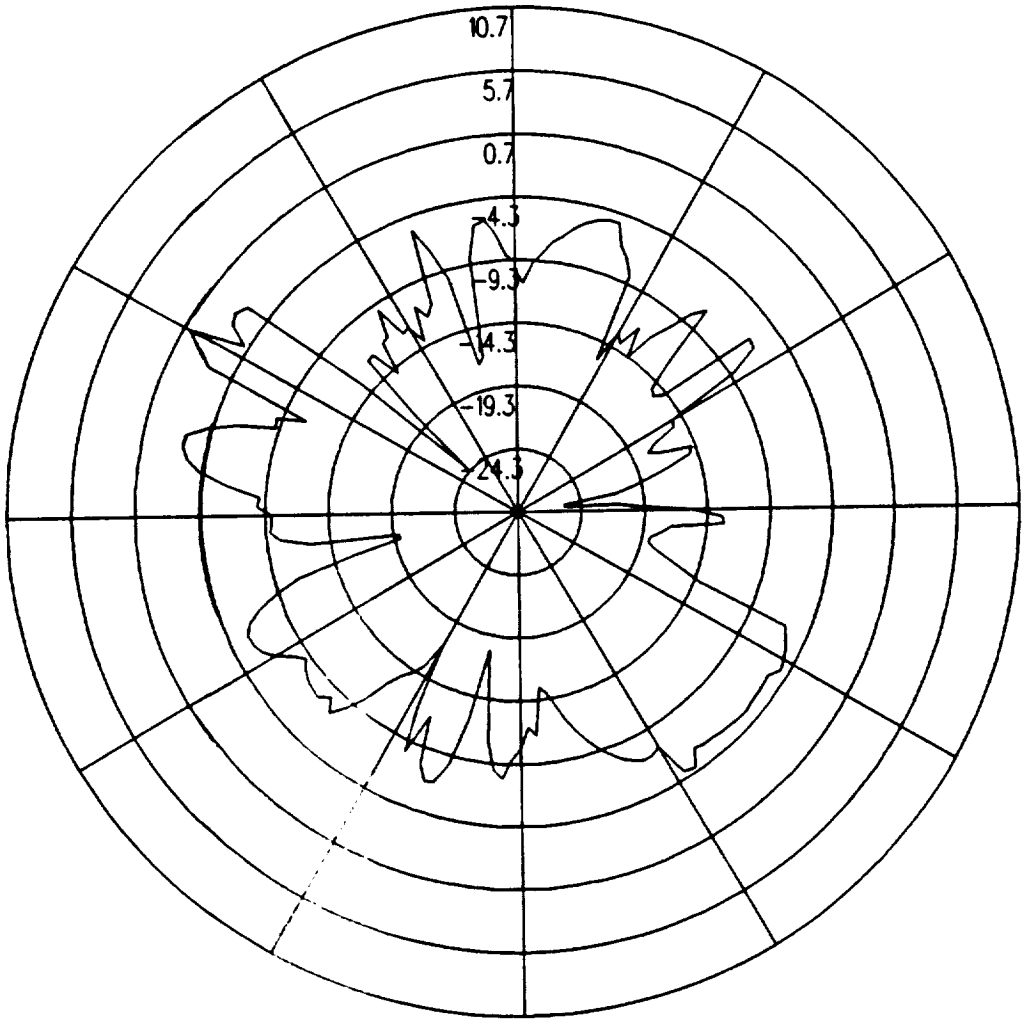

Figure 5.128: UTD calculated conical plane pattern 10° above the horizon for batwing antenna on a P-3C for left hand circular polarization at 300 MHz.(Test Location 10)

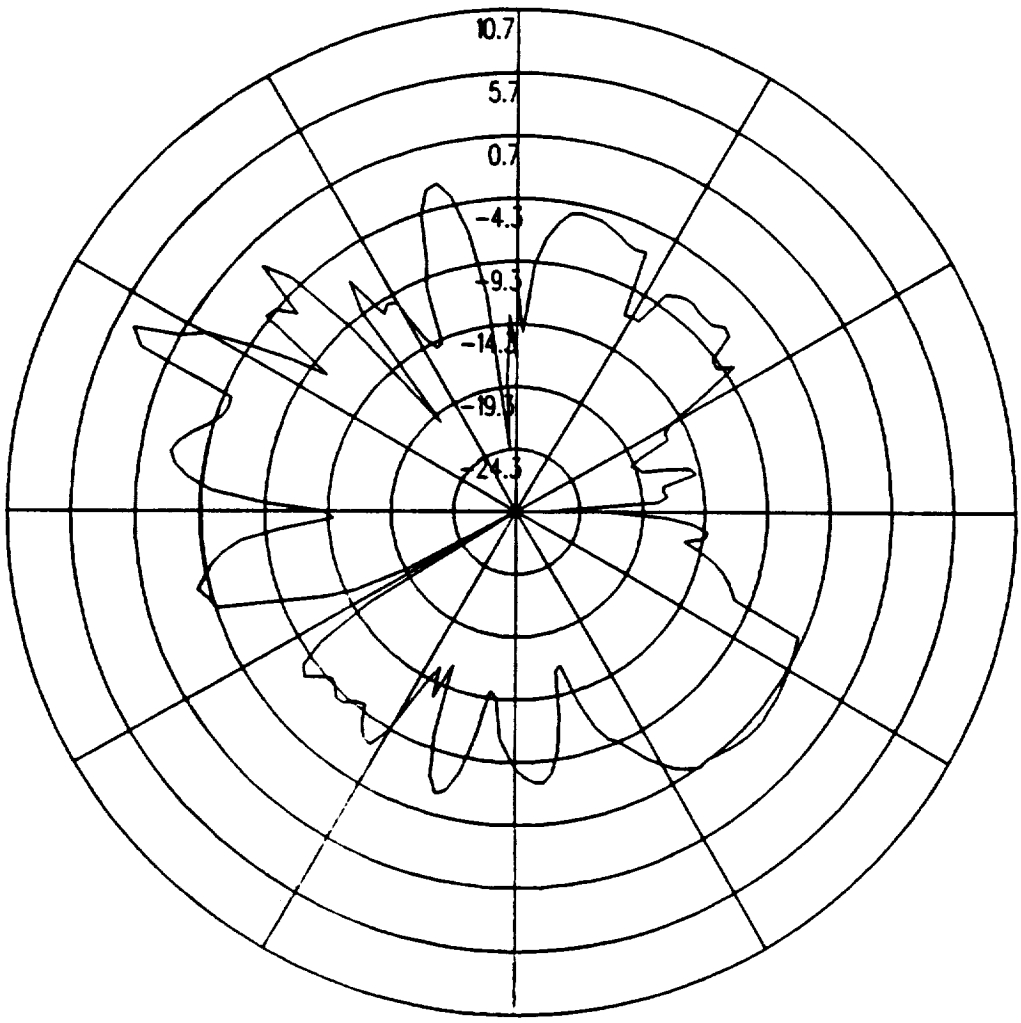

Figure 5.129: UTD calculated conical plane pattern 20° above the horizon for batwing antenna on a P-3C for left hand circular polarization at 300 MHz.(Test Location 10)

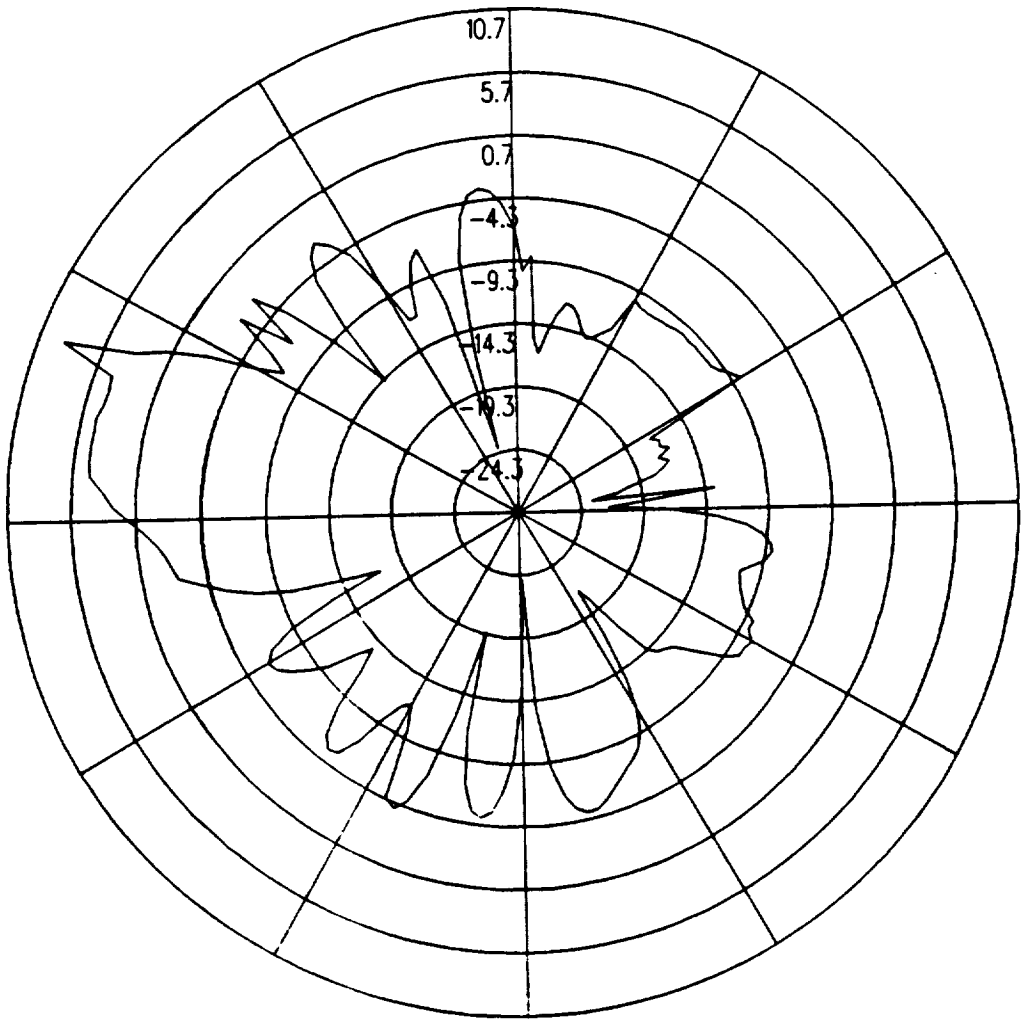

Figure 5.130: UTD calculated conical plane pattern 30° above the horizon for batwing antenna on a P-3C for left hand circular polarization at 300 MHz.(Test Location 10)

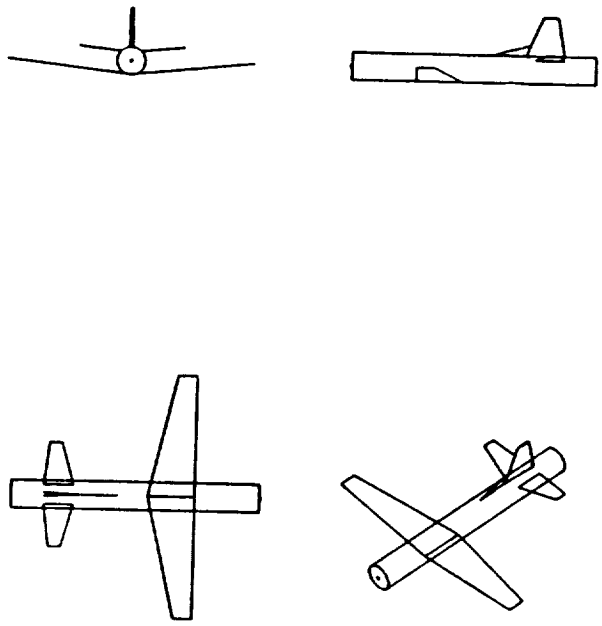

Figure 5.131: Geometry of the model of the P-3C aircraft used in the NEC-BSC code showing the location of the antenna.

5.11 Test Location 11

The antenna is located as illustrated in Figure 5.131, which also shows the computer model used to generate the results. The calculated results at 300 MHz are shown for the roll plane in Figure 5.132, for the azimuth plane in Figure 5.133, for the elevation plane in Figure 5.134, for the conical plane 10° above the horizon in Figure 5.135, for the conical plane 20° above the horizon in Figure 5.136, and for the conical plane 30° above the horizon in Figure 5.137 all for right hand polarization. The cross polarized fields are shown for the roll plane in Figure 5.138, for the azimuth plane in Figure 5.139, for the elevation plane in Figure 5.140, for the conical plane 10° above the horizon in Figure 5.141, for the conical plane 20° above the horizon in Figure 5.142, and for the conical plane 30° above the horizon in Figure 5.143 all for left hand polarization.

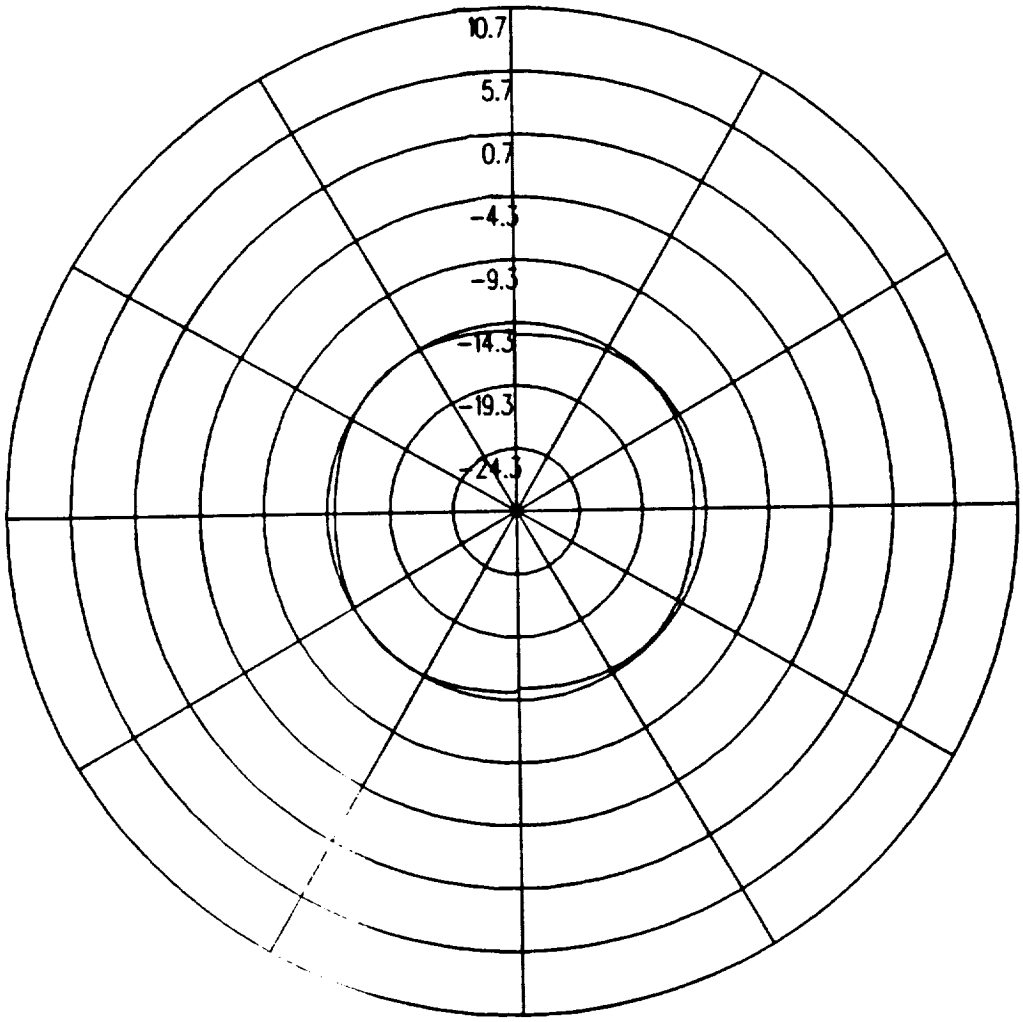

Figure 5.132: UTD calculated roll plane pattern for batwing antenna on a P-3C for right hand circular polarization at 300 MHz. (Test Location 11)

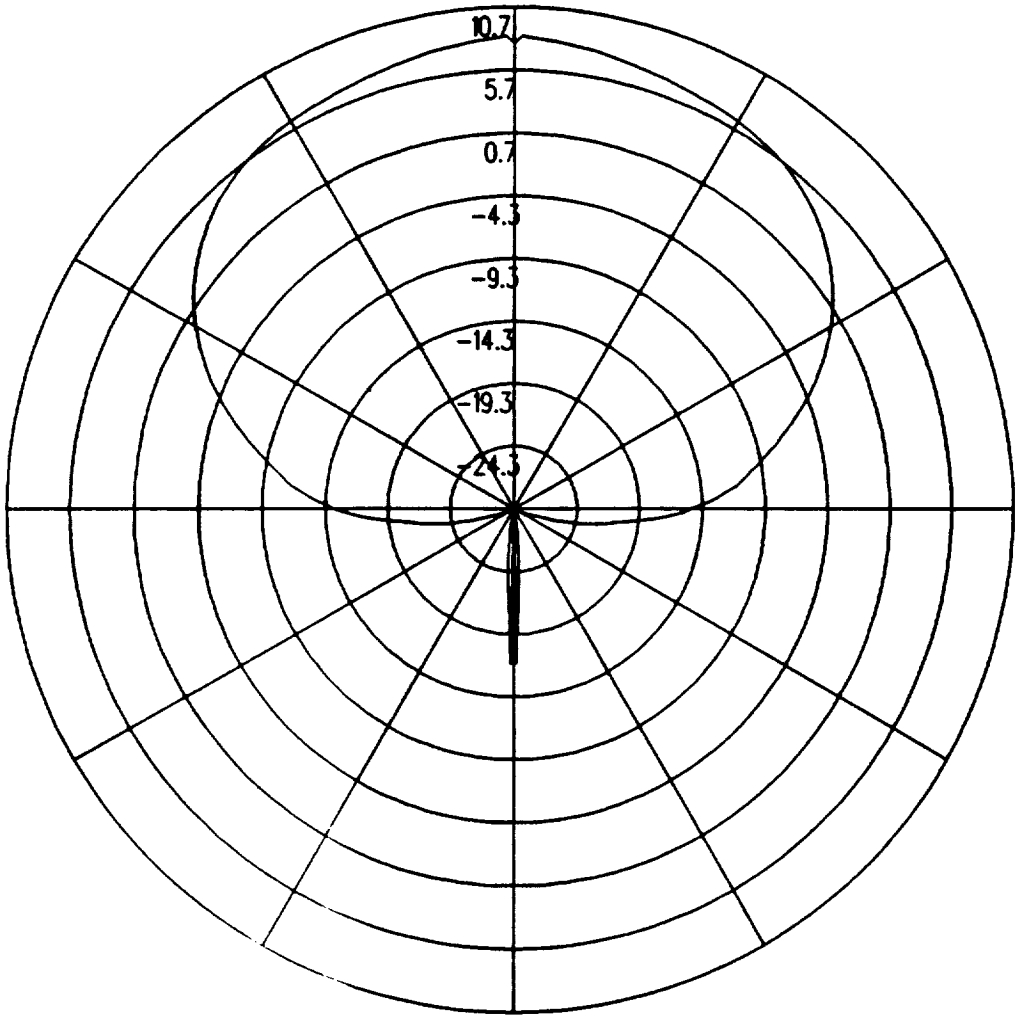

Figure 5.133: UTD calculated azimuth plane pattern for batwing antenna on a P-3C for right hand circular polarization at 300 MHz. (Test Location 11)

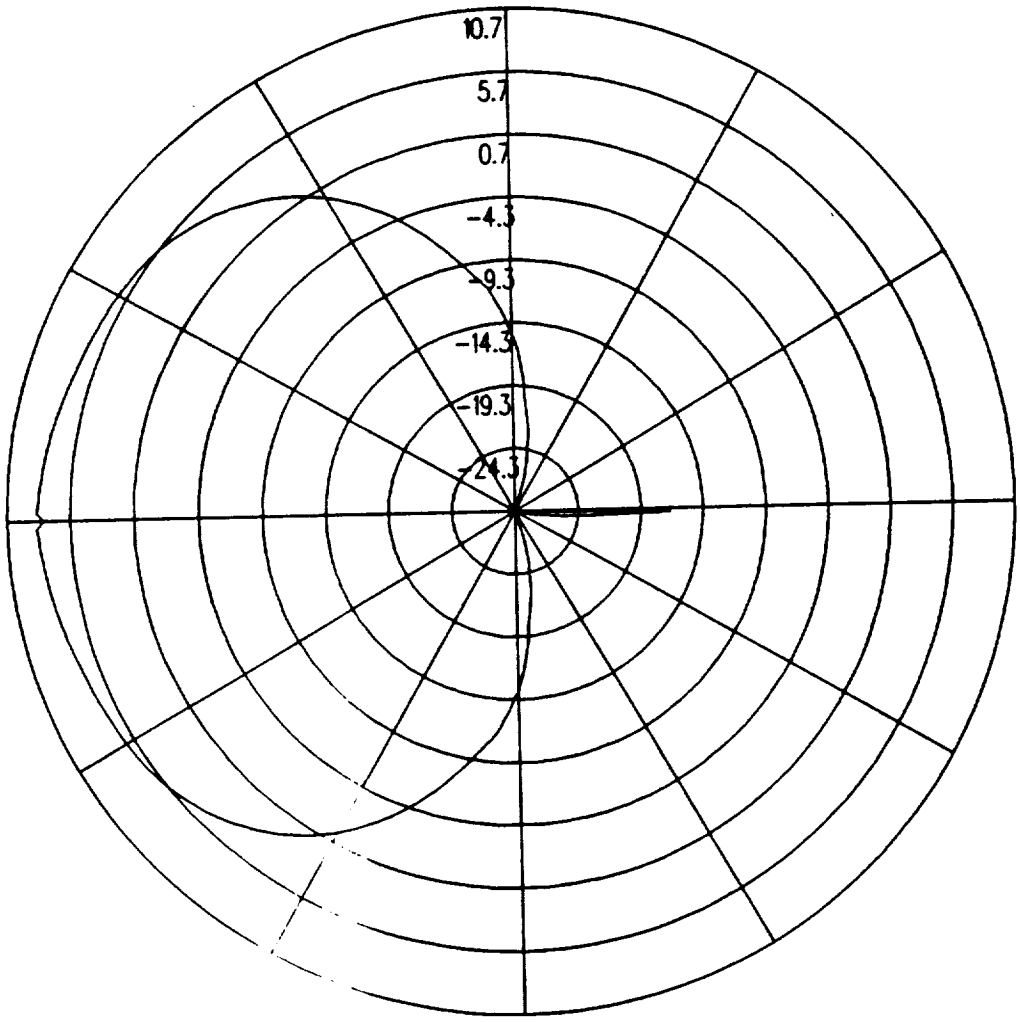

Figure 5.134: UTD calculated elevation plane pattern for batwing antenna on a P-3C for right hand circular polarization at 300 MHz. (Test Location 11)

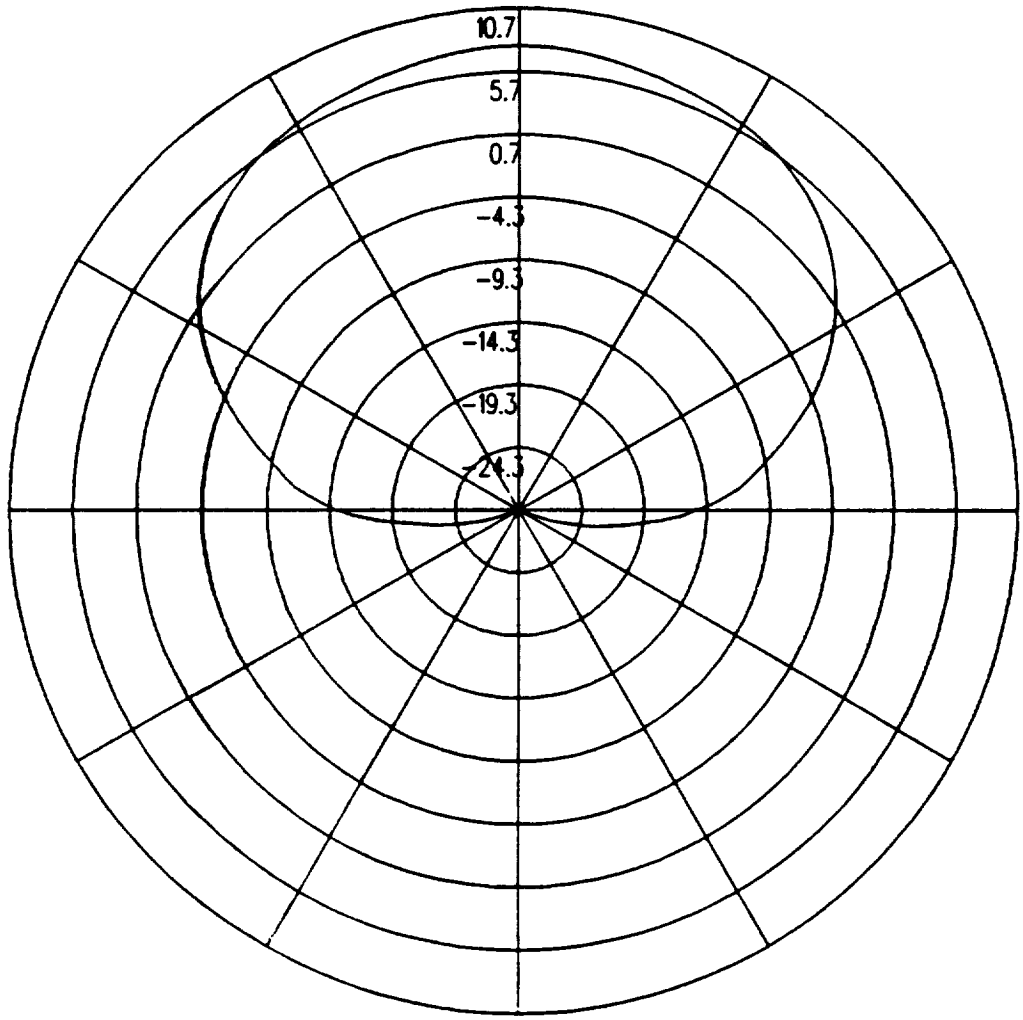

Figure 5.135: UTD calculated conical plane pattern 10° above the horizon for batwing antenna on a P-3C for right hand circular polarization at 300 MHz.(Test Location 11)

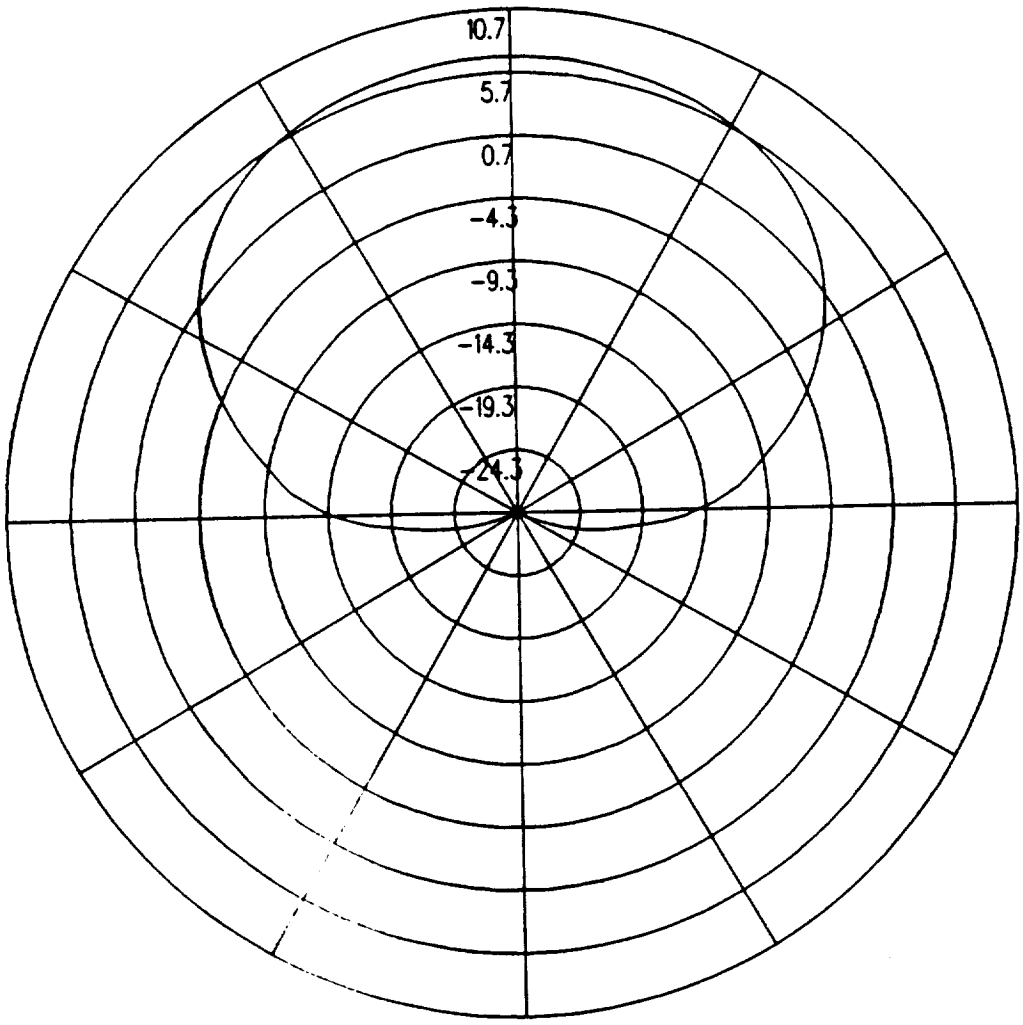

Figure 5.136: UTD calculated conical plane pattern 20° above the horizon for batwing antenna on a P-3C for right hand circular polarization at 300 MHz.(Test Location 11)

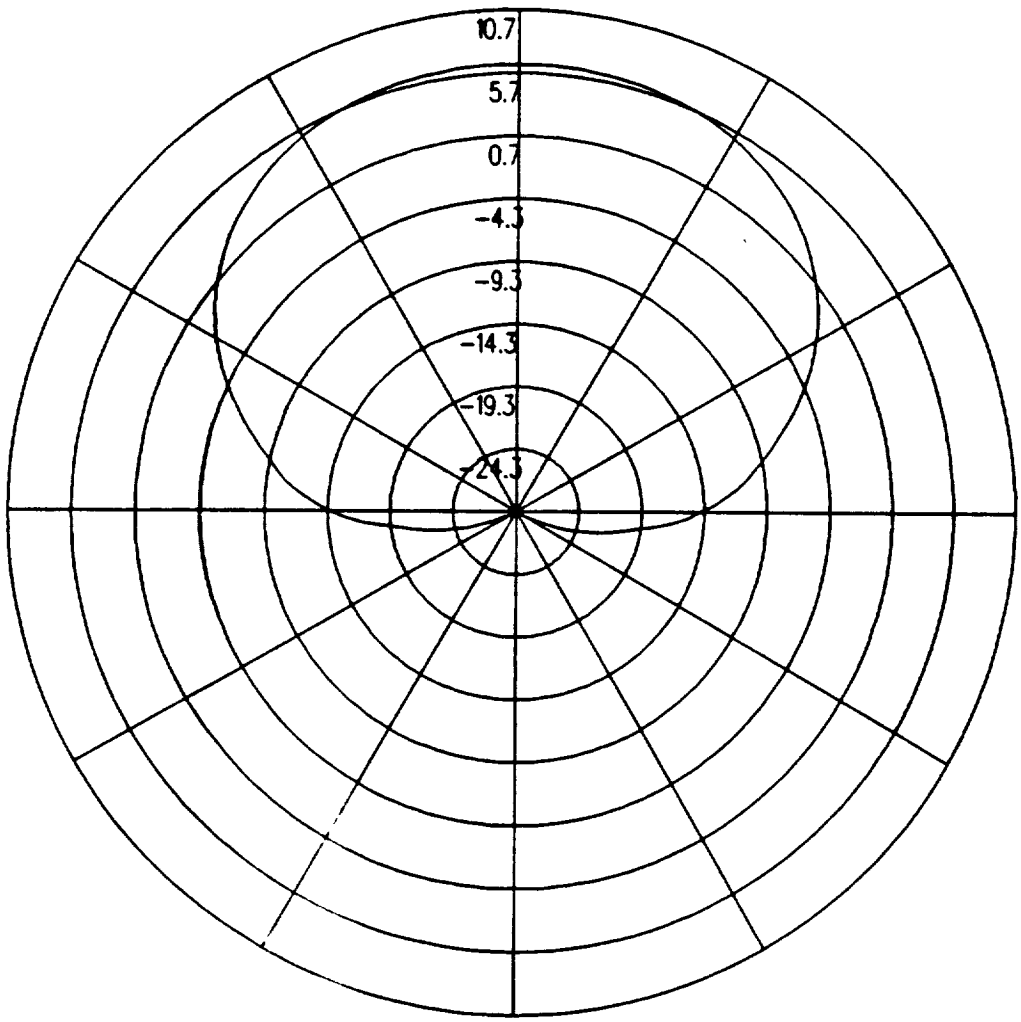

Figure 5.137: UTD calculated conical plane pattern 30° above the horizon for batwing antenna on a P-3C for right hand circular polarization at 300 MHz.(Test Location 11)

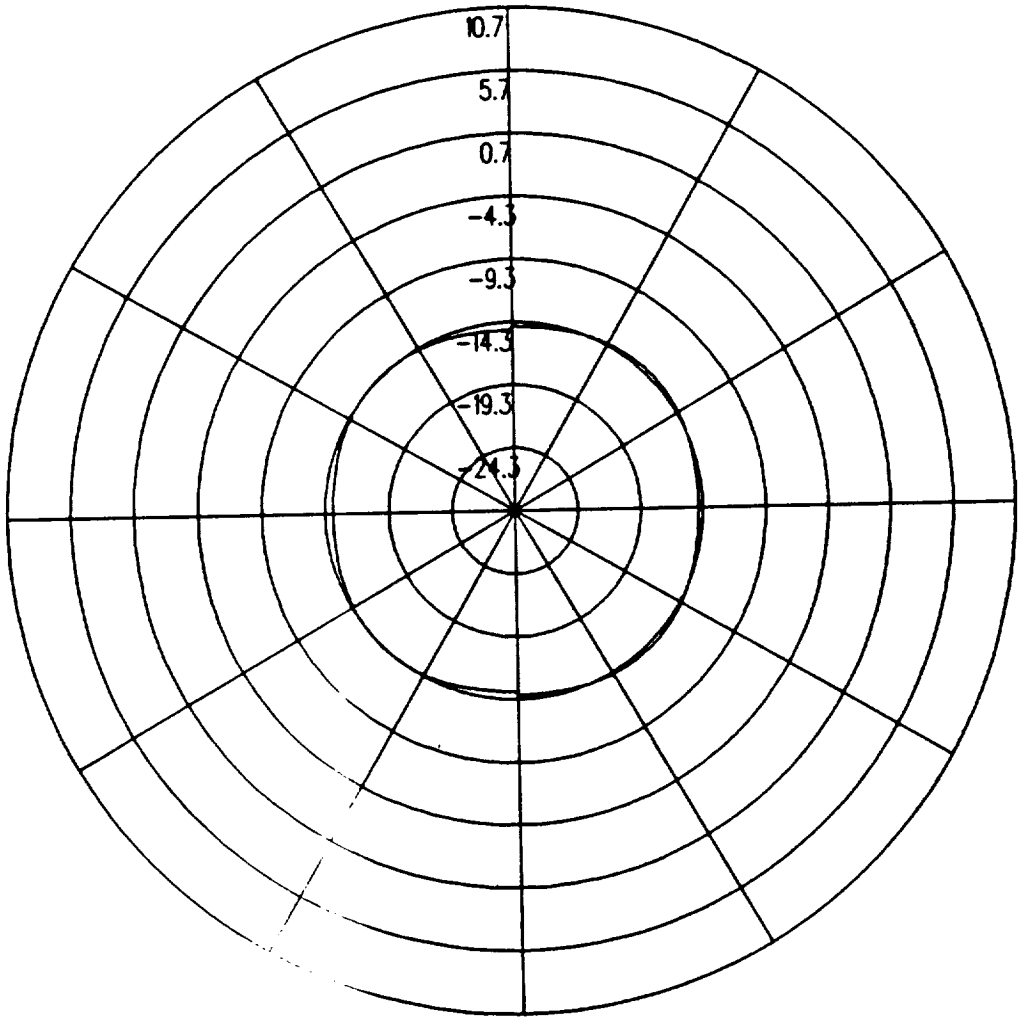

Figure 5.138: UTD calculated roll plane pattern for batwing antenna on a P-3C for left hand circular polarization at 300 MHz. (Test Location 11)

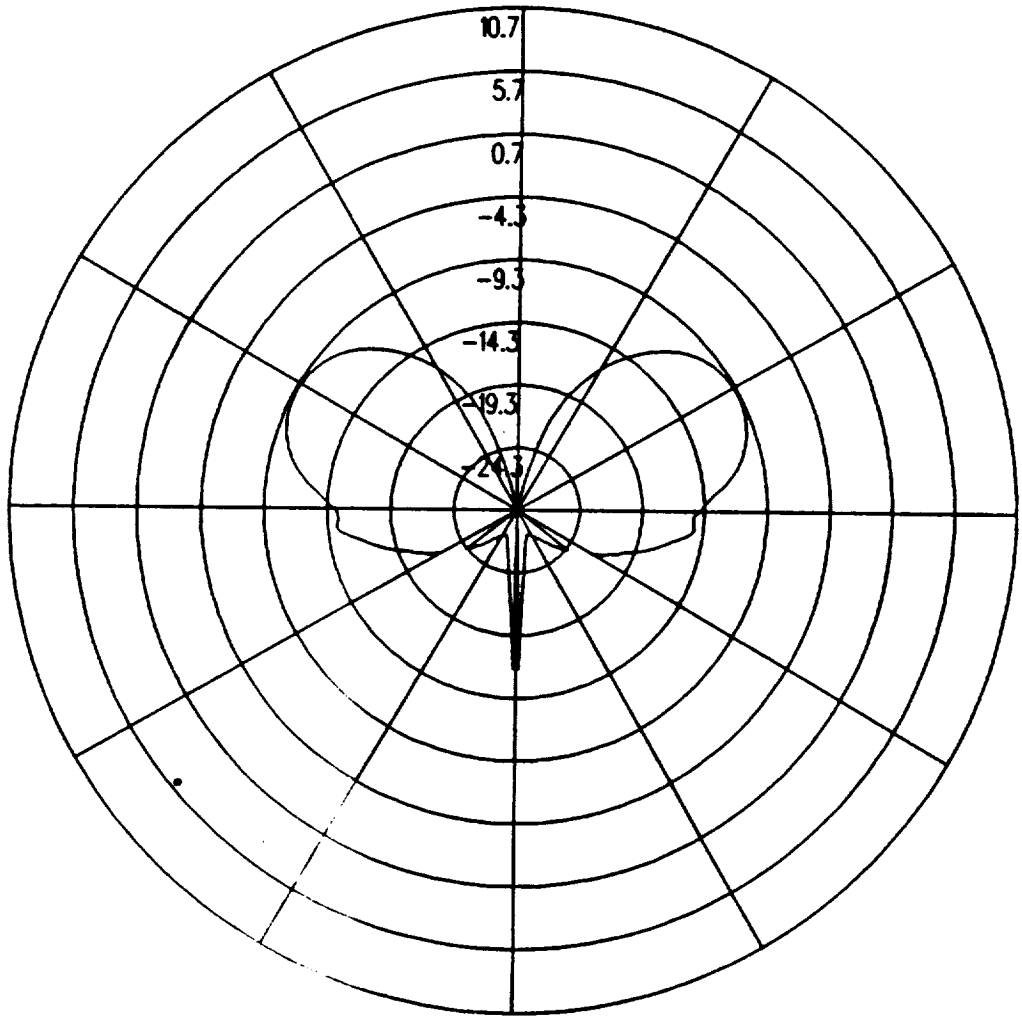

Figure 5.139: UTD calculated azimuth plane pattern for batwing antenna on a P-3C for left hand circular polarization at 300 MHz. (Test Location 11)

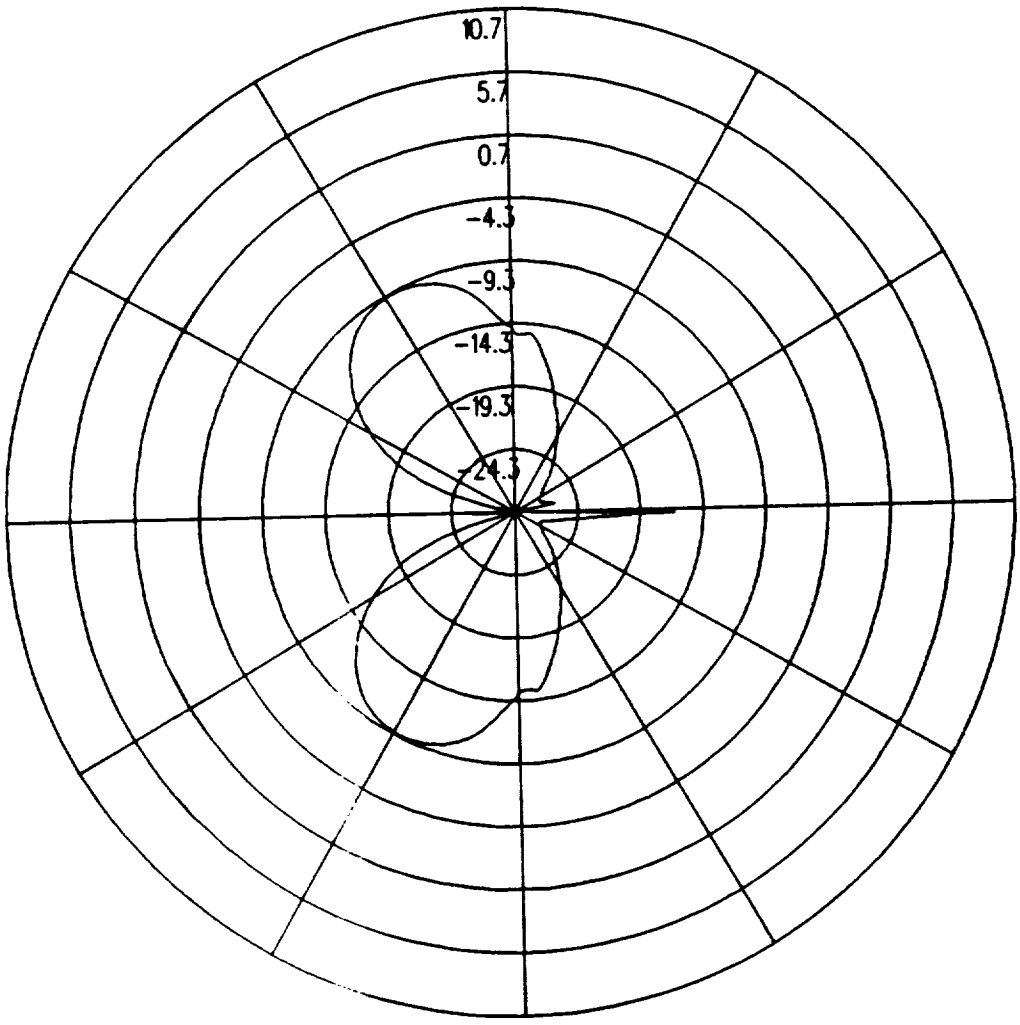

Figure 5.140: UTD calculated elevation plane pattern for batwing antenna on a P-3C for left hand circular polarization at 300 MHz. (Test Location 11)

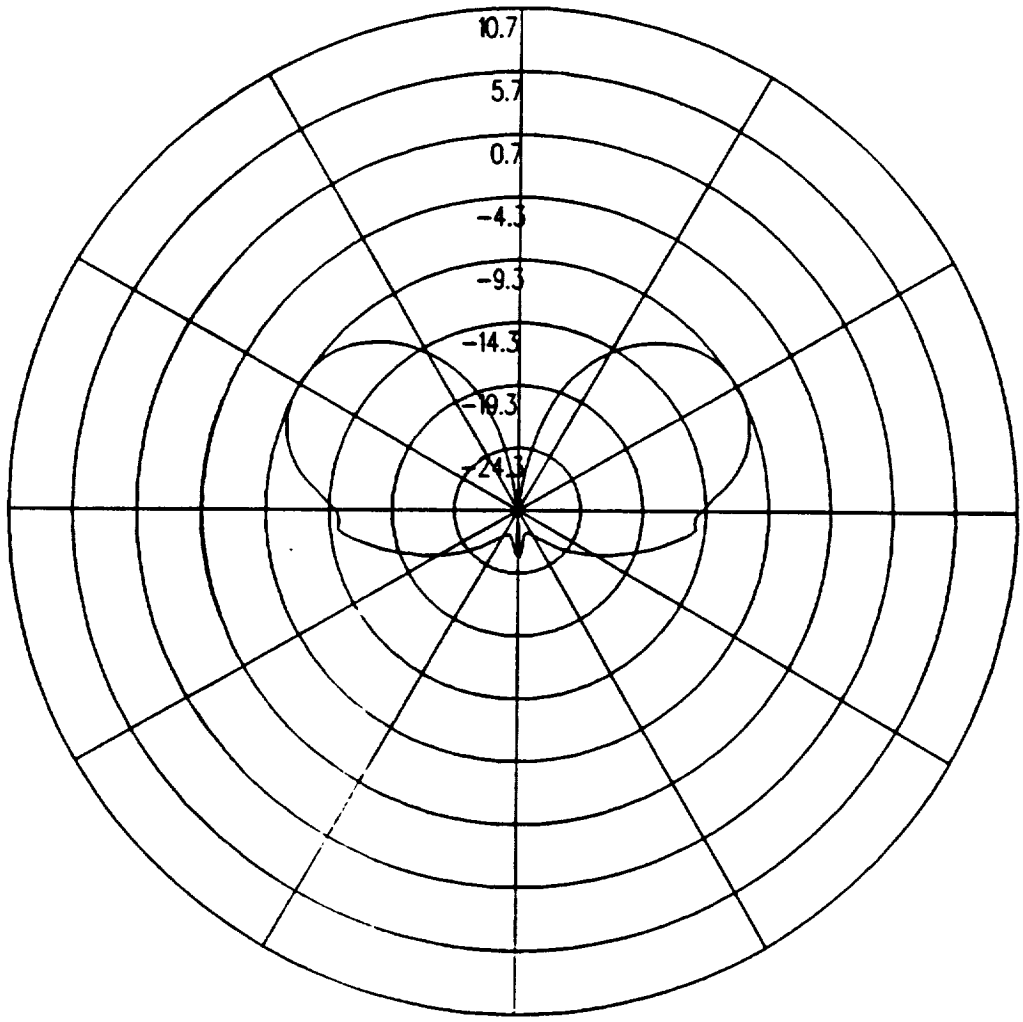

Figure 5.141: UTD calculated conical plane pattern 10° above the horizon for batwing antenna on a P-3C for left hand circular polarization at 300 MHz.(Test Location 11)

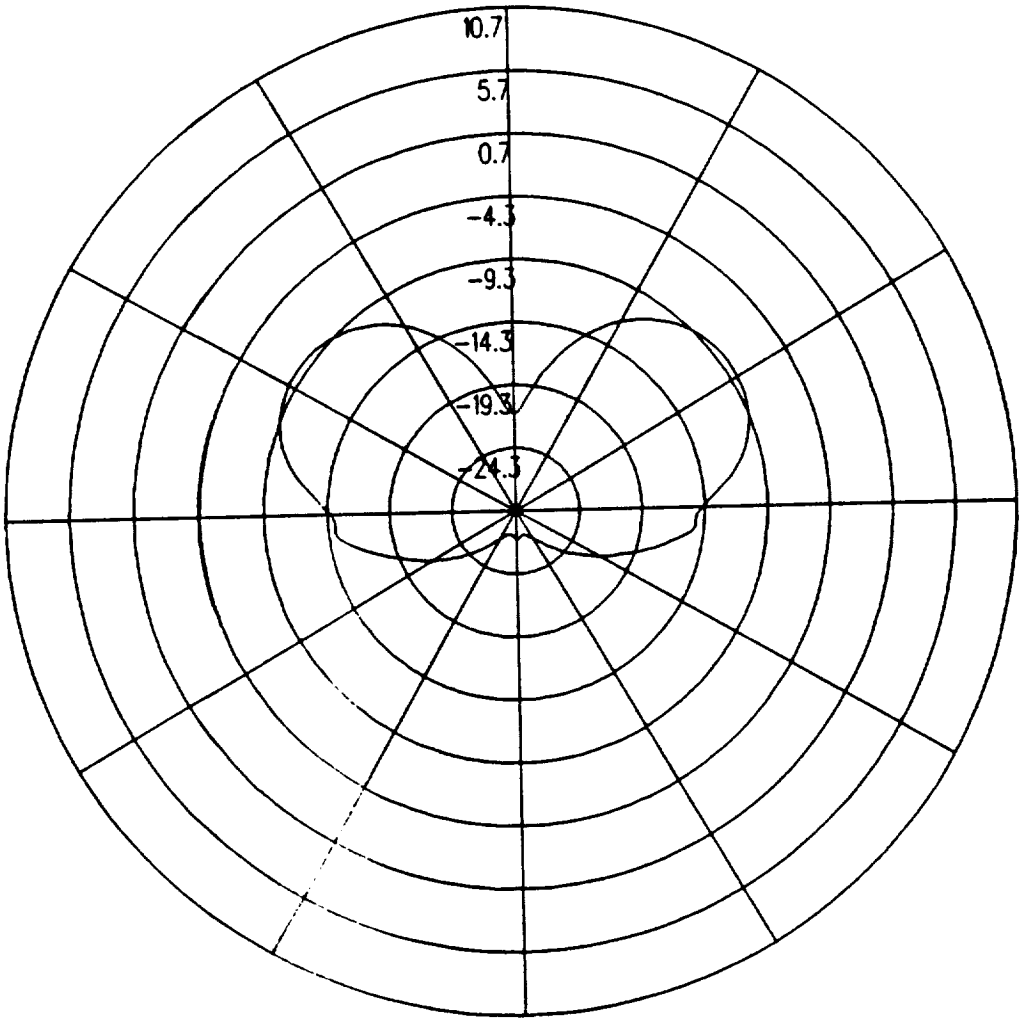

Figure 5.142: UTD calculated conical plane pattern 20° above the horizon for batwing antenna on a P-3C for left hand circular polarization at 300 MHz.(Test Location 11)

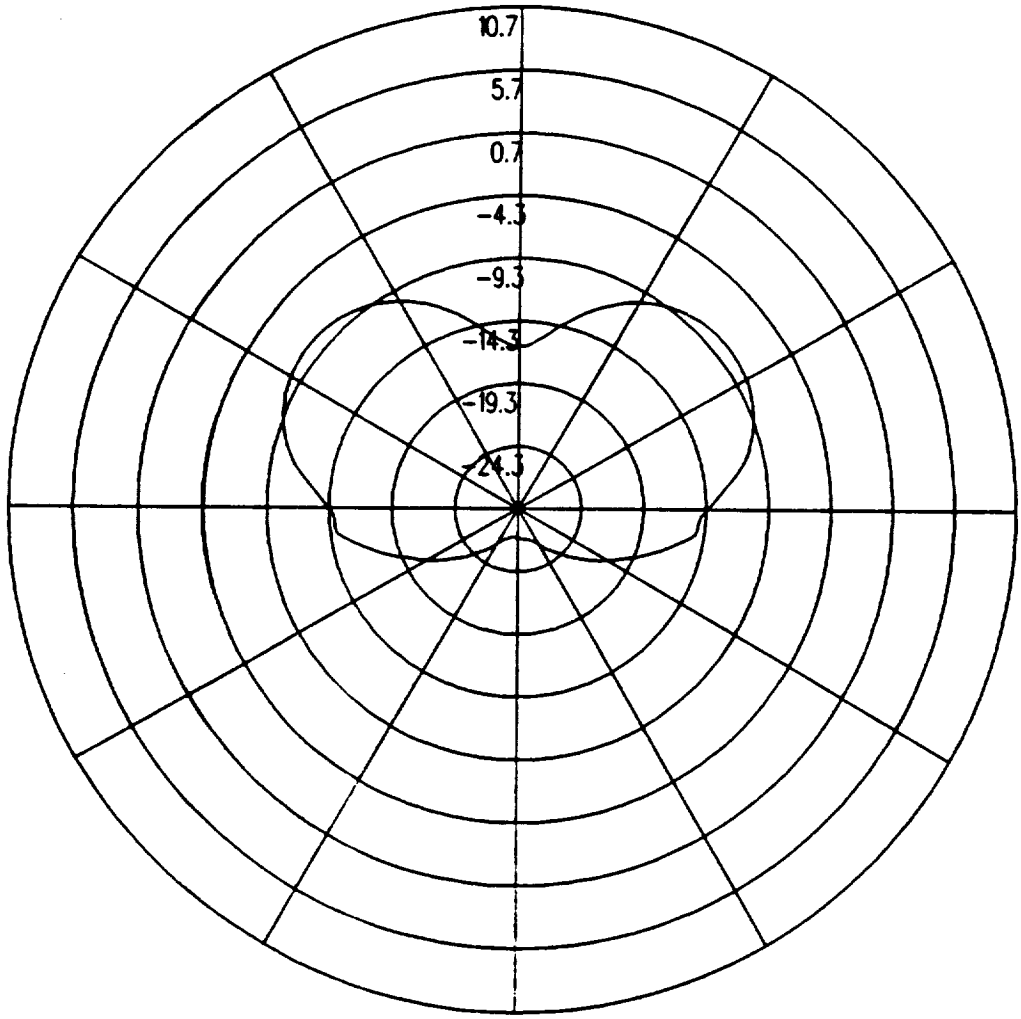

Figure 5.143: UTD calculated conical plane pattern 30° above the horizon for batwing antenna on a P-3C for left hand circular polarization at 300 MHz.(Test Location 11)

Chapter 6

Summary

In this chapter, a summary of the results found in this report and any tentative observations will be given. In the initial parts of this report, the antenna model and the aircraft model which are used in the NEC-BSC code are validated. From the comparisons between the NEC-BSC results and those obtained by other means, the degree of reliability in the computer code models is obtained. In the final parts of this report, an antenna location study is done on the P-3C aircraft. In this study, the antenna is positioned at various alternative locations on the P-3C aircraft to provide trade-off information as to overall pattern and polarization coverage.

6.1 Model Validation

In Chapter 3, the antenna model which has been used in the NEC-BSC code has been validated by comparing the calculated results with those acquired by other means. In the NEC-BSC code, a circular polarized antenna composed of crossed dipoles has been used to represent the Dorne & Margolin DM 1501341 Batwing antenna. In order to validate this model, antenna patterns have been calculated in two elevation cuts, one between the dipole arms and one along a dipole arm. These NEC-BSC calculated patterns for the antenna model have been compared to measured patterns provided by the manufacturer and measured patterns provided by Naval Air Test Center. Also, these NEC-BSC calculated antenna patterns have been compared to results calculated using a moment method solution and an exact eigenvalue solution. In each of these comparisons, the NEC-BSC calcu-

lated antenna patterns have been in good agreement with the corresponding measured patterns or calculated patterns found using other methods. Therefore, there is a high level of confidence in the antenna model which has been used throughout this report.

To validate the aircraft model which has been used in the code, radiation patterns for various antenna locations on the P-3C aircraft model have been compared to corresponding measured radiation patterns provided by Boeing [8] and Lockheed [9] in Chapter 4. Overall, the NEC-BSC calculated patterns show good agreement with the measured results for the various antenna locations throughout the majority of the areas of interest. The sole exception is that the calculated levels by the nose and tail near the horizon of the aircraft are higher by as much as 5–8 dB than the measured levels provided by Boeing and Lockheed. These higher levels near the nose and tail of the aircraft on the horizon have been investigated extensively and are most likely due to the fact that the plate - cylinder interactions which have been simulated using the imaging technique explained in Section 2.2 are only approximations. When the exact plate - cylinder interactions are implemented in the code, the differences between the measured and calculated results are anticipated to be reduced. Therefore, except for small 10° conic regions about the nose and tail near the horizon of the aircraft, there is a high level of confidence that the aircraft model accurately represents the actual P-3C aircraft. Unfortunately, this region is critical to the present siting study. The implementation of the plate - cylinder interactions into the NEC-BSC will be made as soon as possible. It is hoped that the present results can be used temporarily by extrapolating into all regions. This is attempted below.

6.2 Location Study

Chapter 5 details 11 alternative antenna locations on the P-3C aircraft which have been studied. Three of these alternative antenna locations are on the top center line of the aircraft fuselage. The difference between the three locations involves the relative position on the aircraft fuselage. One location is near the nose of the aircraft, the second location is just fore of the wings, and the third location is just aft of the wings. The next two alternative locations studied are on the nose of the aircraft. In these tests,

the composite ellipsoid aircraft model is used because the elliptical nose is critical in the radiation patterns. Two other locations studied are left of the top center line of the fuselage. In the first, the antenna is located directly over the left wing and in the second, the antenna is located half the distance between the wing and the nose of the aircraft. Two additional locations studied are on the vertical stabilizer. One location is parallel to the vertical stabilizer and the other location is on top of the vertical stabilizer. In the next case, the antenna is located on the left tailplane. In the final case studied, the antenna location is on the flat endcap of the aircraft's cylindrical fuselage.

The results found for the three antenna locations on the top center line of the fuselage can be found in Sections 5.1 - 5.3 . The results show that these antenna locations provide good coverage in the main region above the aircraft (i.e., over 30° above the horizon). However, as the pattern approaches the horizon of the aircraft, the coverage decreases to the point that the pattern levels near the horizon of the aircraft are as much as 15 dB below the levels found for the antenna locations used by Boeing and Lockheed in Chapter 4.

The results found for the two antenna locations on the nose of the aircraft can be found in Sections 5.4 and 5.5 . The results show that these antenna locations provide good coverage in the main region above the aircraft (i.e., over 30° above the horizon). Just above the horizon near the nose of the aircraft, these antenna locations also provide good coverage. However, above the horizon near the tail of the aircraft and near the horizon of the aircraft, the pattern levels are as much as 10–15 dB below the levels found for the antenna locations used by Boeing and Lockheed in Chapter 4.

The results found for two additional antenna locations which are left of the top center line of the fuselage can be found in Sections 5.6 and 5.7 . Like the results found in Chapter 4, these antenna locations provide good coverage in the main region above the aircraft (i.e., over 30° above the horizon). These antenna locations also provide good coverage in the region to the left of the aircraft near the horizon. However, near the horizon of the aircraft by the nose and the tail, the pattern levels drop off as much as 10 dB which is the same trend found in the results calculated for the antenna locations used by Boeing and Lockheed in Chapter 4.

The results found for two antenna locations on the vertical stabilizer of the aircraft can be found in Sections 5.8 and 5.9 . The antenna located

parallel to the vertical stabilizer provides good coverage in the region to the left of the aircraft both above and below the horizon. However, in the elevation plane the coverage is very poor. The antenna located on top of the vertical stabilizer provides good coverage in the elevation plane. However, throughout the remainder of the patterns, the coverage provided by this antenna location is not very good.

The results found for the antenna location on the left tailplane of the aircraft can be found in Section 5.10 . The antenna location provides good coverage in the main region above the aircraft (i.e., over 30° above the horizon). However, as the pattern approaches the horizon of the aircraft, the coverage decreases to the point that the pattern levels near the horizon of the aircraft are as much as 20 dB below the levels found for the antenna locations used by Boeing and Lockheed in Chapter 4. The results found for the antenna location on the flat endcap of the cylindrical fuselage can be found in Section 5.11 . This antenna location provides excellent coverage near the nose of the aircraft; however, elsewhere the coverage is very poor.

6.3 Observations

The above antenna location studies have been inspected as separate cases. None of these alternative antenna locations have been able to provide better overall pattern and polarization coverage than the original locations studied by Boeing [8] and Lockheed [9]. However, it is possible to use a combination of these locations, which alone do not provide adequate coverage, to achieve the desired goal. As stated in Chapter 4, the original locations studied by Boeing and Lockheed have good overall pattern and polarization coverage in all areas except for the regions in the horizon near the nose and tail of the aircraft. Therefore, one or a combination of the alternative locations studied in Chapter 5 must provide the desired pattern coverage in these problem regions. The antenna located on the nose of the aircraft which is investigated in Section 5.5 provides the desired pattern coverage for the region in the horizon near the nose of the aircraft, however, this antenna location does nothing to enhance the coverage near the tail. The antenna location which provides the best coverage for the region in the horizon near the tail of the aircraft is the antenna located on top of the vertical stabilizer which is investigated in Section 5.9. Although the levels in this region are

up to 10 dB below the isotropic level, this coverage is adequate for this application. The levels in the horizon near the nose of the aircraft for this antenna location are nearly the same as the levels near the tail, therefore, the levels near the nose will likewise be satisfactory for this application and the antenna location studied in Section 5.5 will not be needed. Therefore, the desired goal of sustaining high levels of coverage throughout the pattern can be achieved by using either of the original antenna locations studied by Boeing or Lockheed along with the antenna location studied in Section 5.9. One problem which may occur in implementing this solution is that little consideration has been given to whether the locations are aerodynamically or economically feasible. Also, no attempt has been made to investigate alternative antenna types at this time.

The code has confirmed the measurement studies. In the future, a computer study such as this can be effectively used in the initial design stages to home in on reasonable siting locations. A limited set of measurements then can be more cost effectively utilized to confirm the prospective locations.